Post-Last Glacial Maximum vegetation and ecosystem responses to climate change and human expansion in the Neotropical realm: land cover changes and megafauna extinctions

By

Antoine Champreux

Thesis submitted to Flinders University for the degree of

Doctor of Philosophy

College of Science and Engineering

24th of February 2024

Post-Last Glacial Maximum vegetation and ecosystem responses to climate change and human expansion in the Neotropical realm: land cover changes and megafauna extinctions

By

Antoine Champreux

Master's degree

Thesis

Submitted to Flinders University

for the degree of

Doctor of Philosophy

College of Science and Engineering

24th of February 2024

Post-Last Glacial Maximum vegetation and ecosystem responses to climate change and human expansion in the Neotropical realm: land cover changes and megafauna extinctions

By

Antoine Champreux

Master's degree

Thesis
Submitted to Flinders University
for the degree of

Doctor of Philosophy

College of Science and Engineering

24th of February 2024

To my parents, Isabelle and Jean-Marc Champreux
À mes parents

Changing landscape after the Ice Age – copyright Fiona Laviano (2024)

TABLE OF CONTENTS

ABSTRACT

The post-Last Glacial Maximum period (~ 19,000 years ago to the present) was characterised by major changes in the global climate and atmospheric CO_2 concentration, such as the general increase in global temperatures and changes in precipitation regimes. In the Neotropical realm, a biogeographical region spanning the southern edge of the USA to Tierra del Fuego in Chile in southernmost South America, this period coincided with widespread ecosystem upheavals, including vegetation changes, the extinction of more than 80% of South American megafauna species (i.e., species weighing > 44 kg), and the increase in population densities of *Homo sapiens*. However, quantifying how the relationships between these events shaped South America's past landscape remains a challenge. The overarching aim of my thesis was to quantify how past environmental changes associated with an increase in human pressure shaped South America's ecosystems. More specifically, I aimed to 1) synthesise knowledge and quantify the effects of post-Last Glacial Maximum climate change and the intensification of human activities on Neotropical ecosystems at broad spatial scales focussing primarily on changes in vegetation, and 2) determine whether climate-induced vegetation changes after the Last Glacial Maximum could have caused megafauna extinctions in the Neotropical realm. To that end, I combined the information provided by palaeo-environment and megafauna fossil records with a spatial and dynamic vegetation modelling approach driven by palaeo-climate simulation experiments. I showed that variation in precipitation, temperature, solar radiation, and atmospheric CO_2 have potentially led to substantial, widespread, and asynchronous increases in regional tree cover, strongly affecting a third of the Neotropical realm mainly prior to the beginning of the Holocene (~11,700 years before present). While the effect of climate appears to be predominant in large-scale ecosystem changes prior to the Holocene, human activities played an increasingly important role during the Holocene, resulting in a progressive decoupling between vegetation patterns and climate, consequently also blurring our current understanding of climate-vegetation relationships. My results also support the hypothesis that climate-induced vegetation changes were likely not the main driver of the demise of most megafauna species in the Southern Cone (latitude > 30 °S) at the very end of the Pleistocene. Overall, my thesis provides a better understanding of the broad-scale mechanisms that shaped Neotropical ecosystems as we know them today, and provides insights to predict the response of these ecosystems to future climate change and the ongoing intensification of human endeavour.

DECLARATION

I certify that this thesis:

1. does not incorporate without acknowledgment any material previously submitted for a degree or diploma in any university
2. and the research within will not be submitted for any other future degree or diploma without the permission of Flinders University; and
3. to the best of my knowledge and belief, does not contain any material previously published or written by another person except where due reference is made in the text.

Signed: Antoine CHAMPREUX
Date: 24.02.202

ACKNOWLEDGEMENTS

I was warned before I embarked on this project: writing a doctoral thesis is like a journey of initiation, an adventure that must be undertaken with courage, patience, determination and certainly a touch of madness. Looking back today (which is a good thing, because I've made it my speciality!), I'm convinced that I could never have predicted what has happened over the last five years. If I had to describe the road I've travelled in three words, it would be something like: "What a hell of a journey!”. It has been a journey filled with discoveries and unexpected events, doubt and *Eureka*, difficulties and wonder. Above all, writing this thesis has been a journey filled with human interaction. I hope to be able to take advantage of this very important section of my thesis to thank those without whom this thesis would undoubtedly not have been what it is today, while hoping not to forget anyone.

First of all, I would like to thank all those who have helped me on a scientific level and during the course of this thesis. I would like to thank the two assessors who agreed to evaluate this work. Thanks to my two thesis supervisors who entrusted me with this subject and followed the progress of this work for five years, even during the last three years when I wrote my thesis from France, thousands of kilometres from our Australian laboratory. Thanks to Dr Frédérik Saltré (Flinders University, Australia) for the many scientific discussions, and for his support and availability at difficult times. Thanks to Prof Corey Bradshaw (Flinders University, Australia) for having confidence in my ability to carry out this 'ambitious' work, and for entrusting me with this subject. Thank you to them for having contributed so much to training me in the challenges of ecosystem modelling, about which I knew very little before starting the project. Thanks to the two assessors, A/Prof Bastien Llamas and A/Prof John Tibby (University of Adelaide, Australia), who patiently re-read my work every year and gave me invaluable advice. Thanks to Prof Catherine Abbott (Flinders University, Australia) for combining administrative support with listening and empathy. Many thanks to Flinders University (Adelaide, Australia) for funding this research.

I would like to thank the researchers at the Senckenberg Biodiversity and Climate Center (SBik-F, Germany) for welcoming me to Frankfurt for a month during my first year of research in order to train me in the use of the LPJ-GUESS dynamic vegetation model, which I was then able to use in several chapters of this thesis. I would particularly like to thank Wolfgang Traylor (SBik-F, Germany), without whom I am sure this thesis would have been very different. Thanks to Wolfgang for sharing with me their passion for things well done, for helping me overcome my fear of computer tools, for their interest in my subject, and for the many scientific and ethical discussions. I would like to thank Dr Matthew Forrest (SBik-F, Germany) for having mainly taken care of my training in the use of LPJ-GUESS during the month I spent in Frankfurt, and for the exchanges that followed. Thank you to Prof Thomas Hickler (SBik-F and Goethe University, Germany) for the valuable scientific discussions, his optimism and his confidence.

Thank you to those who gave me their valuable scientific input during the writing of the various chapters. Thanks to Fiona Laviano (Flinders University, Australia) for our many exchanges on the history of humanity, and for her invaluable advice on radiometric dating techniques. Thanks to Feng He (University of Wisconsin-Madison, USA) for our discussions on palaeo-climate experiments and for his availability during the final months of writing this thesis. Thanks to Agathe Toumoulin (Masaryk University, Czech Republic) for our discussions on palaeo-climates and modelling. Thanks to Dr Erwin González-Guarda (Instituto de Ciencias de la Ingeniería, Universidad de O'Higgins, Chile; Institut Català de Paleoecologia Humana i Evolució Social, Spain) for our discussions and for his advice on the diets of large herbivores in South America. Thanks to A/Prof Michael Dee (Center for Isotope research, University of Groningen, Netherlands) and Dr Gregory Hogdins (University of Arizona AMS Laboratory, USA) for additional information on some of the radiocarbon dating of South American megafaunal remains.

I am very grateful to my fellow researchers who, in addition to my supervisors Frédérik Saltré and Corey Bradshaw, helped me in the writing of certain chapters of this thesis by their proofreading, discussions and comments. I would like to thank Wolfgang Traylor and Thomas Hickler (Chapters 2 and 4), Fiona Laviano (Chapters 3 and 6), and Agathe Toumoulin (Chapter 4).

I would particularly like to thank my two Master's degree supervisors, Dr Brigitte Meyer-Berthaud and Dr Anne-Laure Decombeix (AMAP – botAnique et Modellisation de l'Architecture des Plantes), who passed on to me their passion for palaeobotany, past ecosystems and research in general. Thank you for all your support and advice. In particular, I'd like to thank Brigitte for telling me one day that "a good researcher must above all be resilient". Thanks also to Dr Gilles Le Moguédec (AMAP – botAnique et Modellisation de l'Architecture des Plantes) for our discussions and his advice on statistical methods. Thanks to Dr Vincent Girard (ISEM – Institut des Sciences de l'Évolution de Montpellier, France) for training me to decipher the secrets of fossil macroflora during my Master's degree. Thank you to the CEPAGE Master's team, who gave me many keys to writing this thesis when I was a student at the University of Montpellier, and whom I often thought about.

I would also like to thank my family and friends who have supported me throughout this thesis. Thank you to Fiona for her constant support and interest in my research, without which I might not have finished this project. Thank you to my family, and in particular to my parents who passed on to me their love of nature, their curiosity in all things, and their critical spirit. Thank you to my sisters, my grandparents, and Humbert Marie-Hélène for their uninterrupted support during this project. Thank you to my niece Naomie for her enthusiasm for 'prehistorians' and plants, and for her unexpected, sharp questions about the history of the Earth that often make me think about the origins of knowledge. Thank you for your support during the years of my thesis.

Thank you to those who have encouraged me and who will know why I thank them. Thank you to Agathe, Pierre, Eli, Estelle, Josselin, Luka, Ambre, Aurélien, and Lorenzo. Thank you to those who welcomed me to Australia, Chrissie and Bill, Pete and Rachel, John and Tori, Farzin and Ati, Lisa, Tazrina and Shandra. Thanks also to those who helped me to keep a steady hand on the tiller: Tristan, Valérie, Pierre, Gilles, Natasha, Vincent, Brice, Charlotte, Patrick, Philippe, Steve, Shounta, Nolwenn, Manu and Marianne.

Thank you to my secondary school biology teachers who inspired me to never stop learning about nature and how it works. In particular, thanks to Mrs Cobian, Mrs Perrin and Mr Hazan. Thank you to all those who fight and invest so that knowledge is a common good. Thank you to those who share and popularise scientific knowledge. Thanks also to those who maintain the many online forums, tutorials and blogs that have helped me to unravel many computer science mysteries, particularly in R. Thank you to my scientific peers who built the knowledge on which this thesis is based, and thank you to those who will take an interest in this work and continue to investigate these questions. Finally, thank you to those who fight at all levels for nature to be respected, who give this thesis more meaning.

REMERCIEMENTS

On m'avait prévenu avant que je ne me lance dans ce projet : écrire une thèse de doctorat, c'est comme un voyage initiatique, une aventure qu'il faudra entreprendre avec courage, patience, détermination et certainement un brin de folie. En regardant aujourd'hui vers le passé (ça tombe bien, j'en ai fait ma spécialité !), je suis convaincu que je n'aurais jamais pu prédire ce qu'il s'est passé au cours des cinq dernières années. Si je devais décrire en trois mots le chemin parcouru, ce serait quelque chose comme : “Quel sacré voyage !”. Ce fut un voyage rempli de découvertes et d'évènements inattendus, de doute et d'*Eureka*, de difficultés et d'émerveillements. La rédaction de cette thèse fut surtout un voyage rempli d'interactions humaines. J'espère pouvoir mettre à profit cette section si importante de ma thèse pour remercier ceux sans qui cette thèse n'aurait sans aucun doute pas été ce qu'elle est aujourd'hui en espérant n'oublier personne.

Je remercie d'abord tous ceux qui m'ont aidé sur le plan scientifique et sur le déroulé de cette thèse. Merci d'abord aux deux rapporteurs qui ont accepté de relire et d'évaluer ce travail. Merci à mes deux superviseurs de thèse qui m'ont confié ce sujet et ont suivi l'évolution de ce travail pendant cinq ans, même pendant les trois deniers années ou j'ai rédigé ma thèse depuis la France, a des milliers de kilomètres de notre laboratoire Australien. A Dr Frédérik Saltré (Flinders University, Australie) pour les nombreuses discussions scientifiques, pour son soutien et sa disponibilité dans les moments difficiles. A Prof Corey Bradshaw (Flinders University, Australie) pour avoir eu confiance en mes capacités à effectuer ce travail “ambitieux”. Merci à eux d'avoir beaucoup contribué à me former aux enjeux de la modélisation des écosystèmes à laquelle je ne connaissais pas grand-chose avant de démarrer le projet. Merci aux deux évaluateurs, A/Prof Bastien Llamas et A/Prof John Tibby (University of Adelaide, Australie), qui chaque année ont relu patiemment mon travail et donné de très précieux conseils. Merci à Prof Catherine Abbott (Flinders University, Australie) pour avoir allié soutien administratif avec écoute et empathie. Merci bien-sûr à l'Université Flinders (Adélaïde, Australie) d'avoir financé cette thèse.

Merci aux chercheurs du Centre biodiversité et climat de la Senckenberg (SBiK-F, Allemagne) pour m'avoir accueilli à Francfort pendant un mois au cours de ma première année de thèse afin de me former à l'utilisation du modèle dynamique de végétation LPJ-GUESS que j'ai pu ensuite utiliser dans plusieurs chapitres de cette thèse. Je remercie tout particulièrement Wolfgang Traylor (SBiK-F, Allemagne) sans qui j'en suis certain cette thèse aurait été bien différente. Merci donc à Wolfgang pour m'avoir partagé sa passion pour les choses bien faites, pour m'avoir grandement aidé a dépassé ma peur des outils informatiques, pour son intérêt pour mon sujet, pour les nombreuses discussions scientifiques et éthiques. Je remercie Dr Matthew Forrest (SBiK-F, Allemagne) pour s'être principalement occupé de ma formation à l'utilisation de LPJ-GUESS pendant ce mois passé à Francfort, et pour les échanges qui ont suivi. Merci à Prof Thomas Hickler (Goethe University, SBiK-F, Allemagne) pour les discussions scientifiques précieuses, son optimisme et sa confiance.

Merci à ceux qui m'ont prodigué de précieux conseils scientifiques pendant la rédaction des différents chapitres. Merci à Fiona Laviano (Flinders University, Australie) pour nos nombreux échanges sur l'histoire de l'humanité, pour ses précieux conseils sur les techniques de datation radiométriques. Merci aussi à Feng He (University of Wisconsin-Madison, USA) pour nos échanges sur les expériences de paléoclimat et pour sa disponibilité au cours des derniers mois de la rédaction de cette thèse. Merci à Dr Agathe Toumoulin (Masaryk University, République Tchèque) pour nos discussions sur les paléoclimats et la modélisation. Merci à Dr Erwin Gonzàlez-Guarda (Instituto de Ciencias de la Ingeniería, Universidad de O'Higgins, Chile ; Institut Català de Paleoecologia Humana i Evolució Social, Spain) pour nos échanges et pour ses conseils à propos des régimes alimentaires de grands herbivores d'Amérique du Sud. Merci à A/Prof Michael Dee (Centre pour la recherche sur les isotopes, Université de Groningen, Pays-Bas) et Dr Gregory Hogdins (Laboratoire AMS de l'Université d'Arizona, USA) pour les informations supplémentaires sur certaines datations radiocarbone de restes de mégafaune sud-américaine.

Je remercie grandement mes collègues chercheurs qui, en plus de mes superviseurs Frédérik Saltré et Corey Bradshaw, m'ont aidé dans la rédaction de certains chapitres de cette thèse par leurs relectures, discussions et commentaires. Je remercie Wolfgang Traylor et Thomas Hickler (Chapitres 2 et 4), Matthew Forrest (Chapitre 4), Fiona Laviano (Chapitres 3 et 6), et Agathe Toumoulin (Chapitre 4).

Je remercie particulièrement mes deux superviseurs de Master, Dr Brigitte Meyer-Berthaud et Dr Anne-Laure Decombeix (AMAP – botAnique et Modélisation de l'Architecture des Plantes, France), qui m'ont transmis leur passion pour la paléobotanique, les écosystèmes passés et pour la recherche en général. Merci pour leur soutien et leurs nombreux conseils. Merci notamment Brigitte de m'avoir dit un jour : "un bon chercheur doit avant tout être résilient". Merci aussi à Dr Gilles Le Moguédec (AMAP – botAnique et Modélisation de l'Architecture des Plantes, France) pour nos discussions et ses conseils en statistiques. Merci à Dr Vincent Girard (ISEM – Institut des Sciences de l'Évolution de Montpellier, France) pour m'avoir formé à décrypter les secrets des macroflores fossiles pendant mon Master. Merci à l'équipe du Master CEPAGE qui m'ont donné de nombreuses clés pour écrire cette thèse et à qui j'ai souvent pensé.

Je remercie aussi mes proches qui m'ont accompagné pendant cette thèse. Merci à Fiona pour son soutien de chaque instant et son intérêt pour ma recherche, sans lequel je ne serais peut-être pas aller au bout. Merci à mes parents qui m'ont transmis leur amour de la nature, leur curiosité et l'esprit critique. Merci à mes sœurs et à mes grands-parents. Merci à Humbert Marie-Hélène. Merci à ma nièce Naomie pour son enthousiasme pour "les préhistoriques" et les plantes, et pour ses questions inattendues et aiguisées sur l'histoire de la Terre qui me font souvent réfléchir à l'origine de la connaissance. Merci pour leur soutien pendant ces années de thèse. Merci à ceux qui m'ont encouragé et qui sauront pourquoi je les remercie. Merci à Agathe et Pierre, Eli, Estelle, Josselin, Luka, Ambre, Aurélien, et Lorenzo. Merci à ceux qui m'ont accueilli en Australie, à Chrissie et Bill, Pete et Rachel, John et Tori, Farzin et Ati, Lisa, Tazrina et Shandra. Merci aussi à ceux qui m'ont aidé de ne pas lâcher le gouvernail, merci à Tristan, Valérie, Pierre, Gilles, Natasha, Vincent, Brice, Charlotte, Patrick, Philippe, Steve, Shounta, Nolwenn, Manu et Marianne.

Merci à mes enseignants de biologie du secondaire qui m'ont donné envie de ne jamais cesser d'apprendre sur la nature et son fonctionnement. En particulier, merci à Mme Cobian, Mme Perrin et M. Hazan. Merci à tous ceux qui se battent et s’investissent pour que le savoir soit un bien commun. Merci à ceux qui partagent et vulgarisent la connaissance scientifique. Merci aussi à ceux qui maintiennent les multiples forums, tutoriels, ou blogs en ligne qui m'ont permis d’éclaircir de très nombreux mystères informatiques en particulier sur R. Merci à mes pairs scientifiques qui ont construit les connaissances sur lesquelles cette thèse s’appuie, et merci à ceux qui porteront un intérêt pour ce travail et continuerons à investiguer ces questionnements. Merci à ceux qui se battent à tous les niveaux pour que la nature soit respectée, qui donnent plus de sens à cette thèse.

LIST OF PUBLICATIONS DURING CANDIDATURE

Champreux, A., Meyer-Berthaud, B., & Decombeix, A.-L. (2020). Keraphyton gen. nov., a new Late Devonian fern-like plant from Australia. *PeerJ*, *8*, e9321. https://doi.org/10.7717/peerj.9321

Champreux, A., Saltré, F., & Traylor, W. (2023). *Data and code from: "How to map biomes: quantitative comparison and review of biome-mapping methods."* Zenodo. https://zenodo.org/record/7745096. Accessed 25 March 2023

Champreux, A., Saltré, F., Traylor, W., Forrest, M., Shabani, F., Johnson, C. N., et al. (2019). Post-glacial vegetation changes in Australia. Presented at the CABAH annual symposium, Melbourne, Australia.

Champreux, A., Traylor, W., Toumoulin, A., Forrest, M., Hickler, T., Bradshaw, C. J. A., & Saltré, F. (2023). Neotropical tree cover response to variation in post-Last Glacial Maximum climate and atmospheric CO_2. Presented at the XXI INQUA Congress, Roma, Italia.

Meyer-Berthaud, B., Decombeix, A.-L., Girard, C., Steemans, P., Blanchard, R., Champreux, A., & Evreïnoff, M. (2021a). The Famennian flora of Barraba, New South Wales, Australia. Presented at the Botany 2021, Virtual. https://hal.inrae.fr/hal-03340364. Accessed 30 June 2023

Meyer-Berthaud, B., Decombeix, A.-L., Girard, C., Steemans, P., Blanchard, R., Champreux, A., & Evreïnoff, M. (2021b). A Late Devonian plant assemblage from New South Wales, Australia: Diversity and specificity. *Review of Palaeobotany and Palynology*, *295*, 104535. https://doi.org/10.1016/j.revpalbo.2021.104535

Sayedi, S. S., Abbott, B. W., Vannière, B., Leys, B., Colombaroli, D., Romera, G. G., et al. (2024). Assessing changes in global fire regimes. Fire Ecology, 20(1), 18. https://doi.org/10.1186/s42408-023-00237-9

Shabani, F., Ahmadi, M., Peters, K. J., Haberle, S., Champreux, A., Saltré, F., & Bradshaw, C. J. A. (2019). Climate-driven shifts in the distribution of koala-browse species from the Last Interglacial to the near future. *Ecography*, *42*(9), 1587–1599. https://doi.org/10.1111/ecog.04530

CHAPTER 1

GENERAL INTRODUCTION: BACKGROUND, QUESTIONS, METHODOLOGY, AND CHAPTER PRESENTATION

I. THESIS OBJECTIVES

The overarching aim of my thesis was to quantify how past environmental changes associated with an increase in human pressure shaped South America's ecosystems. I aimed to test the hypothesis that (1) post-Last Glacial Maximum climate changes could have led to large-scale vegetation changes, and that (2) such changes could have facilitated megafauna extinctions.

II. GENERAL BACKGROUND

Climate variation alters ecosystem functioning by changing macroclimates shaping the patterns and positions of biomes worldwide (e.g., Mucina, 2019). Vegetation offers important insights into how ecosystems respond to climate change for two reasons. First, vegetation is one of the main drivers of ecosystem composition, function, and resilience, because it provides shelter and/or nutritional resources for most animals (Tews et al., 2004; Novotny, 2006). Second, vegetation communities are more representative of local climate change than most animal communities, because plants cannot avoid unexpected climate variation by quickly tracking more favourable conditions due to a limited range of movement at sub-generational scales (Wing and Harrington, 2001). Finally, vegetation patterns depend on and are part of a complex association of local abiotic and biotic factors such as temperature (variability and absolute values), humidity (precipitations, evapotranspiration, surface and groundwater), soil properties (granulometry, ability to retain water, nutrients concentration, biodiversity), fire activity (notably ignited by humans, or climatic events such as lightning), human activities (e.g., deforestation, cropping, farming), and megaherbivore browsing/grazing pressure (e.g., feeding, fertilising, trampling, tree killing).

Vegetation growth and composition depends on climate, soil, and perturbation regimes such as fire and herbivory that open the landscapes and facilitate plant growth (e.g., grasses; Bond, 2010). Vegetation structure also affects population growth of herbivore species by being some of their main sources of food (e.g., Rothhammer and Dillehay, 2009; Pachzelt et al., 2013), and fire activity by modifying the amount of fuel available (e.g., Gill, 2014). Changes in vegetation cover also have feedback effects on the climate by modifying albedo, regulating heat fluxes between the Earth's surface and the atmosphere, and altering the hydrological cycle (e.g., Renssen and Lautenschlager, 2000; Bonan, 2008). Reconstructions of palaeo-landscape changes thus provide many examples of large ecosystem changes driven by climate fluctuations over time that are characterised by phenomena like biodiversity richness and abundance loss or gain, leading to local extinctions, mass extinctions, or species turnover (e.g., Jaramillo, 2006; Mayhew, 2011; McInerney and Wing, 2011).

The Last Glacial Maximum (~ 33 to 19–20 thousand years before present [BP]) presented the biggest changes to the palaeo-landscape of the last 120,000 years worldwide, characterised by global dominance of open vegetation (Hooghiemstra and van der Hammen, 1998), and massive ice sheets in the Northern Hemisphere (Clark et al., 2009). In the Northern Hemisphere, the high-magnitude Last Glacial Maximum was followed by a warming period interrupted by a lower-magnitude, but rapid and pronounced, cooling period called the Younger Dryas (12,900 to 11,500 calendar years before present [BP]) (Barnosky and Lindsey, 2010) that resulted in ecotone (i.e., transition area between two vegetation communities) displacements promoting open-vegetation communities (e.g., Peteet, 1995; Reasoner and Jodry, 2000). In South America, high airborne dust concentrations, low pollen and nitrate concentrations in Andean ice cores, and some evidence from rare autochthonous pollen data, indicate that two-thirds of modern Amazonia could have been replaced by savanna-like, semi-open vegetation communities during the Last Glacial Maximum (Marchant et al., 2009; Moore, 2014). A cooling event similar to the Younger Dryas and ending approximately at the same time occurred in South America, with the first glacier advances dated between ~ 15,500 and 14,300 BP in south Patagonia (McCulloch et al., 2005; Sugden et al., 2005). This cooling event, called the Antarctic Cold Reversal Stadial and observed from Antarctic ice cores between ~ 14,700 and 13,000 BP, occurred at the same time as the Bølling-Allerød warm stage in the North Atlantic and affected the entire southern part of the Southern Hemisphere (Pedro et al., 2016).

In the Americas, this deglacial period coincided with the extirpation (i.e., regional extinction) of most megafauna genera (here defined as faunal genera weighing > 44 kg), and the increase in *Homo sapiens* population densities. The Late Pleistocene megafauna extinction worldwide was a global-scale event, with a loss of > 64% of large faunal genera, starting in Australia (61,000 BP; Saltré et al., 2016), then Eurasia and Beringia

(50,000–20,000 BP; Koch and Barnosky, 2006), and finishing in the Americas (15,000 BP; Koch and Barnosky, 2006), and Africa (13,000 BP; Faith, 2014), with variable intensities and extents (Stuart, 2015). These extinctions partly coincided both with climate changes and the major expansion of early *Homo sapiens* across continents, leading to long-standing debates to identify how the megafauna vanished (Barnosky et al., 2004; Goebel et al., 2008; Stuart, 2015). For example, while many studies supported a predominant role of changes in vegetation coverage to explain megafauna extirpation and patterns of *Homo sapiens* expansion (e.g., Tonni et al., 2003; Barnosky et al., 2004; Cione et al., 2009; Rothhammer and Dillehay, 2009), alternative views often singled out the expansion of *Homo sapiens* as a major driver for megafauna extinctions and vegetation changes via hunting and habitat modification (Barnosky et al., 2004; Stuart, 2015). Indeed, one of the major impacts of *Homo sapiens* arrival on its surrounding environment was likely driven by the increase in fire activity (i.e., magnitude and frequency) that promoted grasslands and savannas over forests and dense woodlands. The possible causes of human-induced megafauna extinction include rapid overkill, habitat fragmentation and the introduction of exotic species (Barnosky et al., 2004). However, the relative importance of these factors in explaining megafauna extinctions could have varied or even differed across the world (Stuart, 2015), including between North and Central/South America (i.e., Nearctic and Neotropics, respectively; *sensu* Olson et al., 2001).

The causes of late Pleistocene megafauna extinction are not as clearly identified in the Neotropics as in the Nearctic. In the Nearctic (North America), the chronological pattern of megafauna extinctions was largely contemporaneous with the densification of human remains and the Clovis culture, so that humans have been hypothesised as a contributor or even the main cause of these extinctions, although there is growing suspicion that human populations (non-Clovis) may have reached North America earlier (Waters and Stafford, 2007; Gilbert et al., 2008; Barnosky and Lindsey, 2010; Ardelean et al., 2020; Bennett et al., 2021; Fiedel et al., 2022). In the Neotropics (Central/South America), dates of last appearance for megafauna suggest that the extinction occurred instead within one to three thousand(s) years after the first widespread dispersal of humans into South America, suggesting a different process (Barnosky and Lindsey, 2010; Metcalf et al., 2016). For example, in Patagonia, where the best-preserved megafauna fossil records exist for South America (Barnosky and Lindsey, 2010; Villavicencio et al., 2016; Prates and Perez, 2021), last appearances occurred from 12,500 to 12,200 BP, at least 1000 to 2300 years after the first widespread dispersal of humans, and during the warming phase following the Antarctic Cold Reversal (Metcalf et al., 2016). This rather support that megafauna extinctions coincided with the synergistic effect of human impact and global warming in the Neotropics (Metcalf et al., 2016), corroborating a similar hypothesis for the Nearctic (Cooper et al., 2015), and conflicting global binary hypotheses opposing humans and climate (e.g., Dale Guthrie, 2003; Wroe and Field, 2006; Sandom et al., 2014). While neither human pressure, nor previous global warming through a global rapid increase of forest cover, were alone sufficient to cause extinctions, their first simultaneous occurrence was fateful for the megafauna. If the same phenomena could have caused megafauna extinctions in both the Nearctic and the Neotropics, the scarcity of fossil records is limiting the understanding of processes involved at large scales. Distinguishing climate, human, or synergistic interactions as primary causes thus lies mostly on a comparison of the timing of the climatic, archaeological, or ecosystemic events deduced from fossil records (but see Marshall et al., 2015).

One of the keys to understanding those ecological processes is to examine the regional specificity of extinct megafaunal species, early human populations, and the climate impact on vegetation. In the Neotropics, climate and vegetation changes, megafauna populations and human cultures differed among regions and time, suggesting at least some variations in the processes that caused megafauna extirpations. First, the general climate warming characterising the deglacial period (~19,000 – 11,700 BP) was interrupted by several shorter climate events including the Heinrich Stadial 1 (post-Last Glacial Maximum iceberg discharge, ~ 19,000 – 14,700 BP; Hodell et al., 2017), the Antarctic Cold Reversal (~14,700 – 13,000 BP, affecting all regions of the Southern Hemisphere south of 40°S; Pedro et al., 2016), and the Younger Dryas (~12,900 – 11,700 BP, mainly affecting the Northern Hemisphere as well as tropical and subtropical latitudes of the Southern Hemisphere; Cheng et al., 2020) with regional differences in timing and magnitude (e.g., Maslin et al., 2011; Hodell et al., 2017; Portilho-Ramos et al., 2017; Cheng et al., 2020). Second, the scale of vegetation response to post-Last Glacial Maximum climate changes remains cryptic because of the scarcity of palaeo-environment records (e.g., Mayle et al., 2009; Bush et al., 2011; Flantua et al., 2015).

However, several palaeo-environmental indicators (e.g., pollen, isotopic geochemistry, animal remains) suggest multidirectional and asynchronous tree-cover changes (e.g., Mancini et al., 2005; Metcalfe, 2006; Bush et al., 2011). Third, the Neotropics hosted different animal communities, a higher genera diversity, and different functional groups than in the Nearctic. However, the main ecological differences were the different types of broad-scale ecological engineers like Proboscideans that were able to shape the forests and fertilise the soils (Walter and Breckle, 2004 in Pachzelt et al., 2015; Barnosky and Lindsey, 2010; Barnosky et al., 2016). While the Nearctic had its mastodons (*Mammut* spp.) and woolly mammoths (*Mammuthus primigenius*), one of the most common megafauna fossils found in South America derived from the proboscidean genus *Notiomastodon* that went extinct just prior to the onset of the Holocene (dos Santos Avilla et al., 2013; Gallo et al., 2013). The highly specialised diet of Nearctic proboscideans (i.e., generally grazers) contrasted with the generalist diet of their Neotropical counterparts (i.e., mixt browsing and grazing habits) (Prado et al., 2015, González-Guarda et al., 2017), suggesting that their populations might have shown different responses to vegetation changes and that they affected their habitat in different ways. Moreover, given their more adaptable diet, Neotropical proboscideans should have been less sensitive to environmental changes such as landscape modification (e.g., grassland *versus* forest and woodland). Fourth, the timing of *Homo sapiens* expansion and the interaction with their environments differed between Nearctic and Neotropical realms. *Homo sapiens* appear to have entered North America first via the Bering land bridge between ~ 25,000 and 15,000 BP (i.e., during the last glacial period), and probably expanded into South America between ~ 15,500 and 12,500 BP (see Goebel et al., 2008; Rothhammer and Dillehay, 2009; Prates et al., 2020; Bennett et al., 2021). Archaeological data records show different patterns of toolkit diversity in North and South America in the Late Pleistocene, such as stylistic and technological continuity in bifacial and upper palaeolithic blades (characterising the Clovis culture) in North America (Waters and Stafford, 2007; Goebel et al., 2008; Rothhammer and Dillehay, 2009), and coexisting but distinct, spatially proximate lithic industries (characteristic of isolated cultures) in South America (Dillehay, 1999; Rothhammer and Dillehay, 2009; Moore, 2014; Suárez, 2018). This technological diversity and potential cultural isolation in South America could have been the result of different human adaptations to environmental heterogeneity, and of the low probability of different human groups meeting due to their low density and the geographic barriers of the Andes and the Amazon (Dillehay, 1999; Goldberg et al., 2016).

Potential cultural isolation aside, evidence of megafauna exploitation by humans has been found in many parts of South America, highlighting the potential role of human hunting in late Pleistocene megafauna extinctions (Bampi et al., 2022). Bampi et al. (2022) identified at least 17 sites with clear evidence of megafauna exploitation by humans (i.e., killing and/or scavenging) in South America for at least 15 genera of megafauna, dated over several millennia before their extinction. Among these sites, Lagoa Santa Karst presents clear evidence of killing, i.e., a perforating tool embedded in the skull of a proboscidean calf (*Notiomastodon platensis*) suggesting brain consumption (Mothé et al., 2020). In addition, the sharp temporal decrease in the density of megafaunal remains in South America has been linked to an increase in the density of archaeological sites and fluted projectile points (Fishtail points, Prates and Perez, 2021), a projectile pattern associated with the largest megafauna species (Prates et al., 2022). While *Homo sapiens* and climate change could have interacted to cause the demise of megafauna species throughout the Americas (e.g., Barnosky et al., 2004; Marshall et al., 2015; Cooper et al., 2015; Metcalf et al., 2016; Prates and Perez, 2021), the landscape heterogeneity in South America could have generated more regionally specific causes of extirpation. Shifts in climate conditions together with the expansion of *Homo sapiens* across the Americas probably reshaped vegetation and modified the composition of animal communities such as the proboscideans and other megaherbivores (Metcalf et al., 2016; Villavicencio et al., 2016; Prates and Perez, 2021). However, the relative importance of these factors and the ecological processes involved in the palaeo-vegetation and megaherbivore population dynamics of the Neotropics in the Late Pleistocene are still not clear and should be investigated from different perspectives.

III. ORIGINAL CONTRIBUTION TO KNOWLEDGE

In this PhD thesis I have provided new insights on how past events since the Last Glacial Maximum (~ 19,000 BP) caused megafauna extinctions and shaped the present-day distribution of the Neotropical vegetation such as the emblematic Amazon rainforest, the Cerrado tropical savanna, and the Argentine Pampas. I aimed to synthesise knowledge and quantify the effects of post-Last Glacial Maximum climate change and the intensification of human activities on Neotropical ecosystems at broad spatial scales. I was primarily focused on patterns of changes in vegetation and the extinction of megafauna. Ultimately, this thesis provides new knowledge to elucidate whether climate-induced vegetation changes after the Last Glacial Maximum could have caused megafauna extinctions in the Neotropical realm. To that end, I combined and compared the independent information provided by palaeo-environment and megafauna fossil records with a spatial and dynamic vegetation modelling approach driven by palaeo-climate simulation experiments.

IV. QUESTIONS

(1) Could post-Last Glacial Maximum climate changes have led to large-scale vegetation changes in the Neotropical realm?
(2) Could such vegetation changes have facilitated megafauna extinctions?

To address these questions, I assumed that vegetation patterns depend on climate features and edaphic properties, together with ecological processes such as competition for resources, facilitation, and a set of disturbances regimes (i.e., fire, herbivory and/or human activities impact).

Main hypothesis: I hypothesised that the transition to generally warmer and more humid climate after the Last Glacial Maximum was the main cause of large-scale vegetation changes, generally facilitating the expansion of forests across the Neotropical realm. As recently suggested by other studies regarding the Holarctic region (Cooper et al., 2015), and for South America (Metcalf et al., 2016; Prates and Petez, 2021), I hypothesised that megaherbivore extinctions in the Neotropics were due to the synergistic effect of megafauna habitat loss via climate-induced vegetation changes and the increase in human activities, together with direct killing via human predation. However, at this stage of the research, neither human activities, nor climate change, were alone sufficient to cause eventual extinction. I tested these hypotheses by adapting a dynamic global vegetation model to predict vegetation patterns in the Neotropics during the post-Last

Glacial Maximum period and comparing the results with independent data from fossil records.

V. GENERAL METHODOLOGY

Vegetation is an essential component of an ecosystem because it is the base of all food webs, and it provides structural habitats for all resident wildlife. Vegetation patterns are also closely related to climate, making it an open window on ecosystem functioning. I synthesised the information from satellite observations, and palaeo-environment and megafauna fossil records to describe post-Last Glacial Maximum and modern ecosystems in the Neotropical realm. I used a mechanistic dynamic global vegetation model driven by palaeo-climate simulation experiments to predict the monthly distribution of major plant functional types at a latitude/longitude resolution of 0.5°, considering ecological processes such as fire disturbances, plant competition, and/or facilitation. I adapted this model to the Neotropical realm during the post-Last Glacial Maximum and compared the results with independent information from the fossil record and modern observations.

VI. DESCRIPTION OF CHAPTERS

All the chapters in this thesis are closely interconnected and summarise the development of my reasoning process. As the narrative unfolds, each chapter contributes incrementally toward addressing the general question and testing the main hypotheses. Designed to be both a stand-alone study and an integral component of a broader cohesive argument, each chapter introduces its own set of questions, hypotheses, and implications. Following this introductory segment (Chapter 1), Chapters 2 and 3 review critically some of the fundamental concepts that I use throughout the thesis and identify specific gaps in the existing literature. Chapters 4, 5 and 6 use computer modelling tools (i.e., the dynamic global vegetation model LPJ-GUESS) to quantify the effects of past climate change on ecosystems, and to compare these model outcomes with independent empirical data from the fossil record. In Chapter 7, I discussed my research findings within the framework of my overarching aim and hypotheses outlined in Chapter 1, providing a general conclusion and directions for future research. Below, I present summaries of the five main chapters, illustrating the progression of my arguments and showing the cohesive nature of the thesis. Furthermore, each of the five chapters begins with an abstract that highlights its unique contribution to the scientific literature.

Chapter 2: How to map biomes? Quantitative comparison and review of biome-mapping methods.

Aim: This chapter discusses the interconnections between various biogeographical concepts, the different methodologies to describe past, present, and future vegetation and ecosystems at broad scales, and identifies the primary discrepancies between biome maps. The aim of this chapter was to assess the biome concept critically, a prevalent approach to describe the spatial distribution of ecosystems at broad scales.

Summary: Biomes have been widely used as a synthetical tool to represent past vegetation distribution deduced from palaeo-environment records and palaeo-vegetation simulations. A first glance, mapping past biomes thus represents the best way to study post-Last Glacial Maximum vegetation changes in the Neotropical realm, and should facilitate the comparison of simulations and fossils. In this chapter, I reviewed the various methods to map the distribution of past, present, and future biomes, emphasising the conceptual and methodological divergences. Modern biome maps generally use different sets of biome names and definition criteria, thus preventing their comparison *a priori*. To overcome this bias, I developed an algorithmic approach to compare such biome maps and to identify spatial areas of discrepancies. I demonstrated the usefulness of this protocol by comparing four widely used biome maps and identified the main potential drivers of spatial disagreement. At the global scale, I showed widespread disagreements among biome maps, with notable exceptions in regions around the Equator, the tropics, and boreal latitudes. In the Neotropical realm, only rainforests growing at lower latitudes such as the Amazon and Atlantic rainforests, showed high consistency between maps, while most of the Andes and areas at higher latitudes including in the Southern Cone (e.g., Pampas, Patagonia) showed low agreement. Overall, this chapter highlights that biome maps are not equivalent, and that biome definitions and distribution involve considerable subjectivity. I thus argued that biomes are a biased tool when mapping past vegetation, preventing clear interpretations of the results and comparison. Therefore, using biomes to describe the past and present distribution of ecosystems in the Neotropical realm could result in confusion and complicate comparison with other research studies. In this context, I recommend instead focussing on directly measurable metrics when describing present-day and past vegetation. In the following chapters, I thus tried to describe and compare vegetation changes based on metrics such as the percentage of forest cover, leaf area index, or vegetation net primary productivity.

Chapter 3: Post-Last Glacial Maximum vegetation changes in the Neotropical realm: review of palaeo-environment records.

Aim: In this chapter, I reviewed and described the contributions of palaeo-environmental records to reconstructions of post-Last Glacial Maximum vegetation changes in the Neotropical realm, and identified the potential drivers of these changes.

Summary: I grouped observations into 19 sub-regions grouped in seven main regions: southern North America (mainly the Mexican region), Caribbean (e.g., Central America, northern Venezuela and Colombia, Cuba), Amazon Basin, north-eastern South America (e.g., Caatinga, Cerrado, Atlantic forest), central South America (e.g., Chaco, Pantanal, Pampas, Espinal), the tropical Andes, and Patagonia. For each region, I presented the main characteristics of the physical environment (e.g., climate, topography), modern distribution of vegetation, inputs from palaeo-environment records on post-Last Glacial Maximum vegetation changes, and the main hypotheses on the causes of vegetation changes. I have summarised the main findings through illustrative figures for each area. By focussing on changes in forest cover and floristic composition (see Chapter 2), this chapter shows that while fossil records are rare and heterogeneously distributed in space, it is possible to describe the main trends of vegetation change in most regions. I demonstrated that most vegetation changes occurred in the deglacial period, between the Last Glacial Maximum and the Holocene. These changes were asynchronous among regions, and forest coverage remained relatively stable in large areas such as the southern dry diagonal, the Pampas, and the north-western Amazon Basin. In most cases, changes in moisture are the principal drivers of local vegetation changes, forced by continental-scale shifts in the position and intensity of the inter-tropical convergence zone, and the South Atlantic convergence zone in the tropics, and in the southern westerly winds in Patagonia. However, palaeo-vegetation records are scarce in some regions, and the potential mechanisms contributing to the observed changes are largely inferred via chronological comparison with other events.

Chapter 4: Response of Neotropical tree cover to variation in post-Last Glacial Maximum climate and atmospheric CO_2.

Aim: The aim of this chapter was to investigate the potential response of tree cover to post-Last Glacial Maximum changes in climate and atmospheric CO_2 concentrations in the Neotropical realm. I aimed to quantify the potential range shifts in tree cover, and to identify their potential regional drivers. This chapter was also an opportunity to generate spatially continuous maps of post-Last Glacial Maximum vegetation changes across the Neotropical realm. These maps complement the spatially discrete data presented in Chapter 3, offering a more integrated view of the vegetation dynamic over time.

Summary: In this Chapter, I simulated the potential post-Last Glacial Maximum vegetation changes in the Neotropical realm using the state-of-the-art dynamic global vegetation model LPJ-GUESS, forced by transient palaeo-climate experiment outputs from TraCE-21ka. I simulated vegetation approximately every 3000 years, with simulations corresponding to seven snapshots of interest, including the end of the Last Glacial Maximum (18,500 – 18,400 BP), the end of Heinrich Stadial 1 (15,000 – 14,900 BP), the Younger Dryas (12,000 – 11,900 BP), the Greenlandian (9,000 – 8,900 BP, Early Holocene), the Northgrippian (6,100 – 6,000 BP, mid-Holocene), the Meghalayan (3,000 – 2,900 BP, late Holocene), and the present (1950 – 1990 Anno Domini [AD]). I compared simulation results to palaeo-environmental records (described in Chapter 2) and other palaeo-vegetation simulations. I then identified the processes that best explained forest-cover changes in the seven regions described in Chapter 2, using generalised least-squares models. I showed that my model simulation outputs largely corroborate findings from palaeo-environmental records discussed in Chapter 3 regarding an increase of tree cover at the continental scale mainly during the deglacial period. However, my simulations also described some contrasting patterns among regions, especially during Heinrich Stadial 1 and the Younger Dryas. Changes in precipitation regimes had a more pronounced effect in tropical and subtropical areas, while at higher latitudes (i.e., to the south of the Tropic of Capricorn ~ 23°S) tree-cover changes were more closely associated with temperature shifts. My analyses also indicated that about 67% of the Neotropical realm remained relatively stable since the end of the Last Glacial Maximum (tree-cover standard deviation < 20%). Furthermore, by comparing present-day simulated tree cover against modern satellite-based estimates, I showed that the model overestimated tree cover especially in the areas with high rate of anthropogenic habitat loss. This suggests that human activities have a considerable impact on model accuracy, an aspect that I touched upon in Chapter 2. This chapter provides a novel perspective on post-Last Glacial Maximum vegetation dynamics of vegetation changes across the Neotropical realm, shedding light on the processes that shaped present-day ecosystems. These findings highlight the influence of both climate variations and human activities on vegetation patterns, providing a valuable context for anticipating ecosystem responses to ongoing climate changes and increasing human pressure at regional/continental scales.

Chapter 5: Challenging agreement between simulated post-Last Glacial Maximum biome changes and pollen-based biome reconstruction in the Neotropics.

Aim: The aim of this chapter was to test whether the vegetation simulations presented in Chapter 4 aligned with pollen records at both local scales and the biome level using a detailed, site-by-site comparison. This comparison between simulated and pollen-derived biome reconstruction provided a unique opportunity to (*i*) translate the simulated changes in vegetation into biome categories using biome-mapping criteria based on the definition used for the biomisation of pollen records, (*ii*) quantify the discrepancies between vegetation simulations and biomised pollen data, (*iii*) and discuss the fundamental methodological differences between the vegetation modelling approach, based on palaeo-climate data, and the biomisation approach, predicated on the taxonomical composition of pollen records.

Summary: The BIOME 6000 project provides a database of past biome records at a global scale (Last Glacial Maximum and mid-Holocene), based on standardised translation of pollen records into biomes ('biomisation'). BIOME 6000 was originally designed to facilitate comparisons between pollen records and palaeo-vegetation or climate simulations. In this chapter, I converted LPJ-GUESS palaeo-vegetation outputs from Chapter 4 into biomes, based on equivalencies between pollen and model plant functional types. I thus mapped post-Last Glacial Maximum changes in biome distribution, that I compared with pollen-based biome reconstructions and evaluated their potential agreements and discrepancies in space and time. I revealed many discrepancies between the simulated vegetation outputs and biomised pollen-records with varying agreement across different biomes. These discrepancies highlight the challenges of comparing large-scale vegetation simulations with local-scale records, and suggest that the processes driving vegetation changes at broad scales (e.g., continental, regional) differ from those operating at the local level. This emphasises the need to consider the inherent complexity of the climate-vegetation relationships. However, identifying the areas where simulated and pollen-based biomes match is a powerful method to improve our understanding of past ecosystem function. This chapter highlights the difficulties in comparing pollen and simulation-based information using biomes, including their relative biases and simplification of vegetation representation. My conclusions directly link to those from Chapters 2 and 4, arguing that the biome concept is not an ideal tool for comparisons (Chapter 2), and assessing the potential response of vegetation to post-Last Glacial Maximum climate changes with LPJ-GUESS.

Chapter 6: Climate-induced vegetation changes alone fall short of explaining Late Pleistocene megafauna extinctions in the Southern Cone.

Aim: The aim of this chapter was to explore the extent to which vegetation shifts could be considered as a primary driver explaining megafauna extinctions in the Southern Cone, encompassing regions such as Patagonia and the Pampas. These areas are notable for containing most South American records related to megafauna and vegetation.

Summary: Most post-Last Glacial Maximum megafauna and vegetation remains have been found in the Southern Cone, especially in the Pampas and Patagonia. Previous studies on the cause of megafauna extinction in the Southern Cone suggest that climate change might have facilitated megafauna extinctions by promoting the expansion of forests, thus reducing and fragmenting more-open megafauna habitats. In this chapter, I investigated the potential role of vegetation on megafauna extinctions by examining the correlations between the spatial patterns of megafauna extirpation and simulated vegetation changes. Using a similar modelling approach to that used in Chapters 4 and 5 (i.e., combining the dynamic global vegetation model LPJ-GUESS with palaeo-climate experiments from TraCE-21ka), I simulated the potential vegetation changes in response to climate changes from 15,000 to 11,700 BP (i.e., covering the Antarctic Cold Reversal). I then compared these simulated changes in vegetation against a map of the spatial pattern of megafauna extirpations based only on reliable radiocarbon age estimates. To test the hypothesis that climate change primarily contributed to the late Pleistocene demise of megafauna in the Southern Cone, I used several metrics to characterise the rate of megafauna habitat loss due to climate change and estimated the loss of land areas due to sea-level rise at the time of megafauna extirpation. The results showed that most of the vegetation of the Southern Cone remained relatively stable despite a slight loss of megafauna habitat (see also Chapter 3). The results showed that most of the vegetation of the Southern Cone remained relatively stable despite a minor reduction in megafauna habitat as discussed in Chapter 3. The results of my vegetation simulations, combined with the conclusions from Chapter 3 (which analysed records by sub-region), indicated that attributing large landscapes alterations in the Southern Cone at the time of megafauna extinctions likely stem from an over-extrapolation of the information provided by pollen records. Indeed, most palaeo-vegetation records are located on the slopes of the Andes, areas particularly prone to fluctuations in tree cover. Additionally, the spatial pattern of megafauna extirpation mostly rely on records from Southern Patagonia (because of low reliability elsewhere) so that while most taxa went extinct in the span of a few centuries, there is no support for simultaneous extirpations in the whole Southern Cone, with potentially different timings between the Pampas and southern Patagonia. Overall, I demonstrated that there is little evidence that climate-induced vegetation changes around the Antarctic Cold Reversal were the main causes of megafaunal extinctions in the Southern Cone at the end of the Pleistocene. However, they could have played a facilitating role. This chapter provides a detailed and spatially explicit evaluation of the potential response of vegetation to climate changes around megafauna extinction period, underscoring the need for further research into the impact of human activities on megafauna populations.

CHAPTER 2

HOW TO MAP BIOMES? QUANTITATIVE COMPARISON AND REVIEW OF BIOME-MAPPING METHODS

ABSTRACT

Biomes are large-scale ecosystems occupying large spaces. The biome concept should theoretically facilitate scientific synthesis of global-scale studies of the past, present, and future biosphere. However, there is neither a consensus biome map nor universally accepted definition of terrestrial biomes, making joint interpretation and comparison of biome-related studies difficult. ‘Desert’, ‘rainforest’, ‘tundra’, ‘grassland’ or ‘savanna’, while widely used terms in common language, have multiple definitions and no universally accepted spatial distribution. Fit-for-purpose classification schemes are necessary, so multiple biome-mapping methods should for now co-exist. In this review, I compared biome-mapping methods first conceptually, then quantitatively. To facilitate the description of the diversity of approaches, I grouped the extant diversity of past, present, and future global-scale biome-mapping methods into three main families that differ by the feature captured, the mapping technique, and the nature of observation used: (1) *compilation* biome maps from expert elicitation, (2) *functional* biome maps from vegetation physiognomy, and (3) *simulated* biome maps from vegetation modelling. I designed a protocol to measure and quantify spatially the pairwise agreement between biome maps. I then illustrated the use of such a protocol with a real-world application by investigating the potential ecological drivers of disagreement between four broadly used, modern global biome maps. In this example, I quantified that the strongest disagreement among biome maps generally occurs in landscapes altered by human activities and moderately covered by vegetation. Such disagreements are sources of bias when combining several biome classifications. When aiming to produce realistic biome maps, biases could be minimised by promoting schemes using observations rather than predictions, while simultaneously considering the effect of humans and other ecosystem engineers in the definition. Throughout this review, I provide comparison and decision tools to navigate the diversity of approaches to encourage a more effective use of the biome concept.

KEY WORDS: biogeography, ecology, map comparison, plant functional traits, remote sensing, vegetation, vegetation modelling, palaeo-ecology

Open research statement: All input data, output data, code, and instructions used in this study are provided in a permanent, publicly accessible Zenodo archive (Champreux et al., 2023: https://doi.org/10.5281/zenodo.7745096). This repository enables full reproducibility of the study.

I. INTRODUCTION

'A biome is a large-scale ecosystem occupying large spaces at least at the (sub)continental scale, or found in the form of a complex of small-scale, isolated patches scattered across those large spaces' (Mucina, 2019). Biomes are ecological and biogeographical tools intended to represent the basic biological units of the terrestrial biosphere (Hanks, 2011; Mucina, 2019), such as 'tropical rainforest', 'temperate deciduous forest', 'savanna', or 'grassland'. The biome concept facilitates qualitative and quantitative comparisons of such categories at the global scale. Since the first written mention of the term 'biome' in the early 20th Century (Clements, 1917; Nicholson, 2013; Mucina, 2019), several dozen global biome-classification schemes have emerged (e.g., Mellilo et al., 1993; Running et al., 1995; Myneni et al., 1997; Ellis et al., 2021; and 35 references in Mucina, 2019). The ensuing diversity of biome-delimitation criteria gave rise to various global biome maps (e.g., Walter et al., 1973; Melillo et al., 1993; Leemans, 1990a, b; Prentice et al., 1992; Haxeltine and Prentice, 1996; Olson et al., 2001; Ellis and Ramankutty, 2008; Friedl et al., 2010; Higgins et al., 2016; Fig. 2.1).

Four main drivers are responsible for this diversification: (*i*) the diversity of vegetation, climate, soil and topography that can be interpreted differently depending on expertise, application, and objective (Running et al., 1995; Moncrieff et al., 2016), (*ii*) the rise of analytical tools that facilitate the study of the biosphere at global scales (e.g., remote sensing, vegetation modelling), (*iii*) the evolution of the concept from descriptions of the physical environment toward those quantifying ecosystem functions such as productivity or habitat (Mucina, 2019), and (*iv*) the diversification of uses of biomes from conservation biology to the assessment of global fluxes of matter and energy (Mucina, 2019). Although there are many definitions of biome, for practical reasons I adopt the definition of Mucina (2019) in this review.

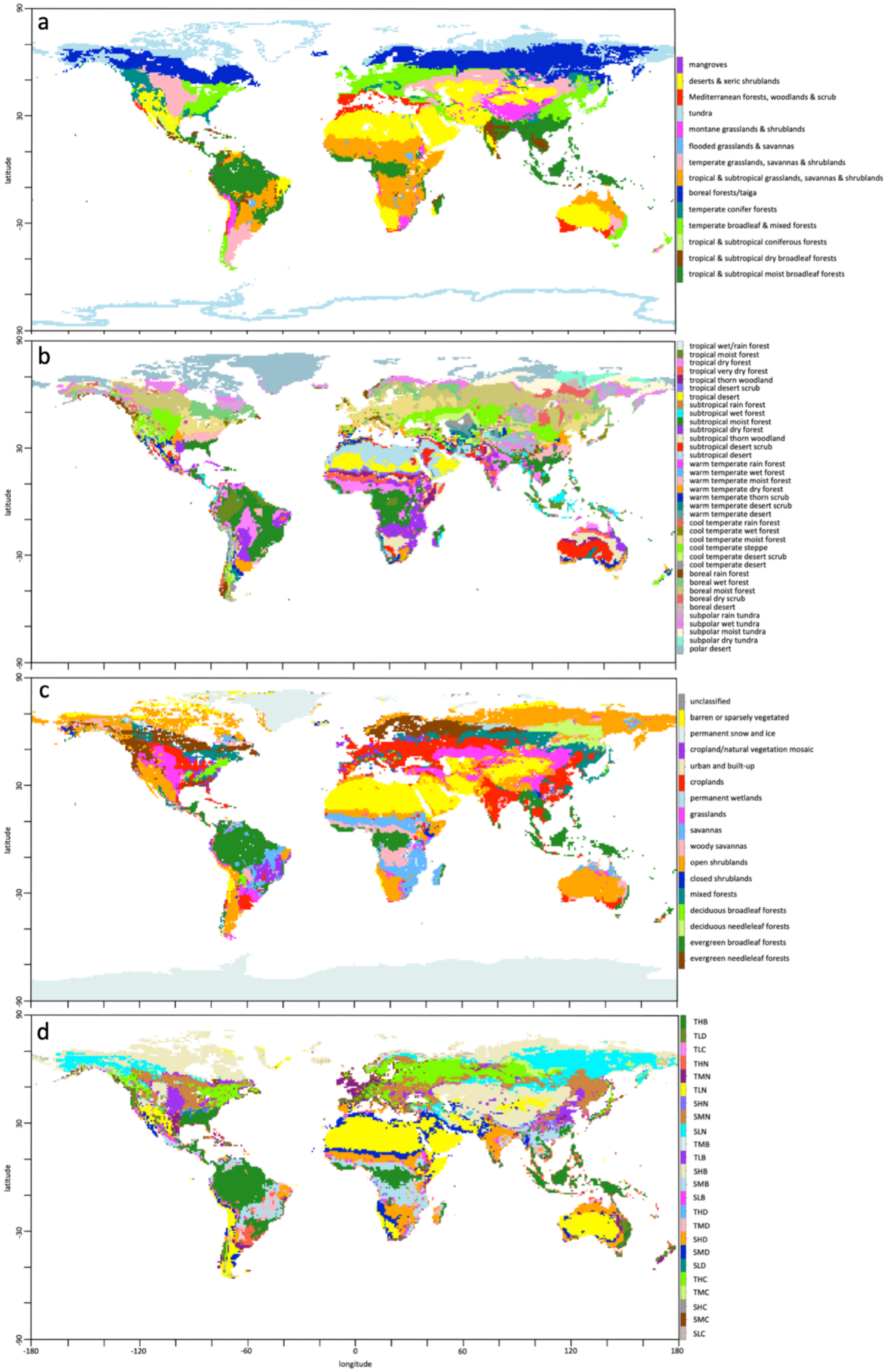
a
mangroves
deserts & xeric shrublands
Mediterranean forests, woodlands & scrub
tundra
montane grasslands & shrublands
flooded grasslands & savannas
temperate grasslands, savannas & shrublands
tropical & subtropical grasslands, savannas & shrublands
boreal forests/taiga
temperate conifer forests
temperate broadleaf & mixed forests
tropical & subtropical coniferous forests
tropical & subtropical dry broadleaf forests
tropical & subtropical moist broadleaf forests
b
tropical wet/rain forest
tropical moist forest
tropical dry forest
tropical very dry forest
tropical thorn woodland
tropical desert scrub
tropical desert
subtropical rain forest
subtropical wet forest
subtropical moist forest
subtropical dry forest
subtropical thorn woodland
subtropical desert scrub
subtropical desert
warm temperate rain forest
warm temperate wet forest
warm temperate moist forest
warm temperate dry forest
warm temperate thorn scrub
warm temperate desert scrub
warm temperate desert
cool temperate rain forest
cool temperate wet forest
cool temperate moist forest
cool temperate steppe
cool temperate desert scrub
cool temperate desert
boreal rain forest
boreal wet forest
boreal moist forest
boreal dry scrub
boreal desert
subpolar rain tundra
subpolar wet tundra
subpolar moist tundra
subpolar dry tundra
polar desert
c
unclassified
barren or sparsely vegetated
permanent snow and ice
cropland/natural vegetation mosaic
urban and built-up
croplands
permanent wetlands
grasslands
savannas
woody savannas
open shrublands
closed shrublands
mixed forests
deciduous broadleaf forests
deciduous needleleaf forests
evergreen broadleaf forests
evergreen needleleaf forests
d
THB
TLD
TLC
THN
TMN
TLN
SHN
SMN
SLN
TMB
TLB
SHB
SMB
SLB
THD
TMD
SHD
SMD
SLD
THC
TMC
SHC
SMC
SLC
latitude
90
30
-30
-90
-180
-120
-60
0
60
120
180
longitude

Figure 2.1. Global biome maps compared in this study. *(**a**) the compilation biome map of the WWF Terrestrial Ecoregions of the World (Olson et al., 2001), (**b**) the simulated biome map from the Holdridge's (1967) life zones (Leemans, 1990a,b), and two functional biome maps: (**c**) MODIS-IGBP land cover-type product (Loveland and Belward, 1997; Friedl et al., 2010), and (**d**) the dominant biome distribution over 31 years from the global functional biome scheme from Higgins et al. (2016, 2017). Biome names are derived from three letters (1) tall vs. short, (2) low, medium, and high vegetation productivity index and (3) cold, dry, both cold and dry, non-seasonal for the growth limitation index.*

In the absence of data on the effect of the diversity of biome-delimitation criteria used on the variability of biome maps, using different criteria to distinguish and map biomes can be an obstacle for effective comparison, validation, understanding, and application of the concept. Results emerging from one type of classification cannot be used when studying another because a universal translation protocol does not yet exist. Studies referring to biomes should therefore acknowledge the assumptions and approaches underlying different biome-classification schemes and the impact of these on ensuing spatial differences. Previous studies have attempted to work around this problem by considering expert knowledge-based equivalencies among categories (Werner et al., 2018), by using low-level classification (i.e., by aggregating biomes into fewer, simplified categories) (Monserud and Leemans, 1992; Harrison and Bartlein, 2012; Dallmeyer et al., 2017), or deciding arbitrarily to use only one set of criteria while ignoring other classification schemes (e.g., Mittermeier et al., 2003; Stocker et al., 2018; da Silva Junior et al., 2020).

However, there is no effort to converge toward a single universal scheme nor to reject others, even with the advent of fully automated classification schemes (i.e., without follow-up expert assessment required for quality control) designed to produce 'objective' biome maps but relying on expert selections of biome-delimitation criteria (e.g., Woodward et al., 2004; Higgins et al., 2016; Moncrieff et al., 2016; Conradi et al., 2020). New biome-classification schemes rather aim to facilitate new applications of the biome concept, but it is sometimes unclear which approach fits which purpose best. In this context, it makes more sense to learn how to navigate carefully through the diversity of approaches, rather than trying to develop a consensus map.

In this review I describe why and how different global-scale terrestrial biome-mapping methods differ. In the first section, I describe the conceptual differences among biome-mapping methods by grouping past, present, and future maps into three main families of methods: (*i*) compilation, (*ii*) functional and (*iii*) simulated biome maps. In the following two sections I aim to quantify the spatial differences among biome maps. In the second section, I provide an algorithmic protocol for comparing existing georeferenced global biome maps spatially. In the third section, I provide a real-world demonstration to illustrate the use of a unified protocol by quantifying and mapping the spatial agreement among classifications to identify the correlations between the spatial distribution of agreement among biome-classification schemes and several environmental descriptors. Ultimately, I discuss how to choose between biome-classification schemes depending on the research question, scope, and audience.

II. MAPPING PAST, PRESENT, AND FUTURE BIOMES: METHODS AND PROXIES

The biome concept engendered dozens of classification schemes and various biome maps. In this section, I first describe how the biome concept fits with other biogeographical concepts. Next, I describe the different methods for mapping the current distribution of biomes by grouping them into three main families of methods: (*i*) *compilation* biome maps from expert elicitation, (*ii*) *functional* biome maps from vegetation physiognomy, and (*iii*) *simulated* biome maps from vegetation modelling. I then use these same families to describe methods for mapping the past and future distribution of biomes. I use these categories to describe the diversity of approaches, although other categorisations could be used based on other criteria.

II.1. Biomes among other biogeographical concepts

The general biome concept is derived from five previous and disconnected, finer-scale notions that all attempted to define a group of life forms living together as a single, universal unit (Mucina, 2019). These were (*i*) *community* (see Clements and Shelford,

1939) — a generic term for a group of organisms at any scale, (*ii*) *association* (von Humboldt and Bonpland, 1805; Nicolson, 2013) — a local-scale community describing a common and predictable grouping of populations of species with consistent physiognomy, (*iii*) *formation* (Grisebach, 1838 in Egerton, 2017; Schimper, 1903; Clements, 1916; Weaver and Clements, 1938 in Whittaker, 1957; Clements and Shelford, 1939; Whittaker, 1957) — a landscape-scale community grouping various associations, characterised by its dominant growth form, developing through a succession of definite stages in response to a specific climate, (*iv*) *biocoenosis* (Möbius, 1877 in Clements and Shelford, 1939) — a term coupling association with the biological interactions within it, and (*v*) *life zone* (Merriam, 1892, 1894; Holdridge, 1967) — representing a finite combination of physical properties of the environment that host a specific biological formation.

The biome concept provides broad-scale studies with a simple, natural 'background' of major ecosystems that transcends parochial community composition, regionally specific species distributions, and other spatially unique processes. Biomes are not uniform in terms of physiognomy. Disturbances such as fires and windstorms in particular create spatial variability by favouring the coexistence of different successional stages in close proximity. Therefore, biomes are large-scale ecosystems incorporating "a complex of fine-scale biotic communities" encompassing both plant and animal life (Mucina, 2019). Additionally, two separate biomes can share common ecological, functional or climatic traits (Moncrieff et al., 2015; Mucina, 2019; Beierkuhnlein and Fischer, 2021).

When it comes to naming and mapping, biomes are usually attributed to the dominant plant formation they host (Box and Fujiwara, 2005). Biome names are often combinations of adjectives describing dominant plant functional (e.g., evergreen, deciduous, broadleaf, woody), or climatic traits (e.g., 'warm', 'dry', 'seasonal', 'tropical', 'boreal') of the communities (Fig. 2.1, Appendix S2.1: Table S2.1.1). Sometimes, biome names refer instead to a specific place that serves as a reference for describing comparable biological communities around the world, such as 'savanna' first used to describe the mixed tree and grass vegetation of the Venezuelan *llanos* (Oviedo, 1535 in Cole, 1960; Balátová-Tuláčková and Surli, 1983), or 'taiga' initially designating northern coniferous forests of Russia (Marcuzzi, 1979). Grouping distinct communities around the world under the banner of a specific place suggests that the definition of such biomes depends on the characteristics of the place of reference, thus representing a challenge to map biomes objectively.

The biome concept complements Earth-scale categorisations of the biosphere that are based more on species identity such as the 846 ‘ecoregions’ distributed across 14 biomes (Olson et al., 2001; Dinerstein et al., 2017), the 198 ‘biotic provinces’ (Dasmann, 1974), the 193 ‘biogeographic provinces’ (Udvardy, 1975), or even the continent-sized ‘realms’ like the six ‘floristic realms’ (Walter and Straka, 1970) or the eight ‘biogeographic realms’ (Udvardy, 1975; Dinerstein et al., 2017). By their very nature, the four latter, region-specific units are based on taxonomic similarity, with a strong imprint of geological history such as continental arrangements, past glaciations, or the establishment of temporary land bridges in the Pleistocene (Olson et al., 2001). But unlike biomes, region-specific units do not consider structural and functional similarities of the vegetation among regions. The biome concept is thus rooted on the phenomenon of functional convergence stating that several taxa from different phylogenetic background can evolve to share some functional traits to adapt to similar environmental conditions (Prentice and Webb III, 1998; Moncrieff et al., 2015).

By grouping spatially distinct biological communities with different species compositions, biomes therefore attempt to make these communities uniform to provide some form of standardised comparison. For example, mapping biome distributions in conservation biology provides the basis for drawing the boundaries of endangered areas and habitats at a global scale in a standardised way (e.g., Olson and Dinerstein, 1998; Olson et al., 2001; Bond and Parr, 2010; Dinerstein et al., 2017; Brancalion et al., 2019). Another example pertains to the assessment of human land-use impacts on the biosphere, which includes the concept of anthropogenically defined biomes (‘anthromes’) (Ellis and Ramankutty, 2008; Dinerstein et al., 2017) that provides a means to compare human-modified systems across regions (Myneni et al., 1997; Loveland et al., 2000; Ellis and Ramankutty, 2008; Bodart et al., 2013). The analogy between the concept of anthromes and biomes can be debated depending on whether one considers people and cultures as part of nature or as an anomaly that merely disrupts it. In this review, I have considered global-scale maps of anthromes and land use as ‘biome’ maps in the broadest sense, following other studies (e.g., Ellis and Ramankutty 2008; Moncrieff et al., 2015; Higgins et al., 2016; Conradi et al., 2020; Ellis et al., 2021). Biomes also provide a framework of homogeneous units to assess and predict the consequences of climate change on the biosphere for both past and future distributions of life on Earth (Prentice et al., 1992; Allen et al., 2010; Gonzalez et al., 2010; Li and Zhang, 2017; Huntley et al., 2021), to compare long-vanished landscapes to modern analogues (e.g., Prentice and Webb III, 1998; Dallmeyer et al., 2017; Sobol et al., 2019), and to represent spatially the global-scale exchanges of matter and energy such as the carbon cycle or nitrogen fixation (e.g., Turner et al., 2006; Yi et al., 2010; Stocker et al., 2018; Zheng et al., 2019; da Silva Junior et al., 2020).

II.2. Approaches to derive modern biome maps

Several classification approaches have facilitated global-scale biome mapping. For describing and subdividing the entirety of nature — from individuals, populations, species, to ecosystems — it might seem desirable to know the distributions of every single species, genotype, or phenotype on the planet. But such information is obviously impossible to acquire, so biome maps must rely instead on the patchy and incomplete data available (Holdridge, 1967; Udvardy, 1975; Moncrieff et al., 2016), even considering the recent advances in data collection and sharing. The resulting maps are thus limited by the quality and completeness of the underlying data, even at local scales. In addition, the diversity of classifications itself stems from the growing diversity of criteria used to define biomes. Biome-mapping criteria often depend on a selection of proxies such as local physical and biological observations of climate, geomorphology, soils, and plant and animal communities (Mucina, 2019). Given the gradual spatial arrangement of biological communities (e.g., Box, 1981; Woodward et al., 2004), mapping biomes commonly involves drawing hard spatial boundaries based on a set of criteria that include precise thresholds, the choice of which is inherently arbitrary and imperfect.

The set of *biomes* used is then designed to match the specific needs of a particular application or research question, assuming explicitly that the definition of biomes cannot be universally useful (Higgins et al., 2016; Conradi et al., 2020). For example, while some biome maps aiming to represent the actual distribution of biological communities facilitate the monitoring of changes in terrestrial ecosystems (e.g., Friedl et al., 2010; Higgins et al., 2016), other biome maps reflecting biome distribution as might be expected when considering only some environmental factors as drivers are more useful for projecting changes in ecosystem distribution through time (e.g., Gonzalez et al., 2010; Huntley et al., 2021). Many biome maps aim to represent the distribution of potential natural vegetation, which is the expected state of mature vegetation without human intervention (Tüxen, 1956; Chiarucci et al., 2010). For example, potential natural vegetation maps would represent an agricultural landscape as a forest or grassland that it once was under similar environmental conditions, or as it would become if human activities ceased. While being a traditional tool in vegetation science, the definition, realism, and usefulness of the potential natural vegetation concept remains strongly debated (e.g., Kowarik, 1987; Box and Fujiwara, 2005; Chiarucci et al., 2010; Mucina, 2010; Loidi and Fernández-González, 2012). Often it is unclear what is 'natural'. For example, it is still debated to what extent the glacial steppes of the Northern Hemisphere disappeared as a result of climate change or because humans drove large megafauna grazers (which acted as ecosystem engineers), such as the woolly mammoth (*Mammuthus primigenius*), to extinction (Owen-Smith, 1987; Zimov et al., 1995; Zimov, 2005). The natural extent of grasslands in Europe is also debated, which has important implications for conservation (Feurdean et al., 2018).

Below I differentiate among three families of methods to map biomes (Table 2.1) that differ by the feature captured, the mapping technique, and the nature of observation used (i.e., *compilation* maps from expert elicitation, *functional* maps from vegetation physiognomy, and *simulated* biome maps from vegetation modelling). I identify the pros and cons of each family of methods. In delineating their specific sources of uncertainty, I use Dietze's (2017) first-principle concepts of prediction uncertainty (Appendix S2.1: Table S2.1.2), which are applicable across the three families of biome-mapping approaches.

II.2.1. Compilation biome maps from expert elicitation

Biome maps derived from ground observations attempt to capture in a single map the real diversity of local perceptions of biological community distributions (i.e., based on local classification systems). Such maps were first generated by expert elicitation, gathering reports of field observations by local experts, and assigning them to particular biomes based on an almost unlimited quantity of ground observations (e.g., plant and animal species composition and diversity, vegetation structure and successional relationships, climate, soil, topography). First, local observations are extrapolated spatially to draw continuous regional biome maps derived from various biome-delimitation criteria. Second, regional maps are combined using category equivalencies defined by expert elicitation to produce global maps (Friedl et al., 2010).

Table 2.1. Biome-classification families and how to apply them. *I grouped existing biome-classifications by how they define and map biomes, i.e., the method and underlying data used for mapping, and the features captured.*

biome-mapping family	**underlying data**	**features captured**	**global mapping method**	**examples of global biome maps**
compilation	unlimited field observations (e.g., plant and animal species composition and diversity, vegetation structure and successional relationships, climate, soil, topography)	subjectively expected state of mature vegetation (i.e., in equilibrium with climate) without human impact global patchwork of local perceptions	compilation of pre-existing regional maps using expert elicitation for category equivalencies	Melillo et al. (1993) Olson et al. (2001)
functional	vegetation physiognomy temperature profiles population density	actual distribution of vegetation functional traits	combinations of vegetation functional traits derived from satellite imagery	Ellis and Ramankutty (2008) Friedl et al. (2010) Higgins et al. (2016, 2017)
simulated	physical environment (e.g., soil, climate, CO_2 concentrations) relationships between vegetation traits and the physical environment	statistically expected vegetation distribution under theoretical assumptions	correlative or mechanistic modelling	Walter (1973) Leemans (1990a,b) and Holdridge (1967) Prentice et al. (1992) Haxeltine and Prentice (1996)

Uncertainty in compiled biome maps then relates predominantly to accuracy and density of underlying observations (driver uncertainty), as well as equivalency definitions (Appendix S2.1: Table S2.1.2). Global biome maps resulting from the compilation of regional maps ensure compatibility with pre-existing regional maps, thus facilitating their broad understanding and acceptance. The large time span among the various observations makes these maps timeless representations of the biosphere, usually focusing on potential natural vegetation. Olson et al. (2001) used this approach by combining observations from over 1000 regional experts to produce one of the most widely used global biome maps in existence today (Fig. 2.1a), endorsed by the World Wildlife Fund and the Intergovernmental Science-Policy Platform of Biodiversity and Ecosystem Services (IPBES 2019). Similarly, Melillo et al. (1993) combined ground-deduced local vegetation maps from 12 different continental-scale sources to produce a global 'potential natural vegetation' map. Pfadenhauer and Klötzli (2014) also combined 16 regional sources to produce a global map of 'Earth's vegetation', with different sources to those used by Melillo et al. (1993). However, Melillo et al. (1993), Olson et al. (2001), and Pfadenhauer and Klötzli (2014) mapped the global distribution of biomes without providing any definition of a biome or vegetation type, even if Melillo et al. (1993) provided some basic, ecosystem-based estimates and predictions regarding their total area, net primary production, and nitrogen uptake.

The absence of proper biome definitions contributes to the general subjectivity and lack of repeatability of compilation biome maps (Moncrieff et al., 2015; Higgins et al., 2016), because such derived, global-scale maps must be necessarily based on the compilation of incompatible, local-scale classifications. Although often considered 'biome' maps by others, compilation biome maps are not based on any generalised classification system and do not 'map' biomes *stricto sensu*. Considering regional map compilation as a proper mapping method can therefore be legitimately debated.

II.2.2. Functional biome maps from vegetation physiognomy

Functional biome maps summarise the distribution of structural and functional attributes of the existing vegetation. Such biomes can be efficiently delineated at the global scale by converting satellite imagery data into vegetation attributes such as plant ground cover (e.g., leaf area index), leaf physiognomy (e.g., needle, broadleaf), leaf phenology (e.g., deciduous, evergreen, semi-evergreen), plant height, or leaf orientation (e.g., erectophile, planophile) (Myneni et al., 1997; Woodward et al., 2004; Friedl et al., 2010; Higgins et al., 2016).

Satellite products also include the impacts of human activities, ultimately culminating in the concept of 'anthromes' (i.e., anthropogenic biomes) that explicitly treat people and cultures as part of nature rather than as an anomaly that merely disrupts it (Ellis and Ramankutty, 2008; Ellis et al., 2021). Some vegetation functional traits can be locally measured from the ground, and increasing data availability, e.g., through the TRY plant functional trait database (Kattge et al., 2020), makes it possible to derive global map estimates (e.g., Butler et al., 2018). Satellite imagery provides measurements in poorly studied areas, such as inaccessible or dangerous places (Popkin, 2015).

Satellite imagery has provided a means to automate the delineation of biomes using standard observations at the global scale, thus reducing subjectivity. The subjectivity in biome classification algorithms based on remote sensing is open to scrutiny, but the observations and analyses are in digital form, as opposed to the personal experiences of local experts. Remote sensing most notably gave rise to the well-known MODIS-IGBP (Moderate Resolution Imaging Spectrometer —International Geosphere Biosphere Programme) land-cover types, using images from MODIS satellites, and following the IGBP biome classification (Loveland and Belward, 1997; Friedl et al., 2010; Fig. 2.1c). Arguing that the IGBP classification uses preconceived ideas of what biomes should look like to decide on their definition, Higgins et al. (2016) more recently developed the global functional biome scheme based on combinations of three global vegetation attributes of height, productivity, and seasonality (Fig. 2.1d). Ellis and Ramankutty (2008) mapped the first global anthrome distribution by combining land-use and land-cover data from satellite imagery with human population-census data.

Satellite-derived functional biome definitions still exclude many data describing botanical, ecological, and some functional characteristics of plants (e.g., Friedl et al., 2010; Higgins et al., 2016; Moncrieff et al., 2016). Limitations also include strict numerical thresholds of ground cover that can only be inferred from space, such as a threshold of 60% of trees used to define 'forest' biomes in the IGBP classification (Loveland and Belward, 1997). Neither does the use of such thresholds consider the large uncertainties associated with the translation of remote-sensing signals into biological descriptors (Houborg et al., 2015). For example, the combination of many factors related to the signal received and its treatment methods can cause > 50% of relative uncertainty in the measurement of the leaf area index from remote sensing (Fang et al., 2019). In summary, correlating remote sensing with ecological 'groundtruthing' hinges on model parametrisation and calibration and could thus suffer from concomitant parameter-related uncertainties (Appendix S2.1: Table S2.1.2). Consequently, this type of classification is difficult to compare to ground observations and is equivocal for vegetation communities scoring close to the threshold.

II.2.3. Simulated biome maps from vegetation modelling

Biome maps from vegetation modelling are predictions of the distribution of vegetation considering a set of precise assumptions. Broad-scale vegetation modelling stems from pre-established climate classifications that have been linked to the global distribution of vegetation types (e.g., Köppen and Geiger, 1954; Bagnouls and Gaussen, 1957; Walter, 1973; Bailey, 1989a, b). When mapping biomes at global scale, vegetation modelling often maps the distribution of biomes predicted from climate, soil, and increasingly, atmospheric chemistry (CO_2 concentration, nitrogen deposition) data (e.g., Smith et al., 2014). Recently, the incorporation of human land use has received more attention (e.g., Yue et al., 2018; Pugh et al., 2019). However, unlike maps from expert-elicitation or vegetation physiognomy, maps from vegetation modelling are statistical or more process-based predictions that do not necessarily aim to represent the current state of vegetation or modern potential natural vegetation. Instead, they often test our current understanding of the role of different drivers, or they are used to project changes in biome distributions through time (e.g., Gonzalez et al., 2010; Huntley et al., 2021).

Modelled predictions often differ from observation-based biome maps because the models try to explain the distribution of biomes rather than mapping them, for example, concerning the role of fire disturbance on global tree cover (Lasslop et al., 2020). When compared to ground- or satellite-based observations, modelled biome maps are means to test hypothetical relationships between environmental factors and the distribution of vegetation types.

One might distinguish approaches that directly correlate biome distribution with environmental conditions from more process-based approaches that consider ecological mechanisms to simulate biome distributions, such as dynamic global vegetation models. However, the distinction blurs where otherwise highly mechanistic models restrict plant distribution by pre-defined bioclimatic limits (e.g., Smith et al., 2001). Both correlative and process-based approaches can aim either to elucidate ecological processes or predict biome distributions accurately. As an example of a correlative approach, Whittaker's broadly used diagram (Whittaker, 1970) considers only mean annual precipitation and temperature to predict a worldwide distribution of biomes. Similarly, Leemans (1990a, b) mapped what Holdridge (1967) described as 'life zones' (a synonym for 'biome') based on actual climate data, where precipitation, evapotranspiration, and altitude are physical limitations of the local environment to support specific life forms (Fig. 2.1b). Prentice et al. (1992) then emphasised the need to consider plant physiological mechanisms explicitly in the choice of predictor variables, such as the minimum winter temperature, which is clearly related to the frost tolerances of different plant or vegetation types, instead of mean annual variables. Recently, it has become more popular to use fewer *a priori* assumptions on drivers, and more potential predictors in combination with advanced 'big data' statistics, including machine learning (Hengl et al., 2018).

On the other hand, process-based biome models map the distribution of biomes by simulating competition among plant types under given environmental conditions based on their physiology. Process-based vegetation models often group plants with similar functional characteristics into a few functional types or growth forms. This approach treats species' groupings functionally as a single 'average' species that ignores phylogenetic relationships (Duckworth et al., 2000). Competition among plant types (defined by a combination of functional traits) is then simulated as a result of simulated physiological processes and competition for resources (water, light, and increasingly also soil nutrients, in particular nitrogen) in dynamic global vegetation models (e.g., Levis et al., 2004; Smith et al., 2014). This simplification predicts the coarse-scale distribution of all plant species by simulating competition among only a few (commonly 5–15) 'virtual' plant functional types. Their high mechanistic detail might cause over-parametrisation in process-based models as a source of uncertainty (Appendix S2.1: Table S2.1.2).

Mechanistic methods provide model-based hypotheses of the ecosystem processes leading to the current distribution of plant types and biomes (e.g., competition for resources, sensitivity to disturbances, where fire is globally of particular importance) (Lasslop et al., 2020). For example, maps produced by Haxeltine and Prentice (1996) and Hickler et al. (2006) agreed approximately ($\kappa > 0.5$) with an expert-based compilation biome map primarily derived from Melillo et al. (1993). Recently, within-plant type trait variability has also been included (e.g., Sakschewski et al., 2016; Dantas de Paula et al., 2021), and the Adaptive dynamic global vegetation model (version 2) also simulates trait inheritance (Scheiter et al., 2013). Together with promising ambitions of including data assimilation in global dynamic vegetation models (Luo and Schuur, 2020), these developments could help reduce uncertainty from parameter variability (*sensu* Dietze, 2017).

Biome maps from correlative or process-based models simplify the relationships between vegetation and environmental conditions. While model simulations might be able to reproduce the general distribution pattern of biomes accurately, they do not account for all processes leading to the actual biome distribution.

II.3. Past and future biomes

The biome concept is a useful tool when reconstructing past or predicting future landscapes because it provides a means to compare long-vanished or expected future landscapes with modern analogues. Past and future biome projections relate to the three families of biome maps, i.e., *compilation* from expert elicitation, *functional* from vegetation physiognomy, and *simulated* from vegetation modelling. Depending on the method used to infer biomes, such reconstructions potentially provide insight into past environmental changes, or on the potential effects of future climate changes on the distribution of biological communities and functional traits at regional to global scales. However, inferring past or future biomes requires hindcasting or predicting characteristics from limited information regarding their extent and properties.

Functional traits and taxonomic diversity of past vegetation remains (e.g., pollen, leaves, phytoliths or leaf waxes) can indicate past biome characteristics. This information provides the valuable evidence of past environments that can be used to infer past biomes. Biome reconstructions based on past vegetation remains or vegetation model simulations assume that at least as far back as the Cretaceous-Palaeogene extinction event (66 million years ago), landscapes hosted modern-analogue floras, even if this assumption weakens with the age of the studied flora due to ensuing evolutionary and environmental changes (Peppe et al., 2011; Carvalho et al., 2021). Past biomes can be inferred from (*i*) expert knowledge combining all the information available from the fossil record (i.e., compiled biomes), (*ii*) functional traits and taxonomic diversity of past vegetation remains (i.e., functional biomes), (*iii*) correlative or mechanistic models based on past climate data deduced from fossil remains or climate model simulations (i.e., simulated biomes). Vegetation modelling also enables future simulated biome projections from simulated climate data.

II.3.1. Past compilation biomes from expert elicitation

Past compilation biomes can be inferred by combining all the information available from a palaeo-environment record (e.g., past vegetation, mammals, climate). Like modern compilation biomes from expert elicitation, the quantity of information is not limited to any standard biome definition, and biomes are defined based on expert elicitation. General functional characteristics and taxonomic diversity of a palaeo-environment record often recall one or several modern associations of local vegetation, formations, or biomes (e.g., Ziegler, 1990; Adams and Faure, 1997; Ray and Adams, 2001; Willis and McElwain, 2002; Dyke, 2007). Experts combine information about the biogeographical origin and/or the modern habitat of the nearest living relative taxa, and/or the environment to which the functional traits are adapted. This approach aims to approximate, albeit subjectively, a natural framework facilitating the interpretation of the data, rather than to describe the environment precisely. Because this approach relies on compiling information from multiple sources using category equivalencies based on expert knowledge, it can be compared to modern compilation biomes (e.g., Olson et al., 2001).

II.3.2. Past functional biomes from proxies of vegetation physiognomy

The general characteristics of past functional biomes can be inferred from leaf compressions, pollen records, and leaf waxes. Like modern ones from remote sensing, past functional biomes focus exclusively on vegetation traits and are independent of estimations of past environmental conditions. For example, information about leaf physiognomy (deciduous, evergreen) can arise from petiole width of leaf compressions, assuming that heavy and thick evergreen leaves have a wider petiole than light and thin deciduous leaves (e.g., Peppe et al., 2018). Leaf physiognomy and the relative proportions of woody and herbaceous vegetation can be deduced from the taxonomic composition of pollen or phytolith records (e.g., Bremond et al., 2008; Forbes et al., 2020). Stable isotope analysis of organic matter ($\delta^{13}C$) like leaf waxes can also provide insights into photosynthetic pathways (i.e., C_3 or C_4) (O'Leary, 1988), potentially indicating the proportion of woody vegetation at the lowest latitudes because C_4 grasses have dominated herbaceous vegetation on all continents since the late Pliocene (e.g., Andrae et al., 2018; Forbes et al., 2020).

While deduced independently from different palaeo-proxies, these vegetation functional traits, once combined, represent functional biome definition criteria. By calibrating biome definitions to local records of modern vegetation, several methods automate the inference process of past functional biomes (Prentice and Webb III, 1998; Sobol and Finkelstein, 2018). Such methods define biomes regionally as combinations of taxa or plant functional types. For example, the BIOME6000 project mapped palaeo-biomes from pollen records for the Last Glacial Maximum and mid-Holocene using a 'biomisation' technique (Prentice and Webb III, 1998; Harrison and Bartlein, 2012). Biomisation is a process where identified pollen taxa are translated into one or more plant functional types for each site. Then the biome with the highest affinity to the composition of specific plant functional types represents that site over the relevant period. Biomisation usually relies on representative plant taxa and expert-based links among pollen taxa, plant functional types, and biomes. Sobol and Finkelstein (2018) alternatively developed a machine-learning method to assign pollen taxa programmatically to biomes. These functional characteristics are comparable to modern functional biomes mapped from remote sensing using the same functional traits (e.g., Friedl et al., 2010; Higgins et al., 2016).

II.3.3. Past and future simulated biomes from vegetation modelling

Past reconstructions of biome changes are an important source to evaluate biome models: an obvious prerequisite to applying such models to project future changes and to inform climate-adaptation and -mitigation measures. However, data from palaeo-environmental records are often very sparse. In the case of deep-time studies going back millions of years, biome models rest on only very few data points (e.g., Salzmann et al., 2008). For time periods with better data coverage, vegetation simulations might actually be able to test hypotheses about what drove past biome shifts. For example, Harrison and Prentice (2003) showed that the BIOME3 model only reproduced landscape openness in the tropics during the Last Glacial Maximum if the model limited C_3 photosynthesis through low atmospheric CO_2. Huntley et al. (2013) showed that glacial variability associated with Heinrich events is crucial to simulate landscape openness comparable to pollen-based reconstructions in western Europe in particular. Forrest et al. (2015) combined fossil plant data, climate, and vegetation modelling to infer that atmospheric CO_2 concentrations during the last Miocene were probably at the low end of current estimates. Future scenarios of biome shifts have been mostly interpreted in terms of climate-adaption needs (e.g., in forestry) and their impact on biodiversity (Gonzalez et al., 2010; Huntley et al., 2021).

To simulate past and future biome distributions, model forcing data can be obtained from various and complementary sources, including model hindcasts and predictions, or palaeo-proxies. First, vegetation models predicting modern biomes from modern climate data can also simulate biomes from hindcasted climate data (e.g., Salzmann et al., 2008; Allen et al., 2010; François et al., 2011; Prentice et al., 2011; Forrest et al., 2015; Allen et al., 2020; Tardif et al., 2021), or future climate scenarios (Leemans 1990a, b; Monserud and Leemans, 1992; Gonzalez et al., 2010; Huntley et al., 2021). Second, many past climate characteristics can be inferred from palaeo-proxies, thus providing independent training data at regional scales against which climate models can be calibrated. For example, past climate characteristics can be deduced from fossil leaf compressions assuming that modern climate dependencies of plant functional traits also apply to the past, and that most plant communities are in equilibrium with their local climates (Peppe et al., 2018 and references therein), regardless of the few exceptions arising from rapidly changing climates (e.g., Davis, 1986; Svenning and Sandel, 2013; Blonder et al., 2015).

II.3.4. Uncertainties of past vegetation palaeo-proxies and biome modelling

The interpretation of palaeo-proxies to infer biomes must also consider the preservation biases resulting from different structural and chemical properties among species or plant parts (Schopf, 1975). Preservation processes prevent several proxies from being recorded simultaneously in the same place, because good preservation conditions for one organism or part of an organism can promote decomposition conditions for others (Schopf, 1975), causing poor taxonomic resolution due to missing identification criteria. Whichever proxy is used, only some organisms are recorded, so that one record represents only a small sample of its original environment, biased toward the most-resistant species (Sangster and Dale, 1964) and deposit environments with high preservation potential (e.g., riparian forests, riverbeds). Finally, whereas microfossil records such as pollen are often assumed to represent the regional environment, macrofossils such as leaves and wood more likely represent the local environment given the latter are not dispersed as much as the former (e.g., DiMichele et al., 2019). Hence, pollen cores can accumulate species-composition information across a much broader spatial range than the immediate vicinity in which the sample was collected. If inferring past biomes from actual vegetation remains is an evidence-based method, the sparse spatial distribution of palaeo-vegetation records provides only temporal snapshots and local reconstructions.

More comprehensive biome maps can only be generated via palaeo-vegetation modelling. Model forcing data, such as palaeo-climate, might diverge from observations (Lorenz et al., 2016). In fore- or hindcasting models, driver uncertainty thus becomes an additional source of uncertainty (Appendix S2.1: Table S2.1.2). Therefore, and in spite of the incomplete process representation in biome models, palaeo-vegetation data and proxies and biome models are sometimes combined to reconstruct past biomes (e.g., Salzmann et al., 2008).

Overall, fossil records represent direct evidence of past environments at a given time period, while model simulations generate past and future biome maps at a regional to global scale. Using a consistent biome-classification scheme for past, modern, and future reconstitutions is essential to assess changes in biome distributions through time and to evaluate climate and biome models that are used for future predictions. Plant remains or simulations can inform different elements of the environment from modern, expert-based analogues and taxonomic diversity to functional traits and palaeo-climate features. Such information must then be combined to describe biomes based on vegetation physiognomy, the physical environment (vegetation modelling), or the compilation of non-standard observations (expert elicitation).

III. COMPARING GLOBAL BIOME MAPS QUANTITATIVELY

The diversity of biome classifications has resulted in various geographic divisions, biome names, and number of biomes (from < 10 to several dozen globally; Beierkuhnlein and Fischer, 2021). Two different biome-classification schemes can even use the same biome name to describe different entities. For example, the ‘tundra’ of Olson et al. (2001) does not correspond to the spatial combination of the four ‘tundra’ biomes of Leemans et al. (1990a, b) (Fig. 2.1). However, the scale and nature of these discrepancies remain cryptic and underestimated (Beierkuhnlein and Fischer, 2021). In this context, it is essential to explore, quantify, and map the global agreement among biome maps. Below, I briefly review published comparison methods and then introduce a new algorithm to quantify pairwise agreement between biome maps.

III.1. Shortcomings of methods to compare biome maps

Several methods can be used to compare biome maps, even if each has its shortcomings. A contingency table is a straightforward tool to illustrate how two classifications overlap spatially (see Higgins et al., 2016). Such a table describes how the distribution of categories in map A relates to that of map B as a fraction of the entire map, with the sum of all fractions = 1 (see also Hagen, 2002). However, summarising the agreement as a single or a few numbers makes the result easier to interpret, especially when there are many categories. Map-comparison measures based on such contingency tables, such as the broadly used Cohen's kappa (κ) (Cohen, 1960; Monserud and Leemans, 1992), or the more recent quantity-and-allocation agreement (Pontius and Millones, 2011), both consider the percentage of pixels of the map attributed to the same category in two maps and take into account the likelihood of agreement occurring by chance.

Quantifying the overall spatial agreement between two biome maps with the methods mentioned above would require classifications to share equivalent sets of categories, which is not the case. Setting up an expert-based equivalency table (or a similarity matrix) between two sets of biomes based on their names or definition similarities, i.e., deciding on theoretical equivalencies among biomes to facilitate map comparison (Fritz and See, 2005; Hagen-Zanker et al., 2005), could be circular, subjective, and non-repeatable. Alternatively, Beierkuhnlein and Fischer (2021) grouped categories from 12 global biome maps based on common climate and environmental characteristics and mapped the frequency of overlap among categories at global scale. This type of approach is effective to identify the existence of differences between biome maps, but their distribution still depends on the criteria chosen to group the categories (here, mainly climate).

To avoid using subjective equivalencies among categories, it is possible to quantify the agreement between each biome pair by measuring their spatial overlap compared to a distribution of overlap occurring by chance. The quantity-and-allocation-agreement statistics suggested by Pontius and Millones (2011) to replace Cohen's κ make sense for global comparisons; unfortunately, Pontius and Millones (2011)'s single-category statistics are weighted by the total number of locations on the map and are therefore not designed for single-category comparisons. In contrast, Cohen's κ on a single category (Monserud and Leemans, 1992) is weighted by the area covered by the category under examination, i.e., weighted by the size of the biome. Because of these challenges, I present here an alternative approach to measure and represent spatially the pairwise agreement between biome maps by merging categories based on spatial overlap and by calculating Cohen's κ on a single category (Monserud and Leemans, 1992), thus considering differences in biome size.

III.2. An algorithmic protocol to represent the spatial distribution of map agreement

III.2.1. Merging biomes based on spatial overlap

To compare two sets of biomes with different category names and numbers (Fig. 2.2a), I must first have the same number of biomes for each set. For each pair of biome classifications, I adjusted the number of biomes of the classification with the highest number of biomes (Map A in Fig. 2.2a) to the classification with the lowest number of biomes (Map B, in Fig. 2.2a,b). To avoid deciding arbitrarily on equivalencies among categories, I merged biomes programmatically based on spatial overlap. Two categories from A were merged if the regions they cover were generally classified in the same category from B, irrespective of biome names or definition similarities. I generated a contingency table between the two rasters, from which I derived the percentage of spatial overlap (ranging from 0 to 100%) for each category from A in categories from B (Fig. 2.2b, left panel). Starting from highest overlap, I then associated each category from A to its highest overlapped category from B. When two categories from A were associated in this way with the same category from B, I merged them, and repeated this process until the two classifications had an equal number of categories (Fig. 2.2b, left panel). The merged biomes from the first map are not biologically equivalent, but the regions they cover are mostly classified in a single category on the second map to which they are compared.

III.2.2. Generating agreement maps

I then generated spatial agreement maps based on Cohen's κ on a single category. I calculated a new contingency table between maps A and B considering merged categories (Fig. 2.2b, right panel). Next, I calculated the κ agreement of a single pair of categories *i,j* ($\kappa_{i,j}$) by successively considering each possible pair of biomes as a single category and compared their distribution against the union of all other categories in both classifications (Fig. 2.2c, left and middle panels). I excluded from the analysis locations not assigned to any terrestrial biomes in at least one of the two maps. I then calculated $\kappa_{i,j}$ of each biome pair (Fig. 2.2c, centre panel) to plot the global distribution of agreement in each a pair of classifications, based on where each pair was located (Fig. 2.2c, right

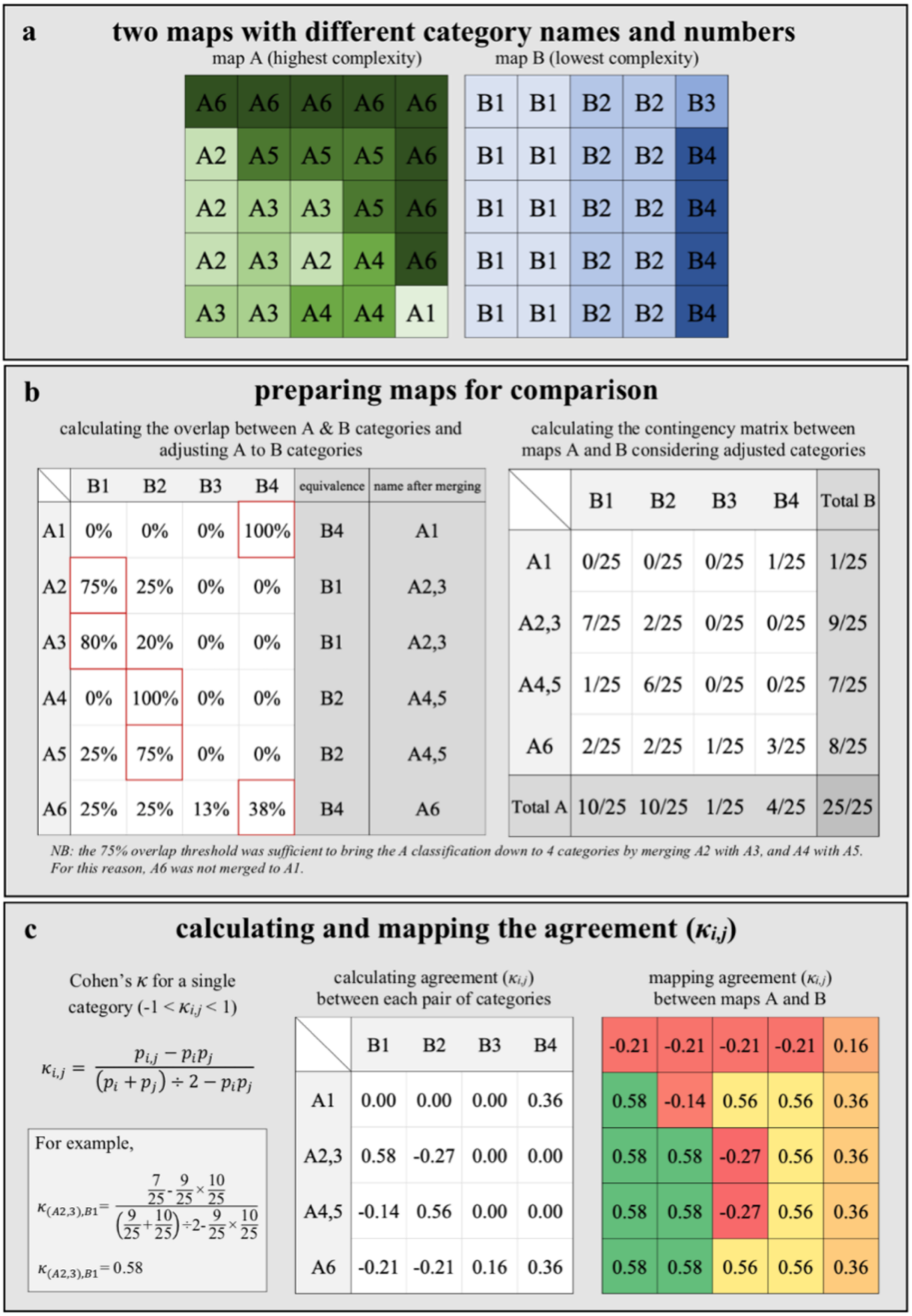

a two maps with different category names and numbers

map A (highest complexity)

A6	A6	A6	A6	A6
A2	A5	A5	A5	A6
A2	A3	A3	A5	A6
A2	A3	A2	A4	A6
A3	A3	A4	A4	A1

map B (lowest complexity)

B1	B1	B2	B2	B3
B1	B1	B2	B2	B4
B1	B1	B2	B2	B4
B1	B1	B2	B2	B4
B1	B1	B2	B2	B4

b preparing maps for comparison

calculating the overlap between A & B categories and adjusting A to B categories

	B1	B2	B3	B4	equivalence	name after merging
A1	0%	0%	0%	100%	B4	A1
A2	75%	25%	0%	0%	B1	A2,3
A3	80%	20%	0%	0%	B1	A2,3
A4	0%	100%	0%	0%	B2	A4,5
A5	25%	75%	0%	0%	B2	A4,5
A6	25%	25%	13%	38%	B4	A6

calculating the contingency matrix between maps A and B considering adjusted categories

	B1	B2	B3	B4	Total B
A1	0/25	0/25	0/25	1/25	1/25
A2,3	7/25	2/25	0/25	0/25	9/25
A4,5	1/25	6/25	0/25	0/25	7/25
A6	2/25	2/25	1/25	3/25	8/25
Total A	10/25	10/25	1/25	4/25	25/25

NB: the 75% overlap threshold was sufficient to bring the A classification down to 4 categories by merging A2 with A3, and A4 with A5. For this reason, A6 was not merged to A1.

c calculating and mapping the agreement ($\kappa_{i,j}$)

Cohen's κ for a single category ($-1 < \kappa_{i,j} < 1$)

$$\kappa_{i,j} = \frac{p_{i,j} - p_i p_j}{(p_i + p_j) \div 2 - p_i p_j}$$

For example,

$$\kappa_{(A2,3),B1} = \frac{\frac{7}{25} - \frac{9}{25} \times \frac{10}{25}}{\left(\frac{9}{25} + \frac{10}{25}\right) \div 2 - \frac{9}{25} \times \frac{10}{25}}$$

$$\kappa_{(A2,3),B1} = 0.58$$

calculating agreement ($\kappa_{i,j}$) between each pair of categories

	B1	B2	B3	B4
A1	0.00	0.00	0.00	0.36
A2,3	0.58	-0.27	0.00	0.00
A4,5	-0.14	0.56	0.00	0.00
A6	-0.21	-0.21	0.16	0.36

mapping agreement ($\kappa_{i,j}$) between maps A and B

-0.21	-0.21	-0.21	-0.21	0.16
0.58	-0.14	0.56	0.56	0.36
0.58	0.58	-0.27	0.56	0.36
0.58	0.58	-0.27	0.56	0.36
0.58	0.58	0.56	0.56	0.36

Figure 2.2. Protocol to spatially compare two raster maps with different classifications. *(**a**) Example of maps to be compared, (**b**) Map preparation procedure including category merging, (**c**) Agreement calculation and mapping.*

panel). $\kappa_{i,j}$ ranges from no agreement ($\kappa_{i,j} < 0.05$) to 'perfect' agreement ($0.99 < \kappa_{i,j} < 1.00$) (*sensu* Monserud and Leemans, 1992).

IV. EXAMPLE OF A REAL-WORLD APPLICATION OF THIS *ALGORITHMIC PROTOCOL*

To demonstrate the utility of quantifying classification agreements, I first compare four global biome maps using the algorithmic protocol presented above. I then discuss the ecological characteristics of areas of low agreement between biome maps, in particular by testing correlations between the agreement and six potential ecological predictors.

IV.1. Comparing four global biome maps

I calculated the similarity between biome pairs for a panel of four broadly used (i.e., biome map or classification cited in thousands of scientific papers and textbooks) or recent georeferenced global biome maps at a 0.5 × 0.5-degree spatial resolution. I compared the compilation biome map from the WWF Terrestrial Ecoregions of the World (Olson et al., 2001; Fig. 2.1a), the simulated biome map from the Holdridge's (1967) life zones (Leemans, 1990a, b; Fig. 2.1b), and two functional biome maps: MODIS-IGBP land cover-type product (Loveland and Belward, 1997; Friedl et al., 2010; Fig. 2.1c), and the dominant biome distribution over 31 years from the global functional biome scheme from Higgins et al. (2016, 2017; Fig. 2.1d) (all biome names for each classification are listed in Appendix S2.1: Table S2.1.1). I did the analysis in R using the `terra` and `diffeR` packages (Pontius and Santacruz, 2019; R Core Team, 2022; Hijmans et al., 2023). All input, output data and code used to run the analyses including original and merged biome maps, contingency matrices, agreement maps, and the algorithm shown in Fig. 2.2 are provided in a Zenodo archive (Champreux et al., 2023).

For each of the six inter-classification comparisons, biomes were merged based on an overlap threshold ranging between 37% (Higgins et al., 2016, 2017 adjusted to Friedl et al., 2010) and 74% (Friedl et al., 2010 adjusted to Olson et al., 2001). The resulting merged categories are based on spatial overlap with a category from the other classification, and thus are not aimed to be ecologically or functionally meaningful. For example, the evergreen needleleaf forests, deciduous needleleaf forests, and permanent wetlands from Friedl et al. (2010) were merged based on their overlap with the boreal forests/taiga from Olson et al. (2001). I merged up to 11 biomes based on a single merging reference, i.e., 11 biomes from Leemans et al. (1990a, b) corresponded to the open shrublands from Friedl et al. (2010) (Fig. 2.3a). In this example, the result shows that the 11 biomes from Leemans et al. (1990a, b), which represent 11 different typical combinations of annual precipitation and potential evapotranspiration, today mainly host vegetation characterised by a 10–60% cover of 1–2-m high woody plants corresponding to the 'open shrublands' of Friedl et al. (2010). I provide all biome-merging settings in Appendix S2.1: Table S2.1.3, as well as all global biome maps with merged categories in Appendix S2.1: Fig. S2.1.1 and S2.1.2.

IV.2. Worldwide pattern of agreement

The global distribution of $\kappa_{i,j}$ demonstrates that the strength of the agreement among global biome maps varies widely across regions. The six inter-classification comparison maps generally share the same spatial distribution pattern of agreement (Fig. 2.4, Appendix S2.1: Fig. S2.1.3). This common pattern is independent of the biome-map family compared. In Fig. 2.4a, I calculated the average $\kappa_{i,j}$ for each grid cell of the world map across the six inter-classification comparisons (Fig. 2.3, Appendix S2.1: Fig. S2.1.3). High mean agreements (> 0.55, *sensu* Monserud and Leemans, 1992) occur in the equatorial rainforests of the Amazon basin, Congo basin and South-East Asia, and tropical deserts of the Sahara and the Arabian Peninsula. Conversely, low or no agreement (< 0.05, *sensu* Monserud and Leemans, 1992) were spread sparsely among many zones of the world, such as in eastern Patagonia, the Caatinga, eastern South Africa and Lesotho, south-eastern and south-western Australia, New Zealand, western Europe, Turkey, and large areas of North America and Asia (Fig. 2.4a).

The worldwide distribution of $\kappa_{i,j}$ also highlights a common latitudinal pattern of agreement among classifications (Fig. 2.4b). At the same latitude, $\kappa_{i,j}$ is generally lower in the Southern Hemisphere than in the Northern Hemisphere. The highest $\kappa_{i,j}$ are located around the Equator, the tropics, and boreal latitudes, despite lower values at temperate latitudes (~ 35° to 60° from the Equator), and in the transition regions between the

Tropics of Cancer and Capricorn and the Equator (~ 5° to 15° from the Equator). Such a pattern suggests that classification agreement depends on one or several latitude-related processes like changes in vegetation cover, species diversity, or natural disturbances.

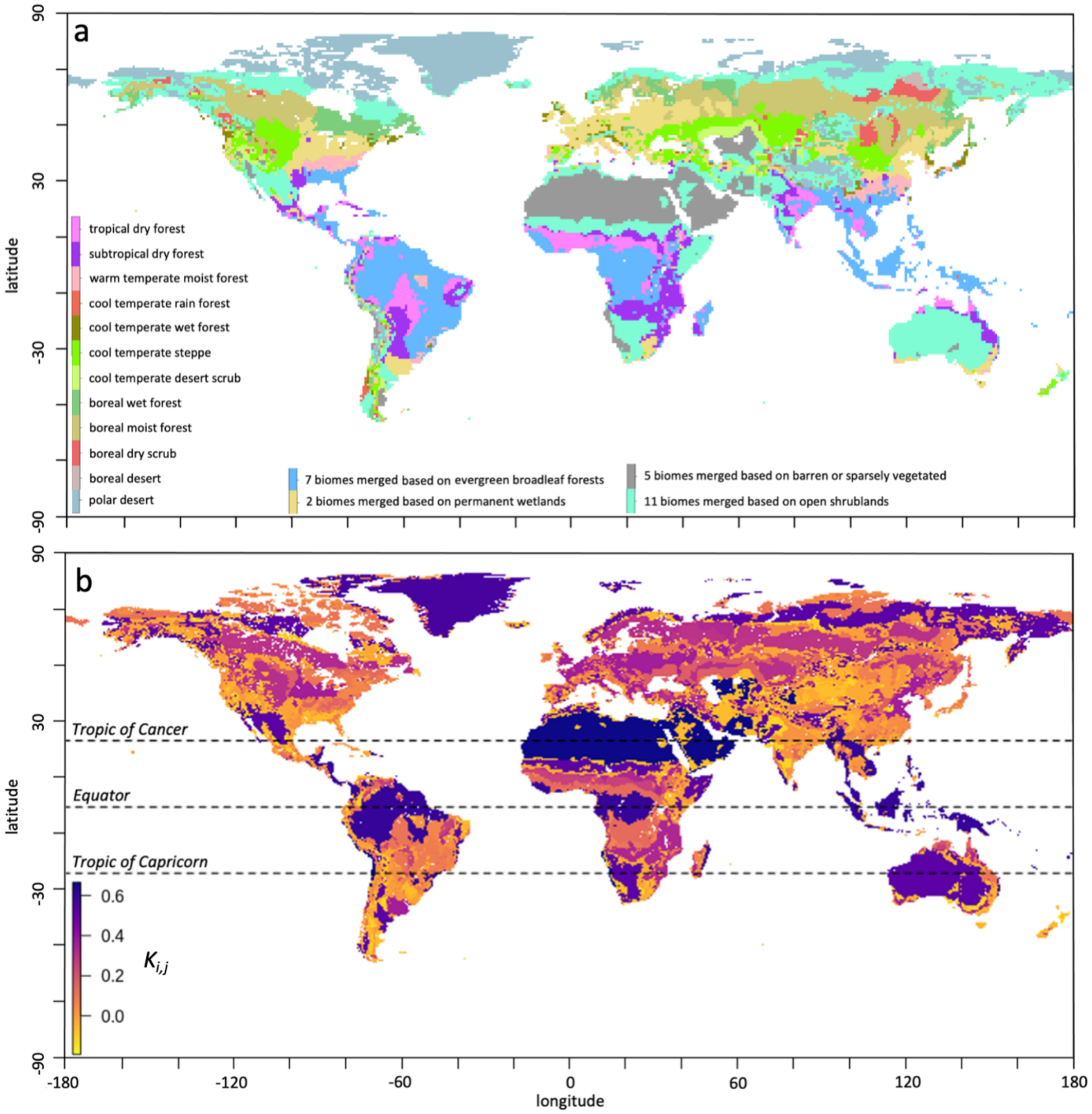

Figure 2.3. Example of biome map comparison. *(**a**) Example of biome map with merged categories. Categories from Leemans (1990a,b, highest complexity) were merged based on their spatial overlap with categories from Friedl et al. (2010, lowest complexity). (**b**) Distribution of the agreement (Cohen's $\kappa_{i,j}$) on a single category between global biome maps from Leemans (1990a,b, with merged categories) and Friedl et al. (2010).*

IV.3. Explaining the distribution of spatial agreement

Discrepancies among biome maps stem from the differences among mapping strategies and illustrate the lack of consensus on how to classify certain areas. Identifying the ecological characteristics of such low-agreement areas optimises the use and further development of the biome concept. In this section, I first discuss theoretically the potential causes of disagreement among biome maps. Then, I quantify the relative effect of six potential predictors in explaining the overall distribution of agreement.

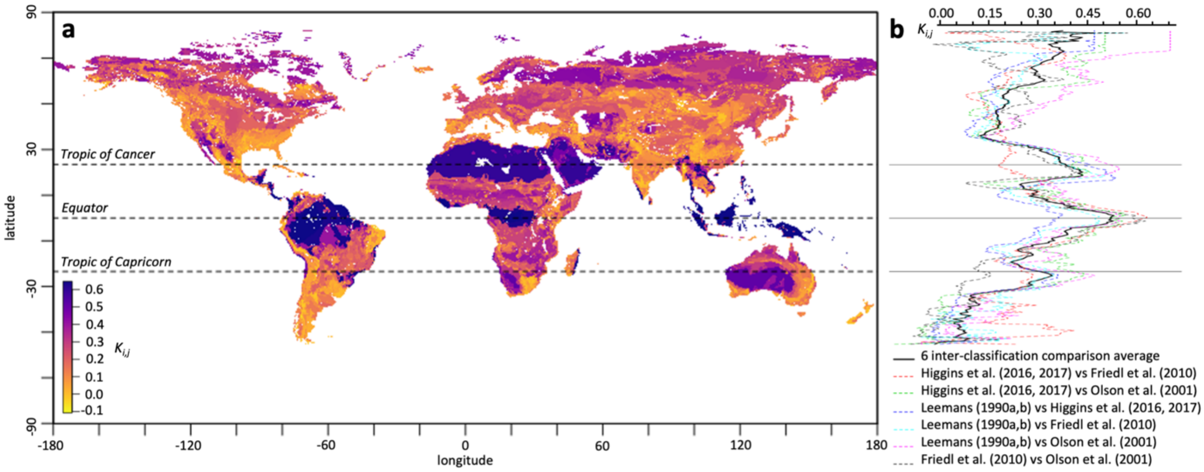

Figure 2.4. Distribution of the mean agreement (Cohen's $\kappa_{i,j}$) on a single category. *Mean $\kappa_{i,j}$ is calculated as the average across the six inter-classification comparison rasters, at a 0.5 × 0.5-degree resolution and ranges from 'no' agreement ($-1 < \kappa_{i,j} < 0.05$) to 'perfect' agreement ($0.99 < \kappa_{i,j} < 1$). (**a**) average for each grid cell of the map, (**b**) average across all the grid cells of the same latitude for the six inter-classification comparisons and their total average.*

IV.3.1. Potential drivers of biome map disagreement

The position of biomes and their boundaries depends on the characteristics of the ecosystems and on the biome-mapping method used (i.e., biome definition and data collection). One of the main conceptual differences between biome maps is whether they consider human activities. As a result, in areas of high human activity, it is likely that biome maps intending to represent potential natural vegetation (Olson et al., 2001; Fig. 2.1a; Leemans, 1990a, b; Fig. 2.1b) should intentionally differ markedly from maps considering the effect of human activities (Loveland and Belward, 1997; Friedl et al., 2010; Fig. 2.1c). Beyond the effect of such conceptual differences, some ecological characteristics could generate disagreement by making the classification of a given area ambiguous. For example, human activities could cause disagreement in any pair of maps if one map unintentionally underestimates them, which could occur between two potential natural vegetation maps.

Weak agreement can also arise in ecosystems that are poorly studied. For example, using the biome map of Ramankutty and Foley (1999), Martin et al. (2012) demonstrated that ecologists focus more on protected natural environments, which could produce disagreements in the most anthropogenically altered areas. Similarly, Martin et al. (2012) demonstrated that relatively open biomes such as 'savanna', 'open shrublands', and 'desert and barren' tend to be under-sampled compared to more forested biomes such as 'tropical deciduous woodland', 'temperate evergreen woodland', and 'temperate deciduous woodland'.

I identified two possible main causes of low agreement among global biome maps: (*i*) high landscape heterogeneity, and (*ii*) impact of landscape-modification processes. First, grid cells hosting landscapes of high heterogeneity such as mixed-tree and grass vegetation (e.g., with intermediate leaf area index), or potentially hosting many different biological associations (e.g., with high mammal or plant species richness) can potentially be classified into several biomes depending on the scale (e.g., one observation on a finer-scale vegetation formation, or average vegetation for the whole grid cell) and the location (e.g., in a mosaic, observation in the more or less forested area) of observations. In such cases, functional and simulated biomes from satellite imagery and modelling might tend to consider average observations, while compilation biomes from field observations could focus on and select localised features. Second, landscapes impacted by modification processes like the effect of ecosystem engineers (e.g., humans via agricultural practices or other effects depending on population density, and/or mammals by their diverse diets and habits) or disturbances (e.g., fire) can potentially elicit gaps between expected and existing biome distributions. When the actual vegetation is different than expected, compilation and simulated biomes theoretically differ from functional biomes, because field observations and model predictions generally downplay the impact of modification processes by focusing on well-preserved, 'natural' landscapes. Additionally, these differences might not be permanent due to the possible temporal variation of disturbance intensity, characterising areas with multiple stable biome states such as in subtropical savannas and forests (Sankaran et al., 2008; Staver et al., 2011; Moncrieff et al., 2014; Dantas et al., 2016).

IV.3.2. Methods: testing correlations with potential ecological drivers of disagreement

Beyond the expected effect of conceptual differences such as the choice either to map or erase the impact of human activities, I assessed the relative effect of (*i*) high landscape heterogeneity and (*ii*) landscape modification on agreement among biome maps. I decomposed the two potential drivers of disagreement into six quantifiable potential predictors, i.e., three landscape-heterogeneity characteristics (leaf area index, mammal species richness, and native plant diversity), and three possible markers of landscape modification including the presence of ecosystem engineers represented by humans (anthropogenic habitat loss, human population density), and a disturbance (monthly burnt area). I included anthropogenic habitat loss in the analysis to account for both its expected effect on biome map agreement when human activities are explicitly considered in only one of the two maps compared, and its potential additional effect when it is unintentionally underestimated in any map, including in potential natural vegetation maps.

I derived data representing the six potential predictors from published sources as follows: (*i*) I calculated the average leaf area index from global remote-sensing data at monthly intervals between 1981 and 2015 (Mao and Yan, 2019). (*ii*) I derived global mammal species richness from the International Union for Conservation of Nature and the Center for International Earth Science Information Network (2015), and (*iii*) the global distribution of native plant species richness and (*iv*) anthropogenic habitat loss from Ellis et al. (2012). Ellis et al. (2012) estimated the distribution of native plant species richness from the species-richness model of Kreft and Jetz (2007), and anthropogenic habitat loss as the sum of the percentage of land use for cultures, urban areas, and two thirds of pasture area from the HYDE 3.1 data model (Klein Goldewijk et al., 2010, 2011). (*v*) I derived human population density in 2015 from the Gridded Population of the World database (Center for International Earth Science Information Network 2018). (*vi*) I calculated the average monthly burnt area from 1997 to 2015 from the remote sensing-derived *Global Fire Emission Database* version 4 (Randerson et al., 2018). I formatted all data to a 0.5 × 0.5-degree resolution, one-year average, and excluded grid cells containing missing data. Missing leaf area index data correspond to low cover, so I replaced missing data on continental areas with an arbitrary low value (= 0.0001) to prevent any statistical misrepresentation.

Relying on these six products can be debated because they are inevitably associated with particular biases and uncertainties. For example, there are uncertainties and differences among available anthropogenic land-cover products depending on the mapping method, including the classification scheme and input data used (Klein Goldewijk et al., 2007, 2011; Buchhorn et al., 2020). The quality of the anthropogenic habitat-loss dataset from Ellis et al. (2012) can be questioned because the input data are not standardised among countries (Klein Goldewijk et al., 2007, 2011). In contrast to Ellis et al. (2012), Buchhorn et al. (2020) provided some estimates of uncertainty and accuracy, and they standardised data collection at the global scale and at high spatial resolution using machine learning. However, the two products have some similarities. For example, despite methodological differences, the estimated total percentage of cropland cover is of the same order of magnitude in the product used by Ellis et al. (2012) (i.e., ~10% in 2000; Klein Goldewijk et al., 2011) to that used by Buchhorn et al. (2020) (i.e., ~12% in 2015; Buchhorn et al., 2019). In this exploratory analysis, I assumed that the product of Ellis et al. (2012) adequately represented the main spatial trends of anthropogenic land cover, but at a low spatial resolution. I also chose to use Ellis et al. (2012) because they explicitly estimated the rate of anthropogenic habitat loss by grid cell, and because they also included an estimate of the percentage of pasture areas. While rarely considered in land-cover products, the percentage of pasture is important for biome distribution because livestock grazing can potentially impact vegetation at broad spatial scales. In addition, I included a measure of the monthly burnt area in the analysis to consider, at least partially, the effect of fire on biome map disagreement. However, such a product does not adequately describe the fire regimes given that some aspects of fire regimes are not specified (e.g., frequency, severity, seasonality) (Hély et al., 2019); as yet there is no global, georeferenced, and gridded dataset representing those aspects. Moreover, the remote-sensing record covers 19 years, so environments with long fire-return intervals are not considered in the burnt area product from Randerson et al. (2018).

The assumption that mammal species richness is related to landscape heterogeneity can be debated. Mammal species richness strongly correlates positively with native plant diversity and leaf area index (Fig. 2.5). I suggest that extremely high or low mammal species richness best characterises 'extreme' biomes (in terms of diversity and vegetation cover), that tend to represent more homogeneous landscapes. Extreme biomes correspond to high mammal richness in equatorial rainforests (> 150 species) or low mammal richness in deserts (< 10 species). In contrast, biome distinction might be more ambiguous in regions with mid-range mammal richness ($50 < S < 100$). Mammal richness generally increases with ecosystem primary productivity (Toszogyova and Storch, 2019). Mid-range mammal richness thus represents mid-range productivity environments. Such environments often correspond to multiple stable biome states, thus heterogeneous landscapes that might prevent agreement on biome identity in large areas, such as in subtropical savannas and forests (Sankaran et al., 2008; Staver et al., 2011; Moncrieff et al., 2014; Dantas et al., 2016). Multiple stable states have mostly been linked to the effects of both fire and herbivores (Dantas et al., 2016). I did not test the effects of herbivores on agreement among biome maps due to the lack of suitable, global-scale data.

I measured the correlations among $\kappa_{i,j}$ and the six potential predictors (Spearman's ρ). Negative values of Spearman's ρ indicated that the selected predictors are likely to affect the agreement among biome classifications negatively. For each of the six pairwise agreement maps and their average, I built and compared 64 generalised least-squares models (accounting for spatial autocorrelation) to identify which predictor among landscape (*i*) heterogeneity and (*ii*) modification variables best described the variation in agreement for a single category $\kappa_{i,j}$ (Appendix S2.1: Table S2.1.4). The 64 models expressed $\kappa_{i,j}$ as a function of all possible combinations of the six potential predictors excluding their interactions, i.e., leaf area index, plant species richness, anthropogenic habitat loss, human population density, mammal species richness and monthly burnt area. To account for computational limitations, I built the generalised least-squares models based on a sample of 471 to 486 grid cells selected at regular intervals of five latitude and five longitude degrees among valid grid cells. I used a metric for the goodness of fit of each model as the difference between the sum of square of the residuals of the generalised least-square model and the sum of squares of the dispersion of the data around the observed mean, divided by the sum of squares of the dispersion of the data around the observed mean (Saltré et al., 2019). High values (> 80%) of the model's goodness of fit indicated that the model performed well in predicting agreement.

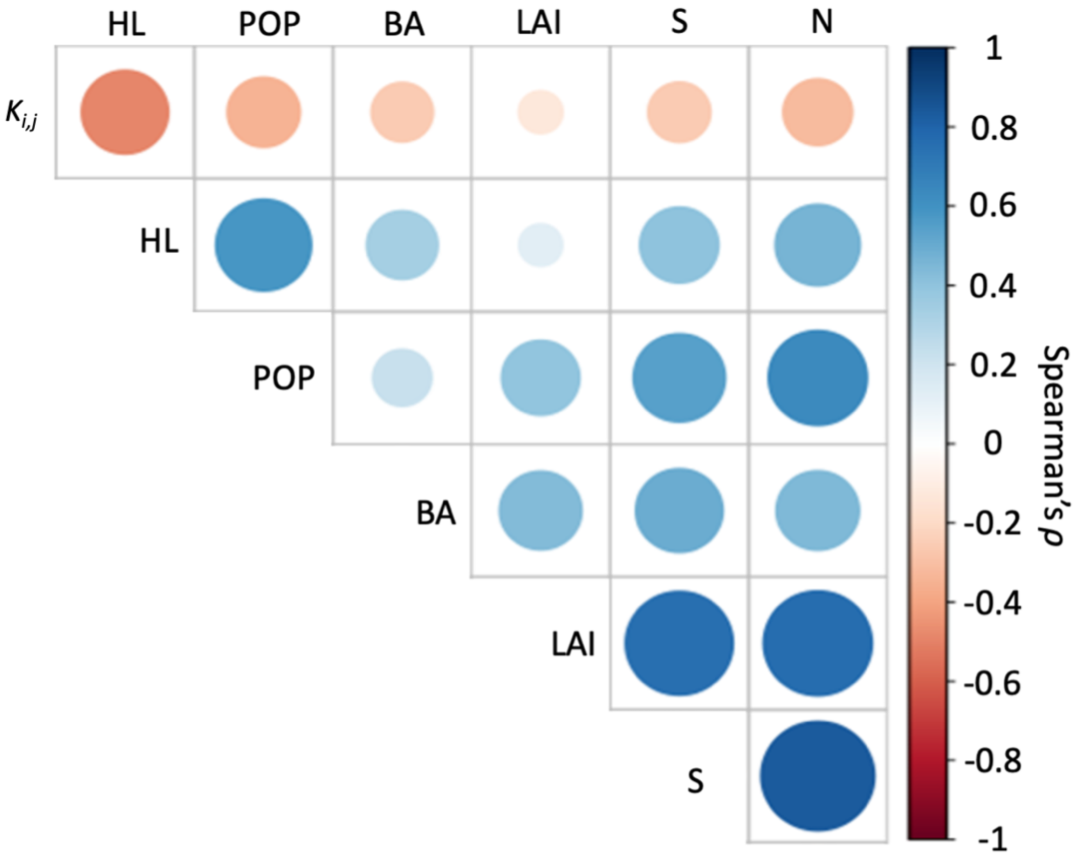

Figure 2.5. Spearman's ρ between variables included in the generalised least-squares models. *Correlations between the mean Cohen's κ (agreement) for a single category ($\kappa_{i,j}$), variables describing landscape modification (HL = Habitat Loss, POP = human population density, BA = yearly burnt area) and landscape heterogeneity (LAI = leaf area index, N = native plant species richness, S = mammal species richness) per grid cell. I used the* `corrplot` *R package (Wei and Simko, 2017). The size of the dots represents the strength of the correlation. Based on uniformly resampled data from the total list of grid cells where I have calculated the mean $\kappa_{i,j}$ across the six inter-classification comparison rasters (×10, 533 grid cells).*

I ranked the 64 models based on their Akaike's information criteria corrected for small samples (AIC_c) (Akaike, 1973; Hurvich and Tsai, 1989). The ranking penalises models with more covariant parameters, thus accounting for collinearity. The top-ranked model indicated the most probable combination of predictors and rejected other hypotheses. From this top-ranked model, I quantified the relative importance of each predictor variable (including their interactions) by measuring the change in the model's goodness of fit and the Nagelkerke pseudo r-squared (R^2; Nagelkerke, 1991) when removing this variable from the model. All input and output data including potential ecological drivers data, resampled data, and generalised least-squares model outputs are provided in a Zenodo archive (Champreux et al., 2023).

IV.3.3. Results: correlations of spatial agreement with landscape heterogeneity and modification factors

All six of this selected predictors were negatively correlated with the average agreement among biome classifications $\kappa_{i,j}$ ($\rho < 0$), with *habitat loss* emerging as the predictor with the greatest explanatory power as expected from discrepancies among biome classification in accounting for human activities (Fig. 2.5). Unsurprisingly, the negative correlations with the six selected predictors confirm the expectations that both landscape heterogeneity and the presence of landscape-modification processes relate to a reduction of the agreement among biome classifications.

In term of average map agreement (Fig. 2.4), generalised least-square models including anthropogenic habitat loss generally explained the distribution of the biome map agreement better than other models (Appendix S2.1: Table S2.1.4A). The top-ranked generalised least-square model included habitat loss, mammal species richness, and leaf area index (> 93% goodness of fit and lowest AIC_c; Table 2.2, Appendix S2.1: Table S2.1.4A). When considering interactions among these three variables, interactions between leaf area index (LAI) and either habitat loss (HL) or mammal species richness (S) had the strongest effect (HL×LAI: highest percent of change of the model's goodness of fit, Δ% goodness of fit = 2.61; LAI×S: highest pseudo R^2 relative to the full model, $R^2 = 0.05$; Tables 2.3, 2.4 and Appendix S2.1: Table S2.1.4).

However, when investigating the six pairwise agreement maps (Table 4, Appendix S2.1: Tables S2.1.5 – S2.1.10), all top-ranked models included anthropogenic habitat loss and the leaf area index. When considering the interaction terms, the most important predictors generally considered anthropogenic habitat loss interacting with another predictor (leaf area index or mammal diversity). High anthropogenic habitat loss was also among the leading ecological characteristics explaining disagreement when comparing the two potential natural vegetation maps (Table 2.4, Appendix S2.1: Table

Table 2.2. Comparison of generalised least-squares models with no interaction terms for the average agreement map. *The generalised least-squares models include measures of landscape modification (HL = habitat Loss, POP = human population density, BA = yearly burnt area) and landscape heterogeneity (LAI = leaf area index, N = native plant species richness, S = mammal richness) per grid cell to describe the mean agreement between the four biome classifications studied. Shown for each model are the number of parameters (k), maximum log-goodness of fit (LL), difference in Akaike's information criterion corrected for small sample sizes relative to the top-ranked model (ΔAIC_c), AIC_c weight (~ model probability; $wAIC_c$). Based on resampled data (× 10,533 grid cells). See details of the full list of generalised least-squares models describing all combinations among predictor variables in Appendix S2.4.*

Model	*k*	LL	ΔAIC_c	$wAIC_c$
~HL+S+LAI	6	295.07	0	0.15
~HL+LAI	5	293.91	0.28	0.13
~HL+S+LAI+POP	7	295.82	0.56	0.11
~HL+LAI+POP	6	294.58	0.99	0.09
~HL+LAI+N	6	294.42	1.32	0.08
~HL+S+LAI+N	7	295.25	1.71	0.06
~HL+S+LAI+BA	7	295.14	1.93	0.06
~HL+LAI+POP+N	7	295	2.2	0.05
~HL+LAI+BA	6	293.91	2.33	0.05
~HL+S+LAI+POP+N	8	295.94	2.4	0.05

Table 2.3. Relative importance of variables including interactions in the top-ranked generalised least-square model for the average agreement map. *These models include measures of landscape modification (HL = habitat loss) and landscape heterogeneity (S = mammal richness, LAI = leaf area index) and their interactions per grid cell to describe the mean agreement between the four biome classifications I examined. Shown for each model are the number of parameters (k), maximum log-goodness of fit (LL), difference in Akaike's information criterion corrected for small sample sizes relative to the top-ranked model (ΔAIC_c), and percent of change in goodness of fit (Δ%GoF) for each model. The goodness of fit is calculated as the difference between the sum of square of the residuals of the generalised least-square model and the sum of squares of the dispersion of the data around the observed mean divided by the sum of squares of the dispersion of the data around the observed mean. The relative importance of each variable is represented by the Nagelkerke pseudo-r square (R^2; Nagelkerke, 1991) and the Δ%GoF of each truncated model (i.e., full model minus one of the predictive variables) relative to the full model, with higher values corresponding to higher importance. Based on resampled data (× 10,533 grid cells).*

variable removed	model	*k*	LL	ΔAIC_c	Δ%GoF	R^2
S×LAI	~HL+S+LAI+(HL×LAI)+(HL×S)	8	308.75	63.24	-2.32	0.05
HL×LAI	~HL+S+LAI+(S×LAI)+(HL×S)	8	333.19	14.37	2.61	0.01
HL×S	~HL+S+LAI+(HL×LAI)+(S×LAI)	8	335.49	9.77	-1.12	0.01
HL	~S+LAI+(HL×LAI)+(S×LAI)+(HL×S)	9	341.41	< 0.001	< 0.001	< 0.001
S	~HL+LAI+(HL×LAI)+(S×LAI)+(HL×S)	9	341.41	< 0.001	< 0.001	< 0.001
none	~HL+S+LAI+(HL×LAI)+(S×LAI)+(HL×S)	9	341.41	< 0.001	< 0.001	< 0.001
LAI	~HL+S+(HL×LAI)+(S×LAI)+(HL×S)	9	341.41	< 0.001	< 0.001	< 0.001

S2.1.11; Olson et al., 2001; Fig. 2.1a; Leemans 1990a, b; Fig. 2.1b). This highlights the difficulties in predicting what nature would look like without the impact of human activities, and suggests their underestimation when mapping potential biome distribution. I provide the details of the generalised least-squares analyses for the pairwise agreement maps in Appendix S2.1: Tables S2.1.5 – S2.1.10.

Table 2.4. General summary of the generalised least-square models. *General summary of the generalised least-squares models for the six pairwise agreement maps and their average. Models include measures of landscape modification (HL = habitat Loss, POP = human population density, BA = yearly burnt area) and landscape heterogeneity (LAI = leaf area index, S = mammal richness) and their interactions per grid cell to describe the mean agreement between the four biome maps I examined. For each agreement map, models are ranked based on the Akaike's information criterion corrected for small sample sizes. For each agreement map, the most important predictor variable (top predictor) is identified by measuring the change in the model's goodness of fit and the Nagelkerke pseudo-r squared (R^2; Nagelkerke, 1991) when removing this variable from the top-ranked model considering pairwise predictor interactions.*

Map A (merged)	**Map B**	**Top-ranked without interactions**	**Top-ranked with interactions**	**Top predictor (Δ%GoF)**	**Top predictor (R^2)**
Average of all agreement maps		~HL + S + LAI	~HL + S + LAI + (HL×LAI) + (S×LAI) + (HL×S)	HL×LAI	S×LAI
Higgins et al., 2016	Friedl et al., 2010	~HL + LAI + POP	~HL + POP + LAI + (HL×LAI)	HL×LAI	HL×LAI
Higgins et al., 2016	Olson et al., 2001	~HL + LAI + BA	~HL + BA + LAI + (HL×LAI) + (HL×BA)	HL×LAI	HL×LAI
Leemans et al., 1990	Higgins et al., 2016	~HL + LAI + POP	~HL + LAI + POP	HL	HL
Leemans et al., 1990	Friedl et al., 2010	~HL + LAI + S	~HL + S + LAI + (HL×LAI) + (S×LAI)	HL×LAI	S×LAI
Leemans et al., 1990	Olson et al., 2001	~HL + LAI + S	~HL + S + LAI + (S×LAI) + (HL×S)	HL×S	S×LAI
Friedl et al., 2010	Olson et al., 2001	~HL + LAI	~HL + LAI + (HL×LAI)	HL×LAI	HL×LAI

The top-ranked models indicate that biome-classification agreement is highest where anthropogenic impacts are lowest. Conversely, areas with more anthropogenic impacts (cultures, pasture, and urban areas) are more likely to correspond to disagreement among different biome classifications. In addition, biome maps often tend to disagree more in areas characterised by mid-range leaf area index. Assuming that areas with high leaf area index are characteristic of forested landscapes and that low values instead reflect more grassland-like ecosystems, I then argue that intermediate leaf area index indicates mixed tree and grass ecosystems, that tend to represent more heterogeneous landscapes. Overall, the results suggest that biome distribution is generally more sensitive to the choice of mapping method in areas with moderate vegetation cover and higher human activity. Further local/regional data and analyses are required to investigate the underlying ecological processes leading to these agreements/disagreements. This protocol helped to identify the areas of focus on a global/continental perspective.

V. CHOOSING A BIOME-CLASSIFICATION SCHEME

Ecology and biogeography studies refer to biomes to summarise fine-scale results at broader scales using established biogeographical units beyond the scope of their study areas, focal species, or ecosystems. This spatial comparison of biome classifications showed widespread discrepancies among biome-classification schemes, suggesting that selecting a specific scheme or map needs careful justification for purpose, although this important aspect is often overlooked (but see Moncrieff et al., 2015; Zizka et al., 2020).

This selection process requires considering several aspects depending on the research question, scope, and audience. By better reflecting the delineation of biomes from regional maps, *compilation* maps should facilitate understanding and acceptance by broad, non-academic audiences, so I recommend that they should be used primarily for science communication. *Functional* maps reflect the actual distribution of biomes at a given time, based on automated and standard observations. Such maps are thus best suited for monitoring biome dynamics (and their potential drivers), and for investigating relationships among vegetation traits and climate, biodiversity, or matter fluxes (e.g., carbon, nitrogen, etc.). Finally, *simulated* biome maps are derived from a set of selected hypotheses on the functioning of the biomes, allowing to test the sensitivity of biome distribution to environmental changes, for example. Such model-generated maps are therefore useful tools to investigate ecological processes underlying present, past, and future biome dynamics. If the latter successfully reproduce the present biome distribution and further benchmarks concerning past vegetation changes (Kelley et al., 2013), they also might be useful to guide climate-adaptation measures, in particular those concerning agriculture, forestry, and conservation (Gonzalez et al., 2010; Martens et al., 2021).

VI. CONCLUSIONS

(**1**) Ideally, the biome concept should be a tool for quantitative comparisons, but it suffers from a diversity of terrestrial biome classifications, which results in various geographic divisions, biome names, and number of categories. Comparing available biome-mapping methods by their definitions and their underlying data, I identified three main families: (1) *compilation* biome maps from expert elicitation, (2) *functional* biome maps from vegetation physiognomy (remote sensing), and (3) *simulated* biome maps from vegetation modelling. Inferring past or future biome distributions requires hindcasting or predicting biome characteristics from limited information based on plant remains or model simulations, such as unlimited observations (compilation), plant functional traits and taxonomic diversity (functional), or physical environment data (simulated).

(**2**) I developed an algorithmic protocol to spatially compare biome-classification schemes with different biome names and numbers. I compared four of the most used modern global biome maps and found strong disagreements among these maps in areas with moderate vegetation cover and in areas where human activities modify ecosystems. While biome-classification schemes agree well in some regions such as equatorial forests and several tropical deserts, they strongly differ in others. I highlighted how quantifying agreement and discrepancies between maps can help evaluate, for example, the impact of humans on global biome distributions. This may inspire further research to refine biome classifications in areas where they diverge.

(**3**) To prevent and acknowledge biases, studies involving several biome classifications should identify areas of disagreement by comparing biome maps spatially. For such spatial comparison, I have provided a protocol, which may also serve to evaluate model outputs against independently produced biome maps. Biome classifications typically disagree in areas of high human impact. These ‘engineered biomes’ or ‘anthromes’ deserve special attention in studies aiming to map modern-day biome distributions. To improve both the accuracy and reproducibility of biome maps, and to promote maps that approach consensus, I advocate data-driven approaches. This could include not only functional biome classifications, but also dynamic global vegetation models that incorporate data on plant functional traits and land use, for example.

(**4**) There is neither a consensus biome map nor universally accepted definitions of biomes. ‘Desert’, ‘rainforest’, ‘tundra’, ‘grassland’ or ‘savanna’ — while being widely used terms in common language — each have multiple definitions and no universally accepted spatial distribution. Because fit-for-purpose classification schemes are necessary, multiple biome maps should continue to co-exist, even within the three main families I identified. As a result, Earth-scale knowledge is still blurred by the extant diversity of approaches. For the time being, consensus seems to be unrealistic aim, and I must instead seek to account for the biases and uncertainties of each map more completely. I have provided comparison and decision tools to navigate this diversity and facilitate a more effective use of the biome concept, emphasising the need for considering the way biomes are defined and mapped when using a specific biome map.

CHAPTER 3

POST-LAST GLACIAL MAXIMUM VEGETATION CHANGES IN THE NEOTROPICAL REALM: REVIEW OF PALAEO-ENVIRONMENT RECORDS

ABSTRACT

The post-Last Glacial Maximum period spans the last ~ 19,000 years and was characterised by a general trend of climate warming until the end of the Pleistocene (11,700 calendar years before present [BP]) with some periods of temporary reversion locally during the Heinrich Stadial 1 (~ 18,100 – 14,700 BP) and the Younger Dryas (~ 12,900 – 11,600 BP). I review the main vegetation changes deduced from palaeo-environment records and their potential drivers. Published analyses of palaeo-environmental records consist mainly of palynological studies, sometimes supplemented by analyses of other proxies such as plant macrofossils, charcoal, phytoliths, isotopic ratios, or faunal remains. Palaeo-environment records suggest asynchronous vegetation changes across the Neotropical realm from the Last Glacial Maximum to the present. While some regions might have fluctuated between dense forests and grass-dominated vegetation, others hosted the gradual development of closed or open landscapes, and some could have remained relatively stable through time. Most vegetation changes are attributed to variation in moisture availability in the environment, with local effect of other factors such as fire regimes, human activities, insolation, and cloud cover. At the continental scale, the main vegetation changes include: (1) the northward retraction and southward expansion of tropical and subtropical forests during Heinrich Stadial 1 and the Younger Dryas following the southward displacement of the inter-tropical convergence zone and the consecutive strengthening of the South Atlantic convergence zone more in the south, (2) the gradual upslope expansion of montane forests in the tropical Andes during the Holocene (11,700 BP to present), and (3) the gradual southward expansion of temperate *Nothofagus* forests, especially on the slopes of the Patagonian Andes, due to the southward displacement of the southern westerly winds after the retreat of the Patagonian ice sheet ~ 15,000 BP until the early Holocene. Despite widespread changes in forest cover and floristic composition, large areas probably maintained a stable tree cover such as the north-western Amazon rain forest, montane forests at lowest elevations in the tropical and subtropical Andes (< 2,000 m above sea level), the Pampas, and the Patagonian dry diagonal. The paucity of palaeo-environment records in some regions, such as in the two South American dry diagonals and in the Amazon Basin, prevents the description of vegetation changes with palaeo-environment records. In the Amazon Basin for example, most recent studies tend to conclude that a drier climate during the Last Glacial Maximum might have been responsible for changes in floristic composition and vegetation structure locally, but the possible widespread replacement of forests by grass-dominated vegetation is still debated. Finally, following European arrival in the Americas, the last ~ 500 years are marked by the massive expansion of land use for cropland and pastures associated with high rates of deforestation and the spread of invasive exotic plant taxa in most Neotropical landscapes.

KEY WORDS: pollen, palaeo-vegetation, Neotropics

I. INTRODUCTION

In this chapter, I review the changes in vegetation that occurred in the Neotropical realm (*sensu* Olson et al., 2001) during the last deglacial and Holocene period spanning 19,000 calendar years before present [BP] to the present based on palaeo-environment records. The Neotropical realm spans from 33 °N to 60 °S, covering the region from southern edge of the USA to Tierra del Fuego in Chile in southernmost South America.

There are various approaches available to describe vegetation. Each study uses its own terminology, which depends on the method and proxy used to infer vegetation changes. I summarise vegetation changes within seven large regions broadly corresponding to a consistent physical-environment context (i.e., influenced by the same climate processes such as rain seasonality, topography, etc.) and covering most of the continent: extended Patagonia, central South America, north-eastern South America, the Amazon Basin, the tropical Andean region, the extended Caribbean region, and the extended Mexican region. Because biome distribution has changed through time and depends to some extent on subjective biome-classification criteria, using modern biome distributions to describe past changes are irrelevant and potentially confounding. In contrast, focusing on patterns expressed across broad spatial scales allows a better appreciation of the movement of ecotones through time, i.e., the transition zones between two adjacent vegetation types. I attempted to describe those regions according to five sections that will summarise the main vegetation shifts that have occurred since the Last Glacial Maximum, highlighting shifts between open/semi-open/closed landscapes, turnover of plant functional type toward more/less drought-tolerant forms, shifts in disturbance regimes such as human and fire, and the main theoretical driving factors for vegetation changes described in the literature:

- Modern physical environment and vegetation, that highlight their main topographic and climatic features, and modern vegetation cover
- Synthesis of main vegetation changes
- Major deglacial vegetation changes (19,000 – 11,700 BP)
- Major Holocene vegetation changes (11,700 BP – present)
- Potential causes of vegetation change

After describing the main environmental characteristics of each region, I first summarise the variety of studies into a single, simple, and intelligible description of the main subregional trends in tree cover changes for each region, and emphasise the debates and uncertainties among studies. Second, I describe the spatio-temporal distribution of the fossil record, and detail tree-cover changes in each site or study used for this review. Finally, I focus on the main potential causes of large-scale vegetation changes in each region.

I.1. Modern physical environment and vegetation

I.1.1. Patagonia

The Patagonia region covers most of Chile to the west and western Argentina to the east, and it is bordered by the Altantic Ocean to the east and the Pacific Ocean the west (Fig. 3.1). The Andes stretch from north to south along the Pacific coast, with highest elevations located in Chile. Western Argentina is covered by medium-height mountain ranges with elevations generally ranging from 500 – 2000 m above sea level. The region is under strong influence from the southern westerly winds bringing precipitation from the Pacific Ocean (Davies et al., 2020). Consequently the western slopes of the Andes are humid, with mean annual precipitation generally ranging from 100 to 900 mm. Conversely, eastern Patagonia is arid, receiving low precipitation (< 100 m year^{-1}) as the south-westerly winds provide highly evaporative conditions at the surface (Davies et al., 2020; Zomer et al., 2022; Fig. 3.1c).

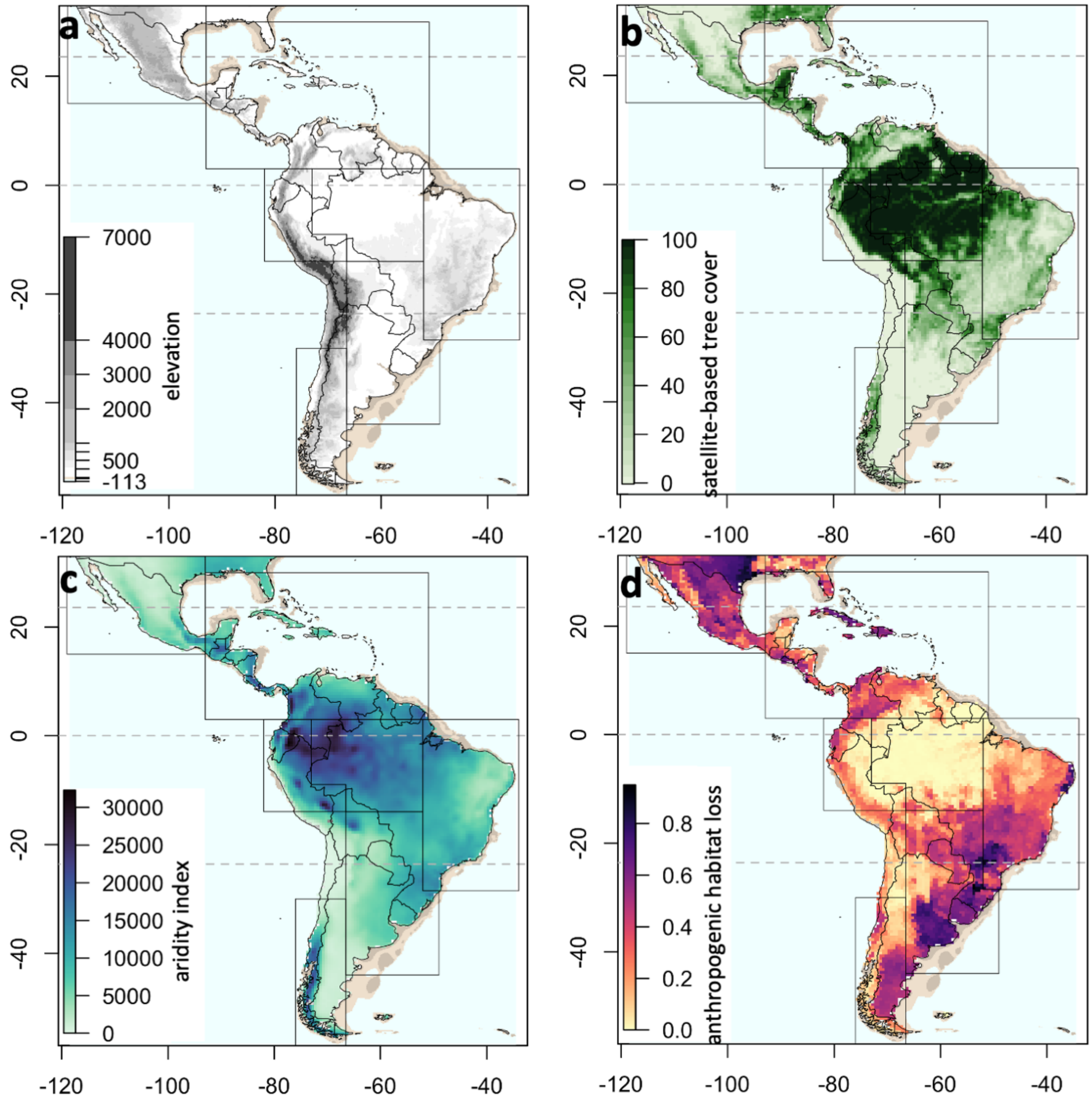

Figure 3.1. ***Modern environment in the Neotropical realm.*** *(a) elevation, (b) satellite-based tree cover derived from Hansen et al. (2013), (c) aridity index derived from Zomer et al. (2022), (d)anthropogenic habitat loss derived from Ellis et al. (2012). Selected regions for this study are outlined in black. (i) Patagonia, (ii) Central South America, (iii) North-eastern South America, (iv) Amazon Basin, (v) Tropical Andean, (vi) Caribbean, (vii) Mexican.*

The Patagonian region is also cold, with mean annual air temperature ranging from 14 °C in the north-eastern lowlands, < 8 °C in the south-eastern lowlands, to below zero at the highest Andean elevations (Davies et al., 2020). Today, broadleaf forests mainly grow on the western slopes of the Andes and steppes cover most of Argentine Patagonia to the east (Fig. 3.1b; Woodward et al., 2004; Hansen et al., 2013; Dinerstein et al., 2017). Western Patagonian forests are divided into two different ecoregions: the Valdivian temperate rainforest and the Magellanic subpolar forests (Dinerstein et al., 2017). Valdivian forests are dominated by evergreen and broadleaf trees, including trees from the genera *Nothofagus, Fitzroya*, and *Araucaria*, with deciduous species more common at the highest elevations. Magellanic forests are characterised by the widespread distribution of trees from the the genus *Nothofagus*, with higher densities of evergreen trees to the west and deciduous trees to the east, while the Chilean Archipelago along the southern Pacific coast is dominated by Magellanic moorland (Fontana and Bennett, 2012). High rates of anthropogenic habitat loss are mainly located on the northern slopes of the Patagonian Andes and in the steppes of eastern Patagonia (Fig. 3.1d; Ellis et al., 2012; Ellis, 2021).

I.1.2. Central South America

The central South American region covers southern Brazil, southern Bolivia, Paraguay, Uruguay, and north-eastern Argentina and is bordered by the Atlantic Ocean to the east and the Amazon Basin to the north (Fig. 3.1). The Brazilian Highlands extend to the northeast of the region along the Atlantic coast in southern Brazil and Uruguay. The rest of the region is mainly composed of a vast plain stretching from north to south, including north-eastern Argentina which is mainly composed of lowlands. The entire region lies to the west of the South Atlantic convergence zone, and the northwest of the region is characterised by high precipitation seasonality influenced by a rainy season from December to January that brings high precipitation to areas that are otherwise arid or semi-arid during the June – August dry season (Villela, 2017; Luebert, 2021).

In contrast, the north-eastern part of the region in the Brazilian Highlands along the Atlantic coast in southern Brazil and Uruguay is always humid, while the south tends to remain arid (Luebert, 2021). Today, low-density dry forests and wood-dominated savannas cover the north of the plains, such as the Chiquitano, Chaco, and Pantanal ecoregions, despite the intense deforestation of some areas in the past decades (Hansen et al., 2013; Dinerstein et al., 2017). Evergreen forests of the Atlantic forest grow in the Brazilian Highlands in southern Brazil, including ecoregions such as the *Araucaria* moist forests, the Serra do Mar coastal forests, and the Alto Paraná Atlantic forests (Hansen et al., 2013; Dinerstein et al., 2017). In the north, the western Cerrado is covered by open savannas. Southern landscapes of the region are vast grasslands with low tree cover. The humid Pampas area in the plains of north-eastern Argentina receives more precipitation and is the most heavily populated area of Argentina, as well as being dedicated to intensive cropping and cattle grazing (Friedl et al., 2010). Consequently, most of the Pampas is subject to extremely high rates of estimated anthropogenic habitat loss (Fig. 3.1d; Ellis et al., 2012; Ellis, 2021). The Argentine Pampas is listed as a fire-dependent/influenced region, meaning that fires are necessary to maintain native plants and animals (Hardesty et al., 2005).

The north-eastern Pampas is characterised by a network of fluvial valleys, and the eastern part has poor drainage that causes frequent flooding during periods of high precipitation (Prieto, 2000). To the west of the Argentine humid Pampas, landscapes become gradually drier and host more xerophytic vegetation including open shrublands such as the Espinal and the Low Monte ecoregions (Prieto, 2000; Prieto et al., 2004; Friedl et al., 2010; Dinerstein et al., 2017). The reason for the absence of trees on the Pampas grasslands is debated, and often considered an anomaly (Chaneton et al., 2012). On the one hand, the area could potentially support deciduous or mixed forests based on its climate, and many introduced tree species grow spontaneously in the region (Chaneton et al., 2012). On the other hand, while the area is characterised by high rates of anthropogenic habitat loss, pristine Pampas landscapes typically host open grasslands, and might have remained open since the Miocene (Chaneton et al., 2012).

Several hypotheses have been posed to explain these observations, including water-limiting characteristics such as soil texture and climate, and woody biomass consumption by fire and herbivores (Bond, 2008). Based on the absence of clear single explanation combined with the continuous historical presence of open landscapes, Chaneton et al. (2012) suggested that the absence of trees resulted from multiple interacting factors, including the absence of adapted tree species in the local species pool, low seed dispersal, abiotic stress such as heavy soil, drought or frost, over-competition by resident grasses, or the absence of appropriate soil microbia such as mycorrhizal fungi.

I.1.3. North-eastern South America

The north-eastern South American region covers north-eastern Brazil exclusively (Fig. 3.1), including the northeast and southeast regions, as well as the eastern parts of the central-west (State of Tocantins and part of Parà) and northern regions (State of Goiás and parts of Mato Grosso). The region is surrounded by the Atlantic Ocean to the north, east, and south and is located between the inter-tropical convergence zone in the north and the South Atlantic convergence zone in the south (Villela, 2017). The region is characterised by medium-height mountain ranges in the southeast and the Brazilian Highlands (or Central Plateau), with increasing elevation toward the southern Atlantic coast and the Pico da Bandeira (2,891 m above sea level) representing the highest summit.

The region comprises four different modern biogeographical regions (ecoregions, *sensu* Olson et al., 2001) — the Caatinga and Cerrado open landscapes, and the Amazon and Atlantic rainforests. The Caatinga and the Cerrado represent a large, dry diagonal stretching from the northeast to the southwest, covering most of the Brazilian Highlands and characterised by a semi-arid to arid climate from June to August and a rainy season corresponding to the South American summer monsoon linked to the southward displacement of the inter-tropical convergence zone (Olson et al., 2001; Luebert, 2021). The aridity index is especially low in the Caatinga (i.e., high aridity; Fig. 3.1c). Today, most of the Caatinga and Cerrado is covered by open, savanna-like landscapes (Fig. 3.1b; Olson et al., 2001; Friedl et al., 2010; Hansen et al., 2013). At finer spatial scales, modern vegetation in the Brazilian Highlands and the Cerrado is a mosaic of vegetation types with various degrees of openness, from sclerophyllous forests and savanna-like vegetation to grasslands and many croplands, with grass-dominated landscapes covering the highest summits above 1,800 – 2,000 m above sea level (Pivello and Coutinho, 1996; Furley 1999; Safford, 1999; Friedl et al., 2010; Pivello, 2011; Hanssen et al., 2013). Like the Pampas (Central South America region), the Cerrado is listed among the fire-dependent/influenced regions (Hardesty et al., 2005).

In the Cerrado, pollen and charcoal records suggest that fire might have shaped grass-dominated landscapes even before the area was populated by humans, with increasing frequencies during the Holocene as the climate dried (Pessenda et al., 2001, 2004, 2005 in Pivello, 2011), and after European settlement (Bond and Keeley, 2005; Pivello, 2011). Around the dry diagonal, the Amazon and Atlantic rainforests cover less arid regions located the north-western corner and a thin strip along the southern and eastern Atlantic coasts, respectively (Fig. 3.1b, c; Dinerstein et al., 2017; Zomer et al., 2022). In the region, the Amazon rainforest notably includes the Xingu-Tocantins-Araguaia, Marajó várzea and the Tocantins/Pindare moist forests connected to the rest of the Amazon forest, as well as smaller patches on mountain-tops considered to be interglacial refugia resulting from the past expansion of the Atlantic rainforest (Ledru et al., 2007; Montade et al., 2014; Ledru et al., 2016; Dinerstein et al., 2017). The Atlantic rainforest can be divided into three latitudinal regions with different climate influences, i.e., the northern region from 5 – 15° S, the central region from 15 – 23° S, and the southern region from 23 – 30° S (Ledru et al., 2016). The northern and central regions are generally characterised by moist, cool, semi-deciduous forest, with patches of dense evergreen forests covering the coast of the central region. The southern region is characterised by a cooler and wetter climate favouring the growth of *Araucaria* and mixed evergreen forests (Ledru et al., 2016). Most of the region is subject to high rates of anthropogenic habitat loss, especially in the Cerrado and the Atlantic rainforest where areas often reach more than 50% of estimated anthropogenic habitat loss (Fig. 3.1d; Ellis et al., 2012).

I.1.4. Amazon Basin

The Amazon Basin is centred on north-western Brazil, including large proportions of the northern region (i.e., States of Acre, Rondônia, Amazonas, and Roraima to the northwest, and Amapá and Pará to the northeast) and the north of the central-west region (i.e., north of the State of Mato Grosso). The Amazon Basin also encompasses parts of surrounding countries including southern Suriname, Guyana, Venezuela, and Colombia, eastern Peru, and northern Bolivia (Fig. 3.1). The region is continental and centred around the vast Amazon River Basin bordered by multiple mountain ranges where the river is sourced. The region overlaps the Equator to the north, which is quasi-paralell to the 6,436 km-long Amazon River located in the Southern Hemisphere. The climate is tropical, with high precipitation especially in the lowlands and in the upper (north-western) Amazon Basin, while the north-eastern and southern parts of the region are generally drier (Fig. 3.1c; Zomer et al., 2022). The southern part of the region is subject to seasonal varition in the position of the inter-tropical convergence zone (Asmerom et al., 2020), which reaches its southernmost margin in January and its northernmost in July. Today, the entire region is covered by moist broadleaf forests and is generally characterised by low rates of anthropogenic habitat loss (Fig. 3.1b, d; Olson et al., 2001; Friedl et al., 2010; Ellis et al., 2012; Hansen et al., 2013; Dinerstein et al., 2017), but the southern and eastern margins bordering more savanna-like landscapes have been subject to intense deforestation since the beginning of the 21st Century (Ellis et al., 2012; Hansen et al., 2013; Fig. 3.1b, d).

I.1.5. Tropical Andean

The tropical Andean region covers southern Colombia, Ecuador, and most of Peru, bordering the Pacific coast to the west and overlapping parts of the Amazon Basin to the east (Fig. 3.1). The Andean cordillera stretches along the Pacific coast, including several parallel and/or successive mountain ranges such as the northern central Cordillera in Colombia and Ecuador, the easten side of the central Andes in Ecuador and Peru, the Tumbesian Mountains in Peru, and the western and central Cordillera of Peru. The region is subject to several distinct climates notably responsible for a large range of aridity indices (Fig. 3.1c; Beck et al., 2018; Zomer et al., 2022). While the east and north of the Andes are humid, the South Pacific coast is arid, especially the Sechura region. The climate on the Pacific coast is strongly influenced by the Humboldt current (or Peruvian current), a cold marine current originating in Antartica that is subject to El Niño-Southern Oscillation (ENSO). During the El Niño phase, sea surface temperature is warmer and rainfall higher in Peru. During La Niña, which lasts a least five months, sea surface temperature cools, the climate aridifies in the Sechura region in Peru, but rainfall increase in the central Andes. Today, moist forests cover most of the region, including the Amazon Basin and eastern slopes of the Andes, as well as the western slopes of the northern central cordillera in Colombia and Ecuador. Thin strips of open landscapes such as grasslands and shrublands dominate the highest elevations in the Andean cordillera (e.g., pàramo grasslands), while the Sechura Desert stretches along the Pacific coast of Peru (Olson et al., 2001; Hansen et al., 2013; Dinerstein et al., 2017; McMichael et al., 2021). In the Sechura desert, scant vegetation is mainly maintained by fog (sea mist), especially in El Niño years due to high sea surface temperatures. Areas of high anthropogenic habitat loss are mainly located in the Andes and on the Pacific coast, whereas the eastern Andean flank and the Western Amazon rainforest remain better preserved (Fig. 3.1d; Ellis et al., 2012; Ellis, 2021).

I.1.6. Caribbean

The Caribbean Sea region encompasses areas with Caribbean coastlines and surroundings, including the Central American countries of Guatemala, Belize, Honduras, El Salvador, Nicaragua, Costa Rica, and Panama, as well as the Yucatan Peninsula (Mexico) and Florida (USA) (Fig. 3.1). The region also includes the northern fringe of South America, including large parts of Colombia, Venezuela, Guyana, Surinam, and French Guyana. Finally, the region includes the West Indies, which is divided into three main Archipelagos: the Greater Antilles, the Lesser Antilles, and the Lucayan Archipelago. The region mainly represents terrestrial areas arranged arround the Carribbean Sea subject to strong coastal influences. Central America is crossed from north to south by the extension of the American cordillera, among which the main mountain ranges include the Sierra Madre de Chiapas crossing southern Mexico, Guatemala, El Salvador, and Honduras, the Cordillera Central and Cordillera de Talamanca crossing Costa Rica, and the Serrania de Tabasara and the Cordillera de San Blas crossing western and Eastern Panama, respectively. On the northern fringe of South America, the American cordillera extends into the western side of Colombia and is divided there into three parallel mountain ranges: the Cordillera Occidental, Central and Oriental. To the east of the Cordillera Oriental lies the vast plains of the Llanos, bordered to the north by the Sierra Merida and the Venezuelan Coastal Range (Cordillera del Norte), and to the east by the Guiana Shield of which the Guiana Highlands to the west are the highest elevations (maximum elevation = 2,995 m at Pico da Neblina). The climate is tropical, meaning constantly high temperatures generally associated with an annual wet and a dry season due to the seasonal migrations of the inter-tropical convergence zone. Today, moist, dry, and pine-oak forests cover most of the region, but tree cover is generally lower at higher elevations (Fig. 3.1b; Olson et al., 2001; Hansen et al., 2013; Dinerstein et al., 2017). The Llanos plains are also mainly devoid of trees and large parts are frequently subject to flooding, especially during the La Niña phase of the El Niño-Southern Oscillation (ENSO) when there are heavy rainfalls in the central Andes. Like the Cerrado (North-eastern South America region) and the Pampas (Central South America region), the Llanos is listed among the fire-dependent/influenced regions (Hasdesy et al., 2005). Dry forests in Colombia and Venezuela have been subject to forest loss and degradation in the past century mainly from inappropriate forest exploitation, fires, and agriculture (Aymard, 2015; Banda-Rodriguez, 2017). Several dry ecosystems stretch along the Caribbean coast of South America, such as the Guajira-Barranquilla xeric scrub and the La Costa xeric shrublands in Venezuela (Dinerstein et al., 2017). High rates of anthropogenic habitat loss are mainly located in the Llanos and Caribbean islands (Fig. 3.1d; Ellis et al., 2012)

I.1.7. Mexican Region

The southern region of North America encompasses Mexico and southern Texas (USA) (Fig. 3.1). The Mexican region is characterised by a strong coastal influence and a succession of mountain ranges with a particularly dry climate (Fig. 3.1c). The region is bordered by the Pacific ocean to the west and the Gulf of Mexico to the east. Mexico is crossed north to south by two main mountain ranges, the Sierra Madre Orientale and Occidental, and in the south by the trans-Mexican volcanic belt bordering in their centre the Mexican Altiplano averaging 1,100 m in elevation. The southern Pacific coast of Mexico is bordered by the Sierra Madre del Sur mountain range. The modern climate mainly varies with seasonal movements of the inter-tropical convergence zone, with winter characterised by high pressures causing dry conditions (Metcalfe, 2006). Today, most forests of the region cover the slopes of the mountain ranges, with largest forests in the occidental region (Hansen et al., 2013). Pine-oak and dry forests represent the two main altitudinal vegetation stages on mountain slopes. In the southeast, a strip of wet forest stretches along the coast of the Gulf of Mexico (Olson et al., 2001; Dinerstein et al., 2017). Inland, higher-elevation areas such as the Mexican Altiplano host more open landscapes, including three large xeric to desertic areas: the north Sonoran, the Chihuahuan, and Baja California. These open landscapes are characterised by typical and distinct floras including cacti, agaves, and yuccas (Metcalfe, 2006). Anthropogenic habitat loss is estimated to reach high rates in most of the region (Fig. 3.1d; Ellis et al., 2012; Ellis, 2021).

II. SYNTHESIS OF THE MAIN VEGETATION CHANGES AND DATA LIMITATION

I synthesised below the main trends of tree-cover changes in each region. Each region is divided into several subregions (Fig. 3.2). Palaeo-environment records are strongly influenced by local rather than regional environments. Grouping records into subregions leads to a better appreciation of larger-scale vegetation change trends. The diversity of deposit contexts and palaeo-vegetation proxies among records is described in Fig. 3.3b and 3c respectively. For each subregion, I summarised the main trend in tree cover changes at large scale using schematic timelines where tree cover is classified into four categories: closed forests, semi-open and mosaic landscapes, open landscapes with sparse trees, and generally treeless landscapes (Fig. 3.4 – 3.11).

To reconstruct the changes in vegetation at regional scale, I mainly used the chronologies provided by original palynological studies and re-estimated their age models using the most recent calibration curve (SHcal20; Hogg et al., 2020) where possible. Sediment cores, which are instrumental to reconstruct past environments, are generally dated using radiocarbon techniques. The sediment is dated at several depths in the core, and the age estimates are then calibrated and used to construct an age-depth model. This approach allows for extrapolating the dates across the entire core while accounting for variation in sedimentation rates. However, given that the calibration curves for age estimates are regularly updated (e.g., Hogg et al., 2020), an age model can become outdated. While the ideal approach would be to reconstruct age models from 'raw' (uncalibrated) ages, such data are not always available in the published

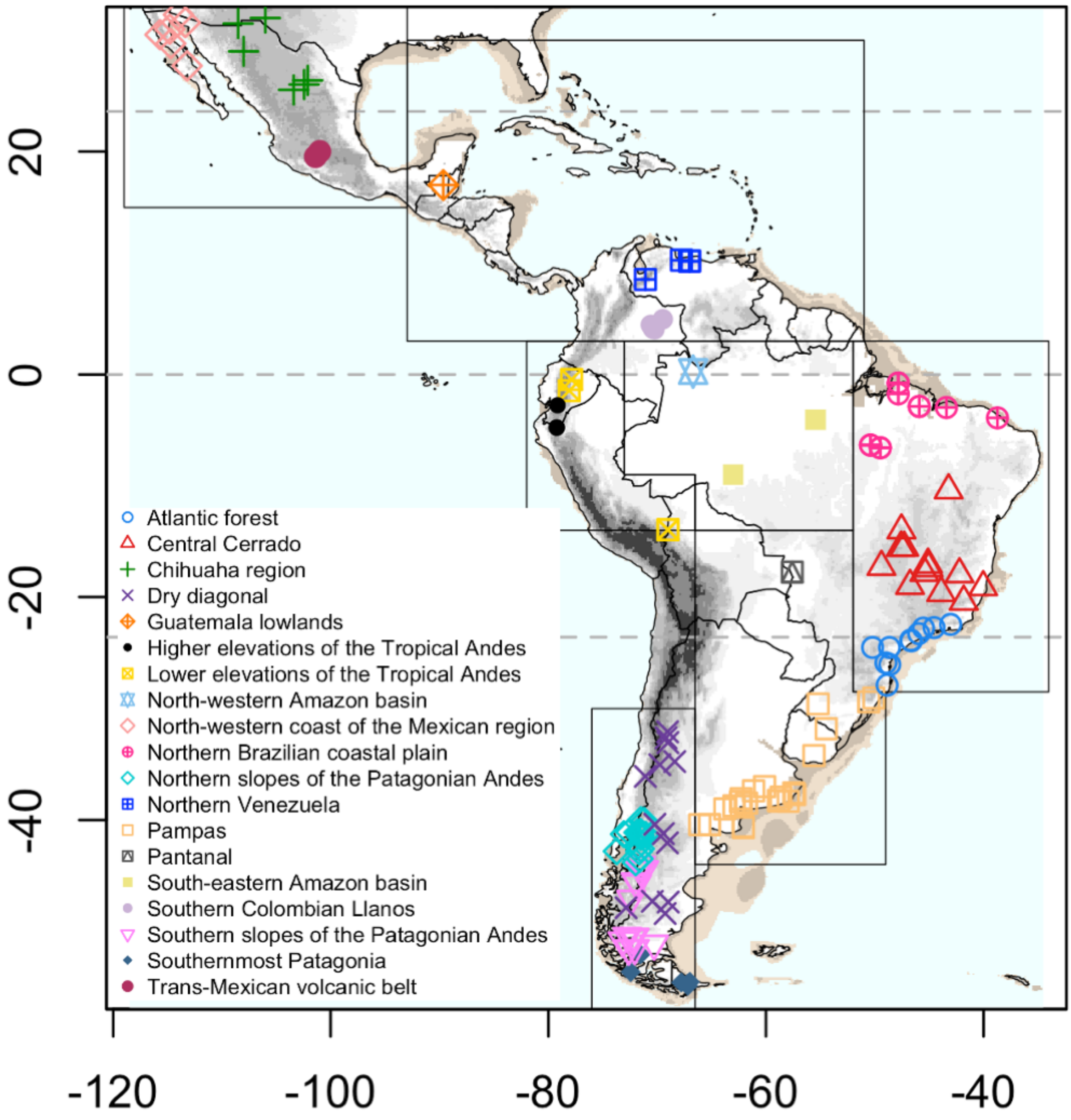

Figure 3.2. Distribution of the palaeo-environment records reviewed in this study classified by subregions. *Selected regions for this study are outlined in black. (i) Patagonia, (ii) Central South America, (iii) North-eastern South America, (iv) Amazon Basin, (v) Tropical Andean, (vi) Caribbean, (vii) Mexican.*

literature. Over the timeframe of this study, the discrepancies between the calibration curves SHcal13 and SHcal20 is typically < 100 years, although it can extend to a few centuries during certain periods (i.e., 12,300–12,500 and 15,100–15,300 radiocarbon years BP; Hogg et al., 2020). Considering that my study focuses on broad, long-term trends in vegetation cover, I assumed that using outdated calibrations would have a

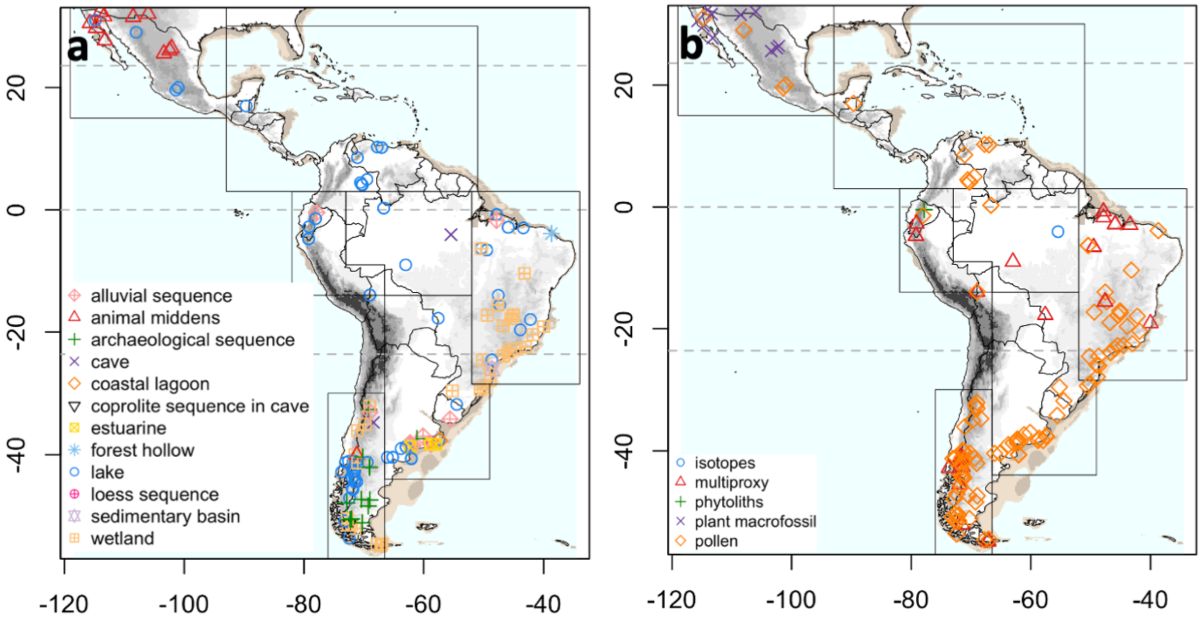

Figure 3.3. Distribution and characteristics of the palaeo-environment records reviewed in this study. *Sites are classified by (a) palaeo-environment proxy, (b) deposit context. Selected regions for this study are outlined in black. (i) Patagonia, (ii) Central South America, (iii) North-eastern South America, (iv) Amazon Basin, (v) Tropical Andean, (vi) Caribbean, (vii) Mexican.*

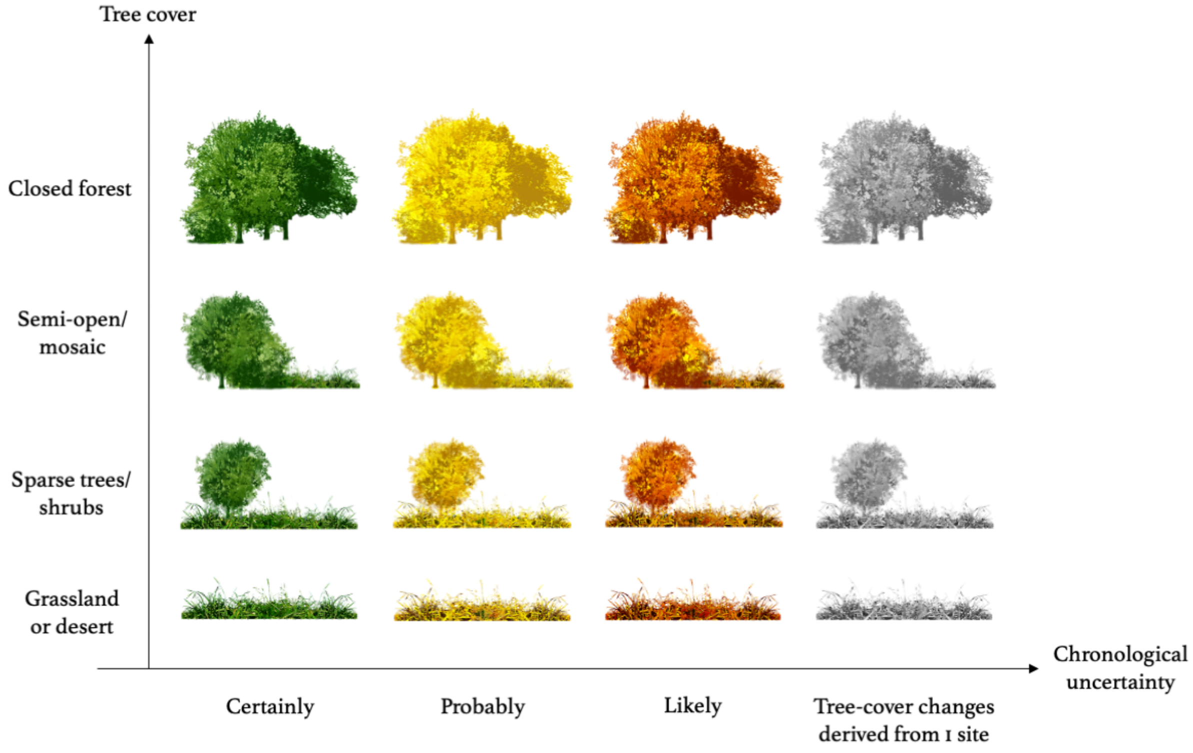

Figure 3.4. Graphic chart used in figures 5 to 11 to represent tree cover changes at subregional scale.

Patagonia

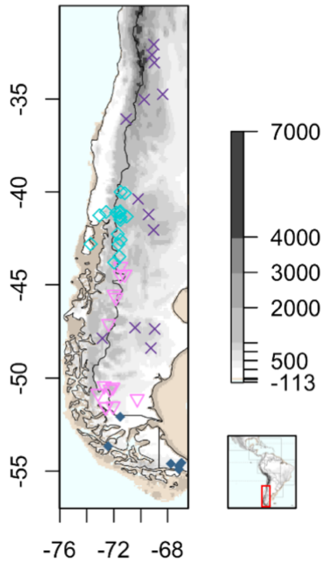

In a nutshell:

- High record density especially on the slopes of the Andes
- Numerous radiocarbon dates, tree-cover changes well chronologically constrained
- North to South gradual expansion of *Nothofagus* forests in the Andes from the Last Glacial Maximum to ~7,000 years BP
- *Nothofagus* forest refugium ~40-43 ° S during the Last Glacial Maximum
- Dry diagonal continuously open

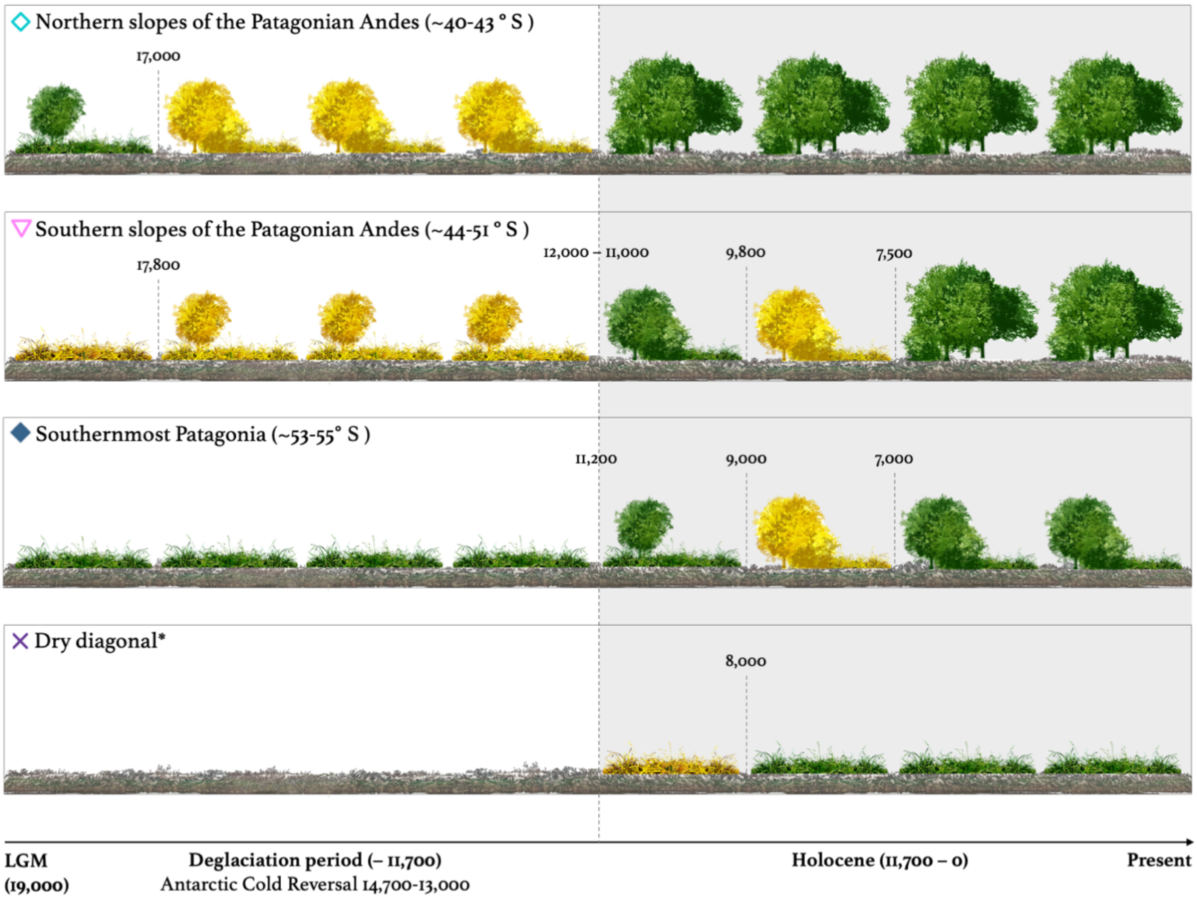

---

* no palaeovegetation records before the early Holocene

Figure 3.5. Summary of the tree-cover changes in Patagonia.

Central South America

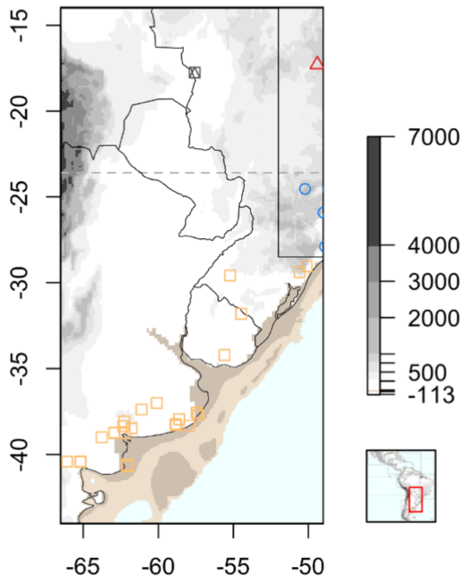

In a nutshell:

- High record density in the Pampas
- Pampas continuously covered with open landscapes with sparse trees
- The presence of megaherbivores adapted to live in open and semi-open environments in the Pampas in the late Pleistocene support the idea that the landscape may have hosted large areas of low tree cover during the deglaciation period

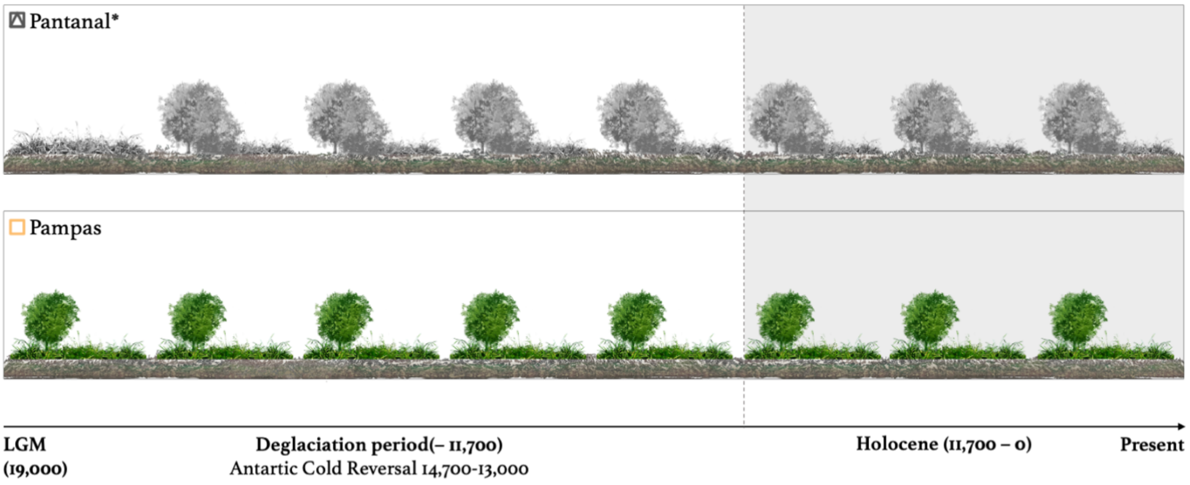

---

* based on a single site: Laguna La Gaiba (Whitney et al., 2011)

Figure 3.6. Summary of the tree-cover changes in Central South America.

North-eastern South America

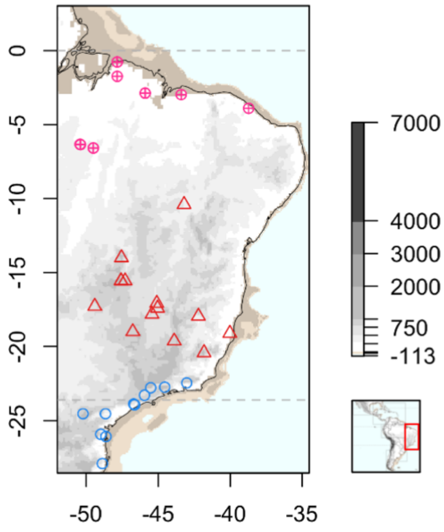

In a nutshell:

- High record density in the Atlantic forest and the Central Cerrado, low record density from 5 to 15 ° S
- Tree-cover changes are poorly geochronologically constrained in the Northern Brazilian coastal plains
- Generally sparse tree cover during the deglaciation period
- Tree cover increased during the Holocene to reach its modern state

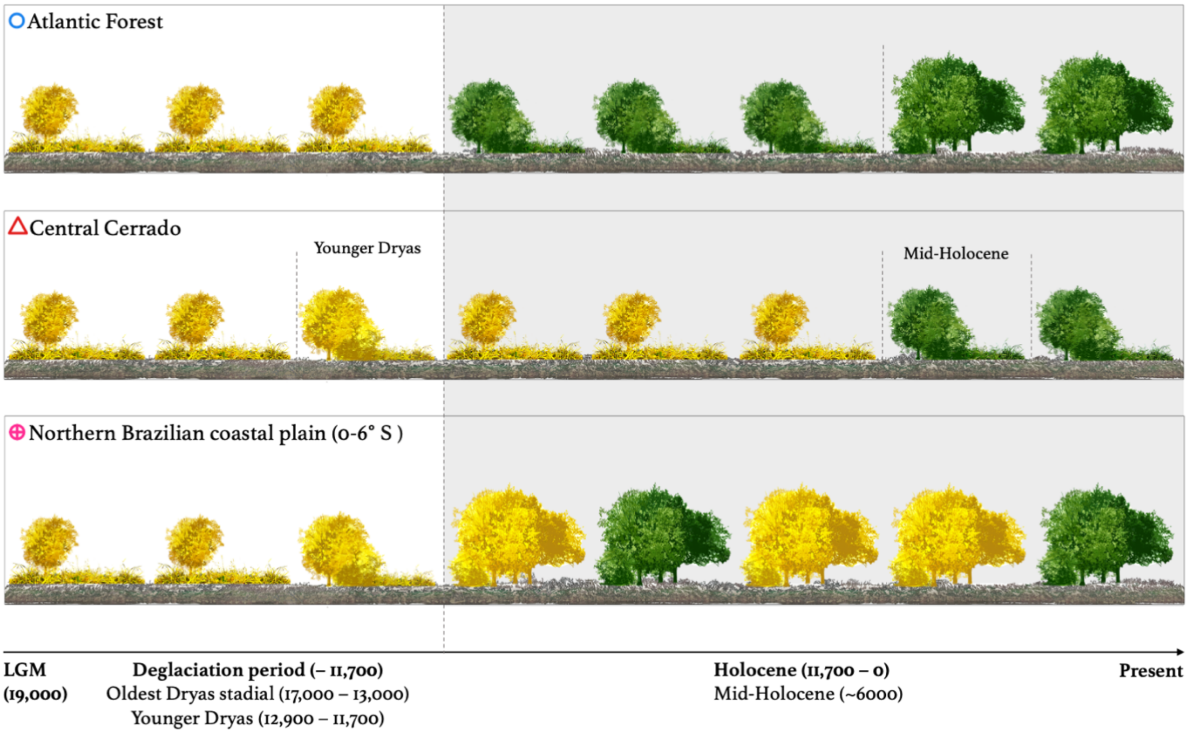

Figure 3.7. Summary of the tree-cover changes in North-eastern South America.

Amazon Basin

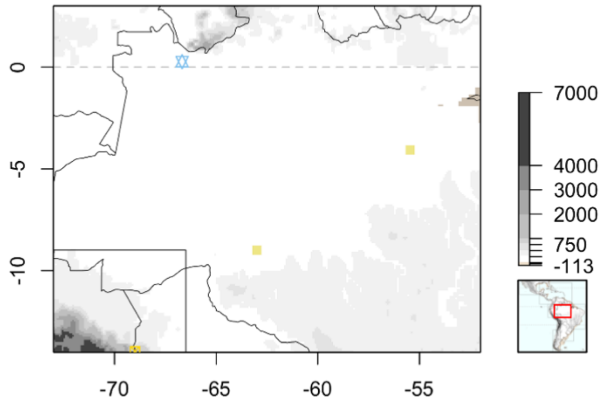

In a nutshell:

- Low record density
- No consensus on post-glacial tree-cover changes
- Closed forests dominate records, but were possibly replaced by grass-dominated vegetation in the South-eastern Amazon Basin until 15,500 years BP

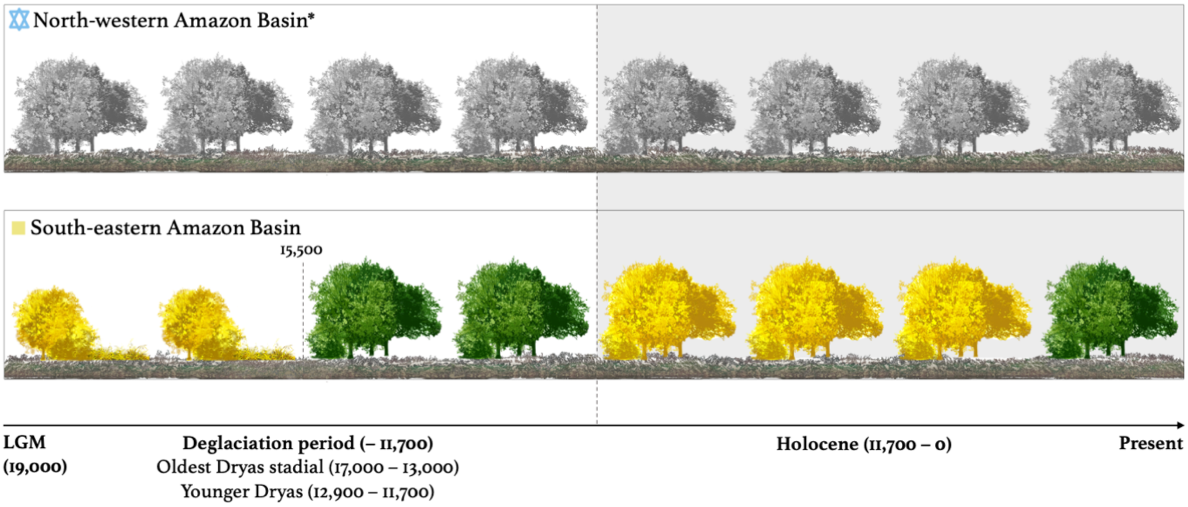

---

* based on a single site: Hill of Six Lakes (Colinvaux et al., 1996; Bush et al., 2004)

Figure 3.8. Summary of the tree-cover changes in the Amazon Basin.

Tropical Andes

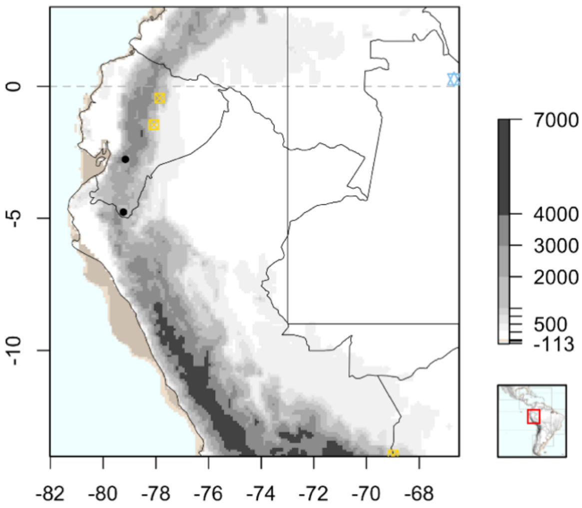

In a nutshell:

- Most records have been well chronologically constrained with radiometric dates
- Lower and mid-elevations(<2000 m) continuously covered with montane forests
- Gradual expansion of montane forests to higher elevations (>3500 m) during the Holocene

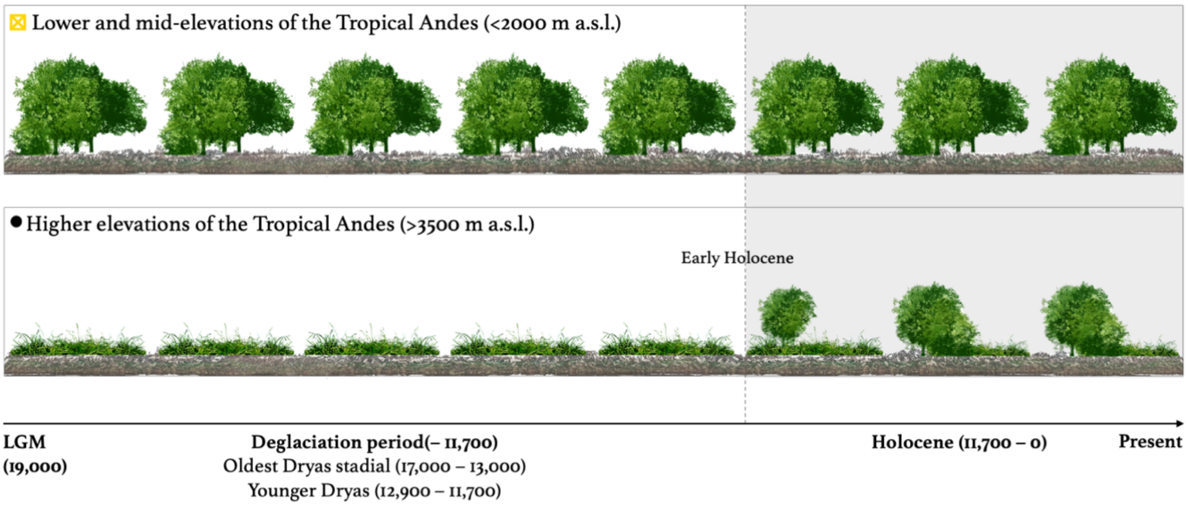

Figure 3.9. Summary of the tree-cover changes in the Tropical Andes.

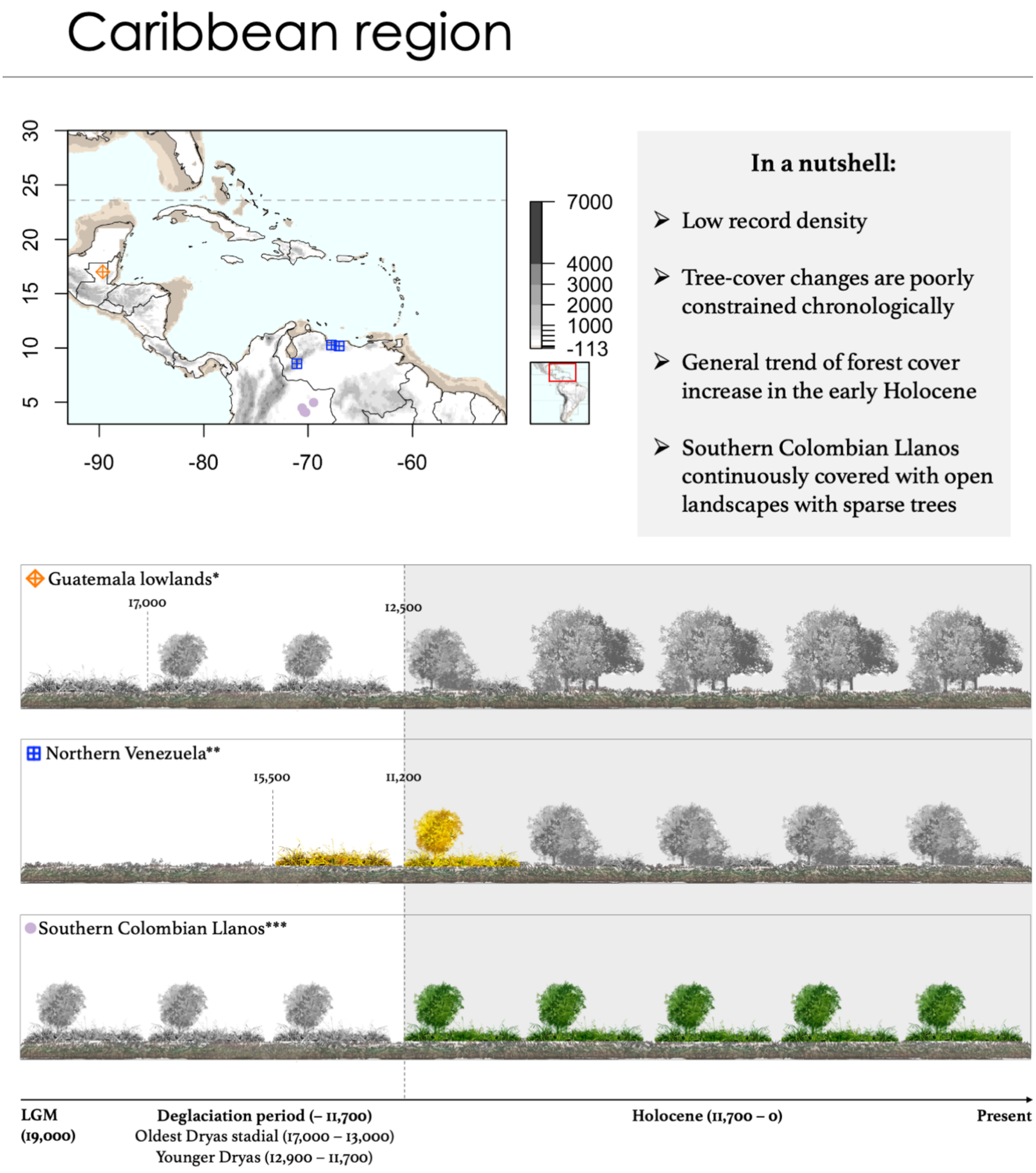

Caribbean region

In a nutshell:

- Low record density
- Tree-cover changes are poorly constrained chronologically
- General trend of forest cover increase in the early Holocene
- Southern Colombian Llanos continuously covered with open landscapes with sparse trees

---

* based on a single site: Lake Quexil (Leyden et al., 1993)

** no palaeovegetation records before ~15,500 cal BP; based on a single site for the Holocene: Lake Valencia (Leyden, 1985)

*** based on a single site for the deglaciation period: Laguna El Pinal (Behling and Hooghiemstra, 1999)

Figure 3.10. Summary of the tree-cover changes in the Caribbean region.

Mexican region

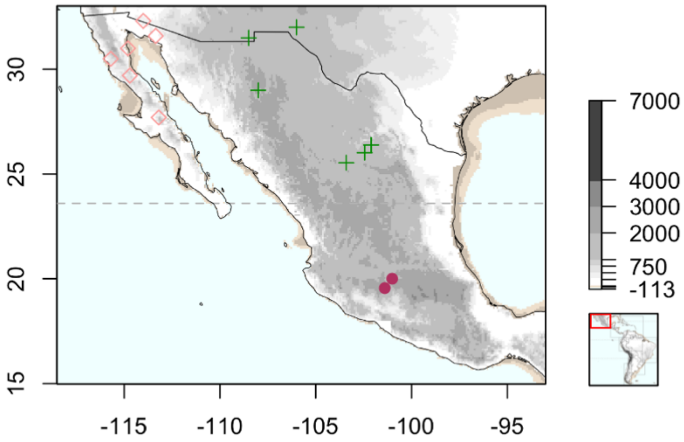

In a nutshell:

- High record density but tree-cover changes often derived from plant macrofossils that better represent local rather than regional trends
- Tree-cover changes are poorly constrained chronologically
- Higher tree cover displaced from North to South during the late Pleistocene-Holocene transition

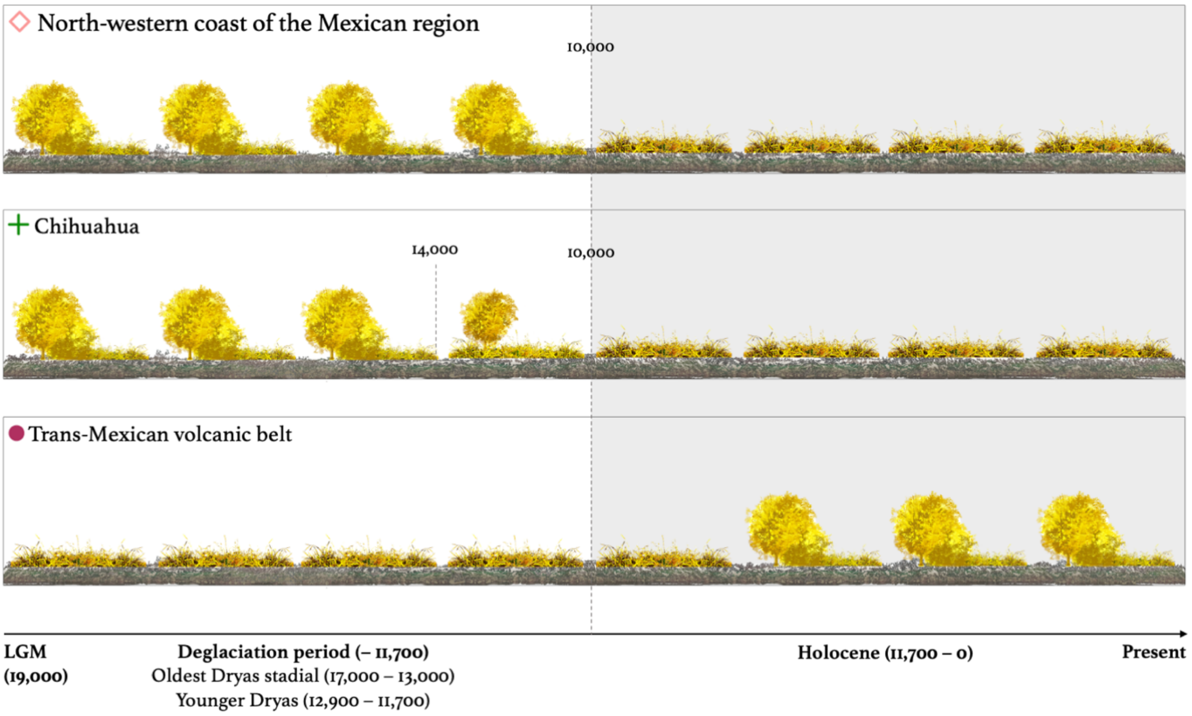

Figure 3.11. Summary of the tree-cover changes in the Mexican region.

minimal impact on the results of the regional syntheses. When uncalibrated radiocarbon age estimates were available, I applied the Southern Hemisphere SHcal20 calibration curve (Hogg et al., 2020) at 1 sigma (68.2% probability), using the OxCal 4.4 software (Bronk Ramsey, 2021). If uncalibrated ages were not provided, I used the calibrated ages from their original study, even though they might have been derived from an older calibration curve such as SHcal13. I represented the chronological uncertainty graphically using a four-colour scheme (Fig. 3.4 – 3.11): (1) where the timing of change in forest cover was well-constrained by radiocarbon dates (i.e., stability of tree-cover category between two dates on all sites, even if categories differ among sites), I represented the vegetation in green ('certainly'); (2) when the date of a change was less well-constrained (i.e., instability of tree-cover category between two dates on all sites, and/or the timing of change differs among sites), I represented the vegetation in yellow ('probable'); (3) when the dating was not based on radiocarbon age estimates, I deferred to the interpretation of the original studies, representing the vegetation in red ('likely'); and (4) when tree-cover changes were derived from a single site, I represented the vegetation in grey.

II.1. Patagonia

The Patagonian region displays a rich set of 50 palaeo-environment records including a large majority of pollen records deposited in various environments (e.g., lakes, wetlands, archaeological sequences) generally occurring in the most humid areas, especially on the eastern and western slopes of the Andes (Fig. 3.1c, 3.2, 3.3, 3.5; see also the *Latin America Pollen Database*; Flantua et al., 2015). The high density of sites and the numerous radiocarbon dates make it possible to describe forest cover changes with low level of uncertainties. Most uncertainties are related to the slight differences among spatially close sites, suggesting spatial heterogeneity due the environment variability among sites.

During the Last Glacial Maximum, large portions of the Patagonian Andes were covered by ice sheets (Patagonian ice sheet) (Davies et al., 2020), but rapid deglaciation started ~18,000 BP, and by 15,000 BP the Patagonian ice Sheet probably separated into several distinct ice masses, creating several large palaeolakes. On the slopes of the

Andes, post-Last Glacial Maximum vegetation changes (~ 19,000 years ago to the present) are characterised by the gradual expansion of *Nothofagus* forests from north to south at a regional scale. Pollen records suggest that some areas in the northern slopes of the Patagonian Andes (40 – 43° S) might have been continuously covered with relatively dense *Nothofagus* forest patches (e.g., Lago Pichilaguna; Moreno et al., 2018), thus representing local refugia during the Last Glacial Maximum. At local scales, discrepancies in the timing of *Nothofagus* arrival among sites and the early occurrence of long-distance, single-grain *Nothofagus* forests suggest that they first established as small patches in a mosaic environment before landscapes gradually became closed forest.

Most pollen records from the northern slopes of the Patagonian Andes (40 – 43° S; Fig. 3.5) have at least sparse *Nothofagus* grains (Iglesias et al., 2014; Pesce and Moreno, 2014), or sometimes continuously high percentages of *Nothofagus* pollen (Moreno et al., 2018). These indicate that some *Nothofagus* populations could have persisted throughout the Last Glacial Maximum in the area. In contrast, other records from the same latitudes on the eastern slopes of the Andes suggest that some areas were instead covered with treeless vegetation during the Last Glacial Maximum (Iglesias et al., 2016). *Nothofagus* expansion and forest establishment occurred asynchronously among sites from the northern slopes of the Patagonian Andes during the late glacial, e.g., as early as 17,000 calibrated years before present (cal. BP, representing the number of years before 1950 obtained after calibrating radiocarbon age estimates) in Lago Lepué (Pesce and Moreno, 2014) and as late as 11,500 cal. BP in Lago Los Niños and Laguna La Pava (Iglesias et al., 2016). This suggests the gradual proliferation and expansion of *Nothofagus* forest patches into a mosaic landscape probably following the high variability among local environments.

On the southern slopes of the Andes (44 – 51° S; Fig. 3.5), palaeo-environment records indicate that the area was covered with open vegetation and some woody taxa, where large, grazing megafauna roamed after retreat of the glaciers. The first *Nothofagus* populations and other woody taxa gradually expanded throughout the deglaciation period, with dense *Nothofagus* forests generally establishing in the early Holocene between 11,800 – 7,500 cal. BP (e.g., Moore, 1978; Heusser et al., 1994; Markgraf et al., 2007; Moreno et al., 2009; Villa-Martínez et al., 2012; Nanavati et al., 2019; McCulloch et al., 2021).

In southernmost Patagonia (Tierra del Fuego; 53 – 55° S; Fig. 3.5), palaeo-environment records suggest that *Nothofagus* populations expanded in the region as late as the early Holocene and that dense forests then established prior to 9,000 cal. BP, rapidly replacing late-glacial treeless landscapes (Markgraf and Huber, 2010; Fontana and Bennett, 2012; Musotto et al., 2017). Pollen records suggest that some *Nothofagus* have been present in the region since the Last Glacial Maximum (Markgraf and Huber, 2010).

In the dry diagonal (Fig. 3.5), pollen records covering only the Holocene indicate that the landscapes of the Patagonian Plateau at ~ 40° S and the northern Santa Cruz region might have remained open or semi-open, alternating between humid grasslands and dry shrub-steppes depending on moisture availability (Mancini,1998; Mancini et al., 2005).

II.2. Central South America

The 26 palaeo-environment records from the Central South America region are exclusively pollen records deposited in a variety of environments including lakes, alluvial and archaeological sequences, estuary, and animal middens (Fig. 3.2, 3.3, 3.6). Records are mainly distributed at the edges of the region, typically in areas that are currently more humid such as in the Pampas and the Pantanal, while there are no records in the Chaco area (Flantua et al., 2015). A single record has been analysed from the Pantanal in the North of the region (Laguna La Gaiba; Whitney et al., 2011). Palaeo-environment records including pollen and faunal records suggest that the Pampas remained approximately stable from the Last Glacial Maximum to today in terms of vegetation structure (Fig. 3.6). Areas located to the south along the Atlantic coast such as southern Brazil, Uruguay, and the Argentine Pampas might have generally been covered by open, grass-dominated vegetation (Prieto, 2000; Mourelle et al., 2017). In Argentina, changes in floristic composition in the pollen records suggest the north-eastern displacement of the arid-semiarid region during the Holocene (Mancini et al., 2005). The only record from the Pantanal in the north-west of the region indicates that tropical forests expanded during the deglacial period and were replaced by seasonally dry tropical forests (i.e., forests generally characterised by a higher proportion of deciduous taxa) during the Late Pleistocene-Holocene transition (Fig. 3.6; Whitney et al., 2011).

II.3. North-eastern South America

North-eastern South America is represented by 36 palaeo-vegetation records consisting mostly of pollen records deposited in a variety of environment including mostly lakes and wetlands together with an alluvial sequence and a forest hollow (Fig. 3.2, 3.3, 3.7). I derived the list of records from Ledru et al. (2016). Pollen records are especially rare in the centre of the region, with most records located in the north and the south, but records are lacking especially between 5° and 15° S (Flantua et al., 2015; Ledru et al., 2016). Records from the Northern Brazilian coastal plain remain poorly dated, thus making it difficult to describe when forest was replaced by more open vegetation.

Palaeo-environmental records suggest relatively open vegetation during the deglaciation period. Then, tree cover generally increased during the Holocene to reach its modern state. Part of the Atlantic forest landscape may have remained relatively stable through time (Ledru et al., 2016; Francisquini et al., 2020). In contrast, generally open vegetation in the Cerrado might have been temporarily replaced by forests during the Younger Dryas and mid-Holocene, possibly linking the Amazon and Atlantic rainforests (Ledru et al., 2016; Cassino et al., 2020). Vegetation from the Northern Brazilian coastal plain was possibly unstable during the Late Pleistocene (Absy et al.,1991; Sifeddine et al., 2001).

II.4. Amazon Basin

The Amazon Basin region is poorly represented in the palaeo-vegetation record, this review including four deposits distributed across three sites located in lowland areas (Fig. 3.2, 3.3, 3.8). Previous studies have analysed pollen records deposited in two lakes including Lake Pata (Colinvaux et al., 1996; Bush et al., 2004; D'Apolito et al., 2013), and Katira (van der Hammen and Absy, 1994), and the isotope composition of speleothems from Paraíso Cave ($\delta^{18}O$; Wang et al., 2017), and of the sediments from Katira ($\delta^{13}C$; van der Hammen and Absy, 1994). This scarcity of palaeo-environment records in the region is mainly due to both low potential for fossil preservation and the current inaccessibility of the Amazonian rainforest. Specifically, Bush et al. (2011) pointed out the scarcity of lakes containing continuous sedimentary sequences, with only a few covering the Last Glacial Maximum. Records are poorly chronologically constrained and changes in tree cover differ among deposits. The Holocene period has been less studied.

Palaeo-environment records are generally located along the Amazon River and on the edges of the Amazon rainforest (Flantua et al., 2015). There is currently no consensus on post-Last Glacial Maximum vegetation changes among Amazon Basin sites, suggesting widespread spatial disparities (van der Hammen and Absy, 1994; Bush et al., 2011). Most debates focus on the possible replacement of parts of the rainforest by more open, grass-dominated vegetation such as tropical savannas during the Last Glacial Maximum. A single site, Hill of Six Lakes, shows that north-western part of the Basin might have hosted large areas of stable forest, with some changes in forest structure and floristic composition (Colinvaux et al., 1996; Bush et al., 2004). In contrast, vast landscapes in the east and the south might have been more unstable (van der Hammen and Absy, 1994; Colinvaux et al., 1996; Bush et al., 2004, 2011; D'Apolito et al., 2013; Wang et al., 2017). Landscapes could then have re-transitioned to forests by 15,500 cal. BP. Such changes are mainly attributed to variation in the position, width, and intensity of the area subject to monsoons.

II.5. Tropical Andean region

The Tropical Andes are represented here by 7 deposits mainly located on the slopes of the Andes at diverse elevations and latitudes especially on the Eastern Andean Flank (Fig. 3.2, 3.3, 3.9, see also the *Latin America Pollen Database*; Flantua et al., 2015). Most palaeo-environment records were deposited in lakes and include pollen records, except for Campo Libre (McMichael et al., 2021) where phytoliths have been analysed in an alluvial sequence. Most records have been chronologically constrained with several radiometric dates (e.g., Hansen et al., 2003; McMichael et al., 2021). Pollen and phytoliths indicate the gradual expansion of montane forests to higher elevations, with lower-elevation landscapes (< 2000 m above sea level) including eastern Andean flank sites remaining covered with relatively stable montane forests (Urrego et al., 2010; Montoya et al., 2018). Forests developed up to high elevations (> 4000 m in Ecuador) mainly during the Holocene (Hansen et al., 2003).

II.6. Caribbean region

The palaeo-environmental record from the Caribbean region includes 9 lake deposits that are all hosting pollen records (Fig. 3.2, 3.3, 3.10). Except for Lake Quexil (Leyden et al., 1993), which is located in the Guatemala Lowlands, the other records are all distributed along the inner or outer edge of the Llanos, i.e., in the Southern Colombian Llanos and in Northern Venezuela. However, there are no records in the heart of the Llanos. Most records are poorly constrained chronologically. Caribbean records thus generally provide insights on the successions of vegetation changes, but with limited dating precision. The documentation of vegetation changes *post*-Last Glacial Maximum is sparse, predominantly sourced from disparate and isolated sites (Fig. 3.10). Palaeo-environmental studies show that the region was generally dominated by open landscapes during the post-Last Glacial Maximum Late Pleistocene, including during Heinrich Stadial 1 (Leyden et al., 1993; Behling and Hooghiemstra, 1999). Forests started to develop at least locally during this period, probably interrupted by the Younger Dryas (12,900 – 11,700 BP) (Leyden, 1985; Leyden et al., 1993; Salgado-Labouriau, 1997; Rull et al., 2015). Holocene records generally suggest the establishment of modern vegetation in the early Holocene characterised by higher forest cover (Leyden, 1985; Leyden et al., 1993; Salgado-Labouriau, 1997; Behling and Hooghiemstra, 1999). However, while changes in tree cover were of high amplitude in Guatemala, records from the Llanos only suggest a slight increase of tree cover near river courses that did not change vegetation structure at larger scale, the regional vegetation probably remaining covered with sparse trees (Behling and Hooghiemstra, 1999).

II.7. Mexican region

The Mexican region is represented by 14 deposits in animal middens and lakes hosting plant macrofossil and pollen records, but records are poorly dated (Fig. 3.2, 3.3, 3.11). Late Pleistocene records suggest a vegetation characterised by higher densities of woody plants in the Chihuahua and along the northwest coast in Sonoran and Baja California, and a more open vegetation to the south in the trans-Mexican volcanic belt compared to the present (Metcalfe, 2006). Open vegetation might have then expanded northward in the early Holocene, while forests expanded in the trans-Mexican volcanic belt (Metcalfe, 2006).

III. MAJOR DEGLACIATION VEGETATION CHANGES (19,000 – 11,700 BP)

III.1. Patagonia

III.1.1. Northern slopes of the Patagonian Andes (40–43°S)

During the deglaciation period, vegetation gradually transitioned from grass-dominated to forest-dominated in records with varying chronologies among records. In Lago Pichilaguna, pollen records indicate the continuous presence of *Nothofagus* forests from the Last Glacial Maximum to the present, despite some changes in floristic composition over that period (Moreno et al., 2018). In Lago Lepué, closed *Nothofagus* forests were established by 17,000 cal. BP and were then continuously present (Pesce and Moreno, 2014). A review of 11 pollen records concluded that a grass-dominated landscape with some *Nothofagus* trees persisted until 15,000 cal. BP (Iglesias et al., 2014). Among the latter 11 records, *Nothofagus* forests then began to expand from ~ 16,500 cal. BP in Lago Mascardi and from ~ 15,000 cal. BP in most of the other sites (Iglesias et al., 2014).

III.1.2. Southern slopes of the Patagonian Andes (44–51°S)

At higher latitudes, on the Southern slopes of the Patagonian Andes, trees tend to establish gradually in most records during the deglaciation period, but their density remain relatively low until the Holocene. In the North of the subregion (44–46°*S*), at Lago Los Niños and Laguna La Pava, pollen records indicate the arrival of trees ~ 14,200 cal. BP, landscapes remaining relatively open prior the Holocene (Iglesias et al., 2016). Pollen records from Mallín Fontanito suggest that the post-Last Glacial Maximum landscape was covered with heath-steppe and sparse *Nothofagus* patches from 17,800 to 13,000 cal. BP. *Nothofagus* forests then began to expand from 13,000 cal. BP (Nanavati et al., 2019). Pollen records from Lake Shaman on the eastern slopes of the Andes suggest that the area was covered with grass steppe, with a high proportion of shrub cover from 19,000 – 14,800 cal. BP (de Porras et al., 2012). Shrubs were then gradually replaced by *Nothofagus* trees to become a forest-steppe ecotone as in the modern landscape. The Holocene vegetation was also highly variable and fire activity increased. At Mallín Pollux, the area was covered with sparse scrub–steppe until 14,000 cal. BP, then plant diversity in the steppe increased from 14,000 cal. BP (Markgraf et al., 2007).

More in the South of the subregion (46–51°*S*), pollen, spore, and charcoal records from Lago Augusta show that the valley was an open landscape covered with herbs, shrubs, and evergreen rainforests taxa ~ 15,600 – 16,000 cal. BP (Villa-Martínez et al., 2012). At Cerro Benítez, pollen and spore records indicate the gradual expansion of *Nothofagus* forests into grass-dominated landscapes after the retraction of the Patagonian ice sheet (McCulloch et al., 2021). Open landscapes expanded after glacier retreat, favoured by large, grazing animals such as *Mylodon darwini*, *Lama gracilis* and *Hippidion saldiasi* that could have arrived in the region as early as ~ 18,000 cal. BP, possibly attracted by open grasslands and freshwater lakes (McCulloch et al., 2021). *Nothofagus* expansion occurred from 14,900 cal. BP, and forest cover increased rapidly by ~ 12,000 cal. BP. In southern Patagonia, pollen records from Lago Guanaco suggest that the area was an open landscape dominated by pre-Andean herbs and shrubs from 12,500 to 11,400 cal. BP. The expansion of *Nothofagus* trees could have begun by ~ 12,300 cal. BP (Moreno et al., 2009). At Cueva del Mylodon, palynological analyses of *Mylodon* dung samples (coprolites) and macrofossils of plants (leaves) suggest that the area was covered with open, treeless vegetation (e.g., grasslands) during the late glacial period, despite the single-grain occurrence of *Nothofagus* possibly indicating long-distance wind transport from some rare *Nothofagus* individuals growing in the region

(Moore, 1978; Heusser et al., 1994). The area remained covered with open landscapes hosting sparse *Nothofagus* trees until the Holocene.

III.1.3. Southernmost Patagonia (52–55°S)

In Southernmost Patagonia, palaeo-vegetation records indicate the persistence of open landscapes until the Holocene, with sporadic records of *Nothofagus* suggesting the persitence of some population at regional scale since the Last Glacial Maximum. Pollen records from La Correntina, Terra Australis and Lake Ballena suggest that the area was a treeless landscape during the deglaciation period (Fontana and Bennett, 2012; Musotto et al., 2017). Well-dated pollen, charcoal, and plant macrofossils records from three peat bogs in Tierra del Fuego and southern Patagonia reveal post-Last Glacial Maximum palaeo-environment changes: Harberton, Río Rubens, and Paso Garibaldi (Markgraf and Huber, 2010). There, pollen records indicate that the area was continuously covered with grass-dominated open landscapes during the deglaciation period. The continuous presence of typical *Nothofagus* elements in the pollen records suggest that some *Nothofagus* trees have occurred in the region since the Last Glacial Maximum.

III.2. Central South America

In Central South America, all but one of the records (Pantanal) are located in the extended Pampas subregion. Records from the extended Pampas reflect an open landscape with sparse trees during the deglaciation period. In the Campos region (southern Brazil and Uruguay), pollen records from Laguna Formosa (here included in the Pampas *lato sensu*) suggest that the area was a mosaic landscape dominated by herbaceous vegetation with some hydrophilous woody taxa mainly distributed along freshwater bodies in the Late Pleistocene and late Holocene (de Oliveira Medeiros, 2011; Mourelle et al., 2017). In the Argentine Pampas, eight pollen sequences provide evidence of past landscape changes (Prieto, 2000) — the area was continuously covered by open vegetation from the Last Glacial Maximum to today, despite some floristic changes. During the Last Glacial Maximum, landscapes in central and south-western Pampas were dominated by psammophytic and shrub steppe. Changes in floristic composition also suggest frequent disturbance events such as flooding. This confirms the information derived from Late Pleistocene vertebrate assemblages in Uruguay that includes both species generally associated with open landscapes: glyptodonts, *Equus* (*A.*) *neogeus*, and *Macrauchenia* spp., and animals preferring freshwater environments such as capybaras (*Hydrochoerus* spp.) and coypus (*Myocastor* spp.) (Mourelle et al., 2017; Ubilla et al., 2018). However, the presence of *Tapirus* spp. and *Tayassu pecari* in southern Brazil during the Late Pleistocene indicates the persistence of some forest areas (Kerber et al., 2014; Mourelle et al., 2017). In addition, many extinct megafauna fossils have been found in the region, especially in the Pampas where several iconic South American species such as *Lama gracilis*, *Doedicurus clavicaudatus*, *Glossotherium robustum*, *Megatherium Americanum*, *Notiomastodon platensis*, and *Equus neogeus* have been described (Prates and Perez, 2021). The presence of such herbivorous taxa adapted to live in open and semi-open environments in the late Pleistocene suggest that the landscape may have hosted large areas of low tree cover during the deglaciation period.

In the Pantanal, information on palaeo-vegetation comes only from the Laguna La Gaiba site (Whitney et al., 2011), and thus should be considered with caution. Records from Laguna La Gaiba suggest that the area was dominated by herbaceous vegetation during the Last Glacial Maximum, then hosted the expansion of tropical forests and floodplain trees during the deglacial period from 19,500 cal. BP, and the landscape re-opening from the Late Pleistocene-early Holocene transition 12,200 cal. BP (Whitney et al., 2011).

III.3. North-eastern South America

I divided North-eastern South America into three subregions including the Northern Brazilian coastal plain to the North, the central Cerrado at mid-latitudes and the Atlantic forest to the South. In this region, Ledru et al. (2016) reviewed 36 sedimentary cores reflecting 169 dated pollen spectra, and reconstructed past forest composition using a statistical probability density function. The authors underlined the lack of palaeo-environment data especially in the north between 5 – 15° S in the current extent of the Atlantic forest. In the Northern Brazilian coastal plain, records generally show a gradual increase in tree cover during the deglaciation period, possibly interrupted by periods of forest re-opening. Ledru et al. (2016) suggested that evergreen and semi-evergreen forests expanded during the deglacial period. In the Carajas area located in the far northwest of the region, geochemical and petrographic organic analyses in the Serra dos Carajas suggest a period of drier conditions during the Last Glacial Maximum until 15,400 cal. BP (Sifeddine et al., 2001). At this site, Absy et al. (1991) documented at least one episode of forest opening in the post-Last Glacial Maximum Late Pleistocene, characterised by the decrease of the proportion of arboreal pollen taxa and the increase of savanna taxa and Poaceae.

In the central Cerrado, Cassino et al. (2020) reviewed pollen records from 6 sites, and speleothem records from 5 sites. Records suggested an increase in monsoon activity in south and central Brazil from 13,000 to 11,200 cal. BP (i.e., around the Younger Dryas), drier conditions in the early Holocene, and wetter conditions around the mid-Holocene. The Late Pleistocene wet period disagrees with earlier studies interpreting a lack of sediment deposition as evidence of aridity from the Last Glacial Maximum to the Holocene (Salgado-Labouriau et al., 1997; Barberi et al., 2000; Cassino et al., 2020). In the south of the Cerrado, moist forests expanded temporarily during the deglacial period, possibly linking the Amazon and Atlantic rainforests (Ledru et al., 2016). In Brejo do Louro, a site located in the south (State of Espírito Santo), palynological, carbon, and nitrogen elemental and isotopic analyses suggest that the Atlantic rainforest remained stable during the deglacial period, despite some floristic composition changes (Francisquini et al., 2020). The forest became gradually more open in the early and mid-Holocene.

More in the South, in the Atlantic forest subregion (22 – 30° S), pollen records suggest that *Araucaria,* evergreen broadleaf forests, and semi-deciduous forests might have been continuously present over the last 17,000 cal. BP (Ledru et al., 2016).

III.4. Amazon Basin

In the Amazon Basin, records suggest that forests continuously covered at least some part of the region in the Northwestern Basin, while parts of the Southeastern Basin may have been more open durin the Last Glacial Maximum. A regional synthesis of palaeo-environment records including palynological, sedimentological and isotopic ($\delta^{13}C$) data from Rondônia, Carajas, and Guyana suggest that the Amazon rainforest might been replaced by more open/savanna-type vegetation in some places where modern rainfall is lowest (van der Hammen and Absy, 1994). In this scenario that assumes a reduction in precipitation is the unique driver of changes in forest cover, a vast north-western patch of forest might have remained stable, as well as several smaller patches distributed along the edges of the modern rainforest. Widespread savanna-type vegetation persisted in the Amazon Basin during the Last Glacial Maximum until ~ 13,000 BP (~ 15,500 cal. BP). At this time, water levels rose in rivers and landscapes gradually started to transform back to forests until the beginning of the Holocene ~ 10,000 BP (~ 11,500 cal. BP).

In Rondônia (southeast), several undated pollen records suggest the replacement of tropical rainforest by grass-dominated savanna. At Katira that is today covered by dense tropical forest, both $\delta^{13}C$ values and pollen composition indicate that an herbaceous savanna covered the area during the Last Glacial Maximum (van der Hammen and Absy, 1994). No data are available to estimate when the forest returned to the region of Katira. In Paraíso cave (south-eastern corner of the region), $\delta^{18}O$ analyses of speleothems suggest the persistence of the tropical forest despite drier conditions, although plant transpiration and water recycling were reduced (Wang et al., 2017). In the north-western Amazon Basin, information on palaeo-vegetation comes only from the Hill of Six Lakes site (Colinvaux et al., 1996; Bush et al., 2004), and thus should be considered with caution. In the equatorial site of Lake Pata in the Hill of Six Lakes (Amazon lowlands, in the North-Western corner of ther region), pollen records suggest that the western Amazonian rainforest was not fragmented and that the region was continuously covered with forests during the last 170,000 years (Colinvaux et al., 1996; Bush et al., 2004). Recent analyses in the same site highlights some changes in forest communities and vegetation structure during the Last Glacial Maximum, including higher proportion herbs and taxa usually characteristic of seasonally dry forests. This suggests greater climate seasonality, contradictiong the notion of a 'wet' Last Glacial Maximum (D'Apolito et al., 2013).

III.5. Tropical Andean region

In the tropical Andean region, records from the deglaciation period show discrepancies in vegetation cover between higher elevation sites (> 3500 m a.s.l) and lower to mid-elevation sites (< 2000 m a.s.l). While forests continuously covered lower and mid-elevations, higher elevations were generally open. At lower and mid-elevations, on the eastern Andean flank, several sites have revealed information about post-Last Glacial Maximum vegetation changes. In a mid-elevation valley of the Ecuadorian Andes (Campo Libre, 1800 m above sea level), phytolith analyses mainly suggest a progressive increase in palm cover reflecting warmer and drier conditions (McMichael et al., 2021). The main increase in general tree cover started at the beginning of the Younger Dryas that was probably related to major drying (12,900 BP). At lower elevations (Laguna Pindo 1,248 m above sea level), pollen records suggest high and stable tropical broadleaf forests during the Last Glacial Maximum and the deglacial period, despite pollen not being preserved during the Younger Dryas (Montoya et al., 2018). In the extreme south of the region, pollen records from Lake Consuelo (Peru; 1,360 m above sea level) suggest persistence of montane cloud forests during the post-Last Glacial Maximum period, with some tree community reorganisation due to drier conditions (Urrego et al., 2010).

At higher elevations, in the western Cordillera of south-western Ecuador, pollen records from the two high-elevation sites of Lagunas Chorreras (3700 m) and Pallcacocha (4060 m) indicate the prevalence of open landscapes corresponding to a cooler and moister climate than today (Hansen et al., 2003). Fluctuations in pollen assemblages suggest that the environment was not stable, possible reflecting changes in wind directions or climate. The charcoal records suggest that fires were not prevalent.

III.6. Caribbean region

In the Caribbean region, records from the deglaciation period show open landscapes until the Holocene, characterised by treeless vegetation the Northern Venezuela (from 15,500 cal. BP) and by sparse trees in Guatemela lowlands and the Southern Colombian Llanos. In Northern Venezuela, records from Lake Anteojos in the Merida Andes show that open landscapes dominated from 14,000 to 10,500 cal. BP, with a decrease in shrub taxa from the onset of the Younger Dryas (Rull et al., 2015). At Lake Valencia, pollen records suggest that grasslands dominated the landscape from 13,000 to 9,800 BP (15,500 – 11,200 cal. BP) (Leyden, 1985).

In Lake Quexil (Guatemala lowlands; Leyden et al., 1993), pollen records were dominated by herbaceous taxa until ~ 14,000 BP (17,000 cal. BP) indicating open landscapes. It should be noted that in the absence of reliable radiocarbon dates, the latter date was estimated via relative dating by Leyden et al. (1985) as corresponding the known end of the Last Glacial Maximum. An initial phase of tree expansion then started, the landscape remaining dominated by herbaceous vegetation. Forest expansion paused before 10,500 BP (~ 12,500 cal. BP) and was followed by the stable settlement of rainforests that remain today.

In the south of the Colombian Llanos, pollen record from Laguna El Pinal suggest that the landscape was covered with grass-dominated vegetation and sparse trees (i.e., savanna) during the last ~ 18,000 BP (~ 22,000 cal. BP), with no marked changes in floral composition (Behling and Hooghiemstra, 1999). There, forested areas are typically located near rivers, including gallery forests growing along river courses.

III.7. Mexican region

In the Mexican region, records from the deglaciation period suggest that the vegetation was rich in woody taxa in the Chihuahua and on the Northwestern coast while it was more open in the Trans-Mexican Volcanic belt. The Sonoran, Baja California and Chihuahua are extremely dry, and associated palaeo-vegetation records are sparse. The regions might have been more humid during the Late Pleistocene, favouring higher densities of woody vegetation (e.g., juniper *Juniperus* spp.; pines *Pinus* spp.) (Metcalfe, 2006). In the Chihuahua, records suggest that more open vegetation started to expand from ~ 12,000 BP (~ 14,000 cal. BP). In contrast, late Pleistocene palaeo-vegetation records from the trans-Mexican volcanic belt, more in the South, tend to describe a dry and open vegetation (Metcalfe, 2006).

IV. MAJOR HOLOCENE VEGETATION CHANGES (11,700 BP – present)

IV.1. Patagonia

IV.1.1. Northern slopes of the Patagonian Andes

On the Northern slopes of the Patagonian Andes, all palaeo-vegetation records indicate the continuous presence of closed *Nothofagus* forests throughout the Holocene (Iglesias et al., 2014; Pesce and Moreno, 2014; Moreno et al., 2018).

IV.1.2. Southern slopes of the Patagonian Andes

On the southern slopes of the Patagonian Andes, palaeo-vegetation records indicate the gradual expansion of *Nothofagus* forests in the first half of the Holocene. While closed *Nothofagus* forests were already established in some areas at the start of the Holocene such as in Mallín Fontanito (Nanavati et al., 2019), dense forests gradually developed in most sites in the first few millennia of the Holocene and covered the whole region from ~ 7,500 BP. At Lago Los Niños and Laguna La Pava, pollen records indicate that closed forests established by the early Holocene ~ 11,500 BP (Iglesias et al., 2016). Some sites such as Lake Shaman (de Porras et al., 2012) rather indicate the development of a forest-steppe ecotone via the expansion of *Nothofagus* forests, suggesting that while forests expanded on the slopes of the Andes, they remained bordered with steppe landscapes. At Mallín Pollux, mixed steppe-*Nothofagus* woodlands expanded from 11,000 to 7,500 BP and closed *Nothofagus* forest became established ~ 7,500 BP (Markgraf et al., 2007). More in the South and on the eastern slopes of the Patagonian Andes, pollen, spore, and charcoal records from Lago Augusta show that dense *Nothofagus* forests established from 11,800 to 9,800 BP (Villa-Martínez et al., 2012). At Cerro Benítez, pollen and spore records indicate that forest cover increased rapidly by ~ 12,000 BP. The area could be considered as an open woodland in the early Holocene, after which the forest expanded again from ~ 7,500 BP (McCulloch et al., 2021). At Cueva del Mylodon, the expansion of closed *Nothofagus* began in the early Holocene (Moore, 1978). Pollen records from Lago Guanaco suggest that the area was an open landscape dominated by pre-Andean herbs and shrubs from 12,500 to 11,400 BP. The expansion of *Nothofagus* trees could have begun by ~ 12,300 BP, and dense forests definitively established at ~ 11,400 BP (Moreno et al., 2009).

IV.1.3. Southernmost Patagonia

In Southernmost Patagonia, records show the expansion of *Nothofagus* forests in the early Holocene. Pollen records from La Correntina and Terra Australis suggest that *Nothofagus* forest began to expand gradually ~ 11,200 BP. Moorland then expanded in the region ~ 9,000 BP to replace the forest at lower elevations, while forests (including the Magellanic rainforest) expanded toward higher elevations (Musotto et al., 2017). Pollen records from Lake Ballena suggest that the expansion of *Nothofagus* forests began ~ 10,500 BP (Fontana and Bennett, 2012); moorland then expanded in the region ~ 9,000 BP. In Harberton, Río Rubens, and Paso Garibaldi (Markgraf and Huber, 2010), well-dated pollen, charcoal, and plant macrofossils records from three peat bogs indicate that dense *Nothofagus* forests definitively established in lowlands and upslopes during the early Holocene, replacing grass-dominated open landscapes.

IV.1.4. Dry diagonal (Holocene only)

In the Patagonian dry diagonal, Mancini et al. (2005) reviewed pollen records 32° – 48° S covering the last ~ 8,000 years, indicating the continuous presence of open landscapes. The Patagonian Plateau at ~ 40° S was gradually populated by grass-steppe with shrubs, suggesting drying conditions. In the northern part of Santa Cruz Province in south-eastern Patagonia, pollen records indicate the continuous presence of open to semi-open vegetation during the Holocene, with some fluctuations in floristic composition during the Holocene, such as the alternance between open grasslands and shrub-steppe vegetation indicating changes in moisture, but not enough for forests to establish (Mancini, 1998).

IV.2. Central South America

Holocene records from the Pampas suggest the continuous presence of open landscapes with sparse trees with some change in vegetation composition. Pollen records from the Pampas suggest a north-eastern displacement of the arid–semiarid region (Mancini et al., 2005). In the Argentine Pampas, psammophytic and shrub steppe that occupied the region during the late glacial period was replaced by humid grasslands during the early Holocene (Prieto, 2000). The only record from the Pantanal shows the continuous presence of closed forests, with typical taxa from seasonally dry tropical forests (Whitney et al., 2011).

IV.3. North-eastern South America

Holocene records from North-eastern South America suggest that modern vegetation was present in the region throughout the Holocene such as tropical forests in the north and the Atlantic forest (Ledru et al., 2016), but with varying proportions including changes in herbaceous-arboreal ratios. Records generally show the gradual establishment of modern vegetation, characterised by a higher tree cover (Ledru et al., 2016).

IV.3.1. Atlantic forest

In the Atlantic forest subregion, tree cover tends to increase in most records especially after the mid-Holocene, but with varying chronologies and amplitude, suggesting an heterogeneous pattern of tree cover changes at regional scale. The chronology of tree cover changes may differ among sites depending on their elevation. Pollen records from Serra dos Órgãos, a relatively high elevation site (2,130 m), show the continuous presence of campos de altitude vegetation (open landscape with sparse trees) throughout the Holocene, and the upslope expansion of the Atlantic rainforest from 5,640 cal. BP (Behling and Safford, 2010). In Serra da Bocaina (1,500 m elevation), the concentration of typical montane forest pollen taxa increased after 7260 cal. BP to gradually form the mosaic landscape of campos vegetation (grasslands) and forest currently present (Behling et al., 2007). Pollen records from Morro de Itapeva (peatbog, 1850 m elevation) show the development of cloud forest during the Holocene (Behling, 1997). Pollen records from Jacarei (550 m elevation) show a generally open landscape with sparse trees during the Holocene. Tree cover increased in the late Holocene, characterised by montane forest taxa (Garcia et al., 2004). In Colônia (900 m elevation), Holocene pollen records show the rapid expansion of rainforest from ~ 9,000 cal. BP. Forest cover then remained relatively high until today despite episodes of forest regressions in the mid-Holocene (~ 6,000–4,000 cal. BP) and the la millennium (Ledru et al., 2009). Pollen records from Curucutu (800 m elevation) show the continuous presence of a mosaic landscape during the Holocene (Pessenda et al., 2009). In Serra Campos Gerais (1200 m elevation), pollen records show that Holocene vegetation was generally characterised by open landscapes with sparse trees and that forest expanded in the valleys in the late Holocene (Behling, 1997). In Lagoa Grande (364 m elevation), pollen records from the last millennium show the dominance of closed forest (Pessenda et al., 2010). In Araçatuba (1,500 m elevation), open landscapes with sparse trees transitioned to a mosaic environment in the late Holocene (Behling, 2007). In Volta Vehla (5 m elevation), mosaic landscapes transitioned to closed forest after the mid-Holocene (Behling and Negrelle, 2001). In Serra do Tabuleiro (861 m elevation), open landscapes with sparse trees transitioned to a mosaic environment after the mid-Holocene (Jeske-Pieruschka et al., 2013).

IV.3.2. Central Cerrado

In the Central Cerrado subregion forest cover increased after the mid-Holocene, mosaic landscapes replacing open landscapes with sparse trees. Reviews of several records (Cassino et al., 2018, 2020) suggest that the subregion was continuously covered with an herbaceous-shrubby vegetation during the Holocene, with variations in composition indicating changes in moisture availability. Records show that tree cover was low in the first part of the Holocene, and the proportion of arboreal taxa increased after the mid-Holocene (~ 6,000 BP). In Brejo do Louro, herbaceous plants dominated the pollen record in the early Holocene, and tree cover increased from 7,300 cal. BP (Francisquini et al., 2020). In Àguas Emendadas, modern vegetation characterised by mosaic vegetation established from the mid-Holocene, replacing more open landscapes (Barberi et al., 2000).

IV.3.3. Northern Brazilian coastal plain

In the Northern Brazilian coastal plain subregion, records indicate the continuous presence of forest taxa and generally high forest cover especially in the early Holocene, but some sites experienced periods of lower forest cover suggesting spatial heterogeneity. Multiproxy records from the Carajas area including well dated records from Pántano da Maurítia show an episode of high moisture availability and dense forest in the early Holocene between 11,400 and 10,200 cal. BP, followed by the expansion of savannas and forest regression until the mid- to late Holocene. Dense rainforest then expanded again and became established by 3,400 cal. BP (Absy et al., 1991; Sifeddine et al., 2001; Hermanowski et al., 2012). In Lagoa da Curuça, high concentrations of Amazonian taxa (trees, shrubs, climbers and epiphytes) in the pollen records show that coastal rainforest dominated the landscape in the early Holocene (Behling, 2001). Subsequent decrease in Amazonian taxa pollen concentrations, contemporaneous with the increase in herbaceous taxa concentrations suggest rainforest opening in the late Holocene. In Rio Curuá, concentrations in tropical rainforest taxa in the pollen record are constantly high (40–80%) throughout the Holocene, indicating the continuous presence of dense forest in the surrounding landscape (Behling and Lima da Costa, 2000). In Lagoa do Caço (Ledru et al., 2006), mosaic landscapes were predominant throughout the Holocene. In Serra de Maranguape, forest taxa dominated the pollen record throughout the Holocene indicating the continuous presence of dense forest with marked changes in forest composition (Montade et al., 2014).

IV.4. Amazon Basin

The Holocene vegetation of the Amazon Basin has attracted less research attention than the deglacial period (Bush et al., 2011). The north-western Amazon Basin is thought to have been continuously covered with forests throughout the Holocene, based on a single site (Hill of Six Lakes; Colinvaux et al., 1996). Sedimentary hiatuses suggest an episode of drying in the mid-Holocene (Bush et al., 2011), which possibly led to less-forested areas.

IV.5. Tropical Andean region

On the eastern Andean flank, the mid-elevation site of Campo Libre that was dominated by forests returned to an open-vegetation floodplain around 7,500 cal. BP as precipitation increased; this floodplain remained stable until the development of maize agriculture around 4,600 cal. BP (McMichael et al., 2021). At lower elevations (Laguna Pindo, 1248 m), tropical broadleaf forest remained stable throughout the Holocene (Montoya et al., 2018). In the far south of the region, pollen records from Lake Consuelo (Peru, 1360 m above sea level) suggest persistence of cloud forests during the Holocene, with most reorganisation of tree communities occurring during the mid-Holocene due to drier conditions (Urrego et al., 2010). At higher elevations, in the western Cordillera of south-western Ecuador, pollen records from the two high-elevation sites of Lagunas Chorreras (3700 m) and Pallcacocha (4060 m) indicate the expansion of montane forests throughout the Holocene (Hansen et al., 2003). The charcoal records suggest the higher prevalence of fire than today.

IV.6. Caribbean region

Modern vegetation, characterised by higher forest cover, generally established in the early Holocene, for example in Lake Quexil (Guatemala lowlands; Leyden et al., 1993), Lake Valencia (Northern Venezuela; Leyden, 1985), and in the south of the Colombian Llanos (Behling and Hooghiemstra, 1999). In the South of the Colombian Llanos, grass-dominated savanna with sparse trees persisted most of the Holocene. Pollen records from Laguna Carimagua, Laguna Sardinas and Laguna Angel show an increase of gallery forest taxa especially palms (*Mauritiella*, *Mauritia*) around study sites in the late Holocene, occurring for example after ~ 4400 BP (~ 5000 cal. BP) in Laguna Carimagua (Behling and Hooghiemstra, 1999).

IV.7. Mexican region

During the Holocene, high precipitation regimes ended on the east coast (Sonoran and Baja Californa) during the early Holocene (~ 9,000 BP, ~ 10,000 cal. BP), causing tree retraction and expansion of more open vegetation northward (Metcalfe, 2006). The same process happened in the Chihuahuan region, but slightly earlier 12,000 to 9,000 BP (14,000 to 10,000 cal. BP) (Metcalfe, 2006). In the trans-Mexican volcanic belt, vegetation changed to a more humid/forested environment in the early Holocene (Metcalfe, 2006).

V. POTENTIAL CAUSES OF VEGETATION CHANGES

V.1. Patagonia

Most studies cite moisture as the primary driver of tree-cover change in western Patagonia, generally driven by changes in precipitation and temperature, the latter having more effect at higher elevations by limiting upslope migration of the treeline (e.g., Markgraf et al., 2007; Markgraf and Huber, 2010). Vegetation flux is tentatively attributed to changes in the influence from the southern westerly winds affecting the precipitation/evaporation balance (Markgraf et al., 2007; Moreno et al., 2018; McCulloch et al., 2021). Increase of precipitation may have been caused by the gradual southward shift of the southern westerly winds resulting from deglaciation (de Porras et al., 2012; Villa-Martínez et al., 2012; Pesce and Moreno, 2014; Iglesias et al., 2016; Nanavati et al., 2019), combined with increasing annual insolation (Iglesias et al., 2016).

Fire disturbance might also have limited the expansion of *Nothofagus* forests in the far south of Patagonia (Musotto et al., 2017). But the effects and ignition sources of fire in Patagonia during the post-Last Glacial Maximum period have been debated (Holz et al., 2017), with changes possibly caused by a more fire-favourable climate and the arrival of humans (Holz et al., 2017 and reference therein). South-western Patagonia (50° S) could have been affected by a cold episode during the Antarctic Cold reversal around 14,800 to 12,600 BP. In north-western Patagonia (~ 40° S), climate might have changed asynchronously with a cold episode at ~ 13,500 – 11,500 BP.

In eastern Patagonia such as in the Patagonian dry diagonal, changes in Holocene vegetation are attributed to variation in the position and seasonal amplitude of latitudinal shifts of the Pacific and Atlantic anticyclones and of the southern westerly winds (Mancini et al., 2005).

In the last 150 – 350 years, most pollen records from the western Andes suggest widespread clearance of *Nothofagus* forests aided by fire, and the spread of invasive exotic species such as *Rumex acetosella* and *Plantago* spp., suggesting the increase of grazing (Markgraf et al., 2007; Villa-Martínez et al., 2012; Moreno et al., 2018; Nanavati et al., 2019). In eastern Patagonia, pollen records indicate the strong and widespread effects of European settlement, such as major changes in floristic composition and fire due to forest clearance and overgrazing. As in the western Andes, pollen records show the massive spread of exotic species such as *Rumex acetosella*, *Plantago* spp., Brassicaceae, and Asteraceae subf. Cichorioideae (Mancini et al., 2005 and reference therein).

V.2. Central South America

Vegetation changes in the Pantanal in the north of the region are attributed to changes in moisture availability driven by changes in precipitation linked to variation in the strength of the monsoon (Whitney et al., 2011; Whitney and Mayle, 2012).

The arrival of Europeans in the last 500 years corresponds to the introduction of many tree species in the Pampas (Chaneton et al., 2012). In Eastern Patagonia, pollen records show the strong and widespread effects of European settlement, such as major changes in floristic composition and fire due to forest clearance and overgrazing. As in the western Andes, pollen records show the spread of exotic species such as *Rumex acetosella*, *Plantago* spp., Brassicaceae, and Asteraceae subf. Cichorioideae (Mancini et al., 2005 and reference therein).

V.3. North-eastern South America

Changes in forest cover in the Atlantic rainforest might have resulted from changes in moisture availability (Francisquini et al., 2020). In the Cerrado, changes are attributed to oscillations of the boundary belt of the South American summer monsoon (Cassino et al., 2020). The main changes include a strengthening of the South Atlantic convergence zone during Heinrich Stadial 1 (‘Mega-SACZ events’; Stríkis et al., 2015).

The arrival of Europeans in the region in the last 500 years was then responsible for drastic changes in tree cover. Today, the region is characterised by high human activity. Large areas in the Cerrado are subject to intense deforestation and agriculture, including livestock pastures and croplands (Friedl et al., 2010; Pivello, 2011). The Atlantic rainforest has experienced high rates of urbanisation, and the Amazon rainforest suffers from much recent deforestation (Hansen et al., 2013). The Atlantic forest was heavily deforested in the 20th Century (Behling, 1995).

V.4. Amazon Basin

Changes in moisture availability is considered as the main driver of post-Last Glacial Maximum tree-cover change in the Amazon Basin (van der Hammen and Absy, 1994; D'Apolito et al., 2013). Evidence of past changes in the South American summer monsoon system have been derived from planktonic foraminiferal oxygen isotope $\delta^{18}O$ records in the Amazon Fan, suggesting the displacement of its northern and southern boundaries and variations in its intensity (Maslin et al., 2011). Temperature gradient forcing in the Northern and Southern hemispheres of Earth could have caused the narrowing of the area subject to monsoon during the Last Glacial Maximum, and a southward displacement of the northern boundary during the Younger Dryas associated with generally lower monsoon intensity. Palaeo-records also suggest episodes of wet Caatinga in north-eastern Brazil associated with the southward displacement of the inter-tropical convergence zone (Wang et al., 2004, 2006, 2007). Overall, data describing post-Last Glacial Maximum climate shifts in the Amazon suggest that changes were not uniform or synchronous across the Basin (Bush et al., 2011). Anthropogenic landscapes occurred in the Amazon Basin from ~ 4,500 BP characterised by polyculture agroforestry, that later intensified with the development of Amazonian dark earths favouring maize cultivation (Maezumi et al., 2018).

V.5. Tropical Andean region

Comparing trends in vegetation changes with speleothem records suggests that mid-elevation forest and palm expansions in the Andes were due to variation in precipitation driven by insolation, solar forcing, and changes in sea-surface temperatures in the equatorial Pacific (McMichael et al., 2021). Similar comparisons suggest that both temperature and precipitation might have been important drivers of vegetation change at lower elevations (Montoya et al., 2018). Urrego et al. (2010) suggested the importance of cloud-driven moisture availability in Lake Consuelo for tree community reorganisation in the context of a stable montane forest cover (Peru; 1360 m).

The first records of human occupation in the tropical Andes date back to 13,000 BP, with the first permanent settlements from 7,000 BP, and exponential growth in the human population and associated activities from 5,000 BP (e.g., Rademaker et al., 2014; Goldberg et al., 2016). Human activities including agriculture may have had an increasing impact of local vegetation. For example, evidence of maize and squash (*Cucurbita*) cultivation in the region was found in phytolith records from the early Holocene between 8,000 and 7,000 years ago in coastal Ecuador (Pearsall, 2008). Evidence of various plant domestication in the early Holocene were also found in the Peruvian Highlands (Pearsall, 2008). While this suggests that human populations started to modify their local environment in the early Holocene in several parts of the Tropical Andes, the effect on tree cover at regional scale may have remained limited before the human population density reached higher values in the late Holocene.

V.6. Caribbean region

Sediment analyses including planktonic foraminifera assemblages in north-eastern Brazil and in the Cariaco and Tobago basins have shown southward displacement of the inter-tropical convergence zone during Heinrich Stadial 1 (post-Last Glacial Maximum iceberg discharge ~ 20,000 – 14,700 BP) and the Younger Dryas (12,900 – 11,700 BP) when the Southern Hemisphere became warmer than the Northern Hemisphere (Peterson et al., 2000; Hodell et al., 2017; Portilho-Ramos et al., 2017). Vegetation changes in the Caribbean region are generally attributed to changes in precipitation regimes responsible for wetter of drier periods (Leyden et al., 1993; Salgado-Labouriau, 1997; Behling and Hooghiemstra, 1999).

Evidence of anthropogenic vegetation change in the early Holocene was found in the region. For example, phytolith records indicate that maize occurred in the Bogotá plains from ~ 8,000 ago, associated with evidence of forest burning and disturbance (Pearsall, 2008). In the Southern Colombian Llanos, the late Holocene increase of a disturbance indicator (*Cecropia*) in the pollen records suggests that the simultaneous increase of palms was caused by increasing human activities (Behling and Hooghiemstra, 1999).

V.7. Mexican region

Shifts in vegetation arose mainly from precipitation changes due to the position of the inter-tropical convergence zone and summer rainfall regimes (Metcalfe, 2006). Evidence of human-related environmental change is visible from 3,500 BP in palaeo-environment records from the Trans-Mexican volcanic belt (Metcalfe, 2006).

VI. SYNTHESIS

Palaeo-environment records suggest asynchronous vegetation changes across the Neotropical realm from the Last Glacial Maximum to the present day. While some areas fluctuated between dense forests and grass-dominated vegetation, others hosted the gradual development of closed or open landscapes, and some could have remained stable through time. Most vegetation changes are attributed to variation in the most influential climate systems, including their position or intensity, such as variation in the position and intensity of the inter-tropical convergence zone, the South Atlantic convergence zone, and the southern westerly winds. Differences in the timing of variation of these climate systems possibly explain the asynchronous vegetation changes. In most regions, vegetation changes respond moisture availability, generally arising from changing precipitation regimes; however, the available studies rarely mention direct effects of temperature variation or the gradual increase in atmospheric CO_2 concentration. Likewise, pollen records are often used as a proxy to infer past precipitation regimes; for example, higher densities of tree pollen are generally considered to be evidence for higher moisture availability, while higher densities of herbaceous vegetation and the presence of xerophytic taxa generally suggest drier environments.

I distinguish two main areas of consistent changes in forest cover. First, forest cover in the tropical and subtropical regions depends on the local intensity of the monsoon regimes characterised by the position and extent of the inter-tropical convergence and the South Atlantic convergence zones. Second, forest cover in the temperate latitudes of South America mainly depends on the intensity of precipitation regimes driven by the position of the southern westerly winds.

VI.1. Tropical and subtropical regions: local intensity of monsoon regimes depending on the position and width of the Intertropical convergence zone and South Atlantic convergence zone

In tropical and subtropical regions, post-Last Glacial Maximum vegetation changes are mainly attributed to variation in the precipitation regimes, including changes in monsoon intensity arising from changing position and extent of the inter-tropical convergence zone — e.g., the Mexican region (Metcalfe, 2006), Caribbean region (Leyden et al., 1993; Salgado-Labouriau, 1997; Behling and Hooghiemstra, 1999; Peterson et al., 2000; Hodell et al., 2017; Portilho-Ramos et al., 2017), and the Amazon Basin (van der Hammen and Absy, 1994; Wang et al., 2004, 2006, 2007; Maslin et al., 2011; D'Apolito et al., 2013). In addition to the changes in the properties of the inter-tropical convergence zone, monsoon intensity in north-eastern South America (Caatinga-Cerrado-Atlantic Forest) and the north-western part of central South America (e.g., Pantanal) could have been affected by variation in the properties of the South Atlantic convergence zone (Whitney et al., 2011; Whitney and Mayle, 2012; Stríkis et al., 2015; Cassino et al., 2020; Francisquini et al., 2020). Forest cover changes in the tropical Andean region have been attributed to changes in moisture availability driven by variation in precipitation (Montoya, 2018; McMichael et al., 2021) and temperature (Montoya et al., 2018). Changes in cloud cover might also have affected forest composition (Urrego et al., 2010).

After the Last Glacial Maximum, the main climate system changes occurred during Heinrich Stadial 1 (~ 18,100 – 14,700 BP; Portilho-Ramos et al., 2017) and the Younger

Dryas (~ 12,900 – 11,600 BP; Cheng et al., 2020), both characterised by the cooling of the Northern Hemisphere (Heinrich, 1988; Broecker, 1994). While the massive post-Last Glacial Maximum iceberg discharges in the North Atlantic (Heinrich events) were primarily responsible climate change during Heinrich Stadial 1, the causes of the Younger Dryas are still debated (Peteet, 1995; van Hoesel et al., 2014; Holliday et al., 2014; Renssen et al., 2015). During those periods, the weakening of the Atlantic meridional overturning circulation (McManus et al., 2004) resulted in the southward displacement of the inter-tropical convergence zone (Peterson et al., 2000; Maslin et al., 2011; Hodell et al., 2017; Portilho-Ramos et al., 2017) and the strengthening of the South Atlantic convergence zone (Chiessi et al., 2009; Stríkis et al., 2015; Bahr et al., 2018). In addition to its displacement during these two periods, the convection zone of the South American summer monsoon might have become wider with the warming of the Northern and Southern Hemispheres, thus progressively affecting a larger area (the 'dynamic boundary-monsoon intensity' hypothesis; Maslin et al., 2011).

Consequently, forests might have temporarily expanded in the tropical and subtropical regions of the Southern Hemisphere (Amazon Basin, Caatinga, Cerrado, Atlantic Forest, and Pantanal) during Heinrich Stadial 1 and the Younger Dryas in response to the increase of moisture availability. Simultaneously, drier conditions in the tropical and subtropical areas of the Northern Hemisphere (i.e., south Mexican and Caribbean regions) might have led to the expansion open landscapes. Pollen records suggest that these trends reversed in the early Holocene in most regions, but that forests remained stable in others such as in the Amazon Basin because the northward migration of the intertropical convergence zone and the weakening of the South Atlantic convergence zone were counter-balanced by the gradual widening of the South American summer monsoon.

Despite widespread forest cover changes and ecotone displacements, forest cover remained relatively stable in several areas throughout the Late Pleistocene and Holocene. Areas continuously covered with forest include the lower elevations of the tropical eastern flank of the Andes, the north-western Amazon Basin, and the southern part of the Atlantic forest in Brazil.

VI.2. Southern temperate region: intensity of precipitation regimes driven by the position and intensity of the southern westerly winds

In the southern temperate region, forest cover changes in Patagonia mainly occurred on the slopes of the Andes and in the far south of Argentina. Such changes are generally attributed to variation in moisture availability driven by the displacement of the southern westerly winds affecting the balance of precipitation and evaporation (Mancini et al., 2005; Markgraf et al., 2007; de Porras et al., 2012; Villa-Martínez et al., 2012; Pesce and Moreno, 2014; Iglesias et al., 2016; Moreno et al., 2018; Nanavati et al., 2019; McCulloch et al., 2021). In addition, several other environmental changes could have driven variation in forest cover. Temperatures are thought to be the dominant limiting factor for the upslope migration of the treeline at higher elevations (Markgraf et al., 2007; Markgraf and Huber, 2010), as well as a driver of the retraction of the Patagonian ice sheet (Davies et al., 2020). Fire might also have limited the development of forests (Musotto et al., 2017; Holz et al., 2017). Finally, insolation increase has been tentatively suggested as a facilitator of forest expansion (Iglesias et al., 2016).

The southward displacement of the southern westerly winds started after the deglaciation from ~ 15,000 BP, driven by the warming of the southern Pacific Ocean (Boex et al., 2013; Davies et al., 2020). Consequently, forests gradually expanded southward and upslope, especially on the slopes of the Patagonian Andes, with higher forest densities to the West. On the eastern side of the Southern Cone, pollen records also suggest the stability of several areas. While evergreen forest continuously covered southern Brazil, the Argentine Pampas remained dominated by herbaceous vegetation, and the Campos region (southern Brazil and Uruguay) might have been continuously covered by a mosaic, semi-open vegetation.

VI.3. Human impacts on vegetation

Evidence for the first human arrival in South America are available in all regions from at least ~ 13,500 cal. BP, with a mean estimated date ~ 15,500 cal. BP at continental scale despite some older, controversial dates (Prates et al., 2020). Human population growth may have then accelerated before slowing down at the end of the Antarctic Cold

Reversal ~ 12,500 cal. BP (Prates et al., 2020). The first human impacts on local vegetation are visible in pollen, phytolith and charcoal records from the early Holocene in some areas, although the effect on tree cover at large scale may have remained limited. Palaeo-environment records suggest the development of agriculture from the early Holocene (e.g., maize in the tropical Andes ~ 8,000 BP; Pearsall, 2008). Charcoal records suggest the increase of fire ignited by humans such as in the eastern Amazon (Absy et al., 1991; Soubies et al., 1991 in Salgado-Labouriau, 1997), the Cerrado (e.g., Pivello, 2011), and the Patagonian Andes (e.g., Iglesias et al., 2016; Méndez et al., 2016; Nanavati et al., 2019), but disentangling the influence of climate and human is difficult.

Later, European arrival was associated with widespread changes in vegetation cover. European arrival in the 15th Century was followed by major changes in vegetation cover associated with broad-scale increases of land use dedicated to. Pollen cores record a sudden decrease in the concentration of tree species, indicating widespread deforestation on the slopes of the Patagonian Andes (Moreno et al., 2018) and the Cerrado (Pivello, 2011), for example. Forest loss has intensified in the 21st Century in the southern and eastern margins of the Amazon Basin, the Cerrado, and the Chaco (Hansen et al., 2013). Pollen cores also indicate the widespread introduction and expansion of exotic species, including both woody taxa in the Pampas (Chaneton et al., 2012), and herbaceous taxa generally associated with land conversion for pasture in eastern Patagonia and the western Andes (e.g., Mancini et al., 2005; Markgraf et al., 2007; Villa-Martínez et al., 2012; Moreno et al., 2018; Nanavati et al., 2019). Finally, records suggest a reduction of natural disturbance regimes (e.g., fire regime) in some regions such as in the Pampas (Chaneton et al., 2012).

VI.4. Concluding remarks and limitations

Overall, Neotropical palaeo-environmental records provide information on post-Last Glacial Maximum vegetation changes and their potential drivers, but this information is limited by the scarcity of records in some regions, and by the difficulties to estimate the effect of each potential driver separately. First, palaeo-vegetation archives are particularly dense in some regions like the slopes of the Andes, along the Atlantic coast in the Brazilian highlands and the Argentine Pampas. Conversely, vast areas of the

Neotropical realm remain under-sampled (e.g., the modern South American dry diagonals and most of the Amazon Basin). In such areas, past vegetation reconstruction mostly depends on information from neighbouring regions and vegetation modelling, often eliciting intense debate; for example, one of the main debates centres on the extent of the Amazon rainforest during the Last Glacial Maximum.

Second, identifying drivers of vegetation changes from palaeo-vegetation records generally relies on comparing the timing of abrupt changes across sites rather than on mechanistic approaches, making it difficult to disentangle autocorrelated drivers. Moreover, such reconstructions are associated with many uncertainties that limit definitive conclusions, such as the feedback effects of vegetation on climate, the role of megafauna and their extinction during ~ 12,700 years, and the timing and impact of human arrival.

CHAPTER 4

RESPONSE OF NEOTROPICAL TREE COVER TO VARIATION IN POST-LAST GLACIAL MAXIMUM CLIMATE AND ATMOSPHERIC CO_2

ABSTRACT

Aim: The post-Last Glacial Maximum period (~ 19,000 years before present to today) was characterised by major changes in the global climate and atmospheric CO_2 concentration. In the Neotropical realm, scattered palaeo-environment records suggest multidirectional and asynchronous tree cover changes among regions. I aim to model the potential tree-cover changes and identify the main regional climatic drivers of tree-cover changes throughout this period.

Location: Neotropical realm.

Time period: 18,500 years before present to today.

Major taxa studied: Spermatophyta (woody trees).

Methods: I applied the dynamic global vegetation model LPJ-GUESS with a set of general circulation model experiments describing seven climate scenarios (Last Glacial Maximum, Heinrich Stadial 1, Younger Dryas, Greenlandian, Northgrippian, Meghalayan, and the present) to hindcast potential tree-cover changes through this interval at a resolution of 0.5° × 0.5°. I then constructed generalised least-squares models to identify which combinations of climate variables (i.e., precipitation, temperature, solar radiation, atmospheric CO_2 concentration) best explained variability in forest cover y within seven large regions covering most of the Neotropical realm.

Results: Average potential tree cover in the Neotropical realm steadily increased from the Last Glacial Maximum (30%) to the present (44%). Only 33% of the areas recorded more than 20% of tree-cover variations, and changes occurred asynchronously among regions during the Heinrich Stadial 1 and the Younger Dryas. Tree cover was closely related to the changes in precipitation regimes in all regions, but none of the tested variables could be discriminated as the 'main' driver of tree-cover changes.

Main conclusions: Variation in climate and atmospheric CO_2 have potentially led to substantial, widespread, and asynchronous increases in tree cover in all regions, strongly affecting a third of the Neotropical realm. Patterns of change suggest the importance of variation in the intensity and position of the inter-tropical convergence zone, the South Atlantic convergence zone, and southern westerly winds.

KEY WORDS: computer modelling, dynamic global vegetation model, forest, leaf area index, palaeo-ecology, pollen, Quaternary, Pleistocene

I. INTRODUCTION

Reconstructing past vegetation response to climate and atmospheric CO_2 changes is essential to understand past ecosystem functioning and to predict future vegetation changes. In response to an increase in northern summer insolation after the Last Glacial Maximum, the post-Last Glacial Maximum period, spanning from the end of the Last Glacial Maximum (~ 19,000 calibrated years before present [BP], corresponding the number of years before 1950) to the present, recorded global rises in temperatures and atmospheric CO_2 concentration. These changes were associated with iceberg discharge mainly in the North Atlantic and changes in precipitation regimes (Clark et al., 2009; He, 2011; Portilho-Ramos et al., 2017). Both palaeo-ecological data and models suggest important vegetation changes at a global scale following the onset of the modern interglacial phase (Nolan et al., 2018).

In the Neotropical realm (Fig. 4.1), major climate variation occurred during the deglacial period (~19,000– 11,700 BP), including Heinrich Stadial 1 (post-Last Glacial Maximum iceberg discharge, ~ 19,000 – 14,700 BP) and the Younger Dryas (12,900 – 11,700 BP), with regional differences in timing and magnitude (e.g., Maslin et al., 2011; Portilho-Ramos et al., 2017). The scale of vegetation response to post-Last Glacial Maximum climate changes remains cryptic because of the scarcity of palaeo-environment records (e.g., Mayle et al., 2009; Bush et al., 2011; Flantua et al., 2015). However, several palaeo-environmental indicators (e.g., pollen, isotopic geochemistry, animal remains) suggest multidirectional and asynchronous tree-cover changes (e.g., Mancini et al., 2005; Metcalfe, 2006; Bush et al., 2011). These vegetation changes were regionally specific, including forest expansion in tropical lowlands (van der Hammen and Absy, 1994; Behling and Hooghiemstra, 1999; Bush et al., 2011) and on the slopes of the tropical and Patagonian Andes (e.g., Hansen et al., 2003; Nanavati et al., 2019), and temporary switches between dense forests and grasslands in most of south-eastern Brazil (e.g., Ledru et al., 2016; Cassino et al., 2020). In contrast, tree cover remained stable despite some changes in the stratification and floristic composition of vegetation in parts of modern tropical forests (e.g., Ledru et al., 2016; Montoya et al., 2018), as in open or mosaic landscapes of southern Brazil and the Pampas (Prieto, 2000; Mourelle et al., 2017) and parts of eastern Patagonia (Mancini et al., 2005).

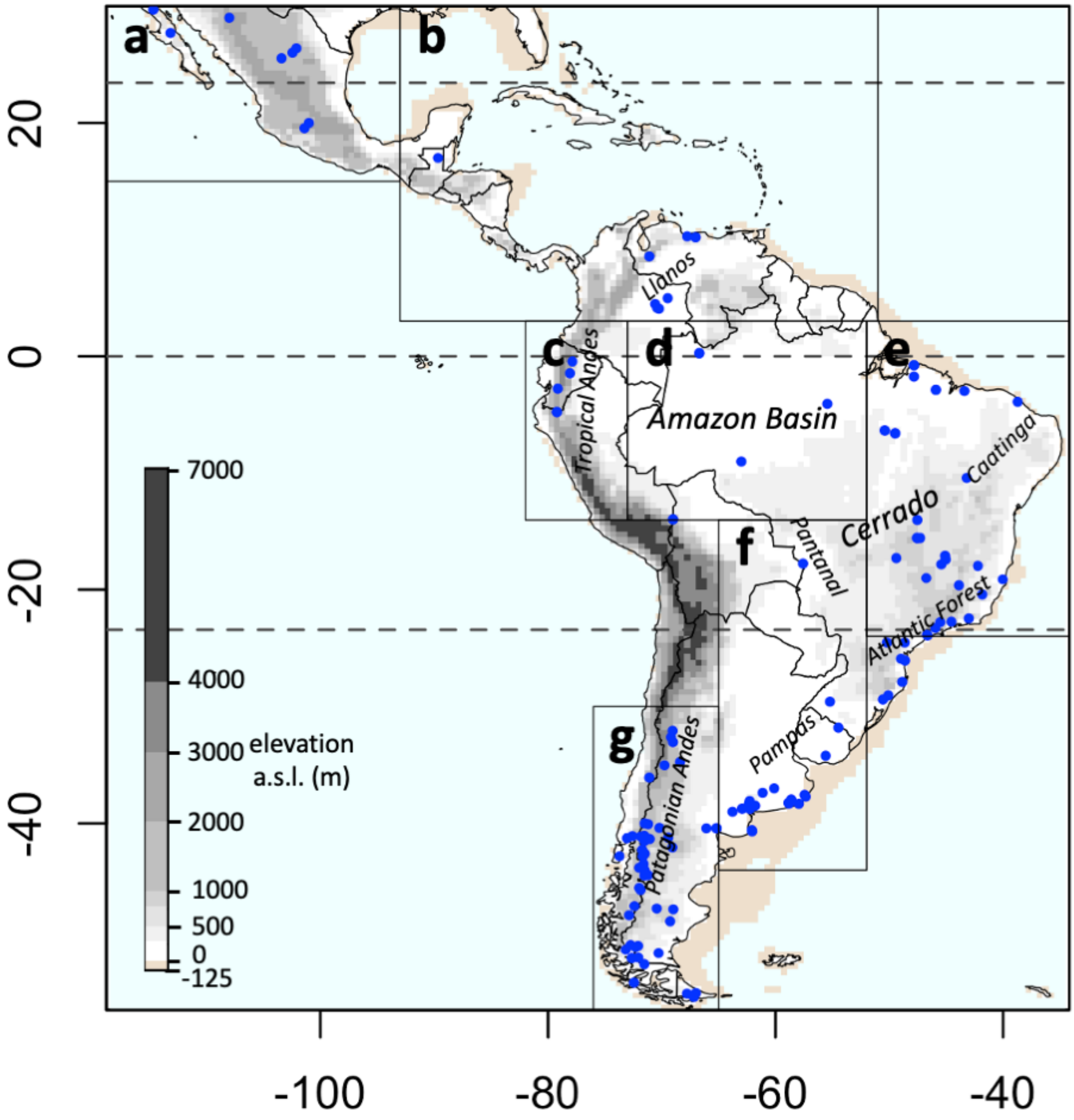

Figure 4.1. Topographical map of the Neotropical realm showing the extent of emerged land during the Last Glacial Maximum (in grey) at a resolution of 0.5° × 0.5° degree*. Selected regions for this study are outlined in black. (a) Mexican, (b) Caribbean, (c) tropical Andes, (d) Amazon Basin, (e) north-eastern South America, (f) central South America, (g) Patagonia. a.s.l. = above sea level. Also indicated are ecoregions mentioned in the main text and palaeo-vegetation records used for comparison with simulated tree cover.*

Local chronological comparisons suggest that changes in moisture availability, derived from variation in precipitation regimes, have strongly affected tree cover during the deglacial period (Behling and Hooghiemstra, 1999; Mancini et al., 2005; Metcalfe, 2006; Whitney et al., 2011; Francisquini et al., 2020). Inter-regional divergence in the trend of tree-cover change could have thus resulted from changes in the position and intensity of the inter-tropical convergence zone and the South Atlantic convergence zone that characterise the South American summer monsoon in tropical and subtropical areas (Metcalfe, 2006; Whitney et al., 2011; Cassino et al., 2020), and the southern westerly winds affecting the precipitation/evaporation balance in temperate South America (Mancini et al., 2005; McCulloch et al., 2021).

Vegetation modelling estimates vegetation distribution as a function of climate variables and can be used as a complementary tool to predict palaeo-vegetation changes and to test the sensitivity of vegetation to changes in climate and atmospheric CO_2 (Salzmann et al., 2008; Allen et al., 2020; Table 4.1). Since the 1990s, three main modelling approaches have been used to simulate past Neotropical vegetation. The first approach is based on correlative models that define the modern living conditions of vegetation types and statistically associate them with estimated palaeo-climate conditions to identify past habitat suitability (Friedlingstein et al., 1992; van der Hammen and Absy, 1994; Werneck et al., 2011; Leite et al., 2016; Costa et al., 2018; Maksic et al., 2019, 2022; details in Table 4.1). The second approach uses equilibrium vegetation models that map biome distributions based on the competitive interaction among simulated plant functional types influenced by climate, atmospheric CO_2 concentration, and soil properties (BIOME model, Prentice et al., 1992, and later versions). Such models have been applied to the Neotropical realm based on various post-Last Glacial Maximum climate scenarios and at various spatial scales, including local studies on the Amazon Basin (Cowling et al., 2001), Colombia (Marchant et al., 2002, 2004, 2006), and global assessments (Prentice et al., 1993; Harrison et al., 1998; Harrison et al., 2004). These two modelling approaches provide a static (i.e., non-dynamic) equilibrium view of the vegetation, representing snapshots of the vegetation distribution at a given time.

Unlike the previous approaches, a third method uses dynamic global vegetation models that are designed to account for successive, interdependent vegetation states over

Table 4.1. Post-Last Glacial Maximum palaeo-vegetation simulations across the Neotropical realm. *Periods: LGM= Last Glacial Maximum, Mid-H= mid-Holocene (6,000 years BP), HE1= Heinrich event 1. Model families:* ^{1}*correlative,* ^{2} *equilibrium vegetation models,* ^{3}*dynamic global vegetation model. Correlative model names correspond to the algorithm used to circumscribe the niche, i.e., RF = random forest, MaxEnt = maximum entropy. *In contrast to other correlative models, CPTEC-PVM2 maps biome distribution based on the calculation of secondary variables such as plant respiration and net and gross primary production. P= precipitations, T= temperature, [CO2]atm= atmospheric* CO_2 *concentrations.*

Reference	**Study region**	**Study period LGM to present**	**Vegetation feature studied**	**Model**	**Input data**	**Past climate input origin**	**Main outputs & results (Neotropics, compared to present)**
Friedlingstein et al., 1992	Global	LGM	biomes	^{1}	annual P, T	/	LGM: forest reduction
van der Hammen & Absy 1994	Amazon Basin	LGM	forest	^{1}	annual P	CLIMAP	LGM: forest reduction in Southeastern Amazon Basin
Werneck et al., 2011	Tropical South America	LGM Mid-H	seasonally dry tropical forests	MaxEnt^{1}	P (×4), T (×5), altitude	ECHAM3	LGM: SDTFs fragmenttion
Leite et al., 2016	Eastern tropical South America	LGM	broadleaf evergreen rainforest	MaxEnt 3.3.3^{1}	19 climate variables from worldclim	3 different GCMs	LGM: Atlantic forest expansion
Costa et al., 2018	South America	LGM to present (1,000 year interval)	biome stability (Olson et al., 2001)	Random Forest^{1}	P, T, seasonality	Simulations using HadCM3	LGM to present: biome instability on Andean slopes, in Caatinga, Cerrado, North Colombia and Venezuela, Chaco, Uruguayan savanna and western Pampas
Maksic et al., 2019	South America	8ka to present (2,000 year interval)	biomes (based on NPP)	CPTEC-PVM2^{1}	P, T, seasonality, [CO2]atm.*	CPTEC-AGCM	Holocene: tropical forest replacement by savanna in the Amazon Basin
Maksic et al., 2022	Brazil	LGM	Biomes (based on NPP)	CPTEC-PVM2^{1}	P, T, seasonality, [CO2]atm.*	8 climate scenarios	LGM: forest persistence in Western and central Amazon, grassland expansion in southern Brazilian Highlands.
Prentice et al., 1993	Global	LGM	Biomes (PFT combinations)	BIOME^{2}	P, T, seasonality, soil texture	climate scenario using ECMWF T21	LGM: forest reduction in Southeastern Amazon Basin and Patagonia
Harrison et al., 1998	Global	Mid-H	biomes	BIOME^{2}	P, T, seasonality, soil texture	10 climate scenarios (from AGCMs)	Mid-H: rainforest replacement by dry forest/savanna in the tropics on northern and Eastern margins in some models particularly
Cowling et al., 2001	Amazon Basin	LGM	LAI, biomes	BIOME3^{2}	P, T, seasonality, clouds, soil texture, [CO2]atm	LGM-GCM	LGM: forest reduction in the Southern Amazon Basin but no widespread invasion of grasslands. LAI sensitive to CO2 variations.
Marchant et al., 2002	Colombia region	LGM	biomes	BIOME3^{2}	P, T, seasonality, clouds, soil texture, [CO2]atm	Modern climate with limited [CO2]atm (200 ppm)	LGM: savanna replacement by xerophytic woods/shrubs
Marchant et al., 2004	Colombia region	LGM	biomes	BIOME3^{2}	P, T, seasonality, clouds, soil texture, [CO2]atm	Modern climate but with limited [CO2]atm (200 ppm)	LGM: moisture is dominant driver at lowest altitudes, but temperatures are more important at higher altitudes

Marchant et al., 2006	Colombia region	LGM	biomes	BIOME3[2]	P, T, seasonality, clouds, soil texture, $[CO_2]_{atm}$	Modern climate but with limited $[CO_2]_{atm}$ (200 ppm)	LGM: moisture is a dominant driver of vegetation changes
Harrison et al., 2003	Global	LGM	biomes	BIOME4[2]	P, T, seasonality, insolation, latitude, soil texture, $[CO_2]_{atm}$	17 climate scenarios (using AGCMs)	LGM: drought-tolerant biomes expansion of in the tropics, forest fragmentation and southward displacement in temperate mid-latitudes
Mayle et al., 2004a	Tropical South America	LGM Mid-H	biomes, NPP	SDGVM[3]	P, T, $[CO_2]_{atm}$	climate scenario using UGAMP-GCM	LGM: forest structure and floristic composition changes in Southeastern Amazon Basin, including lower NPP and forest cover. Holocene: savanna and dry forest expansion due to more frequent fires.
Beerling & Mayle, 2006	Tropical South America	LGM 15ka, 10ka	biomes	SDGVM[3]	P, T, $[CO_2]_{atm}$	climate scenario using UGAMP-GCM	LGM to present: Evergreen rain forests persistence in the Amazon Basin
Cowling & Shin, 2006	Amazon Basin	LGM	PFTs	LPJ[3]	monthly P, T, insolation, $[CO_2]_{atm}$	climate scenarios derived from directly implementing anomalies to modern climate data	LGM: lower forest cover primarily controlled by lower precipitations.
Handiani et al., 2012a	Global	HE1	Biomes, PFTs	TRIFFID[3]	T, moisture, $[CO_2]_{atm}$	UVic ESCM, CCSM3	HE1: forest retraction around tropical Atlantic coast. Southward shift of tropical rainbelt less pronounced in CCSM3 than UVic ESCM.
Werner et al., 2018	Chile	LGM Mid-H	Biomes, PFTs	LPJ-GUESS[3]	monthly P, T, insolation, $[CO_2]_{atm}$	TraCE-21ka climate scenario (using CCSM3)	LGM: coastal cold temperate rainforests northward displacement by about 5°N. Tree line and vegetation zones downslope displacement.
Allen et al., 2020	Global	LGM to present-day (1,000ka intervals)	Biomes	LPJ-GUESS[3]	monthly P, T, insolation, $[CO_2]_{atm}$	88 climate scenarios (using HadCM3)	LGM: forest retraction northward in Patagonia with forest refugia ~40°N in the Andes. Tropical and subtropical biome southward displacement. HE1(17ka): tropical forest southward displacement and minimum forest extent

time (e.g., Scheiter et al., 2013; Smith et al., 2014). These process-based models explicitly simulate the growth and competition of plant functional types (i.e., 'average' species representing all plant species with similar functional characteristics) based on their morphological, physiological, and phenological characteristics, thus simultaneously enabling the prediction of a variety of vegetation and ecosystem properties (Beerling and Mayle, 2006; Cowling and Shin, 2006; Werner et al., 2018). Many dynamic global vegetation models have been used to simulate past vegetation at global (TRIFFID, Handiani et al., 2012a, b; and LPJ-GUESS, Allen et al., 2020) or regional (tropical South America, SDGVM, Mayle et al., 2004; Beerling and Mayle, 2006; LPJ, Cowling and Shin, 2006; Chile, LPJ-GUESS, Werner et al., 2018) scales, but with a particular focus on the Last Glacial Maximum. Simulated tree cover is generally lower during the Last Glacial Maximum than today, especially in the Amazon Basin and southern Patagonia (see Table 4.1). In contrast, the putatively less-atypical post-Last Glacial Maximum period (i.e., from 19,000 BP to the present) is poorly represented in palaeo-vegetation simulations. Therefore, it remains largely unknown how and to what extent the climate modulated Neotropical vegetation at broad spatial scales during several periods of major environmental change such as the Younger-Dryas, the Heinrich Stadial 1, and most of the Holocene. In addition, the aforementioned studies have mainly focused on discrete representations of vegetation such as the distribution of biomes (Table 4.1), rather than on continuous metrics such as the percentage of tree cover.

My aim is to fill that gap by describing the changes of vegetation in the Neotropical realm from the Last Glacial Maximum and by identifying the combination environmental factors that shaped the modification of regional landscapes. I tested the following hypotheses: tree cover changes were mainly due to changes in moisture availability derived from variation in precipitation regimes, but with inter-regional process discrepancies. I simulated the vegetation by applying a state-of-the art dynamic global vegetation model (LPJ-GUESS; Smith et al., 2001, 2014) to several realistic palaeo-climate scenario experiments (TraCE-21ka; He, 2011). I simulated the changes in post-Last Glacial Maximum vegetation, with a focus on the first layer of tree cover, across the Neotropical realm (southern USA at ~ 30° N to the southern tip of South America). Simulations span the end of Last Glacial Maximum to today, by focusing on seven independent, 100-year snapshots every 3000 years, covering the main climate phases of this interval (see Appendix S4.2.5 for the parameters of each selected TraCE-21ka simulation). Snapshots correspond to climate scenarios representing the transition between the Last Glacial Maximum and Heinrich event 1 (~ 18,500 BP), the end of Heinrich Stadial 1 (~ 15,000 BP), the Younger Dryas (~ 12,000 BP), the Greenlandian (early Holocene, ~ 9,000 BP), the Northgrippian (mid-Holocene, ~ 6,000 BP), the Meghalayan (late Holocene, ~3,000 BP), and the present (1951 – 1990 CE). I then evaluated the model projections by comparing the simulated tree cover to analogue information from remote-sensing data (for the present) and palaeo-vegetation records (e.g., pollen, phytoliths, isotopic ratios) for all older periods. Finally, I constructed generalised linear models within seven large regions to identify the main potential regional environmental drivers of tree cover changes and those favouring tree cover stability.

II. MATERIALS ANS METHODS

II.1. The LPJ-GUESS model

I used the dynamic global vegetation model LPJ-GUESS (Smith et al., 2001, 2014) to simulate palaeo-vegetation distribution. LPJ-GUESS is a physiology-based mechanistic model that incorporates explicit relationships between environmental conditions and the biophysical and demographic characteristics of vegetation, and it simulates the dynamic of the vegetation and biogeochemical cycles at regional to global scales. LPJ-GUESS takes as input monthly climate data (precipitation, number of wet days, temperature, solar radiation) and annual atmospheric CO_2 concentration to predict various vegetation and environment characteristics, including leaf area index. LPJ-GUESS is a combination of an individual-based model (GUESS models populations such that all individuals are considered explicitly), and a model based on populations of plant functional types (LPJ classifies plants according to their physical and phenological characteristics). I described the characteristics of the 19 competing plant functional types I used in Appendix S4.1.2 and S4.1.3. Physiological and biogeochemical equations describe processes in the model based on a range of field observations, statistical inferences, and model adjustment validated against empirical observations (Haxeltine and Prentice, 1996; Smith et al., 2001, 2014). Most of the physiological and biogeochemical processes are then simulated at a daily time step (e.g., photosynthesis, respiration, transpiration, soil hydrology, etc.), while individual tree growth and vegetation dynamical processes are modelled annually (Hickler et al., 2004). LPJ-GUESS returns plant functional type (see Appendix S4.1) population characteristics for each cell of a landscape grid (following the resolution of the climate data: 0.5° × 0.5° latitude), where biological entities are individuals for trees and shrubs, and populations for graminoids, or one entity for each of the C_3 and C_4 types in a layer of grasses (Smith et al., 2001; Hickler et al., 2004). LPJ-GUESS has already been used to predict vegetation patterns in northern Eurasia and Chile around the Last Glacial Maximum (Allen et al., 2010; Werner et al., 2018), and to predict global-scale changes in biome distribution every thousand years (Allen et al., 2020).

I computed independently the leaf area index for each grid cell as the mean of five replicate stands of 0.1 ha to balance any stochastically simulated processes including disturbances, plant establishment and mortality. For each replicate stand, the model was run for 549 simulated years to allow the simulated vegetation to reach 'equilibrium' with the conditions. The model was then run for 100 additional years to derive the mean leaf area index for each plant functional type.

II.1.1. Palaeo-climate input data and debiasing approach

I used data describing monthly palaeo-climatic drivers of vegetation dynamics (temperature, solar radiation, precipitation) and annual atmospheric CO_2 concentration derived from TraCE-21ka (He, 2011), a set of experiments done with the general circulation model CCSM3 (Collins et al., 2006; Otto-Bliesner et al., 2006; Yeager et al., 2006), an Earth-system model with coupled atmosphere-ocean-sea ice-land dynamics, and including a dynamic global vegetation module (Fig. 4.2, see Appendix S4.2). CCSM3's horizontal resolution is ~ 3.75° for the atmosphere and ~ 3° for the ocean (Collins et al., 2006).

TraCE-21ka simulations accurately reproduce major climatic features associated with the most recent deglaciation event, and recreate present-day climate patterns (He, 2011; Fordham et al., 2017), with verified hindcast skills such the southward displacement of the inter-tropical convergence zone during Heinrich Stadial 1 (Portilho-Ramos et al., 2017). These simulations were parametrised with several transient forcings including orbitally forced solar radiation changes and changes in the atmospheric concentrations of long-lived greenhouse gases (carbon dioxide, methane, nitrous oxide), and changes in ice sheet volume and topography, as well as freshwater flux (several ocean locations and volumes; see Appendix S4.2).

In TraCE-21ka experiments (He, 2011), the 18,500 BP simulation represents the onset of deglaciation, corresponding to a moderate meltwater discharge into the Atlantic

Ocean (3 metres of equivalent sea-level rise per thousand years 3 m kyr^{-1}; Appendix S4.2.5) associated with an Atlantic meridional overturning circulation comparable to the present (~ 11 – 12 million m^3 sec^{-1}). The 15,000 BP and 12,000 BP experiments both represent periods of intensive deglaciation associated with high Northern Hemisphere meltwater discharge into the Atlantic Ocean (15 and 12 metres of equivalent sea-level rise per thousand years respectively; Appendix S4.2.5), and a slow-down of the Atlantic meridional overturning circulation (~ 4 million m^3 sec^{-1}). The Atlantic meridional overturning circulation then gradually increased until the mid-Holocene to reach its present-day state (~ 11 million m^3 sec^{-1}; Appendix S4.2.5) due to the gradual decrease of the intensity of deglaciation and associated meltwater discharge (Appendix S4.2.5).

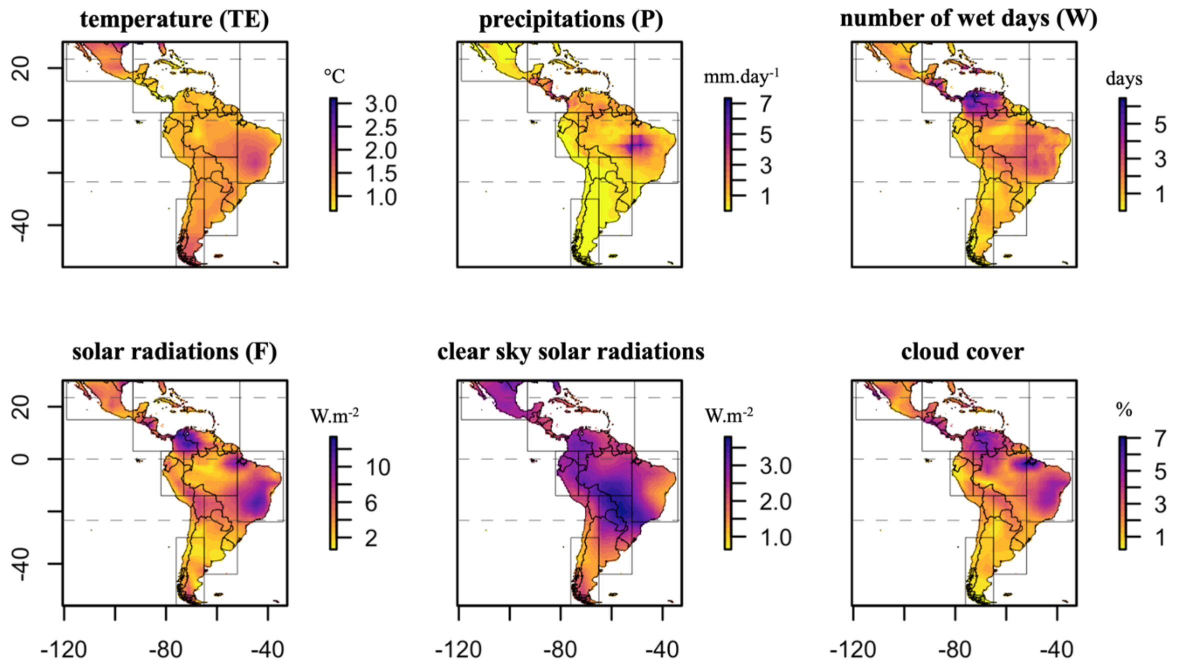

Figure 4.2. Input climate data used in this study, expressed as variation (standard deviation) across the seven simulations (standard deviation) at a resolution of 0.5° × 0.5° degree. *Input data derived from TraCE-21ka (He, 2011) and prepared using the procedure developed by Traylor (2021). For each grid cell, solar radiation was calculated based on cloud cover percentage, clear sky solar radiation, and cloudy sky solar radiation.*

I have improved the realism of the climate inputs by comparing them to observed modern data. Climate models including CCSM3 are biased compared to observations, and their outputs must be debiased prior to being used to hindcast the effect of climate change on biodiversity (He, 2011; Lorenz et al., 2016). For each grid cell, I used the procedure developed by Traylor (2021) for debiasing TraCE-21ka climate data for each input variable (i.e., temperature, solar radiation, precipitation), by downscaling them to a resolution of 0.5° × 0.5° (Appendix S4.2.5), and by considering their anomalies with modern climate datasets based on climate station data (i.e., CRUTS 4.01; Harris et al., 2014) from 1900 to 1990 CE. I complemented the average TraCE-21ka monthly precipitation with a metric of daily variability based on modern observations of the standard deviation of monthly precipitation from the CRU-JRA-55 database (Kobayashi et al., 2015; Harada et al., 2016) covering 1958 to 2017 CE. I describe the input data in Appendix S4.2. In addition to climate and atmospheric CO_2 concentrations, the model incorporates the textural characteristics of the soil to represent the water-retention capacity of the soil layer. However, large uncertainties exist regarding the spatial distribution of textural properties of modern soils (Tafasca et al., 2020), and past variations in soil hydraulic properties remain largely unexplored. Due to the lack of past soil texture data, I used soil texture class data from current CRUNCEP records (Viovy, 2018) as inputs across all periods, assuming that the water-holding capacity of the soil layer remained constant over time. This aligns with the assumptions of prior studies that simulated past vegetation change using LPJ-GUESS (e.g., Allen et al., 2010; Huntley et al., 2023).

II.1.2. Model output analyses

Modelling studies generally transcribe vegetation changes via changes in biome distribution (Table 4.1), thus overlooking more subtle and gradual vegetation changes such as tree cover. In contrast to biome distribution, tree cover can be directly measurable in the field or by satellite, and the main trends of past variation in vegetation openness are detectable in the pollen record. For each input and output variable, I did all analyses based on the annual grid cell average of the 100 simulated years for each independent experiment. For each simulation, the sum of the maximum annual leaf area index of the 12 arboreal plant functional types (Appendix S4.1.2, S4.1.3) is converted to total tree foliar projective cover. Applying the Lambert-Beer law (Monsi and Saeki, 1953), the foliar projective cover represents the percentage of ground area covered by (tree) foliage directly above it (Sitch et al., 2003):

$$f_{\text{tree}} = 1 - e^{-kL_{\text{tree}}}$$

where f_{tree} = tree foliar projective cover, k = 0.5 (extinction coefficient), and L_{tree} = leaf area index of trees. This method is inherently biased due to the choice of a unique extinction coefficient (0.5), which thus remains constant through time and space. At equivalent indices of total tree leaf area, higher or lower vegetation stratification is expected to generate lower or higher tree cover, respectively. While stratification might vary strongly among vegetation types, I assumed that this simplification had only a limited effect on local trends of tree cover variations.

For the present-day simulation, I compared the modern simulated percentage of canopy cover to the canopy cover distribution measured from satellite imagery (Hansen et al., 2013). I then compared differences between observed and simulated vegetation with a map of anthropogenic habitat loss derived from Ellis et al., (2021). I assessed tree cover stability through time using the index of total arboreal leaf area and its standard deviation. To do the analyses, I split the Neotropical realm into seven large subregions (Fig. 4.1): Mexican, Caribbean, tropical Andes, Amazon Basin, north-eastern South America (i.e., Cerrado, Caatinga and Atlantic Forest), central South America (e.g., Chaco, Pantanal, southern Atlantic Forest, Pampas), and Patagonia.

For each of the seven subregions, I built generalised least-squares models to determine which predictor among the climate variables (mean annual precipitation, mean annual temperature, mean annual solar radiation, mean annual number of wet days) and atmospheric CO_2 concentration best described the change in tree cover over time. I first computed and compared the Akaike's information criterion weights (corrected for small sample size: $w\text{AIC}_c$; Burnham and Anderson, 2002) of 32 generalised least-squares models (accounting for spatial autocorrelation) for each region. I selected the top-ranked model based on $w\text{AIC}_c$ from which I evaluated the relative importance of each predictor variable by calculating the information-theoretic evidence ratio of the final model to that without that predictor. Higher evidence ratios indicate stronger evidence for the effect of the removed variable (see Burnham and Anderson, 2002). I did the analyses in R using the packages `nlme` (Pinheiro et al., 2022) and `AICcmodavg` (Mazerolle, 2020).

To assess the sensitivity of Last Glacial Maximum tree cover to simulated fire and low atmospheric CO_2 concentration, I re-ran two simulations for the Last Glacial maximum. In the first simulation, I turned off the fire module in the model. In the second simulation I set the atmospheric CO_2 concentration to the pre-industrial value of 280ppm (instead of ~180 to 190 ppm in the realistic simulation). All other parameters were kept identical to the realistic simulation.

III. RESULTS

III.1 Tree cover response to changes in post-Last Glacial Maximum climate and atmospheric CO_2

Modern simulated tree cover agreed well with satellite imagery data (36.5 % of grid cells with anomalies < 10%, 85.3% with anomalies < 50%; Fig. 4.3a,b). Anomalies are generally inversely proportional to the rate of anthropogenic habitat loss (Fig. 4.3c, d). The simulations tend to underestimate tree cover in preserved landscapes (habitat loss < 25%) while overestimating it in degraded ones (habitat loss > 25%). Tree cover is quasi-systematically overestimated in highly degraded landscapes (habitat loss > 50%) and underestimated in reasonably intact landscapes (habitat loss < 5%) (Fig. 4.3).

Considering the entire Neotropical realm together, the simulations hindcast a steady increase in average tree cover from the Last Glacial Maximum (30%) to the present (44%) (Fig. 4.4, 4.5). In all regions, the simulations predicted lower tree cover during the Last Glacial Maximum compared to the present (Fig. 4.4, 4.5). This overall gradual increase in tree cover was associated to heterogeneous patterns of tree cover and plant functional type distribution changes among regions, in terms of location, magnitude and timing (Fig. 4.4, 4.5; Appendix S4.1.4). The range between minimum and maximum average tree cover across the seven simulations varies considerably across regions, being particularly wide in the Amazon (37%), and narrow in the Mexican region (3%) (Fig. 4.5). While 33% of the grid cells were relatively unstable (SD > 20 %, e.g., Caribbean region, south-eastern Amazon Basin, Cerrado, Patagonian Andes; Fig. 4.6), 17% remained stable (SD < 0.02 %; Fig. 4.6). The most-stable regions correspond either to poorly vegetated regions such as northern Caatinga, northern Venezuela, and

Colombia (regions b, e in Fig. 4.1), or to densely forested regions (i.e., grid cells with > 60% forest cover) such as the southern Atlantic Forest, the north-western Amazon Basin, and tropical forests growing at the lowest altitudes on the slopes of the Andes (regions c, d, e in Fig. 4.1).

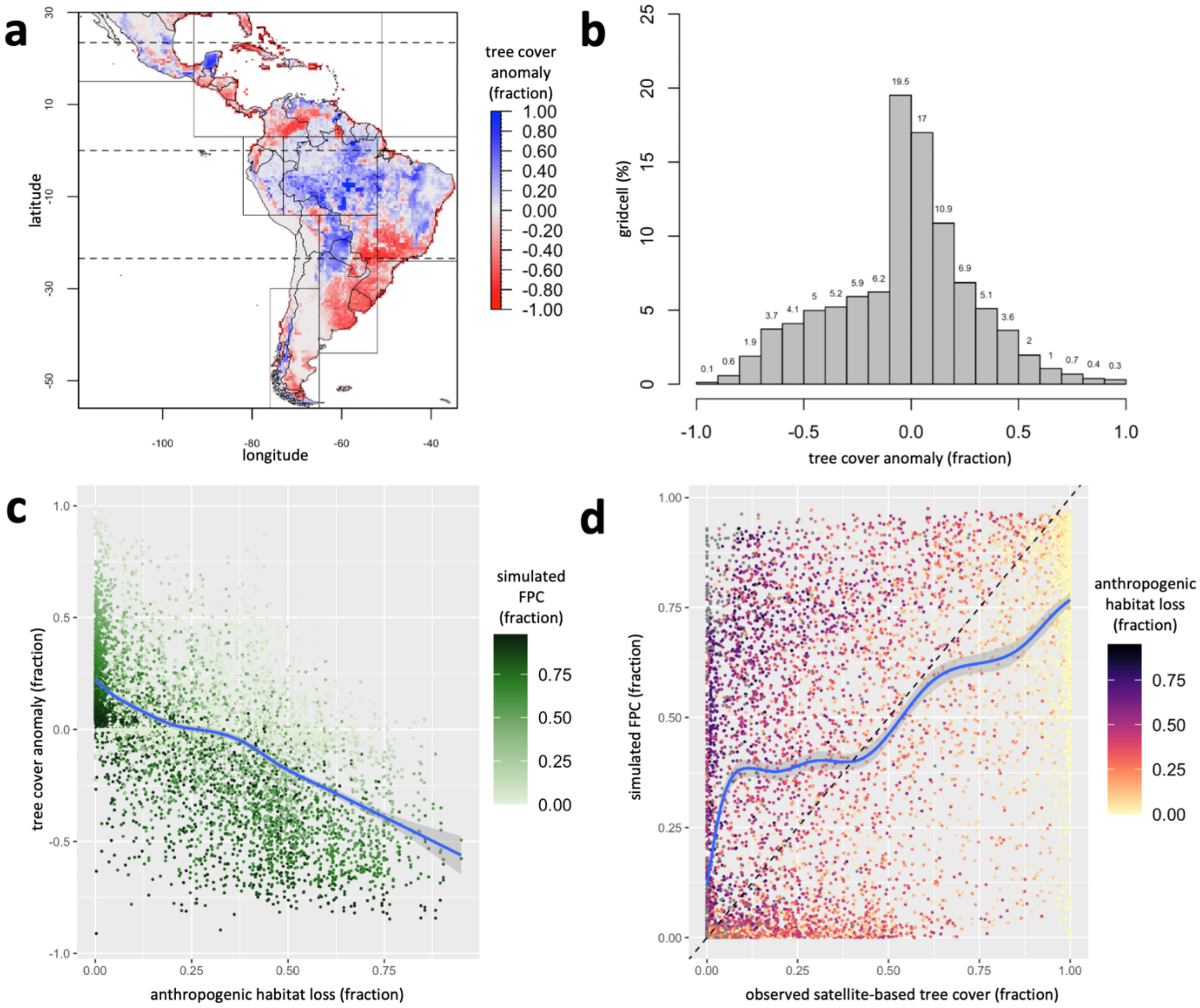

Figure 4.3. Comparison of simulated tree foliar projective cover today (FPC), observed tree cover derived from satellite imagery, and fraction of anthropogenic habitat loss. *(a) spatial distribution of tree-cover anomaly, (b) percentage of simulated grid cells per class of tree-cover anomaly, (c) relationship between tree cover anomaly and fraction of anthropogenic habitat loss, with simulated foliar projective cover indicated for each grid cell, (d) relationship between simulated foliar projective cover and satellite-based fraction of tree cover, with fraction of anthropogenic habitat loss indicated for each grid cell. Tree cover anomaly calculated as the difference between satellite-based tree cover and simulated tree foliar projective cover. Data for the observed tree cover from Hansen et al. (2013). Data for anthropogenic habitat loss from Ellis et al. (2012). Blue curves represent the smoothed relationship obtained from the smooth function in the ggplot2 R package.*

Tree-cover changes were not contemporaneous among all regions (Fig. 4.4). While forests expanded gradually from the Last Glacial Maximum to the present in Patagonia, the Mexican region, and in the tropical Andes, tree cover fluctuated in other regions.

Opposite trends in tree-cover changes among regions mostly occurred during the deglacial period encompassing the Late Pleistocene and early Holocene from 18,500 BP to 9,000 BP (Fig. 4.3, 4.4). Forests expanded rapidly between the Last Glacial Maximum and Heinrich Stadial 1 in tropical areas including the Amazon Basin and north-eastern South America. The simulations subsequently hindcasted periods of temporary forest retraction in several large areas asynchronously. Tree cover decreased most notably in the Caribbean region during Heinrich Stadial 1 and the Younger Dryas, and in central South America during the Younger Dryas and the Greenlandian (see Appendix S4.1 for changes in the distribution of dominant arboreal plant functional types).

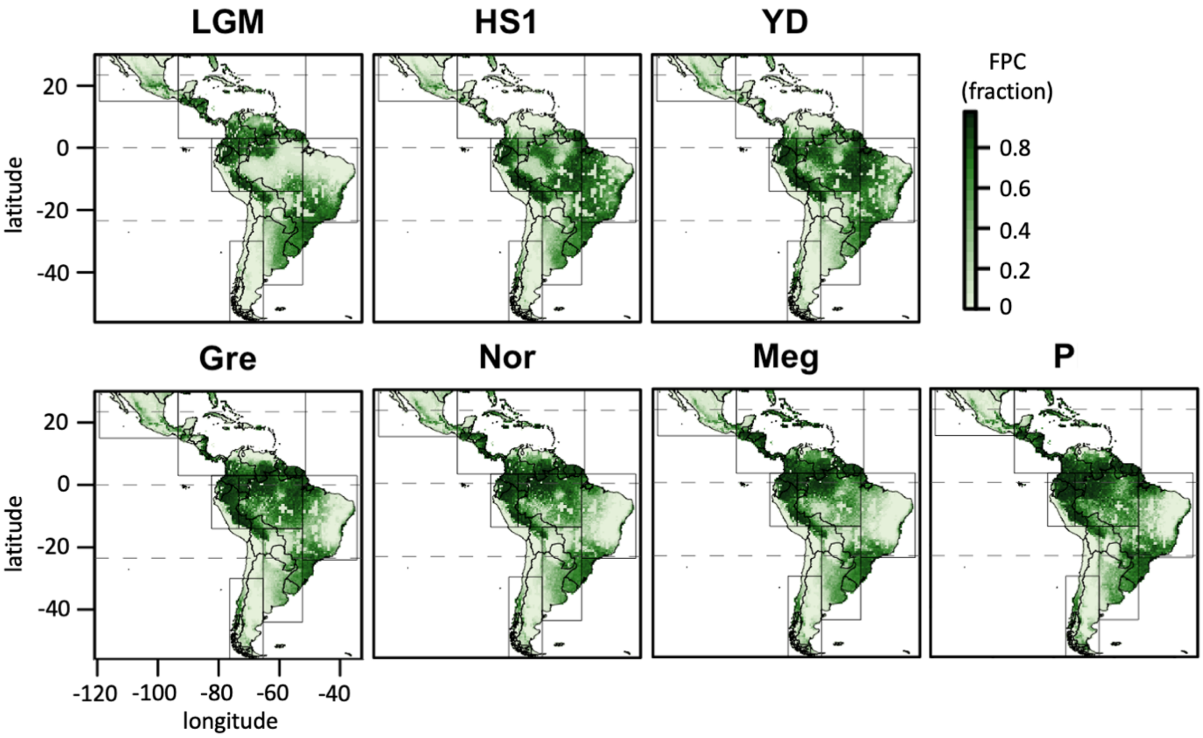

Figure 4.4. Changes in average simulated tree foliar projective cover (FPC) across the simulation experiments. *Snapshots correspond to climate scenarios representing the transition between the Last Glacial Maximum and Heinrich Stadial 1 (LGM: ~18,500 BP), end of Heinrich Stadial 1 (HS1: ~15,000 BP), Younger Dryas (YD: ~12,000 BP), Greenlandian (Gre: early Holocene ~9,000 BP), Northgrippian (Nor: mid-Holocene ~6,000 BP), Meghalayan (Meg: late Holocene ~3,000 BP), and the present (P: 1951 – 1990 CE). Foliar projective cover values represent fractions of ground cover. Squares delimit the seven regions examined.*

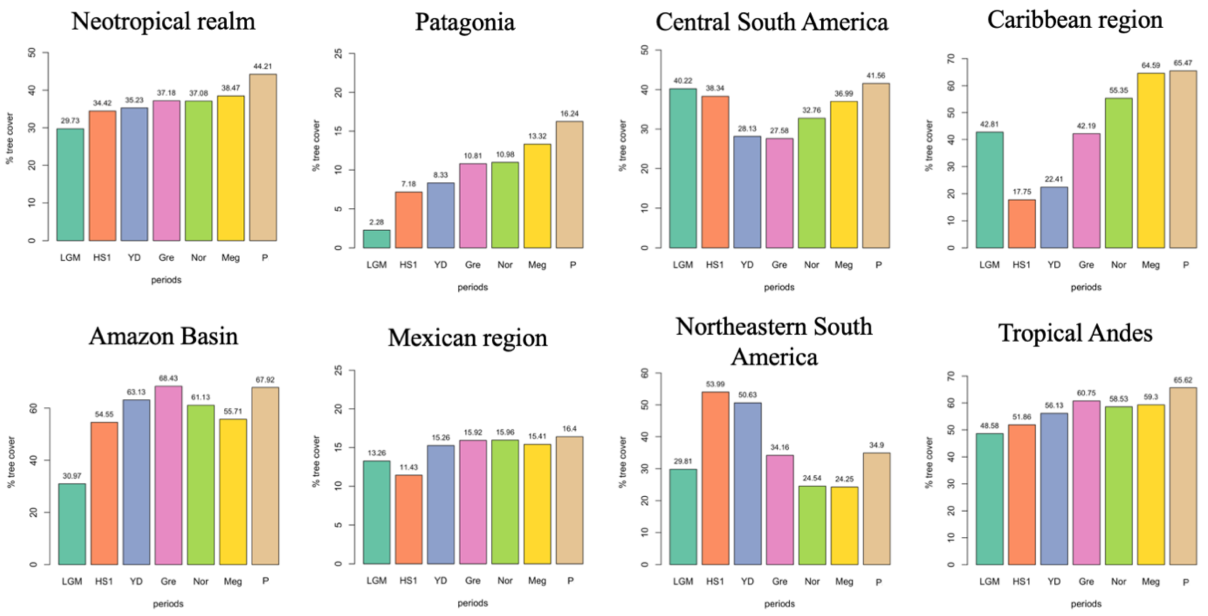

Figure 4.5. Simulated changes in forest-cover changes in the seven sub-regions and the Neotropical realm from 18,500 BP to the present. *Snapshots correspond to the transition between the Last Glacial Maximum and Heinrich event 1 (LGM: 18,500 – 18,400 BP), end of Heinrich Stadial 1 (HS1: 15,000 – 14,900 BP), Younger Dryas (YD: 12,000-11,900 BP), Greenlandian (Gre: 9,000 – 8,900 BP), Northgrippian (Nor: 6,100 – 6,000 BP), Meghalayan (Meg: 3,000 – 2,900 BP), and the present (P: 1950 – 1990 CE).*

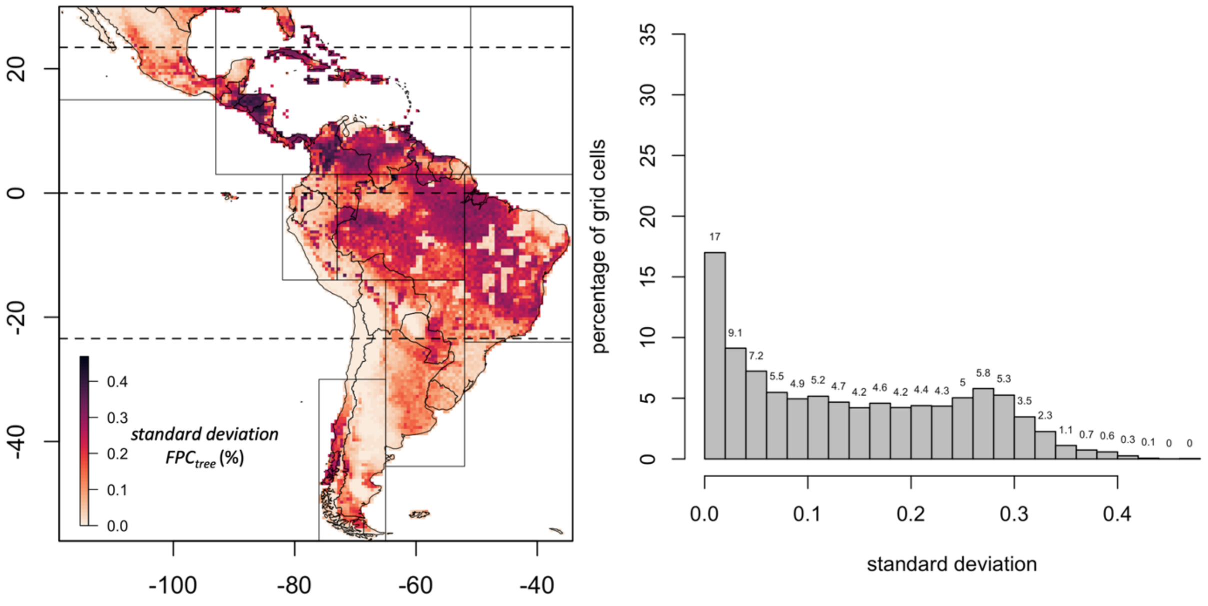

Figure 4.6. Standard deviation of post-Last Glacial Maximum tree-cover across the Neotropics. *(a) spatial distribution of the standard deviation of tree cover, (b) percentage of simulated grid cells per class of tree-cover standard deviation.*

III.2. Main drivers of post-Last Glacial Maximum tree cover changes

In all regions, the top-ranked generalised least-squares model to explain tree cover included the five input variables (precipitation, temperature, number of wet days, atmospheric CO_2 concentration, solar radiation), except for the Mexican region that does not include solar radiation. Precipitation was strongest driver of tree cover in four of seven regions (Caribbean and Mexican regions, north-eastern South America, tropical Andes), and scores close to the top-ranked driver in two others (Amazon Basin and central South America) (Fig. 4.7). In contrast, there is stronger evidence in Patagonia for the effect of temperature than any other explanatory variable, and for solar radiation in the Amazon. In addition, there tended to be stronger support for atmospheric CO_2 concentration in tropical and subtropical regions (central South America, Caribbean, Amazon, north-eastern South America) compared to temperate regions (tropical Andes excepted). There was stronger support for a temperature effect in subtropical and temperate regions (Patagonia, central South America, Mexican region) compared to tropical regions, and stronger relative support for solar radiation in tropical regions

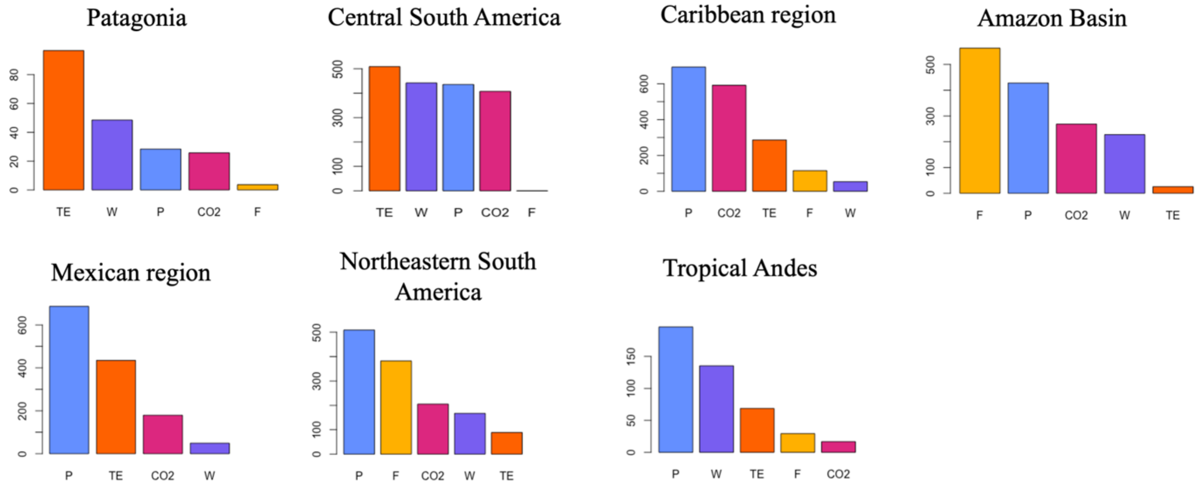

Figure 4.7. Evidence ratio of climate variables in the top-ranked model for each study region to explain changes in the standard deviation of tree foliar projective cover (FPC) across the seven simulation experiments, as derived from generalised least-squares models. *F = solar radiation; P = annual precipitation; D = length of dry season; T = temperature; CO2 = atmospheric* CO_2 *concentration. The evidence ratio measures the strength of evidence for each variable based on the ratio of Akaike's information criterion weights between the top-ranked model and the model without that variable.*

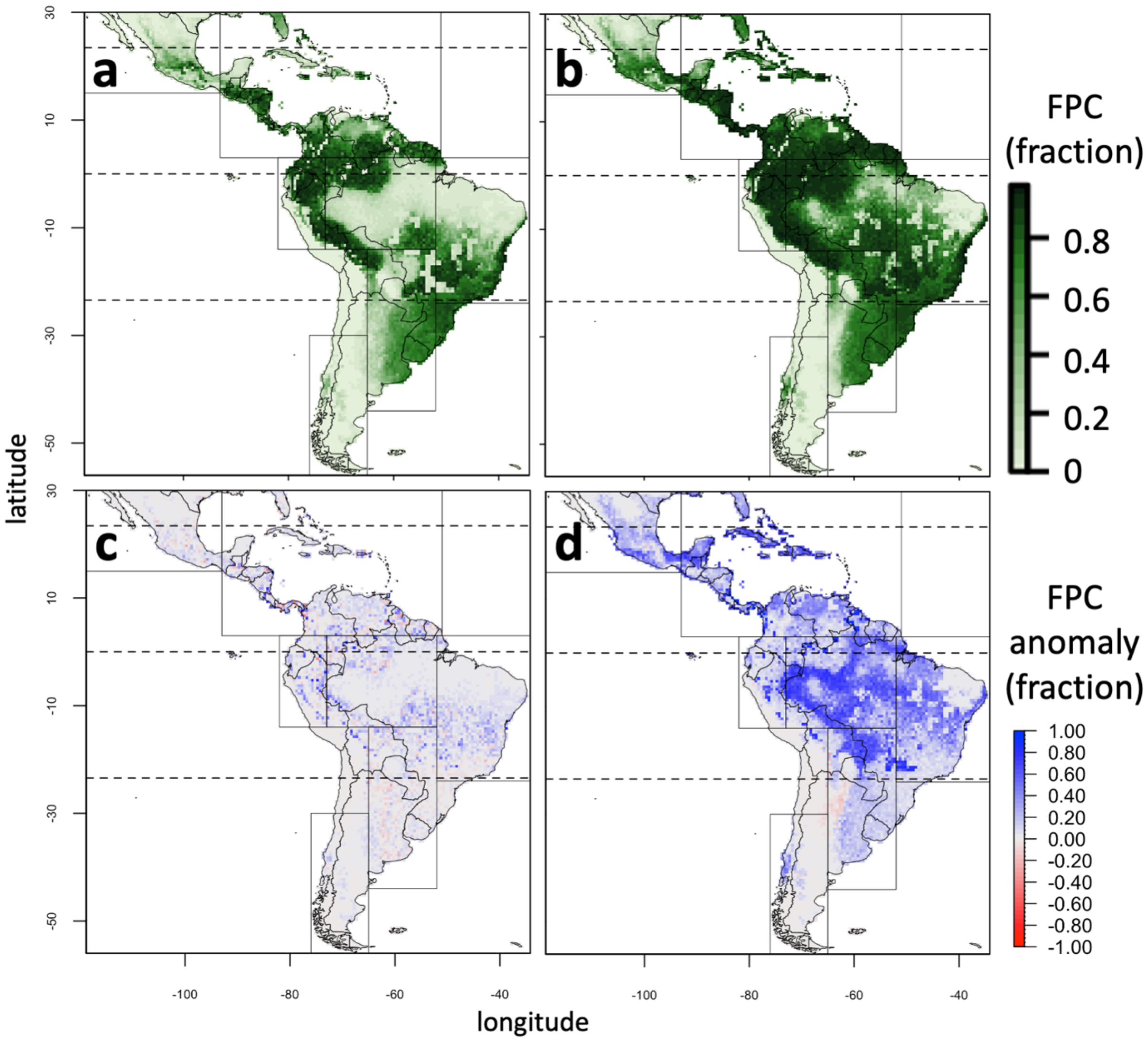

Figure 4.8. Sensitivity of the simulated tree cover (FPC) to changes in model parameters in the Last Glacial Maximum experiment (18,500 BP). *Top maps represent simulated tree cover (a) without simulated fire, and (b) with atmospheric CO_2 concentration set to pre-industrial levels (280 ppm). Bottom maps (c) and (d) respectively represent tree cover (FPC) anomalies between these two simulations and the reference Last Glacial Maximum experiments.*

(Amazon, north-eastern South America) than in subtropical and temperate regions (again, tropical Andes excepted). All details regarding the generalised least-squares models are available in Appendix S4.4.

Turning off fire had a very limited effect on Last Glacial Maximum tree cover, with most effect occurring in the already forested areas (Fig. 4.8a,c). Setting atmospheric CO_2 concentration to pre-industrial levels had a very strong effect on Last Glacial Maximum tree cover especially in the Amazon Basin (Fig. 4.8b,d). There, tree cover increased sharply in areas that were almost treeless in the realistic Last Glacial Maximum simulation. Most grid cells of the Amazon Basin that were treeless gained more than 50% of tree cover, sometimes reaching values close to 100% increase.

IV. DISCUSSION

IV.1. Causes of anomalies in modern simulations

Negative anomalies (lower tree cover than predicted) are largely explained by modern human land-use and therefore probably reflect human-induced forest loss rather than competition between herbaceous and arboreal vegetation. Such anomalies are often consistent with evidence of recent or past deforestation for cultivation, pastures, and urban areas, which I did not consider in the simulations. As evidence, satellite-based measurements of forest loss from the 21st Century highlight ongoing intense deforestation in the south-eastern Amazon Basin and Cerrado (Hansen et al., 2013). Also, historical and palaeo-environment data suggest widespread deforestation in most of the regions where I detected negative anomalies, as in the Atlantic Forest (Behling, 1995), or in Patagonia where the spread of invasive exotic plants indicate increasing grazing pressure (e.g., Mancini et al., 2005; Moreno et al., 2018; Nanavati et al., 2019). In addition to deforestation, anomalies occurring in fire-dependent ecosystems such as the Llanos and the Pampas (Hardesty et al., 2005) reflect the inability of the model to simulate human-ignited and large natural fires (Thonicke et al., 2001).

Several factors that are insufficiently (or even not at all) accounted for in the model could explain the observed tree-cover anomalies, including an inadequate representation of the soil properties or the omission of the impact of large herbivores. First, the lack of data on changes in soil texture, which control water-retention capacity, led me to assume a constant soil water capacity since the Last Glacial Maximum. This is a strong assumption because variation in the intensity of weathering, driven by various environmental changes such as climate and vegetation flux since the Last Glacial Maximum could have affected soil texture. Such soil changes would have more pronounced effects in water-sensitive ecosystems, *i.e.*, during drier periods such as the Last Glacial Maximum, and in regions where water is limiting (e.g., dry diagonals). Second, the model simplistically represents soil properties. Even though these properties can explain some regional difference in vegetation at such as in the Cerrado (Lopes and Cox, 1977), this simplification might prevent the capture of more local vegetation changes. Last, the model does not account for the ecological engineering role of large herbivores (e.g., limiting the development of woody vegetation, soil fertilisation) potentially causing additional discrepancies (Jones et al., 1994; Forbes et al., 2019).

IV.2. Comparison to palaeo-vegetation records

The simulations show a steady increase of the average potential tree cover from the Last Glacial Maximum (30%) to the present (44%) in the Neotropical realm. This increase was associated with heterogeneous patterns of tree-cover changes among regions (Fig. 4.4, 4.5), while about one-third of the simulated grid cells remained relatively stable (Fig. 4.6). These simulated changes in tree cover are generally consistent with the main trends of vegetation changes deduced from palaeo-environment records (Fig. 4.1; Appendix S4.5) and palaeo-vegetation simulations (Table 4.1). Below I compare simulated tree cover with the palaeo-vegetation records in each region.

Patagonia — The extremely low simulated forest cover during the Last Glacial Maximum (i.e., 2.28%, Fig. 4.5) is consistent with hindcasts from previous studies (Table 4.1; Prentice et al., 1993; Werner et al., 2018; Allen et al., 2020). The many and widely distributed palaeo-environment records in the Patagonian Andes facilitate comparisons for the deglacial period and Holocene (Fig. 4.1). The tree fractions of most Patagonian pollen records are dominated today by *Nothofagus* pollen (see Chapter 3), a functionally diverse genus of broadleaved trees typical of the Patagonian forests and represented here by temperate and boreal broadleaved tree plant functional types (Appendix S4.1). In the Patagonian Andes, the simulated and isolated patches of high tree cover ~ 40° S during the Last Glacial Maximum are consistent with abundant *Nothofagus* pollen (Moreno et al., 2018), and sparse *Nothofagus* pollen in other sites located ~ 43 – 45° S (Iglesias et al., 2014; Pesce and Moreno, 2014; Nanavati et al., 2019). The subsequent gradual southward expansion of forests I simulated also corroborates palaeo-vegetation records indicating the primary establishment of dense forests in the northern Patagonian Andes

(~ 43 – 45° S) from ~17,000 (Pesce and Moreno, 2014) to 11,500 BP (Iglesias et al., 2016), and to the secondary establishment in areas located more in the south of Patagonia (~ 47 – 55° S) in the early Holocene between 11,800 and 7,500 BP (Moore, 1978; Heusser et al., 1994; Markgraf et al., 2007; Moreno et al., 2009; Markgraf and Huber, 2010; Fontana and Bennett, 2012; Villa-Martínez et al., 2012; Musotto et al., 2017; McCulloch et al., 2021). While the majority palaeo-vegetation records originate from the Andes region, where tree cover is the most unstable (Figs. 4.1, 4.4, 4.6), the simulations show that tree cover in the vast extra-Andean zones (regions underrepresented in the fossil records) remained consistently low.

Tropical Andes — The gradual expansion of simulated forests (Fig. 4.4, 4.5) is consistent with the trends observed in the fossil record. Model outputs agree with pollen and phytolith records indicating the gradual upward expansion of montane forests from continuously forested areas at the lowest altitudes (< 1400 m above sea level; Urrego et al., 2010; Montoya et al., 2018) to higher altitudes mainly during the Holocene (> 4000 m in Ecuador, Hansen et al., 2003). Although the palaeo-vegetation records are confined to the northern part of the region (Fig. 4.1), the simulations show that the forests also expanded upward in the Peruvian Andes located further to the south.

Amazon Basin — Simulations indicate that most of the Amazon Basin was characterised by open vegetation during the Last Glacial Maximum, despite large and persisting forest in the north-western part of the Basin (Fig. 4.4). These trends generally agree with pollen data also showing some changes in forest floristic composition in stable areas (van der Hammen and Absy, 1994; Colinvaux et al., 1996; Bush et al., 2004, 2011; D'Apolito et al., 2013; Wang et al., 2017). However, most palaeo-vegetation records are located on the edges of this region (Fig. 4.1), thus preventing the description of forest-cover changes in the core of the Basin. Most published palaeo-vegetation simulations also predict similar trends, although the spatial extent of tropical forest during the Last Glacial Maximum varies depending on the vegetation model, the climate inputs, and the criteria used to define tropical biomes (Table 4.1).

Caribbean region and north-western South America — The Caribbean (Northern Hemisphere) and north-western South America (Southern Hemisphere) regions show opposite trends during the deglacial period (Fig. 4.4, 4.5). The temporary southward displacement of tropical and subtropical forests during simulations of Heinrich Stadial 1 and the Younger Dryas is consistent with most observations from the palaeo-vegetation record. In the Northern Hemisphere (Caribbean region), the few arboreal taxa within the palynological record suggest the dominance of open landscapes during these two periods, with modern vegetation characterised by higher tree cover generally establishing from the early Holocene (Leyden et al., 1993; Salgado-Labouriau, 1997; Behling and Hooghiemstra, 1999; Rull et al., 2015). However, the simulated presence of forests in the region during the Last Glacial Maximum is not documented in the vegetation fossil record. In the Southern Hemisphere, pollen records from north-western South America are rare, especially between 5 – 15° S (Flantua et al., 2015; Ledru et al., 2016). Simultaneous to the retraction of tropical forest in the Northern Hemisphere, the simulated temporary expansion of forests in the core of the region (i.e., Cerrado) during Heinrich Stadial 1 and the Younger Dryas is consistent with analyses suggesting recent connections between the Amazon and Atlantic rain forests, especially during the deglacial periods, based on pollen records, speleothems, and the modern occurrence of phylogenetically related species in both forests (Ledru et al., 2016; Thomé et al., 2016; Cassino et al., 2020). The simulated stability of the southern part of the Atlantic Forest from the Last Glacial Maximum to the Meghalayan is consistent with abundant tree pollen persisting until European arrival (Ledru et al., 2016; Francisquini et al., 2020). Finally, the simulated absence of forests during the Last Glacial Maximum in the north of north-western South America could indicate forest cover instability in the palaeo-environment record from the Late Pleistocene (Absy et al.,1991; Sifeddine et al., 2001), but these records are poorly constrained chronologically.

Central South America — In the far north of central South America in the Pantanal, palaeo-vegetation records from Laguna La Gaiba indicate the expansion of tropical forest during the deglacial period (Whitney et al., 2011), consistent with the simulations. Most other palaeo-environment records occur in the Pampas (southeast of the study region), an area dedicated today to intensive cropping and cattle grazing. Pollen and faunal records from Uruguay and the Argentine Pampas indicate that the area was continuously covered with open, grass-dominated vegetation from the Last Glacial Maximum to today (Prieto, 2000; Mourelle et al., 2017). On the contrary, the simulations predict continuous dense forests in this region, dominated by temperate broadleaved evergreen trees (Fig. 4.4; see Appendix S4.1.4). The simulations thus show that this area could climatically support forests as suggested by previous simulations of global biome distribution based on modern climate, predicting the dominance of angiosperm trees (Bond and keeley, 2005) or temperate broadleaved evergreen forests (Allen et al., 2020) according to the biome definition they used (see also Chapter 2). This marked difference between fossil records and climate-based simulations indicates that climate is not the main driver of tree cover in the Pampas. The absence of trees in Pampas grasslands today is debated, suggesting that it arises from multiple interacting factors not considered in the model, including woody biomass consumption by fire and herbivores (e.g., Bond and Keeley, 2005; Allen et al., 2020), over-competition by resident grasses, or low dispersal of tree seeds (Chaneton et al., 2012).

IV.3. Main climate drivers of tree cover changes

As suggested by the fossil record and other models, tree-cover changes are generally associated with variation in precipitation and moisture availability, with lower moisture maintaining lower tree cover, and higher moisture providing the conditions necessary for higher tree cover. This is particularly true in the tropical and subtropical regions (Caribbean, Mexican region, Amazon Basin, north-eastern South America, tropical Andes). The good fit between simulations and palaeo-vegetation records regarding tropical forest contraction in the Northern Hemisphere and expansion in the Southern Hemisphere during Heinrich Stadial 1 and the Younger Dryas confirms the strong implication of southward displacement of the inter-tropical convergence zone, one of the major components of the South American summer monsoon, due to weaker Atlantic meridional overturning circulation inferred from multiple sedimentary and speleothem profiles (e.g., Maslin et al., 2011; Stríkis et al., 2015; Bahr et al., 2018). This result has implications for the future, because climate change could slow Atlantic meridional overturning circulation, with similar consequences on the position of the inter-tropical convergence zone (Jackson et al., 2015).

The difference in the strength of evidence between precipitation and other drivers is not sufficiently high to conclude that tree cover is mostly driven by variation in precipitation, adding more complexity to the general view that most vegetation changes were driven by variation in moisture availability. The results highlight the latitudinal pattern of differential conditions affecting forest cover, with variation in CO_2 concentration having a greater effect on forest cover in lower latitudes (Caribbean, central South America, Amazon Basin, north-eastern South America), while the effect of temperature variation becomes dominant at higher latitudes (e.g., Patagonia). For Patagonia, the results do not agree with most other studies suggesting that *Nothofagus* forests expanded in the Patagonian Andes and south-eastern Patagonia after the southward shift of the southern westerly winds (a classic element of glacial termination; Denton et al., 2009) that affected the precipitation/evaporation balance (Mancini et al., 2005; Markgraf et al., 2007; de Porras et al., 2012; Villa-Martínez et al., 2012; Pesce and Moreno, 2014; Iglesias et al., 2016; Moreno et al., 2018; Nanavati et al., 2019; McCulloch et al., 2021). In the Amazon Basin, the strong support for variation in solar radiation driving forest cover suggests the strong effect of evapotranspiration on tree cover in the region, but this result remains hypothetical because I could not compare it to relevant palaeo-environment records.

The small impact of turning off fire on the simulated Last Glacial Maximum tree cover (Fig. 4.8) suggests that fire might have not been a strong driver of the pattern of tree cover observed at the Last Glacial Maximum. Our results challenge the prevailing view that fire strongly affects the modern distribution of forests (e.g., Bond and Keeley, 2005; Bond, 2010; van Wees et al., 2021). This divergence can be attributed to the variation in vegetation types and the conditions (e.g., human activities, climate) conducive to fires between those periods. First, climate and vegetation were less favourable for fire during the Last Glacial Maximum than they are today (Fig. 4.4). Climate conditions during the Last Glacial Maximum led to generally more open ecosystems characterised by a lower biomass, thus decreasing fuel availability, diminishing the potential impact of fire on the landscape. Turning off fire in the simulations generally favoured higher tree cover during the Last Glacial Maximum, especially in areas with moderate tree cover (Fig. 4.8a,c) while having a minimal effect in areas initially characterised by low tree cover. These results are consistent with studies showing that mixed tree and grassland ecosystems such as savannas are more sensitive to fire than more open ecosystems (Lasslop et al., 2020). For example, present-day wooded grasslands in Africa and South America could transition to forests in the absence of fire (Bond et al., 2005). Second, human activities are a major source of fire ignition (Bowman et al., 2009). In the Neotropical realm, the densification of human populations and their fire-related activities only took place after the Last Glacial Maximum (Goldberg et al., 2016), and their major influence on fire regime state changes in the last 12,500 years most-likely only started at the end of the Holocene (Sayedi et al., 2024), thus considerably limiting the possible ignition sources compared to modern time.

In contrast, experimentally higher atmospheric CO_2 concentrations in the Last Glacial Maximum promoted sharply higher simulated tree cover in tropical areas including in the Amazon Basin, suggesting that the low atmospheric CO_2 characterising the Last Glacial Maximum could have limited the growth of tropical forests, potentially explaining the low tree cover observed in at least some parts of the Amazon Basin in the palaeo-vegetation records (van der Hammen and Absy, 1994; Colinvaux et al., 1996; Bush et al., 2004, 2011; D'Apolito et al., 2013; Wang et al., 2017). Integrating these insights with the results from the generalised least-squares models, I suggest that reduced precipitations and increased solar radiations led to drier conditions in the south and east of the Amazon Basin during the Last Glacial Maximum, hindering the establishment of forests under low atmospheric CO_2 concentrations. However, in scenarios of higher atmospheric CO_2 concentration, the possibility of forest expansion into previously unforested areas of the Amazon Basin emerges (Fig. 4.8). This CO_2 fertilisation effect primarily influenced regions already covered by forests, but its impact was more prominent in the drier areas where tree cover was initially sparse.

V. CONCLUSIONS

Understanding how tree cover responds to variation in climate and atmospheric CO_2 concentration is fundamental for predicting future vegetation changes. The post-Last

Glacial Maximum period offers a wide range of configurations providing a means to test the effect of climate change on tree cover by comparing model outputs to palaeo-environment records. Using palaeo-climate scenarios as realistic experiments of model sensitivity, I demonstrated that tree cover was, as expected, closely related to changes in precipitation regimes. However, I could not identify a single variable as the 'main' driver of tree cover changes across all regions. Simulation results mainly indicate the potential widespread tree cover increasing during the deglacial period, associated with massive vegetation turnover in the tropics. The simulations support the hypotheses that large parts of the Amazon Basin were covered by open, savanna-like vegetation during the Last Glacial Maximum due to variation in the South American summer monsoon, and that the Amazon and Atlantic forests were connected during Heinrich Stadial 1 and the Younger Dryas from the southward displacement of the inter-tropical convergence zone. The model does not include vegetation feedbacks on climate, refined parameterisation of plant functional types based on local vegetation, the effect of human activities, nor the possibility of large herbivores maintaining open landscapes prior to their extinction. While I did estimate the partial effect of modern land use by comparing simulations to satellite data, quantifying the effect of human activities on tree cover after the post-Last Glacial Maximum human expansion remains hypothetical. Finally, the results suggest the potential future direction of tree-cover changes. For example, the expected increases in atmospheric CO_2 and tropical precipitation could theoretically favour higher tree cover in sensitive regions like the Caribbean and central South America. However, I also demonstrated the strong and widespread effect of deforestation in explaining modern tree cover in these regions, highlighting that human endeavour could limit or even reverse the response of vegetation to climate change.

CHAPTER 5

CHALLENGING AGREEMENT BETWEEN SIMULATED POST-LAST GLACIAL MAXIMUM BIOME CHANGES AND POLLEN-BASED BIOME RECONSTRUCTION IN THE NEOTROPICS

ABSTRACT

Reconstructions of palaeo-vegetation changes provide a good overview of the changes in ecosystem composition and functioning as a whole. Reconstructing past vegetation relies on the combination of multiple independent methods including the analysis of pollen records and vegetation modelling. However, vegetation modelling and the analysis of pollen records differ conceptually in the way they describe vegetation, and both are associated with multiple biases. In this study, I aim to test if the vegetation simulations agree with pollen records at local scales and at the biome level using a site-by-site comparison approach focusing on the Neotropical realm. To that aim, I mapped post-Last Glacial Maximum biome distributions in the Neotropical realm based on simulated vegetation cover outputs from a Dynamic Global Vegetation Model (LPJ-GUESS) coupled to palaeo-climate experiments from TraCE-21ka. I then compared simulated biome maps with biomised pollen records of Latin America from the BIOME 6000 project. I built biome definitions based on combinations of pollen-equivalent plant functional types and implemented them in the model by comparison with the biome map associated with the study. To assess the potential of such an approach, I compared simulated and pollen-based biomes by focusing first on biome identity at a given period, then on biome change between two periods. I also compared the two products by classifying biomes into three tree-cover classes. The simulated vegetation for the Last Glacial Maximum depicts a landscape dominated by more open environments compared to the mid-Holocene and the present. During that period, deserts and tropical dry forests covered greater areas, whereas the expanse of other tropical forests was diminished. In contrast to the current distribution, large areas of the Southern Cone were characterised by deserts, and the South-Eastern Amazon Basin predominantly featured tropical dry forests. Meanwhile, regions like the Cerrado were notable for their abundance of tropical rainforests and warm temperate rainforests. Comparisons of simulated biome distribution and pollen-based biomes show moderate agreement increasing towards most recent periods. Site agreement in biome assignment at present (41%), the mid-Holocene (26%) and the Last Glacial Maximum (19 %). The comparison based on the tree-cover classes of biomes led to an increase of 15 to 20 % of agreement. No biome shows high agreement, but forested biomes were generally better predicted than open biomes. In the set of sites compared, the model tended to predict more tropical rainforests and warm temperate rainforests, tropical dry forests, and deserts, while predicting fewer cool grasslands and cool grass shrublands, cool temperate forests, steppes, and tropical seasonal forests than pollen-based biome assignments. This poor agreement may suggest the prevalence of ecological factors not considered in the model, such as megafauna or human land-use, that may affect both the modern calibration and past vegetation hindcasts. However, several steps may also be responsible for the observed disagreement, such as unperfect plant functional type equivalencies, or the absence of a numeric and georeferenced biome calibration map that led us to calibrate biomes by visual comparison. Overall, the results show that palaeo-vegetation simulations moderately agree with pollen-based biome reconstructions at local scale. While such results highlight the need for better model parametrisation, better pollen-based biome assignment and biome definition refinement, the numerous limits and bias associated with such a comparison also demonstrate the difficulties to map the actual past biome changes, as well as the need for more interdisciplinary studies.

KEY WORDS: DGVM, computer modelling, forest, leaf area index, pollen biomisation

I. INTRODUCTION

Vegetation offers important insights into how ecosystems respond to climate change because it is one of the main drivers of ecosystem composition, function, and resilience, and because vegetation communities are more representative of local climate change than most animal communities (Wing and Harrington, 2001; Tews et al., 2004; Novotny, 2006; Chapter 1). Reconstructions of palaeo-vegetation changes thus give a good overview of the changes in ecosystem composition and functioning as a whole. Reconstructing past vegetation relies on the combination of multiple independent methods including the analysis of pollen records and vegetation modelling (see Chapter 2). However, vegetation modelling and the analysis of pollen records differ conceptually in the way they describe vegetation, and both are associated with multiple biases (Chapter 2).

The analysis of pollen records represents vegetation based on the taxonomic composition of the records and on the proportions of the different groups, assuming that the relationship between vegetation and the composition of the pollen rain it produces has remained constant through time (Chapter 2; Chapter 3). Pollen records are often assumed to represent the regional vegetation, but this assumption is undermined by the complexity of the processes shaping the taxonomic composition of the records such as the differences of preservation and dispersal among pollen taxa.

Palaeo-vegetation modelling such as the use of correlative (Leite et al., 2016; Costa et al., 2018; Maksic et al., 2022), process-based (Handiani et al., 2012; Forrest et al., 2015; Werner et al., 2018; Allen et al., 2020; Chapter 4) or equilibrium vegetation (Cowling et al., 2001; Harrison et al., 2003; Marchant et al., 2002, 2004, 2006) models represents the vegetation as it *should be* given a precise set of assumptions embedded in model parameters and inputs, including palaeo-climate, or on the relationships between climate and vegetation (Chapter 2). Vegetation models are thus better designed to test assumptions (for example on climate-vegetation relationships) than to map the "true" past vegetation, so the reliability of their outputs when aiming to map the actual vegetation are open to scrutiny (Chapter 2).

Considering the above-mentioned biases, there is no perfect method to describe the palaeo-vegetation vegetation at regional to global scales, but the analysis of pollen records and vegetation modelling remain two independent methods with different strengths that are often combined to better describe past vegetation changes and investigate the factors driving them (e.g., Marchant et al., 2002, 2004, 2006; Salzmann et al., 2008; Prentice et al., 2011; Maksic et al., 2022 ; Chapter 4). Nonetheless, the conceptual differences between these two methods and their associated biases make their comparison challenging, so expert-based approaches are generally used to design equivalence frameworks (e.g., Marchant et al., 2006; Maksic et al., 2022).

The biome concept (see Mucina, 2019; Chapter 2) is often used as a baseline for data-model comparisons, helping to quantify the rate of agreement and common patterns between the two approaches (e.g., Marchant et al., 2002, 2004, 2006; Maksic et al., 2022). Consequently, past reconstructions of biome changes derived from the analysis of pollen records are an important source to evaluate palaeo-vegetation models. The BIOME 6000 project was designed in the late 1990s to facilitate such palaeo-climate and palaeo-vegetation model validation by providing standardised past biome records (Prentice and Webb III, 1998). For each core site, each pollen taxon is translated into one or more plant functional types (i.e., grouping phylogenetically unrelated taxa sharing similar physiological characteristics; see also Chapter 4), then the biome with the highest affinity with the composition of plant functional types is selected (the biomisation process is described extensively in Prentice and Webb III, 1998). This biomisation technique has been validated with modern pollen data, and biome reconstructions have been done for the Mid-Holocene (~ 6,000 years before present) and the Last Glacial Maximum (~ 18,000 years before present) in most regions of the planet such as Latin America (Marchant et al., 2009), as well as in Africa (Jolly et al., 1998; Elenga et al., 2000), Australia (Pickett et al., 2004), Beringia (Edwards et al., 2000; Bigelow et al., 2003), China (Yu et al., 1998, 2000), Eastern North America (Williams et al., 2000), Eurasia (Tarasov et al., 1998b), Europe (Prentice et al., 1996, 1998; Tarasov et al., 1998b, 1998a; Elenga et al., 2000), Japan (Takahara et al., 2000), and western North America (Thompson and Anderson, 2000).

In Chapter 4, I have compared the main regional trends in post-Last Glacial Maximum tree-cover changes in the Neotropical realm deduced from pollen records (see also Chapter 3) with those simulated with the dynamic global vegetation model LPJ-GUESS (process-based; Smith et al., 2001; Smith et al., 2014) coupled to palaeo-climate data derived from TraCE-21ka, a set of experiments that accurately reproduce major climatic features associated with the most recent deglaciation event, and recreate present-day climate patterns (He, 2011; Fordham et al., 2017). The results of Chapter 4 show that simulations generally agree with the analysis of pollen records at large scales regarding the trends in tree-cover changes. In this Chapter, I aimed to investigate if the same vegetation simulations agree with pollen records at more local scales (i.e., using a site-by-site comparison approach), and at the biome level. I compared simulated biomes with pollen-based biomes to assess the agreement between BIOME6000 reconstructions and model outputs. Comparing simulations of palaeo-vegetation with biomised pollen records first involves calibrating model outputs based on modern biome maps. However, plant functional types and biomes from vegetation models are generally not defined based on the same set of criteria, and model outputs provide only simplistic representations of the vegetation such as the dominant plant functional types representing multiple plant taxa (Chapter 2). I compared the BIOME 6000 biome reconstruction with outputs from the LPJ-GUESS model (see Chapter 4), minimising the above-mentioned biases by deriving biome definition directly from equivalences between modelled and BIOME 6000 plant functional types. I investigated if vegetation simulations agree with pollen-based biome reconstruction at local scale and at the biome level. To that aim, I (1) mapped post-Last Glacial Maximum changes in biome distribution, and (2) compared the simulated biome maps quantitatively to biomised pollen assemblages from the Last Glacial Maximum, mid-Holocene, and the present (Marchant et al., 2009). More specifically, I mapped post-Last Glacial Maximum biome distributions in the Neotropical realm based on simulated vegetation cover outputs from the LPJ-GUESS dynamic global vegetation model coupled to palaeo-climate experiments from TraCE-21ka, Liu et al., 2009; He, 2011; see Chapter 4). I then compared simulated biome maps with biomised pollen records of Latin America from the BIOME 6000 project for the Last Glacial Maximum, the mid-Holocene, and the present (Marchant et al., 2009). I compared the outputs of this data-model comparison using several approaches with various scales of detail, focusing on biome identity, the tree-cover class of biomes, and simulated and observed changes between periods. Coarser classifications are more likely to return similar results, so the less detailed the classification of the entities being compared (i.e., the fewer the categories), the more likely it is that the agreement will be high. Therefore, I hypothesise that the site-by-site agreement between simulated and pollen-based biomes is lower when considering the strict biome identity for a given period than when considering if a biome change occurred between two periods (in particular when the two periods are characterised by strongly different climate contexts such as between the Last Glacial Maximum and the present), and that the agreement is higher when grouping biomes by tree cover (i.e., closed forests, intermediate, or open vegetation). I also hypothesise that palaeo-vegetation simulations reproduce the pollen-based biomes at local scales poorly.

II. METHODS

In this study, I focused on the Neotropical realm, a biogeographical region spanning the southern edge of the USA to Tierra del Fuego in Chile in southernmost South America. Today, the structure of Neotropical vegetation is extremely diverse, including some iconic landscapes such as the Amazon and Atlantic rainforests, the Cerrado, the Venezuelan Llanos, the Argentine Pampas and the *Nothofagus* forests of western Patagonia. In the last ~20,000 years, the Neotropical realm was affected by widespread climate changes, with widespread effects on vegetation and biomes in general. Here, I compared pollen-based biome reconstructions with simulations of the palaeo-vegetation focusing on three time periods, i.e., the end of the Last Glacial Maximum (~21,000–18,000 years before present [BP]), the mid-Holocene (~6,000 BP), and the present.

II.1. Vegetation simulations

II.1.1. Simulating vegetation with LPJ-GUESS

I simulated palaeo-vegetation distribution changes with the mechanistic vegetation model, LPJ-GUESS (Smith et al., 2001, 2014). LPJ-GUESS is a physiology-based mechanistic model that incorporates explicit relationships between environmental conditions and the biophysical and demographic characteristics of vegetation, and it simulates the dynamic of the vegetation and biogeochemical cycles at regional to global scales. LPJ-GUESS takes as input monthly climate data (precipitation, number of wet days, temperature, solar radiation) and annual atmospheric CO_2 concentration to predict various vegetation and environment characteristics, including leaf area index. LPJ-GUESS is a combination of an individual-based model (GUESS models populations such that all individuals are considered explicitly), and a model based on populations of plant functional types (LPJ classifies plants according to their physical and phenological characteristics).

LPJ-GUESS simulates the competition among plant functional types as a result of simulated physiological processes (Smith et al., 2001). I grouped plants with similar functional characteristics into 19 functional types (Table 5.1) assuming that any plant

Table 5.1. List of the plant functional types used in this study.

Acronym	Plant functional type	Life form
BNE	boreal needleleaved evergreen tree	tree
BINE	shade-intolerant boreal needleleaved evergreen tree	tree
BNS	boreal needleleaved summergreen tree	tree
TeNE	temperate needleleaved evergreen tree	tree
TeBS	shade-tolerant temperate broadleaved summergreen tree	tree
IBS	shade-intolerant broadleaved summergreen tree	tree
TeBE	temperate broadleaved evergreen tree	tree
TrBE	tropical broadleaved evergreen tree	tree
TrIBE	tropical broadleaved evergreen tree	tree
TrBR	tropical broadleaved raingreen tree	tree
C3G	C_3 grass	grass
C4G	C_4 grass	grass
TeEsh	temperate evergreen shrub	shrub
TeRSh	temperate raingreen shrub	shrub
TeSSh	temperate raingreen shrub	shrub
TrESh	tropical evergreen shrub	shrub
TrRSh	tropical raingreen shrub	shrub
BESh	boreal evergreen shrub	shrub
BSSh	boreal summergreen shrub	shrub

taxon remains in the same functional group over time. Plant functional types group plants from phylogenetically unrelated taxa but growing in similar environments into a single theoretical taxon, based on the phenomenon of functional convergence stating that several taxa from different phylogenetic background can evolve to share some functional traits to adapt to similar environmental conditions (Prentice and Webb III, 1998). Each plant functional type represents a different combination of functional traits. Model inputs thus include information on plant functional-type traits such as their life form (tree, shrub, grass), bioclimatic range (tropical, temperate, boreal), leaf physiognomy (needleleaf, broadleaf), leaf phenology (evergreen, raingreen, summergreen), body allometry (allocation of the carbon in the plant), tolerance to drought, resistance to fire, maximum crown area, or photosynthetic pathway (C_3 or C_4) (Table 5.2).

Physiological and biogeochemical equations describe processes in the model based on a range of field observations, statistical inferences, and model adjustment validated against empirical observations (Haxeltine and Prentice, 1996; Smith et al., 2001, 2014). Most of the physiological and biogeochemical processes are then

Table 5.2. Plant functional type characteristics used in model simulations. *Characteristics correspond to general traits, temperature ranges, allometric constants describing plant morphology, and life history. Climate classes are associated with differing photosynthesis optimum temperatures and base respiration rates (Smith et al., 2001). Shade tolerance is associated with different regulatory thresholds for recruitment, establishment, and juvenile growth-rates.* $T_{c,min,surv}$ *= minimum coldest-month temperature for survival;* $T_{c,min,est}$ *= minimum coldest-month temperature for establishment;* $T_{c,max,est}$ *= maximum coldest-month temperature for establishment;* $T_{w,min,est}$ *= minimum warmest month mean temperature for establishment (°C);* GDD_5 *= minimum degree-day sum > 5 °C for establishment;* $k_{la:sa}$ *= leaf area to sapwood cross-sectional area ratio;* CA_{max} *= maximum woody crown area;* k_{allom1} *= constant in allometry equations (Smith et al., 2001; higher values = wider crowns);* z_1 *= fraction of roots in first soil layer (remainder allocated to second soil layer);* r_{fire} *= fraction of individuals that survive fire;* $D_{tolerance}$ *= drought sensitivity factor from 0 to 1, where 1 = maximum sensitivity;* a_{leaf} *= leaf longevity;* a_{ind} *= maximum, non-stressed longevity.*

	General traits				temperature range					Allometry constants (PFT morphology)				Life history			
PFT	Climate	Leaf physiognomy	phenology	Shade tolerance	$T_{c,min,surv}$ (°C)	$T_{c,min,est}$ (°C)	$T_{c,max,est}$ (°C)	$T_{w,min,est}$ (°C)	GDD_5 (°C)	k_{la} : sa	CA_{max} (m^2)	k_{allom1}	z_1	r_{fire}	$D_{tolerance}$	A_{leaf} (yr)	A_{ind} (yr)
BNE	boreal	needleleaf	evergreen	tolerant	-31	-30	-1	5	500	5000	50	150	0.6	0.3	0.4	3	500
BINE	boreal	needleleaf	evergreen	intolerant	-31	-30	-1	5	500	5000	50	150	0.6	0.3	0.25	3	500
BNS	boreal	needleleaf	summergreen	intolerant	-1000	-1000	-2	-1000	350	5000	50	150	0.6	0.3	0.2	0.5	300
TeNE	temperate	needleleaf	evergreen	intolerant	-2	-2	10	5	2000	5000	50	150	0.6	0.3	0.3	3	300
TeBS	temperate	broadleaf	summergreen	tolerant	-14	-13	6	5	1100	6000	50	250	0.6	0.1	0.3	0.5	400
IBS	boreal	broadleaf	summergreen	intolerant	-30	-30	7	-1000	350	6000	50	250	0.6	0.1	0.3	0.5	300
TeBE	temperate	broadleaf	evergreen	tolerant	-1	0	18.8	5	2000	6000	50	250	0.6	0.3	0.1	3	300
TrBE	tropical	broadleaf	evergreen	tolerant	15.5	15.5	1000	-1000	0	6000	50	250	0.6	0.1	0.2	2	500
TrIBE	tropical	broadleaf	evergreen	intolerant	15.5	15.5	1000	-1000	0	6000	50	250	0.6	0.1	0.2	2	200
TrBR	tropical	broadleaf	raingreen	intolerant	15.5	15.5	1000	-1000	0	6000	50	250	0.6	0.3	0.1	0.5	400
C3G	-	broadleaf	any	-	-1000	-1000	1000	-1000	0	-	-	-	0.9	0.5	0.01	0.5	-
C4G	-	broadleaf	any	-	15.5	15.5	1000	-1000	0	-	-	-	0.9	0.5	0.01	0.5	-
TeEsh	temperate	broadleaf	evergreen	intolerant	-1000	-1000	1000	-1000	1200	2000	10	100	0.6	0.1	0.1	2	200
TeRSh	temperate	broadleaf	raingreen	intolerant	-1000	-1000	1000	-1000	1200	2000	10	100	0.6	0.4	0.01	1	200
TeSSh	temperate	broadleaf	summergreen	intolerant	-1000	-1000	1000	-1000	1200	2000	10	100	0.6	0.1	0.3	1	100
TrESh	tropical	broadleaf	evergreen	intolerant	15.5	15.5	1000	-1000	0	2000	10	100	0.6	0.1	0.025	2	200
TrRSh	tropical	broadleaf	raingreen	intolerant	15.5	15.5	1000	-1000	0	2000	10	100	0.6	0.1	0.025	1	200
BESh	boreal	broadleaf	evergreen	intolerant	-1000	-1000	-5	-1000	150	2000	10	100	0.6	0.1	0.25	2	200
BSSh	boreal	broadleaf	summergreen	intolerant	-1000	-1000	-5	-1000	150	2000	10	100	0.6	0.1	0.25	0.5	200

simulated at a daily time step (e.g., photosynthesis, respiration, transpiration, soil hydrology, etc.), while individual tree growth and vegetation dynamical processes are modelled annually (Hickler et al., 2004).

LPJ-GUESS returns plant functional type (Tables 5.1 and 5.2) population characteristics for each cell of a landscape grid (following the resolution of the climate data: 0.5° × 0.5° latitude), where biological entities are individuals for trees and shrubs, and populations for graminoids, or one entity for each of the C_3 and C_4 types in a layer of grasses (Smith et al., 2001; Hickler et al., 2004).

LPJ-GUESS has already been used to predict vegetation patterns in northern Eurasia and Chile around the Last Glacial Maximum based on palaeo-climate data derived from HadCM3 and TraCE-21ka (Pope et al., 2000; Liu et al., 2009; Allen et al., 2010; Werner et al., 2018), and to predict changes in biome distribution globally every thousand years since the Last Glacial Maximum based on palaeo-climate data derived from HadCM3 (Pope et al., 2000; Allen et al., 2020), in general visual agreement with palaeo-vegetation records.

I simulated post-Last Glacial Maximum changes in vegetation in the Neotropical realm as 100-year snapshots for the end of Last Glacial Maximum (18,500 – 18,400 BP), the mid-Holocene (6,100 – 6, 000 BP), and the present (1950 – 1990 BP) at a 0.5 × 0.5-degree resolution (see also Chapter 4), with climate data derived mainly from TraCE-21ka (Table 5.3). LPJ-GUESS returns plant functional type population characteristics for each cell of a landscape grid. I calculated the leaf area index for each grid cell by averaging the outcomes from five replicate stands of 0.1 ha. This was designed to mitigate the impact of any stochastically simulated processes including disturbances, plant establishment and mortality. For each replicate stand, I ran the model for 549 simulated years to ensure that the simulated vegetation stabilises and reach 'equilibrium' with the climate conditions. I subsequently ran the model for an additional 100 years to derive the mean leaf area index for each plant functional type.

II.1.2. Palaeo-climate experiments from TraCE-21ka

TraCE-21ka uses the Community Climate System Model ver. 3 (CCSM3; Collins et al., 2006; Otto-Bliesner et al., 2006; Yeager et al., 2006). CCSM3's horizontal resolution is

Table 5.3. TraCE-21ka simulation parameters for the seven selected periods. *BP = before present, CE = common era, NHMW & SHMW= Northern and Southern Hemispheres, respectively; meltwater discharge, expressed in m kyr^{-1} (metres of equivalent sea-level volume per thousand years), with 1 m kyr^{-1} = 0.011 Sv (Sverdrup) representing 3.61×10^{14} m^{3} volume of meltwater in 10^{3} years (He, 2011). AMOC = Atlantic meridional overturning circulation, strength expressed in million m^{3} sec^{-1}.*

Years	**LPJ-GUESS experiment**	**TraCE-21ka experiment**	**TraCE-21ka file prefix**	**NHMW location**	**NHMW (m/kyr)**	**SHMW location**	**SHMW (m/kyr)**	**Geography changes to previous**	**AMOC strength (Million m^{3} sec^{-1})**
18,500-18,400 BP	Last Glacial Maximum (LGM)	TraCE-H1	trace.04	North Atlantic	3				~12
15,000-14,900 BP	Heinrich Stadial 1 (HS1)	TraCE-BA	trace.09	North Atlantic	15				~4
12,000-11,900 BP	Younger Dryas (YD)	TraCE-YD	trace.16	St. Lawrence river	12			Barents Sea and Bering Strait opened	~4
9,000-8,900 BP	Greenlandian (Gre)	TraCE-Holocene	trace.22	Arctic	0.42	Weddell Sea	1.12		~8
				St. Lawrence River	0.42	Ross Sea	1.12		
				Hudson Strait	7.47				
6,100-6,000 BP	Northgrippian (Nor)	TraCE-Holocene	trace.29	Arctic	0.01	Weddell Sea	1.12	Hudson Bay opened, Indonesian Throughflow	~10
				St. Lawrence River	0.01	Ross Sea	1.12		
				Hudson Strait	0.21				
3,000-2900 BP	Meghalayan (Meg)	TraCE-Holocene	trace.33						~11
1950-1990 CE	Present-Day (PD)	TraCE-Holocene	trace.36						~11

~ 3.75° for the atmosphere and ~ 3° for the ocean (Collins et al., 2006). Comparisons with estimations of surface-air temperature from lake sediments and pollen ice cores confirmed the ability of TraCE-21ka to reproduce many major features of the deglacial climate in Greenland, Antarctica, the tropical Pacific, and the Southern Ocean (He, 2011). TraCE-21ka reproduces well the southward displacement of the inter-tropical convergence zone during the Heinrich stadial 1 (post-Last Glacial Maximum iceberg discharge, ~ 19,000 – 14,700 BP; Hodell et al., 2017; Portilho-Ramos et al., 2017), causing changes in precipitation regimes in the tropics with potential strong effect on vegetation (Chapter 3, Chapter 4).

I have improved the realism of the climate inputs by comparing them to observed modern data. Climate models including CCSM3 are biased compared to observations, and their outputs must be debiased prior to being used to hindcast the effect of climate change on biodiversity (He, 2011; Lorenz et al., 2016). I debiased and downscaled the data following the protocol described in Traylor (2021). Following Traylor et al. (2021) (see also Chapter 6), I debiased TraCE-21ka climate data by considering anomalies with modern climate datasets based on climate station data at a 0.5 × 0.5-° latitude resolution (i.e.., CRU TS 4.01 and CRU-JRA-55), thus downscaling the palaeo-climate data to this same resolution. In LPJ-GUESS, monthly precipitations are by default distributed equally among each day of the month, but this could be responsible for over-estimation of the aridity. To correct for this, following Traylor et al. (2021), I added daily rainfall variability to the model input data, based on modern observations of monthly precipitation amount standard deviation gathered in the CRU-JRA-55 database (i.e., 1958 to 2017 CE). In addition to climate and atmospheric CO_2 concentrations, the model incorporates the textural characteristics of the soil to represent the water-retention capacity of the soil layer. However, large uncertainties exist regarding the spatial distribution of textural properties of modern soils (Tafasca et al., 2020), and past variations in soil hydraulic properties remain largely unexplored. Due to the lack of past soil texture data, I used soil texture class data from current CRUNCEP records (Viovy, 2018) as inputs across all periods, assuming that the water-holding capacity of the soil layer remained constant over time. This aligns with the assumptions of prior studies that simulated past vegetation change using LPJ-GUESS (e.g., Allen et al., 2010; Huntley et al., 2023).

II.2. Comparing model outputs with pollen records

I compared model outputs with independent data from pollen records (i.e., not used to build the model). I compared the Last Glacial Maximum and Mid-Holocene outputs with the pollen-based biome record from the BIOME 6000 dataset (Prentice and Webb III, 1998; Marchant et al., 2009).

II.2.1. Defining simulated biome based on equivalencies with pollen-based biomes

I mapped the potential distribution of the biomes simulated with LPG-GUESS by adapting the pollen-based biome classification scheme from Marchant et al. (2009), defining 12 biomes as combinations of 25 pollen plant functional types (Table 5.3, 5.4).

Table 5.4. Equivalencies between pollen and model plant functional types. *Pollen plant functional types (PFT) have been defined in Marchant et al. (2009). LPJ-GUESS plant functional types are described in Table 5.1 and 5.2.*

Name	Growth Habit	climate	Leaf type	Physiology	Pollen PFT	LPJ-GUESS PFT
Tree fern	tree	temperate or tropical	broadleaf	evergreen	tx	TeBE, TrBE
Tropical broad-leaved evergreen tree	tree	tropical	broadleaf	evergreen	Te1	TrBE, TrIBE
Tropical xeric broad-leaved evergreen tree	tree	tropical	broadleaf	evergreen	Te2	TrBE, TrIBE
Tropical rain green tree	tree	tropical	broadleaf	deciduous	Tr1	TrBR
Dry tropical rain green tree	tree	tropical	broadleaf	deciduous	Tr2	TrBR
Tropical xerophytic tree/shrub	tree/shrub	tropical	broadleaf	deciduous	txts	TrRSh (TrESh)
Desert shrub	shrub	tropical	broadleaf	deciduous	ds	TrRSh (TrESh)
Cold temperate conifer	tree	temperate	needleleaf	evergreen	ctc	TeNe
Cool temperate conifer	tree	temperate	needleleaf	evergreen	ctc1	TeNe
Maritime evergreen conifer	tree	temperate	needleleaf	evergreen	ctc2	TeNe
Eurythermic conifer	tree	temperate	needleleaf	evergreen	wtc	TeNe
Temperate evergreen broad-leaved tree	tree	temperate	broadleaf	evergreen	ts1	TeBE (warning: frost tolerant)
Warm temperate evergreen broad-leaved tree	tree	temperate	broadleaf	evergreen	wte	TeBE (warning: frost tolerant)
Temperate summer green tree	tree	boreal	broadleaf	deciduous	ts	IBS, TeBS
Temperate cool deciduous broad-leaved tree	tree	boreal or temperate	broadleaf	deciduous	wte1	IBS, TeBS
Temperate cold-deciduous broad-leaved tree	tree	boreal or temperate	broadleaf	deciduous	wte4	IBS, TeBS
Arctic shrub	shrub	boreal or temperate	broadleaf	deciduous or evergreen	aa	BESh, BSSh,TeESh, TeRSh, TeSSh

This biomisation procedure (derived from Prentice and Webb III, 1998; Marchant et al., 2009) calculates an affinity score of a pollen record with each biome based on the abundance of each pollen taxon. The pollen record is then assigned to the biome with highest affinity score (see Prentice and Webb III, 1998). To make the model outputs directly comparable with maps established by Marchant et al. (2009), I converted model outputs into 9 biomes equivalent to the 12 biomes (3 were merged to others) described in Marchant et al. (2009) as follows:

First, I defined equivalencies between the 25 plant functional types from Marchant et al. (2009) and the 19 simulated plant functional types based on their bioclimatic range and physiological properties (Table 5.4). For example, the desert shrub (ds) from

Marchant et al. (2009) representing woody shrub and cactuses in Mexico and coastal Peru, and grouping the pollen taxa *Agave*, *Atamisquea*, Cactaceae, *Ephedra* and *Monttea aphylla* considered an equivalent to the tropical raingreen shrub (TrRSh) and tropical evergreen shrub (TrESh) from the vegetation model. Similarly, I considered the tropical broad-leaved evergreen tree (Te1) grouping a wide range of pollen taxa such as the Apocynaceae, Arecaceae, Bombacaceae, Melastomatacae, or Rubiaceae, an equivalent in the vegetation model to shade-tolerant and -intolerant tropical broadleaved evergreen tree (TrBE, TrIBE).

Next, I built a biome equivalence table based on similarities among plant functional types defining each biome (Table 5.5). Because the palaeo-vegetation model groups all herbaceous plants into only two plant functional types (i.e., C_4 and C_3 grasses), I only considered woody plant functional types to define biomes. For example, the tropical rainforest biome (TRFO) is represented in Marchant et al. (2009) by a combination of five plant functional types including mangrove (man), tree fern (tx), tropical broad-leaved evergreen tree (Te1), tropical xeric broad-leaved evergreen tree (Te2), and tropical forb (tf) (Table 5.5). In the model, I defined the tropical rainforest biome as the combination of three plant functional types considered equivalent to the above-mentioned pollen plant functional types, i.e., shade-tolerant and -intolerant tropical broadleaved evergreen tree (TrBE, TrIBE), and temperate broadleaved evergreen tree (TeBE). Biome definitions are thus represented by zero (steppe) to seven (cool grass shrublands) plant functional types from the model, with some including only shrubs (i.e., desert, cool grasslands), only trees (i.e., tropical rainforest, tropical seasonal forest, warm temperate forest, warm temperate evergreen broadleaf forest, cool temperate rainforest, warm temperate mixed forest, cool mixed forest), or both (i.e., tropical dry forest, cool grass shrubland). The steppe biome is represented by a single pollen plant functional type in Marchant et al. (2009), the Eurythermic forb, explaining why it is not represented by any woody plant functional type in the model. To limit confusion among biomes, I then grouped biomes sharing a near-common definition (i.e., represented by the almost same combination of plant functional types in the model), leading to a set of nine biomes. Consequently, I grouped cool grass shrublands and cool grasslands (CGSH-CGSS), the tropical rainforests and warm temperate rainforests (TRFO-WTRF), and the

Table 5.5. Biomes as combinations of plant functional types (PFT). *Pollen plant functional types (PFT) have been defined in Marchant et al. (2009). LPJ-GUESS plant functional types are described in Tables 5.1 and 5.2.*

Biome name	Biome acronym	Pollen PFT	LPJ-GUESS shrub PFT	LPJ-GUESS tree PFT
Tropical rainforest	TRFO	man, tx, Te1, Te2, tf	/	TeBE/TrBE, TrBE/TrIBE
Tropical seasonal forest	TSFO	tx, Tr1, Tr2, Te2, tf	/	TeBE/TrBE, TrBR, TrBE/TrIBE
Tropical dry forest	TDFO	Tr2, tf, txts, df	TrRSh (TrESh)	TrBR
Warm temperate rainforest	WTRF	tx, Tr1, Te1, wtc, ctc2, tef, wte	/	TeBE/TrBE, TrBR, TrBE/TrIBE, TeNE, TeBE
Warm temperate evergreen broadleaf forest	WEFO	tx, Tr2, wtc, ctc2, ec,tef,wte	/	TeBE/TrBE, TrBR, TeNE, TeBE
Cool temperate rainforest	CTRF	tx, h, ctc1, tef, wte, wte1	/	TeBE/TrBE, TeNE, TeBE, IBS/TeBS
Warm temperate mixed forest	WAMF	Tr2, wtc, tef, wte, ts	/	TrBR, TeNE, TeBE (IBS/TeBS)
Cool mixed forest	COMI	ctc1, tef, wte1, wte4, ts1	/	TeNE, IBS/TeBS, TeBE
Steppe	STEP	sf	/	/
Desert	DESE	ds, df	TrRSH (TrESh)	/
Cool grass shrublands	CGSH	af, aa, wte4, h	BESh/BSSh/TeESh/TeRSh/TeSSh	IBS/TeBS
Cool grasslands	CGSS	af, aa, cp	BESh/BSSh/TeESh/TeRSh/TeSSh	/

warm-temperate evergreen broadleaf forests and cool mixed forests (WEFO-COMI) (Fig. 5.1).

Finally, I used Table 5.5 to define biomes as combinations of plant functional types based on their leaf area index, by visually defining a threshold of simulated leaf area index for each plant functional type to map the distribution of simulated biomes so they match with the present-day biome map presented in Marchant et al. (2009) (Fig. 5.1). I

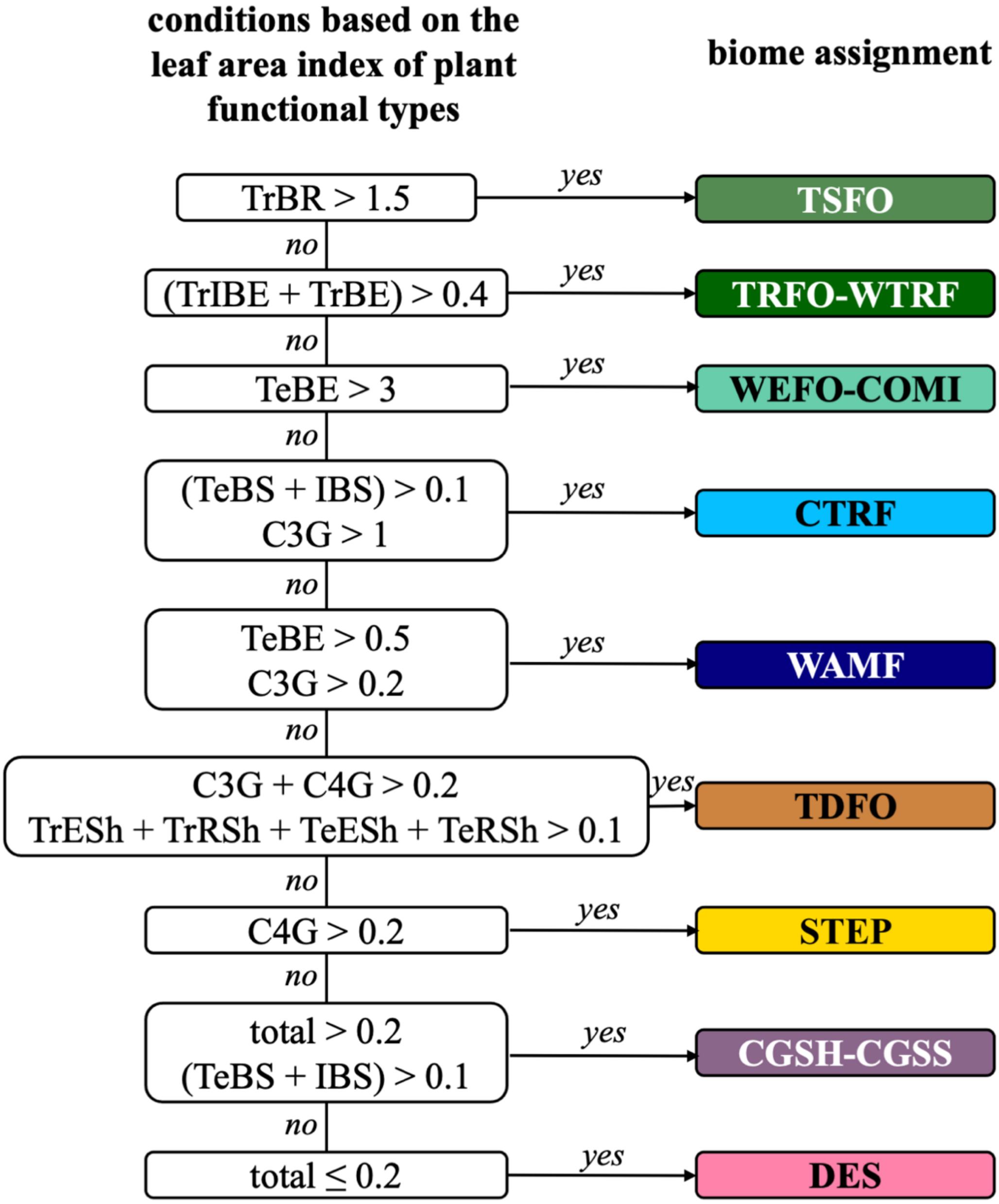

Figure 5.1. Hierarchical algorithm to define biomes based on the average leaf area index of plant functional types as simulated by the model. *The average leaf area index of each plant functional types for each simulation are provided in Figure 5.3-5.5. Plant functional types: BNE = boreal needleleaved evergreen tree, BINE = shade-intolerant boreal needleleaved evergreen tree, BNS = boreal needleleaved summergreen tree, TeNE = temperate needleleaved evergreen tree, TeBS = shade-tolerant temperate broadleaved summergreen tree, IBS = shade-intolerant broadleaved summergreen tree, TeBE = temperate broadleaved evergreen tree, TrBE = tropical broadleaved evergreen tree, TrIBE = tropical broadleaved evergreen tree, TrBR = tropical broadleaved raingreen tree, C3G =* C_3 *grass, C4G =* C_4 *grass, TeEsh = temperate evergreen shrub, TeRSh = temperate raingreen shrub, TeSSh = temperate raingreen shrub, TrESh = tropical evergreen shrub, TrRSh = tropical raingreen shrub, BESh = boreal evergreen shrub, BSSh = boreal summergreen shrub. Biomes: TSFO = tropical seasonal forests, TRFO-WTRF = tropical rainforests and warm temperate rainforests, WEFO-COMI = warm-temperate evergreen broadleaf forests and cool mixed forests, WAMF = warm temperate mixed forests, CTRF = cool temperate rainforests, TDFO = tropical dry forests, STEP = steppes, CGSH-CGSS = cool grass shrublands and cool grasslands, DES = deserts. Plant functional types are described in Tables 5.1 and 5.2.*

calibrated the biome definitions by comparing the modern simulated biome map with the modern potential biome map provided in Marchant et al. (2009), an expert-based compilation of potential natural vegetation maps from Hück (1960) and Schmithüsen (1976) derived from ground observations. I discussed the concept, strengths, and weaknesses of such compilation approach in the Chapter 2. I calibrated biome definitions by visual comparison because a digitised and georeferenced version of the map does not exist. I implemented biome definitions in the model with leaf area index thresholds varying among plant functional types and biomes, and depending on the visual comparison with the reference map. I built a hierarchical algorithm to assign each grid cell to a biome based on the simulated leaf area index of each plant functional types (Fig. 5.1). The model simplifies the representation of vegetation by representing only few dominant plant functional types in a given area. To consider this limitation, I set the leaf area index's threshold of some plant functional types to zero. Model biome definitions are thus often combinations of only a few plant functional types from the initial combination (Fig. 5.1).

II.2.2. Comparing simulated biomes with pollen-based biomes

I obtained simulated tree cover for each site and period by re-classifying each simulated biome into a tree cover category: open, intermediate, or closed following Marchant et al. (2009). I categorised biomes including the terms "closed canopy forest", "closed forest", or "closed canopy" in their definition as "closed"; I categorised those including terms suggesting that the canopy was not completely closed, such as the terms "mixed forest", "semi-closed forest", or "open canopy", as "intermediate". I categorised other biomes dominated by herbaceous vegetation or shrubs as "open". I consequently categorised three biomes as "open" (i.e., cool grass shrublands and cool grasslands, desert, and steppe), two as "intermediate" (i.e., tropical dry forest, and warm-temperate evergreen broadleaf forest and cool mixed forest), and the four others as "closed" (i.e., cool temperate rainforest, tropical rainforest and warm temperate rainforest, tropical seasonal forest, and warm temperate mixed forest).

I calculated the agreement between simulated and pollen-based biomes as well as simulated and pollen-based tree cover at a given period and for changes between any two periods of time. Two present-day biome estimations characterise each pollen site, corresponding to expert-based potential biomes derived from field observation of the present ecosystem surrounding the pollen site, and pollen-based biomes derived from the analysis of the modern sediments (Marchant et al., 2009). I mentioned the total percentage of agreement between the model and either pollen-based biomes, or expert-based biomes, or at least one of them. In addition to the overall agreement, I calculated the agreement between each pair of biomes with Cohen's kappa on a single category ($\kappa_{i,j}$) for each period. This measure facilitates the distinction between biomes that are generally well-predicted and biomes that are poorly predicted. $\kappa_{i,j}$ also allows identifies the most common confusions among biomes (for example, if the simulations often identify a biome "A" in areas where pollen-based biomes rather identify a biome "B") . To facilitate the description of the measure of the Cohen's kappa on a single category ($\kappa_{i,j}$) among biome pairs, I used the terminology of Landis and Koch (1977) who defined classes of agreement based on $\kappa_{i,j}$ ranges: $\kappa_{i,j}$ = 1 = perfect agreement; $\kappa_{i,j}$ = 0 = no agreement; $0 < \kappa_{i,j} < 0.20$ = 'slight' agreement; $0.21 < \kappa_{i,j} < 0.40$ = 'fair' agreement; $0.41 < \kappa_{i,j} < 0.60$ = 'moderate' agreement; $0.61 < \kappa_{i,j} < 0.80$ = 'substantial' agreement; $0.81 < \kappa_{i,j} < 1.00$ = 'almost perfect' agreement.

I next measured the rate of agreement related to change between each two periods. I used four ways of classifying change in biome or tree cover, corresponding to four questions: (*i*) Did the biome change? ('yes' or 'no'); (*ii*) Did the tree-cover class change? ('yes' or 'no'), (*iii*) what was the direction of the change in tree-cover class? ('increase', 'decrease', or 'stable'); and (*iv*) what was the amplitude of the change in tree-cover class (-2, -1, 0, 1, 2). I calculated the amplitude of tree-cover change by considering that "open" = 0, "intermediate" = 1, and "closed" = 2, and by calculating the difference between the youngest and the oldest period. I did all the post-simulation analyses in R (R Core Team, 2022), and I represented the differences in biome or tree-cover assignments using Sankey diagrams using the `ggalluvial` package (Brunson and Read, 2023).

III. RESULTS

III.1. Changes in post-Last Glacial Maximum biome distribution

The Last Glacial Maximum shows important differences in simulated biome distribution with the mid-Holocene and present simulations (Fig. 5.2), with the main changes being the spatial settlement and development of Patagonian forests to replace deserts and cool grassland and cool grass shrubland, and the expansion of the tropical rainforest (TRFO) in the Amazon Basin up to ~10°S replacing tropical dry forests that are limited today to the Cerrado region. Overall, the vegetation cover for most plant functional types during the Last Glacial Maximum was lower compared to contemporary habitats. The total leaf area index in open environments was often < 0.2 (Fig. 5.3), leading to their classification into deserts, especially along the southern dry diagonal in the Southern Cone. During this period, vegetation in the Southern Cone was scarce, dominated by C_3 grass (C3G) and temperate shrubs (TeESh, TeRSh), and a small patch where temperate broadleaf shrubs (TeBS) could thrive sufficiently to maintain the cool temperate rainforest biome (CTRF) in Northern Patagonian Andes. Consequently, cool temperate rainforest (CTRF) was confined to a narrow strip in the northern Patagonian Andes around 40° S, leaving most of the Southern Cone covered with deserts (DES; Fig. 5.2). In contrast, by the mid-Holocene and extending to the present, cool temperate forests (CTRF) have expanded southward, mainly on the slopes of the Andes, while open biomes (i.e., DES, CGSH-CGSS) became less prevalent (Fig. 5.2). During the Last Glacial Maximum, the Amazon Basin was mostly covered with tropical dry forest (TDFO, Fig. 5.2), highlighting the dominance of plant functional types with a raingreen phenology (i.e., losing their leaves during dry periods) at the expense of evergreen plant functional types (Fig. 5.3 – 5.5).

III.2. Pollen-model comparison

III.2.1. Overall comparison between simulated and pollen-based biomes/tree cover

Overall, pollen-model agreement was generally ~ 50%, with a maximum of 61% of the sites for the present-day tree-cover class. The overall agreement tended to increase toward the most recent periods, with the biome agreement reaching 41% for the present-

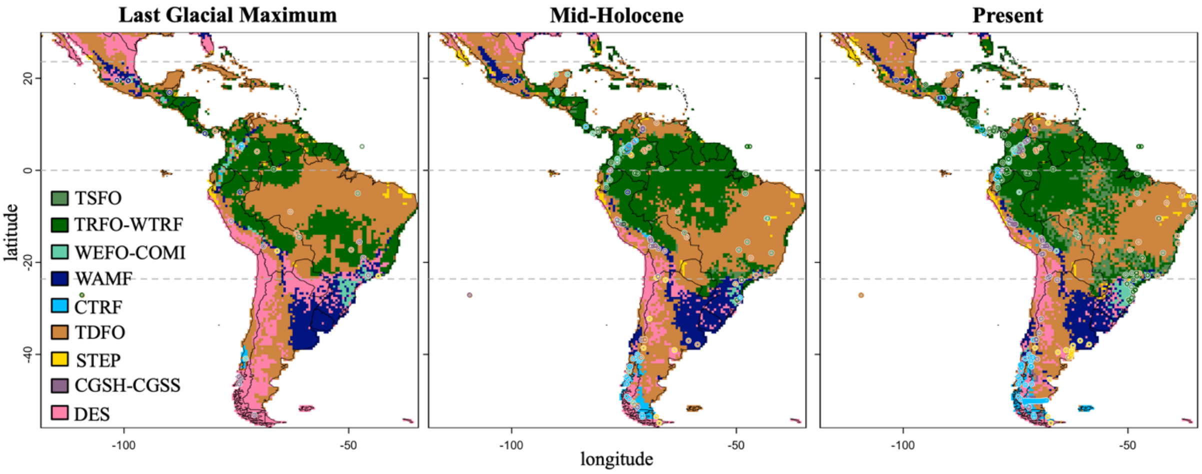

Figure 5.2. Biome distribution as simulated by the model and pollen-based biomes. *Biomes were derived from the leaf area index of plant functional types following the procedure described in Fig. 5.1. Pollen-based biomes were derived from Marchant et al. (2009). TSFO = tropical seasonal forests, TRFO-WTRF = tropical rainforests and warm temperate rainforests, WEFO-COMI = warm-temperate evergreen broadleaf forests and cool mixed forests, WAMF = warm temperate mixed forests, CTRF = cool temperate rainforests, TDFO = tropical dry forests, STEP = steppes, CGSH-CGSS = cool grass shrublands and cool grasslands, DES = deserts.*

day, 26% for the mid-Holocene, and 19% for the Last Glacial Maximum (Fig. 5.6). Overall Cohen's kappa (κ) was 0.05 ('slight') for the Last Glacial Maximum, 0.14 for the Mid-Holocene ('slight'), and 0.19 ('slight') and 0.22 ('fair') for the modern and present-day comparisons, respectively. The comparison of biomes grouped by tree-cover classes had higher agreements, with a gain of 15 to 20% of rate of agreement in time period (Fig. 5.6). The model simulations had higher agreement with modern pollen-based estimations of biomes (biome identity = 41%, tree-cover class identity = 61%, Fig. 5.6) than with the present-day potential biome map derived from ground observations (biome identity = 40%, tree-cover class identity = 55%, Fig. 5.6).

The comparison in terms of biome change (Fig. 5.7) showed that the highest rate of agreement (0.58) corresponded to the estimation of a change in biome between the Last Glacial Maximum and the present. In contrast, the lowest rate of agreement (0.33) corresponded to the estimation of the amplitude of tree-cover change between the Last Glacial Maximum and the mid-Holocene. The rate of agreement in tree-cover change reached very close values when focusing on its occurrence, direction or amplitude between each given pair of periods (difference of rate of agreement < 0.05), apart between the two oldest periods (i.e., the Last Glacial Maximum and mid-Holocene) that

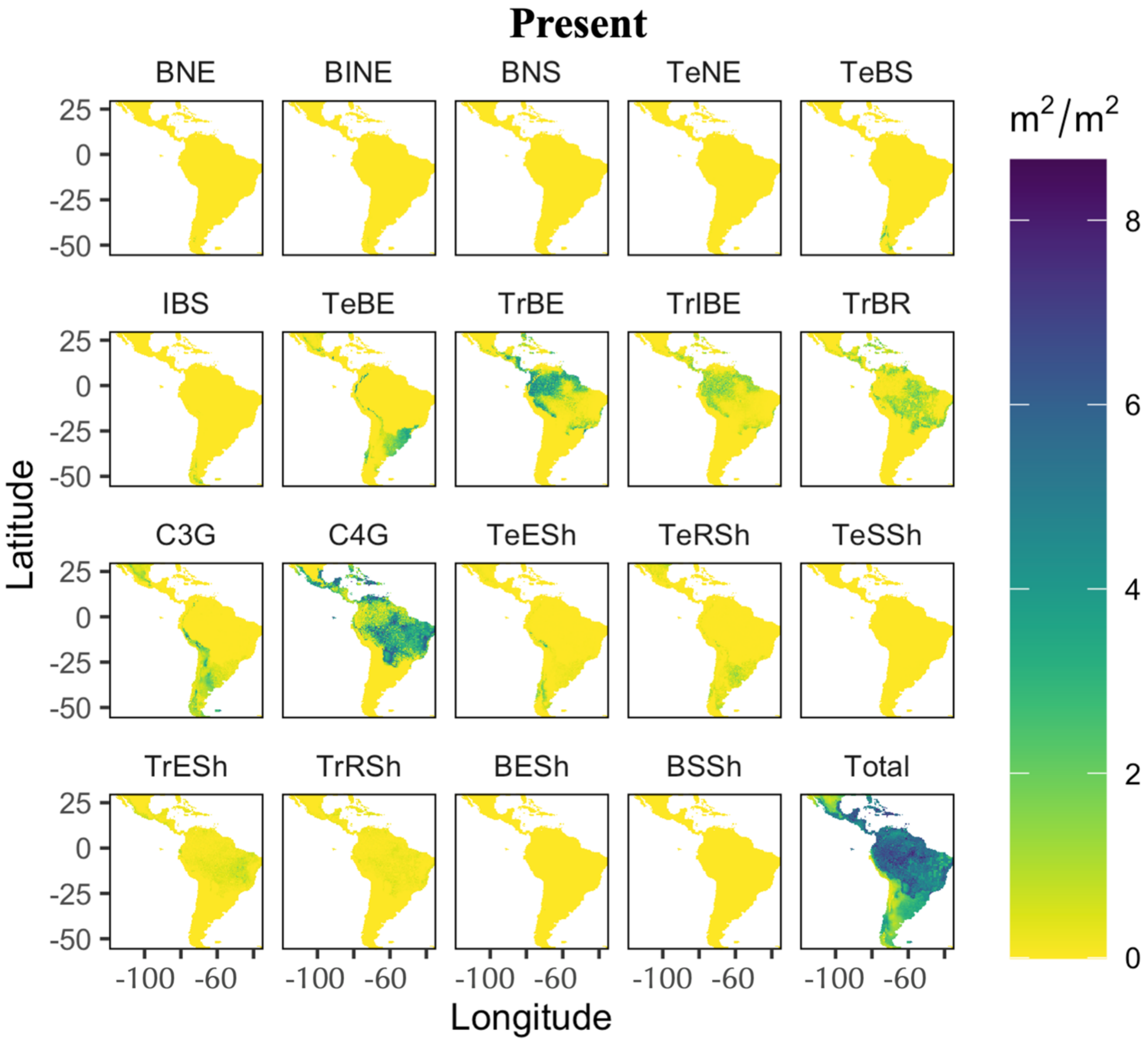

Figure 5.3. Present leaf area index of each plant functional type as simulated by the model. *Plant functional types are described in Tables 5.1 and 5.2. Plant functional types: BNE = boreal needleleaved evergreen tree, BINE = shade-intolerant boreal needleleaved evergreen tree, BNS = boreal needleleaved summergreen tree, TeNE = temperate needleleaved evergreen tree, TeBS = shade-tolerant temperate broadleaved summergreen tree, IBS = shade-intolerant broadleaved summergreen tree, TeBE = temperate broadleaved evergreen tree, TrBE = tropical broadleaved evergreen tree, TrIBE = tropical broadleaved evergreen tree, TrBR = tropical broadleaved raingreen tree, C3G =* C_3 *grass, C4G =* C_4 *grass, TeEsh = temperate evergreen shrub, TeRSh = temperate raingreen shrub, TeSSh = temperate raingreen shrub, TrESh = tropical evergreen shrub, TrRSh = tropical raingreen shrub, BESh = boreal evergreen shrub, BSSh = boreal summergreen shrub. This figure was made using the* `DGVMTools` *R package (accessible at https://github.com/MagicForrest/DGVMTools/releases/tag/v1.0.0).*

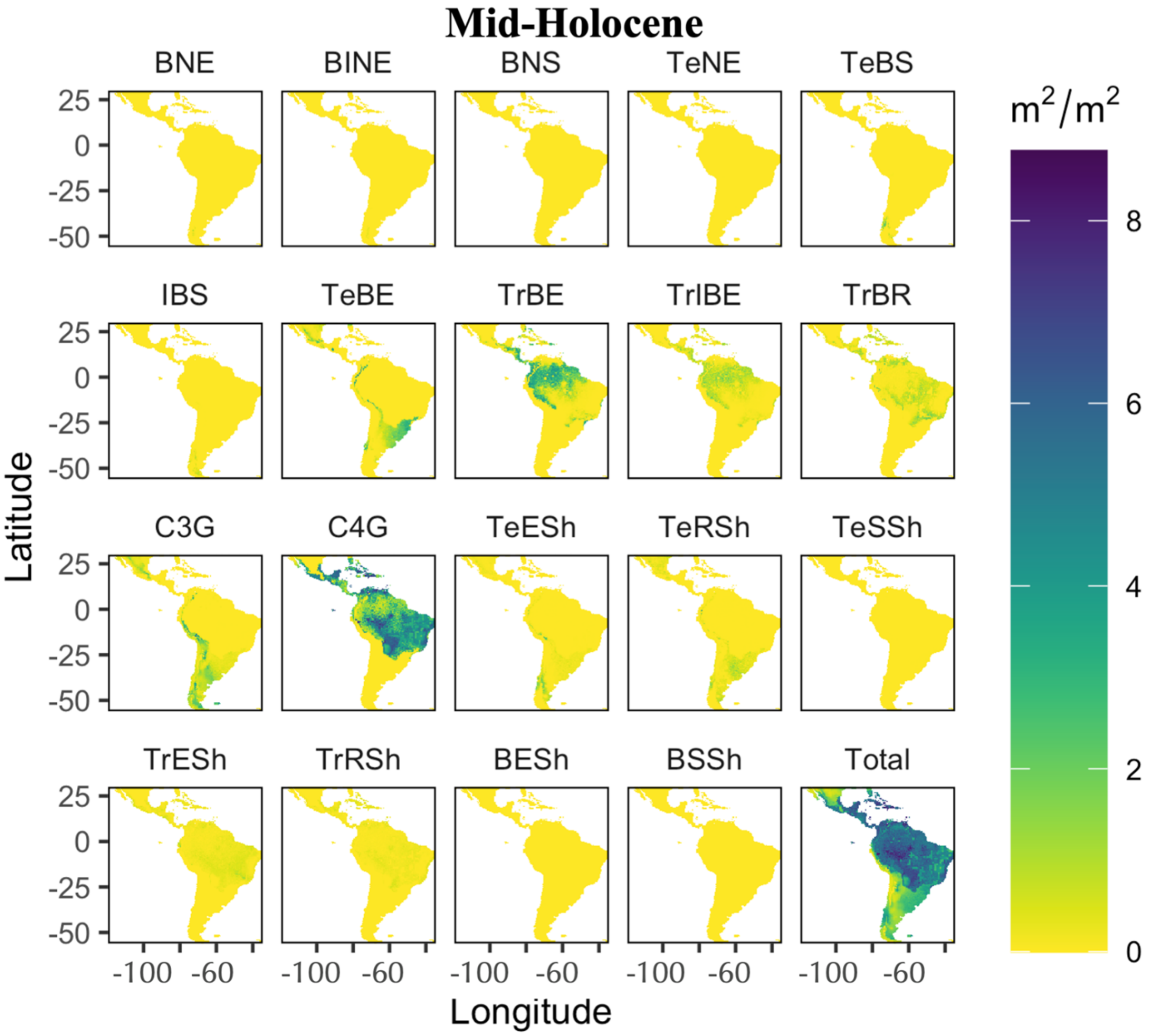

Figure 5.4. Mid-Holocene leaf area index of each plant functional type as simulated by the model. *Plant functional types are described in Tables 5.1 and 5.2. Plant functional types: BNE = boreal needleleaved evergreen tree, BINE = shade-intolerant boreal needleleaved evergreen tree, BNS = boreal needleleaved summergreen tree, TeNE = temperate needleleaved evergreen tree, TeBS = shade-tolerant temperate broadleaved summergreen tree, IBS = shade-intolerant broadleaved summergreen tree, TeBE = temperate broadleaved evergreen tree, TrBE = tropical broadleaved evergreen tree, TrIBE = tropical broadleaved evergreen tree, TrBR = tropical broadleaved raingreen tree, C3G =* C_3 *grass, C4G =* C_4 *grass, TeEsh = temperate evergreen shrub, TeRSh = temperate raingreen shrub, TeSSh = temperate raingreen shrub, TrESh = tropical evergreen shrub, TrRSh = tropical raingreen shrub, BESh = boreal evergreen shrub, BSSh = boreal summergreen shrub. This figure was made using the* `DGVMTools` *R package (accessible at https://github.com/MagicForrest/DGVMTools/releases/tag/v1.0.0).*

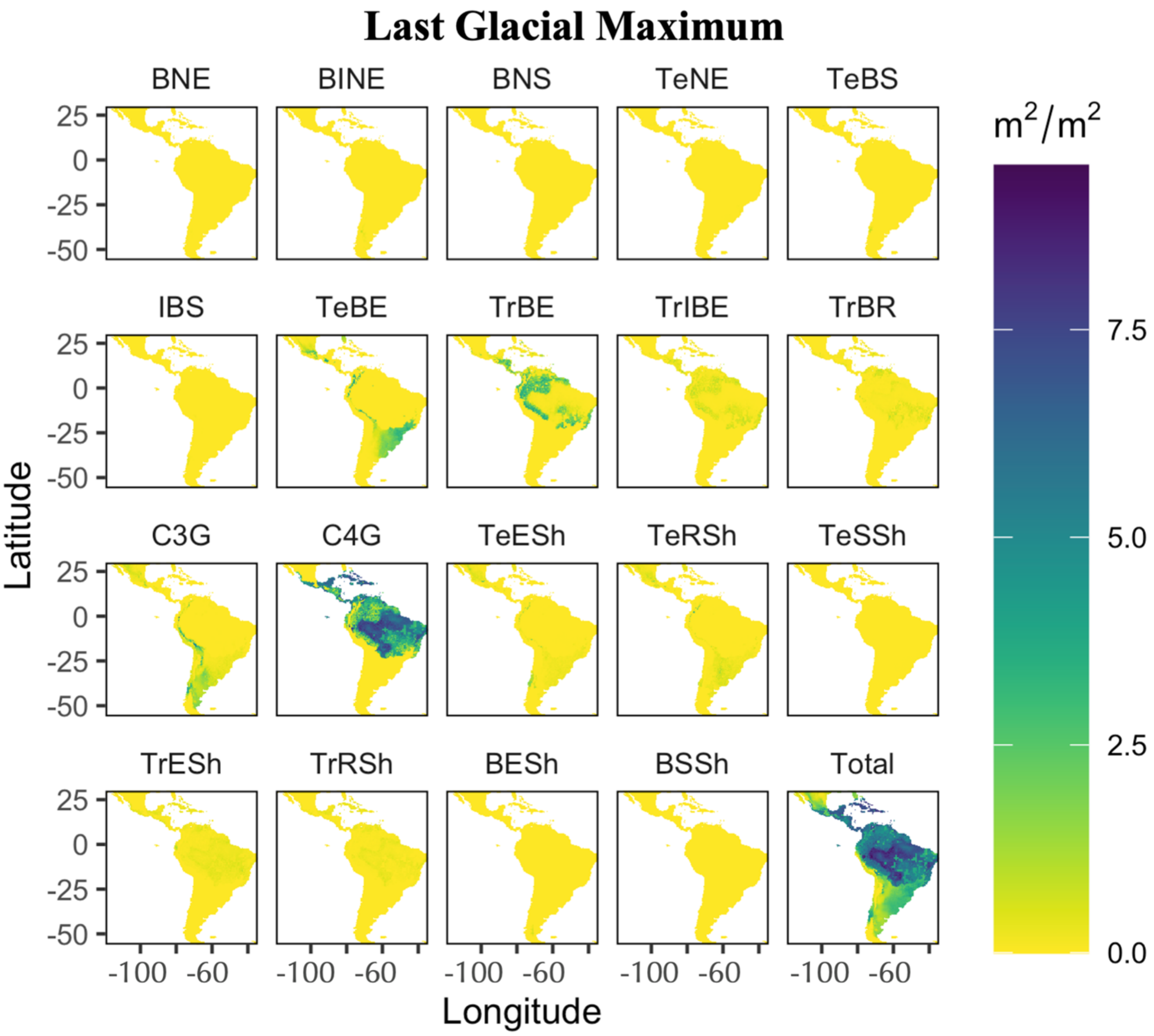

Figure 5.5. Last Glacial Maximum leaf area index of each plant functional type as simulated by the model. *Plant functional types are described in Tables 5.1 and 5.2. Plant functional types: BNE = boreal needleleaved evergreen tree, BINE = shade-intolerant boreal needleleaved evergreen tree, BNS = boreal needleleaved summergreen tree, TeNE = temperate needleleaved evergreen tree, TeBS = shade-tolerant temperate broadleaved summergreen tree, IBS = shade-intolerant broadleaved summergreen tree, TeBE = temperate broadleaved evergreen tree, TrBE = tropical broadleaved evergreen tree, TrIBE = tropical broadleaved evergreen tree, TrBR = tropical broadleaved raingreen tree, C3G =* C_3 *grass, C4G =* C_4 *grass, TeEsh = temperate evergreen shrub, TeRSh = temperate raingreen shrub, TeSSh = temperate raingreen shrub, TrESh = tropical evergreen shrub, TrRSh = tropical raingreen shrub, BESh = boreal evergreen shrub, BSSh = boreal summergreen shrub. This figure was made using the* `DGVMTools` *R package (accessible at https://github.com/MagicForrest/DGVMTools/releases/tag/v1.0.0).*

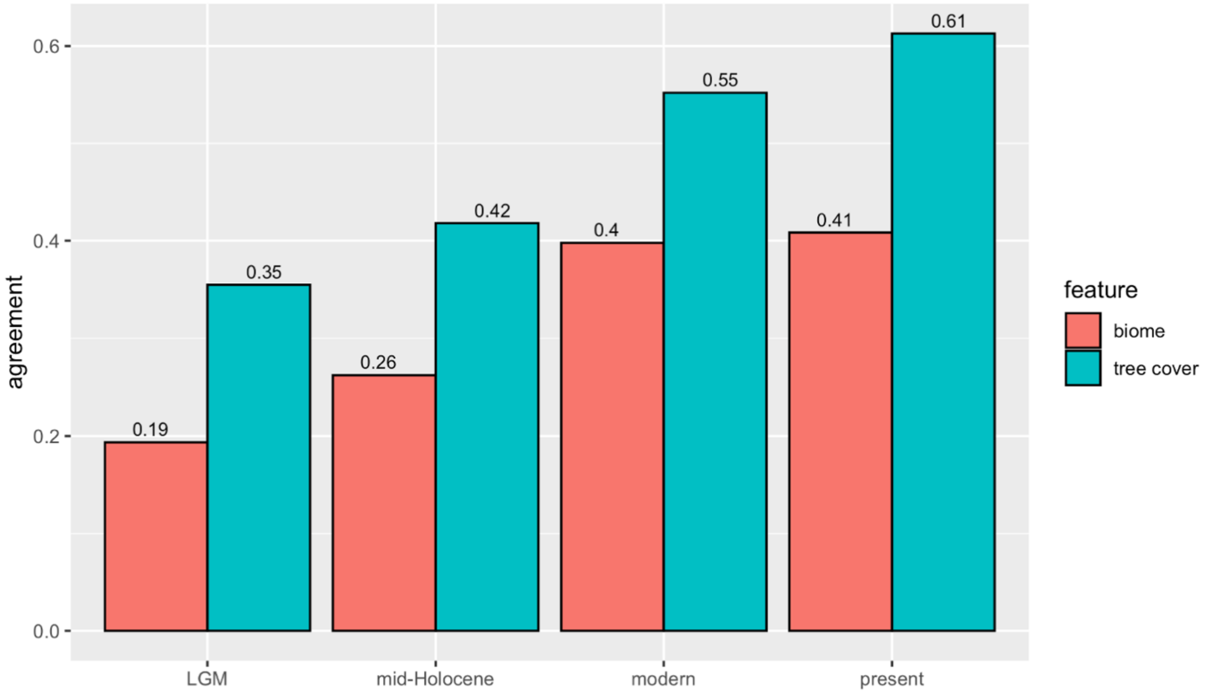

Figure 5.6. General agreement at a given period between the model and the reference data from Marchant et al. (2009). *LGM = Last Glacial Maximum, modern = pollen-based biome reconstruction, present = potential biomes from field observation (Marchant et al., 2009).*

showed more differences (rates of agreement for: occurrence = 0.47, amplitude = 0.33, direction = 0.37). In summary, when a change from past to modern pollen-based biomes is identified, its direction and amplitude are generally also identified in simulations.

III.2.2. Differential agreement among biomes

The comparison of simulated biomes and biomes derived from biomised pollen records shows contrasting agreements among biomes. The pairwise comparison of biomes had the highest Cohen's kappa for a single category ($\kappa_{i,j}$) of 0.51 ('moderate') for tropical rainforests and warm temperate rainforests (TRFO-WTRF) for the present day (Table 5.6). For other periods, the highest $\kappa_{i,j}$ was 0.36 ('fair') for warm temperate mixed forest (WAMF) at the mid-Holocene (Table 5.7), and 0.33 ('fair') for tropical rainforest and warm temperate rainforest (TRFO-WTRF) at the Last Glacial Maximum (Table 5.8).

The Sankey diagrams show that no pollen-based biome perfectly agrees with the vegetation simulations, but the rate of agreement differs among biomes and periods (Fig.

Table 5.6. Cohen's Kappa agreement on a single category ($K_{i,j}$) at present. *Comparison between simulated biomes (columns) and pollen-based biomes (rows). All biome acronyms are described in the caption of Fig. 5.1.*

	CGSH-CGSS	CTRF	STEP	TDFO	TSFO	TRFO-WTRF	WAMF	WEFO-COMI	DES
CGSH-CGSS	0.01	-0.06	-0.01	0.16	-0.05	-0.21	0.05	0.22	0.03
CTRF	0.16	0.45	-0.01	-0.06	-0.05	-0.26	-0.02	-0.09	-0.01
STEP	0.02	-0.07	-0.01	0.26	0.03	-0.1	0.02	-0.11	-0.01
TDFO	-0.07	-0.09	0.1	0.09	-0.04	0.02	-0.01	-0.04	-0.01
TSFO	-0.07	-0.09	-0.01	0.01	0.31	0.03	-0.07	-0.04	-0.01
TRFO-WTRF	-0.12	-0.2	-0.01	-0.22	0.01	0.51	-0.07	-0.06	-0.01
WAMF	-0.01	-0.09	-0.01	-0.08	-0.04	0.04	0.16	0.05	-0.01
WEFO-COMI	0.05	0	-0.01	-0.08	-0.04	-0.05	0.05	0.15	0.09
DES	0	0	0	0	0	0	0	0	0

Table 5.7. Cohen's Kappa agreement on a single category ($K_{i,j}$) at the mid-Holocene. *Comparison between simulated biomes (columns) and pollen-based biomes (rows). All biome acronyms are described in the caption of Fig. 5.1.*

	CGSH-CGSS	CTRF	STEP	TDFO	TSFO	TRFO-WTRF	WAMF	WEFO-COMI	DES
CGSH-CGSS	-0.02	0.03	0	0.11	-0.03	-0.27	0.08	0.07	0.02
CTRF	0.08	0.26	0	-0.13	-0.03	-0.14	-0.05	0.07	0.03
STEP	0.26	-0.09	0	0.12	-0.03	-0.05	-0.1	-0.11	-0.04
TDFO	-0.12	-0.04	0	0.04	0.08	0.1	0.06	-0.12	-0.04
TSFO	-0.1	-0.1	0	0.12	0.12	0.1	-0.12	-0.07	-0.04
TRFO-WTRF	0.01	-0.1	0	-0.16	-0.03	0.31	-0.03	0.01	-0.04
WAMF	-0.06	-0.06	0	-0.08	-0.02	0	0.36	-0.07	-0.03
WEFO-COMI	-0.03	-0.04	0	-0.04	-0.03	0.05	-0.15	0.15	0.07
DES	0	0	NA	0	0	0	0	0	0

Table 5.8. Cohen's Kappa agreement on a single category ($K_{i,j}$) at the Last Glacial Maximum. *Comparison between simulated biomes (columns) and pollen-based biomes (rows). All biome acronyms are described in the caption of Fig. 5.1.*

	CGSH-CGSS	CTRF	STEP	TDFO	TSFO	TRFO-WTRF	WAMF	WEFO-COMI	DES
CGSH-CGSS	0.19	-0.06	0	-0.16	0	-0.4	0	0.25	0.3
CTRF	-0.11	-0.05	0	0.11	0	-0.16	0	-0.08	0.2
STEP	-0.08	-0.04	0	0.02	0	0.11	0	-0.07	-0.09
TDFO	-0.14	-0.06	0	-0.01	0	0.33	0	-0.1	-0.17
TSFO	-0.08	-0.04	0	0.17	0	-0.12	0	-0.07	-0.09
TRFO-WTRF	-0.08	-0.04	0	-0.13	0	0.33	0	-0.07	-0.09
WAMF	0.11	-0.06	0	0.07	0	0.08	0	-0.11	-0.18
WEFO-COMI	-0.05	1	0	-0.06	0	-0.06	0	-0.04	-0.05
DES	0	0	NA	0	NA	0	NA	0	0

5.8). In comparison, data from Marchant et al. (2009) had a high rate of agreement for all biomes between modern biomised pollen records and potential biomes derived from field observations (Fig. 5.8b). The compilation of present, mid-Holocene, and Last Glacial Maximum model-pollen comparisons (Fig. 5.8a) shows that the highest-agreement biomes are tropical rainforests and warm temperate rainforests (TRFO-WTRF),

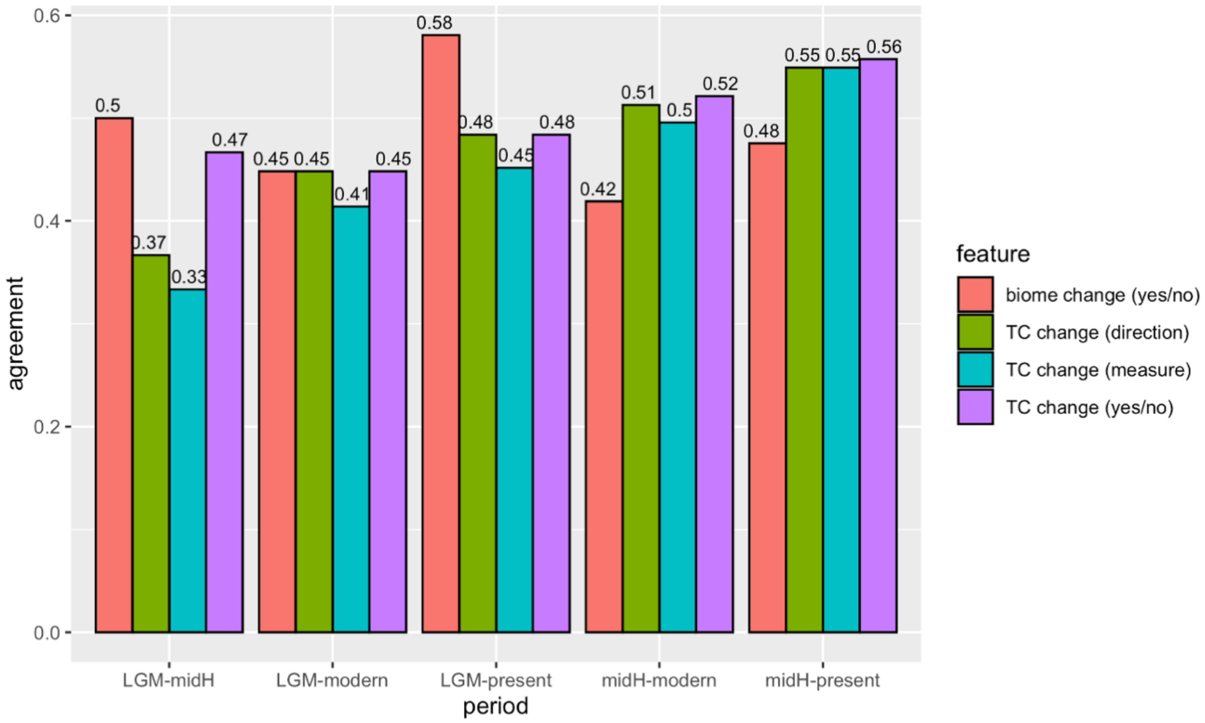

Figure 5.7. General agreement on change between two periods between the model and the reference data from Marchant et al. (2009). *I measured the rate of agreement related to change between each two periods. I used four ways of classifying change in biome or tree cover, corresponding to four questions: "(i) Is there a biome change ("yes" or "no") ?" (red), (ii) "Is there a change in the tree cover class ("yes" or "no")" (purple), (iii) "What is the direction of the change in tree-cover class ("up", "stable", or "down")" (green), and (iv) "What is the amplitude of the change in tree-cover class (-2, -1, 0, 1, 2)" (blue). LGM = Last Glacial Maximum, midH = mid-Holocene, modern = pollen-based biome reconstruction, present = potential biomes from field observation (Marchant et al., 2009), TC = tree cover.*

cool temperate forests (CTRF), warm-temperate evergreen broadleaf forests and cool mixed forests (WEFO-COMI), and to a lesser extent warm temperate mixed forests (WAMF) and tropical dry forests (TDFO). Conversely, the agreement about cool grasslands and cool grass shrublands (CGSH-CGSS), and steppes (STEP) is generally poor. In addition, the Last Glacial Maximum generally differs from the two more recent periods by the nature of inter-biome confusions. When focusing only on the number of sites assigned to each biome, simulated biomes also differ from pollen-based biomes. The model tended to assign more sites to some biomes such as tropical rainforests and warm temperate rainforests (TRFO-WTRF), tropical dry forests (TDFO), and deserts (DES), while assigning fewer sites to others such as cool grasslands and cool grass shrublands (CGSH-CGSS), cool temperate forests (CTRF), steppes (STEP), and tropical

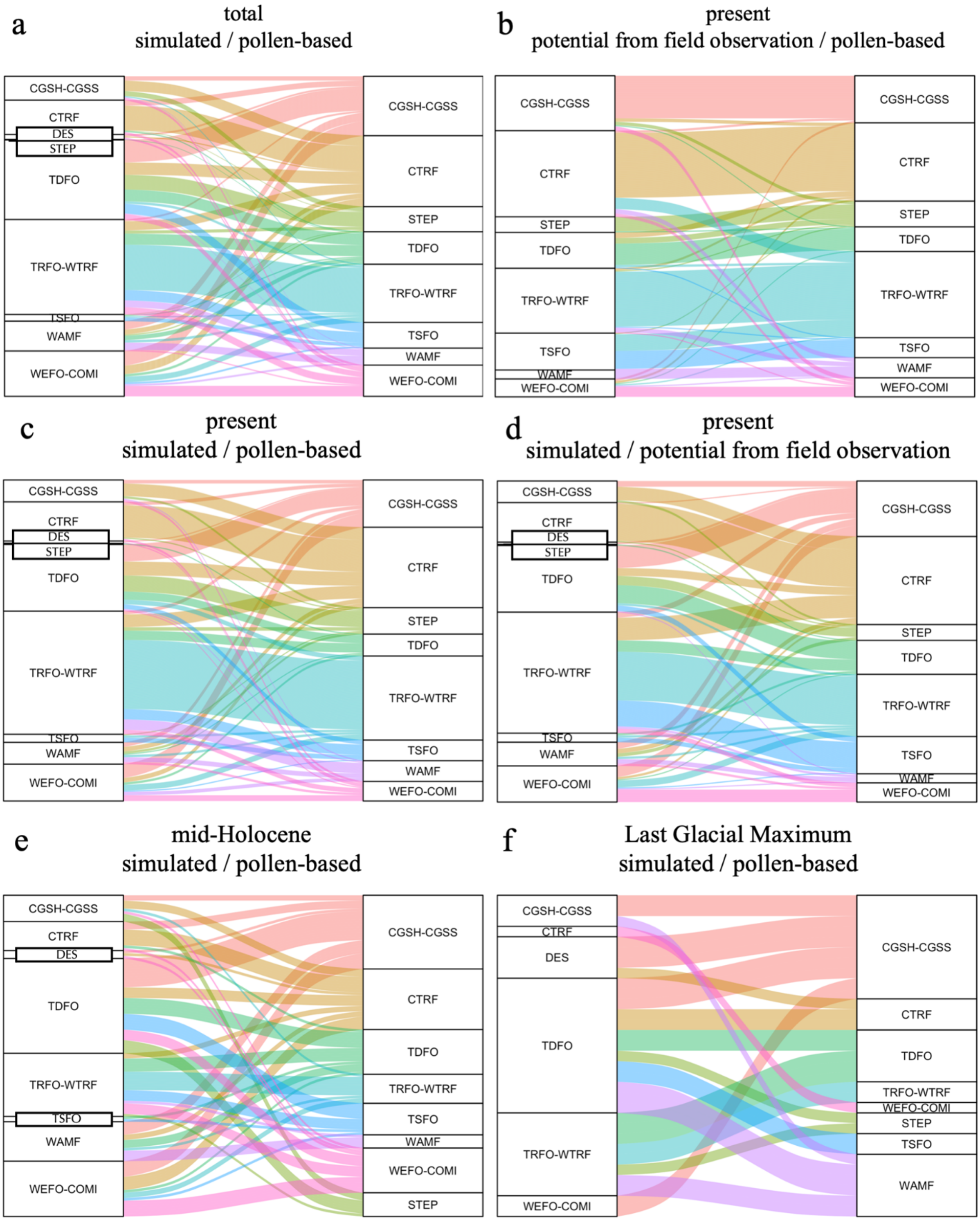

Figure 5.8. Sankey diagrams comparing biome assignments per site by method and period. *Sankey diagrams help visualising changes in categorical data across different conditions. Here, the diagrams show how the method used to determine the type of vegetation (simulation, pollen-based or field observation) affects the result in the sites studied. In each panel, the left column generally indicates simulated biomes, while the right column generally indicates pollen-based biomes. The thickness of a link between a simulated biome and a pollen-based biome is proportional to the number of sites showing this association. The Sankey diagrams were built using the R package* `ggalluvial` *(Brunson and Read, 2023).*

seasonal forests (TSFO). Below, I describe the results of the comparison based on biome identity for each biome.

The comparison between simulated and pollen-based biomes by focusing only on their tree-cover classes shows a relatively high rate of agreement overall, especially for closed forests (Fig. 5.9). The number of pollen records assigned to closed forests by the model is generally consistent with assignments by the biomisation procedure but was lower in the simulations at the Last Glacial Maximum (Fig. 5.9f). In contrast, the model tended to assign many more sites to 'intermediate' tree cover, while assigning fewer sites to 'open' vegetation at all periods as compared to pollen-based biome reconstructions (Fig. 5.9). Records assigned either to intermediate or closed forest cover by the biomisation were generally predicted as not covered with open vegetation by the model. Sites covered with open vegetation were frequently confused by the model with intermediate forest cover. The Last Glacial Maximum comparison shows that open vegetation was relatively better predicted than for the two other periods (Fig. 5.9f).

The data-model comparison of tree-cover change among periods shows that the model tended to overestimate the number of sites that have remained stable (Fig. 5.10). When slight changes (-1 or +1) were detected based on pollen records, the model generally predicted stability. The rate of confusion between negative and positive changes in tree cover is extremely low. Sankey diagrams also show that sites where the model predicted changes were often considered as stable based on pollen records. The spatial distribution of agreement and disagreement for all comparisons shows that pollen-based simulated biomes tended to often agree in some areas such as the slopes of the Southern Patagonian Andes or the Amazon Basin (Fig. 5.11). In contrast, the agreement was generally low in the Cerrado or the region of Mexico (Fig. 5.11).

IV. DISCUSSION

The overall weak agreement between simulated and pollen-based biomes highlights that the two approaches generally disagree at local (site-by-site) scales, contrasting with the general agreement when focusing on the main trends of tree-cover changes at regional scales.

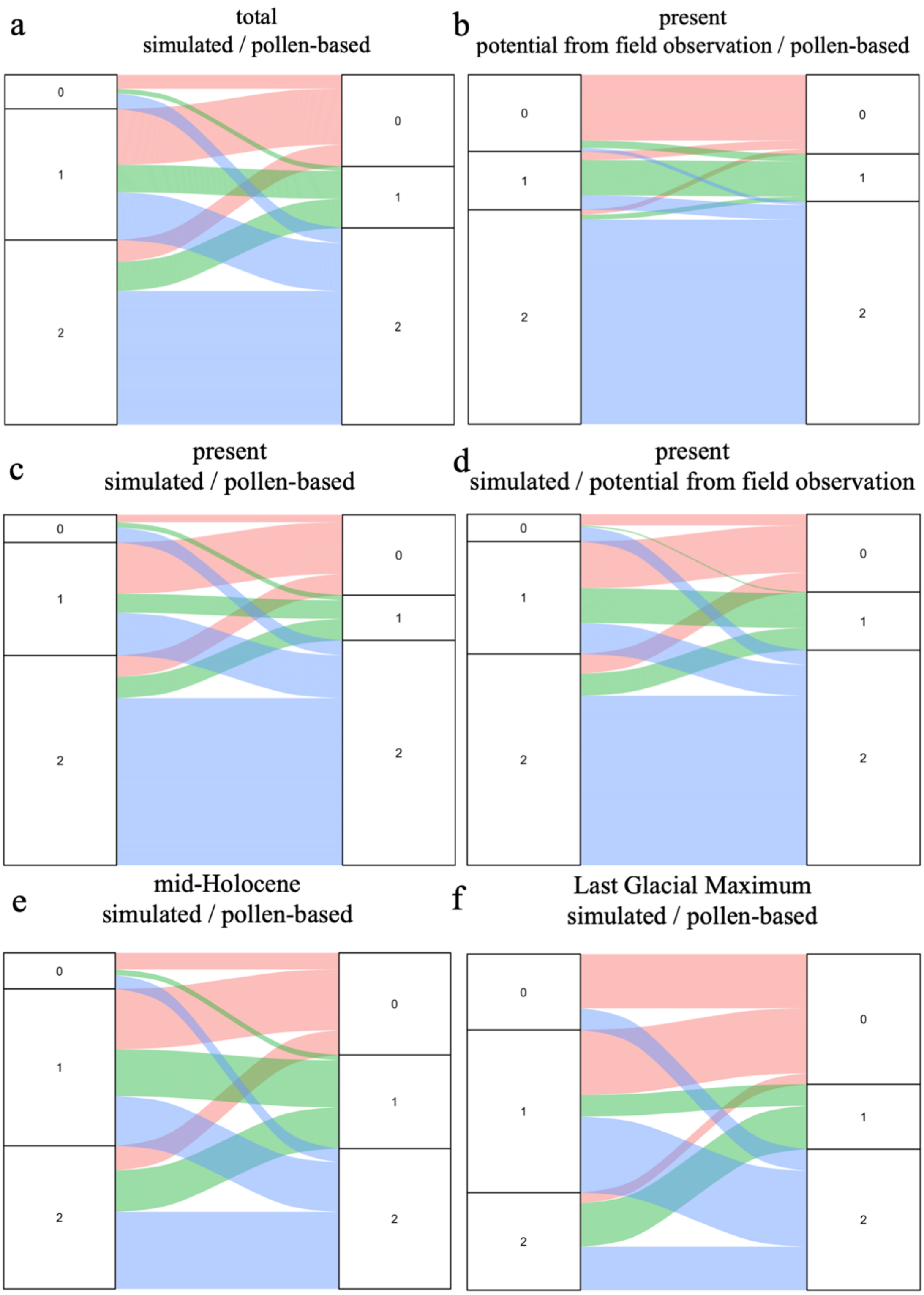

Figure 5.9. Sankey diagrams comparing assignments to a biome tree-cover class per site by method and period. *Sankey diagrams help visualising changes in categorical data across different conditions. Here, the diagrams show how the method used to determine the type of vegetation (simulation, pollen-based or field observation) affects the result in the sites studied. In each panel, the left column generally indicates simulated biomes, while the right column generally indicates pollen-based biomes. The thickness of a link between a simulated biome and a pollen-based biome is proportional to the number of sites showing this association. The Sankey diagrams were built using the R package* `ggalluvial` *(Brunson and Read, 2023).*

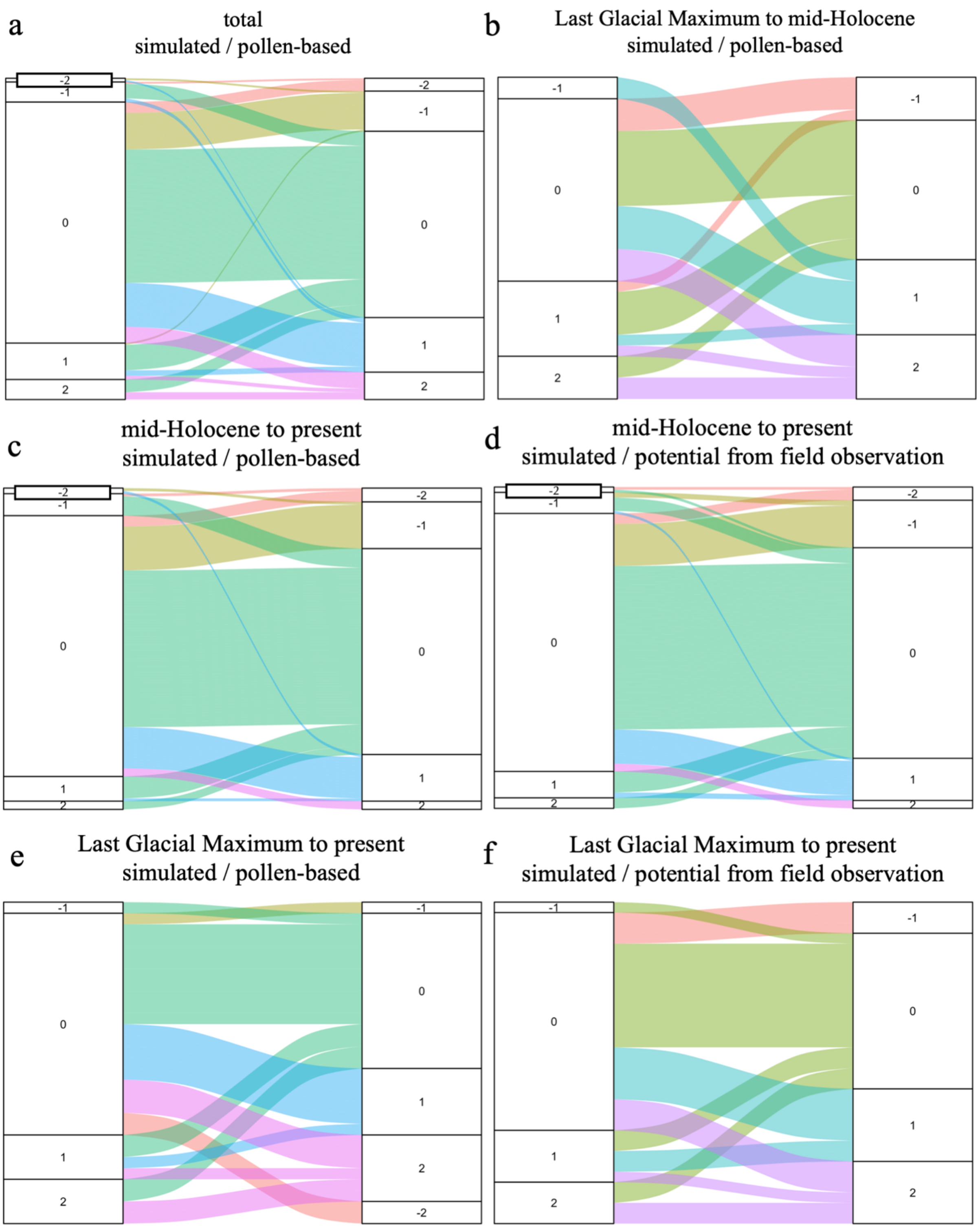

Figure 5.10. Sankey diagrams comparing the amplitude of change in tree-cover class per site by method and period. *Sankey diagrams help visualising changes in categorical data across different conditions. Here, the diagrams show how the method used to determine the type of vegetation (simulation, pollen-based or field observation) affects the result in the sites studied. In each panel, the left column generally indicates simulated biomes, while the right column generally indicates pollen-based biomes. The thickness of a link between a simulated biome and a pollen-based biome is proportional to the number of sites showing this association. The Sankey diagrams were built using the R package* `ggalluvial` *(Brunson and Read, 2023).*

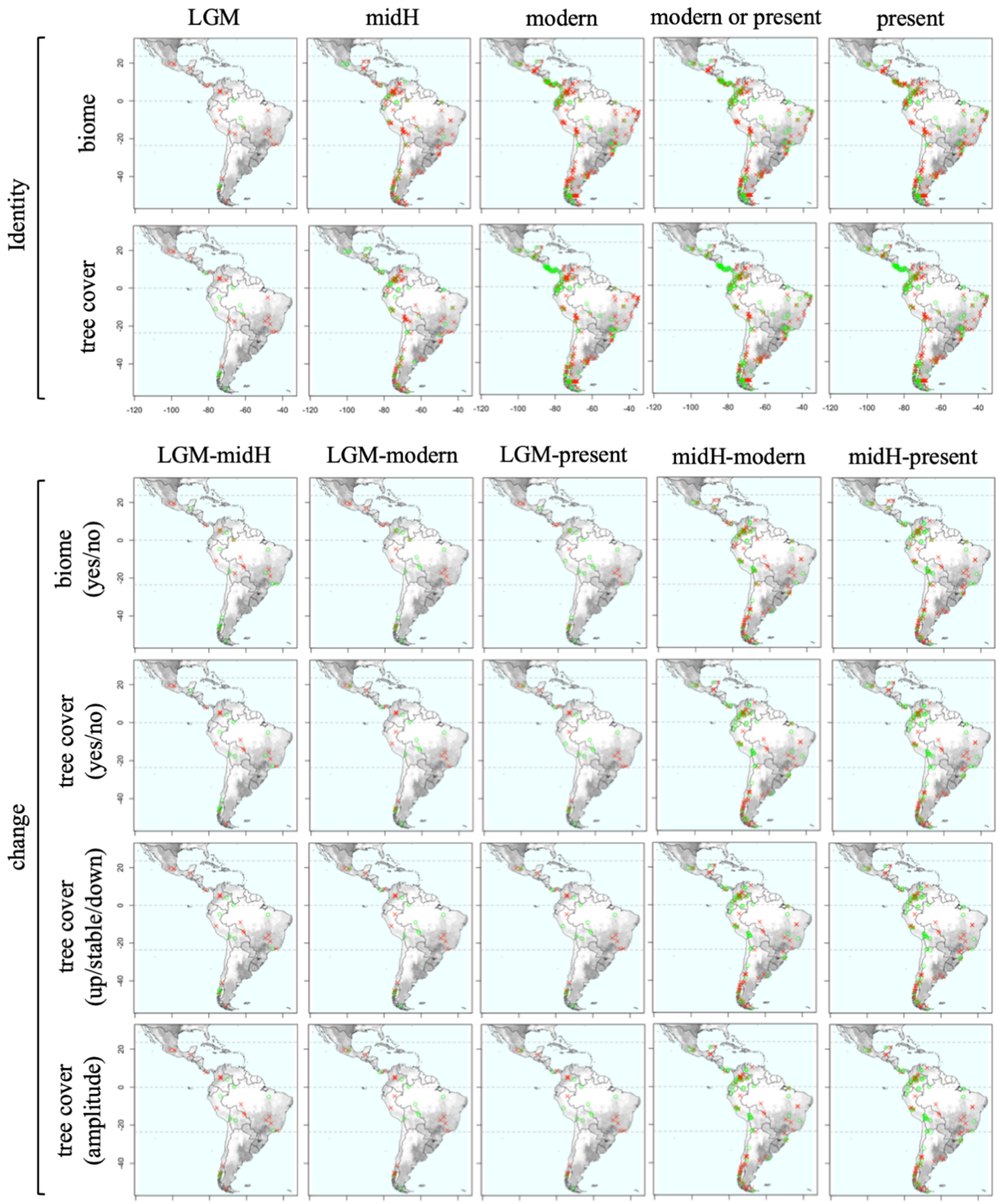

Figure 5.11. Distribution of the agreement for each comparison. *Green circles represent agreement while red cross represent disagreement. LGM = Last Glacial Maximum, midH = mid-Holocene, modern = pollen-based biome reconstruction, present = potential biomes from field observation (Marchant et al., 2009).*

IV.1. Changes in biome distribution

Past biome simulations suggest that post-Last Glacial Maximum climate changes mainly resulted in contractions or expansions biomes (Fig. 5.2). At a continental scale, these simulations agree with the biomisation analyses of Marchant et al. (2009) that characterised the Last Glacial Maximum dominated by more open vegetation compared to the present. More specifically, the simulations match the pollen records in showing that trees were scarce across much of the Southern Cone, except for a limited forested region in the northern Patagonian Andes around 40° S. The simulated range contraction of the Amazon rainforest during the Last Glacial Maximum matches with previous simulations despite various amplitudes (e.g., van der Hammen and Absy 1994; Cowling et al., 2001; Mayle et al., 2004; Maksic et al., 2022). The simulated biome changes in the Cerrado and the Andes agrees with biome stability hindcasts from Costa et al. (2018).

However, these conclusions must be considered carefully given the moderate agreement between the model's predictions and the pollen-record data regarding the periods compared (i.e., Last Glacial Maximum, mid-Holocene and present; Fig. 5.6). The overall agreement based on Cohen’s Kappa at present reached 0.19, which is low compared to other modern data-model comparisons. For example, simulated biomes maps from Haxeltine and Prentice (1996) and Hickler et al. (2006) reached higher Cohen’s Kappa ($\kappa > 0.5$) when compared to the potential biome map from Melillo et al. (1993) derived from the compilation of multiple regional maps. Overall, the differences in prediction potential of the model among biomes (Fig. 5.6 – 5.11) could be attributed to model inaccuracy (under- or over-estimation). For example, sites assigned to tropical rainforests and warm temperate rainforests (TRFO-WTRF) by the pollen record biomisation were also predicted by the model but this must be seen in the context of the large number of sites assigned to this biome by the model in all periods compared to the data from the pollen record biomisation. Similarly, the number of sites covered with cool grasslands and cool grass shrublands (CGSH-CGSS) and steppes (STEP) is lower in the simulations, which explains at least in part why the agreement is so low. In the following paragraphs, I discuss the results of the comparison analysis. First, I discuss the plausible reasons the higher data-model agreement when focusing on the tree-cover classes of biomes, rather than on biome identity. Second, I discuss why the model generally predicted a higher tree cover than pollen record biomisation. Third, I discuss why the agreement was higher towards most recent periods. Finally, I enlarge the discussion to the other sources of disagreement, with a focus on the methodological biases respectively associated with simulated and pollen-based biomes.

IV.2. Tree-cover led to higher agreement than biomes

Unsurprisingly, comparing the three tree-cover classes gives a higher agreement rate than the nine biomes, because tree cover classes comparison is somewhat of an oversimplification of the biome concept. Using the same basic data, the biomes, this comparison could only give a superior or equal agreement. The smaller number of classes also favours a higher agreement. However, the magnitude of the 15-20% difference between the two comparisons (Fig. 5.6) can also be explained by the parameters associated with the tree plant functional types. Indeed, the higher agreement suggests that the two biome assignment methods sometimes agree on the presence of trees, but that the tree plant functional types simulated are not those observed in the pollen records. In such cases, this may mean that the model more correctly simulates competition between trees, shrubs, and grasses, than between different tree plant functional types, in response to various environmental conditions. The parameters differentiating the three growth habits among plant functional types (i.e., trees, shrubs, and grass) are better tuned than those differentiating the tree plant functional types (e.g., tropical, temperate or boreal, deciduous or evergreen). For example, palynological analysis more frequently identify the biome tropical seasonal forest than the model, which tends to classify the relevant sites as belonging to other biomes, in particular to tropical rainforest and warm temperate rainforest (Fig. 5.8). This discrepancy arises because the simulated leaf area index of tropical broadleaved raingreen trees (the plant functional type representative of tropical seasonal forest, Fig. 5.1), does not reach high enough values, in contrast to leaf area index for plant functional type indicative of tropical rainforest and warm temperate rainforest. This issue could likely be explained by the differences in the parameterisation of the plant functional types. In this example, the evergreen phenology of tropical trees, such as tropical broadleaved evergreen trees typical of tropical rainforest and warm temperate rainforest, appear to confer an excessive advantage over the raingreen phenology of other tropical trees such as tropical broadleaved raingreen trees (Fig. 5.3 – 5.5, Table 5.2).

IV.3. Tree cover was generally higher in the model

The model tended to predict higher tree cover relative to pollen records (Fig. 5.9), suggesting that trees are over-competitive in the model, underestimated in the pollen record biomisation, or that biomes were poorly defined. LPJ-GUESS predicted higher tree cover relative to pollen records across all time periods (Fig. 5.9). Dallmeyer et al. (2023) showed a similar trend in Europe over the last 8,000 years. In particular, LPJ-GUESS predicted that more sites were covered with intermediate tree cover, i.e., covered by tropical dry forests (TDFO) or warm-temperate evergreen broadleaf forests and cool mixed forests (WEFO-COMI), at the expense of biomes characterised by open vegetation that include cool grass shrublands and cool grasslands (CGSH-CGSS), steppes (STEP), and deserts (DES) (Fig. 5.8, 5.9). The generally higher tree cover in the model as compared to the pollen records could be counter-intuitive if one considers that arboreal pollen taxa are generally over-represented in the pollen records due to higher pollen dispersal potential. However, higher tree cover could be due at least partially to the poor representation in the model of some processes favouring herbaceous vegetation over trees and shrubs, such as the effect of disturbances increasing tree mortality (e.g., windstorms, fire), or the effect of ecosystem engineers (e.g., human, megafauna) (see also Chapter 2). Another possible reason for the higher tree cover could be the way biomes were defined. In the biome-definition algorithm (Fig. 5.1), "open" biomes (i.e., cool grass shrublands and cool grasslands (CGSH-CGSS), steppes (STEP), and deserts (DES)) were the last to be defined in the hierarchy because their definitions rely mostly on herbaceous and shrub plant functional types. Therefore, this increases the risk of assigning grid cells to other biomes that are higher in the hierarchy. I used several strategies to minimise the bias associated with the use of a hierarchical algorithm for biome classification. First, I calibrated the algorithm visually against a reference map provided in Marchant et al. (2009). Second, 'open' biomes are characterised predominantly by herbaceous vegetation. Thus, if a grid cell, which is in fact 'open' is incorrectly classified as a 'closed' or 'intermediate' biome in the simulations, the discrepancy primarily stems from an overestimation of tree cover rather than a flaw in the classification algorithm itself.

IV.4. Higher agreement towards most recent periods

Differences among periods, and especially between the Last Glacial Maximum and more recent periods, could be related to the site sample size. Indeed, most sites did not provide any record for the Last Glacial Maximum, so the rates of agreement might not be as representative of the reality as the most recent periods. One could also argue that these sample size differences are directly linked to the preservation potential of the environments, which tend to preferentially “select” records from some specific taxa and biomes over others. Therefore, the estimated agreement might be un-representative of the model’s ability to describe vegetation at local scales in the whole Neotropical realm.

The case of the deserts (DES) biome must also be considered carefully. The high proportion of deserts in the simulated biomes from the Last Glacial Maximum is responsible for low agreement with pollen-based biomes. No record was associated with the deserts (DES) biome in the study by Marchant et al. (2009), a feature that could be easily explained by preservation biases, in particular the higher preservation potential in more humid environments (e.g., most post-Last Glacial Maximum palaeo-environments records of the Neotropical realm were deposited in lakes, wetlands or rivers; Chapter 3) that are by their very nature less frequent in desertic contexts. Therefore, the higher proportion of deserts (DES) in the model was to be expected.

In addition to these considerations, the lower rate of agreement for older periods could stem from the fact that biome definitions were based on the assumption that past biomes were analogue to modern biomes, meaning that despite changes in spatial distribution, set of biomes did not change in time (i.e., same set in the past than today), and that biomes kept all their characteristic in time (e.g., functional traits, taxonomic composition, climate; see also Chapter 2). In fact, past landscapes could have hosted biomes with no modern analogue, such as the mammoth’s steppe (Zimov, 2015), potentially characterised by a mix of features from several modern biomes. Some landscapes might have also hosted some plant functional types in regions beyond their modern bioclimatic range. In such cases, model outputs might disagree with pollen records since the model and pollen records do not focus on the same set of features. Mechanistic models should be able to deal with such non-analogue biomes since the simulated composition in plant functional types of a grid cell is based on competition and do not depend on pre-defined ecosystem types. However, converting these compositions into biomes based on modern definitions constrains the model outputs within the range of modern observations.

IV.5. Other sources of disagreement: conceptual differences and methodological biases

This weak rate of agreement generally lower than 0.50 and never reaching higher values than 0.61% whatever the comparison used (Fig. 5.6 – 5.11) might be related to multiple and diverse factors, from the poor representation of some ecological processes in the model, to the poor understanding of the relationships between the composition of the pollen records and the surrounding environment. Biases in the comparison method might also generate "artificial" disagreement and can be related to (i) the spatial and temporal scales used to estimate the biome cover, (ii) the equivalencies among pollen and model plant functional types, and their combination to define biomes, (iii) the use of simulated palaeo-climate data, and (iv) the accuracy of the biome-mapping methods used.

IV.5.1. Differences in the spatial and temporal scales of the biome cover estimation

Simulated biomes and pollen-based biomes focus on different spatial and temporal resolutions, potentially generating disagreement. On the one hand, the LPJ-GUESS model simulations estimate the biome cover as the average biome in a grid cell at a given spatial resolution (here 0.5 × 0.5-degree resolution, large scale) for a given time range (here, 100 simulated years), assuming that the state of vegetation is at equilibrium with climate. On the other hand, pollen-based biomes are estimations of the biome cover in the surrounding environment of a very local record site such a lake, a river, or a bog. In contrast with vegetation simulations, pollen records thus do not represent the average vegetation at a precise resolution and might represent vegetation in a state different from the equilibrium (e.g., vegetation recovering after a disturbance event such as deforestation). The pollen record at a given time results from the part of the local pollen rain that has been deposited and preserved in the record site during a period of time that is difficult to estimate. The pollen composition of a record is thus linked to the compilation of pollen rains reaching the deposition site during an unknown time resulting from multiple drivers such as the composition of the surrounding vegetation that is itself linked to complex processes (e.g., climate, disturbances, evolution history), the seasonality of pollen production, and the rate of sedimentation. Pollen records thus represent a distorting mirror of the actual state of vegetation. While this limits the bias of the short-term variations in vegetation composition, pollen records remain directly dependent of the seasonality of the pollen production, of the configuration of the surrounding environment, and of the vegetation growing directly around the deposition site. In contrast with simulated biomes, the pollen composition might thus be far from representing the highly hypothetical average and equilibrium state of the vegetation.

In addition, the effect of such scale-dependant uncertainties is worsened by the uncertainties in the age of the pollen records, especially at the Last Glacial Maximum. Indeed, Last Glacial Maximum data from Marchant et al. (2009) compile pollen records that have been estimated to represent this period. However, radiocarbon age estimates are often rare in pollen cores, (see Chapter 3 and reference therein), so the ages of large parts of the pollen cores are estimated based on age models. Both radiocarbon age estimates and age models that are associated with uncertainties.

Overall, the differences in the spatial and temporal scales of the biome cover estimation suggest that simulated and pollen-based palaeo-vegetation might tend to agree more when focusing on the main regional trends because synthesising the information across several sites (for pollen-based estimations) or grid cells (for model estimations) is likely to attenuate the above-mentioned biaises.

IV.5.2. Differences in the biome definition and the use of plant functional types

The biome definitions used for simulated biomes have been designed to match those of the pollen-based biomes from Marchant et al. (2009), but this theoretical equivalence relies on a set of assumptions that are difficult to verify, potentially leading to disagreement when comparing the two products. In Chapter 2, I have demonstrated that differences in biome definitions can lead to strong and spatially heterogeneous disagreement when comparing two biome maps, highlighting that such differences must be described and considered carefully. In this study, the equivalencies between simulated and pollen-based biomes were derived from theoretical equivalencies among plant functional types based on their bioclimatic range and physiological properties (Fig. 5.1; Tables 4, 5). However, the equivalencies among plant functional types are open to scrutiny due to the differences in their definition and concept. In the model, a plant functional type groups all plants sharing a precise set of bioclimatic range and physiological properties (Tables 1, 2). Pollen-based plant functional types from Marchant et al. (2009) are identified in the pollen records based on a list of pollen grain taxa also sharing theoretically the same characteristics. However, unlike simulated plant functional types, the pollen taxa considered sometimes represent a wide range of plant species, including some with very different characteristics (Marchant et al., 2009). Although Marchant et al. (2009) have partially limited the effect of this bias by assigning where possible the pollen taxa to the plant functional type corresponding best to the most common taxa of the group, this was sometimes impossible, so some pollen taxa correspond to several plant functional types. For example, the Malvaceae taxa is an extremely diverse family of angiosperms including numerous taxa with various morphologies (including trees, shrubs, and grass), and adapted to a wide range of environments. The Malvaceae family is included in three pollen-based plant functional types in the Marchant et al. (2009), including tropical rain green tree (Tr1), dry tropical rain green tree (Tr2), and temperate forb (tef). In this example, a high frequency of Malvaceae pollen type in the record could thus either be interpreted as a tropical rain green tree or as a temperate forb.

Second, the definition of biomes in the model are based on the equivalent combinations of plant functional types. The estimations of pollen-based biomes are based on an affinity score based on the abundance of each taxon in the pollen record. In the model, I used the leaf area index of each plant functional types associated to a threshold specific to each biome as a substitute to the taxon abundance. While both methods rely on plant functional type abundance, the dominant plant functional types in the simulations might differ from the pollen taxa abundance. In particular, LPJ-GUESS is a simplified representation of the vegetation so the simulated plant functional types growing in a grid cell are less diverse than in the pollen record, and taxa represented in the pollen record are “filtered” for the reasons explained above. Therefore, despite my attempts to define simulated biomes with the same criteria than pollen-based biomes, there is no evidence that these definitions are actually equivalent, which could have generated additional disagreement artificially at rates that are not quantified. However, such biases are not specific to this study as they could apply to any site-by-site comparison approach at the biome level, just as they apply to current biome map comparisons (Chapter 2).

IV.5.3. Differences in the drivers of the relative abundances in plant functional types

Simulated biomes might mismatch with pollen-based biomes because the respective main drivers of the relative abundance in plant functional types are different and are both associated to biases that I detail below.

In the LPJ-GUESS model, the relative abundances in plant functional types result from competition processes that are mainly driven by the climate input, that is derived from palaeo-climate experiments that are biased by their very nature. Here, I used inputs from the TraCE-21ka palaeo-climate experiments that have mainly been validated with palaeo-climate records from the Northern Hemisphere (Liu et al., 2009; He et al., 2011). While I have debiased the data in each grid cell based on a comparison with data from weather stations using the algorithm provided in Traylor et al. (2021), the validity of most of the resulting palaeo-climate data in the Neotropical realm remains unclear. For example, I used past changes in the debiased cloud cover combined to clear sky solar radiations to estimate the amount of solar radiations reaching the ground and available for plants. Despite being highly related to the temperature and the amount of precipitations in the TraCE-21ka palaeo-climate experiments, past changes in the fraction of cloud cover are for now impossible to validate so their effect on vegetation must be considered carefully (Feng He, comm. pers.). In addition, while the ability of LPJ-GUESS to reproduce the main patterns of modern vegetation has been demonstrated (e.g., Smith et al., 2014), the behaviour of the model in environment contexts that have now disappeared is poorly known due to the lack of true validation material, even if some comparison with palaeo-environment records have been performed (e.g., Allen et al., 2010). For example, ecological interactions between vegetation and animals might have been very different in the past. Consequently, the effect of such changes on the distribution of the simulated biomes is unknown, such past changes in animal populations facilitating plant reproduction or dispersal or favouring some types of plant over others (e.g., large browsers facilitating the expansion of herbaceous vegetation; Hyvarinen et al., 2021). It is possible that the Neotropical realm hosted past biomes with no modern equivalent, such megafauna-promoted steppes.

In the pollen records, the relative abundances in plant functional types result from competition processes driven by climate, but also, among other factors, from the differences in pollen production and dispersal of the plant taxa. For example, plant taxa whose pollen is dispersed by the wind such as many trees and shrubs produce larger amount of pollen with higher dispersal distance than plant taxa whose pollen is dispersed by animals (e.g., bees, flies, mammals). Dispersal distance discrepancies among plant taxa have notably been demonstrated by Bush and Rivera (1998) in a forest in the Barro Colorado Island, showing that the pollen dispersal distance was as low as 5 meters for some taxa, while it reached more than 40 meters for others in the same environment. Among the possible consequences of such differences in pollen production and dispersal, the very high pollen production and dispersal of some tree taxa might facilitate the overestimation of forest cover in pollen records deposited in landscapes hosting mixed tree and grass vegetation. Consequently, the model is better suited to assess the large-scale effect of past climate changes on vegetation than to infer past vegetation patterns at local scales.

V. CONCLUSIONS

The simulated vegetation at the Last Glacial Maximum was largely composed by more open environments compared to the mid-Holocene and contemporary periods. The extent of deserts and tropical dry forests was greater, whereas the coverage of other tropical forests was diminished. Unlike the present, large areas of the Southern Cone were dominated by deserts, and most of the south-eastern Amazon Basin featured tropical dry forests. Meanwhile, tropical rainforests and warm temperate rainforests thrived in the Cerrado. However, this study also shows that palaeo-vegetation simulations poorly agree at the biome level with pollen records at local scale. This highlights the difficulties in drawing clear and robust conclusions about past vegetation changes at the local scale and about the processes driving them, in contrast with the relatively better agreement from a regional trend point of view (Chapter 3, Chapter 4). This poor agreement may suggest the prevalence of ecological factors not considered in the model acting at local scales, such as megafauna or human land-use, that may affect both the modern calibration and past vegetation hindcasts. However, several steps may also be responsible for the observed disagreement, such as unperfect plant functional types equivalencies, or the absence of a numeric and georeferenced biome calibration map that led us to calibrate biomes by visual comparison. The differences between simulated biomes and pollen-based biome reconstructions highlight the need for more interdisciplinary studies based on a diversity of independent sources of past biome data to better reconstruct the actual past changes in biome distribution. In this context, future research should focus on comparing several vegetation models, driven by various set of palaeo-climate experiments, with multiple proxies of past environments such as pollen records, plant macrofossils or animal remains. In addition, the translation of the fossil record into biomes might be done using several methods of biomisation.

CHAPTER 6

CLIMATE-INDUCED VEGETATION CHANGES ALONE FALL SHORT OF EXPLAINING LATE PLEISTOCENE MEGAFAUNA EXTINCTIONS IN THE SOUTHERN CONE

ABSTRACT

More than 80% of the South American Pleistocene megafauna species (weighting more than 44 kg) went extinct during the last deglaciation, by the end of the Antarctic Cold Reversal ~ 12,700 years before present (BP). The processes that led to these extinctions are still debated, mainly because several major environmental changes were contemporaneous with those extinctions. South American megafauna extinctions might have resulted from complex mechanisms, including the synergistic effect of rapid climate change, sea-level rise, increasing human activities, and of a possible cosmic impact in southern Patagonia. Most fossil specimens of South American megafauna have been discovered in the Southern Cone (Patagonia and the Pampas). In the Southern Cone, climate change might have facilitated megafauna extinctions by promoting the retraction and fragmentation of the open landscapes that hosted most of the megafauna population. Variation in vegetation properties could have exacerbated extinction risk, including increases in forest cover and grassland fragmentation, and decreases in grass productivity or quality. However, the potential magnitude of this variation has not been quantified. I tested the hypothesis that the spatio-temporal pattern of megafauna extinctions in the Southern Cone is correlated with large vegetation shifts. I first derived the spatio-temporal pattern of megafauna extinctions from pre-published reliable fossil age estimates from radiocarbon dating. I identified 89 reliable age estimates out of 318 radiocarbon dates (28%). I grouped megafauna taxa into four main diet groups (grazers, browsers, generalist-opportunist herbivores, hypercarnivores), and calculated their most probable spatio-temporal pattern of extinction. I then compared these patterns with potential vegetation shifts derived from palaeo-vegetation simulations from the onset of the Antarctic Cold Reversal to the Pleistocene-Holocene boundary (15,000 to 11,700 BP). I applied a dynamic global vegetation model (LPJ-GUESS) forced by transient palaeo-climate data (TraCE-21ka-II). I show that most megafauna taxa associated with reliable age estimates most likely went extinct between 12,700 and 12,600 calibrated years before present (cal BP), and that extirpation (i.e., local extinction) events likely affected the whole Southern Cone from 13,800 to 11,800 cal BP, the last extirpations likely occurring on the Northern slopes of the Patagonian Andes. The responses of areas of open landscapes, and forage productivity and quality, to climate warming after the

Antarctic Cold Reversal were of limited amplitude. The Southern Cone lost around 2.9% of its total emerged land area between 13,000 and 12,000 BP, representing only a maximum of 4.8% of the open landscapes available for megafauna. Evidence of widespread fire following a cosmic impact is limited, and simulated fire risk in vegetation was also low, thereby indicating little opportunity for large fires. I argue that neither climate-driven vegetation changes, loss of emerged area due to sea-level rise, nor outstanding fire activity due a cosmic impact, would have been of sufficient magnitude to be the main cause(s) of the megafauna extinction in the Southern Cone.

KEY WORDS: Patagonia, palaeo-ecology, Quaternary, herbivory, ecological modelling

I. INTRODUCTION

The late Quaternary extinctions affected > 64% of megafauna genera (weighting more than 44 kg) on all continents in the last fifty thousand years, but the causes of these extinctions are still mostly unresolved (Koch and Barnosky, 2006; Johnson, 2009; Stuart, 2015). The extinctions started in Australia (61,000 years before present [BP]; Saltré et al., 2016), then Eurasia and Beringia (50–20,000 BP; Koch and Barnosky, 2006), and finished in the Americas (15,000 BP; Koch and Barnosky, 2006), and Africa (13,000 BP; Faith, 2014), with variable intensities and extents suggesting that they originated from different processes (Stuart, 2015). All these extinctions partly coincided both with climate changes and the arrival of *Homo sapiens* across continents, leading to long-standing debates to identify how megafauna vanished (Barnosky et al., 2004; Goebel et al., 2008). South America was the last, but the most affected continent (Koch and Barnosky, 2006). More than 80% of the South American Pleistocene megafauna species went extinct during the last deglaciation (Cione et al., 2009; Prates and Perez, 2021), but the causes of this extinction remain controversial.

Most remains of extinct megafauna in South America have been found in the Southern Cone (Patagonia and the Pampas) (Barnosky and Lindsey, 2010, Villavicencio et al., 2016, Prates and Perez, 2021). Available radiocarbon dates suggests that most extinctions occurred rapidly around 12,700 calibrated years before present (cal BP, representing the number of years before 1950 obtained after calibrating radiocarbon age estimates) (Metcalf et al., 2016; Pino et al., 2019; Messineo et al., 2021) at the end of the Antarctic Cold Reversal — an event observed in Antarctic ice cores and some palaeoclimate records from the Southern Hemisphere that interrupted the last deglaciation from ~ 14,700 to 13,000 BP (Metcalf et al., 2016; Pedro et al., 2016). Recent studies have suggested that the extinction event resulted from the synergistic role of rapid climate change after the end of the Antarctic Cold Reversal, the development of human culture and population expansion, including specialised hunting (Metcalf et al., 2016; Prates and Perez, 2021), and a possible cosmic impact ~ 12,770 ± 160 cal BP in Chile (Pino et al., 2019; West et al., 2020) concomitantly with multiple other impacts on Earth that are suggested to have triggered both the onset of the Younger Dryas ~ 12,900 BP and a multi-continental fire event (Firestone et al., 2007; Wolbach et al., 2018; Sweatman et al., 2021).

I detail below the scientific facts supporting these hypotheses. First, post-Last Glacial Maximum (~ 19,000 years ago to the present) climate changes including global temperature increase and changes in precipitation regimes promoted the gradual expansion of arboreal vegetation, including *Nothofagus* forests on the slopes of the Andes, in south-eastern Patagonia, and in Tierra del Fuego, but not in the Patagonian plains where the landscape remained open (see Chapter 3; Prentice et al., 1993; Werner et al., 2018; Allen et al., 2020). This forest expansion in the Southern Cone coincides with the southward displacement of the southern westerly winds from ~ 15,000 BP, and was likely driven by the warming of the southern Pacific Ocean (Boex et al., 2013; Davies et al., 2020).

Second, forest changes were accompanied by a 36-m rise in sea level globally between 15,000 and 12,000 BP (Spratt and Lisiecki, 2016) that submerged large portions of the continental shelf potentially reducing the territory available for megafauna populations (Prates and Perez, 2021).

Third, megafauna extinctions are concomitant with one or more possible cosmic impacts that may have caused major fire events (Firestone et al., 2007; Wolbach et al., 2018; Pino et al., 2019; West et al., 2020; Sweatman et al., 2021). To measure the impact of fire on a multi-continental scale around the Younger Dryas boundary ~ 12,800 BP, Wolbach et al. (2018) analysed charcoal and soot records from 152 sites in four continents (South and North America, Europe, Asia), including 13 sites from the Southern Cone, and demonstrated that an anomalous, multi-continental fire event occurred, burning an estimated 10 million km^2 of the Earth's surface and corresponding to ~ 9% of Earth's total biomass. That area estimate was 'considerably more' (Wolbach et al., 2018) than what is estimated to have occurred at the Cretaceous-Palaeogene boundary (i.e., 66 million years ago, when the extinction of all non-avian dinosaurs occurred).

Fourth, the timing of these megafauna extinctions also overlaps with an increase of archaeological evidence of megafauna exploitation by humans. Bampi et al (2022) have identified at least 10 sites in the Southern Cone with reliable evidence of megafauna exploitation by human (killing and/or scavenging). Moreover, megafauna extinctions were associated with a temporary increase in the production of fluted (Fishtail) projectile points, a projectile design associated in time and space with the largest extinct megafauna species, especially in archaeological sites from the Southern Cone, suggesting increasing hunting pressure from humans on megafauna populations (Prates and Perez, 2021; Prates et al., 2022). Forest expansion driven by climatic changes, the spread of megafire, sea-level rise, and increasing human pressure occurring in the same span of time likely facilitated megafauna extinctions via a reduction in and fragmentation of their habitats and possible predation (Metcalf et al., 2016; Villavicencio et al., 2016; Prates and Perez, 2021).

However, none of these hypotheses is yet clearly confirmed to be responsible of the South American megafauna extinction and all hypotheses lack quantification. Even the spatial extent of the Antarctic Cold Reversal is debated because palaeo-climate records have indicated a more intense cooling period in Antarctica and in the South Atlantic (south of 40 °S) relative to the rest of South America (Pedro et al., 2016). Unlike the south of Patagonia, the Pampas might therefore not have been affected as much by the Antarctic Cold Reversal. However, megafauna remains indicate a quasi-simultaneous extinction of all taxa in both regions (Metcalf et al., 2016; Villavicencio, 2016; Prates and Perez, 2021), which de-emphasises a dominant climate-change mechanism. The synergy of events suggests that the causes of extinctions may have varied regionally, promoting a region-based approach to assess the relative impact of each hypothesised mechanisms contributing to the South American megafauna extinction (e.g., Villavicencio, 2016), as also suggested for the other Late Pleistocene extinction worldwide (Stuart, 2015; Saltré et al., 2019).

Overall, several types of environmental change occurred at the time of the extinction of megafauna in the Southern Cone between 13,000 and 12,500 BP, but the relative importance of each remains unclear. This is mostly because the driver of megafauna extinction might vary at a regional scale, and the extent, magnitude, and timing of climate-driven vegetation changes at the end of the Antarctic Cold Reversal have yet to be quantified regionally. Several extinction hypotheses refer to the destruction of megafauna habitat including vegetation changes, thus highlighting the need to compare the timing of extinction of the various taxa based on their preferred habitat, which could partially be achieved by classifying them by diet habit. Different diets should theoretically lead to different response of the taxa to vegetation changes. For example, grazers should be more sensitive to the loss of open landscapes than browsers, generalists should be less affected by vegetation changes, and hypercarnivores should be sensitive to the population of their preys.

Modelling the most-probable spatial pattern of megafauna extirpation (i.e., local extinction) is a useful tool to assess the inter-regional differences in extirpation processes (e.g., Saltré et al., 2019). Such processes can be described via comparisons with spatial patterns of contemporaneous environmental changes (Saltré et al., 2019), including vegetation. Palaeo-vegetation proxies in the Southern Cone are sparsely distributed in space and time (see Chapter 3) and reflect the local state of vegetation resulting from multiple drivers including climate change, the effect of ecological engineers (e.g., human activities, megafauna grazing and browsing), or other external events such as volcanic eruptions or cosmic impacts. In contrast, dynamic global vegetation models provide spatially, and temporally continuous estimations of what vegetation should have been given a known climate pattern (see also chapter 2). Dynamic global vegetation models thus make it possible to discriminate and quantify the effect of climate from other drivers of vegetation changes.

In this chapter, I investigated the megafauna extinction driver from a vegetation change perspective. I tested the hypothesis that the end of the Antarctic Cold Reversal corresponded to large changes in the distribution of habitats used by extinct megafauna — i.e., a reduction and fragmentation of highly productive and nutrient-rich, open landscapes. I (1) compiled all available, reliable radiocarbon age estimates for Southern Cone megafauna to re-calculate an up-to-date pattern of regional disappearance; I then (2) grouped megafauna taxa into four diet categories to identify the differences in their temporal extinction patterns, and (3) inferred the spatio-temporal pattern of extinction of all extinct megafauna taxa using a bias-corrected for the inference of spatial patterns, assuming a single, taxonomically independent extinction event, to estimate extirpation events from fossil records; next, I (4) simulated palaeo-vegetation changes from the onset of the Antarctic Cold Reversal to the end of the Pleistocene (15,000 to 11,700 BP) using a dynamic global vegetation model forced with a transient palaeo-climate experiment, to obtain finer-scale vegetation changes and to compare it with species extirpation ; finally, I (5) compared several metrics of vegetation changes (woody vegetation cover, spatial extent of open landscapes, forage production and quality) with the spatio-temporal patterns of megafauna extinction to identify potential mechanisms related to vegetation changes that could have led to their extinction.

II. METHODS

II.1. Estimating the spatio-temporal patterns of megafauna extinction

II.1.1. Post-glacial megafauna remains

I collected a total of 318 direct radiocarbon age estimates of post-Last Glacial Maximum megafauna remains in the Southern Cone (Appendix S6.1), mainly from the database used in Prates and Perez (2021) that I expanded with cross-referencing of mentioned sources and going through data from original sources. For each age estimate, I checked the information from the original source to identify and correct possible reporting errors such as transcription errors, duplicate age estimates, or misidentified samples such those identified in the Cueva del Mylodon (Chile; Pérez et al., 2021). I collected all raw radiocarbon age estimates (not calibrated) and then calibrated them with the Southern Hemisphere SHcal20 calibration curve (Hogg et al., 2020) at 1 sigma (68.2% probability), using the OxCal 4.4 software (Bronk Ramsey, 2021).

Table 6.1. Megafauna taxa from the Southern Cone considered in this study. *Information was mainly derived from Villavicencio (2016), with additional information from González-Guarda et al. (2017, 2018) for Notiomastodon, and from van Geel et al. (2022) for Mylodon. Proxies used to describe the diet are indicated as follow: [1]morphology (qualitative or via morphometry on cranial or dental traits generally), [2]stable isotope composition, [3]dung composition, [4]dental microwears, [5]extent species.*

Taxon	Family	Estimated Body mass	Diet group	Diet details	Reference
Panthera onca mesembrina	*Felidae* (felid)	190 kg (Prevosti & Martin, 2013)	hypercarnivore	Mainly large preys (e.g., Hippidion, Lama guanicoe, Lama gracilis and possibly Mylodon)	Prevosti & Martin, 2013[1,2]
Smilodon populator	*Felidae* (felid)	220-360 kg (Christiansen and Harris 2005)	hypercarnivore	Mainly large preys (e.g., large camelids, ground sloths)	Prevosti & Martin, 2013[1,2]; Bocherens et al., 2016[2]
***Mylodon* (*darwinii*)**	Mylodontidea (ground sloths)	1,600 kg (Fariña et al., 1998)	grazer	Selective feeders for specific plants or parts of plants Grass and sedges	Moore, 1978[3]; Bargo et al., 2006[1]; Vizcaíno et al., 2006[1]; Bargo & Vizcaíno, 2008[1]; van Geel et al., 2022[3]
Megatherium americanum	Mylodontidea (ground sloths)	3-6 tonnes (Casinos 1996, Fariña et al., 1998)	browser	Woody plants in open habitat	Bargo, 2001[1]; Carretero et al., 2004[3]; Vizcaíno et al., 2006[1]; Green and Kalthoff, 2015[4]
***Glossotherium lettsomi* (synonym of *G. robustum*?)**	Mylodontidea (ground sloths)	(see Pitana et al., 2013)	grazer	Grass and herbaceous plants	Bargo & Vizcaíno, 2008[1]
Notiomastodon platensis	*Gomphoteriidae* (gomphotheres)	7 tonnes (Fariña et al., 2013)	generalist (opportunist herbivore)	Mixed feeder, highly flexible	Sanchez et al., 2004[2]; Domingo et al., 2012[2]; Melo Franca, 2014[2]; González-Guarda et al., 2017[2], 2018[2]
Hippidion saldiasi	*Equidae* (horses)	265 kg (Alberdi and Prado, 1993)	grazers	Herbaceous plants, selective diet	Sanchez et al., 2006[2]; Alberdi et al., 2007[2]
Equus neogeus	*Equidae* (horses)	370 kg (Alberdi and Prado, 1995)	grazers	Herbaceous plants, selective diet	Sánchez et al., 2006[2]
***Hemiauchenia* (*paradoxa*)**	*Camelidae* (camelids)	300 kg (Fariña et al., 2013)	generalist (opportunist herbivore)	Mixed-feeder, highly flexible	Feranec, 2003[1,2]
***Lama guanicoe* Pleistocene**	*Camelidae* (camelids)	100-120 kg (Franklin, 1982)	generalist (mixed, flexible diet)	Intermediate selective foragers, adapt to resource availability	Raedeke and Simonetti, 1988[5]; Fraser, 1998[5]; Puig et al., 1997[5]; Puig et al., 2001[5]
***Vicugna vicugna* (*Lama gracilis*)**	*Camelidae* (camelids)	45-55 kg (Franklin, 1982)	grazer	grazers	Franklin, 1982[5]

To identify possible differences in the temporal pattern of extinction depending on the diet habit of the extinct taxa, I grouped megafauna remains in four different diet groups (Table 6.1): grazers eating mostly herbaceous plants (grass, sedges, forbs, roots), browsers eating mostly woody vegetation (e.g., leaves or bark from trees and shrubs), generalist opportunist herbivores adapting to the type of resource available, and hypercarnivores eating large animals (Table 6.1). To that aim, I mainly derived information on each taxon from Villavicencio (2016), that I complemented with information from González-Guarda et al. (2017, 2018) for *Notiomastodon*, and from van Geel et al. (2022) for *Mylodon*. Diet information was derived from various proxies including cranial and dental morphology, dental microwears, stable isotope composition, dung composition, and knowledge about extent parent species.

II.1.2. Selecting reliable ages

Fossil megafauna bones and teeth are subject to diagenetic alterations and to contamination of collagen material by younger carbon from the surrounding depositional environment (e.g., humic compounds) and from conservation conditions, affecting the quantity and purity of available stable isotopes (Bronk Ramsey et al., 2004; Brock et al., 2013). Sources of contamination for uncharred plant samples, which are the dated material in megafauna excrements, are external humic matter and internal components (e.g., lignin, resins, waxes; Němec et al., 2010) – such samples are rare in comparison to bones and teeth. These contaminants may produce erroneous determinations resulting in underestimation of their age estimates by radiocarbon dating (Higham et al., 2006) thus affecting the estimated extinction timing when combined in a dataset.

Several chemical pre-treatments have been gradually developed to remove such contaminants from fossil and uncharred plant samples prior the measure of carbon isotopes, generally focusing on extracting and purifying the collagen (from bones and teeth) or the cellulose (from plant remains) consisting of large carbon chains (Němec et al., 2010; Brock et al., 2013). It has been demonstrated that the most-recently developed pre-treatments remove the contaminants more efficiently, such as gelatine ultrafiltration (i.e., sequential acid-basic-acid [ABA] pre-treatment adding an ultrafiltration step to purify gelatine; Brown et al., 1988) or Amberlite® XAD®-2 resin purification (i.e., hydrophobic crosslinked polystyrene copolymer resin adsorbent; Stafford et al., 1988) for bones and teeth, and ABA-derived methods (e.g., ABA + Bleach, that is the ABA followed by a bleaching step; Brock et al., 2010) for excrements (i.e., plant remains). Indeed, the XAD-2 method isolates the amino-acids from bones hydrolysed purified collagen using the XAD-2 resin, thus removing high molecular-weight humates and fulvic acids and provides the highest yields of protein from bones (Stafford et al., 1988). Ultrafiltration isolates the larger collagen chains using ultrafilters, thus removing the smaller chains that include most of the contaminants unsuitable for dating. This method removes low molecular-weight contaminants better than less rigorous methods (Brown et al., 1988; Bronk Ramsey et al., 2004; Higham et al., 2006), reducing environmental contaminants from soil-derived amino acids and removing degraded collagens or other short-chain proteins (Brock et al., 2010). The XAD-2 method is more commonly applied to specimens dated in the American laboratories (Herrando-Pérez, 2021), and the ultrafiltration is currently the most-widely used pre-treatment (Villavicencio, 2016).

The reliability of radiocarbon age estimates thus differs depending on the protocol routine applied to the fossil sample prior to estimating age. For example, Messineo et al. (2021) demonstrated that classic pre-treatment techniques could not remove some contaminants from fossil bones such as fulvic acids in the Campo Laborde site (Argentine Pampas). By purifying samples from humates with XAD-2 resin, they showed that the survival of megafauna in the Pampas in the early Holocene was not supported by radiocarbon age estimates based on up-to-date pre-treatment methods. To avoid such biases, I only selected age estimates using up-to-date pre-treatment methods, i.e., ultrafiltration (code AF) or XAD-2 resin purification on bones and teeth, and ABA-derived methods (e.g., ABA + Bleach, code UV) for excrements. Pre-treatment methods using ABA (code AG) and ion exchange gelatin (code AI) are considered outdated (Higham et al., 2006).

Other reliable pre-treatments exist, based on isolation of individual amino acids on collagen (see Brock et al., 2013) or on cellulose dissolution in ionic liquid (Němec et al., 2010), but such methods are not yet widely applied as they are expensive and time-consuming (Herrando-Pérez, 2021) and were not applied to the samples considered in this study.

For each age estimate, I gathered dating information regarding the pre-treatment type by reviewing original sources. In addition, I improved this dataset by collecting not reported pre-treatment information via personal communication from radiocarbon dating laboratory (i.e., Michael Dee for the Center for Isotope research, University of Groningen laboratory [GrA-], and Greg Hogdins for the University of Arizona AMS Laboratory [AA-]), and investigating directly age estimates from the Oxford radiocarbon website/ORAU database (i.e., age with a laboratory code prefix 'OxA-'), which provide preparation code associated to each method (mentionned above); codes are described in Brock et al. (2010) and Bayliss et al. (2016). Age estimates associated with ORAU preparation code NRC and NRC1 are ultrafiltered ages resulting from samples re-dating (Bayliss et al., 2016). I removed 3 age estimates on *Mylodon* remains from Cueva del Mylodon which Metcalf et al. (2016) suggested were ultrafiltered (i.e., OxA-26049, OxA-26048, and OxA-26121), but for which I was unable to confirm such pre-treatment by searching the laboratory code on the Oxford radiocarbon website. I removed from the dataset three age estimates from *Megatherium americanum* that have been rejected by previous studies (Politis et al., 2019; Messineo et al., 2021), despite using the XAD-2 or ultrafiltration pretreatment: (*i*) CAMS-171851 and CAMS-171861 (from Arroyo Seco 2) that had both been made on the same Metacarpal V sample (FCS.CLA.154) as the estimate CAMS-171852, the latter being preferred by Politis et al. (2019) based on its higher bone mass analysed and lower standard deviation, and (*ii*) CAMS-155863 because it was considered unreliable due to contamination by humic substances and appear as an outlier as it was found in a stratigraphic layer where several other dating analyses (using XAD-2) have given age estimates that are several millennia older (Messineo et al., 2021).

Overall, I gathered 318 radiocarbon age estimates representing at least 30 species from 76 sites (Table 6.2; Appendix S6.1), of which 89 ages representing 11 megafauna taxa from 28 sites had reliable ages estimates (28 %) from 19 sites (Table 6.2). The quantity of reliable age estimates available strongly varies among regions of the Southern Cone, with 64 reliable age estimates in Southern Patagonia (10 sites), 19 on the slopes of the Northern Patagonian Andes (16 sites), and only 6 in the Pampas (2 sites). At least 18 taxa were not represented by any reliable age estimate, including the entire Glyptodontidae family (e.g., *Doedicurus clavicaudatus, Glyptodont clavipes, Neosclerocalyptus sp., Neuryurus* sp.*, Sclerocalyptus ornatus*), some Camelidae (e.g., *Macrauchenia patachonica*, *Paleolama*), Equidae (*Equus andium*, *Hippidion principale*), Gomphoteriidae (*Stegomastodon platensis*), Scelidotheriidae (*Sclelidotherium leptocephalum*), Mylondontidae (*Lestodon*, *Glossotherium robustus*), and other phylogenetically isolated species including *Toxodon platensis*, *Arctotherium*, *Dusicyon avus*, *Pseudolopex culpaeus*, and *Eutatus seguini*. Full taxa descriptions are provided in Villavicencio (2016).

II.1.3. Estimating megafauna patterns of extinction

I inferred the spatio-temporal pattern of extinction for all taxa grouped together with the coupled space-time model described in Saltré et al. (2019), assuming a single, taxonomically independent extinction event. Dated fossil remains of extinct megafauna provide the input data to infer spatio-temporal patterns of extinction, but the age of the last occurrence record of a species diverges from the true extinction date due to preservation or sampling biases (the so-called Signor-Lipps effect; Signor et al., 1982). Over the last few decades, many statistical methods have been developed to estimate the dates of extinction of a species, based on the distribution of the dated remains along the time series (e.g., Solow, 1993; Roberts and Solow, 2003; McInerny et al., 2006). While these methods where originally designed to study modern extinctions, they have been adapted to the study of long-disappeared populations (e.g., Solow et al., 2006; Bradshaw et al., 2012; Saltré et al., 2015, 2019). These methods differ by their core assumption about the underlying distribution determining the probability of remains to be deposited, preserved, and found, which is generally unknown (Bradshaw et al., 2012).

Table 6.2. Reliable AMS ^{14}C age estimates (direct ages with pre-treatment information) on megafauna remains (bones, teeth, excrements) of felids, ground sloths, gomphotheres, horses, camelids and indeterminate megafauna from archaeological and palaeontological sites of Southern Patagonia, the Northern slopes of the Patagonian Andes and the Pampas regions (Southern Cone). *Pre-treatment methods with codes: ultrafiltration (code UF, NRC or NRC1), XAD-2 resin (XAD) and acid-base-acid followed by a bleaching step (ABA+Bleach, code UV). Pre-treatments of ages including preparation codes in parenthesis was verified in OxCal/ORAU database; codes are described in Brock et al. (2010) and Bayliss et al. (2016). Some pre-treatment methods were completed via personal communication with dating laboratories. All age estimates are collected non calibrated and then calibrated with Southern Hemisphere SHcal20 curve (Hogg et al., 2020) at 1 sigma (68.2% probability), calibrated with the OxCal 4.4 program (Bronk Ramsey, 2021): mu = mean, sigma = uncertainty. NR = not reported.*

Sites	Latitude (°S)	Longitude (°W)	Family	Taxa	Lab-code	Material	Pre-treatment	^{14}C age BP	error	^{14}C age calBP (mu)	error (1σ)	References
						Southern Patagonia						
Tres Arroyos	-53,38300	-68,78330	Equidae (horses)	*Hippidion saldiasi*	OxA-26123	bone/tooth	UF	10755	45	12730	19	Metcalf et al. 2016
			Equidae (horses)	*Hippidion saldiasi*	OxA-26124	bone/tooth	UF	12530	55	14796	188	Metcalf et al. 2016
			Camelidae (camelids)	*Lama guanicoe* Pleistocene	OxA-21477	bone/tooth	UF	10685	50	12690	42	Metcalf et al. 2016
			Camelidae (camelids)	*Lama guanicoe* Pleistocene	OxA-21371	bone/tooth	UF	10700	50	12699	37	Metcalf et al. 2016
			Camelidae (camelids)	*Lama guanicoe* Pleistocene	OxA-21370	bone/tooth	UF	10730	50	12717	28	Metcalf et al. 2016
			Camelidae (camelids)	*Lama guanicoe* Pleistocene	OxA-21369	bone/tooth	UF	10765	50	12735	24	Metcalf et al. 2016
Cueva del Puma	-52,09400	-69,73300	Camelidae (camelids)	*Lama guanicoe* Pleistocene	OxA-21475	bone/tooth	UF	10960	45	12872	71	Metcalf et al. 2016
Cueva de Los Chingues	-52,09361	-69,74194	Equidae (horses)	*Hippidion saldiasi*	OxA-26127	bone/tooth	UF	11435	50	13306	64	Metcalf et al. 2016
Cueva del Medio	-51,58333	-72,63300	Equidae (horses)	*Hippidion saldiasi*	OxA-26125	bone/tooth	UF	10810	45	12758	28	Metcalf et al. 2016
			Equidae (horses)	*Hippidion saldiasi*	OxA-26126	bone/tooth	UF	11570	50	13429	58	Metcalf et al. 2016
			Camelidae (camelids)	*Lama guanicoe* Pleistocene	OxA-21969	bone/tooth	UF	10630	55	12643	65	Metcalf et al. 2016
			Camelidae (camelids)	*Lama guanicoe* Pleistocene	OxA-21470	bone/tooth	UF	10720	45	12714	25	Metcalf et al. 2016
			Camelidae (camelids)	*Lama guanicoe* Pleistocene	OxA-21385	bone/tooth	UF	10725	45	12717	24	Metcalf et al. 2016
			Camelidae (camelids)	*Lama guanicoe* Pleistocene	OxA-21472	bone/tooth	UF	10740	50	12722	26	Metcalf et al. 2016
			Camelidae (camelids)	*Lama guanicoe* Pleistocene	OxA-21471	bone/tooth	UF	10750	50	12727	24	Metcalf et al. 2016
			Camelidae (camelids)	*Vicugna vicugna* (*Lama gracilis*)	OxA-21469	bone/tooth	UF	10925	45	12831	55	Metcalf et al. 2016
Cueva del Milodon	-51,56500	-72,62028	Felidae (felid)	*Panthera onca mesembrina*	OxA-14451	not reported	UF	11405	55	13274	62	Sagredo 2007, Labarca 2015, Metcalf et al. 2016
			Felidae (felid)	*Panthera onca mesembrina*	OxA-14453	bone/tooth	UF	11925	55	13806	114	Metcalf et al. 2016
			Felidae (felid)	*Panthera onca mesembrina*	OxA-14455	bone/tooth	UF	11995	55	13901	80	Metcalf et al. 2016
			Felidae (felid)	*Panthera onca mesembrina*	OxA-14450	bone/tooth	UF	12610	60	14995	144	Metcalf et al. 2016
			Felidae (felid)	*Panthera onca mesembrina*	OxA-22145	bone/tooth	UF	10905	45	12816	46	Metcalf et al. 2016
			Felidae (felid)	*Panthera onca mesembrina*	OxA-22146	bone/tooth	UF	11260	50	13161	46	Metcalf et al. 2016
			Felidae (felid)	*Panthera onca mesembrina*	OxA-22144	bone/tooth	UF	11305	50	13200	52	Metcalf et al. 2016
			Felidae (felid)	*Smilodon populator*	OxA-13717	bone	UF	11265	45	13162	44	Barnett et al. 2005, Prevosti & Martin 2013
			Felidae (felid)	*Smilodon populator*	OxA-14457	bone	UF	11420	50	13288	62	Barnett et al. 2005, Prevosti & Martin 2013
			Mylodontidea (ground sloths)	*Mylodon darwini*	OXA-26121	excrement	ABA+Bleach (code UV)	13025	50	15597	97	Brock et al. 2010, Metcalf et al. 2016
			Mylodontidea (ground sloths)	*Mylodon darwini*	OXA-26049	excrement	ABA+Bleach (code UV)	13230	75	15891	118	Brock et al. 2010, Metcalf et al. 2016
			Mylodontidea (ground sloths)	*Mylodon darwini*	OXA-26048	excrement	ABA+Bleach (code UV)	13285	75	15967	122	Brock et al. 2010, Metcalf et al. 2016
			Equidae (horses)	*Hippidion saldiasi*	OxA-26120	bone/tooth	UF	13325	60	16024	107	Metcalf et al. 2016
			Camelidae (camelids)	*Lama guanicoe* Pleistocene	OxA-21381	bone/tooth	UF	11875	50	13716	81	Metcalf et al. 2016
			Camelidae (camelids)	*Lama guanicoe* Pleistocene	OxA-21382	bone/tooth	UF	11235	50	13145	40	Metcalf et al. 2016
Cueva Lago Sofia 4	-51,54065	-72,58692	Felidae (felid)	*Smilodon populator*	OxA-22142	bone/tooth	UF	11095	50	13007	62	Metcalf et al. 2016
			Camelidae (camelids)	*Lama guanicoe* Pleistocene	OxA-22057	bone/tooth	UF	10830	100	12808	91	Metcalf et al. 2016
			Camelidae (camelids)	*Lama guanicoe* Pleistocene	OxA-21463	bone/tooth	UF	11370	45	13245	47	Metcalf et al. 2016
			Camelidae (camelids)	*Lama guanicoe* Pleistocene	OxA-21374	bone/tooth	UF	11435	50	13306	64	Metcalf et al. 2016
			Camelidae (camelids)	*Lama guanicoe* Pleistocene	OxA-20853	bone/tooth	UF	12455	55	14630	188	Metcalf et al. 2016
			Camelidae (camelids)	*Lama guanicoe* Pleistocene	OxA-21379	bone/tooth	UF	12470	50	14661	183	Metcalf et al. 2016
			Camelidae (camelids)	*Lama guanicoe* Pleistocene	OxA-21380	bone/tooth	UF	12500	50	14727	183	Metcalf et al. 2016
			Camelidae (camelids)	*Lama guanicoe* Pleistocene	OxA-21376	bone/tooth	UF	12520	55	14770	189	Metcalf et al. 2016
			Camelidae (camelids)	*Lama guanicoe* Pleistocene	OxA-21458	bone/tooth	UF	12545	50	14845	174	Metcalf et al. 2016
			Camelidae (camelids)	*Lama guanicoe* Pleistocene	OxA-21457	bone/tooth	UF	12595	50	14979	132	Metcalf et al. 2016
			Camelidae (camelids)	*Lama guanicoe* Pleistocene	OxA-20705	bone/tooth	UF	12605	60	14984	149	Metcalf et al. 2016
			Camelidae (camelids)	*Lama guanicoe* Pleistocene	OxA-21377	bone/tooth	UF	12650	55	15074	98	Metcalf et al. 2016
			Camelidae (camelids)	*Lama guanicoe* Pleistocene	OxA-20852	bone/tooth	UF	13265	55	15933	97	Metcalf et al. 2016
			Camelidae (camelids)	*Lama guanicoe* Pleistocene	OxA-21373	bone/tooth	UF	13275	55	15948	98	Metcalf et al. 2016

Sites	Latitude (°S)	Longitude (°W)	Family	Taxa	Lab-code	Material	Pre-treatment	^{14}C age BP	error	^{14}C age calBP (mu)	error (1σ)	References
Cueva Lago Sofia 4 *(continued)*	-51,54065	-72,58692	Camelidae (camelids)	*Vicugna vicugna* (*Lama gracilis*)	OxA-21375	bone/tooth	UF	10640	45	12659	55	Metcalf et al. 2016
			Camelidae (camelids)	*Vicugna vicugna* (*Lama gracilis*)	OxA-21466	bone/tooth	UF	10705	45	12706	30	Metcalf et al. 2016
			Camelidae (camelids)	*Vicugna vicugna* (*Lama gracilis*)	OxA-21465	bone/tooth	UF	11050	45	12979	65	Metcalf et al. 2016
			Camelidae (camelids)	*Vicugna vicugna* (*Lama gracilis*)	OxA-21461	bone/tooth	UF	12610	45	15018	102	Metcalf et al. 2016
			Camelidae (camelids)	*Vicugna vicugna* (*Lama gracilis*)	OxA-21467	bone/tooth	UF	13155	50	15785	87	Metcalf et al. 2016
			Camelidae (camelids)	*Vicugna vicugna* (*Lama gracilis*)	OxA-21464	bone/tooth	UF	13210	55	15860	92	Metcalf et al. 2016
			Camelidae (camelids)	*Vicugna vicugna* (*Lama gracilis*)	OxA-21462	bone/tooth	UF	13255	65	15922	107	Metcalf et al. 2016
			Camelidae (camelids)	*Vicugna vicugna* (*Lama gracilis*)	OxA-21378	bone/tooth	UF	13345	55	16054	100	Metcalf et al. 2016
			Camelidae (camelids)	*Vicugna vicugna* (*Lama gracilis*)	OxA-21460	bone/tooth	UF	13365	55	16084	98	Metcalf et al. 2016
			Camelidae (camelids)	*Vicugna vicugna* (*Lama gracilis*)	OxA-21459	bone/tooth	UF	13500	50	16276	89	Metcalf et al. 2016
			Camelidae (camelids)	*Vicugna vicugna* (*Lama gracilis*)	OxA-21967	bone/tooth	UF	13520	65	16308	110	Metcalf et al. 2016
			Camelidae (camelids)	*Vicugna vicugna* (*Lama gracilis*)	OxA-21968	bone/tooth	UF	13915	65	16896	114	Metcalf et al. 2016
Cueva Lago Sofia 1	-51,54065	-72,58692	Equidae (horses)	*Hippidion saldiasi*	OxA-26122	bone/tooth	UF	10750	45	12728	20	Metcalf et al. 2016
			Equidae (horses)	*Hippidion saldiasi*	OXA-9319	bone	UF (code NRC1)	10780	60	12746	36	Borrero 2008, Steele & Politis 2009, Metcalf et al. 2016, Bayliss et al. 2016
Casa del Minero 1	-48,57600	-68,91250	Camelidae (camelids)	*Vicugna vicugna* (*Lama gracilis*)	OxA-26128	bone/tooth	UF	10750	45	12728	20	Metcalf et al. 2016
Piedra Museo	-47,90000	-67,90000	Equidae (horses)	*Hippidion saldiasi*	AA-39362	bone	XAD-2[2]	9952	97	11468	161	Steele & Politis 2009
			Equidae (horses)	*Hippidion saldiasi*	OXA-15870	bone	UF (code NRC)	10675	55	12678	51	Steele & Politis 2009, Bayliss et al. 2016
Baño Nuevo 1	-45,26440	-71,44275	Mylodontidea (ground sloths)	*Mylodontinae*	CAMS-175746	bone	XAD-2	11290	60	13190	56	Labarca 2015, Villavicencio 2016
			Mylodontidea (ground sloths)	*Mylodon* sp.	CAMS-175047	bone	XAD-2	12040	100	13924	125	Labarca 2015, Villavicencio 2016
						Northern slopes of the Patagonian Andes						
Castro, Chiloé[4]	-42,50000	-73,80000	Gomphoteriidae (gomphotheres)	*Notiomastodon platensis*	PSUAMS-2426	tooth	XAD-2	13270	60	15942	103	González-Guarda 2018
Monte Verde	-41,50470	-73,20440	Gomphoteriidae (gomphotheres)	*Gomphotheriidae*	CAMS-175048	bone	XAD-2	13420	120	16161	183	Villavicencio 2016
Nochaco	-41,01900	-73,39000	Gomphoteriidae (gomphotheres)	*Notiomastodon platensis*	PSUAMS-2424	tooth	XAD-2	17130	90	20686	108	González-Guarda 2018
Mulpulmo[4]	-40,83000	-73,50000	Gomphoteriidae (gomphotheres)	*Notiomastodon platensis*	PSUAMS-2425	tooth	XAD-2	19550	130	23511	177	González-Guarda 2018
Choroico[4]	-40,58000	-73,33000	Gomphoteriidae (gomphotheres)	*Notiomastodon platensis*	PSUAMS-2422	tooth	XAD-2	11345	45	13230	47	González-Guarda 2018
Pilauco	-40,56667	-73,11600	Gomphoteriidae (gomphotheres)	*Notiomastodon platensis*	PSUAMS-2415	tooth	XAD-2	13240	60	15901	100	González-Guarda 2018
			Camelidae (camelids)	*Hemiauchenia* sp.	CAMS-175049	bone	XAD-2	11320	90	13220	78	Villavicencio 2016, González-Guarda et al. 2017
Tramalhue	-40,38330	-73,10000	Gomphoteriidae (gomphotheres)	*Notiomastodon platensis*	CAMS-175744	tooth	XAD-2	11380	70	13259	69	Villavicencio 2016
Los Lagos	-40,38330	-73,10000	Gomphoteriidae (gomphotheres)	*Notiomastodon platensis*	CAMS-175749	tooth	XAD-2	11790	80	13654	92	Villavicencio 2016
Río Bueno	-40,37700	-73,02700	Gomphoteriidae (gomphotheres)	*Notiomastodon platensis*	CAMS-175733	tooth	XAD-2	11090	70	12995	77	Villavicencio 2016
El Trébol (Chile)[4]	-40,33000	-73,33000	Gomphoteriidae (gomphotheres)	*Notiomastodon platensis*	UCI-101833	tooth	UF	28760	390	33055	589	González-Guarda 2018
Chan Chan[4]	-40,16000	-73,08000	Gomphoteriidae (gomphotheres)	*Notiomastodon platensis*	PSUAMS-2423	tooth	XAD-2	10250	45	11970	135	González-Guarda 2018
La Plata[4]	-40,08000	-72,50000	Gomphoteriidae (gomphotheres)	*Notiomastodon platensis*	UCI-102088	tooth	UF	12315	40	14344	207	González-Guarda 2018
Alto de Boroa[4]	-38,75000	-72,85000	Gomphoteriidae (gomphotheres)	*Notiomastodon platensis*	PSUAMS-2430	tooth	XAD-2	11875	50	13716	81	González-Guarda 2018
Lonquimay	-37,70890	-71,25730	Mylodontidea (ground sloths)	*Glossotherium lettsomi*	CAMS-175740	bone	XAD-2	10960	70	12892	87	Villavicencio 2016
Tagua Tagua	-34,46889	-71,16639	Gomphoteriidae (gomphotheres)	*Notiomastodon platensis*	CAMS-175743	tooth	XAD-2	12260	80	14298	223	Villavicencio 2016
			Gomphoteriidae (gomphotheres)	*Notiomastodon platensis*	PSUAMS-2429	tooth	XAD-2	11750	60	13616	81	González-Guarda 2018
Quereo	-31,93075	-71,51194	Gomphoteriidae (gomphotheres)	*Notiomastodon* sp.	CAMS-175817	bone	XAD-2	10940	80	12881	89	Villavicencio 2016
			Gomphoteriidae (gomphotheres)	*Notiomastodon* sp.	CAMS-175732	tooth	XAD-2	10970	70	12902	88	Villavicencio 2016
						Pampa						
Arroyo Seco 2	-38,18000	-60,55000	Megatheriidae (ground sloths)	*Megatherium americanum*	OxA-10387	bone	UF	12155	70	14051	138	Politis et al. 2016, Steele & Politis 2009
			Megatheriidae (ground sloths)	*Megatherium americanum*	CAMS-58182	bone	XAD-2	12200	170	14279	330	Politis et al. 2016
			Megatheriidae (ground sloths)	*Megatherium americanum*	OXA-15871	bone	UF (code NRC)	12170	55	14074	107	Steele & Politis 2009, Bayliss et al. 2016
			Equidae (horses)	*Equus neogeus*	UCIAMS-142842	bone	UF	12170	45	14072	81	Politis et al. 2016
			Equidae (horses)	*Hippidion* sp.	AA-39365	bone	XAD-2[2]	11320	110	13223	98	Steele & Politis 2009
Campo Laborde	-37,05000	-61,10000	Megatheriidae (ground sloths)	*Megatherium americanum*	CAMS-171852[1]	bone	XAD-2	10655	35	12680	38	Politis et al. 2019

Footnotes: [1]multi-ages on one sample; [2]University of Arizona AMS laboratory (AA) personal communication; [3]sites not georeferenced in papers (coordonates from the nearest city or from the distribution map of González-Guarda et al. 2017)

Consequently, the performances of these models to infer the actual timing of species extinction differ based on the nature and distribution of the data (Bradshaw et al., 2012; Saltré et al., 2015).

I use the method described by Saltré et al. (2019), which is adapted from the method of Solow et al. (2006) non-spatial approach for the spatial inference of the regional patterns of megafauna extinctions. The non-spatial, maximum-likelihood method to correct for the Signor-Lipps effect developed by Solow et al. (2006) to study the late-Pleistocene extinctions of mammoths and horses in Alaska assumed (*i*) that the radiocarbon ages are independent and uniformly distributed, meaning that there is equal probability of recovering megafauna remains at any time during the interval, and (*ii*) a constant dating error across age estimates. In contrast, the coupled space-time model from Saltré et al. (2019) assumes that the error associated with radiometric age estimates are normally distributed. The coupled space-time model thus combines georeferenced age estimates from fossil remains and their associated standard deviations (laboratory error), to generate continuous maps of unbiased timings of megafauna regional extinction and their associated timing uncertainties.

I estimated the regional timing of megafauna extinction per cell of a spatial grid at a resolution of 0.5° × 0.5° latitude/longitude to match with the resolution of the climate data (see *Palaeo-climate experiments from TraCE-21ka,* below). To estimate an extinction age in each grid cell including in cells without data, I estimated an age based on the entire dataset by weighting each age as a function of its distance to the cell, with the sum of the weights for a given cell equal to 1. The closer the age to the cell, the more weight this age will have on the estimation of the cell's age. For each grid cell without data x, I considered only the ages located within a certain distance of the cell, determined by an optimised bandwidth (of even width across all grid cells) so that the larger the bandwidth, the more neighbouring dated specimens from x are considered in the approximation of the distribution (Silverman, 1986; Härdle et al., 2004). The size of bandwidth is optimised to find a trade-of between the local bias generated by accounting for data far away from the given grid cell (i.e., the larger the bandwidth, the higher the bias) and the local variance that increases when few data are considered (i.e., to narrow bandwidth). I thus ran the model with all possible bandwidth sizes and then selected the size of the bandwidth that was associated with the lower bias and associated variance following the steps described in Saltré et al. (2019). Finally, I subtracted to each grid cell estimate its associated bias to obtain a final, spatially unbiased continuous map of regional megafauna extinction.

II.2. Simulating palaeo-vegetation changes

II.2.1. Palaeo-vegetation simulations from LPJ-GUESS

I used the dynamic global vegetation model LPJ-GUESS (Smith et al., 2001, 2014) to simulate palaeo-vegetation distributions. LPJ-GUESS is a physiology-based mechanistic model that incorporates explicit relationships between environmental conditions and the biophysical and demographic characteristics of vegetation, and simulates the dynamic of the vegetation and biogeochemical cycles at regional to global scales. LPJ-GUESS takes as input monthly climate data (precipitation, number of wet days, temperature, solar radiation) and annual atmospheric CO_2 concentration to predict various vegetation and environment characteristics, including leaf area index. LPJ-GUESS is a combination of an individual-based model (GUESS models populations such that all individuals are considered explicitly), and a model based on populations of plant functional types (LPJ classifies plants according to their physical and phenological characteristics). I described the characteristics of the 19 competing plant functional types I used in Chapter 4.

Physiological and biogeochemical equations describe processes in the model based on a range of field observations, statistical inferences, and model adjustment validated against empirical observations (Haxeltine and Prentice, 1996; Smith et al., 2001, 2014). Most of the physiological and biogeochemical processes are then simulated at a daily time step (e.g., photosynthesis, respiration, transpiration, soil hydrology, etc.), while individual tree growth and vegetation dynamical processes are modelled annually (Hickler et al., 2004). LPJ-GUESS returns plant functional type (see Chapter 4) population characteristics for each cell of a landscape grid (following the resolution of the climate data: 0.5° × 0.5° latitude/longitude, see *Palaeo-climate experiments from TraCE-21ka,* below), where biological entities are individuals for trees and shrubs, and populations for graminoids, or one entity for each of the C_3 and C_4 types in a layer of grasses (Smith et al., 2001; Hickler et al., 2004). LPJ-GUESS has already been used to predict vegetation patterns in northern Eurasia and Chile around the Last Glacial Maximum (Allen et al., 2010; Werner et al., 2018), and to predict global-scale changes in biome distribution every thousand years (Allen et al., 2020).

I computed the leaf area index and annual net primary production for each grid cell independently as the mean of five replicate stands of 0.1 ha to balance any stochastically simulated processes including disturbances, plant establishment, and mortality. For each replicate stand, I ran the model for 500 simulated years to allow the simulated vegetation to reach 'equilibrium' with the conditions. I then ran the model for 3300 additional years (i.e., from 15,000 to 11,701 BP) to derive the annual means leaf area index and annual net primary production for each plant functional type. I also derived the simulated fire-return interval that is based on litter dryness and fuel availability, indicating the risk of fire related to vegetation state.

II.2.2. Palaeo-climate experiments from TraCE-21ka

I used data describing monthly palaeo-climatic drivers of vegetation dynamics (temperature, solar radiation, precipitation) and annual atmospheric CO_2 concentration from 15,000 to 11,700 BP derived from TraCE-21ka-II (He and Clark, 2022), a set of experiments done with the general circulation model CCSM3 (Collins et al., 2006; Otto-Bliesner et al., 2006; Yeager et al., 2006), an Earth-system model with coupled atmosphere-ocean-sea ice-land dynamics, and including a dynamic global vegetation module (see Chapter 4). CCSM3's horizontal resolution is ~ 3.75° for the atmosphere and ~ 3° for the ocean (Collins et al., 2006).

TraCE-21k-II (He and Clark, 2022), also named 'EXP-ACR' in He (2011) and Pedro et al. (2016), is a re-run of TraCE-21k-I, previously called 'TraCE-21ka' (e.g., Liu et al., 2009; He, 2011) from 14,900 BP. I described TraCE-21k-I more extensively in Chapter 4. The same climatic forcing was applied in TraCE-21k-I and TraCE-21k-II, including variation in Earth orbit, greenhouse gases, and ice sheets, but the meltwater forcing was modified in TraCE-21k-II (He and Clark, 2022). In particular, no meltwater flux was applied in TraCE-21k-II from 14,700 to 12,900 BP (He and Clark, 2022). TraCE-21k-II provides a more accurate representation than TraCE-21k-I of the Antarctic Cold Reversal in the Southern Cone (Pedro et al., 2016). TraCE-21k-II corrects for the inaccurate representation of the Antarctic Cold Reversal that is shorter and shows a higher amplitude in TraCE-21k-I than what is observed in the palaeo-climate proxies from Antarctica and the Southern Ocean due to an overestimation of the response of the Atlantic meridional overturning circulation to freshwater forcing in the climate model (He, 2011; Pedro et al., 2016).

I improved the realism of the climate inputs from TraCE-21k-II by comparing them to observed modern climate data. Climate models including CCSM3 are biased compared to observations, and their outputs must be corrected (i.e., debiased) prior to being used to hindcast the effect of climate change on biodiversity (He, 2011; Lorenz et al., 2016). For each grid cell, I used the procedure developed by Traylor (2021) for debiasing TraCE-21ka climate data for each input variable (i.e., temperature, solar radiation, precipitation), by comparison with modern climate datasets based on climate station data (i.e., CRUTS 4.01; Harris et al., 2014) from 1900 to 1990 CE. Traylor (2021)'s procedure consists first of downscaling TraCE-21ka climate data to a resolution of 0.5° × 0.5° latitude/longitude (i.e., the resolution of CRUTS 4.01), and then of considering their anomalies with CRUTS 4.01. Anomalies of temperatures and precipitation were measured by direct comparison with their CRUTS 4.01 equivalents (Fig. 6.1a,b). In TraCE-21k-II, solar radiations (downwelling solar flux at surface in W/m^2) are provided as sum of weighted means of clear sky and cloudy sky surface downwelling shortwave radiation flux, based on the simulated fraction of cloud cover (Traylor, 2021). Since clear-sky radiations originate from space, I assumed that most biases are related to the fraction of cloud cover (Traylor, 2021). To debias the solar radiation data, I first measured the modern anomalies in the total fraction of cloud cover (Fig. 6.1c), then I produced a debiased dataset of past fraction of cloud cover and used it to generate a debiased solar radiation dataset (see Traylor et al., 2021). Following Traylor (2021), I complemented the average TraCE-21k-II monthly precipitation with a metric of daily variability based on modern observations of the standard deviation of monthly precipitation from the CRU-JRA-55 database (Kobayashi et al., 2015; Harada et al., 2016) covering 1958 to 2017 CE.

The procedure developed by Traylor et al. (2021) excludes grid cells that are currently submerged, because no reliable data are available to measure the anomaly between TraCE-21k-II and CRUTS 4.01, since climate processes above land differ from

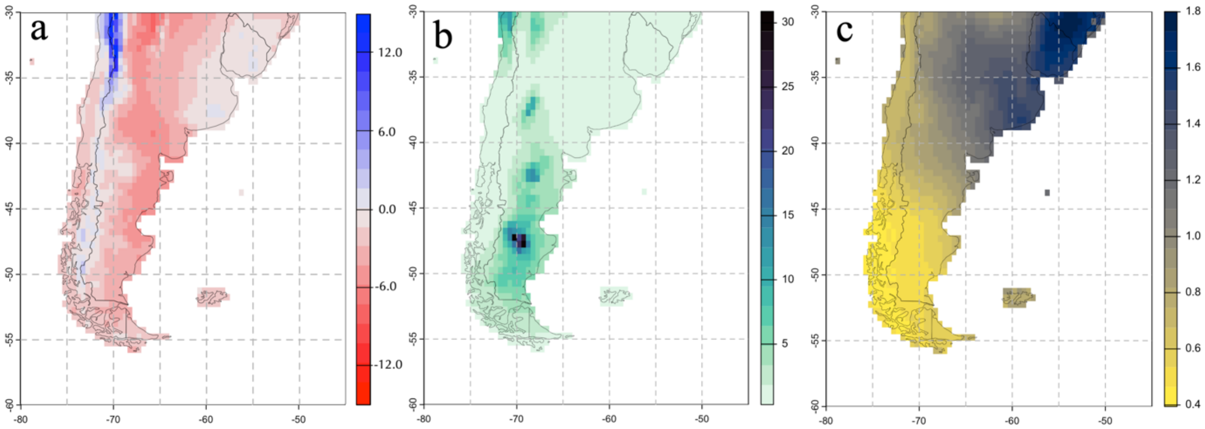

Figure 6.1. Average annual modern bias of the TraCE-21k-II palaeo-climate data. *For each grid cell, the bias between trace (TraCE-21k-II, He and Clark, 2022) and cru (CRUTS 4.01, Harris et al., 2014) are calculated using Traylor (2021). (a) temperatures in °C, where bias = trace − cru, (b) precipitations in fraction, bias = trace / cru, (c) cloud cover, bias = log(trace) / log(cru). See also Traylor (2021) for detailed methods.*

climate processes above oceans. I estimated past changes in emerged land area in the Southern Cone from 15,000 to 11,000 BP by combining elevation data with estimations of past sea levels using the function *expanse* from the R package `terra` (R Core Team 2022; Hijmans et al., 2023). I derived elevation data from the ETOPO-2022 dataset at a 60 arc-second resolution (NOAA National Centers for Environmental Information, 2022), a digital elevation model combining various sources of elevation data including airborne lidar, satellite-derived topography, and shipborne bathymetry datasets (McFerrin et al., 2021). I derived sea level changes every thousand years from Spratt and Lisiecki (2016) that identified statistically the common signal from seven continuous sea-level records derived from marine sediment cores at high temporal resolution (< 5,000 years).

In addition to climate and atmospheric CO_2 concentrations, the model incorporates the textural characteristics of the soil to represent the water-retention capacity of the soil layer. However, large uncertainties exist regarding the spatial distribution of textural properties of modern soils (Tafasca et al., 2020), and past variations in soil hydraulic properties remain largely unexplored. Due to the lack of past soil texture data, I used soil texture class data from current CRUNCEP records (Viovy, 2018) as inputs across all periods, assuming that the water-holding capacity of the soil layer remained constant over time. This aligns with the assumptions of prior studies that simulated past vegetation change using LPJ-GUESS (e.g., Allen et al., 2010; Huntley et al., 2023).

II.2.3. Model output analyses

I measured the simulated changes in vegetation in response to palaeo-climate forcing based on four vegetation features representing the habitat of megafauna species. Most extinct megafauna taxa from the Southern Cone had a diet adapted to open environments as shown by diverse diet proxies including dental or cranial morphology, dental microwears, stable isotope composition, dung composition, and comparison with extent species (Table 6.1). I thus assumed that the habitat from extinct megafauna from the Southern Cone was mainly characterised by open areas, as also suggested by previous studies (e.g., Cione et al., 2009). I focused on several landscape traits characterising open areas, including the woody vegetation cover (i.e., inversely proportional to vegetation openness), as well as forage quantity and quality.

I used the simulated woody (tree and shrub plant functional types) foliar projective cover (see details for foliar projective cover calculation in Chapter 4) to calculate the changes in total grassland and savanna area, using the IGBP biome definition of grasslands (i.e., woody cover < 10%) and savannas (i.e., 10% < woody cover < 30%) (Loveland and Belward, 1997). I also focused on forage quantity (simulated grass net primary production) and forage quality (simulated grass C:N ratio). Lower C:N ratio indicates higher crude protein (i.e., nitrogen-rich molecules) concentration in the plant so higher forage quality, while higher C:N ratio indicates higher carbon chain (e.g., cellulose, lignin) concentration so lower forage quality (Körner, 2002; Schädler et al., 2003; Milchunas et al., 2005).

III. RESULTS

III.1. Spatio-temporal pattern of extinction

The youngest ages of all megafauna taxa fall between ~ 11,500 and 15,600 BP, with two taxa (i.e., *Hippidion saldiasi* and *Notiomastodon platensis*) having their youngest age

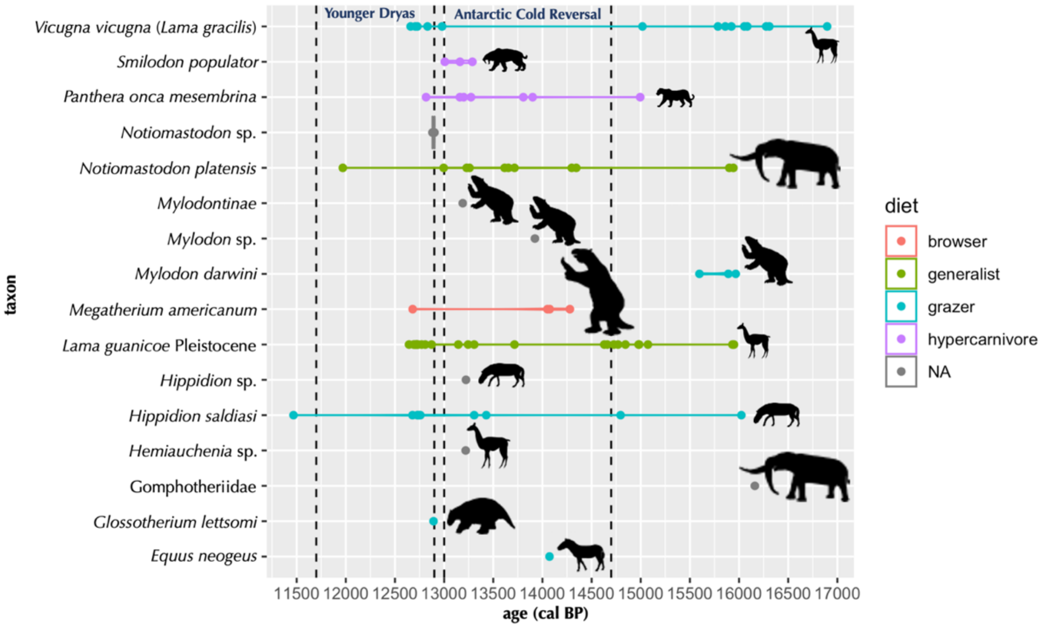

Figure 6.2. Reliable radiocarbon age estimates by megafauna taxon and diet group.

after 12,600 BP (Fig. 6.2). Among the taxa that are associated with > 1 reliable age estimate, the oldest youngest age estimate is associated with a *Mylodon darwini* from Cueva del Milodon (15,967 ± 122 cal BP; OXA-26048) (see site location on Fig. 6.3). Except *Mylodon darwini*, *Hippidion saldiasi* and *Notiomastodon platensis*, the youngest reliable age estimates (> 1) all other taxa fall between ~ 12,200 and 13,000 BP, with no specific pattern regarding megafauna diet (Fig. 6.2).

I estimated that megafauna extinction lasted ~2,000 to less than 1,000 years in the Southern Cone considering the uncertainties (i.e., from 13,800 to 11,800 BP), with a North-South pattern (Fig. 6.3). Megafauna most-likely first extirpated from the Pampas between 13,400 and 13,000 BP, associated with relatively high uncertainty compared to other areas (± 600 to 800 years; Fig. 6.3a,b,c). Then, megafauna extirpated from Southern Patagonia between 12,800 and 12,200 BP, associated with low uncertainty (± 100 to 500 years; Fig. 6.3a,b,c). Finally, megafauna extirpated from Northern slopes of the Patagonian Andes between 12,400 and 11,800 BP, with low uncertainty compared to other areas (± 300 to 500 years; Fig. 6.3a,b,c), representing the last phase of the overall extinction. In addition, several areas are associated with older extirpation events, reaching ~13,800 BP at lower latitudes associated with large uncertainties (± < 900 years; Fig. 6.3a,b,c).

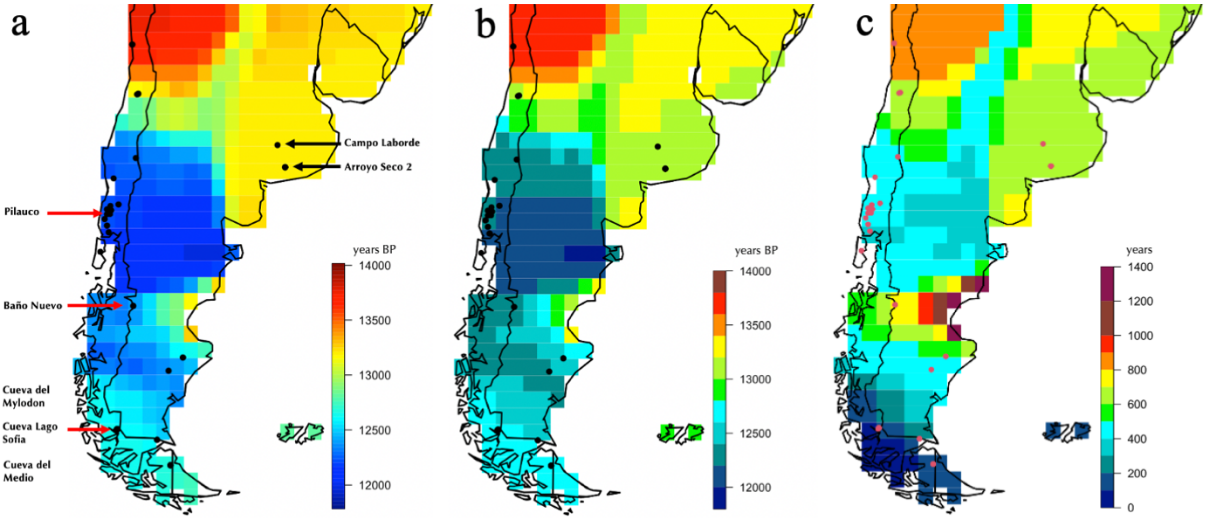

Figure 6.3. Spatial pattern of timing of megafauna extirpation and associated uncertainties. *(a) spatial timing of extirpation, (b) spatial timing of extirpation provided with a discrete scale to facilitate visualisation, (c) associated uncertainties. Time is expressed in calibrated years before present (cal BP). Additional methodological details are provided in Appendix 6.1.2.*

III.2. Environmental changes

Most simulated environmental transitions occurred at the end of the Antarctic Cold Reversal from ~13,000 to 12,700 BP (Fig. 6.4), generally representing rapid, lasting but low-amplitude state changes. During this period, the Southern Cone was characterised by an average 0.8 °C increase in annual temperatures (from ~10.6 °C to 11.4 °C), and an average decrease in monthly precipitation from ~ 2.1×10^{-5} to 1.95×10^{-5} kg m^{-2} s^{-1}. The potential fire-return interval only increased slightly from 500 to 525 years. Tree foliar projective cover decreased slightly from ~ 12 to 9%, while shrub cover increased slightly from 8 to 9%. The total area covered by grasslands decreased by < 7%, changing from ~ 1.6 million to 1.5 million km^2, while the total area covered by savannas increased by ~ 30% from ~ 0.5 million to 0.7 million km^2. Open landscapes thus expanded by around 0.1 million km^2 (10 million ha) in total, with most changes in woody cover occurring in the Pampas and on the slopes of the Andes from 35 to 45 °S (Fig. 6.5, 6.6). The average annual net primary production of grass recorded no substantial change (Fig. 6.4), but most changes occurred in the Pampas, with a decrease after the Antarctic Cold Reversal

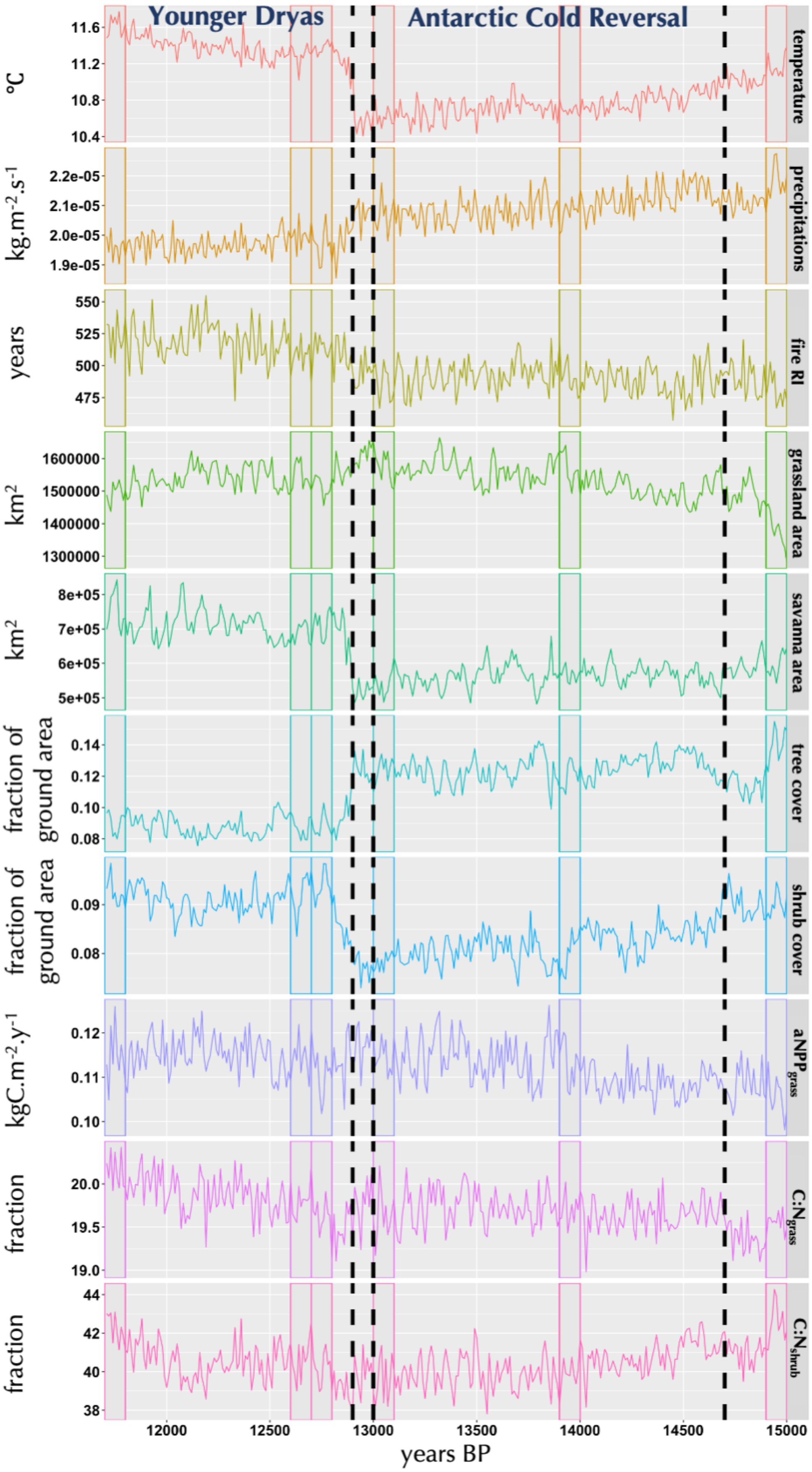
Younger Dryas
Antarctic Cold Reversal
°C
11.6
11.2
10.8
10.4
temperature
kg.m-2.s-1
2.2e-05
2.1e-05
2.0e-05
1.9e-05
precipitations
years
550
525
500
475
fire RI
km2
1600000
1500000
1400000
1300000
grassland area
km2
8e+05
7e+05
6e+05
5e+05
savanna area
fraction of ground area
0.14
0.12
0.10
0.08
tree cover
fraction of ground area
0.09
0.08
shrub cover
kgC.m-2.y-1
0.12
0.11
0.10
aNPPgrass
fraction
20.0
19.5
19.0
C:Ngrass
fraction
44
42
40
38
C:Nshrub
12000
12500
13000
13500
14000
14500
15000
years BP

Figure 6.4. Simulated environmental changes in the Southern Cone from 15,000 to 11,700 BP. *Shown are the changes in decadal means. The values represent the entire study area (i.e., the Southern Cone). Except for the total area covered by savannas and grasslands, the other variables are averages of all simulated gridcells. I used the simulated woody (tree and shrub plant functional types) foliar projective cover (see details for foliar projective cover calculation in Chapter 4) to calculate the changes in total grassland and savanna area, using the IGBP biome definition of grasslands (i.e., woody cover < 10%) and savannas (i.e., 10% < woody cover < 30%) (Loveland and Belward, 1997). For example, the savanna area for a given decade corresponds to the sum of the actual areas of all the grid cells in the Southern Cone where the fraction of woody cover (i.e., woody foliar projective cover) was on average greater than 10% for that decade. fire RI = fire return interval, i.e., the average time between two fires in a given grid cell; aNPP = annual net primary production, i.e., the mass of carbon gained by vegetation (here, by grass or shrubs) per unit area and time, representing the forage production; C:N = carbon-to-nitrogen ratio, i.e., the ratio of the mass of carbon to the mass of nitrogen in vegetation (here, grass or shrubs), representing the forage quality where lower values represent higher forage quality. All the environmental changes presented concern only the land that is currently emerged. Vertical bands correspond to the 100-year snapshots shown in Fig. 6.6–8.*

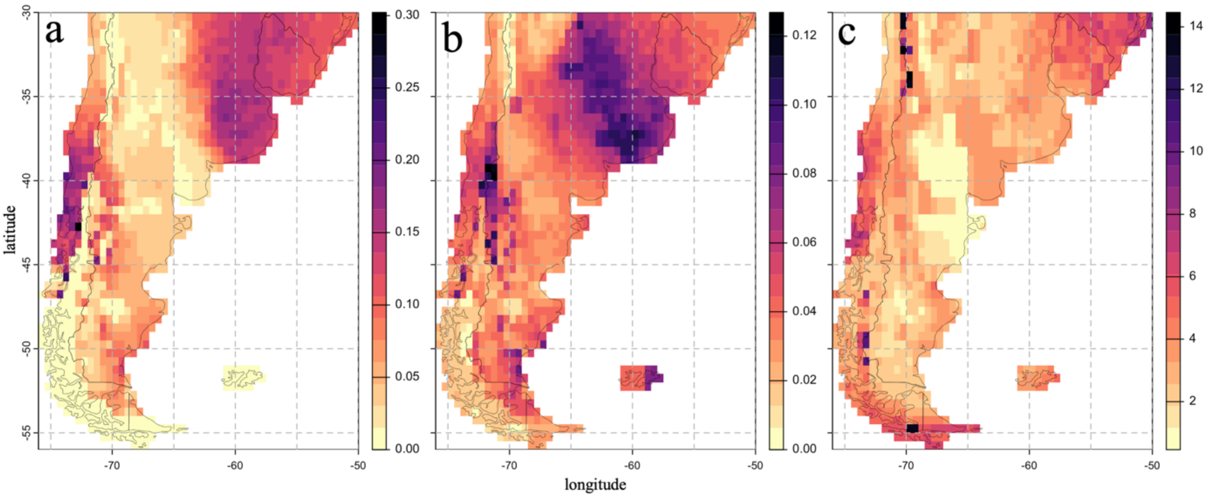

Figure 6.5. Spatial pattern of variation of a selection of simulated vegetation features from 15,000 to 11,700 BP. *(a) Woody foliar projective cover (i.e., tree and shrubs) expressed as a fraction of ground area, (b) grass annual primary production, in kg C m^{-2} $year^{-1}$, (c) forage quality (grass C:N), fraction. Variation is expressed via the standard deviation.*

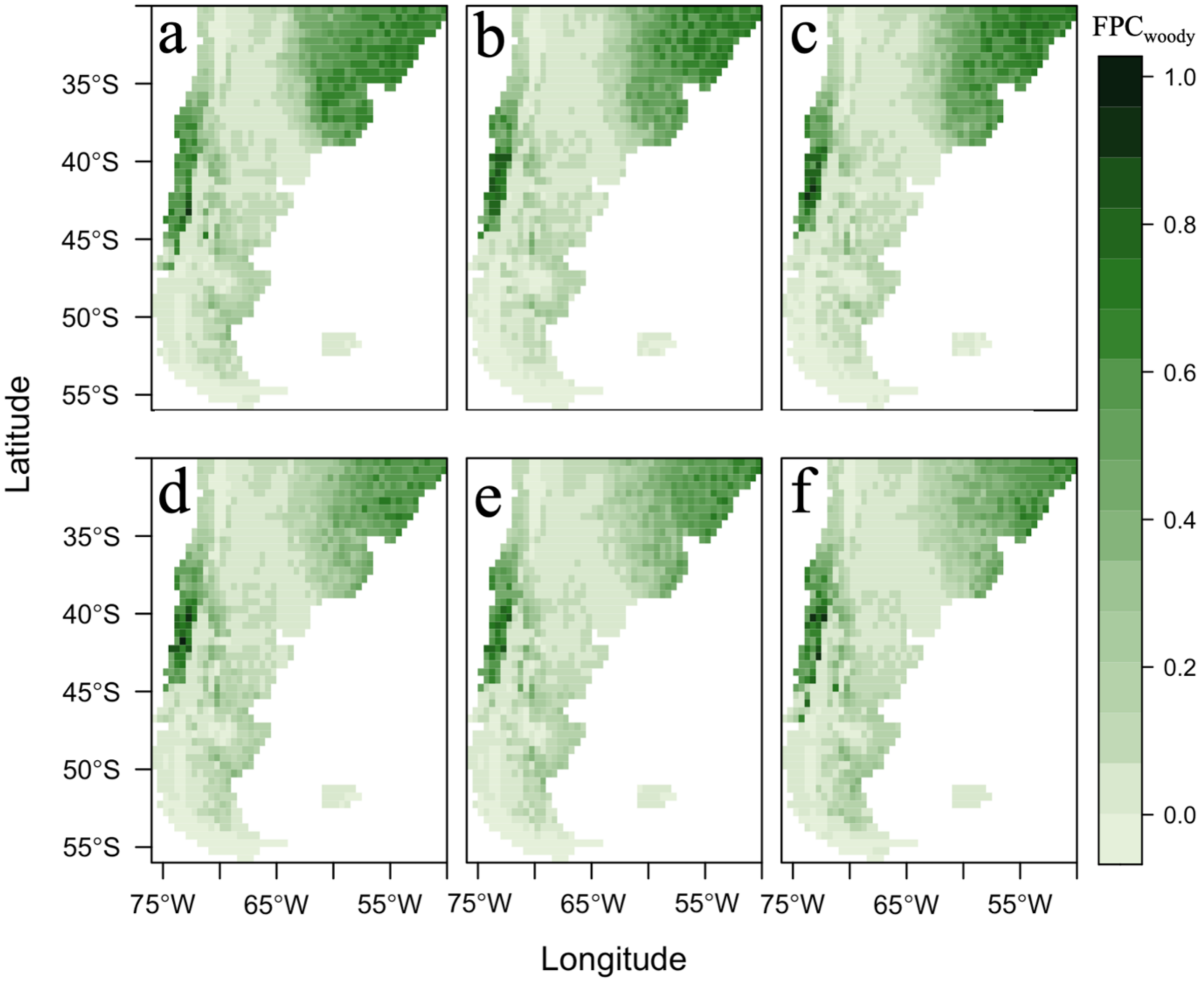

Figure 6.6. 100-year snapshots of the spatial distribution of the woody cover. *Woody cover (FPC$_{woody}$) is expressed as a fraction representing the total foliar projective cover of woody plant functional types (i.e., trees and shrubs), and ranges from the absence of woody plants (FPC$_{woody}$ = 0) to complete coverage by woody plants (FPC$_{woody}$ = 1). Shown are 100-year averages. (a) 15,000–14,901 BP, (b) 14,000–13,901 BP, (c) 13,100–13,001 BP, (d) 12,800–12,701 BP, (e) 13,700–13,601 BP, (f) 11,800–11,701 BP. Snapshots correspond to the vertical bands shown in Figure 6.4.*

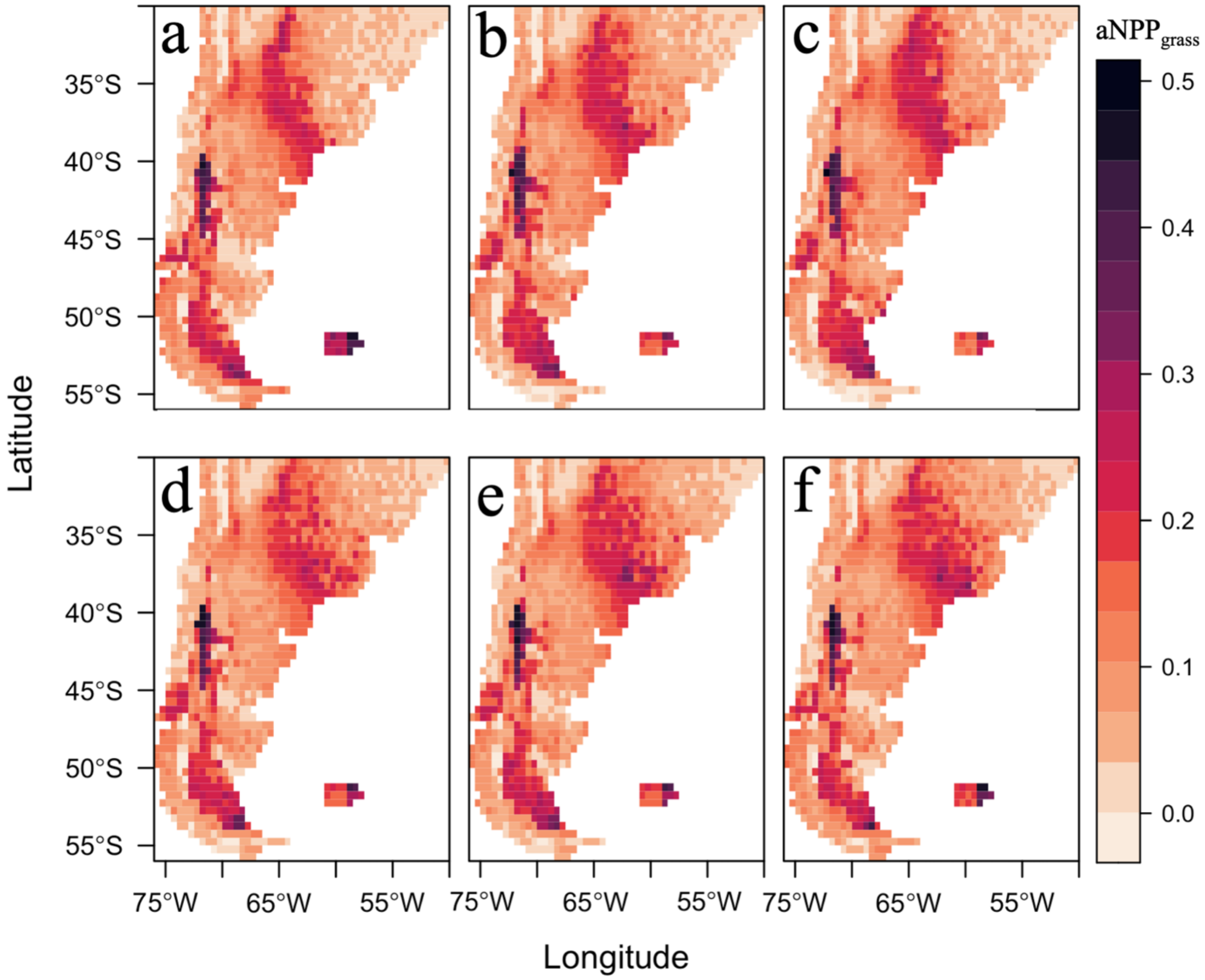

Figure 6.7. 100-year snapshots of the spatial distribution of forage production (grass annual net primary production, aNPP$_{grass}$). *The grass annual net primary production is the mass of carbon gained by herbaceous vegetation per unit area and time, representing the forage production, expressed in kgC.m^{-2}.y^{-1}. Shown are 100-year averages. (a) 15,000–14,901 BP, (b) 14,000–13,901 BP, (c) 13,100–13,001 BP, (d) 12,800–12,701 BP, (e) 13,700–13,601 BP, (f) 11,800–11,701 BP. Snapshots correspond to the vertical bands shown in Figure 6.4.*

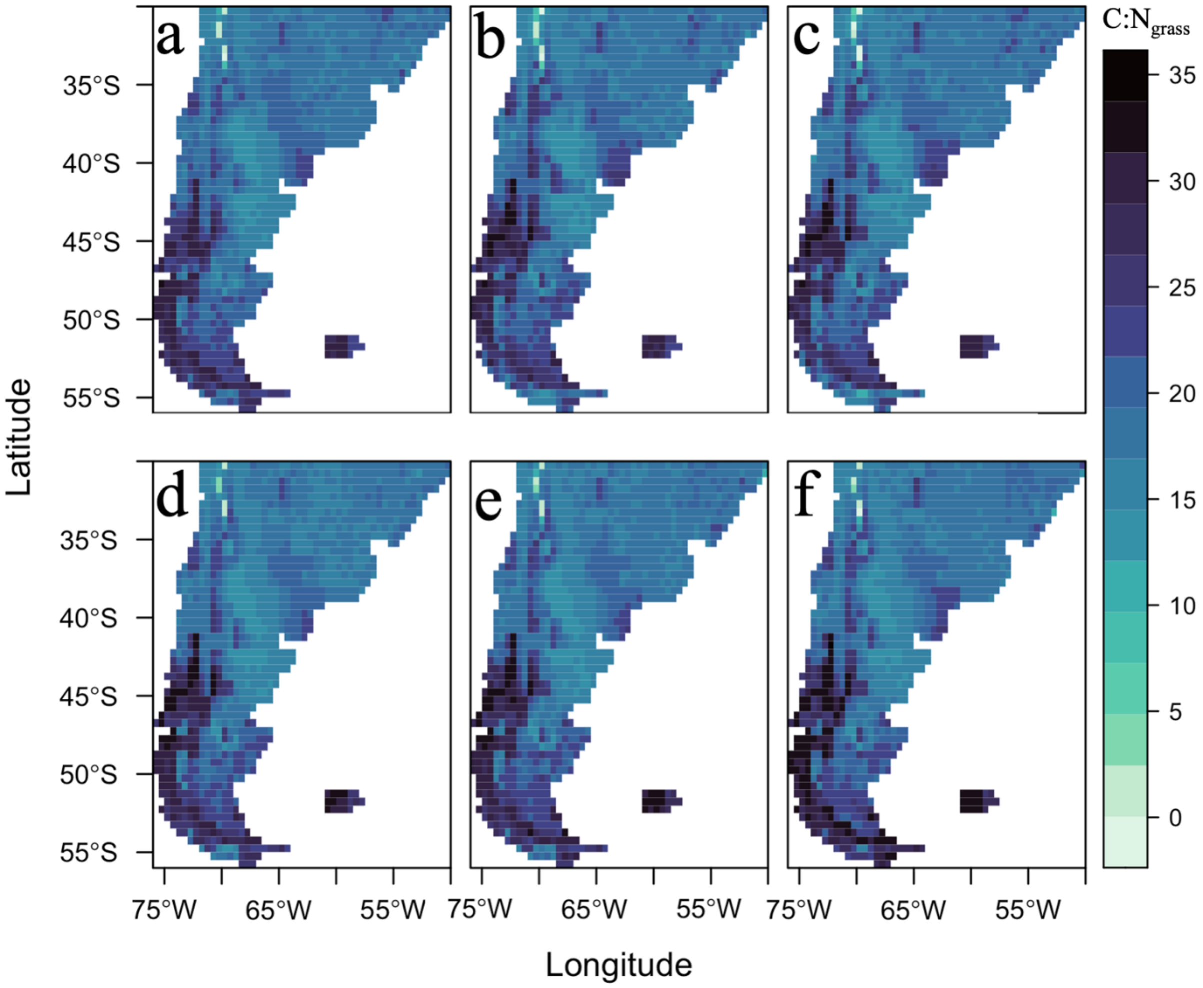

Figure 6.8. 100-year snapshots of the spatial distribution of forage quality (grass carbon-to-nitrogen ratio, C:N$_{grass}$). *The grass carbon-to-nitrogen ratio is the ratio of the mass of carbon to the mass of nitrogen in herbaceous vegetation representing the forage quality where lower values represent higher forage quality. Shown are 100-year averages. (a) 15,000–14,901 BP, (b) 14,000–13,901 BP, (c) 13,100–13,001 BP, (d) 12,800–12,701 BP, (e) 13,700–13,601 BP, (f) 11,800–11,701 BP. Snapshots correspond to the vertical bands shown in Figure 6.4.*

(Fig. 6.5, 6.7c,d). Forage quality (grass C:N) decreased slightly but only temporarily to values equivalent to those at the onset of the Antarctic Cold Reversal 15,000 BP, representing a slight increase in forage quality (Fig. 6.4, 6.5, 6.8c,d).

The increase in sea level caused an important loss of emerged area between 15,000 and 11,000 BP. The Southern Cone was characterised by ~ 605,445 km^2 of additional emerged land 15,000 BP compared to the present (Fig. 6.9), representing ~ 80% of the area of modern Chile. Between 15,000 and 12,000 BP, an estimated 315,947 km^2 of emerged land was lost due to sea level rise, corresponding to ~ 10% of the total area of the Southern Cone at 15,000 BP, and ~ 42% of the area of modern Chile. In the millennium were the core of extinction event likely occurred (i.e., between 13,000 and 12,000 BP), the Southern Cone lost 96,351 km^2.

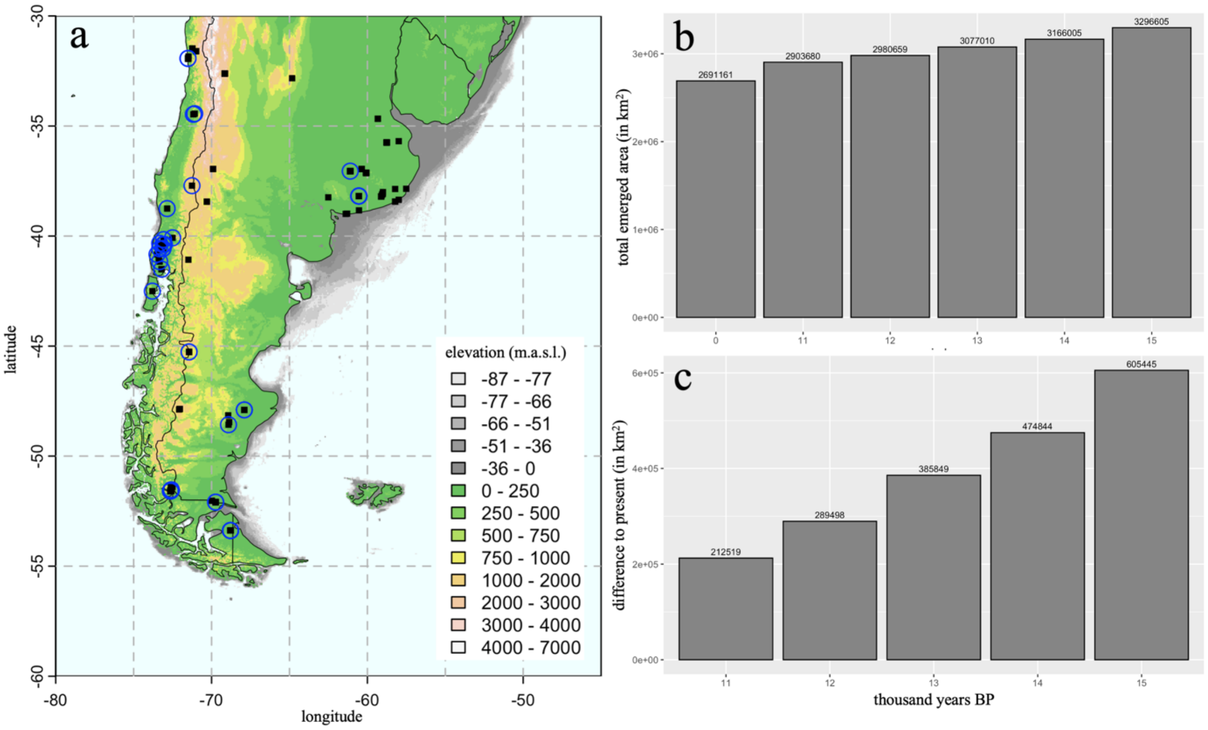

Figure 6.9. Effect of sea-level rise on the total emerged area (in km^2). *(a) Spatial distribution of the changes. The five shades of grey correspond to the estimated emerged area at 15,000, 14,000, 13,000, 12,000 and 11,000 BP, respectively. Black squares = sites with dated megafauna fossils, blue circles = sites with reliable age estimates (i.e., using gelatine ultrafiltration or XAD pre-treatment). m.a.s.l. = m above (modern) sea level. (b) Estimated total emerged area across the five periods mentioned and at present, (c) estimated difference the total emerged area between the five periods and the present.*

IV. DISCUSSION

Our results show that the extinction was most-likely not brutal spatially in the Southern Cone, but rather affected the whole region in ~1,000 to 2,000 years in two or three temporal phases, affecting first the Pampas at the end of the Antarctic Cold Reversal, then Southern Patagonia and the slopes of the Northern Patagonian Andes during the Antarctic Cold Reversal, with the last occurrences of most extinct species occurring during the post-Antarctic Cold Reversal warming (Fig. 6.2 – 6.4). The areas associated with older extirpation age estimates and large uncertainties likely result from the scarcity of the data (e.g., the Pampas; Fig. 6.3). Our results show that the simulated, < 1000 years extinction event affecting most megafauna taxa between ~ 12,800 and 11,800 cal BP (± 100 to 500 years; Fig. 6.3a,b,c) in Southern Patagonia and the Northern slopes of the Patagonian Andes (Fig. 6.2, 6.3) coincides with or occurred just after environmental changes previously mentioned as possible drivers of extinction. I quantified that this extinction event was associated with: (*i*) a climate-induced two-century decrease of 0.1 million km^2 in the area covered by grasslands (i.e., with woody foliar projective cover < 10%; Fig. 6.4) simultaneously with (*ii*) *a* 0.2 million km^2 increase in savanna (i.e., with woody foliar projective cover < 30%; Fig. 6.4) area, and (*iii*) a decrease in the average tree cover (Fig. 6.4). Moreover, I show that the extinction event also coincides with (*iv*) the loss of 96,351 km^2 of emerged area mainly from the Atlantic coast in the span of a millennium (Fig. 6.9).

However, testing the hypothesis that megafauna extinctions were caused by the loss of their habitat due to climate change (i.e., vegetation changes, loss of emerged area and the spread of megafire) requires assessing if the scales of these changes appear sufficiently high to affect 80% of the taxa in such a short timeframe. I describe below why I argue that these changes do not appear to be of sufficiently outstanding nature. First, the effect of warming following the Antarctic Cold Reversal on megafauna habitat was small. Our results support the conclusions of Chapter 3 that the deglacial increase in tree cover was mainly localised on the slopes of the Andes until the early Holocene, with landscapes remaining continuously open in the dry diagonal, southern-most Patagonia and the Pampas, with no substantial effect of the Antarctic Cold Reversal on vegetation (Fig. 6.5a, 6.6). The simulated response of vegetation suggests that while some changes effectively occurred between 13,000 and 12,500 cal BP, there were neither a substantial reduction in the total area covered by open landscapes, nor any reduction in the forage net annual primary production, nor any reduction of the forage quality (C:N) (Fig. 6.4). During the post-Antarctic Cold Reversal warming, the total area covered by grasslands (i.e., with woody foliar projective cover < 10%) would have decreased slightly but rapidly by ~ 7% (excluding currently submerged areas), but the total savanna area (i.e., with woody foliar projective cover < 30%) would have increased substantially, benefitting from the general decrease in tree cover (Fig. 6.4). This contradicts the hypothesis that climate change was responsible for a reduction in megafauna habitat via an increase in tree cover, stemming from the general increase in the extent of *Nothofagus* forests in the deglaciation period (i.e., from the Last Glacial Maximum ~ 19,000 BP to the end of the Pleistocene ~ 11,700 BP) in the Southern Cone observed in pollen records as suggested by Metcalf et al. (2016). In fact, the expansion of *Nothofagus* forests in the Southern Cone is exacerbated in the scientific literature due to the over-representation of the Andean slopes in the fossil record, i.e., where most of the general forest expansion occurred (Fig. 6.5a, 6.6; see also Chapters 3 and 4).

Second, the effect of sea-level rise of the total area of emerged land was of an order of magnitude too small to explain the extinction of the megafauna on its own. In absolute terms, the estimated reduction of the total emerged area between 13,000 and 12,000 BP might appear large (i.e., 96,351 km^2; Fig. 6.9), but it must be compared to the total surface area occupied by the various ecosystems of the Southern Cone. Examined as a percentage, the reduction was only 2.9% of the estimated total emerged area of the Southern Cone at ~ 15,000 BP, and 3.1% of the total emerged area at ~ 13,000 BP. Considering that open landscapes (combining grasslands and savannas), grasslands, and savannas covered an average of 2 million, 1.5 million, and 0.5 million km^2, respectively at ~ 13,000 BP (Fig. 6.9); this reduction of the total emerged area is also equivalent to 4.8% of the total open area, 6.4% of the total grassland area, and 19.3% of the total savanna area. These values indicate that whatever the type of vegetation that would have covered these now-submerged landscapes, most vegetation types would not have been affected, thus preserving most of the habitat. In addition, these changes would not have been extra-ordinary compared to previous millennia through which megafauna taxa persisted. However, my modelling experiments do not indicate if these small *a priori* changes could have represented a tipping point for megafauna populations, so more process-based modelling including megafauna demography are still necessary.

Third, the continuously low flammability of the vegetation seems incompatible with the hypothesis that megafires could have spread to the point of drastically reducing megafauna habitat. Some sites from the Southern Cone had higher fire activity around the Younger Dryas Boundary, but the studies generally do not highlight any link with a cosmic impact (e.g., Lago Eberhard and Pantano Dumestre; Villavicencio, 2016). Such an event would have caused a reduction in the habitat and biomass available to the megafauna; however, evidence of one or several cosmic impacts in the Southern Cone remain limited to one site (Pilauco, Chile; Pino et al., 2019), suggesting a limited event in the region. Moreover, the simulated average potential risk of fire (potential fire return interval > 500 years, based on litter dryness and fuel availability) remained consistently low in the Southern Cone from 15,000 to 11,700 BP (Fig. 6.4), suggesting that despite potentially high rates of ignition due to a cosmic impact, vegetation and climate would have prevented the spread of megafire over large areas. I therefore argue that the current data and my simulations do not support the hypothesis of a widespread fire episode around the Younger Dryas boundary that would have substantially reduced the habitat availability for extinct megafauna taxa.

Our conclusions are still contingent on several sources of uncertainty in most of the Southern Cone, except for the Southern Patagonian plains where age uncertainties are low. In particular, the Pampas is characterised by only 4 age estimates among which only one is < 13,000 cal BP and was considered by the model as an outlier. Despite currently available age estimates indicating a two-phase extinction affecting most of the Southern Cone, the scarcity of reliable data in some regions including in the Pampas, and the absence of age estimates for some widespread megafauna taxa, make it difficult to establish definitive patterns, except for Southern Patagonia.

Our results demonstrate the benefits of vetting the data when combining radiocarbon age estimates. By selecting only radiocarbon ages that were estimated on samples that were prepared using up-to-date pre-treatment methods (i.e., gelatine ultrafiltration or XAD-2 resin), I show that no age estimate was younger than a few centuries after the extinction peak previously estimated by Prates and Perez (2021), i.e., ~12,900 cal BP. This suggests that the numerous younger radiocarbon age estimates might result from polluted, poorly preserved megafauna remains. This support, but at a larger spatial scale the previous findings from Messineo et al. (2021) demonstrating that no megafauna taxa survived in the Holocene in the Pampas site of Campo Laborde, based on a re-analysis using only up-to-date pre-treatments.

V. CONCLUSIONS

Overall, my results support the theory that while climate change coincides temporally with the last occurrence of most megafauna species in the Southern Cone, it did not trigger their extinctions. While it could have slightly facilitated the extinction, the amplitude of changes in vegetation cover after the Antarctic Cold Reversal is not extraordinary. In the broader context of late Quaternary megafauna extinctions, vegetation has rarely been identified as the primary cause (Stuart, 2015). However, vegetation changes are often suggested to have acted as facilitators by reducing the habitat of megafauna populations making them more vulnerable to other events. The expansion of woody vegetation is thought to have fragmented the grass dominated vegetation in Northern Eurasia (e.g., the mammoth steppe) and North America, that are also the two continents with the most reliable chronology (Allen et al., 2010; Stuart, 2015). In contrast with Northern Eurasia, the megafauna extinctions in North and South America share several similarities such as their high intensity (respectively 80% and 69% of the species went extinct; Stuart, 2015), their occurrence a few millennia before the end of the Pleistocene (Faith and Surovell, 2009), and the short durations of the extinction processes (non-staggered, < two millennia). While the precise chronology of human expansion is still debated in the Americas, the rapid megafauna extinctions approximatively coincide with a sharp increase in dated human records on both continents (Goebel et al., 2008; Barnosky and Lindsey, 2010; Prates and Perez, 2021; Fiedl et al., 2022). However, on both continents the evidence of exploitation of megafauna by early human populations are rare and are associated with only a few taxa despite the massive production of hunting tools (Cione et al., 2009; Grayson and Meltzer, 2015; Prates and Perez, 2021; Bampi et al., 2022; Prates et al., 2022). Even a low level of predation by humans on certain species such as the *Lama guanicoe*, could have had a negative impact on the populations of other taxa (Pires et al., 2015; Pires et al., 2020), with potentially dramatic effect if the megafauna populations were already vulnerable. The estimated spatial pattern of megafauna extirpations in the Southern Cone presented in the present study shows that the latest extirpations likely occurred in Southern Patagonia, suggesting that megafauna populations had taken refuge in the South at the end of the Antarctic Cold Reversal, eventually making them highly vulnerable to external, unprecedented events that could at first sight be seen as having a restricted effect, such as the intensification of human hunting activities focusing on large animals (Prates and Perez, 2021; Bampi et al., 2022; Prates et al., 2022) or a cosmic impact (Pino et al., 2019). However, this pattern is associated with larger uncertainties in the North of the Southern Cone than in Southern Patagonia due to the scarcity of reliable age estimates. The Late Pleistocene extinction of most taxa from the Southern Cone remains a mystery, but I argue that neither climate-driven vegetation changes, nor the loss an emerged area due to sea-level rise, nor outstanding fire activity due a cosmic impact would have been sufficiently extraordinary to cause this unpresented extinction.

ACKNOWLEDGEMENTS

I thank Michael Dee and Greg Hogdins for kindly providing pre-treatment details respectively for Groningen (GrA- and GrN-), Arizona Lab (AA-) samples. I am grateful to Erwin González-Guarda for some inputs on megafauna diets.

CHAPTER 7

GENERAL CONCLUSIONS AND PERSPECTIVES

In this PhD thesis, I explored the response of Neotropical ecosystems to changes in post-Last Glacial Maximum climate and atmospheric CO_2 concentration, and the increase of human activities (~ 19,000 years ago to the present). The conclusions of the five core chapters can be grouped into three main themes: (*i*) the effect of climate change on ecosystems, (*ii*) the effect of human activities on ecosystems, (*iii*) the benefits of combining various types of data to study past ecosystems. I detail these three themes below.

I. EFFECT OF POST-LAST GLACIAL MAXIMUM CLIMATE CHANGE ON ECOSYSTEMS

I demonstrated that post-Last Glacial Maximum changes in climate and atmospheric CO_2 concentrations were responsible for widespread changes in tree cover in the Neotropical realm. This response of vegetation was supported by both the synthesis of information from palaeo-vegetation records (Chapter 3) and palaeo-vegetation simulations with the dynamic global vegetation model, LPJ-GUESS, coupled to the palaeo-climate experiments from TraCE-21k-I (Chapter 4, Chapter 5). Tree-cover changes were asynchronous among regions and most changes occurred in the deglacial period from the end of the Last Glacial Maximum to the beginning of the Holocene (Chapter 3, Chapter 4). Changes in precipitation regimes due to the southward displacement of the inter-tropical convergence zone in Heinrich Stadial 1 and the Younger Dryas were responsible for the southward displacement of forests in tropical and subtropical areas, potentially linking the Amazon and Atlantic rainforests via forests bridges in the modern Cerrado (Chapter 3, Chapter 4). The expansion of forests towards higher altitudes in the Andes and their southward expansion in Patagonia were mainly related to the increase in temperatures (Chapter 3, Chapter 4). At the end of the Last Glacial Maximum, the low atmospheric CO_2 concentration and high solar radiation might also have played an important role in the fragmentation of the Amazon rainforest (Chapter 3, Chapter 4).

In contrast with the general view that most of the vegetation from the continent was strongly affected by climate change, my simulations suggest instead that tree cover likely remained approximately stable across large areas, including the north-western part of the modern Amazon rainforest, the southern dry diagonal, and the Argentine Pampas (simulated tree cover standard deviation < 20%; Chapter 4), despite widespread changes in floristic composition (Chapter 3). This difference between the general view and the simulations could be explained by the under-representation of the stable areas in palaeo-vegetation records (Chapter 3), likely because most of these areas have been continuously characterised by dry conditions unsuitable to fossil preservation over the last 20 thousand years. Similarly, the hypothesis that climate change could have caused a large reduction in the habitat of the Late Pleistocene megafauna in the Southern Cone via the expansion of *Nothofagus* forests is likely due to the over-representation of Andean sites in the palaeo-vegetation record (Chapter 6). Despite the scarcity of dated megafauna remains outside the Southern Cone (Chapter 6), it is plausible that the estimated stability of large, open landscapes in the entire Neotropical realm (Chapter 4) provided suitable conditions for megafauna populations to survive climate variation following the Last Glacial Maximum.

II. EFFECT OF HUMAN ACTIVITIES ON ECOSYSTEMS

Although I did not focus primarily on the effect of human activities on Neotropical ecosystems, these activities emerge throughout the chapters as a major player in shaping vegetation patterns in the present and in the past, thereby altering our perception of what is considered as 'natural'.

I showed that modern vegetation simulations in the Neotropical realm tend to overestimate tree cover in areas where the rate of anthropogenic habitat loss is currently highest (Chapter 4). Such overestimates of tree cover occur in the Llanos, Central America, the Pampas, the Atlantic rainforest, the Cerrado, and parts of the Patagonian plains. In these regions, this overestimation suggests that climate could theoretically support denser forests, but that other factors might have prevented forests to develop, such as deforestation, cropping, or pastoralism. These interpretations warrant careful considerations because the over-estimation of tree cover could also be related to prediction error in the model, potentially linked to other ecological variables inadequately represented such as soil characteristics or the impact of large herbivores.

The simulated high tree densities in these areas suggest at least that these open areas are potentially highly productive. Regardless, human activities tend to be highest in areas with the highest primary productivity, suggesting that human populations settled preferentially in productive environments *a priori* suitable to forest growth, and have exploited these areas potentially to the point of modifying them profoundly over broad spatial scales. The effect of human populations on Neotropical ecosystems appeared in palaeo-environment records at least from the early Holocene with the development of agriculture (e.g., maize cropping in the tropical Andes ~ 8,000 BP; Chapter 3). The modification of Neotropical ecosystems by humans intensified in the last few centuries after European arrival with the development of broad-scale deforestation, cropping, and pastoralism, and the expansion of invasive plant species (Chapter 3). The megafauna extinctions of the Late Pleistocene in the Southern Cone suggest that humans might have influenced Neotropical ecosystems prior to the Holocene, but the evidence remains equivocal (Chapter 6). The results of the transient palaeo-vegetation simulations in the Southern Cone from 15,000 to 11,700 BP suggest that climate-induced vegetation changes were not the main drivers of megafauna extinction, bolstering the hypothesis that human endeavour that changed vegetation patterns and/or that directly exploited megafauna species were the main drivers of their demise, despite a lack of clear mechanism (Chapter 6).

In addition, human activities might not only have modified ecosystems, they might have also altered our vision of what ecosystems would be like without human intervention, thereby biassing our understanding of climate-vegetation relationships (Chapter 2). The biome concept is indeed a good illustration of this issue. In Chapter 2, I showed that there is neither a consensus biome map nor a universally accepted definition of terrestrial biomes. ‘Desert’, ‘rainforest’, ‘tundra’, ‘grassland’, or ‘savanna’ — while widely used terms in common language — have multiple definitions and no universally accepted spatial distribution. By quantifying the spatial differences among several widely used biome maps at global scales, I show that the widespread disagreement among biome maps is most likely related to high rates of anthropogenic habitat loss and land-use change, even between maps aiming to infer the distribution of biomes in the absence of human modification. In other words, our perception of what is considered as a ‘natural’ ecosystem remains blurred by the effect of human activities, suggesting that human impacts are largely under-estimated (Chapter 2). Consequently, what we know of the relationships between climate and vegetation is far from complete. The poor understanding of climate-vegetation relationships could also affect the performance of vegetation models, making it difficult to identify accurately the effect of climate changes on vegetation in the past, present, and future (Chapter 4, Chapter 5). More precisely, if the comparison of palaeo-vegetation simulations with palaeo-vegetation records shows good agreement when examining the main regional trends (Chapter 3, Chapter 4), this is potentially also a source of disagreement when looking at the biome level and at more local scales (Chapter 5). Such comparisons provide valuable information on the functioning of ecosystems at different scales, with the many areas of agreement making it possible to robustly identify the climatic origin of the vegetation patterns observed, and the disagreements highlighting the importance of more complex phenomena not taken into account in the model such as the effect of human activities, megafauna, or other local processes.

III. BENEFITS AND DIFFICULTIES OF COMBINING SEVERAL INDEPENDENT SOURCES OF INFORMATION TO ASSESS PAST ECOSYSTEM CHANGES: A MATTER OF SCALE

In this thesis, I adopted a multi-proxy approach by considering and comparing the information provided by the fossil records, simulation or inferences from modelling, and remotely sensed satellite data. Combining these different approaches requires considering their respective biases, the differences between the spatial scales to which they relate, and the ways in which they interpret raw data to describe ecosystems. I highlighted the conceptual and methodological differences between global biome maps (Chapter 2), comparing different approaches used to describe past, present, and future vegetation at broad spatial scales and showed that these approaches are highly complementary.

Current vegetation can be characterised by satellite data providing an overview of the vegetation, described by standardised functional criteria from local to global scales (Chapter 2, Chapter 4). Vegetation modelling, in particular using climate data, provides a better characterisation of the processes driving the observed patterns of current vegetation (Chapter 2, Chapter 4). Field observations complement this information by providing an insight into the complexity of vegetation at a local scale that would not be available in any other way, such as taxonomic diversity and some functional traits (unable to be captured using remote sensing approaches), thus highlighting the specific and functional diversity of ecosystems (Chapter 2, Chapter 3, Chapter 5).

When studying palaeo-vegetation, information is limited to fossil records and to the theoretical results of vegetation modelling. The description of past changes in vegetation at a broad scale is therefore necessarily based on the spatial extrapolation of fossil data, which also gives more support to the results of vegetation simulations when concordant, with simulations being more often used as a predictive tool of vegetation patterns (Chapter 2). In this context, it would be risky to draw hasty conclusions about changes in regional vegetation, for example by spatially extrapolating data from a single fossil site, or by taking the local results of simulations as 'truth'. To limit these biases, I have synthesised the local conclusions drawn from the palaeo-vegetation records by grouping sites by region to obtain the main regional trends (Chapter 3) and focused on the main trends provided by the simulated vegetation (Chapter 4). This regionalisation shows a better agreement between palaeo-vegetation records and simulations in terms of the main trends in forest-cover changes in space and time (Chapter 3, Chapter 4), than when comparing the same raw data at the biome level using a site-by-site approach (Chapter 5). Spatialisation of the fossil data also allows more precise, regional conclusions to be drawn regarding the pattern of extirpation of megafauna in the Southern Cone compared to the non-spatial description of extinction patterns (Chapter 6). Finally, the differences in agreement between these approaches make it possible to distinguish the periods and zones where knowledge is most robust, and those where uncertainties are greatest (Chapter 2, Chapter 3, Chapter 4, Chapter 5), enabling a more in-depth interpretation of past changes in vegetation. The spatial study of fossil records enables to identify the areas most lacking data, which are associated with greater uncertainties (Chapter 3, Chapter 6).

IV. CONCLUSIONS AND PERSPECTIVES

In this thesis, I have provided new insights on the response of ecosystems to post-Last Glacial Maximum changes in climate and atmospheric CO_2 concentrations and the increase in human population densities. I have demonstrated that both climate and humans have shaped vegetation and ecosystems more generally at the continental scale in the Neotropics after the Last Glacial Maximum. While the effect of climate (i.e., changes in temperature, precipitations, solar radiations) and atmospheric CO_2 appear to be predominant in large-scale ecosystem changes prior to the Holocene, human activities played an increasingly central role during the Holocene, resulting in a progressive decoupling between vegetation patterns and climate. This research also identifies several uncertainties in current knowledge, which could be clarified in future studies.

First, the spatio-temporal coverage of fossil data is heterogeneous, evidenced by the high concentration of palaeo-vegetation, archaeological, and megafauna records in Patagonia compared to the rest of the Neotropical realm. Certain regions, such as the Amazon Basin, the Pampas, and the dry diagonals, suffer from a lack of data, leading to major uncertainties about the history and functioning of the ecosystems they host. There is no doubt that the heterogeneous distribution of fossil data in the Neotropical realm is largely due to differences in preservation potential among regions. Moreover, even the most densely represented regions in the fossil record have large uncertainties, which could be partially resolved by adopting more refined methods. More specifically, improving the chronologies of vegetation and megafaunal fossil records by considering the reliability of dating (e.g., Chapter 6) should eventually enable to identify more precisely the relationships between climate, vegetation, megafauna, and human populations through robust chronological comparisons. As vegetation-modelling techniques improve, the methods for comparing palaeo-vegetation records and palaeo-vegetation simulations also need to be updated.

Second, the study of the causes of the extinction of the South American megafauna by chronological comparison is limited by the contemporaneity of multiple events in the last millennia of the Pleistocene, such as the increase in human activities, a hypothesised cosmic impact, climate change (i.e., the Antarctic Cold Reversal and the Younger Dryas), sea-level rises, and vegetation changes. This simultaneity suggests that all these events might have contributed at different scales and proportions to the extinction. Identifying extinction processes should therefore no longer rely solely on non-spatial chronological comparisons. The development and use of mechanistic models could help to test other hypotheses such as the collapse of food webs (Pires et al., 2015, 2020; Llewelyn et al., 2022; Strona and Bradshaw, 2022; Doherty et al., 2023), the effect of complex, taxon-dependent demographic processes (Bradshaw et al., 2021), and the potential effect of low-intensity human activities such as the manipulation of fire regime (e.g., Holz et al., 2016; Nanavati et al., 2019; Rozas-Davila et al., 2023). The development of such models therefore requires a greater understanding of megafauna taxa, for example their physiologies, migratory habits, and reproductive rates.

BIBLIOGRAPHY

Absy, M. L., Cleef, A., Fournier, M., Martin, L., Servant, M., Sifeddine, A., et al. (1991). Mise en évidence de quatre phases d'ouverture de la forêt dense dans le sud-est de l'Amazonie au cours des 60000 dernières années : Première comparaison avec d'autres régions tropicales. *Comptes Rendus de l'Académie des Sciences, Série 2*, *312*(6), 673–678.

Adams, J. M., & Faure, H. (1997). Preliminary Vegetation Maps of the World since the Last Glacial Maximum: An Aid to Archaeological Understanding. *Journal of Archaeological Science*, *24*(7), 623–647. https://doi.org/10.1006/jasc.1996.0146

Akaike, H. (1973). Information theory and an extension of the maximum likelihood principle. In F. Csáki & B. N. Petrov (Eds.), *2nd International Symposium on Information Theory* (pp. 267–281). Budapest, Hungary: Akadémiai Kiadó.

Alberdi, M. T., & Prado, J. L. (2008). Presence of *Stegomastodon* (Gomphotheriidae, Proboscidea) in the Upper Pleistocene of the coastal area of Santa Clara del Mar (Argentina). *Estudios Geológicos*, *64*(2). https://doi.org/10.3989/egeol.08642.044

Alberdi, M. T., & Prado, J. L. (1993). Review of the genus Hippidion Owen, 1869 (Mammalia: Perissodactyla) from the Pleistocene of South America. *Zoological Journal of the Linnean Society*, *108*(1), 1–22.

Alberdi, M. T., & Prado, J. L. (1995). Los mastodontes de América del Sur. *Evolución biológica y climática de la Región Pampeana durante los últimos*, *5*, 277–292.

Alberdi, M. T., & Prado, J. L. (2004). *Caballos fósiles de América del Sur: una historia de tres millones de años*. Olavarría: INCUAPA.

Alberdi, M. T., Prado, J. L., López, P., Labarca, R., & Martínez, I. (2007). *Hippidion saldiasi* Roth, 1899 (Mammalia, Perissodactyla) en el Pleistoceno tardío de Calama, norte de Chile. *Revista chilena de historia natural*, *80*(2), 157–171.

Alberdi, M. T., Miotti, L., & Prado, J. L. (2001). *Hippidion saldiasi* Roth, 1899 (Equidae, Perissodactyla), at the Piedra Museo Site (Santa Cruz, Argentina): Its Implication for the Regional Economy and Environmental Reconstruction. *Journal of Archaeological Science*, *28*(4), 411–419. https://doi.org/10.1006/jasc.2000.0647

Allen, J. R. M., Forrest, M., Hickler, T., Singarayer, J. S., Valdes, P. J., & Huntley, B. (2020). Global vegetation patterns of the past 140,000 years. *Journal of Biogeography*, *47*(10), 2073–2090. https://doi.org/10.1111/jbi.13930

Allen, J. R. M., Hickler, T., Singarayer, J. S., Sykes, M. T., Valdes, P. J., & Huntley, B. (2010). Last glacial vegetation of northern Eurasia. *Quaternary Science Reviews*, *29*(19–20), 2604–2618. https://doi.org/10.1016/j.quascirev.2010.05.031

Andrae, J. W., McInerney, F. A., Polissar, P. J., Sniderman, J. M. K., Howard, S., Hall, P. A., & Phelps, S. R. (2018). Initial Expansion of C_4 Vegetation in Australia

During the Late Pliocene. *Geophysical Research Letters*, *45*(10), 4831–4840. https://doi.org/10.1029/2018GL077833

Aramayo, S. A., Téllez, B. G., & Schillizzi, R. A. (2005). Sedimentologic and paleontologic study of the southeast coast of Buenos Aires province, Argentina: A late Pleistocene–Holocene paleoenvironmental reconstruction. *Journal of South American Earth Sciences*, *20*(1), 65–71. https://doi.org/10.1016/j.jsames.2005.05.002

Ardelean, C. F., Becerra-Valdivia, L., Pedersen, M. W., Schwenninger, J.-L., Oviatt, C. G., Macías-Quintero, J. I., et al. (2020). Evidence of human occupation in Mexico around the Last Glacial Maximum. *Nature*, *584*(7819), 87–92. https://doi.org/10.1038/s41586-020-2509-0

Arnold, J. R., & Libby, W. F. (1951). Radiocarbon dates. *Science*, *113*(2927), 111–120.

Asmerom, Y., Baldini, J. U. L., Prufer, K. M., Polyak, V. J., Ridley, H. E., Aquino, V. V., et al. (2020). Intertropical convergence zone variability in the Neotropics during the Common Era. *Science Advances*, *6*(7), eaax3644. https://doi.org/10.1126/sciadv.aax3644

Aymard, G. (2015). Bosques de los Llanos de Venezuela: estructura, composición florística, diversidad y estado actual de conservación. En: Tierras Llaneras de Venezuela, pp. 241-268. R. López F. et al. (eds.), 2° Edición, IRD-CIDIAT. Mérida, Venezuela.

Bagnouls, F., & Gaussen, H. (1957). Les climats biologiques et leur classification. *Annales de géographie*, *66*(355), 193–220. https://doi.org/10.3406/geo.1957.18273

Bahr, A., Hoffmann, J., Schönfeld, J., Schmidt, M. W., Nürnberg, D., Batenburg, S. J., & Voigt, S. (2018). Low-latitude expressions of high-latitude forcing during Heinrich Stadial 1 and the Younger Dryas in northern South America. *Global and Planetary Change*, *160*, 1–9. https://doi.org/10.1016/j.gloplacha.2017.11.008

Bailey, R. G. (1989a). *Ecoregions of the Continents: Map of Physical Environment: World*. Washington, USA: US Department of Agriculture, Forest Service.

Bailey, R. G. (1989b). Explanatory Supplement to Ecoregions Map of the Continents. *Environmental Conservation*, *16*(4), 307–309. https://doi.org/10.1017/S0376892900009711

Balátová-Tuláčková, E., & Surli, M. (1983). Contribution to the phytosociological characteristics of the Yaguaramas savanna (Cienfuegos Province, Cuba). *Folia Geobotanica et Phytotaxonomica*, *18*(1), 1–12. https://doi.org/10.1007/BF02855631

Bampi, H., Barberi, M., & Lima-Ribeiro, M. S. (2022). Megafauna kill sites in South America: A critical review. *Quaternary Science Reviews*, *298*, 107851. https://doi.org/10.1016/j.quascirev.2022.107851

Banda Rodriguez, K. P. (2017). *Phytogeography and conservation of neotropical dry forest, with emphasis on Columbia* (Ph.D.). University of Edinburgh. Retrieved from http://hdl.handle.net/1842/28955

Barberena, R. (2015). Cueva Huenul 1 Archaeological Site, Northwestern Patagonia, Argentina: Initial Colonization and Mid-Holocene Demographic Retraction. *Latin American Antiquity*, *26*(3), 304–318. https://doi.org/10.7183/1045-6635.26.3.304

Barberena, R., de la Paz Pompei, M., Otaola, C., Neme, G., Gil, A., Borrazo, K., et al. (2010). *Current Research in the Pleistocene*, *27*, 5–8.

Barberi, M., Salgado-Labouriau, M. L., & Suguio, K. (2000). Paleovegetation and paleoclimate of "Vereda de Águas Emendadas", central Brazil. *Journal of South American Earth Sciences*, *13*(3), 241–254. https://doi.org/10.1016/S0895-9811(00)00022-5

Bargo, M. S. (2001). The ground sloth Megatherium americanum: skull shape, bite forces, and diet. *Acta Palaeontologica Polonica*, *46*(2).

Bargo, M. S., De Iuliis, G., & Vizcaíno, S. F. (2006). Hypsodonty in Pleistocene ground sloths. *Acta Palaeontologica Polonica*, *51*(1).

Bargo, M. S., & Vizcaíno, S. F. (2008). Paleobiology of Pleistocene ground sloths (Xenarthra, Tardigrada): biomechanics, morphogeometry and ecomorphology applied to the masticatory apparatus, 23.

Barnett, R., Barnes, I., Phillips, M. J., Martin, L. D., Harington, C. R., Leonard, J. A., & Cooper, A. (2005). Evolution of the extinct Sabretooths and the American cheetah-like cat. *Current Biology*, *15*(15), R589–R590.

Barnosky, A. D., Koch, P. L., Feranec, R. S., Wing, S. L., & Shabel, A. B. (2004). Assessing the causes of Late Pleistocene extinctions on the continents. *science*, *306*(5693), 70–75. https://doi.org/10.1126/science.1101476

Barnosky, A. D., & Lindsey, E. L. (2010). Timing of Quaternary megafaunal extinction in South America in relation to human arrival and climate change. *Quaternary International*, *217*(1–2), 10–29. https://doi.org/10.1016/j.quaint.2009.11.017

Barnosky, A. D., Lindsey, E. L., Villavicencio, N. A., Bostelmann, E., Hadly, E. A., Wanket, J., & Marshall, C. R. (2016). Variable impact of late-Quaternary megafaunal extinction in causing ecological state shifts in North and South America. *Proceedings of the National Academy of Sciences*, *113*(4), 856–861. https://doi.org/10.1073/pnas.1505295112

Bayliss, A., Bronk Ramsey, C., Cook, G., Marshall, P., McCormac, G., & van der Plicht, J. (2016). Radiocarbon dates from samples funded by English Heritage between 1998 and 2003. Historic England, Swindon.

Beck, H. E., Zimmermann, N. E., McVicar, T. R., Vergopolan, N., Berg, A., & Wood, E. F. (2018). Present and future Köppen-Geiger climate classification maps at 1-km resolution. *Scientific Data*, *5*(1), 180214. https://doi.org/10.1038/sdata.2018.214

Beerling, D. J., & Mayle, F. E. (2006). Contrasting effects of climate and CO_2 on Amazonian ecosystems since the last glacial maximum. *Global Change Biology*, *12*(10), 1977–1984. https://doi.org/10.1111/j.1365-2486.2006.01228.x

Behling, H. (1995). A high resolution Holocene pollen record from Lago do Pires, SE Brazil: vegetation, climate and fire history. *Journal of Paleolimnology*, *14*(3), 253–268. https://doi.org/10.1007/BF00682427

Behling, H. (1997a). Late Quaternary vegetation, climate and fire history of the Araucaria forest and campos region from Serra Campos Gerais, Paran/t State (South Brazil). *Review of Palaeobotany and Palynology*, 13.

Behling, H. (1997b). Late Quaternary vegetation, climate and fire history from the tropical mountain region of Morro de Itapeva, SE Brazil. *Palaeogeography, Palaeoclimatology, Palaeoecology*, *129*(3–4), 407–422. https://doi.org/10.1016/S0031-0182(97)88177-1

Behling, H. (2001). Late Quaternary environmental changes in the Lagoa da Curuça region (eastern Amazonia, Brazil) and evidence of Podocarpus in the Amazon lowland. *Vegetation History and Archaeobotany*, *10*(3), 175–183.

Behling, H. (2007). Late Quaternary vegetation, fire and climate dynamics of Serra do Araçatuba in the Atlantic coastal mountains of Paraná State, southern Brazil. *Vegetation History and Archaeobotany*, *16*(2), 77–85. https://doi.org/10.1007/s00334-006-0078-2

Behling, H., Dupont, L., DeForest Safford, H., & Wefer, G. (2007). Late Quaternary vegetation and climate dynamics in the Serra da Bocaina, southeastern Brazil. *Quaternary International*, *161*(1), 22–31. https://doi.org/10.1016/j.quaint.2006.10.021

Behling, H., & Hooghiemstra, H. (1999). Environmental history of the Colombian savannas of the Llanos Orientales since the Last Glacial Maximum from lake records El Pinal and Carimagua. *Journal of Paleolimnology*, *21*(4), 461–476.

Behling, H., & Lima da Costa, M. (2000). Holocene Environmental Changes from the Rio Curuá Record in the Caxiuanã Region, Eastern Amazon Basin. *Quaternary Research*, *53*(3), 369–377. https://doi.org/10.1006/qres.1999.2117

Behling, H., & Negrelle, R. R. B. (2001). Tropical Rain Forest and Climate Dynamics of the Atlantic Lowland, Southern Brazil, during the Late Quaternary. *Quaternary Research*, *56*(3), 383–389. https://doi.org/10.1006/qres.2001.2264

Behling, H., & Safford, H. D. (2010). Late-glacial and Holocene vegetation, climate and fire dynamics in the Serra dos Órgãos, Rio de Janeiro State, southeastern Brazil. *Global Change Biology*, *16*(6), 1661–1671. https://doi.org/10.1111/j.1365-2486.2009.02029.x

Beierkuhnlein, C., & Fischer, J.-C. (2021). Global biomes and ecozones – Conceptual and spatial communalities and discrepancies. *Erdkunde*, *75*(4), 249–270. https://doi.org/10.3112/erdkunde.2021.04.01

Bennett, M. R., Bustos, D., Pigati, J. S., Springer, K. B., Urban, T. M., Holliday, V. T., et al. (2021). Evidence of humans in North America during the Last Glacial Maximum. *Science*, *373*(6562), 1528–1531. https://doi.org/10.1126/science.abg7586

Bigelow, N. H., Brubaker, L. B., Edwards, M. E., Harrison, S. P., Prentice, I. C., Anderson, P. M., et al. (2003). Climate change and Arctic ecosystems: 1. Vegetation changes north of 55°N between the last glacial maximum, mid-Holocene, and present. *Journal of Geophysical Research: Atmospheres*, *108*(D19). https://doi.org/10.1029/2002JD002558

Blonder, B., Nogués-Bravo, D., Borregaard, M. K., Donoghue, J. C., Jørgensen, P. M., Kraft, N. J. B., et al. (2015). Linking environmental filtering and disequilibrium to biogeography with a community climate framework. *Ecology*, *96*(4), 972–985. https://doi.org/10.1890/14-0589.1

Bocherens, H., Cotte, M., Bonini, R., Scian, D., Straccia, P., Soibelzon, L., & Prevosti, F. J. (2016). Paleobiology of sabretooth cat *Smilodon populator* in the Pampean Region (Buenos Aires Province, Argentina) around the Last Glacial Maximum: Insights from carbon and nitrogen stable isotopes in bone collagen. *Palaeogeography, Palaeoclimatology, Palaeoecology*, *449*, 463–474. https://doi.org/10.1016/j.palaeo.2016.02.017

Bodart, C., Brink, A. B., Donnay, F., Lupi, A., Mayaux, P., & Achard, F. (2013). Continental estimates of forest cover and forest cover changes in the dry ecosystems of Africa between 1990 and 2000. *Journal of Biogeography*, *40*(6), 1036–1047. https://doi.org/10.1111/jbi.12084

Boex, J., Fogwill, C., Harrison, S., Glasser, N. F., Hein, A., Schnabel, C., & Xu, S. (2013). Rapid thinning of the late Pleistocene Patagonian Ice Sheet followed migration of the Southern Westerlies. *Scientific Reports*, *3*(1), 2118. https://doi.org/10.1038/srep02118

Bonan, G. B. (2008). Forests and Climate Change: Forcings, Feedbacks, and the Climate Benefits of Forests. *Science*, *320*(5882), 1444–1449. https://doi.org/10.1126/science.1155121

Bond, W. (2010). Consumer control by megafauna and fire. In J. Terborgh & J. A. Estes (Eds.), *Trophic Cascades: Predators, Prey, and the Changing Dynamics of Nature* (2nd ed. (9 june 2010)., pp. 275–285). Washington DC: Island Press.

Bond, W. J. (2008). What Limits Trees in C_4 Grasslands and Savannas? *Annual Review of Ecology, Evolution, and Systematics*, *39*(1), 641–659. https://doi.org/10.1146/annurev.ecolsys.39.110707.173411

Bond, W. J., & Keeley, J. E. (2005). Fire as a global 'herbivore': the ecology and evolution of flammable ecosystems. *Trends in Ecology & Evolution*, *20*(7), 387–394. https://doi.org/10.1016/j.tree.2005.04.025

Bond, W. J., & Parr, C. L. (2010). Beyond the forest edge: Ecology, diversity and conservation of the grassy biomes. *Biological Conservation*, *143*(10), 2395–2404. https://doi.org/10.1016/j.biocon.2009.12.012

Borrero, L. A. (1999). The faunas of the Pleistocene/Holocene boundary in the Seno de la Ultima Esperanza, Chile. *Zooarchaeology of the Pleistocene/Holocene Boundary (JC Driver, ed.). BAR Internacional Series*, *800*, 59–62.

Borrero, L. A., Martin, F. M., & Prieto, Y. A. (1997). La Cueva Lago Sofía 4, Última Esperanza, Chile: Una Madriguera de Felino del Pleistoceno Tardío. *Anales del Instituto de la Patagonia*, *25*, 103–122.

Borrero, L. A. (2003). Taphonomy of the Tres Arroyos 1 Rockshelter, Tierra del Fuego, Chile. *Quaternary International*, *109–110*, 87–93. https://doi.org/10.1016/S1040-6182(02)00205-7

Borrero, L. A. (2008). Extinction of Pleistocene megamammals in South America: The lost evidence. *Quaternary International*, *185*(1), 69–74. https://doi.org/10.1016/j.quaint.2007.10.021

Borrero, L. A., Lanata, J. L., & Cárdenas, P. (1991). Reestudiando cuevas: nuevas excavaciones en Ultima Esperanza, Magallanes. In *Anales del Instituto de la Patagonia*.

Borrero, L. A., & Martin, F. M. (2012). Ground sloths and humans in southern Fuego-Patagonia: taphonomy and archaeology. *World Archaeology*, *44*(1), 102–117. https://doi.org/10.1080/00438243.2012.646145

Bowman, D. M., Balch, J. K., Artaxo, P., Bond, W. J., Carlson, J. M., Cochrane, M. A., et al. (2009). Fire in the Earth system. *science*, *324*(5926), 481–484. https://doi.org/10.1126/science.1163886

Box, E. O. (1981). Predicting physiognomic vegetation types with climate variables. *Vegetatio*, *45*(2), 127–139. https://doi.org/10.1007/BF00119222

Box, E. O., & Fujiwara, K. (2005). Vegetation types and their broad-scale distribution. In E. van der Maarel (Ed.), *Vegetation ecology* (pp. 106–128). Oxford, UK: Blackwell Publishing.

Bradshaw, C. J. A., Cooper, A., Turney, C. S. M., & Brook, B. W. (2012). Robust estimates of extinction time in the geological record. *Quaternary Science Reviews*, *33*, 14–19. https://doi.org/10.1016/j.quascirev.2011.11.021

Bradshaw, C. J. A., Johnson, C. N., Llewelyn, J., Weisbecker, V., Strona, G., & Saltré, F. (2021). Relative demographic susceptibility does not explain the extinction chronology of Sahul's megafauna. *eLife*, *10*, e63870. https://doi.org/10.7554/eLife.63870

Brancalion, P. H. S., Niamir, A., Broadbent, E., Crouzeilles, R., Barros, F. S. M., Zambrano, A. M. A., et al. (2019). Global restoration opportunities in tropical rainforest landscapes. *Science Advances*, *5*(7), eaav3223. https://doi.org/10.1126/sciadv.aav3223

Bremond, L., Alexandre, A., Peyron, O., & Guiot, J. (2008). Definition of grassland biomes from phytoliths in West Africa. *Journal of Biogeography*, *35*(11), 2039–2048. https://doi.org/10.1111/j.1365-2699.2008.01944.x

Brock, F., Geoghegan, V., Thomas, B., Jurkschat, K., & Higham, T. F. G. (2013). Analysis of Bone “Collagen” Extraction Products for Radiocarbon Dating. *Radiocarbon*, *55*(2), 445–463. https://doi.org/10.1017/S0033822200057581

Brock, F., Higham, T., Ditchfield, P., & Ramsey, C. B. (2010). Current pretreatment methods for AMS radiocarbon dating at the Oxford Radiocarbon Accelerator Unit (ORAU). *Radiocarbon*, *52*(1), 103–112.

Broecker, W. S. (1994). Massive iceberg discharges as triggers for global climate change. *Nature*, *372*(6505), 421–424. https://doi.org/10.1038/372421a0

Bronk Ramsey, C. (2021). OxCal program ver. 4.4. *Radiocarbon Accelerator Unit, University of Oxford. Retrieved from https://c14. arch. ox. ac. uk/oxcal. html*.

Bronk Ramsey, C., Higham, T., Bowles, A., & Hedges, R. (2004). Improvements to the Pretreatment of Bone at Oxford. *Radiocarbon*, *46*(1), 155–163. https://doi.org/10.1017/S0033822200039473

Brown, T. A., Nelson, D. E., Vogel, J. S., & Southon, J. R. (1988). Improved Collagen Extraction by Modified Longin Method. *Radiocarbon*, *30*(2), 171–177. https://doi.org/10.1017/S0033822200044118

Brunson, J. C., & Read, Q. D. (2023). *ggalluvial: Alluvial Plots in “ggplot2”. R package version 0.12.5*. R. http://corybrunson.github.io/ggalluvial/

Burleigh, R., Hewson, A., & Meeks, N. (1977). British Museum natural radiocarbon measurements IX. *Radiocarbon*, *19*(2), 143–160.

Burleigh, R., & Matthews, K. (1982). British Museum natural radiocarbon measurements XIII. *Radiocarbon*, *24*(2), 151–170.

Burnham, K. P., & Anderson, D. R. (2002). *Model selection and multimodel inference: a practical information-theoretic approach* (2nd ed.). New York: Springer.

Bush, M. B., De Oliveira, P. E., Colinvaux, P. A., Miller, M. C., & Moreno, J. E. (2004). Amazonian paleoecological histories: one hill, three watersheds. *Palaeogeography, Palaeoclimatology, Palaeoecology*, *214*(4), 359–393. https://doi.org/10.1016/j.palaeo.2004.07.031

Bush, M., Flenley, J., & Gosling, W. (Eds.). (2011). *Tropical Rainforest Responses to Climatic Change*. Berlin, Heidelberg: Springer Berlin Heidelberg. https://doi.org/10.1007/978-3-642-05383-2

Bush, M. B., & Rivera, R. (1998). Pollen Dispersal and Representation in a Neotropical Rain Forest. *Global Ecology and Biogeography Letters*, *7*(5), 379–392. https://doi.org/10.2307/2997685

Butler, E. E., Datta, A., Flores-Moreno, H., Chen, M., Wythers, K. R., Fazayeli, F., et al. (2017). Mapping local and global variability in plant trait distributions. *Proceedings of the National Academy of Sciences*, *114*(51), E10937–E10946. https://doi.org/10.1073/pnas.1708984114

Carretero, D. D., García, A., & Dacar, M. A. (2004). First data on differential use of the environment by Pleistocene megafauna species (San Juan, Argentina). *Current Research in the Pleistocene*, *21*, 91–92.

Carvalho, M. R., Jaramillo, C., de la Parra, F., Caballero-Rodríguez, D., Herrera, F., Wing, S., et al. (2021). Extinction at the end-Cretaceous and the origin of modern Neotropical rainforests. *Science*, *372*(6537), 63–68. https://doi.org/10.1126/science.abf1969

Casamiquela, R. t. (1969). Enumeración crítica de los mamíferos continentales pleistocenos de Chile. *Rehue (Revista del Centro de Antropología, Universidad de Concepción)*, *2*, 143–172.

Casinos, A. (1996). Bipedalism and quadrupedalism in *Megatherium*: an attempt at biomechanical reconstruction. *Lethaia*, *29*(1), 87–96.

Cassino, R. F., Ledru, M.-P., Santos, R. de A., & Favier, C. (2020). Vegetation and fire variability in the central Cerrados (Brazil) during the Pleistocene-Holocene transition was influenced by oscillations in the SASM boundary belt. *Quaternary Science Reviews*, *232*, 106209. https://doi.org/10.1016/j.quascirev.2020.106209

Cassino, R. F., Martinho, C. T., & da Silva Caminha, S. A. F. (2018). A Late Quaternary palynological record of a palm swamp in the Cerrado of central Brazil interpreted using modern analog data. *Palaeogeography, Palaeoclimatology, Palaeoecology*, *490*, 1–16. https://doi.org/10.1016/j.palaeo.2017.08.036

Center For International Earth Science Information Network-CIESIN-Columbia University. (2017). Gridded Population of the World, Version 4 (GPWv4): Population Density, Revision 11. Palisades, NY: Socioeconomic Data and Applications Center (SEDAC). https://doi.org/10.7927/H49C6VHW

Champreux, A., Saltré, F., & Traylor, W. (2023). *Data and code from: "How to map biomes: quantitative comparison and review of biome-mapping methods."* Zenodo. https://zenodo.org/record/7745096. Accessed 25 March 2023

Chaneton, E. J., Mazía, N., Batista, W. B., Rolhauser, A. G., & Ghersa, C. M. (2012). Woody plant invasions in Pampa grasslands: a biogeographical and community assembly perspective. In *Ecotones between forest and grassland* (pp. 115–144). Springer.

Chang, J., Ciais, P., Herrero, M., Havlik, P., Campioli, M., Zhang, X., et al. (2016). Combining livestock production information in a process-based vegetation model to reconstruct the history of grassland management. *Biogeosciences*, *13*(12), 3757–3776. https://doi.org/10.5194/bg-13-3757-2016

Chang, J., Ciais, P., Wang, X., Piao, S., Asrar, G., Betts, R., et al. (2017). Benchmarking carbon fluxes of the ISIMIP2a biome models. *Environmental Research Letters*, *12*(4), 045002. https://doi.org/10.1088/1748-9326/aa63fa

Cheng, H., Zhang, H., Spötl, C., Baker, J., Sinha, A., Li, H., et al. (2020). Timing and structure of the Younger Dryas event and its underlying climate dynamics. *Proceedings of the National Academy of Sciences*, *117*(38), 23408–23417. https://doi.org/10.1073/pnas.2007869117

Chiarucci, A., Araújo, M. B., Decocq, G., Beierkuhnlein, C., & Fernández-Palacios, J. M. (2010). The concept of potential natural vegetation: an epitaph? *Journal of Vegetation Science*, *21*(6), 1172–1178. https://doi.org/10.1111/j.1654-1103.2010.01218.x

Chiessi, C. M., Mulitza, S., Pätzold, J., Wefer, G., & Marengo, J. A. (2009). Possible impact of the Atlantic Multidecadal Oscillation on the South American summer monsoon. *Geophysical Research Letters*, *36*(21). https://doi.org/10.1029/2009GL039914

Christiansen, P., & Harris, J. M. (2005). Body size of *Smilodon* (Mammalia: Felidae). *Journal of Morphology*, *266*(3), 369–384.

Cione, A. L., Tonni, E. P., & Soibelzon, L. (2009a). Did Humans Cause the Late Pleistocene-Early Holocene Mammalian Extinctions in South America in a Context of Shrinking Open Areas? In G. Haynes (Ed.), *American Megafaunal Extinctions at the End of the Pleistocene* (pp. 125–144). Dordrecht: Springer Netherlands. https://doi.org/10.1007/978-1-4020-8793-6_7

Cione, A. L., Tonni, E. P., & Soibelzon, L. (2009b). Did humans cause the Late Pleistocene-Early Holocene mammalian extinctions in South America in a context of shrinking open areas? In *American megafaunal extinctions at the end of the Pleistocene* (pp. 125–144). Springer.

Civalero, M. T., Borrazo, K., Bozzuto, D., Vruno, A. D., Dolce, V., & Limbrunner, P. (2007). ¿ Ultimas? excavaciones en Cerro Casa de Piedra 7, Santa Cruz. In *rqueología Argentina en los inicios de un nuevo siglo, Rosario, Laborde Libros* (pp. 329–335).

Clapperton, C. M. (1993). Nature of environmental changes in South America at the Last Glacial Maximum. *Palaeogeography, Palaeoclimatology, Palaeoecology*, *101*(3), 189–208. https://doi.org/10.1016/0031-0182(93)90012-8

Clark, P. U., Dyke, A. S., Shakun, J. D., Carlson, A. E., Clark, J., Wohlfarth, B., et al. (2009). The Last Glacial Maximum. *Science*, *325*(5941), 710–714. https://doi.org/10.1126/science.1172873

Clements, F. E. (1917). The development and structure of biotic communities. *Journal of Ecology*, *5*, 12–21.

Clements, F. E. (1916). *Plant succession: an analysis of the development of vegetation* (Vol. 242). Washington, USA: Carnegie Institution of Washington.

Clements, Frederic Edward, & Shelford, V. E. (1939). *Bio-ecology*. New York, USA: John Wiley & Sons, Ltd. http://archive.org/details/bioecology00clem. Accessed 15 July 2019

Cohen, J. (1960). A Coefficient of Agreement for Nominal Scales. *Educational and Psychological Measurement*, *20*(1), 37–46. https://doi.org/10.1177/001316446002000104

Cole, M. M. (1960). Cerrado, Caatinga and Pantanal: the distribution and origin of the savanna vegetation of Brazil. *The Geographical Journal*, *126*(2), 168–179. http://dx.doi.org/10.2307/1793957

Colinvaux, P. A., De Oliveira, P. E., Moreno, J. E., Miller, M. C., & Bush, M. B. (1996). A Long Pollen Record from Lowland Amazonia: Forest and Cooling in Glacial Times. *Science*, *274*(5284), 85–88. https://doi.org/10.1126/science.274.5284.85

Collins, W. D., Bitz, C. M., Blackmon, M. L., Bonan, G. B., Bretherton, C. S., Carton, J. A., et al. (2006). The Community Climate System Model Version 3 (CCSM3). *Journal of Climate*, *19*(11), 2122–2143. https://doi.org/10.1175/JCLI3761.1

Collinson, M. E., & Hooker, J. J. (2003). Paleogene vegetation of Eurasia: framework for mammalian faunas. *Deinsea*, *10*(1), 41–84.

Coni, J. F., Cassiodoro, G., Agnolin, A., & Goñi, R. (2020). Differential Distribution of Projectile Points in Southern Patagonia during the Early Holocene: Peopling Implications? *PaleoAmerica*, *6*(3), 250–267. https://doi.org/10.1080/20555563.2020.1757859

Conradi, T., Slingsby, J. A., Midgley, G. F., Nottebrock, H., Schweiger, A. H., & Higgins, S. I. (2020). An operational definition of the biome for global change research. *New Phytologist*, *227*(5), 1294–1306. https://doi.org/10.1111/nph.16580

Cooper, A., Turney, C., Hughen, K. A., Brook, B. W., McDonald, H. G., & Bradshaw, C. J. A. (2015). Abrupt warming events drove Late Pleistocene Holarctic megafaunal turnover. *Science*, *349*(6248), 602–606. https://doi.org/10.1126/science.aac4315

Costa, G. C., Hampe, A., Ledru, M., Martinez, P. A., Mazzochini, G. G., Shepard, D. B., et al. (2018). Biome stability in South America over the last 30 kyr: Inferences from long-term vegetation dynamics and habitat modelling. *Global Ecology and Biogeography*, *27*(3), 285–297. https://doi.org/10.1111/geb.12694

Cowling, S. A., Maslin, M. A., & Sykes, M. T. (2001). Paleovegetation Simulations of Lowland Amazonia and Implications for Neotropical Allopatry and Speciation. *Quaternary Research*, *55*(2), 140–149. https://doi.org/10.1006/qres.2000.2197

Cowling, S. A., & Shin, Y. (2006). Simulated ecosystem threshold responses to co-varying temperature, precipitation and atmospheric CO_2 within a region of Amazonia: Modelling ecosystem thresholds in Amazonia. *Global Ecology and Biogeography*, *15*(6), 553–566. https://doi.org/10.1111/j.1466-8238.2006.00256.x

Craney, T. A., & Surles, J. G. (2002). Model-Dependent Variance Inflation Factor Cutoff Values. *Quality Engineering*, *14*(3), 391–403. https://doi.org/10.1081/QEN-120001878

Cruz, L. E., Bargo, M. S., Tonni, E. P., & Figini, A. J. (2010). Radiocarbon date on megafauna from the late Pleistocene-early Holocene of Córdoba province, Argentina: stratigraphic and paleoclimatic significance. *Revista mexicana de ciencias geológicas*, 27(3), 470–476.

da Silva Junior, C. A., Teodoro, P. E., Delgado, R. C., Teodoro, L. P. R., Lima, M., de Andréa Pantaleão, A., et al. (2020). Persistent fire foci in all biomes undermine the Paris Agreement in Brazil. *Scientific Reports*, *10*(1), 16246. https://doi.org/10.1038/s41598-020-72571-w

Dale Guthrie, R. (2003). Rapid body size decline in Alaskan Pleistocene horses before extinction. *Nature*, *426*(6963), 169–171. https://doi.org/10.1038/nature02098

Dallmeyer, A., Claussen, M., Ni, J., Cao, X., Wang, Y., Fischer, N., et al. (2017). Biome changes in Asia since the mid-Holocene – an analysis of different transient Earth system model simulations. *Climate of the Past*, *13*(2), 107–134. https://doi.org/10.5194/cp-13-107-2017

Dallmeyer, A., Poska, A., Marquer, L., Seim, A., & Gaillard-Lemdahl, M.-J. (2023). The challenge of comparing pollen-based quantitative vegetation reconstructions with outputs from vegetation models-a European perspective. *Climate of the Past Discussions*, 1–50. https://doi.org/10.5194/cp-2023-16

Dantas de Paula, M., Forrest, M., Langan, L., Bendix, J., Homeier, J., Velescu, A., et al. (2021). Nutrient cycling drives plant community trait assembly and ecosystem functioning in a tropical mountain biodiversity hotspot. *New Phytologist*, *232*(2), 551–566. https://doi.org/10.1111/nph.17600

Dantas, V. L., Hirota, M., Oliveira, R. S., & Pausas, J. G. (2016). Disturbance maintains alternative biome states. *Ecology Letters*, *19*(1), 12–19. https://doi.org/10.1111/ele.12537

Dantas, V. L., & Pausas, J. G. (2020). Megafauna biogeography explains plant functional trait variability in the tropics. *Global Ecology and Biogeography*, *29*(8), 1288–1298. https://doi.org/10.1111/geb.13111

D'Apolito, C., Absy, M. L., & Latrubesse, E. M. (2013). The Hill of Six Lakes revisited: new data and re-evaluation of a key Pleistocene Amazon site. *Quaternary Science Reviews*, *76*, 140–155. https://doi.org/10.1016/j.quascirev.2013.07.013

Dasmann, R. F. (1974). *Biotic provinces of the world: further development of a system for defining and classifying natural regions for purposes of conservation* (Vol. IUCN Occasional Paper 9). Morges, Switzerland: International Union for Conservation of Nature and Natural Resources.

Davies, B. J., Darvill, C. M., Lovell, H., Bendle, J. M., Dowdeswell, J. A., Fabel, D., et al. (2020). The evolution of the Patagonian Ice Sheet from 35 ka to the present day (PATICE). *Earth-Science Reviews*, *204*, 103152. https://doi.org/10.1016/j.earscirev.2020.103152

Davis, M. B. (1986). Climatic instability, time lags, and community disequilibrium. In J. Diamond & T. J. Case (Eds.), *Community ecology* (pp. 269–284). Harper & Row, New York.

De Oliveira, K., García, J., Daners, G., Ubilla, M., Goso, C., & Bistrichi, C. (2011). Contribuicao palinoflorística para o cenario do Pleistoceno superior-Holoceno inferior na bacia do Rio Santa Lucia, sul de Uruguai. *Paleontologıa: cená rios de vida. Interciencia*, 175–187.

de Porras, M. E., Maldonado, A., Abarzúa, A. M., Cárdenas, M. L., Francois, J. P., Martel-Cea, A., et al. (2012). Postglacial vegetation, fire and climate dynamics at Central Chilean Patagonia (Lake Shaman, 44°S). *Quaternary Science Reviews*, *50*, 71–85. https://doi.org/10.1016/j.quascirev.2012.06.015

Dillehay, T. D. (1999). The late Pleistocene cultures of South America. *Evolutionary Anthropology: Issues, News, and Reviews*, *7*(6), 206–216. https://doi.org/10.1002/(SICI)1520-6505(1999)7:6<206::AID-EVAN5>3.0.CO;2-G

DiMichele, W. A., Hotton, C. L., Looy, C. V., & Hook, R. W. (2019). Paleoecological and paleoenvironmental interpretation of three successive macrofloras and palynofloras from the Kola Switch locality, lower Permian (Archer City Formation, Bowie Group) of Clay County, Texas, USA. *PalZ*, *93*(3), 423–451. https://doi.org/10.1007/s12542-019-00485-8

Dinerstein, E., Olson, D., Joshi, A., Vynne, C., Burgess, N. D., Wikramanayake, E., et al. (2017). An Ecoregion-Based Approach to Protecting Half the Terrestrial Realm. *BioScience*, *67*(6), 534–545. https://doi.org/10.1093/biosci/bix014

Doherty, S., Saltré, F., Llewelyn, J., Strona, G., Williams, S. E., & Bradshaw, C. J. A. (2023). Estimating co-extinction threats in terrestrial ecosystems. *Global Change Biology*. https://doi.org/doi:10.1111/gcb.16836

Dormann, C. F., Schymanski, S. J., Cabral, J., Chuine, I., Graham, C., Hartig, F., et al. (2012). Correlation and process in species distribution models: bridging a dichotomy. *Journal of Biogeography*, *39*(12), 2119–2131. https://doi.org/10.1111/j.1365-2699.2011.02659.x

dos Santos Avilla, L., Figueiredo, A. M. G., Kinoshita, A., Bertoni-Machado, C., Mothé, D., Asevedo, L., et al. (2013). Extinction of a gomphothere population from southeastern Brazil: taphonomic, paleoecological and chronological remarks. *Quaternary international*, *305*, 85–90. https://doi.org/10.1016/j.quaint.2012.09.015

Dubois, C. F., & Borrero, L. A. (1997). Geoarchaeological perspectives on late Pleistocene faunas from ultima Esperanza sound. Magallanes, Chile. *Anthropologie (1962-)*, *35*(2), 207–213.

Duckworth, J. C., Kent, M., & Ramsay, P. M. (2000). Plant functional types: an alternative to taxonomic plant community description in biogeography? *Progress in Physical Geography: Earth and Environment*, *24*(4), 515–542. https://doi.org/10.1177/030913330002400403

Dyke, A. S. (2007). Late Quaternary Vegetation History of Northern North America Based on Pollen, Macrofossil, and Faunal Remains. *Géographie physique et Quaternaire*, *59*(2–3), 211–262. https://doi.org/10.7202/014755ar

Edwards, M. E., Anderson, P. M., Brubaker, L. B., Ager, T. A., Andreev, A. A., Bigelow, N. H., et al. (2000). Pollen-based biomes for Beringia 18,000, 6000 and 0 14C yr bp. *Journal of Biogeography*, *27*(3), 521–554. https://doi.org/10.1046/j.1365-2699.2000.00426.x

Egerton, F. N. (2017). History of Ecological Sciences, Part 59: Niches, Biomes, Ecosystems, and Systems. *The Bulletin of the Ecological Society of America*, *98*(4), 298–337. https://doi.org/10.1002/bes2.1337

Elenga, H., Peyron, O., Bonnefille, R., Jolly, D., Cheddadi, R., Guiot, J., et al. (2000). Pollen-based biome reconstruction for southern Europe and Africa 18,000 yr BP. *Journal of Biogeography*, *27*(3), 621–634. https://doi.org/10.1046/j.1365-2699.2000.00430.x

Ellis, E. C. (2021). Replication Data for: Ellis et al. (2012). Harvard Dataverse. https://doi.org/10.7910/DVN/PDNWKL

Ellis, E. C., Antill, E. C., & Kreft, H. (2012). All Is Not Loss: Plant Biodiversity in the Anthropocene. *PLOS One*, *7*(1), e30535. https://doi.org/10.1371/journal.pone.0030535

Ellis, E. C., Gauthier, N., Klein Goldewijk, K., Bliege Bird, R., Boivin, N., Díaz, S., et al. (2021). People have shaped most of terrestrial nature for at least 12,000 years. *Proceedings of the National Academy of Sciences*, *118*(17), e2023483118. https://doi.org/10.1073/pnas.2023483118

Ellis, E. C., & Ramankutty, N. (2008). Putting people in the map: anthropogenic biomes of the world. *Frontiers in Ecology and the Environment*, *6*(8), 439–447. https://doi.org/10.1890/070062

Faith, J. T. (2014). Late Pleistocene and Holocene mammal extinctions on continental Africa. *Earth-Science Reviews*, *128*, 105–121. https://doi.org/10.1016/j.earscirev.2013.10.009

Faith, J. T., & Surovell, T. A. (2009). Synchronous extinction of North America's Pleistocene mammals. *Proceedings of the National Academy of Sciences*, *106*(49), 20641–20645. https://doi.org/10.1073/pnas.0908153106

Fang, H., Baret, F., Plummer, S., & Schaepman-Strub, G. (2019). An Overview of Global Leaf Area Index (LAI): Methods, Products, Validation, and Applications. *Reviews of Geophysics*, *57*(3), 739–799. https://doi.org/10.1029/2018RG000608

Fariña, R. A., Vizcaíno, S. F., & Bargo, M. S. (1998). Body mass estimations in Lujanian (late Pleistocene-early Holocene of South America) mammal megafauna. *Mastozoología Neotropical*, *5*(2), 87–108.

Fariña, R. A., Vizcaíno, S. F., & De Iuliis, G. (2013). *Megafauna: giant beasts of pleistocene South America*. Indiana University Press.

Feranec, R. S. (2003). Stable Isotopes, Hypsodonty, and the Paleodiet of *Hemiauchenia* (Mammalia: Camelidae): A Morphological Specialization Creating Ecological Generalization. *Paleobiology*, *29*(2), 230–242.

Feurdean, A., Ruprecht, E., Molnár, Z., Hutchinson, S. M., & Hickler, T. (2018). Biodiversity-rich European grasslands: Ancient, forgotten ecosystems. *Biological Conservation*, *228*, 224–232. https://doi.org/10.1016/j.biocon.2018.09.022

Fiedel, S. J. (2022). Initial human colonization of the Americas, redux. *Radiocarbon*, *64*(4), 845–897. https://doi.org/10.1017/RDC.2021.103

Firestone, R. B., West, A., Kennett, J. P., Becker, L., Bunch, T. E., Revay, Z. S., et al. (2007). Evidence for an extraterrestrial impact 12,900 years ago that contributed to the megafaunal extinctions and the Younger Dryas cooling. *Proceedings of the National Academy of Sciences*, *104*(41), 16016–16021. https://doi.org/10.1073/pnas.0706977104

Flantua, S. G. A., Hooghiemstra, H., Grimm, E. C., Behling, H., Bush, M. B., González-Arango, C., et al. (2015). Updated site compilation of the Latin American Pollen Database. *Review of Palaeobotany and Palynology*, *223*, 104–115. https://doi.org/10.1016/j.revpalbo.2015.09.008

Fontana, S. L., & Bennett, K. (2012). Postglacial vegetation dynamics of western Tierra del Fuego. *The Holocene*, *22*(11), 1337–1350. https://doi.org/10.1177/0959683612444144

Forbes, E. S., Cushman, J. H., Burkepile, D. E., Young, T. P., Klope, M., & Young, H. S. (2019). Synthesizing the effects of large, wild herbivore exclusion on ecosystem function. *Functional Ecology*, *33*(9), 1597–1610. https://doi.org/10.1111/1365-2435.13376

Forbes, M., Jankowski, N., Cohen, T., Hopf, F., Mueller, D., Bird, M., et al. (2020). Palaeochannels of Australia's Riverine Plain - Reconstructing past vegetation environments across the Late Pleistocene and Holocene. *Palaeogeography, Palaeoclimatology, Palaeoecology*, *545*, 109533. https://doi.org/10.1016/j.palaeo.2019.109533

Fordham, D. A., Saltré, F., Haythorne, S., Wigley, T. M. L., Otto-Bliesner, B. L., Chan, K. C., & Brook, B. W. (2017). PaleoView: a tool for generating continuous climate projections spanning the last 21 000 years at regional and global scales. *Ecography*, *40*(11), 1348–1358. https://doi.org/10.1111/ecog.03031

Forrest, M., Eronen, J. T., Utescher, T., Knorr, G., Stepanek, C., Lohmann, G., & Hickler, T. (2015). Climate-vegetation modelling and fossil plant data suggest low atmospheric CO_2 in the late Miocene. *Climate of the Past*, *11*(12), 1701–1732. https://doi.org/10.5194/cp-11-1701-2015

Francisquini, M. I., Lorente, F. L., Ruiz Pessenda, L. C., Buso Junior, A. A., Mayle, F. E., Lisboa Cohen, M. C., et al. (2020). Cold and humid Atlantic Rainforest during the last glacial maximum, northern Espírito Santo state, southeastern Brazil. *Quaternary Science Reviews*, *244*, 106489. https://doi.org/10.1016/j.quascirev.2020.106489

François, L., Utescher, T., Favre, E., Henrot, A.-J., Warnant, P., Micheels, A., et al. (2011). Modelling Late Miocene vegetation in Europe: Results of the CARAIB model and comparison with palaeovegetation data. *Palaeogeography, Palaeoclimatology, Palaeoecology*, *304*(3), 359–378. https://doi.org/10.1016/j.palaeo.2011.01.012

Franklin, W. L. (1982). Biology, ecology, and relationship to man of the South American camelids. *Mammalian Biology in South America*, *6*, 457–489.

Fraser, M. D. (1998). Diet composition of guanacos (*Lama guanicoe*) and sheep (*Ovis aries*) grazing in grassland communities typical of UK uplands. *Small Ruminant Research*, *29*(2), 201–212. https://doi.org/10.1016/S0921-4488(97)00133-8

Friedl, M. A., Sulla-Menashe, D., Tan, B., Schneider, A., Ramankutty, N., Sibley, A., & Huang, X. (2010). MODIS Collection 5 global land cover: Algorithm refinements and characterization of new datasets. *Remote Sensing of Environment*, *114*(1), 168–182. https://doi.org/10.1016/j.rse.2009.08.016

Friedlingstein, P., Delire, C., Müller, J. F., & Gérard, J. C. (1992). The climate induced variation of the continental biosphere: A model simulation of the Last Glacial Maximum. *Geophysical Research Letters*, *19*(9), 897–900. https://doi.org/10.1029/92GL00546

Fritz, S., & See, L. (2005). Comparison of land cover maps using fuzzy agreement. *International Journal of Geographical Information Science*, *19*(7), 787–807. https://doi.org/10.1080/13658810500072020

Furley, P. A. (1999). The nature and diversity of neotropical savanna vegetation with particular reference to the Brazilian cerrados. *Global Ecology and Biogeography*, *8*(3–4), 223–241. https://doi.org/10.1046/j.1466-822X.1999.00142.x

Gallo, V., Avilla, L. S., Pereira, R. C. L., & Absolon, B. A. (2013). Distributional patterns of herbivore megamammals during the Late Pleistocene of South America. *Anais da Academia Brasileira de Ciências*, *85*(2), 533–546. https://doi.org/10.1590/S0001-37652013000200005

García, A. (2003). On the Coexistence of Man and Extinct Pleistocene Megafauna at Gruta Del Indio (Argentina). *Radiocarbon*, *45*(1), 33–39. https://doi.org/10.1017/S0033822200032379

Garcia, M. J., De Oliveira, P. E., de Siqueira, E., & Fernandes, R. S. (2004). A Holocene vegetational and climatic record from the Atlantic rainforest belt of coastal State of São Paulo, SE Brazil. *Review of Palaeobotany and Palynology*, *131*(3–4), 181–199. https://doi.org/10.1016/j.revpalbo.2004.03.007

Gilbert, M. T. P., Jenkins, D. L., Götherstrom, A., Naveran, N., Sanchez, J. J., Hofreiter, M., et al. (2008). DNA from Pre-Clovis Human Coprolites in Oregon, North America. *Science*, *320*(5877), 786–789. https://doi.org/10.1126/science.1154116

Goebel, T., Waters, M. R., & O'Rourke, D. H. (2008). The Late Pleistocene Dispersal of Modern Humans in the Americas. *Science*, *319*(5869), 1497–1502. https://doi.org/10.1126/science.1153569

Goldberg, A., Mychajliw, A. M., & Hadly, E. A. (2016). Post-invasion demography of prehistoric humans in South America. *Nature*, *532*(7598), 232–235. https://doi.org/10.1038/nature17176

Gonzalez, P., Neilson, R. P., Lenihan, J. M., & Drapek, R. J. (2010). Global patterns in the vulnerability of ecosystems to vegetation shifts due to climate change: Global vulnerability to climate change. *Global Ecology and Biogeography*, *19*(6), 755–768. https://doi.org/10.1111/j.1466-8238.2010.00558.x

González-Guarda, E. A. G. (2018). *La autoecología delos gonfoterios (Gomphotheriidae) del Pleistoceno superior de Chile*. Universidad Complutense de Madrid, Madrid.

González-Guarda, E., Domingo, L., Tornero, C., Pino, M., Hernández Fernández, M., Sevilla, P., et al. (2017). Late Pleistocene ecological, environmental and climatic reconstruction based on megafauna stable isotopes from northwestern Chilean Patagonia. *Quaternary Science Reviews*, *170*, 188–202. https://doi.org/10.1016/j.quascirev.2017.06.035

González-Guarda, E., Petermann-Pichincura, A., Tornero, C., Domingo, L., Agustí, J., Pino, M., et al. (2018). Multiproxy evidence for leaf-browsing and closed habitats in extinct proboscideans (Mammalia, Proboscidea) from Central Chile. *Proceedings of the National Academy of Sciences*, *115*(37), 9258–9263. https://doi.org/10.1073/pnas.1804642115

Grayson, D. K., & Meltzer, D. J. (2015). Revisiting Paleoindian exploitation of extinct North American mammals. *Journal of Archaeological Science*, *56*, 177–193. https://doi.org/10.1016/j.jas.2015.02.009

Green, J. L., & Kalthoff, D. C. (2015). Xenarthran dental microstructure and dental microwear analyses, with new data for *Megatherium americanum* (Megatheriidae). *Journal of Mammalogy*, *96*(4), 645–657. https://doi.org/10.1093/jmammal/gyv045

Guisan, A., & Zimmermann, N. E. (2000). Predictive habitat distribution models in ecology. *Ecological Modelling*, *135*(2), 147–186. https://doi.org/10.1016/S0304-3800(00)00354-9

Hagen-Zanker, A., Straatman, B., & Uljee, I. (2005). Further developments of a fuzzy set map comparison approach. *International Journal of Geographical Information Science*, *19*(7), 769–785. https://doi.org/10.1080/13658810500072137

Hajduk, A., Albornoz, A., & Lezcano, M. J. (2006). Levels with Extinct Fauna in the Forest Rockshelter El Trébol (Northwest Patagonia, Argentina), 3.

Håkansson, S. (1976). University of Lund radiocarbon dates IX. *Radiocarbon*, *18*(3), 290–320.

Handiani, D., Paul, A., & Dupont, L. (2012). Tropical climate and vegetation changes during Heinrich Event 1: a model-data comparison. *Climate of the Past*, *8*(1), 37–57. https://doi.org/10.5194/cp-8-37-2012

Hanks, R. R. (2011). *Encyclopedia of geography terms, themes, and concepts*. Santa Barbara, USA: ABC-CLIO.

Hansen, B. C. S., Rodbell, D. T., Seltzer, G. O., León, B., Young, K. R., & Abbott, M. (2003). Late-glacial and Holocene vegetational history from two sites in the western Cordillera of southwestern Ecuador. *Palaeogeography, Palaeoclimatology, Palaeoecology*, *194*(1), 79–108. https://doi.org/10.1016/S0031-0182(03)00272-4

Hansen, M. C., Potapov, P. V., Moore, R., Hancher, M., Turubanova, S. A., Tyukavina, A., et al. (2013). High-Resolution Global Maps of 21st-Century Forest Cover Change. *Science*, *342*(6160), 850–853. https://doi.org/10.1126/science.1244693

Harada, Y., Kamahori, H., Kobayashi, C., Endo, H., Kobayashi, S., Ota, Y., et al. (2016). The JRA-55 Reanalysis: Representation of Atmospheric Circulation and Climate Variability. *Journal of the Meteorological Society of Japan. Ser. II*, *94*(3), 269–302. https://doi.org/10.2151/jmsj.2016-015

Hardesty, J., Myers, R., & Fulks, W. (2005). Fire, Ecosystems, and People: A Preliminary Assessment of Fire as a Global Conservation Issue. *The George Wright Forum*, *22*(4), 78–87.

Härdle, W., Müller, M., Sperlich, S., & Werwatz, A. (2004). *Nonparametric and semiparametric models* (Vol. 1). Springer.

Harris, I., Jones, P. D., Osborn, T. J., & Lister, D. H. (2014). Updated high-resolution grids of monthly climatic observations – the CRU TS3.10 Dataset. *International Journal of Climatology*, *34*(3), 623–642. https://doi.org/10.1002/joc.3711

Harrison, S. P., Jolly, D., Laarif, F., Abe-Ouchi, A., Dong, B., Herterich, K., et al. (1998). Intercomparison of Simulated Global Vegetation Distributions in Response to 6 kyr BP Orbital Forcing. *Journal of Climate*, *11*(11), 2721–2742. https://doi.org/10.1175/1520-0442(1998)011<2721:IOSGVD>2.0.CO;2

Harrison, S. P., Kutzbach, J. E., Liu, Z., Bartlein, P. J., Otto-Bliesner, B., Muhs, D., et al. (2003). Mid-Holocene climates of the Americas: a dynamical response to changed seasonality. *Climate Dynamics*, *20*(7), 663–688. https://doi.org/10.1007/s00382-002-0300-6

Harrison, S. P., & Bartlein, P. (2012). Records from the Past, Lessons for the Future: What the Palaeorecord Implies about Mechanisms of Global Change. In A. Henderson-Sellers & K. McGuffie (Eds.), *The Future of the World's Climate (Second Edition)* (pp. 403–436). Boston: Elsevier. https://doi.org/10.1016/B978-0-12-386917-3.00014-2

Harrison, S. P., & Prentice, C. I. (2003). Climate and CO2 controls on global vegetation distribution at the last glacial maximum: analysis based on palaeovegetation data, biome modelling and palaeoclimate simulations. *Global Change Biology*, *9*(7), 983–1004. https://doi.org/10.1046/j.1365-2486.2003.00640.x

Haxeltine, A., & Prentice, I. C. (1996a). BIOME3: An equilibrium terrestrial biosphere model based on ecophysiological constraints, resource availability, and competition among plant functional types. *Global biogeochemical cycles*, *10*(4), 693–709. https://doi.org/10.1029/96GB02344

Haxeltine, A., & Prentice, I. C. (1996b). BIOME3: An equilibrium terrestrial biosphere model based on ecophysiological constraints, resource availability, and competition among plant functional types. *Global Biogeochemical Cycles*, *10*(4), 693–709. https://doi.org/10.1029/96GB02344

He, F. (2011). *Simulating transient climate evolution of the last deglaciation with CCSM 3* (PhD thesis). University of Wisconsin-Madison, Madison, Wisconsin, United States of America.

He, F., & Clark, P. U. (2022). Freshwater forcing of the Atlantic Meridional Overturning Circulation revisited. *Nature Climate Change*, *12*(5), 449–454. https://doi.org/10.1038/s41558-022-01328-2

Heinrich, H. (1988). Origin and Consequences of Cyclic Ice Rafting in the Northeast Atlantic Ocean During the Past 130,000 Years. *Quaternary Research*, *29*(2), 142–152. https://doi.org/10.1016/0033-5894(88)90057-9

Hengl, T., Walsh, M. G., Sanderman, J., Wheeler, I., Harrison, S. P., & Prentice, I. C. (2018). Global mapping of potential natural vegetation: an assessment of machine learning algorithms for estimating land potential. *PeerJ*, *6*, e5457. https://doi.org/10.7717/peerj.5457

Herrando-Pérez, S. (2021). Bone need not remain an elephant in the room for radiocarbon dating. *Royal Society Open Science*, *8*(1), 201351. https://doi.org/10.1098/rsos.201351

Heusser, C. J., Borrero, L. A., & Lanata, A. (1994). Late glacial vegetation at Cueva del Mylodon. *Anales del Instituto de la Patagonia*, 6.

Hickler, T., Prentice, I. C., Smith, B., Sykes, M. T., & Zaehle, S. (2006). Implementing plant hydraulic architecture within the LPJ Dynamic Global Vegetation Model. *Global Ecology and Biogeography*, *15*(6), 567–577. https://doi.org/10.1111/j.1466-8238.2006.00254.x

Hickler, T., Smith, B., Sykes, M. T., Davis, M. B., Sugita, S., & Walker, K. (2004). Using a generalized vegetation model to simulate vegetation dynamics in Northeastern USA. *Ecology*, *85*(2), 519–530. https://doi.org/10.1890/02-0344

Higgins, S. I., Buitenwerf, R., & Moncrieff, G. R. (2016). Defining functional biomes and monitoring their change globally. *Global Change Biology*, *22*(11), 3583–3593. https://doi.org/10.1111/gcb.13367

Higgins, S. I., Buitenwerf, R., & Moncrieff, G. R. (2017). Data from: Defining functional biomes and monitoring their change globally. *Dryad*. https://doi.org/10.5061/dryad.3pm63

Higham, T. F., Jacobi, R. M., & Ramsey, C. B. (2006). AMS radiocarbon dating of ancient bone using ultrafiltration. *Radiocarbon*, *48*(2), 179–195.

Hijmans, R. J., Bivand, R., Pebesma, E., & Sumner, M. D. (2023). *terra: Spatial Data Analysis*. https://CRAN.R-project.org/package=terra. Accessed 14 March 2023

Hijmans, R. J., & van Etten, J. (2012). *raster: Geographic analysis and modeling with raster data. R package version 2.0-12*. R.

Hodell, D. A., Nicholl, J. A., Bontognali, T. R. R., Danino, S., Dorador, J., Dowdeswell, J. A., et al. (2017). Anatomy of Heinrich Layer 1 and its role in the last deglaciation. *Paleoceanography*, *32*(3), 284–303. https://doi.org/10.1002/2016PA003028

Hofreiter, M., Betancourt, J. L., Sbriller, A. P., Markgraf, V., & McDonald, H. G. (2003). Phylogeny, diet, and habitat of an extinct ground sloth from Cuchillo Curá, Neuquén Province, southwest Argentina. *Quaternary Research*, *59*(3), 364–378. https://doi.org/10.1016/S0033-5894(03)00030-9

Hogg, A. G., Heaton, T. J., Hua, Q., Palmer, J. G., Turney, C. S., Southon, J., et al. (2020). SHCal20 Southern Hemisphere calibration, 0–55,000 years cal BP. *Radiocarbon*, *62*(4), 759–778.

Holdridge, L. R. (1967). *Life zone ecology*. San Jose, Costa Rica: Tropical Science Centre.

Holliday, V. T., Surovell, T., Meltzer, D. J., Grayson, D. K., & Boslough, M. (2014). The Younger Dryas impact hypothesis: a cosmic catastrophe. *Journal of Quaternary Science*, *29*(6), 515–530. https://doi.org/10.1002/jqs.2724

Holz, A., Méndez, C., Borrero, L., Prieto, A., Torrejón, F., & Maldonado, A. (2016). Fires: the main human impact on past environments in Patagonia? *Past Global Change Magazine*, *24*(2), 72–73.

Hooghiemstra, H., & van der Hammen, T. (1998). Neogene and Quaternary development of the neotropical rain forest: the forest refugia hypothesis, and a literature overview. *Earth-Science Reviews*, *44*(3), 147–183. https://doi.org/10.1016/S0012-8252(98)00027-0

Houborg, R., Fisher, J. B., & Skidmore, A. K. (2015). Advances in remote sensing of vegetation function and traits. *International Journal of Applied Earth Observation and Geoinformation*, *43*, 1–6. https://doi.org/10.1016/j.jag.2015.06.001

Hück, K. (1960). Die waldgeographische Regionen und Unterregionen von Südamerika (with map 1: 55,000,000). *Geographische Taschenbuch*.

Huntley, B., Allen, J. R. M., Collingham, Y. C., Hickler, T., Lister, A. M., Singarayer, J., et al. (2013). Millennial Climatic Fluctuations Are Key to the Structure of Last Glacial Ecosystems. *PLOS One*, *8*(4), e61963. https://doi.org/10.1371/journal.pone.0061963

Huntley, B., Allen, J. R. M., Forrest, M., Hickler, T., Ohlemüller, R., Singarayer, J. S., & Valdes, P. J. (2023). Global biome patterns of the Middle and Late Pleistocene. *Journal of Biogeography*, *50*(8), 1352–1372. https://doi.org/10.1111/jbi.14619

Huntley, B., Allen, J. R. M., Forrest, M., Hickler, T., Ohlemüller, R., Singarayer, J. S., & Valdes, P. J. (2021). Projected climatic changes lead to biome changes in areas of previously constant biome. *Journal of Biogeography*, *48*(10), 2418–2428. https://doi.org/10.1111/jbi.14213

Hurvich, C. M., & Tsai, C.-L. (1989). Regression and time series model selection in small samples. *Biometrika*, *76*(2), 297–307. http://dx.doi.org/10.1093/biomet/76.2.297

Hyvarinen, O., Te Beest, M., le Roux, E., Kerley, G., de Groot, E., Vinita, R., & Cromsigt, J. P. G. M. (2021). Megaherbivore impacts on ecosystem and Earth system functioning: the current state of the science. *Ecography*, *44*(11), 1579–1594. https://doi.org/10.1111/ecog.05703

Iglesias, V., Markgraf, V., & Whitlock, C. (2016). 17,000 years of vegetation, fire and climate change in the eastern foothills of the Andes (lat. 44°S). *Palaeogeography, Palaeoclimatology, Palaeoecology*, *457*, 195–208. https://doi.org/10.1016/j.palaeo.2016.06.008

Iglesias, V., Whitlock, C., Markgraf, V., & Bianchi, M. M. (2014). Postglacial history of the Patagonian forest/steppe ecotone (41–43°S). *Quaternary Science Reviews*, *94*, 120–135. https://doi.org/10.1016/j.quascirev.2014.04.014

International Union for Conservation of Nature - IUCN, & Center for International Earth Science Information Network - CIESIN - Columbia University. (2015). Gridded Species Distribution: Global Mammal Richness Grids, 2015 Release. Palisades, NY: NASA Socioeconomic Data and Applications Center (SEDAC). https://doi.org/10.7927/H4N014G5

IPBES. (2019). *Global assessment report on biodiversity and ecosystem services of the Intergovernmental Science-Policy Platform on Biodiversity and Ecosystem Services* (p. 1144). Bonn, Germany: IPBES secretariat. https://doi.org/10.5281/zenodo.5657041

Jaramillo, C. (2006). Cenozoic Plant Diversity in the Neotropics. *Science*, *311*(5769), 1893–1896. https://doi.org/10.1126/science.1121380

Jeske-Pieruschka, V., Pillar, V. D., De Oliveira, M. A. T., & Behling, H. (2013). New insights into vegetation, climate and fire history of southern Brazil revealed by a 40,000 year environmental record from the State Park Serra do Tabuleiro. *Vegetation History and Archaeobotany*, *22*(4), 299–314. https://doi.org/10.1007/s00334-012-0382-y

Johnson, C. N. (2009). Ecological consequences of Late Quaternary extinctions of megafauna. *Proceedings of the Royal Society B: Biological Sciences*, *276*(1667), 2509–2519. https://doi.org/10.1098/rspb.2008.1921

Jolly, D., Prentice, I. C., Bonnefille, R., Ballouche, A., Bengo, M., Brenac, P., et al. (1998). Biome reconstruction from pollen and plant macrofossil data for Africa and the Arabian peninsula at 0 and 6000 years. *Journal of Biogeography*, *25*(6), 1007–1027. https://doi.org/10.1046/j.1365-2699.1998.00238.x

Jones, C. G., Lawton, J. H., & Shachak, M. (1994). Organisms as ecosystem engineers. *Oikos*, 373–386.

Kattge, J., Bönisch, G., Díaz, S., Lavorel, S., Prentice, I. C., Leadley, P., et al. (2020). TRY plant trait database–enhanced coverage and open access. *Global change biology*, *26*(1), 119–188. https://doi.org/10.1111/gcb.14904

Kelley, D. I., Prentice, I. C., Harrison, S. P., Wang, H., Simard, M., Fisher, J. B., & Willis, K. O. (2013). A comprehensive benchmarking system for evaluating global vegetation models. *Biogeosciences*, *10*(5), 3313–3340. https://doi.org/10.5194/bg-10-3313-2013

Kerber, L., Pitana, V. G., Ribeiro, A. M., Hsiou, A. S., & Oliveira, E. V. (2014). Late Pleistocene vertebrates from Touro Passo Creek (Touro Passo Formation), southern Brazil: a review. *Revista mexicana de ciencias geológicas*, *31*(2), 248–259.

Klein Goldewijk, K., Beusen, A., Drecht, G. van, & Vos, M. de. (2011). The HYDE 3.1 spatially explicit database of human-induced global land-use change over the past 12,000 years. *Global Ecology and Biogeography*, *20*(1), 73–86. https://doi.org/10.1111/j.1466-8238.2010.00587.x

Klein Goldewijk, K., Beusen, A., & Janssen, P. (2010). Long-term dynamic modeling of global population and built-up area in a spatially explicit way: HYDE 3.1. *The Holocene*, *20*(4), 565–573. https://doi.org/10.1177/0959683609356587

Kobayashi, S., Ota, Y., Harada, Y., Ebita, A., Moriya, M., Onoda, H., et al. (2015). The JRA-55 Reanalysis: General Specifications and Basic Characteristics. *Journal of the Meteorological Society of Japan. Ser. II*, *93*(1), 5–48. https://doi.org/10.2151/jmsj.2015-001

Koch, P. L., & Barnosky, A. D. (2006). Late Quaternary Extinctions: State of the Debate. *Annual Review of Ecology, Evolution, and Systematics*, *37*(1), 215–250. https://doi.org/10.1146/annurev.ecolsys.34.011802.132415

Köppen, W., & Geiger, R. (1954). *Klima der Erde (Climate of the earth) Wall Map*. Gotha, Germany: Klett-Perthes.

Körner, C. (2002). Grassland in a CO_2-enriched world. In *Multi-function grasslands: quality forages, animal products and landscapes* (pp. 611–624). Presented at the 19th General Meeting of the European Grassland Federation, La Rochelle, France: Organizing Committee of the European Grassland Federation. https://www.cabdirect.org/cabdirect/abstract/20023148914

Kowarik, I. (1987). Kritische Anmerkungen zum theoretischen Konzept der potentiellen natürlichen Vegetation mit Anregungen zu einer zeitgemäßen Modifikation. *Tuexenia*, *7*, 53–67.

Kreft, H., & Jetz, W. (2007). Global patterns and determinants of vascular plant diversity. *Proceedings of the National Academy of Sciences*, *104*(14), 5925–5930. https://doi.org/10.1073/pnas.0608361104

Labarca, R. E. (2015). La Meso y megafauna terrestre extinta del Pleistoceno de Chile. *Publicación Ocasional del Museo Nacional de Historia Natural*, 65.

Landis, J. R., & Koch, G. G. (1977). The Measurement of Observer Agreement for Categorical Data. *Biometrics*, *33*(1), 159–174. https://doi.org/10.2307/2529310

Lasslop, G., Hantson, S., Harrison, S. P., Bachelet, D., Burton, C., Forkel, M., et al. (2020). Global ecosystems and fire: Multi-model assessment of fire-induced tree-cover and carbon storage reduction. *Global Change Biology*, *26*(9), 5027–5041. https://doi.org/10.1111/gcb.15160

Ledru, M.-P., Ceccantini, G., Gouveia, S. E. M., López-Sáez, J. A., Pessenda, L. C. R., & Ribeiro, A. S. (2006). Millenial-scale climatic and vegetation changes in a northern Cerrado (Northeast, Brazil) since the Last Glacial Maximum. *Quaternary Science Reviews*, *25*(9–10), 1110–1126. https://doi.org/10.1016/j.quascirev.2005.10.005

Ledru, M.-P., Montade, V., Blanchard, G., & Hély, C. (2016). Long-term Spatial Changes in the Distribution of the Brazilian Atlantic Forest. *Biotropica*, *48*(2), 159–169. https://doi.org/10.1111/btp.12266

Ledru, M.-P., Mourguiart, P., & Riccomini, C. (2009). Related changes in biodiversity, insolation and climate in the Atlantic rainforest since the last interglacial. *Palaeogeography, Palaeoclimatology, Palaeoecology*, *271*(1–2), 140–152. https://doi.org/10.1016/j.palaeo.2008.10.008

Ledru, M.-P., Salatino, M. L. F., Ceccantini, G., Salatino, A., Pinheiro, F., & Pintaud, J.-C. (2007). Regional assessment of the impact of climatic change on the distribution of a tropical conifer in the lowlands of South America. *Diversity and Distributions*, *13*(6), 761–771. https://doi.org/10.1111/j.1472-4642.2007.00389.x

Leemans, R. (1990a). *Global data sets collected and compiled by the Biosphere Project* (IIASA Working Paper). Laxenburg, Austria: International Institute for Applied Analysis.

Leemans, R. (1990b). *Possible Changes in Natural Vegetation Patterns due to Global Warming* (IIASA Working Paper No. WP-90-008). Laxenburg, Austria: International Institute for Applied Analysis.

Leite, Y. L. R., Costa, L. P., Loss, A. C., Rocha, R. G., Batalha-Filho, H., Bastos, A. C., et al. (2016). Neotropical forest expansion during the last glacial period challenges refuge hypothesis. *Proceedings of the National Academy of Sciences*, *113*(4), 1008–1013. https://doi.org/10.1073/pnas.1513062113

Levis, S., Bonan, G. B., Vertenstein, M., & Oleson, K. W. (2004). *The Community Land Model's Dynamic Global Vegetation Model (CLM-DGVM): Technical Description and User's Guide* (NCAR Technical Note No. TN-459+ IA) (p. 50). Boulder, USA: National Center for Atmospheric Research.

Leyden, B. W. (1985). Late Quaternary Aridity and Holocene Moisture Fluctuations in the Lake Valencia Basin, Venezuela. *Ecology*, *66*(4), 1279–1295. https://doi.org/10.2307/1939181

Leyden, B. W., Brenner, M., Hodell, D. A., & Curtis, J. H. (1993). Late Pleistocene Climate in the Central American Lowlands. In P. K. Swart, K. C. Lohmann, J.

Mckenzie, & S. Savin (Eds.), *Geophysical Monograph Series* (pp. 165–178). Washington, D. C.: American Geophysical Union. https://doi.org/10.1029/GM078p0165

Li, F., & Zhang, X. (2017). Heat response of global vegetation biomes to ongoing climate warming based on remote sensing. *Geosciences*, *7*(3), 83. https://doi.org/10.3390/geosciences7030083

Lindeskog, M., Arneth, A., Bondeau, A., Waha, K., Seaquist, J., Olin, S., & Smith, B. (2013). Implications of accounting for land use in simulations of ecosystem carbon cycling in Africa. *Earth System Dynamics*, *4*(2), 385–407. https://doi.org/10.5194/esd-4-385-2013

Liu, Z., Otto-Bliesner, B. L., He, F., Brady, E. C., Tomas, R., Clark, P. U., et al. (2009). Transient Simulation of Last Deglaciation with a New Mechanism for Bølling-Allerød Warming, *325*, 26.

Llewelyn, J., Strona, G., McDowell, M. C., Johnson, C. N., Peters, K. J., Stouffer, D. B., et al. (2022). Sahul's megafauna were vulnerable to plant-community changes due to their position in the trophic network. *Ecography*, *2022*(1), ecog.06089. https://doi.org/10.1111/ecog.06089

Loidi, J., & Fernández-González, F. (2012). Potential natural vegetation: reburying or reboring? *Journal of Vegetation Science*, *23*(3), 596–604. https://doi.org/10.1111/j.1654-1103.2012.01387.x

Long, A., & Martin, P. S. (1974). Death of American Ground Sloths. *Science*, *186*(4164), 638–640. https://doi.org/10.1126/science.186.4164.638

Long, A., Martin, P. S., & Lagiglia, H. A. (1997). Ground sloth extinction and human occupation at Gruta del Indio, Argentina. *Radiocarbon*, *40*(2), 693–700.

Lopes, A. S., & Cox, F. R. (1977). Cerrado Vegetation in Brazil: An Edaphic Gradient1. *Agronomy Journal*, *69*(5), 828–831. https://doi.org/10.2134/agronj1977.00021962006900050025x

Lorenz, D. J., Nieto-Lugilde, D., Blois, J. L., Fitzpatrick, M. C., & Williams, J. W. (2016). Downscaled and debiased climate simulations for North America from 21,000 years ago to 2100AD. *Scientific Data*, *3*. https://doi.org/10.1038/sdata.2016.48

Loveland, T. R., & Belward, A. S. (1997). The IGBP-DIS global 1km land cover data set, DISCover: First results. *International Journal of Remote Sensing*, *18*(15), 3289–3295. https://doi.org/10.1080/014311697217099

Loveland, T. R., Reed, B. C., Brown, J. F., Ohlen, D. O., Zhu, Z., Yang, L., & Merchant, J. W. (2000). Development of a global land cover characteristics database and IGBP DISCover from 1 km AVHRR data. *International Journal of Remote Sensing*, *21*(6–7), 1303–1330. https://doi.org/10.1080/014311600210191

Luebert, F. (2021). The two South American dry diagonals. *Frontiers of Biogeography*, *0*(0). https://doi.org/10.21425/F5FBG51267

MacFerrin, M., Amante, C., Stroker, K., Carignan, K., Love, M., & Lim, E. (2021). ETOPO 2022: An Updated NOAA Global Relief Model. In *AGU Fall Meeting Abstracts* (Vol. 2021, pp. NH25B-0560). Presented at the AGU Fall Meeting, New Orleans, LA, USA. https://ui.adsabs.harvard.edu/abs/2021AGUFMNH25B0560M

Maezumi, S. Y., Alves, D., Robinson, M., de Souza, J. G., Levis, C., Barnett, R. L., et al. (2018). The legacy of 4,500 years of polyculture agroforestry in the eastern Amazon. *Nature Plants*, *4*(8), 540–547. https://doi.org/10.1038/s41477-018-0205-y

Maksic, J., Venancio, I. M., Shimizu, M. H., Chiessi, C. M., Piacsek, P., Sampaio, G., et al. (2022). Brazilian biomes distribution: Past and future. *Palaeogeography, Palaeoclimatology, Palaeoecology*, *585*, 110717. https://doi.org/10.1016/j.palaeo.2021.110717

Maksic, J., Shimizu, M. H., de Oliveira, G. S., Venancio, I. M., Cardoso, M., & Ferreira, F. A. (2019). Simulation of the Holocene climate over South America and impacts on the vegetation. *The Holocene*, *29*(2), 287–299. https://doi.org/10.1177/0959683618810406

Mancini, M. V., Paez, M. M., Prieto, A. R., Stutz, S., Tonello, M., & Vilanova, I. (2005). Mid-Holocene climatic variability reconstruction from pollen records (32°–52°S, Argentina). *Quaternary International*, *132*(1), 47–59. https://doi.org/10.1016/j.quaint.2004.07.013

Mancini, M. V. (1998). Vegetational changes during the Holocene in Extra-Andean Patagonia, Santa Cruz Province, Argentina. *Palaeogeography, Palaeoclimatology, Palaeoecology*, *138*(1), 207–219. https://doi.org/10.1016/S0031-0182(97)00119-3

Mao, J., & Yan, B. (2019). Global Monthly Mean Leaf Area Index Climatology, 1981-2015. *ORNL DAAC, Oak Ridge, Accessed 14 October 2019*. https://doi.org/10.3334/ORNLDAAC/1653

Marchant, R., Cleef, A., Harrison, S. P., Hooghiemstra, H., Markgraf, V., van Boxel, J., et al. (2009). Pollen-based biome reconstructions for Latin America at 0, 6000 and 18 000 radiocarbon years ago. *Climate of the Past*, *5*(4), 725–767. https://doi.org/10.5194/cp-5-725-2009

Marchant, R., Behling, H., Berrio, J.-C., Cleef, A., Duivenvoorden, J., Hooghiemstra, H., et al. (2002). Pollen-based biome reconstructions for Colombia at 3000, 6000, 9000, 12 000, 15 000 and 18 000 14C yr ago: Late Quaternary tropical vegetation dynamics. *Journal of Quaternary Science*, *17*(2), 113–129. https://doi.org/10.1002/jqs.669

Marchant, R., Berrío, J. C., Behling, H., Boom, A., & Hooghiemstra, H. (2006). Colombian dry moist forest transitions in the Llanos Orientales—A comparison of model and pollen-based biome reconstructions. *Palaeogeography,* *Palaeoclimatology, Palaeoecology*, *234*(1), 28–44. https://doi.org/10.1016/j.palaeo.2005.10.028

Marchant, R., Boom, A., Behling, H., Hooghiemstra, H., Melief, B., Geel, B. V., et al. (2004). Colombian vegetation at the Last Glacial Maximum: a comparison of model- and pollen-based biome reconstructions. *Journal of Quaternary Science*, *19*(7), 721–732. https://doi.org/10.1002/jqs.878

Marcuzzi, G. (1979). *European ecosystems*. The Hague, Netherlands: W. Junk.

Markgraf, V. (1983). Late and postglacial vegetational and paleoclimatic changes in subantarctic, temperate, and arid environments in Argentina. *Palynology*, *7*(1), 43–70. https://doi.org/10.1080/01916122.1983.9989252

Markgraf, V. (1985). Late Pleistocene faunal extinctions in southern Patagonia. *Science*, *228*(4703), 1110–1112.

Markgraf, V., Betancourt, J., & Rylander, K. A. (1997). Late-Holocene rodent middens from Rio Limay, Neuquen Province, Argentina. *The Holocene*, *7*(3), 325–329. https://doi.org/10.1177/095968369700700308

Markgraf, V., & Huber, U. M. (2010). Late and postglacial vegetation and fire history in Southern Patagonia and Tierra del Fuego. *Palaeogeography, Palaeoclimatology, Palaeoecology*, *297*(2), 351–366. https://doi.org/10.1016/j.palaeo.2010.08.013

Markgraf, V., Whitlock, C., & Haberle, S. (2007). Vegetation and fire history during the last 18,000 cal yr B.P. in Southern Patagonia: Mallín Pollux, Coyhaique, Province Aisén (45°41′30″ S, 71°50′30″ W, 640 m elevation). *Palaeogeography, Palaeoclimatology, Palaeoecology*, *254*(3–4), 492–507. https://doi.org/10.1016/j.palaeo.2007.07.008

Marshall, C. R., Lindsey, E. L., Villavicencio, N. A., & Barnosky, A. D. (2015). A Quantitative Model for Distinguishing Between Climate Change, Human Impact, and Their Synergistic Interaction as Drivers of the Late Quaternary Megafaunal Extinctions. *The Paleontological Society Papers*, *21*, 1–20. https://doi.org/10.1017/S1089332600002941

Martens, C., Hickler, T., Davis-Reddy, C., Engelbrecht, F., Higgins, S. I., Maltitz, G. P., et al. (2021). Large uncertainties in future biome changes in Africa call for flexible climate adaptation strategies. *Global Change Biology*, *27*(2), 340–358. https://doi.org/10.1111/gcb.15390

Martin, F. M. (2008). Bone-Crunching Felids at the End of the Pleistocene in Fuego-Patagonia, Chile. *Journal of taphonomy*, *6*(3–4), 337–372.

Martin, F., San Román, M., Morello, F., Todisco, D., Prevosti, F. J., & Borrero, L. A. (2013). Land of the ground sloths: Recent research at Cueva Chica, Ultima Esperanza, Chile. *Quaternary International*, *305*, 56–66. https://doi.org/10.1016/j.quaint.2012.11.003

Martin, F. M., Prieto, A., Román, M. S., Prevosti, F., Cárdena, P., & Borrero, L. A. (2004). Late-Pleistocene Megafauna at Cueva del Puma, Pali-Aike Lava Field, Chile. *Current Research in the Pleistocene*, (21), 101–103.

Martínez, G. A. (2001). 'Fish-tail' projectile points and megamammals: new evidence from Paso Otero 5 (Argentina). *Antiquity*, *75*(289), 523–528. https://doi.org/10.1017/S0003598X00088736

Martínez, G., Gutierrez, M. A., & Prado, J. L. (2004). New Archaeological Evidences from the Late- Pleistocene/Early-Holocene Paso Otero 5 Site (Pampean Region, Argentina). *Latin America*, 4.

Martínez, G., & Gutiérrez, M. A. (2011). Paso Otero 5 : a summary of the interdisciplinary lines of evidence for reconstructing early human occupation and paleoenvironment in the Pampean region, Argentina, 15.

Martinić, M. (1996). La Cueva del Milodon (Ultima Esperanza, Patagonia chilena). Un siglo de descubrimientos y estudios referidos a la vida primitiva en el sur de America. *Journal de la société des américanistes*, *82*(1), 311–323.

Maslin, M. A., Ettwein, V. J., Wilson, K. E., Guilderson, T. P., Burns, S. J., & Leng, M. J. (2011). Dynamic boundary-monsoon intensity hypothesis: evidence from the deglacial Amazon River discharge record. *Quaternary Science Reviews*, *30*(27), 3823–3833. https://doi.org/10.1016/j.quascirev.2011.10.007

Massone, M., & Prieto, A. (2004). Evaluación de la modalidad cultural Fell 1 en Magallanes. *Chungará (Arica)*, *36*, 303–315. https://doi.org/10.4067/S0717-73562004000300033

Mayhew, P. J. (2011). Global climate and extinction: evidence from the fossil record. In T. R. Hodkinson, M. B. Jones, S. Waldren, & J. A. N. Parnell (Eds.), *Climate Change, Ecology and Systematics* (Vol. 78, pp. 99–121). Cambridge: Cambridge University Press.

Mayle, F. E., Beerling, D. J., Gosling, W. D., & Bush, M. B. (2004). Responses of Amazonian ecosystems to climatic and atmospheric carbon dioxide changes since the last glacial maximum. *Philosophical Transactions of the Royal Society of London. Series B: Biological Sciences*, *359*(1443), 499–514. https://doi.org/10.1098/rstb.2003.1434

Mayle, F. E., Burn, M. J., Power, M., & Urrego, D. H. (2009). Vegetation and Fire at the Last Glacial Maximum in Tropical South America. In F. Vimeux, F. Sylvestre, & M. Khodri (Eds.), *Past Climate Variability in South America and Surrounding Regions* (Vol. 14, pp. 89–112). Dordrecht: Springer Netherlands. https://doi.org/10.1007/978-90-481-2672-9_4

McCulloch, R. D., Fogwill, C. J., Sugden, D. E., Bentley, M. J., & Kubik, P. W. (2005). Chronology of the last glaciation in central Strait of Magellan and Bahía Inútil, southernmost South America. *Geografiska Annaler: Series A, Physical Geography*, *87*(2), 289–312. https://doi.org/10.1111/j.0435-3676.2005.00260.x

McCulloch, R. D., Mansilla, C. A., Martin, F., Borrero, L., Staff, R. A., & Tisdall, E. W. (2021). The nature and timing of landscape change at Cerro Benítez, Última Esperanza, southern Patagonia (52°S): New insights into the history of megafaunal extinctions and human occupation. *Quaternary International*, *601*, 116–129. https://doi.org/10.1016/j.quaint.2021.07.018

McInerney, F. A., & Wing, S. L. (2011). The Paleocene-Eocene Thermal Maximum: A perturbation of carbon cycle, climate, and biosphere with implications for the future. *Annual Review of Earth and Planetary Sciences*, *39*, 489–516. https://doi.org/10.1146/annurev-earth-040610-133431

McInerny, G. J., Roberts, D. L., Davy, A. J., & Cribb, P. J. (2006). Significance of Sighting Rate in Inferring Extinction and Threat. *Conservation Biology*, *20*(2), 562–567. https://doi.org/10.1111/j.1523-1739.2006.00377.x

McManus, J. F., Francois, R., Gherardi, J.-M., Keigwin, L. D., & Brown-Leger, S. (2004). Collapse and rapid resumption of Atlantic meridional circulation linked to deglacial climate changes. *Nature*, *428*(6985), 834–837. https://doi.org/10.1038/nature02494

McMichael, C. N. H., Witteveen, N. H., Scholz, S., Zwier, M., Prins, M. A., Lougheed, B. C., et al. (2021). 30,000 years of landscape and vegetation dynamics in a mid-elevation Andean valley. *Quaternary Science Reviews*, *258*, 106866. https://doi.org/10.1016/j.quascirev.2021.106866

Melillo, J. M., McGuire, A. D., Kicklighter, D. W., Moore, B., Vorosmarty, C. J., & Schloss, A. L. (1993). Global climate change and terrestrial net primary production. *Nature*, *363*(6426), 234–240. https://doi.org/10.1038/363234a0

Mena, F., & Stafford, T. W. (2006). Contexto estratigráfico y fechación directa de esqueletos humanos del Holoceno Temprano en Cueva Baño Nuevo 1 (Patagonia Central, Chile). In *Segundo Simposio Internacional del Hombre Temprano en América* (pp. 139–154). INAH: Ciudad de México.

Méndez, C., de Porras, M. E., Maldonado, A., Reyes, O., Nuevo Delaunay, A., & García, J.-L. (2016). Human Effects in Holocene Fire Dynamics of Central Western Patagonia (~44° S, Chile). *Frontiers in Ecology and Evolution*, *4*, 100. https://doi.org/10.3389/fevo.2016.00100

Méndez, C., Quintana, R. S., Nuevo-Delaunay, A., Murillo, I., Mendoza, P. L., Jackson, D., & Maldonado, A. (2020). Depositional Contexts and New Age Controls for Terminal-Pleistocene Megafauna in North-central Chile (31°50′S). *PaleoAmerica*, *6*(4), 357–373. https://doi.org/10.1080/20555563.2020.1733384

Merriam, C. H. (1894). Laws of temperature control of the geographic distribution of terrestrial animals and plants. *National Geographic Magazine*, *6*, 229–238.

Merriam, C. H. (1892). The geographic distribution of life in North America: with special reference to the Mammalia. *Proceedings of the Biological Society of Washington*, *7*, 1–64.

Messineo, P. G., Favier Dubois, C. M., Politis, G. G., & Vitale, P. (2021). Site formation process and megamammal bone radiocarbon dates in Campo Laborde (Pampas of Argentina): Contribution towards a research methodology. *Quaternary International*, *586*, 53–65. https://doi.org/10.1016/j.quaint.2021.01.007

Metcalf, J. L., Turney, C., Barnett, R., Martin, F., Bray, S. C., Vilstrup, J. T., et al. (2016). Synergistic roles of climate warming and human occupation in Patagonian megafaunal extinctions during the Last Deglaciation. *Science Advances*, *2*(6), e1501682. https://doi.org/10.1126/sciadv.1501682

Metcalfe, S. E. (2006). Late Quaternary Environments of the Northern Deserts and Central Transvolcanic Belt of Mexico. *Annals of the Missouri Botanical Garden*, *93*(2), 258–273.

Milchunas, D. G., Mosier, A. R., Morgan, J. A., LeCain, D. R., King, J. Y., & Nelson, J. A. (2005). Elevated CO_2 and defoliation effects on a shortgrass steppe: Forage quality versus quantity for ruminants. *Agriculture, Ecosystems & Environment*, *111*(1–4), 166–184. https://doi.org/10.1016/j.agee.2005.06.014

Mittermeier, R. A., Mittermeier, C. G., Brooks, T. M., Pilgrim, J. D., Konstant, W. R., da Fonseca, G. A. B., & Kormos, C. (2003). Wilderness and biodiversity conservation. *Proceedings of the National Academy of Sciences*, *100*(18), 10309–10313. https://doi.org/10.1073/pnas.1732458100

Moncrieff, G. R., Bond, W. J., & Higgins, S. I. (2016). Revising the biome concept for understanding and predicting global change impacts. *Journal of Biogeography*, *43*(5), 863–873. https://doi.org/10.1111/jbi.12701

Moncrieff, G. R., Hickler, T., & Higgins, S. I. (2015). Intercontinental divergence in the climate envelope of major plant biomes. *Global Ecology and Biogeography*, *24*(3), 324–334. https://doi.org/10.1111/geb.12257

Moncrieff, G. R., Scheiter, S., Bond, W. J., & Higgins, S. I. (2014). Increasing atmospheric CO_2 overrides the historical legacy of multiple stable biome states in Africa. *New Phytologist*, *201*(3), 908–915. https://doi.org/10.1111/nph.12551

Monserud, R. A., & Leemans, R. (1992). Comparing global vegetation maps with the Kappa statistic. *Ecological modelling*, *62*(4), 275–293. http://dx.doi.org/10.1016/0304-3800(92)90003-W

Montade, V., Ledru, M.-P., Burte, J., Martins, E. S. P. R., Verola, C. F., Costa, I. R. da, & Magalhães e Silva, F. H. (2014). Stability of a Neotropical microrefugium during climatic instability. *Journal of Biogeography*, *41*(6), 1215–1226. https://doi.org/10.1111/jbi.12283

Montgomery, D. C., & Peck, E. A. (1982). *Introduction to linear regression analysis*. New York: Wiley.

Montoya, E., Keen, H. F., Luzuriaga, C. X., & Gosling, W. D. (2018). Long-Term Vegetation Dynamics in a Megadiverse Hotspot: The Ice-Age Record of a Pre-montane Forest of Central Ecuador. *Frontiers in Plant Science*, *9*, 196. https://doi.org/10.3389/fpls.2018.00196

Moore, D. M. (1978). Post-glacial vegetation in the South Patagonian territory of the giant ground sloth, Mylodon. *Botanical Journal of the Linnean Society*, *77*(3), 177–202. https://doi.org/10.1111/j.1095-8339.1978.tb01398.x

Moreno, P. I., Videla, J., Valero-Garcés, B., Alloway, B. V., & Heusser, L. E. (2018). A continuous record of vegetation, fire-regime and climatic changes in northwestern Patagonia spanning the last 25,000 years. *Quaternary Science Reviews*, *198*, 15–36. https://doi.org/10.1016/j.quascirev.2018.08.013

Moreno, P. I., Kaplan, M. R., François, J. P., Villa-Martínez, R., Moy, C. M., Stern, C. R., & Kubik, P. W. (2009). Renewed glacial activity during the Antarctic cold reversal and persistence of cold conditions until 11.5 ka in southwestern Patagonia. *Geology*, *37*(4), 375–378. https://doi.org/10.1130/G25399A.1

Mothé, D., Avilla, L. S., Araújo-Júnior, H. I., Rotti, A., Prous, A., & Azevedo, S. A. K. (2020). An artifact embedded in an extinct proboscidean sheds new light on human-megafaunal interactions in the Quaternary of South America. *Quaternary Science Reviews*, *229*, 106125. https://doi.org/10.1016/j.quascirev.2019.106125

Mourelle, D., Prieto, A. R., & García-Rodríguez, F. (2017). Riparian woody vegetation history in the campos region, southeastern South America, during two time windows: late Pleistocene and late Holocene. *Quaternary Science Reviews*, *167*, 14–29. https://doi.org/10.1016/j.quascirev.2017.04.024

Mucina, L. (2010). Floristic-phytosociological approach, potential natural vegetation, and survival of prejudice. *Lazaroa*, *31*, 173–182. https://doi.org/10.5209/rev_LAZA.2010.v31.13

Mucina, L. (2019). Biome: evolution of a crucial ecological and biogeographical concept. *New Phytologist*, *222*(1), 97–114. https://doi.org/10.1111/nph.15609

Musotto, L. L., Borromei, A. M., Bianchinotti, M. V., & Coronato, A. (2017). Late Quaternary palaeoenvironmental reconstruction of central Tierra del Fuego (Argentina) based on pollen and fungi. *Quaternary International*, *442*, 13–25. https://doi.org/10.1016/j.quaint.2016.01.071

Myneni, R. B., Ramakrishna, R., Nemani, R., & Running, S. W. (1997). Estimation of global leaf area index and absorbed par using radiative transfer models. *IEEE Transactions on Geoscience and Remote Sensing*, *35*(6), 1380–1393. https://doi.org/10.1109/36.649788

Nagelkerke, N. J. (1991). A note on a general definition of the coefficient of determination. *Biometrika*, *78*(3), 691–692. http://dx.doi.org/10.1093/biomet/78.3.691

Nami, H. G., & Nakamura, T. (1995). Cronología radiocarbonica con AMS sobre muestras de hueso procedentes del sitio Cueva del Medo (Ultima Esperanza, Chile). *Anales del Instituto de la Patagonia*, *23*, 125–133.

Nanavati, W. P., Whitlock, C., Iglesias, V., & de Porras, M. E. (2019). Postglacial vegetation, fire, and climate history along the eastern Andes, Argentina and Chile (lat. 41–55°S). *Quaternary Science Reviews*, *207*, 145–160. https://doi.org/10.1016/j.quascirev.2019.01.014

Němec, M., Wacker, L., Hajdas, I., & Gäggeler, H. (2010). Alternative Methods for Cellulose Preparation for AMS Measurement. *Radiocarbon*, *52*(3), 1358–1370. https://doi.org/10.1017/S0033822200046440

Nicolson, M. (2013). Community concepts in plant ecology: from Humboldtian plant geography to the superorganism and beyond. *Web Ecology*, *13*(1), 95–102. https://doi.org/10.5194/we-13-95-2013

NOAA National Centers for Environmental Information. (2022). *ETOPO 2022 15 Arc-Second Global Relief Model*. NOAA Boulder, CO, USA.

Novotny, V. (2006). Why Are There So Many Species of Herbivorous Insects in Tropical Rainforests? *Science*, *313*(5790), 1115–1118. https://doi.org/10.1126/science.1129237

O'Leary, M. H. (1988). Carbon isotopes in photosynthesis. *Bioscience*, *38*(5), 328–336. http://dx.doi.org/10.2307/1310735

Olson, D. M., & Dinerstein, E. (1998). The Global 200: a representation approach to conserving the Earth's most biologically valuable ecoregions. *Conservation biology*, *12*(3), 502–515.

Olson, D. M., Dinerstein, E., Wikramanayake, E. D., Burgess, N. D., Powell, G. V. N., Underwood, E. C., et al. (2001). Terrestrial Ecoregions of the World: A New Map of Life on Earth: A new global map of terrestrial ecoregions provides an innovative tool for conserving biodiversity. *BioScience*, *51*(11), 933–938. https://doi.org/10.1641/0006-3568(2001)051[0933:TEOTWA]2.0.CO;2

Otto-Bliesner, B. L., Tomas, R., Brady, E. C., Ammann, C., Kothavala, Z., & Clauzet, G. (2006). Climate Sensitivity of Moderate- and Low-Resolution Versions of CCSM3 to Preindustrial Forcings. *Journal of Climate*, *19*(11), 2567–2583. https://doi.org/10.1175/JCLI3754.1

Owen-Smith, N. (1987). Pleistocene extinctions: the pivotal role of megaherbivores. *Paleobiology*, *13*(3), 351–362. https://doi.org/10.1017/S0094837300008927

Pachzelt, A., Forrest, M., Rammig, A., Higgins, S. I., & Hickler, T. (2015). Potential impact of large ungulate grazers on African vegetation, carbon storage and fire regimes. *Global Ecology and Biogeography*, *24*(9), 991–1002. https://doi.org/10.1111/geb.12313

Pachzelt, A., Rammig, A., Higgins, S., & Hickler, T. (2013). Coupling a physiological grazer population model with a generalized model for vegetation dynamics. *Ecological Modelling*, *263*, 92–102. https://doi.org/10.1016/j.ecolmodel.2013.04.025

Paskoff, R. (1971). Edad radiométrica del mastodonte de Los Vilos: 9.100±300 años BP. *Noticiario Mensual del Museo Nacional de Historia Natural*, *15*(11).

Paunero, R., Davis, C. V., Rindel, D., Tessone, A., Paunero, R., Davis, C. V., et al. (2017). La fauna Pleistocénica: evidencias zooarqueológicas en la Meseta Central de Santa Cruz, los sitios de La María. *Magallania (Chile)*, *45*(2), 181–198. https://doi.org/10.4067/S0718-22442017000200181

Paunero, R. S., Rosales, G., Prado, J. L., & Alberdi, M. T. (2008). Cerro Bombero: record of *Hippidion saldiasi* Roth, 1899 (Equidae, Perissodactyla) in the Early Holocene of Patagonia (Santa Cruz, Argentina). *Estudios Geológicos*, *64*(1), 89–98. https://doi.org/10.3989/egeol.08641430

Paunero, R. S., Frank, A., Skarbun, F., Rosales, G., Zapata, G., Cueto, M., et al. (2005). Arte rupestre en estancia La María, Meseta Central de Santa Cruz: sectorización y contextos arqueológicos. In *Relaciones de la Sociedad Argentina de Antropología* (pp. 147–168). Buenos Aires.

Pearsall, D. M. (2008). Plant Domestication and the Shift to Agriculture in the Andes. In H. Silverman & W. H. Isbell (Eds.), *Handbook of South American archaeology* (pp. 105–120). New York: Springer.

Pedro, J. B., Bostock, H. C., Bitz, C. M., He, F., Vandergoes, M. J., Steig, E. J., et al. (2016). The spatial extent and dynamics of the Antarctic Cold Reversal. *Nature Geoscience*, *9*(1), 51–55. https://doi.org/10.1038/ngeo2580

Peppe, D. J., Baumgartner, A., Flynn, A., & Blonder, B. (2018). Reconstructing Paleoclimate and Paleoecology Using Fossil Leaves. In D. A. Croft, D. F. Su, & S. W. Simpson (Eds.), *Methods in Paleoecology* (pp. 289–317). Cham, Switzerland: Springer International Publishing. https://doi.org/10.1007/978-3-319-94265-0_13

Peppe, D. J., Royer, D. L., Cariglino, B., Oliver, S. Y., Newman, S., Leight, E., et al. (2011). Sensitivity of leaf size and shape to climate: global patterns and paleoclimatic applications. *New Phytologist*, *190*(3), 724–739. https://doi.org/10.1111/j.1469-8137.2010.03615.x

Pérez, L. M., Toledo, N., Mari, F., Echeverría, I., Tonni, E. P., & Toledo, M. J. (2021). Radiocarbon dates of fossil record assigned to mylodontids (Xenarthra - Folivora) found in Cueva del Milodón, Chile. *Quaternary Science Reviews*, *251*, 106695. https://doi.org/10.1016/j.quascirev.2020.106695

Pesce, O. H., & Moreno, P. I. (2014). Vegetation, fire and climate change in central-east Isla Grande de Chiloé (43°S) since the Last Glacial Maximum, northwestern Patagonia. *Quaternary Science Reviews*, *90*, 143–157. https://doi.org/10.1016/j.quascirev.2014.02.021

Pessenda, L. C. R., De Oliveira, P. E., Mofatto, M., de Medeiros, V. B., Francischetti Garcia, R. J., Aravena, R., et al. (2009). The evolution of a tropical rainforest/grassland mosaic in southeastern Brazil since 28,000 ^{14}C yr BP based on carbon isotopes and pollen records. *Quaternary Research*, *71*(3), 437–452. https://doi.org/10.1016/j.yqres.2009.01.008

Pessenda, L. C. R., Saia, S. E. M. G., Gouveia, S. E. M., Ledru, M.-P., Sifeddine, A., Amaral, P. G. C., & Bendassolli, J. A. (2010). Last millennium environmental changes and climate inferences in the Southeastern Atlantic forest, Brazil. *Anais da Academia Brasileira de Ciências*, *82*(3), 717–729. https://doi.org/10.1590/S0001-37652010000300019

Peteet, D. (1995). Global Younger Dryas? *Quaternary International*, *28*, 93–104. https://doi.org/10.1016/1040-6182(95)00049-O

Peterson, L. C., Haug, G. H., Hughen, K. A., & Röhl, U. (2000). Rapid Changes in the Hydrologic Cycle of the Tropical Atlantic During the Last Glacial. *Science*, *290*(5498), 1947–1951. https://doi.org/10.1126/science.290.5498.1947

Pickett, E. J., Harrison, S. P., Hope, G., Harle, K., Dodson, J. R., Peter Kershaw, A., et al. (2004). Pollen-based reconstructions of biome distributions for Australia, Southeast Asia and the Pacific (SEAPAC region) at 0, 6000 and 18,000 ^{14}C yr BP. *Journal of Biogeography*, *31*(9), 1381–1444. https://doi.org/10.1111/j.1365-2699.2004.01001.x

Pino, M. (Ed.). (2016). *El Sitio Pilauco: Osorno, Patagonia Noroccidental de Chile*.

Pino, M., Abarzúa, A. M., Astorga, G., Martel-Cea, A., Cossio-Montecinos, N., Navarro, R. X., et al. (2019). Sedimentary record from Patagonia, southern Chile supports cosmic-impact triggering of biomass burning, climate change, and megafaunal extinctions at 12.8 ka. *Scientific Reports*, *9*(1), 4413. https://doi.org/10.1038/s41598-018-38089-y

Pino, M., Chávez-Hoffmeister, M., Navarro-Harris, X., & Labarca, R. (2013). The late Pleistocene Pilauco site, Osorno, south-central Chile. *Quaternary International*, *299*, 3–12. https://doi.org/10.1016/j.quaint.2012.05.001

Pires, M. M., Koch, P. L., Fariña, R. A., de Aguiar, M. A. M., dos Reis, S. F., & Guimarães, P. R. (2015). Pleistocene megafaunal interaction networks became more vulnerable after human arrival. *Proceedings of the Royal Society B: Biological Sciences*, *282*(1814), 20151367. https://doi.org/10.1098/rspb.2015.1367

Pires, M. M., Rindel, D., Moscardi, B., Cruz, L. R., Guimarães, P. R., dos Reis, S. F., & Perez, S. I. (2020). Before, during and after megafaunal extinctions: Human impact on Pleistocene-Holocene trophic networks in South Patagonia. *Quaternary Science Reviews*, *250*, 106696. https://doi.org/10.1016/j.quascirev.2020.106696

Pitana, V. G., Esteban, G. I., Ribeiro, A. M., & Cartelle, C. (2013). Cranial and dental studies of *Glossotherium robustum* (Owen, 1842)(Xenarthra: Pilosa: Mylodontidae) from the Pleistocene of southern Brazil. *Alcheringa: An Australasian Journal of Palaeontology*, *37*(2), 147–162.

Pivello, V. R. (2011). The Use of Fire in the Cerrado and Amazonian Rainforests of Brazil: Past and Present. *Fire Ecology*, *7*(1), 24–39. https://doi.org/10.4996/fireecology.0701024

Pivello, V. R., & Coutinho, L. M. (1996). A qualitative successional model to assist in the management of Brazilian cerrados. *Forest Ecology and Management*, *87*(1), 127–138. https://doi.org/10.1016/S0378-1127(96)03829-7

Politis, G. G., Bonomo, M., & Prates, L. (2003). Politis, G. G., Bonomo, M., & Prates, L. (2003). Território y mobilidad entre la costa atlantica y el interior de la región pampeana (Argentina). *Estudos Ibero-Americanos*, *29*(1), 11–35.

Politis, G. G., & Steele, J. (2014). Cronología radiocarbónica. *Estado Actual de las investigaciones en el sitio Arroyo Seco*, *2*, 57e66.

Politis, G. G., & Lindsey, E. (2012). *Humans and Pleistocene megamammals in the Pampean Region. Trabajo presentado en el 77th Annual Meeting of the Society for American Archaeology*. Memphis, Tennesse.

Politis, G. G., Gutiérrez, M. A., Rafuse, D. J., & Blasi, A. (2016). The Arrival of Homo sapiens into the Southern Cone at 14,000 Years Ago. *PLOS ONE*, *11*(9), e0162870. https://doi.org/10.1371/journal.pone.0162870

Politis, G. G., Messineo, P. G., Stafford, T. W., & Lindsey, E. L. (2019). Campo Laborde: A Late Pleistocene giant ground sloth kill and butchering site in the Pampas. *Science Advances*, *5*(3), eaau4546. https://doi.org/10.1126/sciadv.aau4546

Pontius Jr, R. G., & Santacruz, A. (2019). *Differ: Metrics of difference for comparing pairs of maps or pairs of variables. R package version 0.0-6*. R.

Pontius Jr, R. G., & Millones, M. (2011). Death to Kappa: birth of quantity disagreement and allocation disagreement for accuracy assessment. *International Journal of Remote Sensing*, *32*(15), 4407–4429. https://doi.org/10.1080/01431161.2011.552923

Pope, V. D., Gallani, M. L., Rowntree, P. R., & Stratton, R. A. (2000). The impact of new physical parametrizations in the Hadley Centre climate model: HadAM3. *Climate Dynamics*, *16*(2–3), 123–146. https://doi.org/10.1007/s003820050009

Popkin, G. (2015). The hunt for the world's missing carbon. *Nature News*, *523*(7558), 20–22. https://doi.org/10.1038/523020a

Portilho-Ramos, R. C., Chiessi, C. M., Zhang, Y., Mulitza, S., Kucera, M., Siccha, M., et al. (2017). Coupling of equatorial Atlantic surface stratification to glacial shifts in the tropical rainbelt. *Scientific Reports*, *7*(1), 1561. https://doi.org/10.1038/s41598-017-01629-z

Prado, J. L., Martinez-Maza, C., & Alberdi, M. T. (2015). Megafauna extinction in South America: A new chronology for the Argentine Pampas. *Palaeogeography, Palaeoclimatology, Palaeoecology*, *425*, 41–49. https://doi.org/10.1016/j.palaeo.2015.02.026

Prado, J. L., Alberdi, M. T., & Martino, V. J. D. (2012). Équidos y Gonfoterios del Pleistoceno Tardío del Sudeste de la Provincia de Buenos Aires. *Ameghiniana*, *49*(4), 623. https://doi.org/10.5710/AMGH.28.4.2011.559

Prates, L., & Perez, S. I. (2021). Late Pleistocene South American megafaunal extinctions associated with rise of Fishtail points and human population. *Nature Communications*, *12*(1), 2175. https://doi.org/10.1038/s41467-021-22506-4

Prates, L., Politis, G. G., & Perez, S. I. (2020). Rapid radiation of humans in South America after the last glacial maximum: A radiocarbon-based study. *PLOS ONE*, *15*(7), e0236023. https://doi.org/10.1371/journal.pone.0236023

Prates, L., Rivero, D., & Perez, S. I. (2022). Changes in projectile design and size of prey reveal the central role of Fishtail points in megafauna hunting in South America. *Scientific Reports*, *12*(1), 16964. https://doi.org/10.1038/s41598-022-21287-0

Prentice, I. C., Harrison, S. P., & Bartlein, P. J. (2011). Global vegetation and terrestrial carbon cycle changes after the last ice age. *New Phytologist*, *189*(4), 988–998. https://doi.org/10.1111/j.1469-8137.2010.03620.x

Prentice, I. C., Cramer, W., Harrison, S. P., Leemans, R., Monserud, R. A., & Solomon, A. M. (1992). Special paper: a global biome model based on plant physiology and dominance, soil properties and climate. *Journal of biogeography*, *9*(2), 117–134. http://dx.doi.org/10.2307/2845499

Prentice, I. C., Sykes, M. T., Lautenschlager, M., Harrison, S. P., Denissenko, O., & Bartlein, P. J. (1993). Modelling Global Vegetation Patterns and Terrestrial Carbon Storage at the Last Glacial Maximum. *Global Ecology and Biogeography Letters*, *3*(3), 67. https://doi.org/10.2307/2997548

Prentice, I. C., & Webb III, T. (1998). BIOME 6000: reconstructing global mid-Holocene vegetation patterns from palaeoecological records. *Journal of Biogeography*, *25*(6), 997–1005. https://doi.org/10.1046/j.1365-2699.1998.00235.x

Prevosti, F. J., & Martin, F. M. (2013). Paleoecology of the mammalian predator guild of Southern Patagonia during the latest Pleistocene: Ecomorphology, stable isotopes, and taphonomy. *Quaternary International*, *305*, 74–84. https://doi.org/10.1016/j.quaint.2012.12.039

Prieto, A., Labarca, R., & Sierpe, V. (2010). New evidence of the sabertooth cat *Smilodon* (Carnivora: Machairodontinae) in the late Pleistocene of southern Chilean Patagonia. *Revista chilena de historia natural*, *83*(2). https://doi.org/10.4067/S0716-078X2010000200010

Prieto, A. R. (2000). Vegetational history of the Late glacial–Holocene transition in the grasslands of eastern Argentina. *Palaeogeography, Palaeoclimatology, Palaeoecology*, *157*(3–4), 167–188. https://doi.org/10.1016/S0031-0182(99)00163-7

Prieto, A. R., Blasi, A. M., De Francesco, C. G., & Fernández, C. (2004). Environmental history since 11,000 ^{14}C yr B.P. of the northeastern Pampas, Argentina, from alluvial sequences of the Luján River. *Quaternary Research*, *62*(2), 146–161. https://doi.org/10.1016/j.yqres.2004.04.006

Prieto, A. (1991). Cazadores tempranos y tardíos en la cueva 1 del Lago Sofía. In Anales del Instituto de la Patagonia (Vol. 20, pp. 75–99). Punta Arenas, Chile.

Pugh, T. A. M., Lindeskog, M., Smith, B., Poulter, B., Arneth, A., Haverd, V., & Calle, L. (2019). Role of forest regrowth in global carbon sink dynamics. *Proceedings of the National Academy of Sciences*, *116*(10), 4382–4387. https://doi.org/10.1073/pnas.1810512116

Puig, S., Videla, F., Cona, M. I., & Monge, S. A. (2001). Use of food availability by guanacos (Lama guanicoe) and livestock in Northern Patagonia (Mendoza, Argentina). *Journal of Arid Environments*, *47*(3), 291–308. https://doi.org/10.1006/jare.2000.0677

Puig, S. V., F., & Cona, M. I. (1997). Diet and abundance of the guanaco (*Lama guanicoe* Müller 1776) in four habitats of northern Patagonia, Argentina. *Journal of Arid Environments*, *36*(2), 343–357. https://doi.org/10.1006/jare.1996.0186

R Core Team. (2022). *R: A language and environment for statistical computing*. Vienna, Austria: R Foundation for Statistical Computing. https://www.R-project.org/

Rademaker, K., Hodgins, G., Moore, K., Zarrillo, S., Miller, C., Bromley, G. R. M., et al. (2014). Paleoindian settlement of the high-altitude Peruvian Andes. *Science*, *346*(6208), 466–469. https://doi.org/10.1126/science.1258260

Raedeke, K. J., & Simonetti, J. A. (1988). Food Habits of *Lama guanicoe* in the Atacama Desert of Northern Chile. *Journal of Mammalogy*, *69*(1), 198–201. https://doi.org/10.2307/1381777

Randerson, J. T., van der Werf, G. R., Giglio, L., Collatz, G. J., & Kasibhatla, P. S. (2017). Global Fire Emissions Database, Version 4.1 (GFEDv4). *ORNL DAAC, Oak Ridge, Accessed 14 October 2019*. https://doi.org/10.3334/ORNLDAAC/1293

Ray, N., & Adams, J. (2001). A GIS-based vegetation map of the world at the last glacial maximum (25,000-15,000 BP). *Internet archaeology*, *11*. https://doi.org/10.11141/ia.11.2

Reasoner, M. A., & Jodry, M. A. (2000). Rapid response of alpine timberline vegetation to the Younger Dryas climate oscillation in the Colorado Rocky Mountains, USA. *Geology*, *28*(1), 51–54. https://doi.org/10.1130/0091-7613(2000)28<51:RROATV>2.0.CO;2

Renssen, H., & Lautenschlager, M. (2000). The effect of vegetation in a climate model simulation on the Younger Dryas. *Global and Planetary Change*, *26*(4), 423–443. https://doi.org/10.1016/S0921-8181(00)00054-0

Renssen, H., Mairesse, A., Goosse, H., Mathiot, P., Heiri, O., Roche, D. M., et al. (2015). Multiple causes of the Younger Dryas cold period. *Nature Geoscience*, *8*(12), 946–949. https://doi.org/10.1038/ngeo2557

Roberts, D. L., & Solow, A. R. (2003). When did the dodo become extinct? *Nature*, *426*(6964), 245–245. https://doi.org/10.1038/426245a

Rossello, E. A., Jahn, B., Liu, T.-K., & Petrocelli, J. L. (1999). New 4,300 yr ^{14}C age of Glyptodonts at Luján River (Buenos Aires, Argentina) and its implications. In *II*

South American Symposium on Isotope Geology (Villa Carlos Paz, Argentina)(Villa Carlos Paz, Argentina: Villa Carlos Paz, Argentina).

Rothhammer, F., & Dillehay, T. D. (2009). The Late Pleistocene Colonization of South America: An Interdisciplinary Perspective. *Annals of Human Genetics*, *73*(5), 540–549. https://doi.org/10.1111/j.1469-1809.2009.00537.x

Rozas-Davila, A., Valencia, B. G., & Bush, M. B. (2016). The functional extinction of Andean megafauna. *Ecology*, *97*(10), 2533–2539. https://doi.org/10.1002/ecy.1531

Rull, V., Vegas-Vilarrúbia, T., & Montoya, E. (2015). Neotropical vegetation responses to Younger Dryas climates as analogs for future climate change scenarios and lessons for conservation. *Quaternary Science Reviews*, *115*, 28–38. https://doi.org/10.1016/j.quascirev.2015.03.003

Running, S. W., Loveland, T. R., Pierce, L. L., Nemani, R. R., & Hunt, E. R. (1995). A remote sensing based vegetation classification logic for global land cover analysis. *Remote Sensing of Environment*, *51*(1), 39–48. https://doi.org/10.1016/0034-4257(94)00063-S

Safford, H. D. (1999). Brazilian Páramos I. An introduction to the physical environment and vegetation of the campos de altitude. *Journal of Biogeography*, *26*(4), 693–712. https://doi.org/10.1046/j.1365-2699.1999.00313.x

Sagredo, E. A. (2007). Geomorfología, estratigrafía y geocronología de la Última Terminación glacial en Última Esperanza (51°S): Implicancias paleoecológicas y paleoclimáticas. *Santiago, Universidad de Chile. MS*.

Sakschewski, B., von Bloh, W., Boit, A., Poorter, L., Peña-Claros, M., Heinke, J., et al. (2016). Resilience of Amazon forests emerges from plant trait diversity. *Nature Climate Change*, *6*(11), 1032–1036. https://doi.org/10.1038/nclimate3109

Salgado-Labouriau, M. L. (1997). Late quaternary palaeoclimate in the savannas of South America. *Journal of Quaternary Science*, *12*(5), 371–379. https://doi.org/10.1002/(SICI)1099-1417(199709/10)12:5<371::AID-JQS320>3.0.CO;2-3

Saltré, F., Brook, B. W., Rodríguez-Rey, M., Cooper, A., Johnson, C. N., Turney, C. S. M., & Bradshaw, C. J. A. (2015). Uncertainties in dating constrain model choice for inferring extinction time from fossil records. *Quaternary Science Reviews*, *112*, 128–137. https://doi.org/10.1016/j.quascirev.2015.01.022

Saltré, F., Chadoeuf, J., Peters, K. J., McDowell, M. C., Friedrich, T., Timmermann, A., et al. (2019). Climate-human interaction associated with southeast Australian megafauna extinction patterns. *Nature Communications*, *10*(1), 5311. https://doi.org/10.1038/s41467-019-13277-0

Saltré, F., Rodríguez-Rey, M., Brook, B. W., Johnson, C. N., Turney, C. S. M., Alroy, J., et al. (2016). Climate change not to blame for late Quaternary megafauna extinctions in Australia. *Nature Communications*, *7*, 10511. https://doi.org/10.1038/ncomms10511

Salzmann, U., Haywood, A. M., Lunt, D. J., Valdes, P. J., & Hill, D. J. (2008). A new global biome reconstruction and data-model comparison for the Middle Pliocene. *Global Ecology and Biogeography*, *17*(3), 432–447. https://doi.org/10.1111/j.1466-8238.2008.00381.x

Sánchez, B., Prado, J. L., & Alberdi, M. T. (2006). Ancient feeding, ecology and extinction of Pleistocene horses from the Pampean Region, Argentina, 10.

Sandom, C., Faurby, S., Sandel, B., & Svenning, J.-C. (2014). Global late Quaternary megafauna extinctions linked to humans, not climate change. *Proceedings of the Royal Society B: Biological Sciences*, *281*(1787), 20133254. https://doi.org/10.1098/rspb.2013.3254

Sangster, A. G., & Dale, H. M. (1964). Pollen grain preservation of underrepresented species in fossil spectra. *Canadian Journal of Botany*, *42*(4), 437–449. http://dx.doi.org/10.1139/b64-044

Sankaran, M., Ratnam, J., & Hanan, N. (2008). Woody cover in African savannas: the role of resources, fire and herbivory. *Global Ecology and Biogeography*, *17*(2), 236–245. https://doi.org/10.1111/j.1466-8238.2007.00360.x

Saxon, E. C. (1979). Natural prehistory: the archeology of Fuego-Patagonian ecology. *Quaternaria Roma*, *21*.

Sayedi, S. S., Abbott, B. W., Vannière, B., Leys, B., Colombaroli, D., Romera, G. G., et al. (2024). Assessing changes in global fire regimes. Fire Ecology, 20(1), 18. https://doi.org/10.1186/s42408-023-00237-9

Scanferla, A., Bonini, R., Pomi, L., Fucks, E., & Molinari, A. (2013). New Late Pleistocene megafaunal assemblage with well-supported chronology from the Pampas of southern South America. *Quaternary International*, *305*, 97–103. https://doi.org/10.1016/j.quaint.2012.08.005

Schäbitz, F. (1991). Holocene vegetation and climate in southern Santa Cruz, Argentina. *Südamerika: Geomorphologie und Paläökologie im jüngeren Quartär*, 235–244.

Schädler, M., Jung, G., Auge, H., & Brandl, R. (2003). Palatability, decomposition and insect herbivory: patterns in a successional old-field plant community. *Oikos*, *103*(1), 121–132. https://doi.org/10.1034/j.1600-0706.2003.12659.x

Scheiter, S., Langan, L., & Higgins, S. I. (2013). Next-generation dynamic global vegetation models: learning from community ecology. *New Phytologist*, *198*(3), 957–969. https://doi.org/10.1111/nph.12210

Schimper, A. F. W. (1903). *Plant-geography Upon a Physiological Basis*. Oxford, UK: Clarendon Press.

Schmithüsen, J. (1976). Atlas zur Biogeographie (Meyers großer phys Weltatlas, Bd. 3). Bibliogr. Inst., Mannheim—Wien—Zürich.

Schopf, J. M. (1975). Modes of fossil preservation. *Review of Palaeobotany and Palynology*, *20*(1–2), 27–53. http://dx.doi.org/10.1016/0034-6667(75)90005-6

Shelford, V. E., & Olson, S. (1935). Sere, climax and influent animals with special reference to the transcontinental coniferous forest of North America. *Ecology*, *16*(3), 375–402. http://dx.doi.org/10.2307/1930076

Sifeddine, A., Martin, L., Turcq, B., Volkmer-Ribeiro, C., Soubiès, F., Cordeiro, R. C., & Suguio, K. (2001). Variations of the Amazonian rainforest environment: a sedimentological record covering 30,000 years. *Palaeogeography, Palaeoclimatology, Palaeoecology*, *168*(3), 221–235. https://doi.org/10.1016/S0031-0182(00)00256-X

Signor, P. W., Lipps, J. H., Silver, L. T., & Schultz, P. H. (1982). Sampling bias, gradual extinction patterns, and catastrophes in the fossil record. In *Geological implications of impacts of large asteroids and comets on the Earth* (Vol. 190, pp. 291–296). Geological Society of America Special Publication.

Silverman, B. W. (1986). *Density estimation for statistics and data analysis* (Vol. 26). CRC press.

Smith, B., Wårlind, D., Arneth, A., Hickler, T., Leadley, P., Siltberg, J., & Zaehle, S. (2014). Implications of incorporating N cycling and N limitations on primary production in an individual-based dynamic vegetation model. *Biogeosciences*, *11*(7), 2027–2054. https://doi.org/10.5194/bg-11-2027-2014

Smith, B., Prentice, I. C., & Sykes, M. T. (2001). Representation of vegetation dynamics in the modelling of terrestrial ecosystems: comparing two contrasting approaches within European climate space. *Global Ecology*, 25. https://doi.org/10.1046/j.1466-822X.2001.t01-1-00256.x

Sobol, M. K., & Finkelstein, S. A. (2018). Predictive pollen-based biome modeling using machine learning. *PLOS One*, *13*(8), e0202214. https://doi.org/10.1371/journal.pone.0202214

Sobol, M. K., Scott, L., & Finkelstein, S. A. (2019). Reconstructing past biomes states using machine learning and modern pollen assemblages: A case study from Southern Africa. *Quaternary Science Reviews*, *212*, 1–17. https://doi.org/10.1016/j.quascirev.2019.03.027

Solow, A. R., Roberts, D. L., & Robbirt, K. M. (2006). On the Pleistocene extinctions of Alaskan mammoths and horses. *Proceedings of the National Academy of Sciences*, *103*(19), 7351–7353. https://doi.org/10.1073/pnas.0509480103

Solow, A. R. (1993). Inferring Extinction from Sighting Data. *Ecology*, *74*(3), 962–964. https://doi.org/10.2307/1940821

Spratt, R. M., & Lisiecki, L. E. (2016). A Late Pleistocene sea level stack. *Climate of the Past*, *12*(4), 1079–1092. https://doi.org/10.5194/cp-12-1079-2016

Stafford, T. W., Brendel, K., & Duhamel, R. C. (1988). Radiocarbon, ^{13}C and ^{15}N analysis of fossil bone: Removal of humates with XAD-2 resin. *Geochimica et Cosmochimica Acta*, *52*(9), 2257–2267. https://doi.org/10.1016/0016-7037(88)90128-7

Staver, A. C., Archibald, S., & Levin, S. A. (2011). The Global Extent and Determinants of Savanna and Forest as Alternative Biome States. *Science*, *334*(6053), 230–232. https://doi.org/10.1126/science.1210465

Steele, J., & Politis, G. (2009). AMS ^{14}C dating of early human occupation of southern South America. *Journal of Archaeological Science*, *36*(2), 419–429. https://doi.org/10.1016/j.jas.2008.09.024

Stern, C. R., Moreno, P. I., Villa-Martínez, R., Sagredo, E. A., Prieto, A., & Labarca, R. (2011). Evolution of ice-dammed proglacial lakes in Última Esperanza, Chile: implications from the late-glacial R1 eruption of Reclús volcano, Andean Austral Volcanic Zone. *Andean Geology*, 17.

Stocker, B. D., Zscheischler, J., Keenan, T. F., Prentice, I. C., Peñuelas, J., & Seneviratne, S. I. (2018). Quantifying soil moisture impacts on light use efficiency across biomes. *New Phytologist*, *218*(4), 1430–1449. https://doi.org/10.1111/nph.15123

Stríkis, N. M., Chiessi, C. M., Cruz, F. W., Vuille, M., Cheng, H., de Souza Barreto, E. A., et al. (2015). Timing and structure of Mega-SACZ events during Heinrich Stadial 1. *Geophysical Research Letters*, *42*(13), 5477-5484A. https://doi.org/10.1002/2015GL064048

Strona, G., & Bradshaw, C. J. A. (2022). Coextinctions dominate future vertebrate losses from climate and land use change. *Science Advances*, *8*(50), eabn4345. https://doi.org/10.1126/sciadv.abn4345

Stuart, A. J. (2015). Late Quaternary megafaunal extinctions on the continents: a short review. *Geological Journal*, *50*(3), 338–363. https://doi.org/10.1002/gj.2633

Suárez, R. (2018). The Peopling of Southeastern South America: Cultural Diversity, Paleoenvironmental Conditions, and Lithic Technological Organization During the Late Pleistocene and Early Holocene. In E. Robinson & F. Sellet (Eds.), *Lithic Technological Organization and Paleoenvironmental Change* (Vol. 9, pp. 281–300). Cham: Springer International Publishing. https://doi.org/10.1007/978-3-319-64407-3_13

Sugden, D. E., Bentley, M. J., Fogwill, C. J., Hulton, N. R. J., McCulloch, R. D., & Purves, R. S. (2005). Late-glacial glacier events in southernmost South America: a blend of ‘northern’ and 'southern’ hemispheric climatic signals? *Geografiska Annaler: Series A, Physical Geography*, *87*(2), 273–288. https://doi.org/10.1111/j.0435-3676.2005.00259.x

Svenning, J.-C., & Sandel, B. (2013). Disequilibrium vegetation dynamics under future climate change. *American Journal of Botany*, *100*(7), 1266–1286. https://doi.org/10.3732/ajb.1200469

Sweatman, M. B. (2021). The Younger Dryas impact hypothesis: Review of the impact evidence. *Earth-Science Reviews*, *218*, 103677. https://doi.org/10.1016/j.earscirev.2021.103677

Tafasca, S., Ducharne, A., & Valentin, C. (2020). Weak sensitivity of the terrestrial water budget to global soil texture maps in the ORCHIDEE land surface model. *Hydrology and Earth System Sciences*, *24*(7), 3753–3774. https://doi.org/10.5194/hess-24-3753-2020

Takahara, H., Sugita, S., Harrison, S. P., Miyoshi, N., Morita, Y., & Uchiyama, T. (2000). Pollen-based reconstructions of Japanese biomes at 0, 6000 and 18,000 ^{14}C yr BP. *Journal of Biogeography*, *27*(3), 665–683. https://doi.org/10.1046/j.1365-2699.2000.00432.x

Tarasov, P. E., Cheddadi, R., Guiot, J., Bottema, S., Peyron, O., Belmonte, J., et al. (1998). A method to determine warm and cool steppe biomes from pollen data; application to the Mediterranean and Kazakhstan regions. *Journal of Quaternary Science: Published for the Quaternary Research Association*, *13*(4), 335–344. https://doi.org/10.1002/(SICI)1099-1417(199807/08)13:43.3.CO;2-1

Tarasov, P. E., Webb III, T., Andreev, A. A., Afanas' eva, N. B., Berezina, N. A., Bezusko, L. G., et al. (1998). Present-day and mid-Holocene biomes reconstructed from pollen and plant macrofossil data from the former Soviet Union and Mongolia. *Journal of Biogeography*, *25*(6), 1029–1053. https://doi.org/10.1046/j.1365-2699.1998.00236.x

Tardif, D., Toumoulin, A., Fluteau, F., Donnadieu, Y., Le Hir, G., Barbolini, N., et al. (2021). Orbital variations as a major driver of climate and biome distribution during the greenhouse to icehouse transition. *Science Advances*, *7*(43), eabh2819. https://doi.org/10.1126/sciadv.abh2819

Tews, J., Brose, U., Grimm, V., Tielbörger, K., Wichmann, M. C., Schwager, M., & Jeltsch, F. (2004). Animal species diversity driven by habitat heterogeneity/diversity: the importance of keystone structures: Animal species diversity driven by habitat heterogeneity. *Journal of Biogeography*, *31*(1), 79–92. https://doi.org/10.1046/j.0305-0270.2003.00994.x

Thomé, M. T. C., Sequeira, F., Brusquetti, F., Carstens, B., Haddad, C. F. B., Rodrigues, M. T., & Alexandrino, J. (2016). Recurrent connections between Amazon and Atlantic forests shaped diversity in Caatinga four-eyed frogs. *Journal of Biogeography*, *43*(5), 1045–1056. https://doi.org/10.1111/jbi.12685

Thompson, R. S., & Anderson, K. H. (2000). Biomes of western North America at 18,000, 6000 and 0 ^{14}C yr BP reconstructed from pollen and packrat midden data. *Journal of Biogeography*, *27*(3), 555–584. https://doi.org/10.1046/j.1365-2699.2000.00427.x

Tonni, E. P., Carlini, A. A., Yané, G. J. S., & Figini, A. J. (2003). Cronología radiocarbónica y condiciones climáticas en la "Cueva del Milodón"(sur de Chile) durante el Pleistoceno Tardío. *Ameghiniana*, *40*(4), 609–615.

Tonni, E. P., Huarte, R. A., Carbonari, J. E., & Figini, A. J. (2003). New radiocarbon chronology for the Guerrero Member of the Luján Formation (Buenos Aires, Argentina): palaeoclimatic significance. *Quaternary International*, *109–110*, 45–48. https://doi.org/10.1016/S1040-6182(02)00201-X

Tonni, E. P., Cione, A. L., & Soibelzon, L. H. (2003). The broken zig-zag: Late Cenozoic large mammal and tortoise extinction in South America. *Revista del Museo Argentino de Ciencias Naturales*, *5*. https://doi.org/10.22179/REVMACN.5.26

Toszogyova, A., & Storch, D. (2019). Global diversity patterns are modulated by temporal fluctuations in primary productivity. *Global Ecology and Biogeography*, *28*(12), 1827–1838. https://doi.org/10.1111/geb.12997

Townshend, J., Justice, C., Li, W., Gurney, C., & McManus, J. (1991). Global land cover classification by remote sensing: present capabilities and future possibilities. *Remote Sensing of Environment*, *35*(2–3), 243–255. http://dx.doi.org/10.1016/0034-4257(91)90016-Y

Traylor, W. (2021). *wtraylor/trace21ka_for_lpjguess: Version 0.3.0*. Zenodo. https://zenodo.org/record/5060115. Accessed 21 June 2022

Turner, D. P., Ritts, W. D., Cohen, W. B., Gower, S. T., Running, S. W., Zhao, M., et al. (2006). Evaluation of MODIS NPP and GPP products across multiple biomes. *Remote Sensing of Environment*, *102*(3–4), 282–292. https://doi.org/10.1016/j.rse.2006.02.017

Tüxen, R. (1956). Die huetige potentielle naturliche Vegetation als Gegestand der Vegetationskarierung. *Angewandte Pflanzensozioligie*, *13*, 5–42.

Ubilla, M., Rinderknecht, A., Corona, A., & Perea, D. (2018). Mammals in Last 30 to 7 ka Interval (Late Pleistocene-Early Holocene) in Southern Uruguay (Santa Lucía River Basin): Last Occurrences, Climate, and Biogeography. *Journal of Mammalian Evolution*, *25*(2), 291–300. https://doi.org/10.1007/s10914-017-9380-2

Udvardy, M. D. F. (1975). *A Classification of the Biogeographical Provinces of the World* (IUCN Occasional Paper No. 18) (p. 49). Morges, Switzerland: International Union for Conservation of Nature and Natural Resources.

Urrego, D. H., Bush, M. B., & Silman, M. R. (2010). A long history of cloud and forest migration from Lake Consuelo, Peru. *Quaternary Research*, *73*(2), 364–373. https://doi.org/10.1016/j.yqres.2009.10.005

Urrego, D. H., Silman, M. R., & Bush, M. B. (2005). The Last Glacial Maximum: stability and change in a western Amazonian cloud forest. *Journal of Quaternary Science*, *20*(7–8), 693–701. https://doi.org/10.1002/jqs.976

van der Hammen, T., & Absy, M. L. (1994). Amazonia during the last glacial. *Palaeogeography, Palaeoclimatology, Palaeoecology*, *109*(2–4), 247–261. https://doi.org/10.1016/0031-0182(94)90178-3

van Geel, B., van Leeuwen, J. F. N., Nooren, K., Mol, D., den Ouden, N., van der Knaap, P. W. O., et al. (2022). Diet and environment of *Mylodon darwinii* based on pollen of a Late-Glacial coprolite from the Mylodon Cave in southern Chile.

Review of Palaeobotany and Palynology, *296*, 104549. https://doi.org/10.1016/j.revpalbo.2021.104549

van Hoesel, A., Hoek, W. Z., Pennock, G. M., & Drury, M. R. (2014). The Younger Dryas impact hypothesis: a critical review. *Quaternary Science Reviews*, *83*, 95–114. https://doi.org/10.1016/j.quascirev.2013.10.033

van Wees, D., van der Werf, G. R., Randerson, J. T., Andela, N., Chen, Y., & Morton, D. C. (2021). The role of fire in global forest loss dynamics. *Global Change Biology*, *27*(11), 2377–2391. https://doi.org/10.1111/gcb.15591

Velásquez, H., & Mena, F. (2006). VELÁSQUEZ, Héctor et MENA, Francisco. Distribuciones óseas de ungulados en la cueva Baño Nuevo-1 (XI Región, Chile): un primer acercamiento. *Magallania (Punta Arenas)*, *34*(2), 91–106. https://doi.org/10.4067/S0718-22442006000200009

Villa-Martínez, R., Moreno, P. I., & Valenzuela, M. A. (2012). Deglacial and postglacial vegetation changes on the eastern slopes of the central Patagonian Andes (47°S). *Quaternary Science Reviews*, *32*, 86–99. https://doi.org/10.1016/j.quascirev.2011.11.008

Villavicencio, N. A., Lindsey, E. L., Martin, F. M., Borrero, L. A., Moreno, P. I., Marshall, C. R., & Barnosky, A. D. (2016). Combination of humans, climate, and vegetation change triggered Late Quaternary megafauna extinction in the Última Esperanza region, southern Patagonia, Chile. *Ecography*, *39*(2), 125–140. https://doi.org/10.1111/ecog.01606

Villavicencio, N. A. (2016). *Late Quaternary Megafaunal Extinctions in South America: Chronology, environmental changes and human impacts at regional scales.* (PhD thesis). University of California, Berkeley.

Villela, R. J. (2017). The South Atlantic Convergence Zone: a critical view and overview. *Revista do Instituto Geológico*, *38*(2). https://doi.org/10.5935/0100-929X.20170006

Viovy, N. (2018). CRUNCEP Version 7 - Atmospheric Forcing Data for the Community Land Model. Research Data Archive at the National Center for Atmospheric Research, Computational and Information Systems Laboratory. http://rda.ucar.edu/datasets/ds314.3/

Vizcaíno, S. F., Bargo, M. S., & Cassini, G. H. (2006). Dental occlusal surface area in relation to body mass, food habits and other biological features in fossil xenarthrans, 16.

von Humboldt, A., & Bonpland, A. (1805). *Essai sur la géographie des plantes : accompagné d'un tableau physique des régions équinoxiales*. Paris, France: Levrault, Schoell et Compagnie. https://gallica.bnf.fr/ark:/12148/bpt6k977938. Accessed 16 August 2019

Walter, H. (1973). *Vegetation of the earth in relation to climate and the eco-physiological conditions.* New York, USA: Springer-Verlag.

Walter, H., & Straka, H. (1970). *Arealkunde: Floristisch-Historische Geobotanik* (2nd ed., Vol. 3). Stuttgart, Germany: Eugen Ulmer.

Wang, X., Auler, A. S., Edwards, R. L., Cheng, H., Cristalli, P. S., Smart, P. L., et al. (2004). Wet periods in northeastern Brazil over the past 210 kyr linked to distant climate anomalies. *Nature*, *432*(7018), 740–743. https://doi.org/10.1038/nature03067

Wang, X., Auler, A. S., Edwards, R. L., Cheng, H., Ito, E., & Solheid, M. (2006). Interhemispheric anti-phasing of rainfall during the last glacial period. *Quaternary Science Reviews*, *25*(23), 3391–3403. https://doi.org/10.1016/j.quascirev.2006.02.009

Wang, X., Auler, A. S., Edwards, R. L., Cheng, H., Ito, E., Wang, Y., et al. (2007). Millennial-scale precipitation changes in southern Brazil over the past 90,000 years. *Geophysical Research Letters*, *34*(23). https://doi.org/10.1029/2007GL031149

Wang, X., Edwards, R. L., Auler, A. S., Cheng, H., Kong, X., Wang, Y., et al. (2017). Hydroclimate changes across the Amazon lowlands over the past 45,000 years. *Nature*, *541*(7636), 204–207. https://doi.org/10.1038/nature20787

Warming, E., Balfour, I. B., Groom, P., & Vahl, M. (1909). *Oecology of plants; an introduction to the study of plant-communities*. Oxford, UK: Clarendon Press. http://archive.org/details/oecologyofplants00warmiala. Accessed 15 July 2019

Waters, M. R., & Stafford, T. W. (2007). Redefining the Age of Clovis: Implications for the Peopling of the Americas. *Science*, *315*(5815), 1122–1126. https://doi.org/10.1126/science.1137166

Wei, T., & Simko, V. (2017). *R package "corrplot": Visualization of a Correlation Matrix. R package version 0.84*. R.

Werneck, F. P., Costa, G. C., Colli, G. R., Prado, D. E., & Sites Jr, J. W. (2011). Revisiting the historical distribution of Seasonally Dry Tropical Forests: new insights based on palaeodistribution modelling and palynological evidencegeb: Palaeodistributions of Seasonally Dry Tropical Forests. *Global Ecology and Biogeography*, *20*(2), 272–288. https://doi.org/10.1111/j.1466-8238.2010.00596.x

Werner, C., Schmid, M., Ehlers, T. A., Fuentes-Espoz, J. P., Steinkamp, J., Forrest, M., et al. (2018). Effect of changing vegetation and precipitation on denudation – Part 1: Predicted vegetation composition and cover over the last 21 thousand years along the Coastal Cordillera of Chile. *Earth Surface Dynamics*, *6*(4), 829–858. https://doi.org/10.5194/esurf-6-829-2018

West, A., Bunch, T., Lecompte, M. A., Adedeji, V., Moore, C. R., & Wolbach, W. S. (2020). Evidence from Pilauco, Chile Suggests a Catastrophic Cosmic Impact Occurred Near the Site ~ 12,800 Years Ago. In *Pilauco: A Late Pleistocene Archaeo-paleontological Site* (pp. 249–270). Springer.

Whitney, B. S., & Mayle, F. E. (2012). Pediastrum species as potential indicators of lake-level change in tropical South America. *Journal of Paleolimnology*, *47*(4), 601–615. https://doi.org/10.1007/s10933-012-9583-8

Whitney, B. S., Mayle, F. E., Punyasena, S. W., Fitzpatrick, K. A., Burn, M. J., Guillen, R., et al. (2011). A 45kyr palaeoclimate record from the lowland interior of tropical South America. *Palaeogeography, Palaeoclimatology, Palaeoecology*, *307*(1–4), 177–192. https://doi.org/10.1016/j.palaeo.2011.05.012

Whittaker, R. H. (1957). Recent evolution of ecological concepts in relation to the eastern forests of North America. *American Journal of Botany*, *44*(2), 197–206. http://dx.doi.org/10.1002/j.1537-2197.1957.tb08230.x

Whittaker, R. H. (1970). *Communities and ecosystems.* New York, USA: MacMillan.

Williams, J. W., Webb III, T., Richard, P. H., & Newby, P. (2000). Late Quaternary biomes of Canada and the eastern United States. *Journal of Biogeography*, *27*(3), 585–607. https://doi.org/10.1046/j.1365-2699.2000.00428.x

Wing, S. L., & Harrington, G. J. (2001). Floral response to rapid warming in the earliest Eocene and implications for concurrent faunal change. *Paleobiology*, *27*(3), 539–563. https://doi.org/10.1666/0094-8373(2001)027<0539:FRTRWI>2.0.CO;2

Wolbach, W. S., Ballard, J. P., Mayewski, P. A., Parnell, A. C., Cahill, N., Adedeji, V., et al. (2018). Extraordinary Biomass-Burning Episode and Impact Winter Triggered by the Younger Dryas Cosmic Impact ~12,800 Years Ago. 2. Lake, Marine, and Terrestrial Sediments. *The Journal of Geology*, *126*(2), 185–205. https://doi.org/10.1086/695704

Woodward, F. I., Lomas, M. R., & Kelly, C. K. (2004). Global climate and the distribution of plant biomes. *Philosophical Transactions of the Royal Society of London. Series B: Biological Sciences*, *359*(1450), 1465–1476. https://doi.org/10.1098/rstb.2004.1525

Wroe, S., & Field, J. (2006). A review of the evidence for a human role in the extinction of Australian megafauna and an alternative interpretation. *Quaternary Science Reviews*, *25*(21), 2692–2703. https://doi.org/10.1016/j.quascirev.2006.03.005

Yeager, S. G., Shields, C. A., Large, W. G., & Hack, J. J. (2006). The Low-Resolution CCSM3. *Journal of Climate*, *19*(11), 2545–2566. https://doi.org/10.1175/JCLI3744.1

Yi, C., Ricciuto, D., Li, R., Wolbeck, J., Xu, X., Nilsson, M., et al. (2010). Climate control of terrestrial carbon exchange across biomes and continents. *Environmental Research Letters*, *5*(3), 034007. https://doi.org/10.1088/1748-9326/5/3/034007

Yu, G., Chen, X., Ni, J., Cheddadi, R., Guiot, J., Han, H., et al. (2000). Palaeovegetation of China: a pollen data-based synthesis for the mid-Holocene and last glacial maximum. *Journal of Biogeography*, *27*(3), 635–664. https://doi.org/10.1046/j.1365-2699.2000.00431.x

Yu, G., Prentice, I. C., Harrison, S. P., & Sun, X. (1998). Pollen-based biome reconstructions for China at 0 and 6000 years. *Journal of Biogeography*, *25*(6), 1055–1069. https://doi.org/10.1046/j.1365-2699.1998.00237.x

Yue, C., Ciais, P., Luyssaert, S., Li, W., McGrath, M. J., Chang, J., & Peng, S. (2018). Representing anthropogenic gross land use change, wood harvest, and forest age dynamics in a global vegetation model ORCHIDEE-MICT v8.4.2. *Geoscientific Model Development*, *11*(1), 409–428. https://doi.org/10.5194/gmd-11-409-2018

Zheng, M., Zhou, Z., Luo, Y., Zhao, P., & Mo, J. (2019). Global pattern and controls of biological nitrogen fixation under nutrient enrichment: A meta-analysis. *Global Change Biology*, *25*(9), 3018–3030. https://doi.org/10.1111/gcb.14705

Zhu, D., Ciais, P., Chang, J., Krinner, G., Peng, S., Viovy, N., et al. (2018). The large mean body size of mammalian herbivores explains the productivity paradox during the last glacial maximum. *Nature ecology & evolution*, *2*(4), 640–649. https://doi.org/10.1038/s41559-018-0481-y

Zimov, S. A., Chuprynin, V. I., Oreshko, A. P., Chapin, F. S., Reynolds, J. F., & Chapin, M. C. (1995). Steppe-Tundra Transition: A Herbivore-Driven Biome Shift at the End of the Pleistocene. *The American Naturalist*, *146*(5), 765–794. https://doi.org/10.1086/285824

Zimov, S. A. (2005). Pleistocene Park: Return of the Mammoth's Ecosystem. *Science*, *308*(5723), 796–798. https://doi.org/10.1126/science.1113442

Zizka, A., Carvalho-Sobrinho, J. G., Pennington, R. T., Queiroz, L. P., Alcantara, S., Baum, D. A., et al. (2020). Transitions between biomes are common and directional in Bombacoideae (Malvaceae). *Journal of Biogeography*, *47*(6), 1310–1321. https://doi.org/10.1111/jbi.13815

Zomer, R. J., Xu, J., & Trabucco, A. (2022). Version 3 of the Global Aridity Index and Potential Evapotranspiration Database. *Scientific Data*, *9*(1), 409. https://doi.org/10.1038/s41597-022-01493-1

LIST OF FIGURES

LIST OF TABLES

APPENDICES

To

Post-Last Glacial Maximum vegetation and ecosystem responses to climate change and human expansion in the Neotropical realm: land cover changes and megafauna extinctions

By

Antoine Champreux
Master's degree

Thesis
Submitted to Flinders University
for the degree of

Doctor of Philosophy

College of Science and Engineering
24th of February 2024

List of Appendices:

Appendix S2. Chapter 2 – How to map biomes: quantitative comparison and review of biome-mapping methods

Appendix S4. Chapter 4 – Response of Neotropical tree cover to variation in post-Last Glacial Maximum climate and atmospheric CO_2

Appendix S6. Chapter 6 – Climate-induced vegetation changes alone do not explain Late Pleistocene megafauna extinctions in the Southern Cone

APPENDIX S2

Chapter 2 – How to map biomes: quantitative comparison and review of biome-mapping methods

The following Supporting Information is available for this chapter:

Appendix S2.1.

Table S2.1.1. List of biomes for the four biome classifications studied. *Ranks do not indicate any relationship. In Higgins et al. (2016, 2017), the biome names are derived from three letters (1) tall vs. short, (2) low, medium, and high vegetation productivity index, and (3) cold, dry, both cold and dry, non-seasonal for the growth limitation index.*

Leemans (1990a,b)	Higgins et al. (2016, 2017)	Friedl et al. (2010)	Olson et al. (2001)
polar desert	SLC	evergreen needleleaf forests	tropical & subtropical moist broadleaf forests
subpolar dry tundra	SMC	evergreen broadleaf forests	tropical & subtropical dry broadleaf forests
subpolar moist tundra	SHC	deciduous needleleaf forests	tropical & subtropical coniferous forests
subpolar wet tundra	TMC	deciduous broadleaf forests	temperate broadleaf & mixed forests
subpolar rain tundra	THC	mixed forests	temperate conifer forests
boreal desert	SLD	closed shrublands	boreal forests/taiga
boreal dry scrub	SMD	open shrublands	tropical & subtropical grasslands, savannas & shrublands
boreal moist forest	SHD	woody savannas	temperate grasslands, savannas & shrublands
boreal wet forest	TMD	savannas	flooded grasslands & savannas
boreal rain forest	THD	grasslands	montane grasslands & shrublands
cool temperate desert	SLB	permanent wetlands	tundra
cool temperate desert scrub	SMB	croplands	Mediterranean forests, woodlands & scrub
cool temperate steppe	SHB	urban and built-up	deserts & xeric shrublands
cool temperate moist forest	TLB	cropland/natural vegetation mosaic	mangroves
cool temperate wet forest	TMB	permanent snow and ice	
cool temperate rain forest	SLN	barren or sparsely vegetated	
warm temperate desert	SMN	unclassified	
warm temperate desert scrub	SHN		
warm temperate thorn scrub	TLN		
warm temperate dry forest	TMN		
warm temperate moist forest	THN		
warm temperate wet forest	TLC		
warm temperate rain forest	TLD		
subtropical desert	THB		
subtropical desert scrub			
subtropical thorn woodland			
subtropical dry forest			
subtropical moist forest			
subtropical wet forest			
subtropical rain forest			
tropical desert			
tropical desert scrub			
tropical thorn woodland			
tropical very dry forest			
tropical dry forest			
tropical moist forest			
tropical wet forest			
tropical rain forest			

Table S2.1.2. Summary of the main sources of uncertainty associated with each of the three families of biome-mapping methods described here. *I associated each source of uncertainty with the corresponding uncertainty concept using the terminology of Dietze (2017), who stated that uncertainty in ecological prediction can be partitioned into four main concepts (Dietze 2017, Table 2.1 therein): (1) initial condition uncertainty (endogenous stability), (2) driver uncertainty (exogenous stability), (3) parameter uncertainty, and (4) parameter variability and process error. The initial condition uncertainty does not apply to biome-mapping methods because they assume that ecosystems are in a state of equilibrium, taking into account the inherent instability of biomes.*

biome map family	common practice (source of uncertainty)	prevalent uncertainty concept
compilation	extrapolate from punctual observations	driver uncertainty
	compile disparate regional maps by equating biomes	process error (model structure)
	use observations made at different times	driver uncertainty
functional	discrete classification thresholds	parameter variability and sensitivity
	average predictions over large scales	parameter variability
	correlate remote sensing with groundtruthing	parameter variability and uncertainty
	only remote sensing as a driver	process error due to unconsidered covariates
simulated	plant functional types with many parameters	parameter uncertainty, sensitivity, and variability
	extrapolation (fore-/hindcasting)	driver sensitivity and uncertainty
	only climate as a driver	process error due to unconsidered covariates
	average predictions over large scales	parameter variability
	use parsimonious set of mechanisms	process error due to unconsidered mechanisms

Table S2.1.3. Biome merging settings for the six inter-classification comparisons. *For each comparison, I adjusted the number of biomes of the classification with the highest complexity (Map A in Fig. 2.2a) to the classification with lower complexity (Map B in Fig. 2.2a). Starting from highest overlap, I associated each category from A to its highest overlapped category from B. When two categories from A were associated with the same category from B, I merged them, and repeated the operation until the two classifications had an equal number of categories (Fig. 2.2b, left panel). Merged Biomes overlap their merging reference from 100% to the overlap threshold. In Higgins et al. (2016, 2017), the biome names are derived from three letters (1) tall vs. short, (2) low, medium, and high vegetation productivity index, and (3) cold, dry, both cold and dry, non-seasonal for the growth limitation index.*

highest complexity	**lowest complexity**	**overlap threshold**	**biomes merged**	**merging reference**
Friedl et al. (2010)	Olson et al. (2001)	74%	evergreen needleleaf forests	boreal forests/taiga
			deciduous needleleaf forests	
			permanent wetlands	
			permanent snow and ice	tundra
			unclassified	
Higgins et al. (2016, 2017)	Olson et al. (2001)	39%	SLD	temperate broadleaf & mixed forests
			SHN	
			SMC	boreal forests/taiga
			TMC	
			THC	
			SLN	
			SHD	tropical & subtropical grasslands, savannas & shrublands
			TMD	
			SMB	
			SHC	temperate grasslands, savannas & shrublands
			TLB	
			TMB	
			SLC	tundra
			SHB	
			SMD	deserts & xeric shrublands
			TLN	
Leemans (1990a,b)	Olson et al. (2001)	49%	warm temperate wet forest	tropical & subtropical moist broadleaf forests
			warm temperate rain forest	
			subtropical moist forest	
			subtropical wet forest	
			subtropical rain forest	
			tropical moist forest	
			tropical wet forest	
			cool temperate moist forest	temperate broadleaf & mixed forests
			cool temperate wet forest	
			cool temperate rain forest	
			subpolar rain tundra	boreal forests/taiga
			boreal desert	
			boreal dry scrub	
			boreal moist forest	
			boreal wet forest	
			subtropical dry forest	tropical & subtropical grasslands, savannas & shrublands
			tropical thorn woodland	
			tropical very dry forest	
			tropical dry forest	
			polar desert	tundra
			subpolar moist tundra	
			cool temperate desert	deserts & xeric shrublands
			cool temperate desert scrub	
			warm temperate desert	
			warm temperate desert scrub	
			subtropical desert	
			subtropical desert scrub	
			tropical desert	
			tropical desert scrub	

highest complexity	lowest complexity	overlap threshold	biomes merged	merging reference
Leemans (1990a,b)	Friedl et al. (2010)	41%	warm temperate wet forest	evergreen broadleaf forests
			warm temperate rain forest	
			subtropical moist forest	
			subtropical wet forest	
			subtropical rain forest	
			tropical moist forest	
			tropical wet forest	
			subpolar dry tundra	open shrublands
			subpolar moist tundra	
			subpolar wet tundra	
			subpolar rain tundra	
			boreal rain forest	
			warm temperate desert scrub	
			warm temperate thorn scrub	
			subtropical desert scrub	
			subtropical thorn woodland	
			tropical thorn woodland	
			tropical very dry forest	
			cool temperate moist forest	permanent wetlands
			warm temperate dry forest	
			cool temperate desert	barren or sparsely vegetated
			warm temperate desert	
			subtropical desert	
			tropical desert	
			tropical desert scrub	
Higgins et al. (2016, 2017)	Friedl et al. (2010)	37%	SLC	open shrublands
			SMD	
			THD	
			SHB	
			SLN	
			TLN	
			TLC	
			TLB	permanent wetlands
			TMB	
			TMN	
Leemans (1990a,b)	Higgins et al. (2016, 2017)	52%	polar desert	SHB
			cool temperate desert	
			cool temperate desert scrub	
			subpolar dry tundra	SLN
			subpolar moist tundra	
			boreal desert	
			subtropical desert	TLN
			subtropical desert scrub	
			tropical desert	
			tropical desert scrub	
			tropical thorn woodland	
			warm temperate wet forest	THB
			warm temperate rain forest	
			subtropical wet forest	
			subtropical rain forest	
			tropical moist forest	
			tropical wet forest	

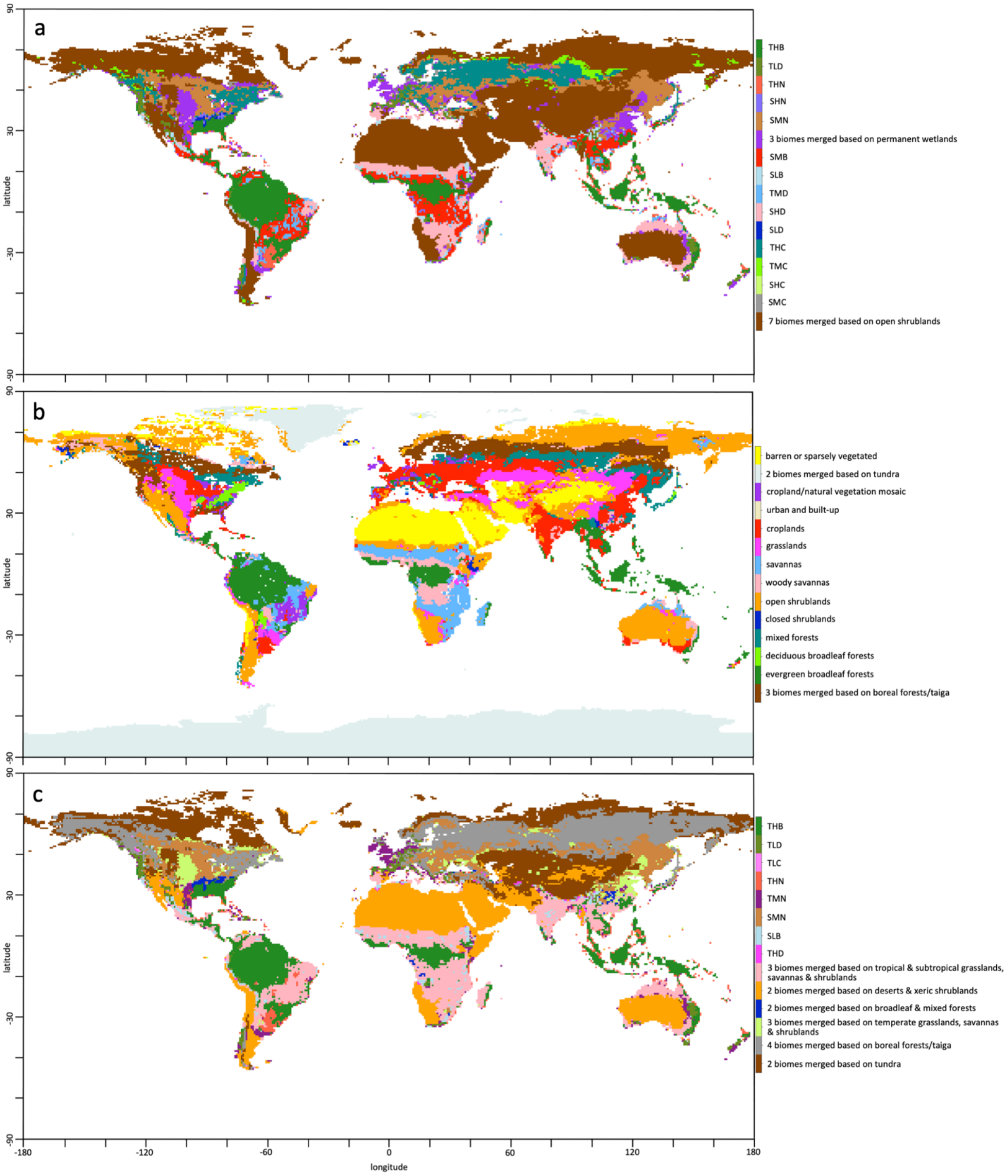

Figure S2.1.1. Global biome maps with merged categories for each of the six comparisons (part 1). *(**a**) Higgins et al. (2016, 2017) with categories merged based on Friedl et al. (2010), (**b**) Friedl et al. (2010) with categories merged based on Olson et al. (2001), (**c**) Higgins et al. (2016, 2017) with categories merged based on Olson et al. (2001). Higgins et al. (2016, 2017)'s biome names are derived from three letters (1) tall vs. short, (2) low, medium, and high vegetation productivity index, and (3) cold, dry, both cold and dry, non-seasonal for the growth limitation index.*

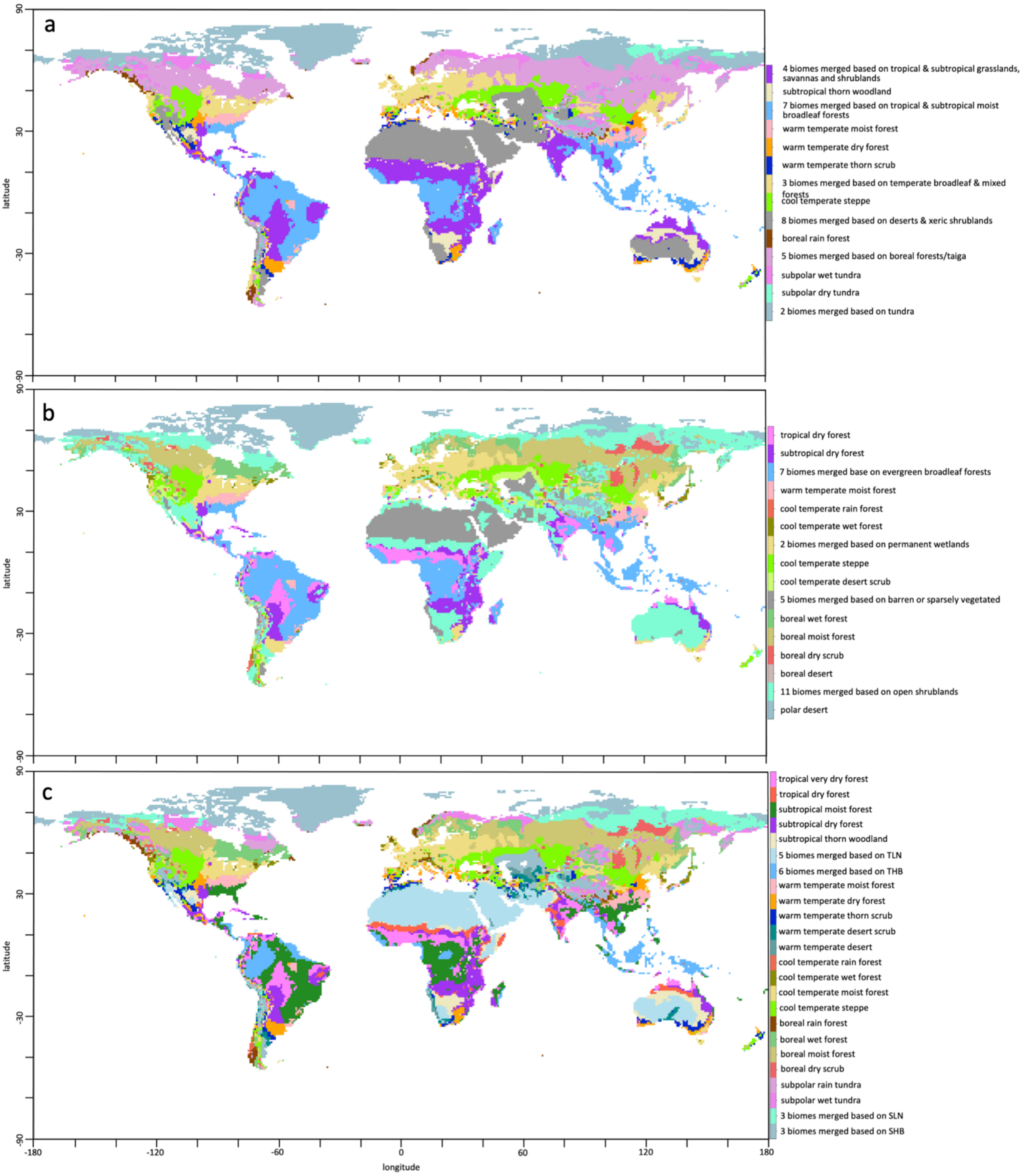

Figure S2.1.2. Global biome maps with merged categories for each of the six comparisons (part 2). *(**a**) Leemans (1990a,b) with categories merged based on Olson et al. (2001), (**b**) Leemans (1990a,b) with categories merged based on Friedl et al. (2010), (**c**) Leemans (1990a,b) with categories merged based on Higgins et al. (2016, 2017). Higgins et al. (2016, 2017)'s biome names are derived from three letters (1) tall vs. short, (2) low, medium, and high vegetation productivity index, and (3) cold, dry, both cold and dry, non-seasonal for the growth limitation index.*

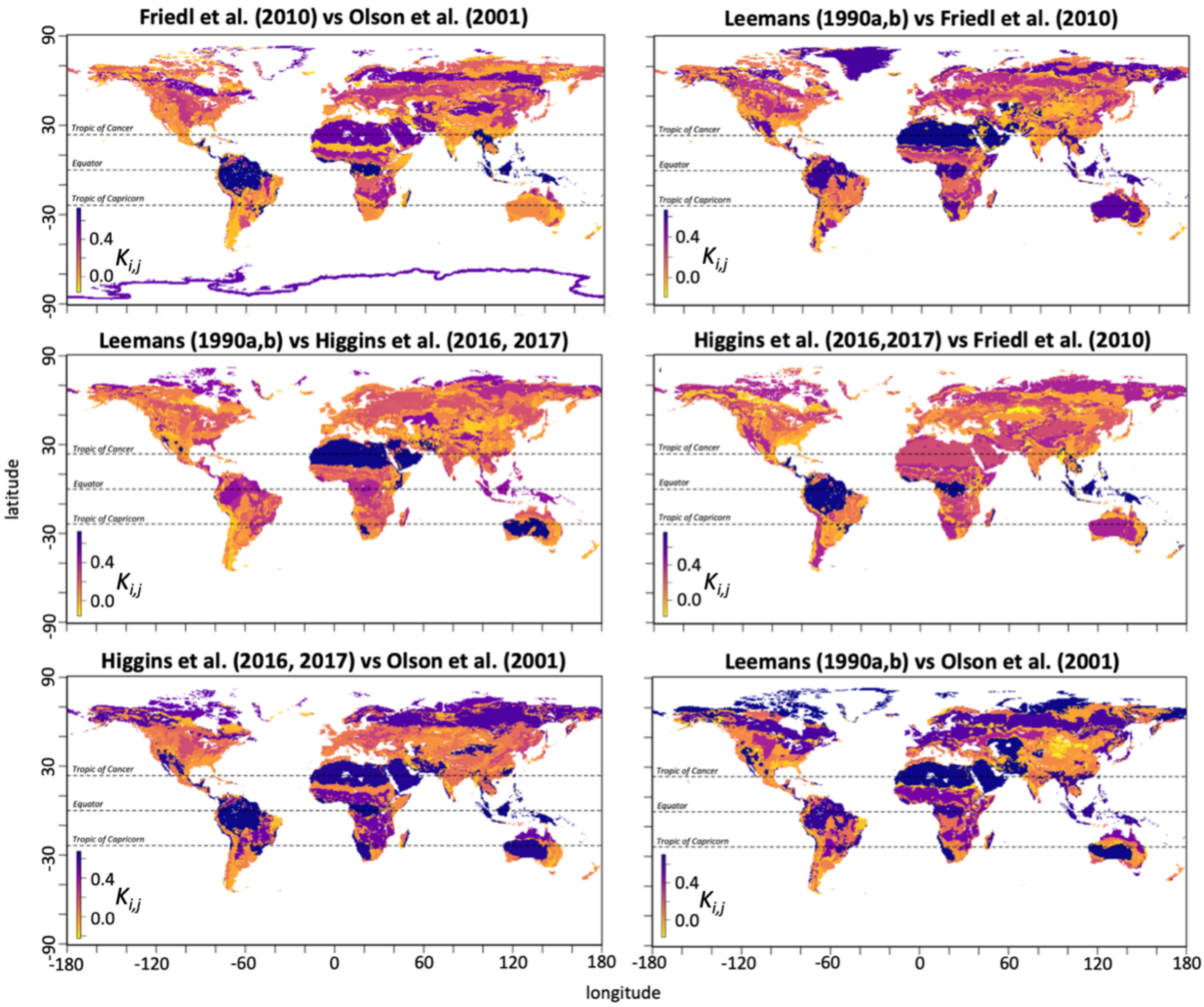

Figure S2.1.3. Distribution of the agreement (Cohen's $\kappa_{i,j}$) on a single category for the six inter-classification comparisons. *$\kappa_{i,j}$ is calculated at a 0.5° × 0.5° resolution and ranges from no agreement ($-1 < \kappa_{i,j} < 0.05$) to perfect agreement ($0.99 < \kappa_{i,j} < 1$). The method employed to calculate $\kappa_{i,j}$ is described in Figure 2.1.*

Table S2.1.4. Comparison of generalised least-squares models to explain the average agreement map. (A) comparison of generalised least-squares models with no interaction terms, (B) comparison of generalised least-squares models including interaction terms, as derived from the top-ranked model in A, and (C) relative importance of variables in the top-ranked generalised least-square model in B. *The generalised least-squares models include measures of landscape modification (HL = habitat Loss, POP = human population density, BA = yearly burnt area) and landscape heterogeneity (LAI = leaf area index, N = native plant species richness, S = mammal richness) per grid cell to describe the agreement between the two biome maps I examined. Shown for each model are the number of parameters (k), Akaike's information criterion (AIC_c), difference in Akaike's information criterion corrected for small sample sizes relative to the top-ranked model (ΔAIC_c), the relative goodness of fit (ModLL), AIC_c weight (~ model probability; $wAIC_c$), maximum log-goodness of fit (LL), the cumulative weights (CumWt), and a metric of the model's structural goodness of fit (%GoF). Shown for C are the percent of change in goodness of fit (Δ%GoF), and Nagelkerke pseudo-r square (R^2). The goodness of fit is calculated as the difference between the sum of square of the residuals of the generalised least-square model and the sum of squares of the dispersion of the data around the observed mean divided by the sum of squares of the dispersion of the data around the observed mean. In C, the relative importance of each variable is represented by Δ%GoF and R^2 of each truncated model (i.e., full model minus one of the predictive variables) relative to the full model with higher absolute values corresponding to higher importance. Based on resampled data (× 10,533 grid cells).*

S2.1.4A.

model	*k*	AIC$_c$	ΔAIC$_c$	ModLL	*w*AIC$_c$	LL	CumWt	%GoF
~HL+S+LAI	6	-577.97	0	1	0.15	295.07	0.15	93.02
~HL+LAI	5	-577.68	0.28	0.87	0.13	293.91	0.28	98.44
~HL+S+LAI+POP	7	-577.41	0.56	0.76	0.11	295.82	0.4	94.45
~HL+LAI+POP	6	-576.98	0.99	0.61	0.09	294.58	0.49	99.11
~HL+LAI+N	6	-576.65	1.32	0.52	0.08	294.42	0.57	99.41
~HL+S+LAI+N	7	-576.26	1.71	0.43	0.06	295.25	0.64	95.24
~HL+S+LAI+BA	7	-576.04	1.93	0.38	0.06	295.14	0.69	93.5
~HL+LAI+POP+N	7	-575.77	2.2	0.33	0.05	295	0.74	99.73
~HL+LAI+BA	6	-575.64	2.33	0.31	0.05	293.91	0.79	98.53
~HL+S+LAI+POP+N	8	-575.57	2.4	0.3	0.05	295.94	0.84	96.02
~HL+S+LAI+POP+BA	8	-575.42	2.54	0.28	0.04	295.87	0.88	94.77
~HL+LAI+POP+BA	7	-574.92	3.05	0.22	0.03	294.58	0.91	99.13
~HL+LAI+BA+N	7	-574.59	3.38	0.18	0.03	294.42	0.94	99.42
~HL+S+LAI+BA+N	8	-574.27	3.7	0.16	0.02	295.29	0.97	95.4
~HL+LAI+POP+BA+N	8	-573.7	4.27	0.12	0.02	295.01	0.98	99.71
~HL+S+LAI+POP+BA+N	9	-573.54	4.43	0.11	0.02	295.97	1	96.13
~S+LAI+POP	6	-551.95	26.01	0	0	282.07	1	89.37
~S+LAI+POP+N	7	-551.89	26.08	0	0	283.07	1	95.97
~S+LAI+POP+BA+N	8	-550.03	27.94	0	0	283.17	1	95.7
~LAI+POP+N	6	-549.99	27.98	0	0	281.08	1	99.8
~S+LAI+POP+BA	7	-549.99	27.98	0	0	282.11	1	88.85
~LAI+POP+BA+N	7	-548.67	29.3	0	0	281.46	1	99.98
~LAI+POP	5	-547.42	30.54	0	0	278.78	1	99.62
~S+LAI+N	6	-547.35	30.61	0	0	279.77	1	93.86
~S+LAI	5	-546.2	31.77	0	0	278.17	1	82.4
~LAI+POP+BA	6	-545.98	31.99	0	0	279.08	1	99.13
~HL+N	5	-545.83	32.13	0	0	277.98	1	91.65
~LAI+N	5	-545.77	32.2	0	0	277.95	1	100
~S+LAI+BA+N	7	-545.48	32.49	0	0	279.86	1	93.52
~HL+POP+N	6	-544.87	33.1	0	0	278.53	1	92.97
~HL+S+N	6	-544.75	33.22	0	0	278.46	1	96.76
~LAI+BA+N	6	-544.37	33.59	0	0	278.28	1	99.87
~S+LAI+BA	6	-544.21	33.76	0	0	278.19	1	81.81
~HL+BA+N	6	-544.11	33.85	0	0	278.15	1	92.86
~HL+S+POP+N	7	-543.65	34.31	0	0	278.95	1	97.28
~HL+POP+BA+N	7	-543.08	34.89	0	0	278.66	1	93.91
~HL+S+BA+N	7	-542.82	35.15	0	0	278.53	1	96.89
~HL+S+POP+BA+N	8	-541.68	36.28	0	0	279	1	97.37
~LAI	4	-541.5	36.47	0	0	274.79	1	97.92
~LAI+BA	5	-539.97	38	0	0	275.05	1	96.93
~HL+S	5	-539.06	38.91	0	0	274.59	1	99.48
~HL+S+POP	6	-537.37	40.6	0	0	274.78	1	99.22
~HL+S+BA	6	-537.02	40.94	0	0	274.6	1	99.52
~HL+S+POP+BA	7	-535.34	42.62	0	0	274.79	1	99.28
~HL	4	-529.42	48.55	0	0	268.75	1	96.48
~HL+POP	5	-527.63	50.34	0	0	268.88	1	96.96
~HL+BA	5	-527.47	50.5	0	0	268.8	1	96.92
~HL+POP+BA	6	-525.66	52.31	0	0	268.92	1	97.3
~POP+N	5	-495.66	82.3	0	0	252.9	1	93.67
~S+POP+N	6	-494.42	83.55	0	0	253.3	1	98.23
~POP+BA+N	6	-493.84	84.13	0	0	253.01	1	92.64
~S+POP+BA+N	7	-492.82	85.15	0	0	253.53	1	98.02
~S+POP	5	-490.25	87.72	0	0	250.19	1	98.43
~S+POP+BA	6	-489.31	88.66	0	0	250.75	1	99
~N	4	-488.76	89.21	0	0	248.42	1	89.2
~S+N	5	-487.85	90.12	0	0	248.99	1	96.66
~BA+N	5	-486.88	91.09	0	0	248.5	1	88
~S+BA+N	6	-486.21	91.76	0	0	249.19	1	96.35
~S	4	-485.52	92.45	0	0	246.8	1	99.79
~S+BA	5	-484.39	93.58	0	0	247.26	1	99.96
~POP	4	-483.19	94.78	0	0	245.64	1	97.86
~POP+BA	5	-481.52	96.45	0	0	245.83	1	97.04
~1	3	-479.11	98.86	0	0	242.58	1	95.25
~BA	4	-477.36	100.61	0	0	242.72	1	94.15

S2.1.4B.

model	*k*	AIC_c	ΔAIC_c	ModLL	$wAIC_c$	LL	CumWt	%GoF
~HL+S+LAI+(HL×LAI)+(S×LAI)+(HL×S)	9	-664.43	0	1	0.99	341.41	0.99	96.11
~HL+S+LAI+(HL×LAI)+(S×LAI)	8	-654.66	9.77	0.01	0.01	335.49	1	97.22
~HL+S+LAI+(S×LAI)	7	-650.64	13.79	0	0	332.44	1	94.79
~HL+S+LAI+(HL×S) + (S×LAI)	8	-650.06	14.37	0	0	333.19	1	93.5
~HL+S+LAI+(HL×LAI)	7	-603.23	61.2	0	0	308.74	1	98.45
~HL+S+LAI+(HL×LAI)+(HL×S)	8	-601.19	63.24	0	0	308.75	1	98.42
~ HL+S+LAI+(HL×S)	7	-586.99	77.44	0	0	300.62	1	96.41
~HL+S+LAI	6	-577.97	86.46	0	0	295.07	1	93.02

S2.1.4C.

variable removed	model	*k*	AIC_c	ΔAIC_c	ModLL	$wAIC_c$	LL	CumWt	%GoF	Δ%GoF	R^2
S×LAI	~HL+S+LAI+(HL×LAI)+(HL×S)	8	-601.19	63.24	0	0	308.75	1	98.42	-2.32	0.05
HL×LAI	~HL+S+LAI+(S×LAI)+(HL×S)	8	-650.06	14.37	0	0	333.19	1	93.5	2.61	0.01
HL×S	~HL+S+LAI+(HL×LAI)+(S×LAI)	8	-654.66	9.77	0.01	0	335.49	1	97.22	-1.12	0.01
HL	~S+LAI+(HL×LAI)+(S×LAI)+(HL×S)	9	-664.43	0	1	0.25	341.41	0.75	96.11	0	0
S	~HL+LAI+(HL×LAI)+(S×LAI)+(HL×S)	9	-664.43	0	1	0.25	341.41	1	96.11	0	0
none	~HL+S+LAI+(HL×LAI)+(S×LAI)+(HL×S)	9	-664.43	0	1	0.25	341.41	0.25	96.11	0	0
LAI	~HL+S+(HL×LAI)+(S×LAI)+(HL×S)	9	-664.43	0	1	0.25	341.41	0.5	96.11	0	0

Table S2.1.5. Map comparisons between merged Higgins et al. (2016, 2017) and Friedl et al. (2010). (A) comparison of generalised least-squares models with no interaction terms, (B) comparison of generalised least-squares models including interaction terms, as derived from the top-ranked model in A, and (C) relative importance of variables in the top-ranked generalised least-square model in B. *The generalised least-squares models include measures of landscape modification (HL = habitat Loss, POP = human population density, BA = yearly burnt area) and landscape heterogeneity (LAI = leaf area index, N = native plant species richness, S = mammal richness) per grid cell to describe the agreement between the two biome maps I examined. Shown for each model are the number of parameters (k), Akaike's information criterion (*AIC_c*), difference in Akaike's information criterion corrected for small sample sizes relative to the top-ranked model (*ΔAIC_c*), the relative goodness of fit (ModLL),* AIC_c *weight (~ model probability;* $wAIC_c$*), maximum log-goodness of fit (LL), the cumulative weights (CumWt), and a metric of the model's structural goodness of fit (%GoF). Shown for C are the percent of change in goodness of fit (Δ%GoF), and Nagelkerke pseudo-r square (*R^2*). The goodness of fit is calculated as the difference between the sum of square of the residuals of the generalised least-square model and the sum of squares of the dispersion of the data around the observed mean divided by the sum of squares of the dispersion of the data around the observed mean. In C, the relative importance of each variable is represented by Δ%GoF and* R^2 *of each truncated model (i.e., full model minus one of the predictive variables) relative to the full model with higher absolute values corresponding to higher importance. Based on resampled data (× 10,533 grid cells).*

S2.1.5A.

model	*k*	AIC_c	ΔAIC_c	ModLL	$wAIC_c$	LL	CumWt	%GoF
~HL+LAI+POP	6	-143.91	0	1	0.23	78.04	0.23	80.62
~HL+LAI	5	-142.73	1.18	0.55	0.13	76.43	0.36	83.43
~HL+LAI+POP+BA	7	-142.46	1.45	0.48	0.11	78.35	0.47	81.76
~HL+LAI+POP+N	7	-141.95	1.96	0.38	0.09	78.09	0.56	79.4
~HL+S+LAI+POP	7	-141.88	2.03	0.36	0.08	78.06	0.64	81.68
~HL+LAI+BA	6	-141.1	2.81	0.25	0.06	76.64	0.7	84.41
~HL+LAI+N	6	-140.9	3.01	0.22	0.05	76.54	0.75	81.67
~HL+S+LAI	6	-140.69	3.22	0.2	0.05	76.43	0.8	83.94
~HL+LAI+POP+BA+N	8	-140.54	3.37	0.19	0.04	78.43	0.84	80.33
~HL+S+LAI+POP+BA	8	-140.39	3.52	0.17	0.04	78.35	0.88	82
~HL+S+LAI+POP+N	8	-139.89	4.02	0.13	0.03	78.1	0.91	80.05
~HL+LAI+BA+N	7	-139.34	4.57	0.1	0.02	76.79	0.94	82.52
~HL+S+LAI+BA	7	-139.04	4.87	0.09	0.02	76.64	0.96	84.26
~HL+S+LAI+N	7	-138.85	5.06	0.08	0.02	76.54	0.98	81.24
~HL+S+LAI+POP+BA+N	9	-138.48	5.43	0.07	0.02	78.43	0.99	79.6
~HL+S+LAI+BA+N	8	-137.31	6.6	0.04	0.01	76.81	1	80.89
~LAI+POP+N	6	-125.74	18.17	0	0	68.96	1	70.43
~LAI+POP+BA+N	7	-125.64	18.27	0	0	69.94	1	73.07
~LAI+POP	5	-125.33	18.58	0	0	67.73	1	76.57
~HL+S+POP+N	7	-125.21	18.7	0	0	69.73	1	81.73
~LAI+POP+BA	6	-125.01	18.9	0	0	68.6	1	79.1
~HL+POP+N	6	-124.91	19	0	0	68.55	1	91.53
~HL+S+N	6	-124.59	19.32	0	0	68.39	1	82.67
~S+LAI+POP	6	-124.56	19.35	0	0	68.37	1	84.12
~S+LAI+POP+N	7	-124.08	19.83	0	0	69.16	1	76.58
~HL+N	5	-123.87	20.03	0	0	67	1	93
~S+LAI+POP+BA	7	-123.75	20.16	0	0	68.99	1	84.69
~S+LAI+POP+BA+N	8	-123.68	20.23	0	0	69.99	1	76.13
~HL+S+POP+BA+N	8	-123.67	20.24	0	0	69.99	1	81.24
~HL+POP+BA+N	7	-122.96	20.95	0	0	68.6	1	91.84
~HL+S+BA+N	7	-122.95	20.96	0	0	68.59	1	82.28
~HL+S	5	-122.32	21.59	0	0	66.23	1	65.13
~HL+S+POP	6	-121.98	21.93	0	0	67.08	1	62.15
~HL+BA+N	6	-121.87	22.04	0	0	67.02	1	93.2
~HL+S+BA	6	-121.34	22.57	0	0	66.76	1	66.02
~HL+S+POP+BA	7	-121.2	22.71	0	0	67.72	1	62.95
~LAI+N	5	-119.44	24.47	0	0	64.78	1	73.95
~LAI+BA+N	6	-119.11	24.8	0	0	65.65	1	76.44
~S+LAI+N	6	-117.63	26.28	0	0	64.91	1	78.68
~LAI	4	-117.27	26.64	0	0	62.68	1	81.88
~S+LAI+BA+N	7	-117.09	26.82	0	0	65.67	1	78.36
~LAI+BA	5	-116.65	27.26	0	0	63.39	1	84.12
~S+LAI	5	-116.58	27.33	0	0	63.35	1	88.83
~S+LAI+BA	6	-115.5	28.41	0	0	63.84	1	89.39
~HL	4	-108.96	34.95	0	0	58.52	1	85
~HL+POP	5	-108.29	35.62	0	0	59.21	1	83.09
~HL+BA	5	-107.12	36.79	0	0	58.62	1	85.71
~HL+POP+BA	6	-106.52	37.39	0	0	59.35	1	83.9
~S+POP+N	6	-92.59	51.32	0	0	52.39	1	75.91
~S+POP+BA+N	7	-92.53	51.38	0	0	53.39	1	75.29
~POP+N	5	-92.36	51.55	0	0	51.25	1	88.27
~S+POP+BA	6	-91.91	52	0	0	52.04	1	59.4
~POP+BA+N	6	-91.35	52.56	0	0	51.77	1	89.66
~S+POP	5	-91.02	52.89	0	0	50.57	1	57.43
~S+BA	5	-84.81	59.1	0	0	47.47	1	66.98
~S	4	-84.4	59.51	0	0	46.24	1	65.04
~S+N	5	-84.28	59.63	0	0	47.2	1	78.04
~S+BA+N	6	-84.05	59.86	0	0	48.11	1	77.57
~N	4	-83.27	60.64	0	0	45.68	1	91.63
~BA+N	5	-82.05	61.86	0	0	46.09	1	92.79
~POP	4	-80.23	63.68	0	0	44.16	1	80.27
~POP+BA	5	-79.46	64.45	0	0	44.79	1	82.41
~1	3	-74.65	69.26	0	0	40.35	1	85.17
~BA	4	-73.65	70.26	0	0	40.87	1	86.99

S2.1.5B.

model	*k*	AIC_c	ΔAIC_c	ModLL	$wAIC_c$	LL	CumWt	%GoF
~HL+POP+LAI+(HL×LAI)	7	-169.39	0	1	0.35	91.81	0.35	63.91
~HL+POP+LAI+(HL×LAI)+(HL×POP)	8	-168.58	0.81	0.67	0.23	92.44	0.58	62.17
~HL+POP+LAI+(HL×LAI)+(POP×LAI)	8	-168.41	0.97	0.61	0.21	92.36	0.8	68.35
~HL+POP+LAI+(HL×LAI)+(POP×LAI)+(HL×POP)	9	-168.31	1.08	0.58	0.2	93.35	1	67.79
~HL+POP+LAI	6	-143.91	25.48	0	0	78.04	1	80.62
~HL+POP+LAI+(HL×POP)	7	-142.97	26.41	0	0	78.61	1	79.55
~HL+POP+LAI+(POP×LAI)	7	-142.59	26.8	0	0	78.41	1	77.18
~HL+POP+LAI+(POP×LAI)+(HL×POP)	8	-141.32	28.07	0	0	78.81	1	76.99

S2.1.5C.

variable removed	model	*k*	AIC_c	ΔAIC_c	ModLL	$wAIC_c$	LL	CumWt	%GoF	Δ%GoF	R^2
HL×LAI	~HL+POP+LAI	6	-143.91	26.26	0	0	78.04	1	80.62	-16.71	0.13
POP	~HL+LAI+(HL×LAI)	6	-170.17	0	1	0.33	91.17	0.33	65.7	-1.79	0.01
none	~HL+POP+LAI+(HL×LAI)	7	-169.39	0.78	0.68	0.22	91.81	0.55	63.91	0	0
HL	~POP+LAI+(HL×LAI)	7	-169.39	0.78	0.68	0.22	91.81	0.78	63.91	0	0
LAI	~HL+POP+(HL×LAI)	7	-169.39	0.78	0.68	0.22	91.81	1	63.91	0	0

Table S2.1.6. Map comparisons between merged Higgins et al. (2016, 2017) and Olson et al. (2001). (A) comparison of generalised least-squares models with no interaction terms, (B) comparison of generalised least-squares models including interaction terms, as derived from the top-ranked model in A, and (C) relative importance of variables in the top-ranked generalised least-square model in B. *The caption to Table S2.1.5 describes the terms used in this table.*

S2.1.6A.

model	k	AIC_c	ΔAIC_c	ModLL	$w\text{AIC}_c$	LL	CumWt	%GoF
~HL+LAI+BA	6	-30.75	0	1	0.21	21.46	0.21	89.11
~HL+LAI	5	-29.75	1	0.61	0.13	19.94	0.33	84.68
~HL+LAI+POP+BA	7	-29.17	1.58	0.45	0.09	21.7	0.43	90.48
~HL+S+LAI+BA	7	-28.89	1.85	0.4	0.08	21.56	0.51	86.7
~HL+LAI+BA+N	7	-28.8	1.95	0.38	0.08	21.52	0.59	90
~HL+LAI+POP	6	-28.36	2.39	0.3	0.06	20.27	0.65	86.81
~HL+LAI+N	6	-27.95	2.8	0.25	0.05	20.06	0.7	86.4
~HL+S+LAI	6	-27.72	3.02	0.22	0.05	19.95	0.75	83.63
~HL+S+LAI+POP+BA	8	-27.37	3.38	0.18	0.04	21.83	0.79	87.99
~HL+LAI+POP+BA+N	8	-27.17	3.58	0.17	0.03	21.74	0.82	91.1
~HL+S+LAI+BA+N	8	-26.87	3.88	0.14	0.03	21.59	0.85	87.71
~HL+LAI+POP+N	7	-26.47	4.28	0.12	0.02	20.35	0.87	88.04
~HL+S+LAI+POP	7	-26.35	4.39	0.11	0.02	20.29	0.9	85.38
~HL+S+LAI+N	7	-25.89	4.86	0.09	0.02	20.06	0.92	86.26
~HL+S+LAI+POP+BA+N	9	-25.3	5.45	0.07	0.01	21.84	0.93	88.49
~HL+BA+N	6	-25.07	5.68	0.06	0.01	18.62	0.94	84.65
~HL+S+LAI+POP+N	8	-24.42	6.33	0.04	0.01	20.36	0.95	87.22
~HL+S+BA	6	-23.84	6.91	0.03	0.01	18.01	0.96	94.3
~HL+POP+BA+N	7	-23.47	7.28	0.03	0.01	18.85	0.96	86.06
~HL+S	5	-23.44	7.31	0.03	0.01	16.78	0.97	92.45
~HL+N	5	-23.38	7.37	0.03	0.01	16.75	0.97	78.76
~HL+S+BA+N	7	-23.34	7.41	0.02	0.01	18.79	0.98	88.63
~HL+BA	5	-22.74	8.01	0.02	0	16.43	0.98	87.87
~HL+S+N	6	-22.3	8.45	0.01	0	17.24	0.98	87.32
~HL+POP+N	6	-21.96	8.79	0.01	0	17.07	0.99	80.95
~HL+S+POP+BA	7	-21.92	8.83	0.01	0	18.08	0.99	94.83
~HL+S+POP+BA+N	8	-21.65	9.1	0.01	0	18.97	0.99	89.29
~HL+S+POP	6	-21.62	9.13	0.01	0	16.9	0.99	93.28
~HL	4	-21.44	9.31	0.01	0	14.76	1	82.78
~HL+POP+BA	6	-20.83	9.92	0.01	0	16.5	1	88.66
~HL+S+POP+N	7	-20.7	10.05	0.01	0	17.47	1	88.12
~HL+POP	5	-19.65	11.09	0	0	14.89	1	84.17
~LAI+POP+N	6	8.89	39.64	0	0	1.64	1	90.37
~S+LAI+POP+N	7	10.01	40.76	0	0	2.11	1	81.7
~LAI+POP+BA+N	7	10.51	41.25	0	0	1.86	1	91.71
~S+LAI+POP	6	10.62	41.37	0	0	0.78	1	66.29
~LAI+N	5	11.02	41.77	0	0	-0.45	1	85.56
~LAI+POP	5	11.05	41.79	0	0	-0.46	1	82.04
~S+LAI+POP+BA+N	8	11.29	42.04	0	0	2.51	1	82.52
~S+LAI+POP+BA	7	11.57	42.32	0	0	1.33	1	69
~S+LAI+N	6	12.49	43.23	0	0	-0.16	1	77.34
~LAI+POP+BA	6	12.54	43.29	0	0	-0.18	1	84.34
~LAI+BA+N	6	12.55	43.3	0	0	-0.19	1	87.45
~S+LAI+BA+N	7	13.73	44.48	0	0	0.25	1	78.35
~S+LAI	5	14.69	45.43	0	0	-2.28	1	52.8
~LAI	4	14.82	45.57	0	0	-3.37	1	71.41
~S+LAI+BA	6	15.49	46.24	0	0	-1.66	1	56.61
~LAI+BA	5	16.18	46.93	0	0	-3.03	1	74.92
~S+POP	5	27.91	58.66	0	0	-8.89	1	88.39
~POP+N	5	28.14	58.89	0	0	-9.01	1	73.32
~POP	4	28.2	58.95	0	0	-10.06	1	77.66
~POP+BA+N	6	29.48	60.23	0	0	-8.65	1	76.55
~S+POP+N	6	29.53	60.28	0	0	-8.68	1	83.26
~POP+BA	5	29.6	60.35	0	0	-9.74	1	80.51
~S+POP+BA	6	29.62	60.37	0	0	-8.72	1	89.34
~S	4	30.63	61.38	0	0	-11.28	1	80.87
~1	3	30.91	61.66	0	0	-12.43	1	67.51
~S+POP+BA+N	7	31.12	61.86	0	0	-8.44	1	83.83
~N	4	31.76	62.51	0	0	-11.84	1	62.63
~BA	4	32.18	62.92	0	0	-12.05	1	71.57
~S+BA	5	32.24	62.98	0	0	-11.06	1	82.42
~S+N	5	32.63	63.38	0	0	-11.25	1	78.68
~BA+N	5	32.97	63.72	0	0	-11.42	1	67.08
~S+BA+N	6	34.18	64.93	0	0	-11	1	79.39

S2.1.6B.

model	*k*	AIC_c	ΔAIC_c	ModLL	$wAIC_c$	LL	CumWt	%GoF
~HL+BA+LAI+(HL×LAI)+(HL×BA)	8	-41.84	0	1	0.66	29.07	0.66	93.2
~HL+BA+LAI+(HL×LAI)+(BA×LAI)+(HL×BA)	9	-39.95	1.89	0.39	0.26	29.16	0.91	93.45
~HL+BA+LAI+(HL×LAI)	7	-36.53	5.3	0.07	0.05	25.38	0.96	94.37
~HL+BA+LAI+(HL×LAI)+(BA×LAI)	8	-34.59	7.25	0.03	0.02	25.45	0.97	94.19
~HL+BA+LAI+(HL×BA)	7	-34.46	7.37	0.03	0.02	24.35	0.99	86.96
~HL+BA+LAI+(BA×LAI)+(HL×BA)	8	-32.42	9.41	0.01	0.01	24.36	1	86.91
~HL+BA+LAI	6	-30.75	11.09	0	0	21.46	1	89.11
~HL+BA+LAI+(BA×LAI)	7	-29.32	12.51	0	0	21.78	1	88.89

S2.1.6C.

variable removed	model	*k*	AIC_c	ΔAIC_c	ModLL	$wAIC_c$	LL	CumWt	%GoF	Δ%GoF	R^2
HL×LAI	**~HL+BA+LAI+(HL×BA)**	7	-34.46	7.37	0.03	0.01	24.35	1	86.96	6.24	0.15
HL×BA	**~HL+BA+LAI+(HL×LAI)**	7	-36.53	5.3	0.07	0.02	25.38	0.99	94.37	-1.17	0.12
HL	**~BA+LAI+(HL×LAI)+(HL×BA)**	8	-41.84	0	1	0.24	29.07	0.24	93.2	0	0
none	**~HL+BA+LAI+(HL×LAI)+(HL×BA)**	8	-41.84	0	1	0.24	29.07	0.49	93.2	0	0
BA	**~HL+LAI+(HL×LAI)+(HL×BA)**	8	-41.84	0	1	0.24	29.07	0.73	93.2	0	0
LAI	**~HL+BA+(HL×LAI)+(HL×BA)**	8	-41.84	0	1	0.24	29.07	0.98	93.2	0	0

Table S2.1.7. Map comparisons between merged Leemans et al. (1990a,b) and Higgins et al. (2016, 2017). (A) comparison of generalised least-squares models with no interaction terms, (B) comparison of generalised least-squares models including interaction terms, as derived from the top-ranked model in A, and (C) relative importance of variables in the top-ranked generalised least-square model in B. *The caption to Table S2.1.5 describes the terms used in this table.*

S2.1.7A.

model	k	AIC_c	$\Delta\mathrm{AIC}_c$	ModLL	$w\mathrm{AIC}_c$	LL	CumWt	%GoF
~HL+LAI+POP	6	-309.51	0	1	0.1	160.84	0.1	90.88
~HL+POP	5	-308.69	0.82	0.66	0.07	159.41	0.17	91.68
~HL+LAI	5	-308.69	0.82	0.66	0.07	159.41	0.24	91.59
~HL	4	-308.34	1.17	0.56	0.06	158.21	0.3	92.29
~HL+LAI+POP+N	7	-307.92	1.59	0.45	0.05	161.08	0.35	88.84
~HL+LAI+POP+BA	7	-307.85	1.66	0.44	0.05	161.05	0.39	91.23
~HL+S+POP	6	-307.66	1.85	0.4	0.04	159.92	0.43	88.47
~HL+LAI+N	6	-307.57	1.94	0.38	0.04	159.88	0.47	88.71
~HL+S+LAI+POP	7	-307.52	1.99	0.37	0.04	160.88	0.51	91.87
~HL+POP+N	6	-307.24	2.27	0.32	0.03	159.71	0.54	92.83
~HL+S	5	-307.23	2.28	0.32	0.03	158.68	0.58	89.25
~HL+LAI+BA	6	-306.94	2.57	0.28	0.03	159.56	0.61	91.91
~HL+POP+BA	6	-306.87	2.64	0.27	0.03	159.52	0.63	91.97
~HL+S+LAI	6	-306.67	2.84	0.24	0.03	159.42	0.66	92.24
~HL+N	5	-306.52	2.99	0.22	0.02	158.33	0.68	93
~HL+BA	5	-306.47	3.04	0.22	0.02	158.3	0.71	92.54
~HL+LAI+POP+BA+N	8	-306.33	3.18	0.2	0.02	161.32	0.73	89.09
~HL+S+POP+BA	7	-306.03	3.48	0.18	0.02	160.14	0.75	88.51
~HL+LAI+BA+N	7	-305.91	3.6	0.17	0.02	160.08	0.76	88.93
~HL+S+LAI+POP+N	8	-305.86	3.65	0.16	0.02	161.08	0.78	89.21
~HL+S+LAI+POP+BA	8	-305.81	3.7	0.16	0.02	161.06	0.8	91.86
~LAI+POP	5	-305.8	3.71	0.16	0.02	157.97	0.81	87.42
~HL+S+POP+N	7	-305.62	3.89	0.14	0.01	159.93	0.83	89.27
~HL+S+LAI+N	7	-305.52	3.99	0.14	0.01	159.88	0.84	88.19
~HL+S+BA	6	-305.52	3.99	0.14	0.01	158.85	0.86	89.3
~HL+POP+BA+N	7	-305.42	4.09	0.13	0.01	159.83	0.87	93.11
~LAI+POP+N	6	-305.38	4.13	0.13	0.01	158.78	0.88	83.65
~HL+S+N	6	-305.22	4.29	0.12	0.01	158.7	0.89	88.22
~HL+S+LAI+BA	7	-304.89	4.62	0.1	0.01	159.56	0.9	92.23
~HL+BA+N	6	-304.64	4.87	0.09	0.01	158.41	0.91	93.24
~S+LAI+POP	6	-304.59	4.92	0.09	0.01	158.38	0.92	91.5
~LAI+POP+BA	6	-304.49	5.02	0.08	0.01	158.33	0.93	88.1
~HL+S+LAI+POP+BA+N	9	-304.26	5.25	0.07	0.01	161.32	0.94	88.78
~LAI+POP+BA+N	7	-304.17	5.34	0.07	0.01	159.2	0.95	84.29
~HL+S+POP+BA+N	8	-303.97	5.54	0.06	0.01	160.14	0.95	88.86
~HL+S+LAI+BA+N	8	-303.89	5.62	0.06	0.01	160.1	0.96	87.74
~S+LAI+POP+N	7	-303.59	5.92	0.05	0.01	158.91	0.96	87.09
~HL+S+BA+N	7	-303.54	5.98	0.05	0.01	158.89	0.97	87.8
~S+LAI+POP+BA	7	-303.03	6.48	0.04	0	158.64	0.97	91.5
~POP	4	-302.87	6.64	0.04	0	155.48	0.98	88.15
~LAI+N	5	-302.72	6.79	0.03	0	156.42	0.98	81.57
~S+LAI+POP+BA+N	8	-302.21	7.3	0.03	0	159.26	0.98	86.58
~S+POP	5	-301.53	7.98	0.02	0	155.83	0.98	84.97
~LAI+BA+N	6	-301.47	8.04	0.02	0	156.83	0.99	82.24
~POP+N	5	-301.31	8.2	0.02	0	155.72	0.99	89.35
~POP+BA	5	-301.3	8.21	0.02	0	155.72	0.99	88.7
~LAI	4	-301.26	8.26	0.02	0	154.67	0.99	87.12
~S+LAI+N	6	-300.84	8.67	0.01	0	156.51	0.99	84.57
~S+LAI	5	-300.22	9.29	0.01	0	155.18	0.99	91.82
~S+POP+BA	6	-300.2	9.31	0.01	0	156.19	0.99	85.1
~LAI+BA	5	-299.86	9.65	0.01	0	154.99	1	87.8
~POP+BA+N	6	-299.75	9.76	0.01	0	155.96	1	89.91
~S+POP+N	6	-299.51	10	0.01	0	155.85	1	86.11
~S+LAI+BA+N	7	-299.47	10.04	0.01	0	156.86	1	84.01
~1	3	-298.61	10.9	0	0	152.33	1	88
~S+LAI+BA	6	-298.59	10.92	0	0	155.38	1	91.83
~S+POP+BA+N	7	-298.15	11.36	0	0	156.19	1	85.59
~S	4	-297.09	12.42	0	0	152.59	1	85.11
~BA	4	-296.98	12.53	0	0	152.53	1	88.54
~N	4	-296.61	12.9	0	0	152.35	1	88.3
~S+BA	5	-295.64	13.87	0	0	152.89	1	85.25
~S+N	5	-295.19	14.32	0	0	152.66	1	82.73
~BA+N	5	-294.97	14.54	0	0	152.55	1	88.85
~S+BA+N	6	-293.83	15.68	0	0	153	1	82.15

model	***k***	**AIC_c**	**ΔAIC_c**	**ModLL**	**$wAIC_c$**	**LL**	**CumWt**	**%GoF**
~HL+POP+LAI	6	-309.51	0	1	0.32	160.84	0.32	90.88
~HL+POP+LAI+(HL×LAI)	7	-308.5	1.01	0.6	0.19	161.37	0.51	89.73
~HL+POP+LAI+(HL×POP)	7	-307.82	1.69	0.43	0.14	161.03	0.64	92.06
~HL+POP+LAI+(POP×LAI)	7	-307.48	2.03	0.36	0.11	160.86	0.76	90.4
~HL+POP+LAI+(HL×LAI)+(HL×POP)	8	-306.96	2.55	0.28	0.09	161.63	0.85	91.11
~HL+POP+LAI+(HL×LAI)+(POP×LAI)	8	-306.51	3	0.22	0.07	161.41	0.92	90.46
~HL+POP+LAI+(POP×LAI)+(HL×POP)	8	-305.89	3.62	0.16	0.05	161.1	0.97	91.23
~HL+POP+LAI+(HL×LAI)+(POP×LAI)+(HL×POP)	9	-304.89	4.62	0.1	0.03	161.64	1	91.26

S2.1.7B.

S2.1.7C.

variable removed	**model**	***k***	**AIC_c**	**ΔAIC_c**	**ModLL**	**$wAIC_c$**	**LL**	**CumWt**	**%GoF**	**Δ%GoF**	**R^2**
HL	**~LAI+POP**	5	-305.8	3.71	0.16	0.06	157.97	1	87.42	3.46	0.01
POP	**~HL+LAI**	5	-308.69	0.82	0.66	0.27	159.41	0.94	91.59	-0.72	0.01
LAI	**~HL+POP**	5	-308.69	0.82	0.66	0.27	159.41	0.67	91.68	-0.81	0.01
none	**~HL+LAI+POP**	6	-309.51	0	1	0.4	160.84	0.4	90.88	0	0

Table S2.1.8. Map comparisons between merged Leemans et al. (1990a,b) and Friedl et al. (2010). (A) comparison of generalised least-squares models with no interaction terms, (B) comparison of generalised least-squares models including interaction terms, as derived from the top-ranked model in A, and (C) relative importance of variables in the top-ranked generalised least-square model in B. *The caption to Table S2.1.5 describes the terms used in this table.*

S2.1.8A.

model	*k*	AIC_c	ΔAIC_c	ModLL	$wAIC_c$	LL	CumWt	%GoF
~HL+S+LAI	6	-90.42	0	1	0.13	51.3	0.13	95.1
~S+LAI	5	-89.55	0.87	0.65	0.09	49.84	0.22	93.76
~S+LAI+POP	6	-89.28	1.14	0.56	0.07	50.73	0.29	95.35
~HL+S+LAI+POP	7	-89.12	1.3	0.52	0.07	51.68	0.36	95.88
~HL+LAI	5	-88.74	1.68	0.43	0.06	49.43	0.42	99.07
~HL+S+LAI+BA	7	-88.7	1.72	0.42	0.06	51.47	0.47	94.58
~HL+S+LAI+N	7	-88.37	2.05	0.36	0.05	51.31	0.52	95.33
~S+LAI+BA	6	-87.98	2.45	0.29	0.04	50.08	0.56	93.06
~S+LAI+N	6	-87.8	2.62	0.27	0.04	49.99	0.6	95.32
~S+LAI+POP+BA	7	-87.76	2.66	0.26	0.03	51	0.63	94.78
~HL+LAI+BA	6	-87.55	2.87	0.24	0.03	49.86	0.66	98.52
~HL+S+LAI+POP+BA	8	-87.45	2.98	0.23	0.03	51.88	0.69	95.41
~S+LAI+POP+N	7	-87.32	3.1	0.21	0.03	50.78	0.72	96.08
~HL+LAI+POP	6	-87.26	3.16	0.21	0.03	49.72	0.75	99.36
~HL+LAI+N	6	-87.14	3.28	0.19	0.03	49.66	0.77	99.47
~HL+S+LAI+POP+N	8	-87.05	3.37	0.19	0.02	51.68	0.8	95.88
~HL+S+LAI+BA+N	8	-86.67	3.75	0.15	0.02	51.49	0.82	95.05
~S+LAI+BA+N	7	-86.33	4.09	0.13	0.02	50.29	0.83	94.96
~HL+LAI+POP+BA	7	-86.16	4.26	0.12	0.02	50.2	0.85	98.92
~LAI	4	-86.12	4.3	0.12	0.02	47.1	0.86	98.98
~HL+LAI+BA+N	7	-86.07	4.35	0.11	0.01	50.15	0.88	99.09
~LAI+POP	5	-85.9	4.52	0.1	0.01	48.01	0.89	99.49
~S+LAI+POP+BA+N	8	-85.87	4.56	0.1	0.01	51.09	0.91	95.78
~LAI+N	5	-85.84	4.58	0.1	0.01	47.98	0.92	99.7
~HL+LAI+POP+N	7	-85.58	4.84	0.09	0.01	49.91	0.93	99.65
~LAI+BA	5	-85.4	5.03	0.08	0.01	47.76	0.94	98.25
~HL+S+LAI+POP+BA+N	9	-85.38	5.04	0.08	0.01	51.88	0.95	95.63
~LAI+POP+BA	6	-85.27	5.15	0.08	0.01	48.73	0.96	98.97
~LAI+BA+N	6	-85.26	5.16	0.08	0.01	48.72	0.97	99.3
~LAI+POP+N	6	-85.11	5.32	0.07	0.01	48.64	0.98	99.86
~LAI+POP+BA+N	7	-84.59	5.83	0.05	0.01	49.41	0.99	99.58
~HL+LAI+POP+BA+N	8	-84.59	5.84	0.05	0.01	50.45	1	99.34
~HL+N	5	-80.1	10.32	0.01	0	45.11	1	97.58
~HL+POP+N	6	-78.57	11.86	0	0	45.37	1	98.01
~HL+BA+N	6	-78.48	11.94	0	0	45.33	1	96.97
~HL+S+N	6	-78.34	12.08	0	0	45.26	1	96.04
~HL+POP+BA+N	7	-77	13.42	0	0	45.62	1	97.46
~HL+S+POP+N	7	-76.87	13.56	0	0	45.55	1	96.47
~HL+S+BA+N	7	-76.57	13.85	0	0	45.41	1	95.84
~HL	4	-76.22	14.2	0	0	42.15	1	98.79
~HL+S	5	-75.64	14.78	0	0	42.89	1	99.75
~HL+S+POP+BA+N	8	-75.12	15.3	0	0	45.72	1	96.29
~HL+BA	5	-74.72	15.7	0	0	42.42	1	98.3
~HL+S+BA	6	-74.48	15.95	0	0	43.33	1	99.56
~HL+POP	5	-74.34	16.09	0	0	42.23	1	98.97
~HL+S+POP	6	-73.78	16.64	0	0	42.98	1	99.84
~POP+N	5	-73.33	17.1	0	0	41.73	1	98.35
~N	4	-73.14	17.28	0	0	40.61	1	97.52
~HL+POP+BA	6	-72.87	17.56	0	0	42.52	1	98.53
~HL+S+POP+BA	7	-72.66	17.76	0	0	43.45	1	99.69
~POP+BA+N	6	-72.27	18.15	0	0	42.23	1	97.61
~BA+N	5	-72.01	18.41	0	0	41.07	1	96.59
~S+POP+N	6	-71.62	18.8	0	0	41.9	1	96.94
~S+N	5	-71.31	19.11	0	0	40.72	1	96.16
~1	3	-70.78	19.64	0	0	38.42	1	98.65
~S+POP+BA+N	7	-70.34	20.08	0	0	42.29	1	96.68
~POP	4	-70.07	20.35	0	0	39.08	1	99.17
~S+BA+N	6	-70.02	20.41	0	0	41.1	1	95.84
~S	4	-69.84	20.58	0	0	38.96	1	99.6
~BA	4	-69.73	20.69	0	0	38.91	1	97.94
~S+POP	5	-69.23	21.19	0	0	39.68	1	99.87
~S+BA	5	-69.19	21.23	0	0	39.66	1	99.29
~POP+BA	5	-69.09	21.33	0	0	39.61	1	98.61
~S+POP+BA	6	-68.69	21.73	0	0	40.43	1	99.69

S2.1.8B.

model	*k*	AIC_c	$\Delta\mathrm{AIC}_c$	ModLL	$w\mathrm{AIC}_c$	LL	CumWt	%GoF
~HL+S+LAI+(HL×LAI)+(S×LAI)	8	-128.96	0	1	0.43	72.63	0.43	97.02
~HL+S+LAI+(HL×LAI)+(S×LAI)+(HL×S)	9	-128.31	0.65	0.72	0.31	73.35	0.75	96.77
~HL+S+LAI+(S×LAI)	7	-127.23	1.73	0.42	0.18	70.74	0.93	95
~HL+S+LAI+(S×LAI)+(HL×S)	8	-125.24	3.72	0.16	0.07	70.78	1	95.27
~HL+S+LAI+(HL×LAI)	7	-104.48	24.48	0	0	59.36	1	98.55
~HL+S+LAI+(HL×LAI)+(HL×S)	8	-103.02	25.94	0	0	59.67	1	98.58
~HL+S+LAI+(HL×S)	7	-99.31	29.65	0	0	56.77	1	97.54
~HL+S+LAI	6	-90.42	38.54	0	0	51.3	1	95.1

S2.1.8C.

variable removed	model	*k*	AIC_c	$\Delta\mathrm{AIC}_c$	ModLL	$w\mathrm{AIC}_c$	LL	CumWt	%GoF	Δ%GoF	R^2
S×LAI	**~HL+S+LAI+(HL×LAI)**	7	-104.48	24.48	0	0	59.36	1	98.55	-1.53	0.16
HL×LAI	**~HL+S+LAI+(S×LAI)**	7	-127.23	1.73	0.42	0.1	70.74	1	95	2.03	0.02
HL	**~S+LAI+(HL×LAI)+(S×LAI)**	8	-128.96	0	1	0.23	72.63	0.23	97.02	0	0
S	**~S+LAI+(HL×LAI)+(S×LAI)**	8	-128.96	0	1	0.23	72.63	0.45	97.02	0	0
none	**~HL+S+LAI+(HL×LAI)+(S×LAI)**	8	-128.96	0	1	0.23	72.63	0.68	97.02	0	0
LAI	**~HL+S+(HL×LAI)+(S×LAI)**	8	-128.96	0	1	0.23	72.63	0.9	97.02	0	0

Table S2.1.9. Map comparisons between merged Leemans et al. (1990a,b) and Olson et al. (2001). (A) comparison of generalised least-squares models with no interaction terms, (B) comparison of generalised least-squares models including interaction terms, as derived from the top-ranked model in A, and (C) relative importance of variables in the top-ranked generalised least-square model in B. *The caption to Table S2.1.5 describes the terms used in this table.*

S2.1.9A.

model	*k*	AIC_c	$\Delta\mathrm{AIC}_c$	ModLL	$w\mathrm{AIC}_c$	LL	CumWt	%GoF
~HL+S+LAI	6	83.17	0	1	0.19	-35.5	0.19	99.97
~HL+S+LAI+N	7	83.49	0.32	0.85	0.16	-34.63	0.35	98.53
~HL+LAI+N	6	84.57	1.4	0.5	0.09	-36.19	0.44	90.14
~HL+S+LAI+BA	7	85.15	1.98	0.37	0.07	-35.46	0.51	99.95
~HL+S+LAI+POP	7	85.22	2.05	0.36	0.07	-35.49	0.58	99.98
~HL+S+LAI+POP+N	8	85.49	2.32	0.31	0.06	-34.59	0.64	98.66
~HL+S+LAI+BA+N	8	85.54	2.37	0.31	0.06	-34.62	0.7	98.52
~HL+LAI	5	85.98	2.81	0.25	0.05	-37.93	0.74	95.07
~HL+LAI+POP+N	7	86.39	3.22	0.2	0.04	-36.08	0.78	91.17
~HL+LAI+BA+N	7	86.55	3.38	0.18	0.03	-36.16	0.82	90.56
~HL+S+LAI+POP+BA	8	87.21	4.04	0.13	0.03	-35.45	0.84	99.96
~HL	4	87.44	4.27	0.12	0.02	-39.68	0.86	95.95
~HL+S+LAI+POP+BA+N	9	87.55	4.38	0.11	0.02	-34.59	0.89	98.65
~HL+LAI+POP	6	87.95	4.78	0.09	0.02	-37.89	0.9	95.56
~HL+LAI+BA	6	88.01	4.84	0.09	0.02	-37.92	0.92	95.22
~HL+LAI+POP+BA+N	8	88.4	5.23	0.07	0.01	-36.05	0.93	91.49
~HL+POP	5	89.27	6.11	0.05	0.01	-39.57	0.94	96.61
~HL+S	5	89.28	6.11	0.05	0.01	-39.58	0.95	97.19
~HL+N	5	89.48	6.31	0.04	0.01	-39.68	0.96	96
~HL+BA	5	89.48	6.31	0.04	0.01	-39.68	0.97	96
~HL+LAI+POP+BA	7	90	6.83	0.03	0.01	-37.88	0.97	95.67
~HL+S+POP	6	91.13	7.96	0.02	0	-39.48	0.98	97.72
~HL+S+N	6	91.17	8	0.02	0	-39.5	0.98	98.32
~HL+POP+N	6	91.32	8.16	0.02	0	-39.57	0.98	96.6
~HL+POP+BA	6	91.32	8.16	0.02	0	-39.57	0.99	96.63
~HL+S+BA	6	91.33	8.16	0.02	0	-39.58	0.99	97.17
~HL+BA+N	6	91.52	8.36	0.02	0	-39.67	0.99	96.05
~HL+S+POP+N	7	93.08	9.91	0.01	0	-39.42	0.99	98.51
~HL+S+POP+BA	7	93.18	10.02	0.01	0	-39.48	0.99	97.69
~HL+S+BA+N	7	93.22	10.05	0.01	0	-39.49	1	98.31
~HL+POP+BA+N	7	93.38	10.21	0.01	0	-39.57	1	96.61
~S+LAI+N	6	94.32	11.15	0	0	-41.07	1	98.8
~HL+S+POP+BA+N	8	95.14	11.97	0	0	-39.42	1	98.51
~S+LAI+POP+N	7	96.08	12.91	0	0	-40.92	1	98.52
~S+LAI+BA+N	7	96.29	13.13	0	0	-41.03	1	98.84
~LAI+N	5	96.78	13.61	0	0	-43.33	1	86.92
~S+LAI	5	97.33	14.16	0	0	-43.6	1	99.08
~S+LAI+POP+BA+N	8	98.05	14.88	0	0	-40.87	1	98.55
~LAI+BA+N	6	98.28	15.11	0	0	-43.05	1	88.43
~S+LAI+POP	6	98.44	15.27	0	0	-43.13	1	99.68
~LAI+POP+N	6	98.71	15.54	0	0	-43.27	1	86.05
~S+LAI+BA	6	99.37	16.2	0	0	-43.6	1	99.06
~LAI+POP+BA+N	7	100.21	17.04	0	0	-42.99	1	87.57
~S+LAI+POP+BA	7	100.49	17.32	0	0	-43.13	1	99.67
~LAI	4	103.78	20.61	0	0	-47.85	1	95.86
~LAI+POP	5	105.11	21.94	0	0	-47.49	1	94.16
~LAI+BA	5	105.47	22.3	0	0	-47.67	1	96.66
~LAI+POP+BA	6	106.76	23.6	0	0	-47.29	1	95.12
~1	3	109.11	25.94	0	0	-51.53	1	97.25
~POP	4	110.62	27.45	0	0	-51.27	1	96.11
~S	4	110.82	27.65	0	0	-51.37	1	98.63
~BA	4	110.85	27.68	0	0	-51.38	1	97.84
~N	4	110.99	27.82	0	0	-51.45	1	96.82
~POP+BA	5	112.34	29.17	0	0	-51.11	1	96.8
~S+POP	5	112.34	29.17	0	0	-51.11	1	97.8
~POP+N	5	112.59	29.42	0	0	-51.23	1	95.82
~S+BA	5	112.65	29.48	0	0	-51.26	1	98.86
~BA+N	5	112.73	29.56	0	0	-51.3	1	97.44
~S+N	5	112.86	29.69	0	0	-51.37	1	98.48
~S+POP+BA	6	114.15	30.98	0	0	-50.99	1	98.08
~POP+BA+N	6	114.3	31.13	0	0	-51.06	1	96.53
~S+POP+N	6	114.38	31.21	0	0	-51.1	1	98.04
~S+BA+N	6	114.68	31.51	0	0	-51.25	1	98.55
~S+POP+BA+N	7	116.21	33.04	0	0	-50.99	1	98.11

S2.1.9B.

model	*k*	AIC_c	ΔAIC_c	ModLL	$wAIC_c$	LL	CumWt	%GoF
~HL+S+LAI+(S×LAI)+(HL×S)	8	73.67	0	1	0.51	-28.68	0.51	99.97
~HL+S+LAI+(HL×LAI)+(S×LAI)+(HL×S)	9	74.63	0.96	0.62	0.32	-28.13	0.83	100
~HL+S+LAI+(S×LAI)	7	76.68	3.01	0.22	0.11	-31.22	0.94	99.94
~HL+S+LAI+(HL×LAI)+(S×LAI)	8	78.51	4.83	0.09	0.05	-31.1	0.99	99.98
~HL+S+LAI	6	83.17	9.5	0.01	0	-35.5	1	99.97
~HL+S+LAI+(HL×LAI)	7	84.85	11.18	0	0	-35.31	1	99.89
~HL+S+LAI+(HL×S)	7	85.03	11.36	0	0	-35.4	1	99.99
~HL+S+LAI+(HL×LAI)+(HL×S)	8	85.62	11.95	0	0	-34.66	1	99.91

S2.1.9C.

variable removed	model	*k*	AIC_c	ΔAIC_c	ModLL	$wAIC_c$	LL	CumWt	%GoF	Δ%GoF	R^2
S×LAI	**~HL+S+LAI+(HL×S)**	7	85.03	11.36	0	0	-35.4	1	99.99	-0.02	-0.25
HL×S	**~HL+S+LAI+(S×LAI)**	7	76.68	3.01	0.22	0.05	-31.22	1	99.94	0.03	-0.09
none	**~HL+S+LAI+(S×LAI)+(HL×S)**	8	73.67	0	1	0.24	-28.68	0.24	99.97	0	0
HL	**~S+LAI+(S×LAI)+(HL×S)**	8	73.67	0	1	0.24	-28.68	0.47	99.97	0	0
S	**~HL+LAI+(S×LAI)+(HL×S)**	8	73.67	0	1	0.24	-28.68	0.71	99.97	0	0
LAI	**~HL+S+(S×LAI)+(HL×S)**	8	73.67	0	1	0.24	-28.68	0.95	99.97	0	0

Table S2.1.10. Map comparisons between merged Friedl et al. (2010) and Olson et al. (2001). (A) comparison of generalised least-squares models with no interaction terms, (B) comparison of generalised least-squares models including interaction terms, as derived from the top-ranked model in A, and (C) relative importance of variables in the top-ranked generalised least-square model in B. *The caption to Table S2.1.5 describes the terms used in this table.*

S2.1.10A.

model	*k*	AIC$_c$	ΔAIC$_c$	ModLL	wAIC$_c$	LL	CumWt	%GoF
~HL+LAI	5	-178.13	0	1	0.17	94.13	0.17	93.73
~HL+LAI+BA	6	-177.91	0.22	0.89	0.15	95.05	0.32	94.61
~HL+LAI+POP	6	-176.86	1.27	0.53	0.09	94.52	0.4	94.3
~HL+LAI+POP+BA	7	-176.45	1.69	0.43	0.07	95.34	0.48	95.03
~HL+S+LAI+BA	7	-176.42	1.72	0.42	0.07	95.33	0.55	93.47
~HL+S+LAI	6	-176.31	1.82	0.4	0.07	94.25	0.61	92.89
~HL+LAI+N	6	-176.12	2.01	0.37	0.06	94.15	0.68	93.39
~HL+LAI+BA+N	7	-175.95	2.18	0.34	0.06	95.1	0.73	94.15
~HL+S+LAI+POP	7	-175.09	3.05	0.22	0.04	94.66	0.77	93.44
~HL+S+LAI+POP+BA	8	-175	3.13	0.21	0.03	95.66	0.8	93.9
~HL+LAI+POP+N	7	-174.88	3.26	0.2	0.03	94.56	0.84	93.89
~HL+S+LAI+BA+N	8	-174.72	3.42	0.18	0.03	95.51	0.87	92
~HL+LAI+POP+BA+N	8	-174.52	3.62	0.16	0.03	95.42	0.89	94.52
~HL+S+LAI+N	7	-174.38	3.75	0.15	0.03	94.31	0.92	91.96
~HL+S+LAI+POP+BA+N	9	-173.39	4.74	0.09	0.02	95.89	0.93	92.32
~HL+S+LAI+POP+N	8	-173.23	4.9	0.09	0.01	94.77	0.95	92.33
~LAI+POP	5	-172.11	6.03	0.05	0.01	91.12	0.96	94
~LAI	4	-171.25	6.89	0.03	0.01	89.67	0.96	92.59
~S+LAI+POP	6	-171.21	6.92	0.03	0.01	91.7	0.97	92.06
~LAI+POP+BA	6	-170.97	7.17	0.03	0	91.57	0.97	94.6
~S+LAI+POP+BA	7	-170.6	7.53	0.02	0	92.42	0.98	92.48
~S+LAI	5	-170.36	7.77	0.02	0	90.25	0.98	90.38
~LAI+POP+N	6	-170.3	7.83	0.02	0	91.24	0.98	94.77
~LAI+BA	5	-170.29	7.85	0.02	0	90.21	0.99	93.4
~S+LAI+BA	6	-169.98	8.15	0.02	0	91.08	0.99	90.99
~LAI+N	5	-169.8	8.33	0.02	0	89.97	0.99	94.06
~S+LAI+POP+N	7	-169.17	8.97	0.01	0	91.7	0.99	92.4
~LAI+POP+BA+N	7	-169.11	9.02	0.01	0	91.68	0.99	95.25
~LAI+BA+N	6	-168.75	9.38	0.01	0	90.47	1	94.63
~S+LAI+POP+BA+N	8	-168.53	9.6	0.01	0	92.42	1	92.39
~S+LAI+N	6	-168.49	9.65	0.01	0	90.33	1	91.76
~S+LAI+BA+N	7	-167.98	10.15	0.01	0	91.11	1	91.77
~HL+BA+N	6	-138.22	39.91	0	0	75.2	1	80.02
~HL+S+BA+N	7	-138.12	40.01	0	0	76.18	1	87.51
~HL+S+N	6	-137.92	40.21	0	0	75.05	1	87.24
~HL+POP+BA+N	7	-136.7	41.44	0	0	75.47	1	80.85
~HL+N	5	-136.7	41.44	0	0	73.41	1	76.3
~HL+S+POP+BA+N	8	-136.47	41.67	0	0	76.39	1	87.88
~HL+S+POP+N	7	-136.4	41.74	0	0	75.32	1	87.68
~HL+POP+N	6	-135.4	42.73	0	0	73.79	1	77.56
~HL+S	5	-118.7	59.43	0	0	64.42	1	98.99
~HL+S+BA	6	-117.01	61.13	0	0	64.59	1	99.13
~S+POP+N	6	-116.79	61.35	0	0	64.48	1	86.53
~HL+S+POP	6	-116.65	61.48	0	0	64.42	1	99
~POP+N	5	-115.96	62.17	0	0	63.05	1	74.33
~S+POP+BA+N	7	-115.5	62.64	0	0	64.87	1	86.66
~POP+BA+N	6	-115.46	62.68	0	0	63.82	1	77.01
~HL+S+POP+BA	7	-114.95	63.19	0	0	64.59	1	99.13
~S+N	5	-114.73	63.4	0	0	62.43	1	84.9
~S+BA+N	6	-113.54	64.59	0	0	62.86	1	85.08
~N	4	-113.35	64.78	0	0	60.72	1	69.99
~BA+N	5	-113.08	65.06	0	0	61.6	1	73.34
~S	4	-100.43	77.71	0	0	54.26	1	98.57
~S+POP	5	-100.09	78.05	0	0	55.11	1	99.12
~S+BA	5	-98.43	79.71	0	0	54.28	1	98.64
~S+POP+BA	6	-98.06	80.08	0	0	55.12	1	99.15
~HL+BA	5	-82.37	95.76	0	0	46.25	1	83.32
~HL	4	-82.17	95.97	0	0	45.13	1	79.66
~HL+POP+BA	6	-80.36	97.78	0	0	46.27	1	83.06
~HL+POP	5	-80.13	98.01	0	0	45.13	1	79.54
~1	3	-68.92	109.21	0	0	37.49	1	77.89
~BA	4	-68.07	110.06	0	0	38.08	1	80.82
~POP	4	-67.97	110.16	0	0	38.03	1	79.92
~POP+BA	5	-67.02	111.11	0	0	38.57	1	82.49

S2.1.10B.

model	*k*	AIC_c	ΔAIC_c	ModLL	$wAIC_c$	LL	CumWt	%GoF
~HL+LAI+ (HL×LAI)	6	-198.12	0	1	1	105.15	1	97.16
~HL+LAI	5	-178.13	19.98	0	0	94.13	1	93.73

S2.1.10C.

variable removed	model	*k*	AIC_c	ΔAIC_c	ModLL	$wAIC_c$	LL	CumWt	%GoF	Δ%GoF	R^2
HL×LAI	**~HL+LAI**	5	-178.13	19.98	0	0	94.13	1	93.73	3.44	0.09
none	**~HL+LAI+ (HL×LAI)**	6	-198.12	0	1	0.33	105.15	0.33	97.16	0	0
HL	**~LAI+ (HL×LAI)**	6	-198.12	0	1	0.33	105.15	0.67	97.16	0	0
LAI	**~HL+ (HL×LAI)**	6	-198.12	0	1	0.33	105.15	1	97.16	0	0

APPENDIX S4

Chapter 4 – Response of Neotropical tree cover to variation in post-Last Glacial Maximum climate and atmospheric CO_2

The following Supporting Information is available for this chapter:

Appendix S4.1. Description of plant functional types and model outputs.

In the model, I grouped plants with similar functional characteristics into 19 functional types (Table S4.1.2). Each plant functional type represents a different combination of functional traits (Table S4.1.3). Model inputs therefore include information on plant functional-types traits such as their life form (tree, shrub, grass), bioclimatic range (tropical, temperate, boreal), leaf physiognomy (needleleaf, broadleaf), leaf phenology (evergreen, raingreen, summergreen), body allometry (allocation of the carbon in the plant), tolerance to drought, resistance to fire, maximum crown area, or photosynthetic pathway (C_3 or C_4).

For each of the seven simulations, I mapped the distribution of dominant tree functional types by selecting the functional type with the highest leaf area index in each grid cell (Fig. S4.1.4). Such maps represent the most abundant type of tree in a landscape whatever the percentage of forest cover. This provides information on the potential type of forest, and on the possibility for landscapes to host at least some tree populations, even if forest cover is close to zero.

Simulated changes in the distribution of dominant arboreal plant functional types mainly show the competition between deciduous and evergreen trees within the tropical, temperate, and boreal climate zones (Figure S4.1.4). Climate zones were displaced through time, mainly characterised by the enlargement of the tropical zone, and the southward expansion of the temperate and boreal zones. Tropical and temperate trees also expanded upslope in the tropical Andes at the expense of boreal deciduous trees. Most of these climate zone displacements occurred between the Last Glacial Maximum and the end of Heinrich Stadial 1, followed by gradual but slower displacements until the present. Within the tropical zone during the Last Glacial Maximum, evergreen trees (tropical broadleaved evergreen trees, TrIBE and TrBE; Tables S.2 and S2.3) were dominant in the landscape compared to deciduous trees (tropical broadleaved raingreen trees, TrBR; Tables S2.2 and S2.3) in several distinct areas including Central America, along the western flank of the Andes, the north-western Amazon Basin, and the Cerrado. The area dominated by tropical evergreen trees was then displaced southward during Heinrich Stadial 1, to the benefit of tropical deciduous trees in the north-western Amazon Basin. Evergreen tree-dominated areas then gradually moved back northward from the Younger Dryas to the present. In Patagonia, temperate (temperate broadleaved evergreen tree, TeBE, and shade-tolerant temperate broadleaved summergreen tree, TeBS; Tables S2.2 and S2.3) and boreal deciduous boreal broadleaved trees gradually expanded southward at the expense of boreal needleleaved evergreen trees (shade-intolerant boreal needleleaved evergreen tree, BINE and boreal needleleaved evergreen tree, BNE; Tables S2.2 and S2.3).

Table S4.1.2. *List of the plant functional types used in this study.*

Acronym	*Plant functional type*	*Life form*
BNE	boreal needleleaved evergreen tree	tree
BINE	shade-intolerant boreal needleleaved evergreen tree	tree
BNS	boreal needleleaved summergreen tree	tree
TeNE	temperate needleleaved evergreen tree	tree
TeBS	shade-tolerant temperate broadleaved summergreen tree	tree
IBS	shade-intolerant broadleaved summergreen tree	tree
TeBE	temperate broadleaved evergreen tree	tree
TrBE	tropical broadleaved evergreen tree	tree
TrIBE	tropical broadleaved evergreen tree	tree
TrBR	tropical broadleaved raingreen tree	tree
C3G	C_3 grass	grass
C4G	C_4 grass	grass
TeEsh	temperate evergreen shrub	shrub
TeRSh	temperate raingreen shrub	shrub
TeSSh	temperate raingreen shrub	shrub
TrESh	tropical evergreen shrub	shrub
TrRSh	tropical raingreen shrub	shrub
BESh	boreal evergreen shrub	shrub
BSSh	boreal summergreen shrub	shrub

Table S4.1.3. Plant functional type characteristics used in model simulations. *Characteristics correspond to general traits, temperature ranges, allometry constants describing plant morphology, and life history. Climate classes are associated with differing photosynthesis optimum temperatures and base respiration rates (Smith et al., 2001). Shade tolerance is associated with different regulatory thresholds for recruitment, establishment, and juvenile growth-rates. $T_{c,min,surv}$ = minimum coldest-month temperature for survival; $T_{c,min,est}$ = minimum coldest-month temperature for establishment; $T_{c,max,est}$ = maximum coldest-month temperature for establishment; $T_{w,min,est}$ = minimum warmest month mean temperature for establishment (°C); GDD_5 = minimum degree-day sum > 5 °C for establishment; $k_{la:sa}$ = leaf area to sapwood cross-sectional area ratio; CA_{max} = maximum woody crown area; k_{allom1} = constant in allometry equations (Smith et al., 2001; higher values = wider crowns); z_1 = fraction of roots in first soil layer (remainder allocated to second soil layer); r_{fire} = fraction of individuals that survive fire; $D_{tolerance}$ = drought sensitivity factor from 0 to 1, where 1 = maximum sensitivity; a_{leaf} = leaf longevity; a_{ind} = maximum, non-stressed longevity.*

	General traits				temperature range					Allometry constants (PFT morphology)				Life history			
PFT	Climate	Leaf physiognomy	phenology	Shade tolerance	$T_{c,min,surv}$ (°C)	$T_{c,min,est}$ (°C)	$T_{c,max,est}$ (°C)	$T_{w,min,est}$ (°C)	GDD_5 (°C)	k_{la} : sa	CAmax (m^2)	k_{allom1}	z_1	r_{fire}	Dtolerance	A_{leaf} (yr)	A_{ind} (yr)
BNE	boreal	needleleaf	evergreen	tolerant	-31	-30	-1	5	500	5000	50	150	0.6	0.3	0.4	3	500
BINE	boreal	needleleaf	evergreen	intolerant	-31	-30	-1	5	500	5000	50	150	0.6	0.3	0.25	3	500
BNS	boreal	needleleaf	summergreen	intolerant	-1000	-1000	-2	-1000	350	5000	50	150	0.6	0.3	0.2	0.5	300
TeNE	temperate	needleleaf	evergreen	intolerant	-2	-2	10	5	2000	5000	50	150	0.6	0.3	0.3	3	300
TeBS	temperate	broadleaf	summergreen	tolerant	-14	-13	6	5	1100	6000	50	250	0.6	0.1	0.3	0.5	400
IBS	boreal	broadleaf	summergreen	intolerant	-30	-30	7	-1000	350	6000	50	250	0.6	0.1	0.3	0.5	300
TeBE	temperate	broadleaf	evergreen	tolerant	-1	0	18.8	5	2000	6000	50	250	0.6	0.3	0.1	3	300
TrBE	tropical	broadleaf	evergreen	tolerant	15.5	15.5	1000	-1000	0	6000	50	250	0.6	0.1	0.2	2	500
TrIBE	tropical	broadleaf	evergreen	intolerant	15.5	15.5	1000	-1000	0	6000	50	250	0.6	0.1	0.2	2	200
TrBR	tropical	broadleaf	raingreen	intolerant	15.5	15.5	1000	-1000	0	6000	50	250	0.6	0.3	0.1	0.5	400
C3G	-	broadleaf	any	-	-1000	-1000	1000	-1000	0	-	-	-	0.9	0.5	0.01	0.5	-
C4G	-	broadleaf	any	-	15.5	15.5	1000	-1000	0	-	-	-	0.9	0.5	0.01	0.5	-
TeEsh	temperate	broadleaf	evergreen	intolerant	-1000	-1000	1000	-1000	1200	2000	10	100	0.6	0.1	0.1	2	200
TeRSh	temperate	broadleaf	raingreen	intolerant	-1000	-1000	1000	-1000	1200	2000	10	100	0.6	0.4	0.01	1	200
TeSSh	temperate	broadleaf	summergreen	intolerant	-1000	-1000	1000	-1000	1200	2000	10	100	0.6	0.1	0.3	1	100
TrESh	tropical	broadleaf	evergreen	intolerant	15.5	15.5	1000	-1000	0	2000	10	100	0.6	0.1	0.025	2	200
TrRSh	tropical	broadleaf	raingreen	intolerant	15.5	15.5	1000	-1000	0	2000	10	100	0.6	0.1	0.025	1	200
BESh	boreal	broadleaf	evergreen	intolerant	-1000	-1000	-5	-1000	150	2000	10	100	0.6	0.1	0.25	2	200
BSSh	boreal	broadleaf	summergreen	intolerant	-1000	-1000	-5	-1000	150	2000	10	100	0.6	0.1	0.25	0.5	200

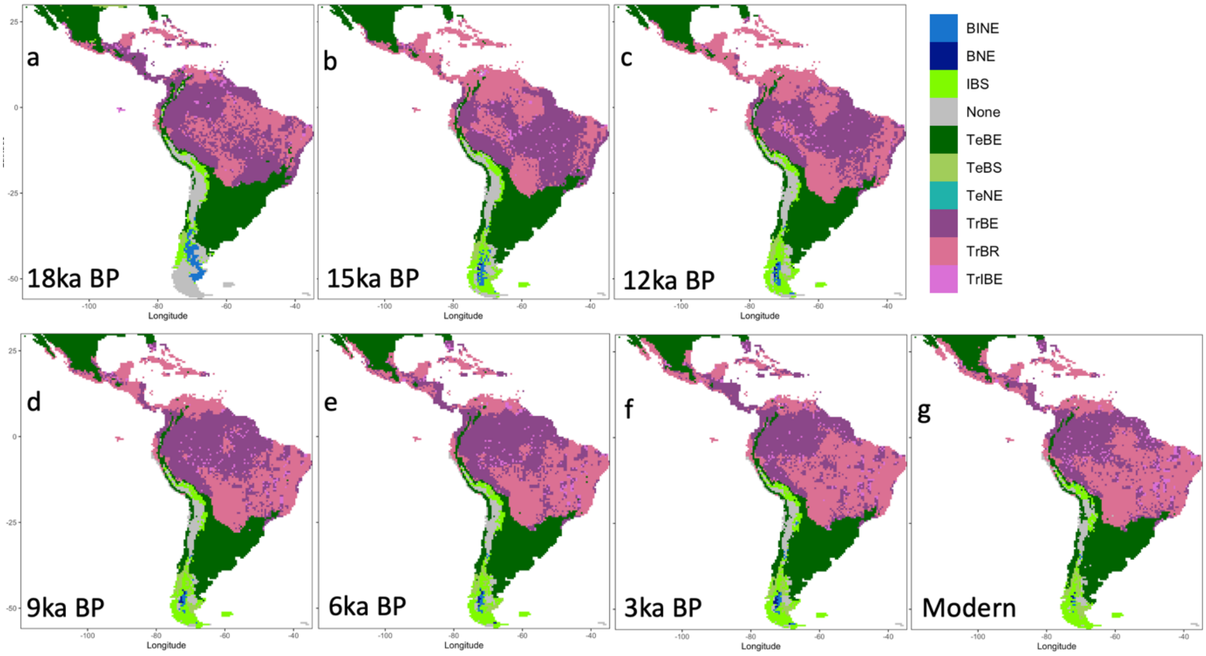

Figure S4.1.4. *Leaf area index-dominant arboreal plant functional type as simulated with LPJ-GUESS under climate scenarios corresponding to (a) 18,500 years BP, Last Glacial Maximum, (b) 15,000 years BP, Heinrich Stadial 1, (c) 12,000 years BP, Younger Dryas, (d) 9,000 years BP, Greenlandian, (e) 6,000 years BP, Northgrippian, and (f) 3,000 years BP, Meghalayan. Colours correspond to the plant functional types described in Tables S2.2 and S2.3.*

Appendix S4.2. Description of the palaeo-climate input data.

I used palaeo-climate input data from the TraCE-21ka experiments (He, 2011). I downscaled and debiased the data based on Traylor et al. (2021).

Table S4.2.5. TraCE-21ka simulation parameters for the seven selected periods. *BP = before present, CE = common era, NHMW & SHMW= Northern and Southern Hemispheres, respectively; meltwater discharge, expressed in m kyr^{-1} (metres of equivalent sea-level volume per thousand years), with 1 m kyr^{-1} = 0.011 Sv (Sverdrup) representing 3.61×10^{14} m^3 volume of meltwater in 10^3 years (He, 2011). AMOC = Atlantic meridional overturning circulation, strength expressed in million m^3 sec^{-1}.*

Years	**LPJ-GUESS experiment**	**TraCE-21ka experiment**	**TraCE-21ka file prefix**	**NHMW location**	**NHMW (m/kyr)**	**SHMW location**	**SHMW (m/kyr)**	**Geography changes to previous**	**AMOC strength (million m^3 sec^{-1})**
18,500-18,400 BP	Last Glacial Maximum (LGM)	TraCE-H1	trace.04	North Atlantic	3				~12
15,000-14,900 BP	Heinrich Stadial 1 (HS1)	TraCE-BA	trace.09	North Atlantic	15				~4
12,000-11,900 BP	Younger Dryas (YD)	TraCE-YD	trace.16	St. Lawrence river	12			Barents Sea and Bering Strait opened	~4
9,000-8,900 BP	Greenlandian (Gre)	TraCE-Holocene	trace.22	Arctic	0.42	Weddell Sea	1.12		~8
				St. Lawrence River	0.42	Ross Sea	1.12		
				Hudson Strait	7.47				
6,100-6,000 BP	Northgrippian (Nor)	TraCE-Holocene	trace.29	Arctic	0.01	Weddell Sea	1.12	Hudson Bay opened, Indonesian Throughflow	~10
				St. Lawrence River	0.01	Ross Sea	1.12		
				Hudson Strait	0.21				
3,000-2900 BP	Meghalayan (Meg)	TraCE-Holocene	trace.33						~11
1950-1990 CE	Present (P)	TraCE-Holocene	trace.36						~11

Figure S4.2.6. Summary of the input data used in this study for the seven selected periods, expressed as total average. *Input data represented here are (a) "precipitations", total convective and large-scale precipitation rate including liquid and ice in mm.day^{-1}, (b) number of wet days per month, (c) "temperature", near surface air temperature at 2 meters in degree Celsius, (d) "solar radiations", mean daily surface incident shortwave radiations in W.m^{-2} calculated from (e) clearsky downwelling solar flux at surface W.m^{-2} and (f) "cloud cover", vertically integrated total cloud in percent. Snapshots correspond to the transition between the Last Glacial Maximum and Heinrich event 1 (LGM: 18,500 – 18,400 years BP), end of Heinrich Stadial 1 (HS1: 15,000 – 14,900 years BP), Younger Dryas (YD: 12,000-11,900 years BP), Greenlandian (Gre: 9,000 – 8,900 years BP), Northgrippian (Nor: 6,100 – 6,000 years BP), Meghalayan (Meg: 3,000 – 2,900 years BP), and the present (P: 1950 – 1990 CE).*

(a)

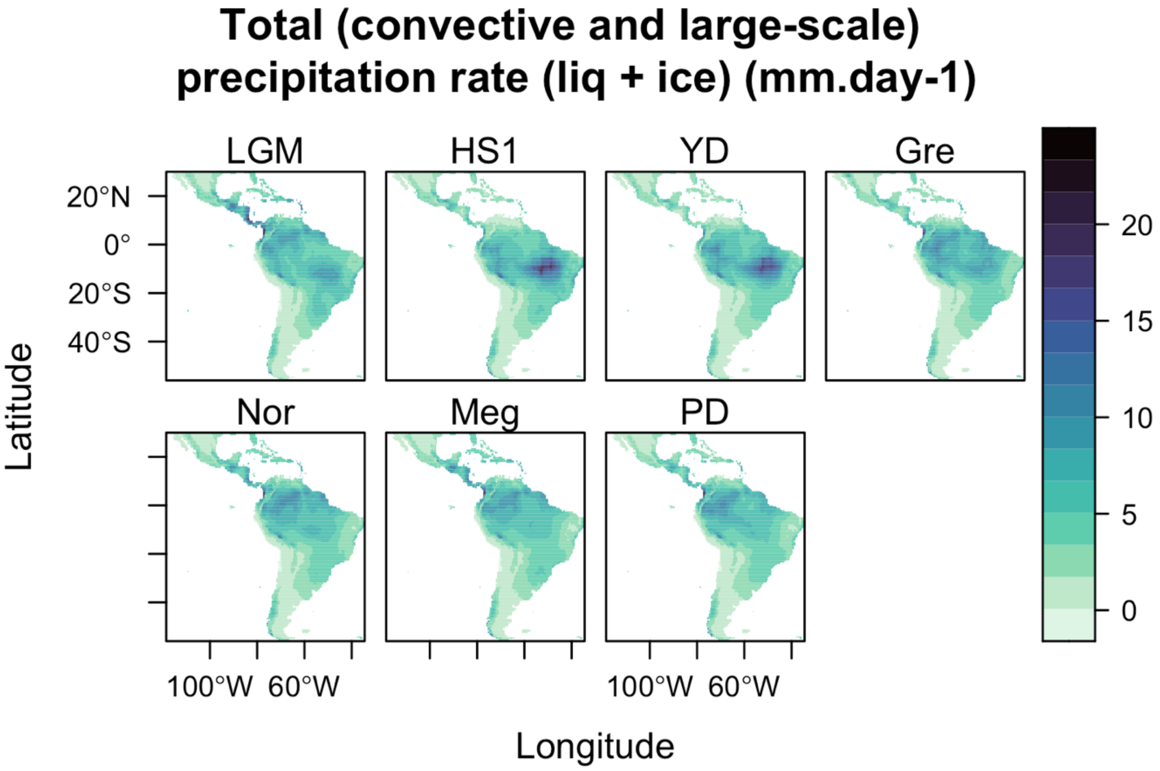

(b)

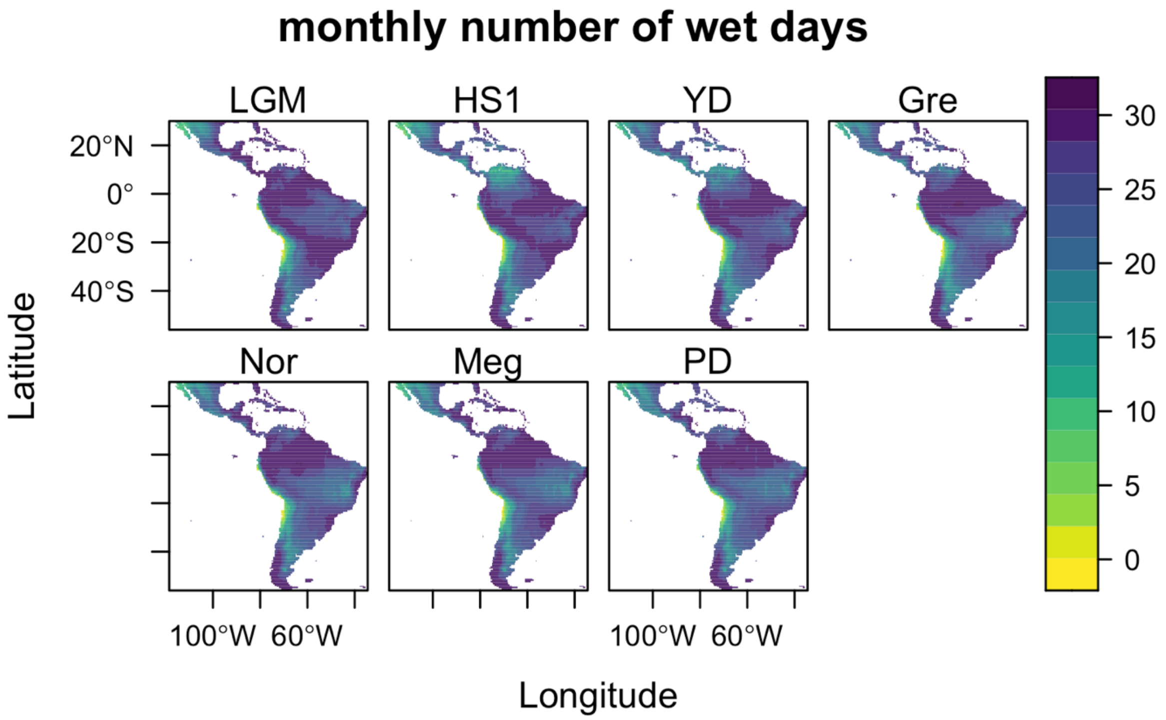
monthly number of wet days
LGM
HS1
YD
Gre
Nor
Meg
PD
20°N
0°
20°S
40°S
Latitude
100°W
60°W
100°W
60°W
Longitude
30
25
20
15
10
5
0

(c)

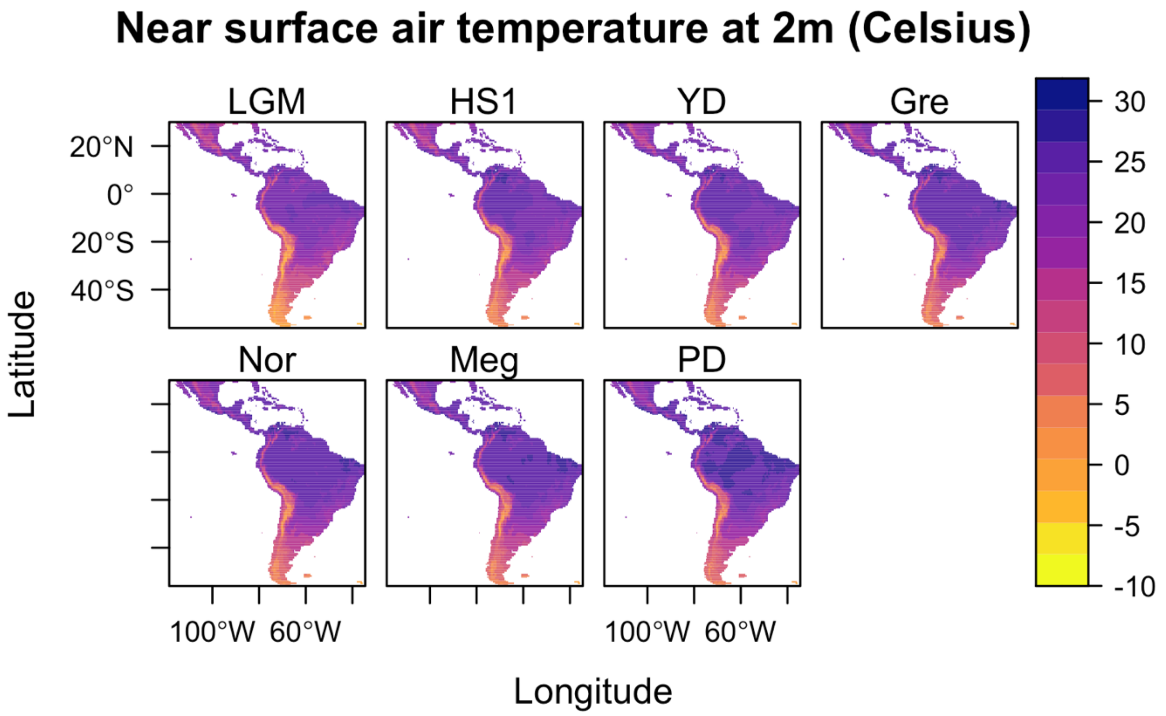
Near surface air temperature at 2m (Celsius)
LGM
HS1
YD
Gre
Nor
Meg
PD
20°N
0°
20°S
40°S
Latitude
100°W
60°W
100°W
60°W
Longitude
30
25
20
15
10
5
0
-5
-10

(d)

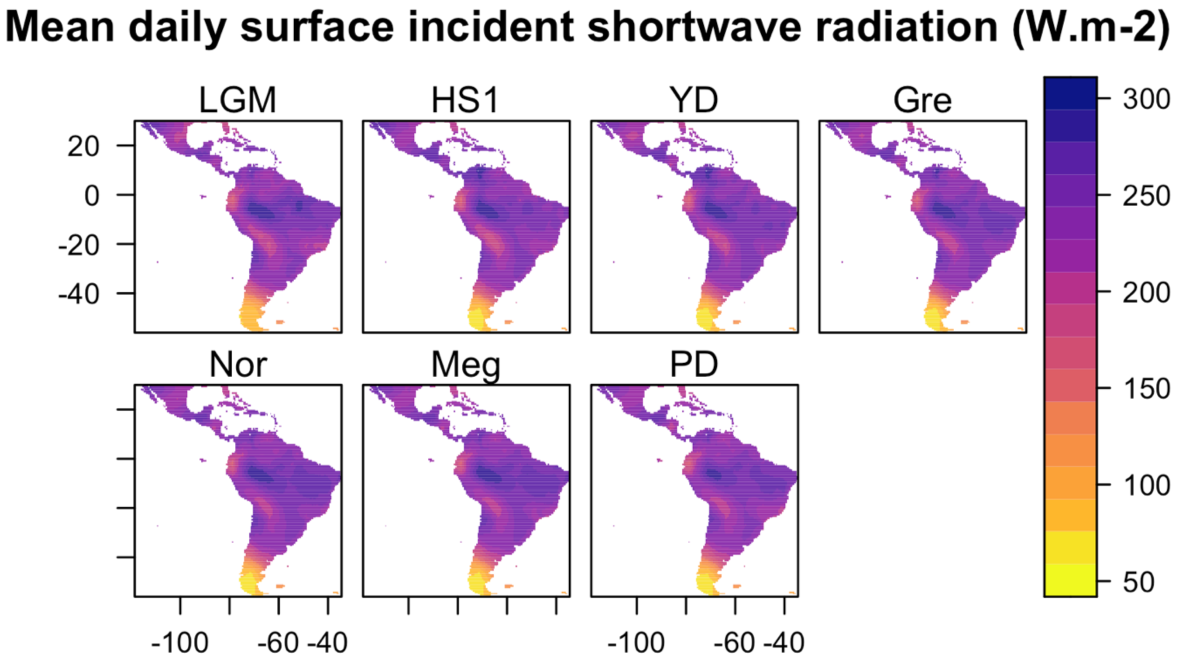
Mean daily surface incident shortwave radiation (W.m-2)
LGM
HS1
YD
Gre
Nor
Meg
PD
20
0
-20
-40
-100
-60 -40
-100
-60 -40
300
250
200
150
100
50

(e)

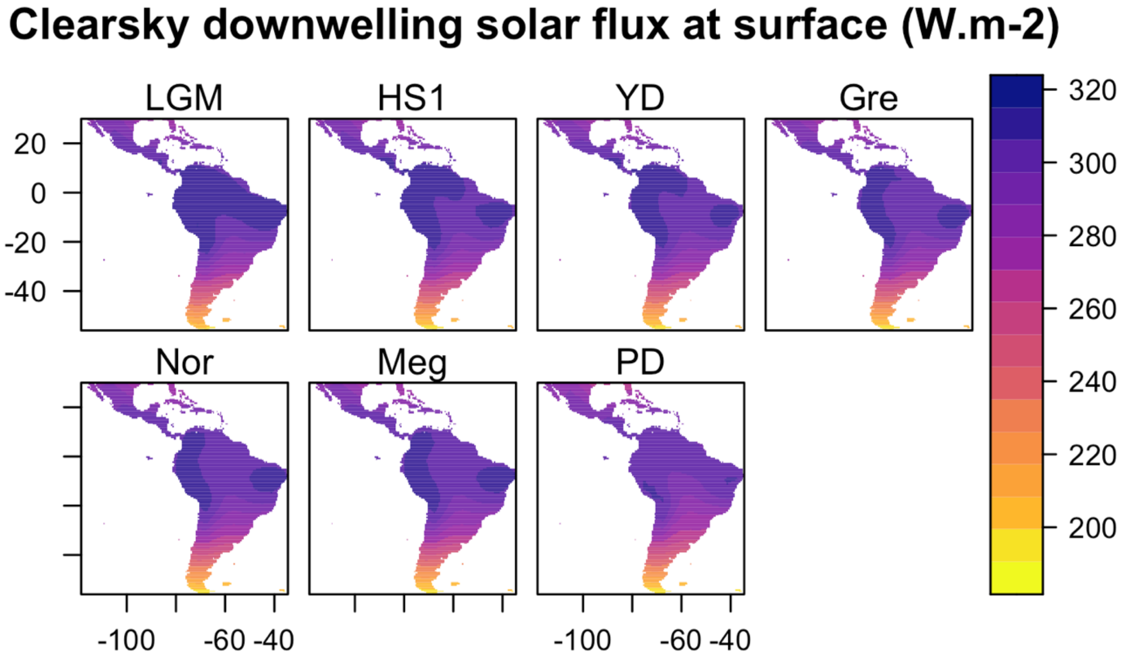
Clearsky downwelling solar flux at surface (W.m-2)
LGM
HS1
YD
Gre
Nor
Meg
PD
20
0
-20
-40
-100
-60 -40
-100
-60 -40
320
300
280
260
240
220
200

(f)

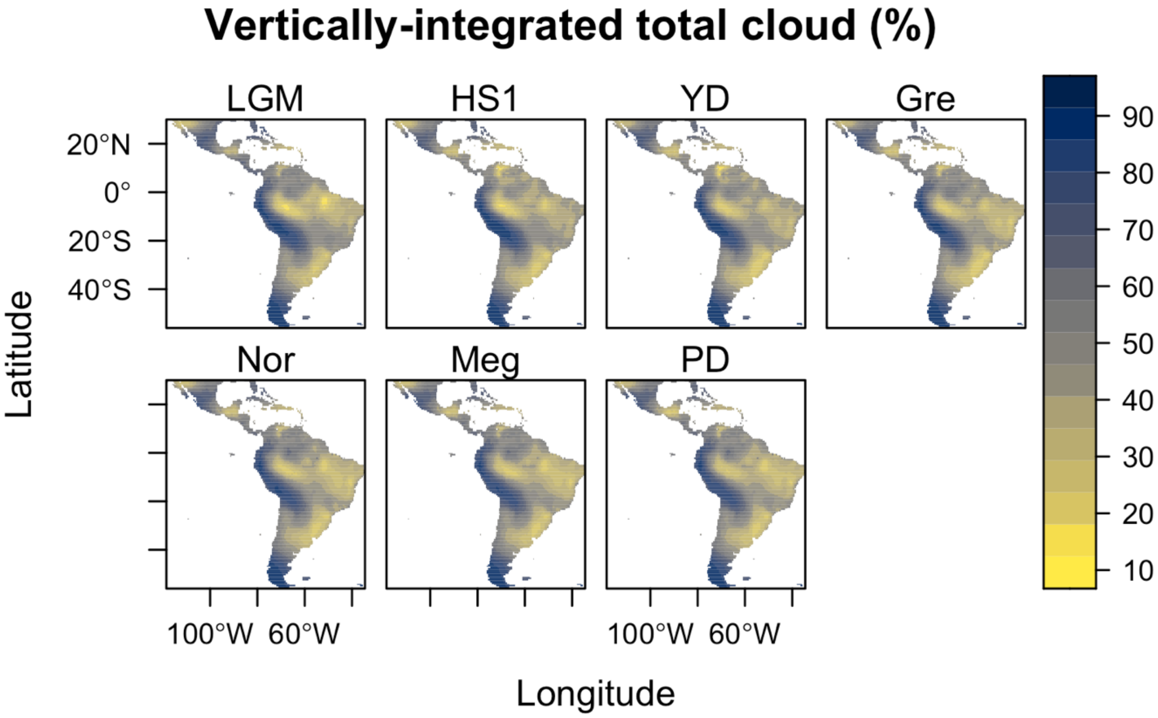
Vertically-integrated total cloud (%)
LGM
HS1
YD
Gre
Nor
Meg
PD
20°N
0°
20°S
40°S
Latitude
100°W
60°W
100°W
60°W
Longitude
90
80
70
60
50
40
30
20
10

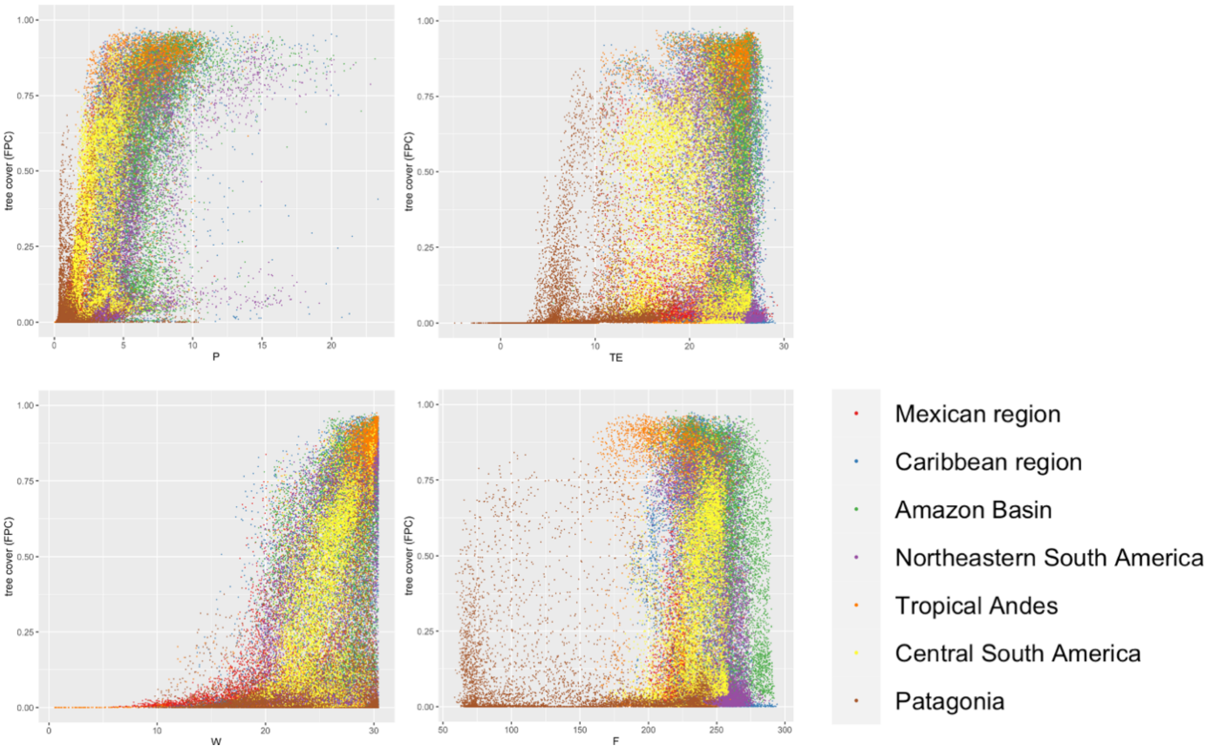

Figure S4.2.7. Relationships between simulated tree foliar projective cover (FPC) and climate input. *P: precipitations, TE: temperature, W: number of wet days, F: solar radiations.*

Appendix S4.4. Comparison of generalised least square models to explain tree cover (FPC) in the seven regions I examined.

Table S4.4.8. Comparison of generalised least-squares models to explain the tree cover (FPC) in Patagonia. *The generalised least-squares models were built based on mean annual averages of model input data including the four climate variables (P = mean annual precipitation, TE = mean annual temperature, F = mean annual solar radiation, W = mean annual number of wet days) and atmospheric* CO_2 *concentration (CO2) per grid cell to describe the tree cover (TC = mean annual tree foliar projective cover) for each region I examined. Shown for each model are the number of parameters (k), Akaike's information criterion (*AIC_c*), difference in Akaike's information criterion corrected for small sample sizes relative to the top-ranked model (*ΔAIC_c*), the relative likelihood (ModLL),* AIC_c *weight (~ model probability;* $wAIC_c$*), maximum log-likelihood (LL), the cumulative weights (CumWt).*

Model	k	AICc	∆AICc	ModLL	wAICc	LL	CumWt
~TE+P+W+F+CO2	8	-9404.27	0	1	0.97	4710.15	0.97
~TE+P+W+CO2	7	-9396.96	7.32	0.03	0.03	4705.49	1
~TE+P+W+F	7	-9352.84	51.43	0	0	4683.43	1
~TE+W+F+CO2	7	-9347.57	56.7	0	0	4680.8	1
~TE+W+CO2	6	-9345.71	58.56	0	0	4678.86	1
~TE+P+W	6	-9335.35	68.92	0	0	4673.68	1
~TE+P+F+CO2	7	-9307.2	97.07	0	0	4660.61	1
~TE+W+F	6	-9297.35	106.92	0	0	4654.68	1
~TE+P+F	6	-9257.32	146.95	0	0	4634.67	1
~P+W+F+CO2	7	-9210.91	193.36	0	0	4612.46	1
~TE+P+co2	6	-9199.35	204.92	0	0	4605.68	1
~P+W+CO2	6	-9199.12	205.15	0	0	4605.57	1
~P+F+CO2	6	-9150.7	253.57	0	0	4581.36	1
~W+F+CO2	6	-9148.64	255.63	0	0	4580.33	1
~P+CO2	5	-9144.64	259.64	0	0	4577.32	1
~TE+F+CO2	6	-9136.64	267.64	0	0	4574.33	1
~W+CO2	5	-9123.94	280.33	0	0	4566.98	1
~TE+P	5	-9109.8	294.47	0	0	4559.91	1
~TE+F	5	-9091.04	313.23	0	0	4550.53	1
~P+W+F	6	-9064.63	339.65	0	0	4538.32	1
~P+W	5	-9056.57	347.7	0	0	4533.29	1
~P+F	5	-9015.21	389.07	0	0	4512.61	1
~P	4	-9009.09	395.18	0	0	4508.55	1
~W+F	5	-9003.61	400.66	0	0	4506.81	1
~F+CO2	5	-8993.58	410.69	0	0	4501.8	1
~TE+CO2	5	-8986.98	417.3	0	0	4498.49	1
~TE+CO2	5	-8986.98	417.3	0	0	4498.49	1
~W	4	-8984.65	419.62	0	0	4496.33	1
~CO2	4	-8962.94	441.33	0	0	4485.47	1
~TE	4	-8897.38	506.89	0	0	4452.69	1
~F	4	-8869.66	534.61	0	0	4438.83	1
~1	3	-8840.24	564.04	0	0	4423.12	1

Table S4.4.9. Comparison of generalised least-squares models to explain the tree cover (FPC) in the tropical Andes. *The caption to Table S4.4.8 describes the terms used in this table*.

Model	**k**	**AICc**	**ΔAICc**	**ModLL**	**wAICc**	**LL**	**CumWt**
~TE+P+W+F+CO2	8	-2129.62	0	1	1	1072.84	1
~TE+P+W+F	7	-2096.19	33.43	0	0	1055.11	1
~TE+P+W+CO2	7	-2071.27	58.35	0	0	1042.65	1
~TE+P+W	6	-2044.01	85.62	0	0	1028.02	1
~P+W+F+CO2	7	-1992.26	137.37	0	0	1003.15	1
~P+W+CO2	6	-1935.15	194.47	0	0	973.59	1
~P+W+F	6	-1934.43	195.19	0	0	973.23	1
~P+W	5	-1885.46	244.17	0	0	947.74	1
~TE+P+F+CO2	7	-1858.91	270.71	0	0	936.47	1
~P+F+CO2	6	-1818.03	311.59	0	0	915.03	1
~TE+P+F	6	-1817.53	312.09	0	0	914.78	1
~TE+P+co2	6	-1787.8	341.82	0	0	899.92	1
~P+F	5	-1761.97	367.65	0	0	886	1
~TE+P	5	-1753.62	376.01	0	0	881.82	1
~P+CO2	5	-1748.34	381.28	0	0	879.18	1
~TE+W+F+CO2	7	-1737.27	392.35	0	0	875.65	1
~TE+W+F	6	-1727.45	402.17	0	0	869.74	1
~TE+W+CO2	6	-1726.78	402.84	0	0	869.41	1
~P	4	-1700.85	428.78	0	0	854.43	1
~W+CO2	5	-1118.95	1010.68	0	0	564.48	1
~W+F+CO2	6	-1116.96	1012.66	0	0	564.49	1
~W	4	-1087.58	1042.05	0	0	547.8	1
~W+F	5	-1085.59	1044.03	0	0	547.81	1
~TE+F+CO2	6	-904.14	1225.49	0	0	458.08	1
~TE+CO2	5	-902.25	1227.38	0	0	456.13	1
~TE+CO2	5	-902.25	1227.38	0	0	456.13	1
~TE+F	5	-897.58	1232.04	0	0	453.8	1
~TE	4	-896.12	1233.51	0	0	452.06	1
~CO2	4	-420.51	1709.11	0	0	214.26	1
~F+CO2	5	-418.63	1711	0	0	214.32	1
~1	3	-395.27	1734.35	0	0	200.64	1
~F	4	-393.63	1735.99	0	0	200.82	1

Table S4.4.10. Comparison of generalised least-squares models to explain the tree cover (FPC) in the Amazon Basin. *The caption to Table S4.4.8 describes the terms used in this table.*

Model	k	AICc	ΔAICc	ModLL	wAICc	LL	CumWt
~TE+P+W+F+CO2	8	-9146.17	0	1	1	4581.09	1
~P+W+F+CO2	7	-9095.3	50.87	0	0	4554.66	1
~TE+P+F+CO2	7	-8690.77	455.4	0	0	4352.39	1
~TE+P+W+F	7	-8609.16	537.01	0	0	4311.58	1
~P+F+CO2	6	-8561.51	584.67	0	0	4286.76	1
~TE+P+F	6	-8322.36	823.81	0	0	4167.18	1
~TE+W+F+CO2	7	-8289.99	856.18	0	0	4152	1
~W+F+CO2	6	-8256.12	890.05	0	0	4134.06	1
~P+W+F	6	-8188.66	957.51	0	0	4100.34	1
~TE+P+W+CO2	7	-8019.8	1126.37	0	0	4016.91	1
~P+W+CO2	6	-7980.35	1165.82	0	0	3996.18	1
~P+F	5	-7819.87	1326.3	0	0	3914.94	1
~TE+W+F	6	-7819.67	1326.5	0	0	3915.84	1
~TE+F+CO2	6	-7549.91	1596.26	0	0	3780.96	1
~W+F	5	-7479.62	1666.55	0	0	3744.81	1
~TE+P+co2	6	-7472.01	1674.16	0	0	3742.01	1
~P+CO2	5	-7468.98	1677.19	0	0	3739.5	1
~F+CO2	5	-7422.87	1723.3	0	0	3716.44	1
~TE+W+CO2	6	-7335.77	1810.4	0	0	3673.89	1
~TE+P+W	6	-7328.05	1818.12	0	0	3670.03	1
~W+CO2	5	-7297.88	1848.29	0	0	3653.94	1
~TE+F	5	-7286.39	1859.78	0	0	3648.2	1
~P+W	5	-7283.76	1862.41	0	0	3646.88	1
~TE+P	5	-6979.5	2166.67	0	0	3494.75	1
~P	4	-6905.17	2241	0	0	3456.59	1
~F	4	-6849.15	2297.02	0	0	3428.58	1
~W	4	-6680.27	2465.9	0	0	3344.14	1
~CO2	4	-6502.22	2643.95	0	0	3255.11	1
~TE+CO2	5	-6501	2645.18	0	0	3255.5	1
~TE+CO2	5	-6501	2645.18	0	0	3255.5	1
~TE	4	-6125.12	3021.05	0	0	3066.56	1
~1	3	-6050.35	3095.82	0	0	3028.18	1

Table S4.4.11. Comparison of generalised least-squares models to explain the tree cover (FPC) in the Caribbean region*. The caption to Table S4.4.8 describes the terms used in this table.*

Model	k	AICc	∆AICc	ModLL	wAICc	LL	CumWt
~TE+P+W+F+CO2	8	-7096.53	0	1	1	3556.28	1
~TE+P+F+CO2	7	-6990.25	106.29	0	0	3502.13	1
~TE+P+W+CO2	7	-6866.6	229.94	0	0	3440.3	1
~TE+P+co2	6	-6601.26	495.27	0	0	3306.64	1
~P+W+F+CO2	7	-6523.64	572.9	0	0	3268.83	1
~P+F+CO2	6	-6347.09	749.45	0	0	3179.55	1
~P+W+CO2	6	-6290.71	805.82	0	0	3151.36	1
~TE+P+W+F	7	-5913.1	1183.43	0	0	2963.56	1
~P+CO2	5	-5911.83	1184.71	0	0	2960.92	1
~TE+P+F	6	-5736.65	1359.89	0	0	2874.33	1
~P+W+F	6	-5705.78	1390.75	0	0	2858.9	1
~TE+P+W	6	-5688.73	1407.81	0	0	2850.37	1
~P+F	5	-5480.88	1615.65	0	0	2745.45	1
~P+W	5	-5480.45	1616.08	0	0	2745.23	1
~TE+P	5	-5321.98	1774.56	0	0	2665.99	1
~P	4	-5038.65	2057.88	0	0	2523.33	1
~TE+W+F+CO2	7	-4696.05	2400.49	0	0	2355.03	1
~TE+W+CO2	6	-4675.49	2421.05	0	0	2343.75	1
~W+F+CO2	6	-4496.06	2600.48	0	0	2254.03	1
~W+CO2	5	-4469.83	2626.7	0	0	2239.92	1
~TE+W+F	6	-4063.06	3033.48	0	0	2037.53	1
~W+F	5	-4000.13	3096.41	0	0	2005.07	1
~W	4	-3963.03	3133.51	0	0	1985.52	1
~TE+F+CO2	6	-3602.63	3493.91	0	0	1807.32	1
~TE+CO2	5	-3411.82	3684.71	0	0	1710.92	1
~TE+CO2	5	-3411.82	3684.71	0	0	1710.92	1
~F+CO2	5	-3347.46	3749.08	0	0	1678.73	1
~CO2	4	-3138.48	3958.05	0	0	1573.24	1
~TE+F	5	-2940.55	4155.98	0	0	1475.28	1
~F	4	-2837.94	4258.6	0	0	1422.97	1
~TE	4	-2712.27	4384.26	0	0	1360.14	1
~1	3	-2601.36	4495.17	0	0	1303.68	1

***Table S4.4.12. Comparison of generalised least-squares models to explain the tree cover (FPC) in north-western South America**. The caption to Table S4.4.8 describes the terms used in this table.*

Model	**k**	**AICc**	**ΔAICc**	**ModLL**	**wAICc**	**LL**	**CumWt**
~TE+P+W+F+CO2	8	-9755.01	0	1	1	4885.51	1
~P+W+F+CO2	7	-9578.03	176.98	0	0	4796.02	1
~TE+P+F+CO2	7	-9420.2	334.81	0	0	4717.11	1
~TE+P+W+F	7	-9343.89	411.12	0	0	4678.95	1
~P+W+F	6	-9322.41	432.6	0	0	4667.21	1
~P+F+CO2	6	-9299.91	455.1	0	0	4655.96	1
~TE+P+F	6	-9170.17	584.84	0	0	4591.09	1
~P+F	5	-9149.69	605.32	0	0	4579.85	1
~TE+P+W+CO2	7	-8990.67	764.34	0	0	4502.34	1
~TE+P+W	6	-8485.13	1269.88	0	0	4248.57	1
~P+W+CO2	6	-8329.66	1425.35	0	0	4170.84	1
~TE+W+F+CO2	7	-8313.83	1441.18	0	0	4163.92	1
~TE+W+F	6	-8197.06	1557.95	0	0	4104.53	1
~P+W	5	-8182.85	1572.16	0	0	4096.43	1
~W+F+CO2	6	-8173.82	1581.19	0	0	4092.92	1
~W+F	5	-8136.49	1618.52	0	0	4073.25	1
~TE+P+co2	6	-8064.75	1690.26	0	0	4038.38	1
~TE+W+CO2	6	-7952.89	1802.12	0	0	3982.45	1
~TE+P	5	-7843.96	1911.05	0	0	3926.98	1
~TE+F+CO2	6	-7738.17	2016.84	0	0	3875.09	1
~TE+F	5	-7728.14	2026.87	0	0	3869.07	1
~F	4	-7662.47	2092.54	0	0	3835.24	1
~F+CO2	5	-7660.59	2094.42	0	0	3835.3	1
~W+CO2	5	-7511.49	2243.52	0	0	3760.75	1
~W	4	-7483.87	2271.14	0	0	3745.94	1
~P+CO2	5	-7414.38	2340.63	0	0	3712.2	1
~P	4	-7403.76	2351.25	0	0	3705.88	1
~TE+CO2	5	-6883.75	2871.26	0	0	3446.88	1
~TE+CO2	5	-6883.75	2871.26	0	0	3446.88	1
~TE	4	-6865.38	2889.63	0	0	3436.69	1
~CO2	4	-6454.1	3300.91	0	0	3231.05	1
~1	3	-6431.06	3323.95	0	0	3218.53	1

Table S4.4.13. Comparison of generalised least-squares models to explain the tree cover (FPC) in central South America*. The caption to Table S4.4.8 describes the terms used in this table.*

Model	k	AICc	∆AICc	ModLL	wAICc	LL	CumWt
~TE+P+W+F+CO2	8	-13142.93	0	1	0.54	6579.47	0.54
~TE+P+W+CO2	7	-13142.58	0.35	0.84	0.46	6578.3	1
~TE+P+W+F	7	-12327.98	814.94	0	0	6171	1
~TE+P+W	6	-12318.97	823.96	0	0	6165.49	1
~TE+W+F+CO2	7	-12271.37	871.56	0	0	6142.69	1
~TE+P+F+CO2	7	-12258.45	884.48	0	0	6136.23	1
~TE+P+co2	6	-12257.63	885.3	0	0	6134.82	1
~TE+W+CO2	6	-11991.8	1151.13	0	0	6001.9	1
~TE+P+F	6	-11900.92	1242.01	0	0	5956.47	1
~TE+P	5	-11899.53	1243.4	0	0	5954.77	1
~TE+W+F	6	-11746.78	1396.15	0	0	5879.39	1
~P+W+F+CO2	7	-11464.02	1678.91	0	0	5739.02	1
~P+W+CO2	6	-11460.45	1682.47	0	0	5736.23	1
~P+W	5	-11305.12	1837.81	0	0	5657.56	1
~P+W+F	6	-11303.12	1839.8	0	0	5657.57	1
~W+F+CO2	6	-11247.93	1895	0	0	5629.97	1
~W+CO2	5	-11189.89	1953.03	0	0	5599.95	1
~W+F	5	-11104.73	2038.2	0	0	5557.37	1
~W	4	-10998.79	2144.14	0	0	5503.4	1
~P+F+CO2	6	-10920.01	2222.92	0	0	5466.01	1
~P+CO2	5	-10916.44	2226.49	0	0	5463.22	1
~P	4	-10892.35	2250.58	0	0	5450.18	1
~P+F	5	-10891.96	2250.97	0	0	5450.98	1
~TE+F+CO2	6	-10484.6	2658.33	0	0	5248.3	1
~TE+F	5	-10472.71	2670.21	0	0	5241.36	1
~F	4	-10121.81	3021.12	0	0	5064.91	1
~F+CO2	5	-10120.84	3022.09	0	0	5065.42	1
~TE+CO2	5	-9744.22	3398.7	0	0	4877.11	1
~TE+CO2	5	-9744.22	3398.7	0	0	4877.11	1
~TE	4	-9738.05	3404.88	0	0	4873.03	1
~1	3	-9663.85	3479.08	0	0	4834.93	1
~CO2	4	-9662.16	3480.77	0	0	4835.08	1

Table S4.4.14. Comparison of generalised least-squares models to explain the tree cover (FPC) in the Mexican region*. The caption to Table S4.4.8 describes the terms used in this table.*

Model	k	AICc	ΔAICc	ModLL	wAICc	LL	CumWt
~TE+P+W+CO2	7	-8523.05	0	1	0.73	4268.54	0.73
~TE+P+W+F+CO2	8	-8521.05	2	0.37	0.27	4268.54	1
~TE+P+F+CO2	7	-8468.55	54.51	0	0	4241.29	1
~TE+P+co2	6	-8424.99	98.06	0	0	4218.5	1
~TE+P+W	6	-8163.71	359.35	0	0	4087.86	1
~TE+P+W+F	7	-8162.01	361.04	0	0	4088.02	1
~TE+P+F	6	-8121.18	401.88	0	0	4066.6	1
~TE+P	5	-8080.37	442.68	0	0	4045.19	1
~P+W+F+CO2	7	-7665.69	857.36	0	0	3839.86	1
~P+W+CO2	6	-7653.55	869.5	0	0	3832.78	1
~P+F+CO2	6	-7632.69	890.36	0	0	3822.35	1
~P+W+F	6	-7593.1	929.96	0	0	3802.56	1
~P+W	5	-7582.35	940.7	0	0	3796.18	1
~P+F	5	-7562.58	960.47	0	0	3786.3	1
~P+CO2	5	-7529.29	993.76	0	0	3769.65	1
~P	4	-7468.18	1054.87	0	0	3738.09	1
~TE+W+F+CO2	7	-7416.55	1106.51	0	0	3715.29	1
~TE+W+F	6	-7218.92	1304.14	0	0	3615.47	1
~TE+W+CO2	6	-7150.06	1373	0	0	3581.04	1
~W+F+CO2	6	-6915.75	1607.3	0	0	3463.88	1
~W+F	5	-6871.47	1651.59	0	0	3440.74	1
~W+CO2	5	-6796.83	1726.23	0	0	3403.42	1
~W	4	-6755.46	1767.59	0	0	3381.73	1
~TE+F+CO2	6	-6167.5	2355.55	0	0	3089.76	1
~TE+CO2	5	-6156.25	2366.8	0	0	3083.13	1
~TE+CO2	5	-6156.25	2366.8	0	0	3083.13	1
~TE+F	5	-6101.94	2421.12	0	0	3055.97	1
~TE	4	-6090.01	2433.04	0	0	3049.01	1
~F+CO2	5	-5945.32	2577.73	0	0	2977.67	1
~F	4	-5932.51	2590.54	0	0	2970.26	1
~CO2	4	-5910.7	2612.35	0	0	2959.35	1
~1	3	-5899.55	2623.51	0	0	2952.78	1

Appendix S4.5. Palaeo-vegetation records used for comparison with simulated tree cover (FPC).

Table S4.5.15. List of palaeo-vegetation records covering the post-Last Glacial Maximum. *Most records were derived from the Latin America Pollen Database (Flantua et al., 2015).*

Region	Site name	Latitude	Longitude	environment	proxie_list	Reference
Patagonia	Haberton	-54.90	-67.17	wetland	pollen, charcoal, plant macrofossils	Markgraf and Huber, 2010
Patagonia	Paso Garibaldi	-54.72	-67.17	wetland	pollen, charcoal, plant macrofossils	Markgraf and Huber, 2010
Patagonia	Lake Ballena	-53.66	-72.42	lake	pollen	Fontana and Bennett, 2012
Patagonia	La Correntina	-54.55	-66.98	wetland	pollen	Musotto et al., 2017
Patagonia	Terra Australis	-54.60	-67.77	wetland	pollen	Musotto et al., 2017
Patagonia	Rio Rubens	-52.08	-71.52	wetland	pollen, charcoal, plant macrofossils	Markgraf and Huber, 2010
Patagonia	Cerro Benítez	-51.55	-72.58	wetland	pollen	McCulloch et al., 2021
Patagonia	Cueva del Mylodon	-51.56	-72.62	coprolite sequence in cave	pollen	Moore, 1978; Heusser et al., 1994
Patagonia	Meseta Latorre 1-2	-51.52	-72.05	wetland	pollen	Mancini et al., 2005; Schäbitz, 1991
Patagonia	Lago Guanaco	-50.83	-73.17	lake	pollen	Moreno et al., 2009
Patagonia	Cerro Frías	-50.43	-72.72	wetland	pollen	Mancini et al., 2005
Patagonia	Chorrillo Malo 2	-50.50	-72.07	archaeological sequence	pollen	Mancini et al., 2005
Patagonia	Cerro Verlika 1	-50.60	-72.28	archaeological sequence	pollen	Mancini et al., 2005
Patagonia	Cueva Las Buitreras	-51.12	-70.27	archaeological sequence	pollen	Mancini et al., 2005
Patagonia	Lago Los Niños	-44.02	-71.48	lake	pollen	Iglesias et al., 2016
Patagonia	Laguna La Pava	-44.47	-71.52	lake	pollen	Iglesias et al., 2016
Patagonia	Lake Shaman	-44.43	-71.18	lake	pollen	de Porras et al., 2012
Patagonia	Mallín Fontanito	-45.52	-71.97	lake	pollen, charcoal	Nanavati et al., 2019
Patagonia	Mallín Pollux	-45.69	-71.84	lake	pollen	Markgraf et al., 2007
Patagonia	Lago Augusta	-47.08	-72.38	lake	pollen	Villa-Martínez et al., 2012
Patagonia	Mallín Aguado	-40.00	-71.48	wetland	pollen	Iglesias et al., 2014
Patagonia	Laguna El Trebol	-41.12	-71.82	lake	Pollen, plant macrofossils, charcoal, magnetic susceptibility	Iglesias et al., 2014
Patagonia	Lago Moreno (Morenito)	-41.05	-71.52	lake	pollen	Mancini et al., 2005
Patagonia	Lago Mascardi	-41.13	-71.57	lake	Pollen, chironomids, isotopes	Iglesias et al., 2014
Patagonia	Laguna Padre Laguna	-41.36	-71.51	lake	pollen, charcoal	Iglesias et al., 2014
Patagonia	Mallin Book	-41.33	-71.58	wetland	pollen	Mancini et al., 2005; Markgraf, 1983

Patagonia	Huala Hué	-41.51	-71.51	lake	pollen, charcoal	Iglesias et al., 2014
Patagonia	Lago Cóndor	-42.58	-71.48	lake	pollen, charcoal	Iglesias et al., 2014
Patagonia	Lago Mosquito	-42.82	-71.65	lake	pollen	Iglesias et al., 2014
Patagonia	Mallín Serrucho	-42.27	-71.70	lake	pollen	Iglesias et al., 2014
Patagonia	La Zeta	-43.48	-71.58	lake	pollen	Iglesias et al., 2014
Patagonia	Lago Theobald	-43.80	-71.97	lake	pollen	Iglesias et al., 2014
Patagonia	Lago Lepué	-42.80	-73.71	lake	pollen, charcoal	Pesce and Moreno, 2014
Patagonia	Lago Pichilaguna	-41.27	-73.06	lake	Pollen	Moreno et al., 2018
Patagonia	Primavera	-40.07	-71.18	animal middens	pollen	Mancini et al., 2005; Markgraf et al., 1997
Patagonia	Lago Escondido	-41.08	-72.57	lake	pollen	Iglesias et al., 2014
Patagonia	Lago Mascardi-Gutierrez	-41.33	-71.05	wetland	pollen	Mancini et al., 2005; Markgraf, 1983
Patagonia	Epullán Grande	-40.38	-70.20	archaeological sequence	pollen	Mancini et al., 2005
Patagonia	Laguna Cari Laufquén Chica	-41.22	-69.42	lake	pollen	Mancini et al., 2005
Patagonia	Campo Moncada 2	-42.05	-69.05	archaeological sequence	pollen	Mancini et al., 2005
Patagonia	Salina 2	-32.08	-69.03	wetland	pollen	Mancini et al., 2005; Markgraf, 1983
Patagonia	Agua de la Cueva	-32.63	-69.17	archaeological sequence	pollen	Mancini et al., 2005
Patagonia	La Estacada	-33.05	-69.00	alluvial sequence	pollen	Mancini et al., 2005
Patagonia	Gruta del Indio	-34.75	-68.37	cave	pollen	Mancini et al., 2005
Patagonia	Salado	-35.03	-69.75	wetland	pollen	Mancini et al., 2005; Markgraf, 1983
Patagonia	Vaca Lauquén	-36.08	-71.08	wetland	pollen	Mancini et al., 2005
Patagonia	Alero Cárdenas	-47.30	-70.43	archaeological sequence	pollen	Mancini et al., 2005
Patagonia	Los Toldos	-47.37	-68.97	archaeological sequence	pollen	Mancini et al., 2005
Patagonia	Parque Nacional Perito Moreno	-47.88	-72.85	archaeological sequence	pollen	Mancini et al., 2005
Patagonia	La Martita cave 4	-48.40	-69.25	archaeological sequence	pollen	Mancini et al., 2005
Central South America	Laguna Formosa	-31.81	-54.48	lake	pollen	Mourelle et al., 2017; Barberi et al., 2000
Central South America	Rio Santa Lucia	-34.21	-55.60	alluvial sequence	pollen	de Oliveira et al., 2011
Central South America	Empalme Querandies	-37.00	-60.12	alluvial sequence	pollen	Prieto, 2000
Central South America	Cerro La China	-37.95	-58.62	loess sequence	pollen	Prieto, 2000
Central South America	La Horqueta II	-38.30	-58.82	alluvial sequence	pollen	Prieto, 2000
Central South America	Arroyo Las Brusquitas	-38.23	-58.86	estuarine	pollen	Mancini et al., 2005

Central South America	Laguna Hinojales	-37.56	-57.45	lake	pollen	Mancini et al., 2005
Central South America	La Lagunita, Mar Chiquita	-37.71	-57.35	coastal lagoon	pollen	Mancini et al., 2005
Central South America	Arroyo La Ballenera	-38.32	-57.95	estuarine	pollen	Mancini et al., 2005
Central South America	Fortín Necochea	-37.38	-61.13	archaeological sequence	pollen	Mancini et al., 2005
Central South America	Sauce Grande	-38.48	-61.78	alluvial sequence	pollen	Prieto, 2000
Central South America	Naposta Grande	-38.35	-62.33	alluvial sequence	pollen	Prieto, 2000
Central South America	Arroyo Sauce Chico	-38.08	-62.27	alluvial sequence	pollen	Mancini et al., 2005
Central South America	Salinas Chicas 1	-38.73	-62.93	lake	pollen	Mancini et al., 2005
Central South America	Salinas Chicas 4	-38.75	-62.92	lake	pollen	Mancini et al., 2005
Central South America	Napostá Grande Profile III	-38.77	-62.25	estuarine	pollen	Mancini et al., 2005
Central South America	Salina Anzoátegui	-39.00	-63.77	lake	pollen	Mancini et al., 2005
Central South America	Salina Gualicho 1	-40.43	-65.18	lake	pollen	Mancini et al., 2005
Central South America	Salina Gualicho 2	-40.40	-65.18	lake	pollen	Mancini et al., 2005
Central South America	Laguna Indio Muerto	-40.42	-66.07	lake	pollen	Mancini et al., 2005
Central South America	Salina Piedra	-40.58	-62.07	lake	pollen	Mancini et al., 2005
Central South America	Salina Inglés	-40.68	-62.05	lake	pollen	Mancini et al., 2005
Central South America	Cambara do Sul	-29.05	-50.10	wetland	pollen	Ledru et al., 2016
Central South America	São Francisco de Paula	-29.40	-50.57	wetland	pollen	Ledru et al., 2016
Central South America	São Francisco de Assis	-29.59	-55.22	wetland	pollen	Ledru et al., 2016
Central South America	Laguna La Gaiba	-17.75	-57.58	lake	Pollen, Diatoms	Whitney et al.,2011
North-eastern South America	Serra dos Órgãos	-22.46	-43.03	wetland	pollen	Ledru et al., 2016
North-eastern South America	Serra da Bocaina	-22.74	-44.56	wetland	pollen	Ledru et al., 2016
North-eastern South America	Morro de Itapeva	-22.78	-45.53	wetland	pollen	Ledru et al., 2016
North-eastern South America	Jacareí	-23.28	-45.97	wetland	pollen	Ledru et al., 2016
North-eastern South America	Colônia	-23.87	-46.71	wetland	pollen	Ledru et al., 2016
North-eastern South America	Curucutu	-23.93	-46.65	wetland	pollen	Ledru et al., 2016
North-eastern South America	Serra Campos Gerais	-24.53	-50.22	wetland	pollen	Ledru et al., 2016

North-eastern South America	Lagoa Grande	-24.53	-48.66	lake	pollen	Ledru et al., 2016
North-eastern South America	Araçatuba	-25.92	-48.98	wetland	pollen	Ledru et al., 2016
North-eastern South America	Volta Velha	-26.07	-48.63	sedimentary basin	pollen	Ledru et al., 2016
North-eastern South America	Serra do Tabuleiro	-27.90	-48.88	wetland	pollen	Ledru et al., 2016
North-eastern South America	Brejo do Louro	-19.11	-40.03	wetland	palynological, carbon and nitrogen elemental and isotopic analyses	Francisquini et al., 2020
North-eastern South America	Saquinho	-10.40	-43.22	wetland	pollen	Ledru et al., 2016
North-eastern South America	Chapada dos Veadeiros	-14.00	-47.56	lake	pollen	Ledru et al., 2016
North-eastern South America	Fazenda Urbano	-17.41	-45.06	wetland	pollen	Ledru et al., 2016
North-eastern South America	Vereda Laçador	-17.82	-45.44	wetland	pollen	Ledru et al., 2016; Cassino et al 2018
North-eastern South America	São José	-17.08	-45.11	wetland	pollen	Cassino et al., 2018
North-eastern South America	Lago do Pires	-17.95	-42.22	lake	pollen	Ledru et al., 2016
North-eastern South America	Salitre	-19.00	-46.77	wetland	pollen	Ledru et al., 2016
North-eastern South America	Lagoa Santa	-19.63	-43.90	lake	pollen	Ledru et al., 2016
North-eastern South America	Primeiro Rancho	-20.41	-41.83	wetland	pollen	Ledru et al., 2016
North-eastern South America	Crominia	-17.28	-49.40	wetland	pollen	Ledru et al., 2016
North-eastern South America	Lagoa Feia	-15.57	-47.30	lake	pollen	Ledru et al., 2016
North-eastern South America	Aguas Emendadas VAE2	-15.57	-47.58	wetland	Palynomorphs, charcoal	Cassino et al., 2020
North-eastern South America	Aguas Emendadas VAEI	-15.57	-47.58	wetland	Pollen, charcoal	Cassino et al., 2020; Barberi et al., 2000
North-eastern South America	Carajas CSS 10	-6.58	-49.50	lake	Pollen, TOM	Sifeddine et al., 2001
North-eastern South America	Carajas CSS 2	-6.58	-49.50	lake	Pollen, TOM	Sifeddine et al., 2001
North-eastern South America	Serra dos Carajas	-6.33	-50.42	lake	pollen	Absy et al.,1991
North-eastern South America	Pantano da Mauritia	-6.35	-50.39	wetland	pollen	Ledru et al., 2016
North-eastern South America	Lagoa da Curuça Core A	-0.77	-47.85	lake	Pollen, charcoal	Ledru et al., 2016
North-eastern South America	Lagoa da Curuça Core B	-0.77	-47.85	lake	Pollen, charcoal	Ledru et al., 2016; Behling, 1996; Behling ,1998; Behling, 2001
North-eastern South America	Rio Curua	-1.74	-47.85	alluvial sequence	Pollen, Charcoal, XRD	Ledru et al., 2016; Behling, 2001
North-eastern South America	Lagoa do Caço MA97-1	-2.97	-43.42	lake	Pollen, Lithology	Ledru et al., 2016

North-eastern South America	Lake Caco MA98-4	-2.87	-45.92	lake	Pollen, C Isotopes, Algae	Ledru et al., 2016
North-eastern South America	Lake Caco MA98-5	-2.87	-45.92	lake	Pollen, C Isotopes	Ledru et al., 2016
North-eastern South America	Serra de Maranguape	-3.89	-38.72	forest hollow	Pollen	Ledru et al., 2016
Amazon Basin	Katira - Rondonia	-9.00	-63.00	lake	Pollen, Isotopes C13	Van der Hammen and Absy, 1994
Amazon Basin	Paraíso Cave	-4.07	-55.45	cave	speleothem δ18O	Wang et al., 2017
Amazon Basin	Lagoa (da) Pata I (Lake Pata)	0.27	-66.68	lake	pollen	Colinvaux et al., 1996; Bush et al., 2004
Amazon Basin	Lagoa (da) Pata II (Lake Pata)	0.27	-66.68	lake	pollen	D'Apolito et al.,2013
Tropical Andes	Campo Libre	-0.45	-77.86	alluvial sequence	phytoliths	McMichael et al., 2021
Tropical Andes	Laguna Pindo	-1.45	-78.08	lake	pollen	Montoya et al., 2018
Tropical Andes	Lake Consuelo-CON1	-13.95	-68.99	lake	Pollen, Lithostratigraphy, LOI	Bush et al.,2004; Urrego et al.,2005; Urrego et al.,2010
Tropical Andes	Lake Consuelo-CON2	-13.95	-69.00	lake	Pollen	Urrego et al.,2010
Tropical Andes	Laguna Chorreras	-2.77	-79.16	lake	pollen, charcoal	Hansen et al.,2003; Rodbell et al.,2002
Tropical Andes	Laguna Pallcacocha 1	-4.77	-79.23	lake	Pollen, magnetic susp., organic content	Rodbell et al.,1999
Tropical Andes	Laguna Pallcacocha 2	-4.77	-79.23	lake	Pollen, charcoal	Hansen et al.,2003
Caribbean region	Laguna El Pinal	4.13	-70.38	lake	pollen	Behling and Hooghiemstra ,1999
Caribbean region	Laguna Carimagua	4.07	-70.23	lake	pollen	Behling and Hooghiemstra ,1999
Caribbean region	Laguna Angel	4.47	-70.57	lake	pollen	Behling and Hooghiemstra ,1999
Caribbean region	Laguna Sardinas	4.97	-69.47	lake	pollen	Behling and Hooghiemstra ,1999
Caribbean region	Lake Quexil	17.00	-89.67	lake	pollen	Leyden et al., 1993
Caribbean region	Laguna de los Anteojos	8.54	-71.07	lake	pollen	Rull et al., 2015
Caribbean region	Lake Valencia 1-14-77	10.27	-67.75	lake	pollen	Leyden, 1985
Caribbean region	Lake Valencia 76V 7-11	10.18	-67.01	lake	pollen	Leyden,1985
Caribbean region	Lake Valencia 76V 1-5	10.18	-67.01	lake	pollen	Leyden,1985
Mexican region	Lake Pátzcuaro	19.55	-101.39	lake	pollen	Metcalfe et al., 2006
Mexican region	Lake Cuitzeo	20.00	-101.00	lake	pollen	Metcalfe et al., 2006
Mexican region	Sierra Cataviña	29.70	-114.70	animal middens	plant macrofossil	Metcalfe et al., 2006
Mexican region	San Fernando	30.50	-115.70	animal middens	plant macrofossil	Metcalfe et al., 2006

Mexican region	Tinajas Mountains	32.30	-114.00	animal middens	plant macrofossil	Metcalfe et al., 2006
Mexican region	Sierra San Francisco	27.70	-113.20	animal middens	plant macrofossil	Metcalfe et al., 2006
Mexican region	Laguna Seca San Felipe	31.00	-114.80	lake	pollen	Metcalfe et al., 2006
Mexican region	Hornaday Mountains	31.59	-113.36	animal middens	plant macrofossil	Metcalfe et al., 2006
Mexican region	Sierra de La Misericordia	25.54	-103.40	animal middens	plant macrofossil	Metcalfe et al., 2006
Mexican region	Puerto de La Ventanillas	26.02	-102.44	animal middens	plant macrofossil	Metcalfe et al., 2006
Mexican region	Cañon de La Fragua	26.39	-102.10	animal middens	plant macrofossil	Metcalfe et al., 2006
Mexican region	Lake Babicora	29.00	-108.00	lake	pollen	Metcalfe et al., 2006
Mexican region	Playas Valley	31.50	-108.50	animal middens	plant macrofossil	Metcalfe et al., 2006
Mexican region	Hueco Mountains	32.00	-106.00	animal middens	plant macrofossil	Metcalfe et al., 2006

APPENDIX S6

Chapter 6 – Climate-induced vegetation changes alone do not explain Late Pleistocene megafauna extinctions in the Southern Cone

The following Supporting Information is available for this chapter:

Appendix S6.1.

Table S6.1.1. Unreliable ^{14}C age estimates (direct AMS and conventional radiocarbon ages with pre-treatment information) on megafauna remains (bones, teeth, excrements) of felids, ground sloths, gomphotheres, horses, camelids, canids, bears, rheids, macrauquenids, armadillo and indeterminate megafauna from archaeological and palaeontological sites of Southern Patagonia, the Northern slopes of the Patagonian Andes and the Pampas regions (Southern Cone). *Age measurement by Accelerator Mass Spectrometry (AMS), by conventional spectrometry (conv.) and Liquid Scitillation Counting (LSC). Pre-treatment methods with codes: ultrafiltration (code UF), XAD-2 resin (XAD), acid-base-acid (ABA, code AG) and ion exchange gelatin (code AI). Pre-treatments of ages including preparation codes in parenthesis was verified in OxCal/ORAU database; codes are described in Brock et al. (2010). Some pre-treatment methods were completed via personal communication with AA and GrA dating laboratories. All age estimates are collected non calibrated and then calibrated with Southern Hemisphere SHcal20 curve (Hogg et al., 2020) at 1 sigma (68.2% probability), calibrated with the OxCal 4.4 program (Bronk Ramsey, 2021): mu = mean, sigma = uncertainty. NR = not reported.*

Sites	Latitude (°S)	Longitude (°W)	Family	Taxa	Lab-code	Material	Measure	Pre-treatment	^{14}C age BP	error	^{14}C age calBP (mu)	error (1σ)	References
Southern Patagonia													
Tres Arroyos	-53,38300	-68,78330	Felidae (felid)	*Panthera onca mesembrina*	OxA-9248	bone	AMS	ABA (code AG)	11085	70	12991	77	Borrero 2003, Massone & Prieto 2004, Steele & Politis 2009, Prevosti & Martin 2013
			Equidae (horses)	*Hippidion saldiasi*	Beta-123152	bone	AMS	NR	12540	70	14800	208	Borrero 2003, Massone 2004, Paunero et al. 2008, Labarca 2015
			Camelidae (camelids)	*Vicugna vicugna (Lama gracilis)*	OxA-9246	bone	AMS	ABA (code AG)	10630	70	12632	78	Steele & Politis 2009
			Canidae (canids)	*Dusicyon avus*	OxA-9245	tooth	AMS	ABA (code AG)	10575	65	12587	94	Borrero 2003, Steele & Politis 2009
Cueva del Puma	-52,09400	-69,73300	Ursidae (bears)	*Arctotherium tarijense*	Ua-21033	bone/tooth	NR	NR	10345	75	12203	179	Martin et al. 2004, Labarca 2015
Cueva de Los Chingues	-52,09361	-69,74194	Mylodontidea (ground sloths)	*Mylodon darwini*	Ua-32861	bone	conv.	NR	12165	80	14084	170	Martín 2008, Labarca 2015
			Equidae (horses)	*Hippidion saldiasi*	Beta-147744	bone	NR	NR	11210	50	13130	39	Labarca 2015
			Equidae (horses)	*Hippidion saldiasi*	Ua-24685	NR	NR	NR	11990	90	13880	114	Martin 2008, Labarca 2015
			Camelidae (camelids)	*Camelidae*	GX-32664	bone	NR	NR	10890	60	12820	59	Prevosti & Martin 2013
			Ursidae (bears)	*Arctotherium* sp.	GX-32665	bone/tooth	NR	NR	11360	70	13245	70	Prevosti & Martin 2013, Metcalf et al. 2016
			Canidae (canids)	*Dusicyon avus*	GX-32663	bone	NR	NR	10490	80	12417	180	Prevosti & Martin 2013
			Rheidae (rheids)	*Rheidae*	Ua-24684	bone	NR	NR	10165	70	11784	166	Prevosti & Martin 2013
Cueva Fell	-52,02981	-69,98463	Mylodontidea (ground sloths)	*Mylodontidae*	Beta-284446	bone	conv.	NR	10340	50	12199	158	Borrero and Martin 2012
			Mylodontidea (ground sloths)	*Mylodon darwini*	Ua-34249	NR	NR	NR	10295	65	12122	184	Martín 2008, Labarca 2015
Pozo consuelo	-51,59976	-72,65227	Mylodontidea (ground sloths)	*Mylodon darwini*	SD (no detail)	bone	NR	NR	12125	85	14010	146	Stern 2011, Labarca 2015
Cueva del Medio	-51,58333	-72,63300	Felidae (felid)	*Smilodon populator*	Ua-37622	bone	NR	NR	11100	80	12999	84	Prieto et al. 2010
			Mylodontidea (ground sloths)	*Mylodon darwini*	NUTA-2341	bone	AMS	base-acid washes	12720	300	15058	512	Nami & Nakamura 1995, Labarca 2015
			Equidae (horses)	*Hippidion saldiasi*	Beta-58105	bone	conv.	NR	10350	130	12188	248	Nami & Nakamura 1995, Labarca 2015
			Equidae (horses)	*Hippidion saldiasi*	NUTA-1811	bone/tooth	AMS	base-acid washes	10710	100	12677	98	Nami & Nakamura 1995, Metcalf et al. 2016
			Equidae (horses)	*hippidion saldiasi*	NUTA-2331	bone	AMS	base-acid washes	10860	160	12840	152	Nami & Nakamura 1995, Metcalf et al. 2016
			Equidae (horses)	*Hippidion saldiasi*	A-7341 (AA-12578)	bone	NR	pretreatment by user (unknown)[2]	11570	100	13433	101	Martinic 1996, Labarca 2015
			Equidae (horses)	*Hippidion saldiasi*	A-7240 (AA-12577)	bone	NR	pretreatment by user (unknown)[2]	11990	100	13877	124	Martinic 1996, Labarca 2015
			Camelidae (camelids)	*Lama* cf. *owenii*	NUTA-2197	bone	AMS	base-acid washes	11040	250	12978	232	Nami & Nakamura 1995
			Camelidae (camelids)	*Lama* cf. *owenii*	NUTA-1734	bone	AMS	base-acid washes	10430	100	12305	199	Nami & Nakamura 1995
			Camelidae (camelids)	*Lama* cf. *owenii*	NUTA-1737	bone	AMS	base-acid washes	11120	130	13016	124	Nami & Nakamura 1995
Cueva Chica	-51,57331	-72,58603	Mylodontidea (ground sloths)	*Mylodon darwini*	Beta-288227	bone	NR	NR	10780	50	12743	26	Martin et al. 2013
			Mylodontidea (ground sloths)	*Mylodon darwini*	Beta-284437	bone	NR	NR	13970	70	16979	124	Martin et al. 2013
			Mylodontidea (ground sloths)	*Mylodon darwini*	Beta-288230	bone	NR	NR	14240	60	17280	108	Martin et al. 2013
			Camelidae (camelids)	*Vicugna vicugna (Lama gracilis)*	Beta-288231	bone	NR	NR	14870	70	18180	89	Martin et al. 2013
Cueva del Milodon	-51,56500	-72,62028	Mylodontidea (ground sloths)	*Mylodon* sp.	BM-1210B	excrement	conv.	NR	12308	288	14489	456	Saxon 1979, Burleigh & Matthews 1982, Markgraf 1985, Tonni et al. 2003a
			Mylodontidea (ground sloths)	*Mylodon* sp.	Beta-164895	bone	conv.	NR	13630	50	16464	91	Martin 2010, Borrero & Martin 2012
			Mylodontidea (ground sloths)	*Mylodon* sp.	LP-49	bone	conv.	NR	10377	481	12061	630	Tonni et al. 2003a
			Mylodontidea (ground sloths)	*Mylodon* sp.	A-1391	leather	conv.	NR	10400	330	12126	459	Long & Martin 1974, Tonni et al. 2003a
			Mylodontidea (ground sloths)	*Mylodon* sp.	GX-6248	excrement	conv.	NR	10575	400	12308	525	Markgraf 1985, Tonni et al. 2003a
			Mylodontidea (ground sloths)	*Mylodon* sp.	C-484	excrement	conv.	NR	10832	400	12644	510	Arnold & Libby 1951, Markgraf 1985, Tonni et al. 2003a
			Mylodontidea (ground sloths)	*Mylodon* sp.	GX-6243	excrement	conv.	NR	10880	300	12769	362	Markgraf 1985, Tonni et al. 2003a
			Mylodontidea (ground sloths)	*Mylodon* sp.	LP-255	excrement	conv.	NR	11330	140	13232	130	Borrero et al. 1991, Tonni et al. 2003a
			Mylodontidea (ground sloths)	*Mylodon* sp.	GX-6246	excrement	conv.	NR	11775	480	13936	653	Markgraf 1985, Tonni et al. 2003a
			Mylodontidea (ground sloths)	*Mylodon* sp.	BM-1210	excrement	conv.	NR	11810	229	13739	290	Saxon 1979, Burleigh & Matthews 1982, Markgraf 1985, Tonni et al. 2003a
			Mylodontidea (ground sloths)	*Mylodon* sp.	GX-6247	excrement	conv.	NR	11905	335	13979	485	Markgraf 1985, Tonni et al. 2003a
			Mylodontidea (ground sloths)	*Mylodon* sp.	GX-6244	excrement	conv.	NR	12020	460	14228	647	Markgraf 1985, Tonni et al. 2003a
			Mylodontidea (ground sloths)	*Mylodon* sp.	A-2447	excrement	conv.	NR	12240	150	14335	307	Markgraf 1985, Tonni et al. 2003a
			Mylodontidea (ground sloths)	*Mylodon* sp.	A-2445	excrement	conv.	NR	12270	350	14469	528	Markgraf 1985, Tonni et al. 2003a
			Mylodontidea (ground sloths)	*Mylodon* sp.	GX-6245	excrement	conv.	NR	12285	480	14559	689	Markgraf 1985, Tonni et al. 2003a
			Mylodontidea (ground sloths)	*Mylodon* sp.	BM-1209	excrement	conv.	NR	12496	148	14688	297	Saxon 1979, Burleigh & Matthews 1982, Markgraf 1985, Tonni et al. 2003a
			Mylodontidea (ground sloths)	*Mylodon* sp.	BM-1375	excrement	conv.	NR	12552	128	14780	282	Saxon 1979, Burleigh & Matthews 1982, Markgraf 1985, Tonni et al. 2003a
			Mylodontidea (ground sloths)	*Mylodon* sp.	LP-257	excrement	conv.	NR	12570	160	14805	323	Borrero et al. 1991, Tonni et al. 2003a
			Mylodontidea (ground sloths)	*Mylodon* sp.	A-2448	excrement	conv.	NR	12870	100	15390	149	Markgraf 1985, Tonni et al. 2003a

Sites	Latitude (°S)	Longitude (°W)	Family	Taxa	Lab-code	Material	Measure	Pre-treatment	^{14}C age BP	error	^{14}C age calBP (mu)	error (1σ)	References
Cueva del Milodon *(continued)*	-51,56500	-72,62028	Mylodontidea (ground sloths)	*Mylodon darwini*	BM-728	bone	conv.	NR	12984	76	15530	126	Burleigh et al. 1977, Tonni et al. 2003a
			Mylodontidea (ground sloths)	*Mylodon darwini*	W-2998	leather	conv.	NR	13040	300	15612	482	Martinic 1996
			Mylodontidea (ground sloths)	*Mylodon darwini*	BM-1208	bone	conv.	ABA	13183	202	15836	298	Burleigh & Matthews 1982, Tonni et al. 2003a
			Mylodontidea (ground sloths)	*Mylodon darwini*	LU-794	bone	conv.	ABA	13260	115	15939	171	Håkansson 1976, Tonni et al. 2003a
			Mylodontidea (ground sloths)	*Mylodon* sp.	A-2446	excrement	conv.	NR	13470	180	16253	277	Markgraf 1985, Tonni et al. 2003a
			Mylodontidea (ground sloths)	*Mylodon darwini*	Beta-164896	bone	conv.	NR	13490	40	16261	76	Martin 2010, Borrero & Martin 2012
			Mylodontidea (ground sloths)	*Mylodon darwini*	NZ-1680	leather	conv.	NR	13500	470	16319	695	Tonni et al. 2003a
			Mylodontidea (ground sloths)	*Mylodon darwini*	A-1390	excrement	conv.	NR	13560	190	16391	292	Long & Martin 1974, Tonni et al. 2003a
			Mylodontidea (ground sloths)	*Mylodon* sp.	LP-34	excrement	conv.	NR	10812	325	12656	416	Tonni et al. 2003a
			Mylodontidea (ground sloths)	*Mylodon* sp.	LP-3671	bone	LSC	acid wash	11370	90	13258	82	Pérez et al. 2021
			Mylodontidea (ground sloths)	*Mylodon* sp.	AA-112450	skin	AMS	AAA & soxhlet	13263	42	15927	82	Pérez et al. 2021
			Mylodontidea (ground sloths)	*Mylodon* sp.	GrM-21338	excrement	AMS	NR	13140	55	15724	202	van Geel et al. 2022
			Equidae (horses)	*Hippidion saldiasi*	GrA-510	bone (and hair?)	AMS	NR[3]	11480	60	13357	67	Alberdi & Prado 2004, Paunero et al. 2008
			Ursidae (bears)	*Arctotherium* sp.	WK-20234	bone/tooth	NR	NR	13257	147	15937	216	Metcalf et al. 2016
Cueva Lago Sofia 1	-51,54065	-72,58692	Mylodontidea (ground sloths)	*Mylodon darwini*	GX-31641	NR	NR	NR	9700	100	11030	160	Martín 2008, Labarca 2015
			Mylodontidea (ground sloths)	*Mylodon darwini*	OxA-9506	bone/tooth	AMS	ABA (code AG)	12250	110	14320	261	Steele & Politis 2009, Metcalf et al. 2016
			Mylodontidea (ground sloths)	*Mylodon darwini*	PITT-0939	bone	conv.	NR	12990	490	15519	777	Prieto Iglesias et al. 1991, Labarca 2015
			Equidae (horses)	*Hippidion* sp.	OxA-9504	bone	AMS	ABA (code AG)	10310	160	12105	305	Borrero 2008, Steele & Politis 2009, Barnosky & Lindsey 2010
Cueva Lago Sofia 2	-51,54065	-72,58692	Camelidae (camelids)	*Lama guanicoe* (?)	OxA-8635	bone	AMS	ABA (code AG)	10710	70	12692	56	Steele & Politis 2009
Cueva Lago Sofia 3	-51,54065	-72,58692	Canidae (canids)	*Pseudolopex culpaeus*	OxA-9505	bone	AMS	ABA (code AG)	10140	120	11759	267	Steele & Politis 2009
Cueva Lago Sofia 4	-51,54065	-72,58692	Mylodontidea (ground sloths)	*Mylodon darwini*	PITT-0940	bone	conv.	NR	11590	100	13452	104	Borrero et al. 1997, Labarca 2015
			Mylodontidea (ground sloths)	*Mylodon darwini*	AA-11498	bone	conv.	pretreatment by user (unknown)[2]	13400	90	16129	140	Borrero et al. 1997, Labarca 2015
			Camelidae (camelids)	*Vicugna vicugna (Lama gracilis)*	OxA-20708	bone/tooth	AMS	ABA (code AG)	13270	65	15943	109	Metcalf et al. 2016
SA Patagonia	-51,40000	-72,50000	Mylodontidea (ground sloths)	*Mylodon* sp.	NSRL-3341	bone	NR	NR	11050	60	12971	74	Borrero 1999, Barnosky & Lindsey 2010
Aleros Dos Herradura	-51,40000	-72,60000	Mylodontidea (ground sloths)	*Mylodon* sp.	LP-421	bone	conv.	NR	11380	150	13276	137	Martinic 1996, Dubois & Borrero 1997
			Mylodontidea (ground sloths)	*Mylodon darwini*	AA-12574	bone	AMS	pretreatment by user (unknown)[2]	12825	110	15329	168	Borrero & Martin 1994, Dubois & Borrero 1997, Labarca 2015
Cueva Túnel	-48,45750	-68,87200	Equidae (horses)	*Hippidion saldiasi*	AA-71148	bone	AMS	ABA[2]	10400	100	12267	199	Paunero et al. 2005, Paunero et al. 2017
Cerro Bombero	-48,14900	-68,93300	Equidae (horses)	*Hippidion saldiasi*	LP-1528	bone	LSC	NR	8850	80	9930	155	Paunero et al. 2008
Piedra Museo	-47,90000	-67,90000	Equidae (horses)	*Hippidion* sp.	OxA-8528	bone	AMS	ABA (code AG)	10925	65	12855	77	Alberdi et al. 2001, Barnosky & Lindsey 2010
			Camelidae (camelids)	*Lama guanicoe*	OxA-8527	bone	AMS	ABA (code AG)	10390	70	12261	168	Steele & Politis 2009
			Camelidae (camelids)	*Lama* sp.	OxA-9507	bone	AMS	ABA (code AG)	10100	110	11668	225	Steele & Politis 2009
			Camelidae (camelids)	*Camelidae*	AA-8428	bone	AMS	pretreatment by user (unknown)[2]	10400	80	12272	178	Borrero 1999
Casa de Piedra 7	-47,88333	-72,08333	indeterminate	Megafauna	UGA-7385	excrement	NR	NR	10530	620	12239	810	Civalero et al. 2007
Destacamento Guardaparques	-47,86184	-72,04117	Mylodontidea (ground sloths)	*Mylodon darwini*	AA-96293	bone	AMS	ABA[2]	11680	120	13553	130	Coni et al. 2020
			Mylodontidea (ground sloths)	*Mylodon darwini*	AA-96296	bone	AMS	ABA[2]	11780	120	13655	134	Coni et al. 2020
			Equidae (horses)	*Hippidion saldiasi*	AA-87694	bone	AMS	supplied as prepared collagen[2]	11000	110	12931	101	Coni et al. 2020
			indeterminate	Megafauna	AA-96294	bone	AMS	ABA[2]	12130	120	14075	232	Coni et al. 2020
			indeterminate	Megafauna	AA-96295	bone	AMS	ABA[2]	12420	120	14581	259	Coni et al. 2020
Baño Nuevo 1	-45,26440	-71,44275	Mylodontidea (ground sloths)	*Mylodon darwini*	UCIAMS-10105	bone	AMS	NR	11255	30	13145	29	Velásquez & Mena 2006, Labarca 2015
			Mylodontidea (ground sloths)	*Mylodon darwini*	UCIAMS-10106	bone	AMS	NR	11265	35	13155	37	Velásquez & Mena 2006, Labarca 2015
			Mylodontidea (ground sloths)	*Mylodon darwini*	UCIAMS-10104	NR	AMS	NR	11410	25	13272	39	Mena & Stafford 2006, Labarca 2015
			Mylodontidea (ground sloths)	*Mylodon darwini*	CAMS-32685	bone	AMS	NR	11480	50	13360	58	Velásquez & Mena 2006, Labarca 2015
			Mylodontidea (ground sloths)	*Mylodon darwini*	UCIAMS-10107	bone	AMS	NR	12510	30	14779	153	Velásquez & Mena 2006, Labarca 2015
			Macraucheniidae (macrauquenids)	*Macrauchenia patachonica*	UCIAMS-19491	tooth	AMS	NR	11665	50	13528	56	Velásquez & Mena 2006, Labarca 2015
			indeterminate	Ungulate	UCIAMS-10111	bone	AMS	NR	12400	30	14525	170	Velásquez & Mena 2006
			indeterminate	Ungulate	UCIAMS-10109	bone	AMS	NR	12320	30	14345	204	Velásquez & Mena 2006
Baño Nuevo 2	-45,26440	-71,44275	indeterminate	Ungulate	UCIAMS-10110	bone	AMS	NR	12000	35	13904	71	Velásquez & Mena 2006
Baño Nuevo 3	-45,26440	-71,44275	Canidae (canids)	*Dusicyon avus*	UCIAMS-19490	bone	AMS	NR	7070	25	7897	34	Velásquez & Mena 2006

Sites	Latitude (°S)	Longitude (°W)	Family	Taxa	Lab-code	Material	Measure	Pre-treatment	^{14}C age BP	error	^{14}C age calBP (mu)	error (1σ)	References
Northern slopes of the Patagonian Andes													
Monte Verde	-41,50470	-73,20440	Gomphoteriidae (gomphotheres)	*Notiomastodon platensis*	TX-3760	bone	AMS	NR	unclear^5	200	13952	310	Labarca 2015, González-Guarda 2018
			Gomphoteriidae (gomphotheres)	*Notiomastodon platensis*	OxA-105	tooth	AMS	NR	unclear^5	unclear^5	14029	393	Labarca 2015, González-Guarda 2018
El Trébol (Argentina)	-41,07330	-71,48660	Mylodontidea (ground sloths)	*Mylodontinae*	AA-65707	bone (burnt?)	AMS	ABA^2	10570	130	12464	208	Hajduk et al. 2006
Nochaco	-41,01900	-73,39000	Gomphoteriidae (gomphotheres)	*Notiomastodon platensis*	SD (no detail)	NR	NR	NR	16150	750	19730	911	Casamiquela 1969, Labarca 2015
Los Notros	-40,56944	-73,10417	Gomphoteriidae (gomphotheres)	*Notiomastodon platensis*	AA-109501	tooth	AMS	ABA^2	13585	81	16409	132	González-Guarda 2018, Lira et al. 2020
Pilauco	-40,56667	-73,11600	Gomphoteriidae (gomphotheres)	*Notiomastodon platensis*	TO-11477	bone	AMS	NR	12540	90	14779	235	González-Guarda et al. 2017
			Gomphoteriidae (gomphotheres)	*Notiomastodon platensis*	PSUAMS-2416	bone	AMS	NR	13040	60	15617	107	González-Guarda 2018
			Gomphoteriidae (gomphotheres)	*Notiomastodon platensis*	PSUAMS-2418	bone	AMS	NR	13210	60	15861	98	González-Guarda 2018
			Gomphoteriidae (gomphotheres)	*Notiomastodon platensis*	PSUAMS-2419	bone	AMS	NR	13260	70	15931	114	González-Guarda 2018
			Gomphoteriidae (gomphotheres)	*Notiomastodon platensis*	PSUAMS-2420	bone	AMS	NR	13240	60	15901	100	González-Guarda 2018
			Gomphoteriidae (gomphotheres)	*Notiomastodon platensis*	PSUAMS-2421	bone	AMS	NR	13135	50	15756	87	González-Guarda 2018
			Gomphoteriidae (gomphotheres)	*Notiomastodon platensis*	UCIAMS-101670	bone	AMS	NR	12725	40	15175	69	Pino et al. 2016
			Gomphoteriidae (gomphotheres)	*Notiomastodon platensis*	UCIAMS-101830	bone	AMS	NR	12760	50	15221	85	Pino et al. 2016
			Gomphoteriidae (gomphotheres)	*Notiomastodon platensis*	UCIAMS-101831	bone	AMS	NR	13220	60	15874	98	Pino et al. 2016
			Equidae (horses)	*Equus andium*	AA-81810	tooth	AMS	ABA^2	11457	140	13339	128	Pino et al. 2013
			Equidae (horses)	*Equus andium*	PSUAMS-2417	bone	AMS	NR	12035	50	13917	73	González-Guarda 2018
Cuchillo Curá	-38,43543	-70,30563	indeterminate	*Phyllophaga* sp. (ground sloth)	GX-21149	excrement	conv.	NR	13750	230	16655	331	Hofreiter et al. 2003
			indeterminate	*Phyllophaga* sp. (ground sloth)	Ua-13871	excrement	AMS	NR	14665	150	17900	220	Hofreiter et al. 2004
Cueva Huenul	-36,95000	-69,90000	indeterminate	Megafauna	AA-85720	excrement	AMS	ABA^2	11841	56	13689	74	Barberena et al. 2010, Barberena 2015
			indeterminate	Megafauna	AA-85722	excrement	AMS	ABA^2	13844	75	16803	129	Barberena et al. 2010, Barberena 2015
Río Cuarto (Córdoba)	-32,83000	-64,83000	Mylodontidea (ground sloths)	*Sclelidotherium leptocephalum*	LP-1407	bone	conv.	NR	7550	60	8342	68	Cruz et al. 2010
Gruta del Indio	-32,61600	-69,15000	indeterminate	Megafauna	LP-925	excrement	conv.	NR	8990	90	10083	141	García 2003, Gil 2005
			indeterminate	Megafauna	A-1351	excrement	conv.	NR	10610	210	12442	300	Long et al. 1997, García 2003, Gil 2005
			indeterminate	Megafauna	A-9493	excrement	conv.	NR	10900	185	12869	173	Long et al. 1997, García 2003, Gil 2005
			indeterminate	Megafauna	GRN-5558	excrement	conv.	acid wash^3	10950	60	12875	80	Long & Martin 1974, Long et al. 1997, Gil 2005
			indeterminate	Megafauna	A-9570	excrement	conv.	NR	11040	130	12958	114	Long et al. 1997, García 2003, Gil 2005
			indeterminate	Megafauna	A-1371	excrement	conv.	NR	11820	180	13716	209	Long et al. 1997, García 2003, Gil 2005
			indeterminate	Megafauna	A-9571	excrement	conv.	NR	12375	115	14520	255	Long et al. 1997, Gil 2005
			indeterminate	Megafauna	LP-929	excrement	NR	NR	30200	800	34742	874	García 2003
			indeterminate	Megafauna	LP-918	excrement	NR	NR	30800	700	35326	698	García 2003
			indeterminate	Megafauna	LP-1072	excrement	NR	NR	28670	720	32983	839	García 2003
			indeterminate	Megafauna	LP-1075	excrement	NR	NR	24140	510	28413	523	García 2003
			indeterminate	Megafauna	Beta-152588	excrement	NR	NR	29530	540	33939	632	García 2003
			indeterminate	Megafauna	Beta-152589	excrement	NR	NR	36400	200	41420	193	García 2003
			Mylodontidea (ground sloths)	Sloth	GrN-5772	bone	conv.	acid wash^3	9560	60	10914	129	García 2003
			Mylodontidea (ground sloths)	Sloth	A-1282	excrement	conv.	NR	9650	800	11224	1071	Long et al. 1997
			Mylodontidea (ground sloths)	Sloth	A-1636	excrement	conv.	NR	10200	300	11905	456	Long et al. 1997
			Mylodontidea (ground sloths)	Sloth	A-9494	excrement	conv.	NR	10285	240	12026	387	Long et al. 1997
Piedra Escarbada	-31,95192	-71,49403	Mylodontidea (ground sloths)	*Mylodontinae*	UGAMS-18379	bone	AMS	ABA	12410	35	14544	171	Méndez et al. 2020
Lazareto	-31,95081	-71,49925	Camelidae (camelids)	*Paleolama* sp.	UGAMS-11818	tooth	AMS	ABA	11160	30	13097	33	Méndez et al. 2020
			indeterminate	*Xenartra*	UGAMS-11820	bone	AMS	ABA	11300	30	13191	43	Méndez et al. 2020
Valle de los Caballos 266	-31,94611	-71,50511	indeterminate	Megamammal	UGAMS-19986	tooth	AMS	ABA	9770	30	11208	21	Méndez et al. 2020
			indeterminate	Megamammal	UGAMS-19984	bone	AMS	ABA	10280	30	12023	127	Méndez et al. 2020
			indeterminate	Megamammal	UGAMS-19985	bone	AMS	ABA	10390	30	12274	121	Méndez et al. 2020
Las Higrófilas	-31,94583	-71,49811	indeterminate	*Xenartra*	UGAMS-18378	bone	AMS	ABA	9670	30	11065	113	Méndez et al. 2020
El Avistadero	-31,93589	-71,50053	Equidae (horses)	*Equus* sp.	UGAMS-11545	bone	AMS	ABA	9770	30	11208	21	Méndez et al. 2020
			Camelidae (camelids)	*Paleolama* sp.	UGAMS-11547	bone	AMS	ABA on bioapatite	10920	30	12814	38	Méndez et al. 2020
			Camelidae (camelids)	*Paleolama* sp.	UGAMS-11546	bone	AMS	ABA on bioapatite	11190	30	13120	24	Méndez et al. 2020

Sites	Latitude (°S)	Longitude (°W)	Family	Taxa	Lab-code	Material	Measure	Pre-treatment	^{14}C age BP	error	^{14}C age calBP (mu)	error (1σ)	References
Quereo	-31,93075	-71,51194	Gomphoteriidae (gomphotheres)	*Notiomastodon platensis*	GAK-2984	bone	NR	NR	9100	300	10286	421	Paskoff 1971, Labarca 2015
El Membrillo	-31,92853	-71,48842	Mylodontidea (ground sloths)	*Mylodon* sp.	NSRL-11081	bone	AMS	ABA	13500	65	16276	110	Méndez et al. 2020
			Camelidae (camelids)	*Paleolama* sp.	UGAMS-9451	bone	AMS	ABA on bioapatite	10830	40	12768	29	Méndez et al. 2020
Las Vegas	-31,92247	-71,49814	Mylodontidea (ground sloths)	*Mylodontinae*	UGAMS-7593	bone	AMS	ABA	12280	40	14251	172	Méndez et al. 2020
			Mylodontidea (ground sloths)	*Mylodontidae*	UGAMS-6195	bone	AMS	ABA	7190	30	7994	31	Méndez et al. 2020
			Equidae (horses)	*Equus* sp.	UGAMS-7593	bone	AMS	ABA	13430	40	16174	77	Méndez et al. 2020
			Equidae (horses)	*Equus* sp.	UGAMS-7594	bone	AMS	ABA	9500	30	10822	135	Méndez et al. 2020
El Boldo	-31,90881	-71,48125	indeterminate	*Xenartra*	UGAMS-9450	bone	AMS	ABA on bioapatite	11970	30	13894	78	Méndez et al. 2020
Las Terrazas	-31,84000	-71,48000	Equidae (horses)	*Equidae*	UGAMS-11162	bone	AMS	ABA on bioapatite	25860	90	30113	79	Méndez et al. 2020
Las Monedas	-31,60000	-71,00000	Equidae (horses)	*Equus* sp.	UGAMS-18377	bone	AMS	ABA on bioapatite	10430	30	12338	132	Méndez et al. 2020
			Equidae (horses)	*Equus* sp.	UGAMS-18376	bone	AMS	ABA on bioapatite	10750	30	12731	11	Méndez et al. 2020
			Equidae (horses)	*Equus* sp.	UGAMS-7605	bone	AMS	ABA	10950	35	12848	54	Méndez et al. 2020
			Camelidae (camelids)	*Paleolama* sp.	UGAMS-7606	bone	NR	ABA	10310	30	12120	153	Méndez et al. 2020
Santa Julia	-31,48330	-71,23000	Equidae (horses)	*Equus* sp.	UGAMS-9447	tooth	AMS	ABA on bioapatite	11590	30	13453	47	Méndez et al. 2020
			Camelidae (camelids)	*Palaeolama* sp.	UGAMS-9449	bone	AMS	ABA on bioapatite	11770	30	13629	74	Méndez et al. 2020
			indeterminate	*Xenartra*	UGAMS-9448	bone	AMS	ABA on bioapatite	11490	35	13371	44	Méndez et al. 2020
							Pampa						
Conglomerado (Monte Hermoso)	-38,99000	-61,39000	Gomphoteriidae (gomphotheres)	*Stegomastodon platensis*	GrA-42388	tooth	AMS	acid etching^{3}	17600	135	21300	232	Prado et al. 2012
Pehuen-Có	-38,98000	-61,30000	Mylodontidea (ground sloths)	*Lestodon* sp.	NR	bone	AMS	NR	16440	320	19877	390	Aramayo et al. 2005
Paleolama (Monte Hermoso)	-38,83000	-60,54000	Equidae (horses)	*Equus neogeus*	GrA-47265	tooth	AMS	acid wash^{3}	14020	60	17075	110	Prado et al. 2012
Centinela del Mar	-38,43000	-58,22000	Equidae (horses)	*Hippidion principale*	GrA-49337	tooth	AMS	acid etching^{3}	15130	60	18467	118	Prado et al. 2015
			Macraucheniidae (macrauquenids)	*Macrauchenia patachonica*	GrA-49321	tooth	AMS	acid etching^{3}	9890	50	11317	83	Prado et al. 2015
Arroyo La Carolina, Mar del Sur	-38,35000	-57,99000	Equidae (horses)	*Hippidion principale*	GrA-48962	bone	AMS	acid etching^{3}	13450	60	16200	100	Prado et al. 2015
Arroyo Chasicó	-38,24000	-62,51000	Gomphoteriidae (gomphotheres)	*Stegomastodon platensis*	GrA-47267	tooth	AMS	acid wash^{3}	10710	50	12705	34	Prado et al. 2015
Río Quequén Grande	-38,19667	-59,11556	Equidae (horses)	*Equus neogeus*	LP-1235	bone	conv.	NR	10290	130	12093	274	Tonni et al. 2003b, Barnosky & Lindsey 2010
			Equidae (horses)	*Equus neogeus*	GrA-47132	bone	AMS	ABA^{3}	13930	60	16921	107	Prado et al. 2015
			Equidae (horses)	*Equus neogeus*	GrA-49125	tooth	AMS	acid etching^{3}	10150	55	11758	128	Prado et al. 2015
			Mylodontidea (ground sloths)	*Glossotherium robustum*	GrA-47131	bone	AMS	ABA^{3}	14160	60	17215	88	Prado et al. 2015
Arroyo Seco 2	-38,18000	-60,55000	Megatheriidae (ground sloths)	*Megatherium americanum*	AA-62514	bone	AMS	NR	11770	120	13645	134	Politis et al. 2016
			Megatheriidae (ground sloths)	*Megatherium americanum*	LP-53	bone	conv.	NR	8470	240	9480	328	Politis et al. 2019
			Megatheriidae (ground sloths)	*Megatherium americanum*	TO-1506	bone	conv.	NR	7320	50	8116	64	Politis et al. 2019
			Megatheriidae (ground sloths)	*Megatherium americanum*	SI-5481	bone	AMS	NR	1800	110	1706	131	Politis & Steele 2014
			Mylodontidea (ground sloths)	*Glossotherium robustum*	OxA-4591	bone	AMS	ion exchange gelatin (code AI)	12240	110	14300	261	Politis et al. 2016
			Mylodontidea (ground sloths)	*Glossotherium robustum*	AA-9049	bone	AMS	pretreatment by user (unknown)^{2}	10500	90	12420	187	Politis et al. 2003, Politis et al. 2016
			Toxodontidae (toxodontids)	*Toxodon* sp.	CAMS-16389	bone	AMS	base wash	11750	70	13618	85	Barnosky & Lindsey 2010, Politis et al. 2016
			Toxodontidae (toxodontids)	*Toxodon platensis*	AA-7964	bone	AMS	pretreatment by user (unknown)^{2}	11590	90	13451	93	Politis et al. 2016
			Equidae (horses)	*Equus neogeus*	AA-7965	bone	AMS	pretreatment by user (unknown)^{2}	11250	105	13158	103	Politis et al. 2016
			Equidae (horses)	*Equus neogeus*	OxA-4590	bone	AMS	ion exchange gelatin (code AI)	11000	100	12930	97	Politis et al. 2016
			Equidae (horses)	*Equus neogeus*	TO-1504	bone	AMS	NR	8890	90	9970	152	Politis et al. 2016
			Equidae (horses)	*Equidae*	AA-90118	bone	AMS	ABA^{2}	11190	110	13087	116	Politis et al. 2016
			Camelidae (camelids)	*Camelidae* cf. *Hemiauchenia*	GrA-47340	tooth	AMS	acid wash^{3}	9775	45	11203	46	Prado et al. 2015
			Chlamyphoridae (armadillo)	*Eutatus seguini*	AA-90117	bone	AMS	ABA^{2}	7388	74	8200	94	Politis et al. 2016
			indeterminate	Megafauna	OxA-9242	bone	AMS	ABA (code AG)	11730	70	13599	85	Steele & Politis 2009, Politis et al. 2016
			indeterminate	Megafauna	OxA-9243	bone	AMS	ABA (code AG)	12070	140	13999	233	Steele & Politis 2009, Politis et al. 2016
Río Quequén Salado	-38,12000	-59,06000	Chlamyphoridae (armadillo)	*Neuryurus* sp.	GrA-48668	bone	AMS	ABA^{3}	10480	50	12452	148	Prado et al. 2015
Paso Otero 5	-38,08000	-59,02000	Megatheriidae (ground sloths)	*Megatherium americanum*	GX-29795	bone	AMS	NR	9560	100	10902	161	Martínez et al. 2004, Martínez & Gutiérrez 2011
			Equidae (horses)	*Equus neogeus*	GX-29794	bone	AMS	NR	2110	30	2077	61	Martínez & Gutiérrez 2011
			Macraucheniidae (macrauquenids)	*Macrauchenia* cf. *patachonica*	GX-29792	bone	AMS	NR	4130	30	4678	83	Martínez & Gutiérrez 2011

Sites	Latitude (°S)	Longitude (°W)	Family	Taxa	Lab-code	Material	Measure	Pre-treatment	^{14}C age BP	error	^{14}C age calBP (mu)	error (1σ)	References
Paso Otero 5 *(continued)*	-38,08000	-59,02000	indeterminate	Megamammal	AA-19291	bone	AMS	pretreatment by user (unknown)[2]	10190	120	11877	285	Martínez & Gutiérrez 2011
			indeterminate	Megamammal	AA-39363	bone	AMS	ABA[2]	10440	100	12318	199	Martínez 2001, Martínez & Gutiérrez 2011
Campo del Arce	-38,00000	-59,00000	Megatheriidae (ground sloths)	*Megatherium americanum*	LP-174	bone	conv.	NR	13070	120	15659	185	Tonni et al. 2003b, Barnosky & Lindsey 2010
Arroyo Grande, Balcarce	-37,86000	-58,22000	Canidae (canids)	*Dusicyon avus*	GrA-49126	tooth	AMS	acid etching[3]	6250	50	7153	80	Prado et al. 2015
Santa Clara del Mar	-37,85000	-57,51000	Gomphoteriidae (gomphotheres)	*Stegomastodon platensis*	GrA-37641	tooth	AMS	base-acid washes[3]	17880	60	21719	152	Alberti and Prado 2008
La Moderna	-37,13000	-60,08000	Chlamyphoridae (armadillo)	*Doedicurus clavicaudatus*	Beta-7824	bone	conv.	NR	6550	160	7434	149	Politis et al. 2019
			Chlamyphoridae (armadillo)	*Doedicurus clavicaudatus*	TO-1507	bone	AMS	NR	12350	370	14577	557	Politis et al. 2019
			Chlamyphoridae (armadillo)	*Doedicurus clavicaudatus*	TO-1507-1	bone	AMS	NR	7010	100	7833	94	Politis et al. 2019
			Chlamyphoridae (armadillo)	*Doedicurus clavicaudatus*	TO-1507-2	bone	AMS	NR	7510	370	8415	413	Politis et al. 2019
			Chlamyphoridae (armadillo)	*Doedicurus clavicaudatus*	TO-2610	bone	AMS	NR	7460	80	8262	85	Politis et al. 2019
			Chlamyphoridae (armadillo)	*Glyptodont* sp.	CAMS-155869	bone	AMS	NR	7890	330	8812	382	Politis & Lindsey 2012
			Chlamyphoridae (armadillo)	*Neosclerocalyptus* sp.	CAMS-155871	bone	AMS	NR	4820	250	5527	311	Politis & Lindsey 2012
			Chlamyphoridae (armadillo)	*Neosclerocalyptus* sp.	CAMS-155870	bone	AMS	NR	4680	120	5373	164	Politis & Lindsey 2012
			Chlamyphoridae (armadillo)	*Doedicurus clavicaudatus*	AA-55120	bone	AMS	acid wash[2]	494	53	529	49	Politis & Lindsey 2012
Campo Laborde	-37,05000	-61,10000	Megatheriidae (ground sloths)	*Megatherium americanum*	AA-71665	bone (burnt?)	AMS	ABA[2]	9730	290	11191	471	Politis et al. 2019
			Megatheriidae (ground sloths)	*Megatherium americanum*	AA-71667	bone	AMS	ABA	6740	480	7624	503	Politis et al. 2019
			Megatheriidae (ground sloths)	*Megatherium americanum*	AA-71666	bone	AMS	ABA	7630	460	8584	517	Politis et al. 2019
			Megatheriidae (ground sloths)	*Megatherium americanum*	AA-55117	bone	AMS	acid wash	7750	250	8641	300	Politis et al. 2019
			Megatheriidae (ground sloths)	*Megatherium americanum*	AA-55118	bone	AMS	acid wash	8080	200	8984	260	Politis et al. 2019
			Megatheriidae (ground sloths)	*Megatherium americanum*	CAMS-171851[1]	bone	AMS	XAD	10570	170	12420	253	Politis et al. 2019
			Megatheriidae (ground sloths)	*Megatherium americanum*	CAMS-171861[1]	bone	AMS	XAD	10690	380	12459	498	Politis et al. 2019
			Megatheriidae (ground sloths)	*Megatherium americanum*	CAMS-155863[4]	bone	AMS	UF	7380	410	8293	445	Politis et al. 2019
			indeterminate	Megamammal	AA-55119	bone	AMS	acid wash	8720	190	9812	235	Politis et al. 2019
Arroyo Tapalqué	-36,95000	-60,37000	Felidae (felid)	*Smilodon populator*	GrA-49131	tooth	AMS	acid etching[3]	10140	60	11731	141	Prado et al. 2015
			Mylodontidea (ground sloths)	*Scelidotherium leptocephalum*	GrA-48388	bone	AMS	acid wash[3]	7615	85	8419	89	Prado et al. 2015
			Equidae (horses)	*Equus neogeus*	GrA-47178	tooth	AMS	acid wash[3]	13590	60	16413	101	Prado et al. 2015
Salto de Piedra	-36,94740	-60,37500	Mylodontidea (ground sloths)	*Mylodontinae*	LP-1193	bone	conv.	NR	11940	80	13828	122	Tonni et al. 2003b
Río Salado	-35,75000	-58,76000	Felidae (felid)	*Smilodon populator*	LP-2184	bone	conv.	NR	13400	200	16153	301	Scanferla et al. 2013
			Megatheriidae (ground sloths)	*Megatherium americanum*	GrA-49130	tooth	AMS	acid etching[3]	11590	60	13448	67	Prado et al. 2015
			Equidae (horses)	*Hippidion principale*	GrA-49323	bone	AMS	ABA[3]	14190	60	17233	91	Prado et al. 2015
			Equidae (horses)	*Hippidion principale*	LP-2259	bone	conv.	NR	12860	120	15376	177	Scanferla et al. 2013
			Equidae (horses)	*Hippidion principale*	Beta-311032	tooth	AMS	NR	14120	50	17192	86	Prado et al. 2013
			Chlamyphoridae (armadillo)	*Doedicurus clavicaudatus*	GrA-48480	bone	AMS	ABA[3]	14140	60	17204	88	Prado et al. 2015
			Chlamyphoridae (armadillo)	*Doedicurus clavicaudatus*	GrA-48961	bone	AMS	ABA[3]	12860	50	15375	96	Prado et al. 2015
			Chlamyphoridae (armadillo)	*Doedicurus* sp.	LP-2568	bone	conv.	NR	12380	190	14548	337	Scanferla et al. 2013
Chascomús	-35,69000	-57,99000	Chlamyphoridae (armadillo)	*Sclerocalyptus ornatus*	GrA-48955	bone	AMS	ABA[3]	13370	55	16091	97	Prado et al. 2015
Río Luján	-34,67000	-59,33000	Toxodontidae (toxodontids)	*Toxodon platensis*	Beta-305155	tooth	AMS	NR	11920	50	13794	111	Prado et al. 2015
			Chlamyphoridae (armadillo)	*Glyptodont clavipes*	NR	bone	AMS	NR	4370	90	5011	145	Rossello et al. 1999

Footnotes: [1]multi-ages on one sample; [2]University of Arizona AMS laboratory (AA) personal communication; [3]Center for isotope research, University of Groningen laboratory (GrA) personal communication; [4]clear outlier; [5]The results of the two age estimates are different in two publications, with the two source reports being unavailable online: TX-3760 = 11.990 ± 200 years BP and OxA-105 = 12.000 ± 250 years BP (Dillehay 2000 in Labarca 2015), TX-3760 = 13,860 ± 200 years BP and OxA-105 = 12,250 ± 200 years BP (Dillehay and Pino 1989 in González-Guarda 2018).

Appendix 6.1.2. Methodological details related to the spatial pattern of timing of megafauna extirpation and associated uncertainties. *(a) distribution of the error associated with each reliable age estimate (it is to be expected that the younger the age estimates, the smaller the associated error), (b) bandwidth optimisation. The optimal bandwidth selected (54) is associated with the lower integrated mean squared error representing a combination of the average bias and variance (see Saltré et al., 2019). The size of bandwidth is optimised to find a trade-of between the local bias generated by accounting for data far away from the focal grid cell (i.e., the larger the bandwidth, the higher the bias) and the local variance that increases when few data are considered (i.e., too narrow a bandwidth). SdAge = error associated with each reliable age estimate, imse= integrated mean squared error (see Saltré et al., 2019). Age is expressed in calibrated years before present (cal BP).*

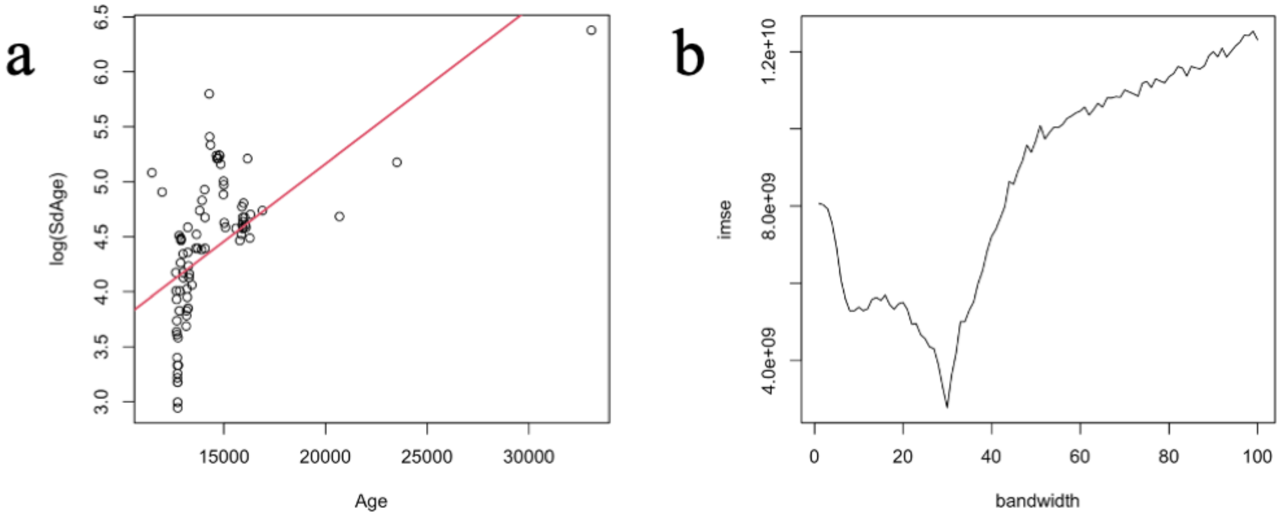

RÉSUMÉ

La période qui a suivi le dernier maximum glaciaire (il y a environ 19 000 ans jusqu'à aujourd'hui) a été caractérisée par des changements majeurs dans le climat mondial et la concentration de CO_2 dans l'atmosphère, tels que l'augmentation générale des températures mondiales et des changements dans les régimes de précipitations. Dans l'écozone néotropicale, une région biogéographique qui s'étend du sud des États-Unis à la Terre de Feu au Chili, à l'extrême sud de l'Amérique du Sud, cette période a coïncidé avec des bouleversements généralisés des écosystèmes, notamment des changements dans la végétation, l'extinction de plus de 80 % des espèces de la mégafaune sud-américaine (c'est-à-dire des espèces pesant plus de 44 kg) et l'augmentation des densités de population d'*Homo sapiens*. Cependant, quantifier comment les relations entre ces événements ont façonné le paysage passé de l'Amérique du Sud reste un défi. L'objectif principal de ma thèse était de quantifier la manière dont les changements environnementaux passés associés à une augmentation de la pression humaine ont façonné les écosystèmes d'Amérique du Sud. Plus précisément, l'objectif était de 1) synthétiser les connaissances et quantifier les effets des changements climatiques postérieurs au dernier maximum glaciaire et de l'intensification des activités humaines sur les écosystèmes néotropicaux à de larges échelles spatiales, en me concentrant principalement sur les changements de végétation, et 2) déterminer si les changements de végétation induits par le climat après le dernier maximum glaciaire auraient pu provoquer l'extinction de la mégafaune dans l'écozone néotropicale. Dans ce but, j'ai combiné les informations fournies par les archives fossiles des paléoenvironnements et de la mégafaune avec une approche de modélisation spatiale et dynamique de la végétation basée sur des expériences de simulation du paléoclimat. J'ai montré que les variations des précipitations, de la température, du rayonnement solaire et des concentrations de CO_2 dans l'atmosphère ont potentiellement conduit à des augmentations substantielles, étendues et asynchrones de la couverture arborée régionale, affectant fortement un tiers de l'écozone néotropicale principalement avant le début de l'Holocène (il y a environ 11 700 ans). Alors que l'effet du climat semble prédominant dans les changements à grande échelle des écosystèmes avant l'Holocène, les activités humaines ont joué un rôle de plus en plus important pendant l'Holocène, entraînant un découplage progressif entre la distribution de la végétation et le climat, brouillant ainsi notre compréhension actuelle des relations entre le climat et la végétation. Mes résultats soutiennent également l'hypothèse selon laquelle les changements de végétation induits par le climat n'ont probablement pas été la principale cause de la disparition de la plupart des espèces de mégafaune dans le Cône Sud (latitude > 30 °S) à la toute fin du Pléistocène. Dans l'ensemble, ma thèse permet de mieux comprendre les mécanismes à grande échelle qui ont façonné les écosystèmes néotropicaux tels que nous les connaissons aujourd'hui, et de prévoir la réponse de ces écosystèmes aux futurs changements climatiques et à l'intensification continue des activités humaines.

Post-Last Glacial Maximum vegetation and ecosystem responses to climate change and human expansion in the Neotropical realm: land cover changes and megafauna extinctions

Thesis submitted by Antoine Champreux to Flinders University for the degree of Doctor of Philosophy

SUMMARY

The last Ice Age ended around 19,000 years ago and was followed by a global warming that lasted around 7,000 years, giving rise to major vegetation changes on all continents. It was during this warming period that South America saw most of the large animal species that used to populate it disappear, and human population densities explode. However, the extent of the changes in vegetation, the effect of human on nature and the causes of the extinction are still poorly understood. By comparing the information provided by the fossil record and computer simulations of ecosystems, I show that climate change may have caused major changes in vegetation, but that their scale was probably insufficient to cause extinction. I also show that humans have had an increasingly important effect on nature over the last 12,000 years, to the point of disturbing our current understanding of the links between climate and vegetation.

ABRÉGÉ

Réponse de la végétation et des écosystèmes au changement climatique et à l'expansion humaine après le dernier maximum glaciaire dans l'écozone néotropicale : modifications de la couverture terrestre et extinctions de la mégafaune – Thèse présentée par Antoine Champreux à l'Université Flinders en vue de l'obtention du titre de Docteur en Philosophie

La dernière période glaciaire s'est achevée il y a environ 19 000 ans et a été suivie d'un réchauffement global qui a duré environ 7 000 ans, donnant lieu à des changements majeurs de la végétation sur tous les continents. C'est au cours de cette période de réchauffement que l'Amérique du Sud a vu disparaître la plupart des espèces animales de grande taille qui la peuplaient et que les densités de population humaine ont explosé. Cependant, l'ampleur des changements de végétation, l'effet de l'homme sur la nature et les causes de l'extinction sont encore mal connus. En comparant les informations fournies par les archives fossiles et les simulations informatiques des écosystèmes, je montre que le changement climatique a pu provoquer des changements majeurs dans la végétation, mais que leur ampleur était probablement insuffisante pour provoquer l'extinction. Je montre également que l'homme a eu un effet de plus en plus important sur la nature au cours des 12 000 dernières années, au point de perturber notre compréhension actuelle des liens entre le climat et la végétation.